Stony Brook University

NEW CRANIAL AND POSTCRANIAL REMAINS OF LATE PALEOCENE PLESIADAPIDAE ("PLESIADAPIFORMES," MAMMALIA) FROM NORTH AMERICA AND EUROPE: DESCRIPTION AND EVOLUTIONARY IMPLICATIONS

A Dissertation Presented

by

Douglas Martin Boyer

to

The Graduate School

in Partial Fulfillment of the

Requirements

for the Degree of

Doctor of Philosophy

in

Anatomical Sciences

Stony Brook University

May 2009

Stony Brook University

The Graduate School

Douglas Martin Boyer

We the dissertation committee for the above candidate for the

Doctor of Philosophy degree, hereby recommend

acceptance of this dissertation

David W. Krause – Dissertation Advisor
Distinguished Service Professor, Department of Anatomical Sciences

Maureen A. O'Leary – Chairperson of Defense
Associate Professor, Department of Anatomical Sciences

John G. Fleagle
Distinguished Professor, Department of Anatomical Sciences

William L. Jungers
Distinguished Teaching Professor and Chairman, Department of Anatomical Sciences

Philip D. Gingerich
E. C. Case Professor of Paleontology, Professor of Geology, Biology, and Anthropology, Director of Museum of Paleontology, University of Michigan, Ann Arbor

This dissertation is accepted by the Graduate School

Lawrence Martin
Dean of the Graduate School

Abstract of the Dissertation

NEW CRANIAL AND POSTCRANIAL REMAINS OF LATE PALEOCENE PLESIADAPIDAE ("PLESIADAPIFORMES," MAMMALIA) FROM NORTH AMERICA AND EUROPE: DESCRIPTION AND EVOLUTIONARY IMPLICATIONS

by

Douglas Martin Boyer

Doctor of Philosophy

in

Anatomical Sciences

Stony Brook University

2009

Plesiadapidae are a diverse monophyletic family of primate-like mammals that existed during the Paleogene in Europe and North America. They are thought to be nested within the Plesiadapoidea, which are in turn a member of a larger group of fossil mammals called the Plesiadapiformes. An understanding of plesiadapid evolutionary history is important for investigations into the origin of extant primates (including humans, apes, monkeys, lemurs, etc.) plus anatomically modern, extinct primates (euprimates). Specifically, this dissertation accumulates evidence bearing on the hypothesis that the ancestor of euprimates inherited a big toe that (1) is divergent from the lateral digits, (2) exhibits lateral torsion, and (3) has a nail, from its common ancestor with the Plesiadapoidea, in which these features were adaptations to foraging for angiosperm products in a fine branche niche. New information on plesiadapid skeletons may alter views on the phylogenetic relationship of various plesiadapiforms to euprimates. Altered phylogenetic arrangements of plesiadapids, other plesiadapiforms, and euprimates, are likely to indicate that the unusual features of the feet of euprimates were not inherited from plesiadapiforms and evolved at roughly the same time as forward facing orbits and other euprimate novelties. This would re-open the possibility that euprimate features are adaptations for a behavior besides foraging among small branches for angiosperm products.

I describe the first known crania of *Pronothodectes gaoi*, a species of the most basal plesiadapid genus known; a skull of *Nannodectes intermedius*, the oldest known for a plesiadapid; and the first skull and postcranial skeleton of the large, late-occurring North American species *Plesiadapis cookei*. I provide new morphological observations for a cranial specimen of *Nannodectes gidleyi* and several specimens of *Plesiadapis tricuspidens*. These new data document basic characteristics of plesiadapid cranial and

postcranial anatomy more accurately and comprehensively than previously possible. I use quantitative comparative and cladistic methodologies to (1) reconstruct cranial characteristics for the ancestral node of the family Plesiadapidae, (2) generate hypotheses regarding phylogenetic relationships of various plesiadapid species to each other, and (3) test hypotheses regarding the phylogenetic relationship of Plesiadapidae and other plesiadapiforms to extant euarchontan mammals (Primates, Scandentia, and Dermoptera). I use quantitative comparative morphology to reconstruct functional and behavioral features of various plesiadapid species.

The ancestral node of the family Plesiadapidae is reconstructed as having an enlarged premaxilla that contacts the frontal; a laterally-positioned, intratympanic, transpromontorial route for the internal carotid plexus; a non-functional internal carotid artery; a non-tubular external auditory meatus; and an auditory bulla, the composition of which is uncertain, but best interpreted as petrosal. *P. cookei* and *P. tricuspidens* appear derived in having external auditory meati that are tubular and in having a maxilla that lacks extensive dorsal exposure of the molar tooth roots within the orbit. *P. tricuspidens* is apparently autapomorphic among plesiadapids in having an increased relative size and posterior projection of the premaxilla, consequent narrowing of the frontal contact with the nasal, an increased relative size of the glenoid fossae of the squamosal and decreased prominence and posterior projection of the nuchal crests. *N. gidleyi* is autapomorphic in having an increased relative size of the glenoids, and in the apparent lack of an intratympanic route for the internal carotid plexus.

P. cookei and *P. tricuspidens* have been traditionally thought to be close relatives. *P. tricuspidens* is also thought to be closely related to *Platychoerops.* The skull of *P. cookei* differs from that of *P. tricuspidens* in ways that make it similar to earlier-occurring North American plesiadapids. Unlike *P. tricuspidens* or other North American plesiadapids, *P. cookei* has a dentition indicating it had a diet focused on leaves. These features and a cladistic analysis of other dental characters suggest that *P. cookei* is a closer relative of *Platychoerops* than is *P. tricuspidens.*

The postcranial skeleton of *Plesiadapis cookei*, while generally similar to that of other plesiadapids, has more elongate limbs, possibly reflecting a more specialized arboreal habitus.

Finally, new information from plesiadapid skulls and postcrania increases cladistic support for previously proposed higher-level clades. Specifically, the new data support the hypotheses that plesiadapids, carpolestids, saxonellids and *Chronolestes* comprise the Plesiadapoidea, and that Plesiadapoidea is the sister taxon to Euprimates. Therefore the results of this dissertation corroborate the hypothesis that euprimates evolved their grasping features from a fine-branch foraging, common ancestor with plesiadapoids.

Dedication:

This dissertation is dedicated to my family, especially my father, Martin Boyer; my mother, Lyle (Hillman) Lad; and my grandparents - Thomas and Theresa Boyer, and William and June Hillman. These people have always been my primary role models and sources of inspiration. They have always loved, encouraged, and supported me.

Table of Contents

Figure list

Chapter 1

Chapter 2

Chapter 3

Chapter 4

Chapter 5

Chapter 6

Table List

Chapter 2

Chapter 3

Chapter 4

Chapter 5

Acknowledgments

This dissertation is organized so that each chapter is followed by acknowledgments of those individuals and funding agencies that made the research presented there possible. However, a few general thanks are stated here. First, I thank those who have provided me with my foundation in science, many unique opportunities, and critical assistance and guidance over the years including William Sanders, Jonathan Bloch, Philip Gingerich, and David Krause. Joseph Groenke is another person who has been particularly important in the accomplishments partly represented by this dissertation.

My dissertation committee has been a cohesive team, each member fulfilling a critical and unique role to improve the scientific quality, presentational quality, and scientific relevance of the work represented by this document. Together they have helped to hone the many projects in which I am involved down to a select few that constitute this dissertation.

I must additionally acknowledge the Stony Brook University faculty who did not serve on my committee but have provided many important or foundational learning, teaching, and research experiences. These include Jack Stern, Susan Larson, Brigitte Demes, Stefan Judex, Patricia Wright, James Rohlf, Nate Kley, Troy Rasbury, Randy Susman, Erik Sieffert, James Rossie, Elizabeth Stone, Fred Grine, Lawrence Martin, Callum Ross, Cathy Forster, and Alan Turner. I am grateful and honored to have participated in the tradition of academic excellence that this University and its faculty represent.

Making a large contribution to the success of Stony Brook University's anatomy program are secretaries Linda Benson and Chris Johnson, who have gone out of their way to help me and many others over the years. Furthermore, Stony Brook could not function the way it does without the skilled artistry of Luci Betti-Nash and Stephen Nash. Cindy Stauch, the Museum Business Administrator at the University of Michigan Museum of Paleontology helped usher in my career in paleontology by putting me in contact with the Museum's fossil preparator, Dr. William Sanders, upon hearing of my interests from Jackie Pozniack, the mutual veterinarian and friend of Cindy and my mother Lyle Lad, in 1997.

Generally speaking, I am in debt to many people at the University of Michigan, Stony Brook University, and elsewhere who have written letters of recommendation for my graduate school applications, grant and fellowship applications, and job applications; and/or those who have taken the time to review the various manuscripts and project proposals I have written. I must acknowledge my peers in the Stony Brook University Anatomical Sciences and Anthropology graduate programs who were a source of inspiration and camaraderie while we learned to become professional scientists together. I hope that I continue to work with many of these people well into the future. Finally, the most inspiring and supportive people in my life, without whom the completion of this dissertation would have had much less meaning for me, include members of my family (to whom this document is dedicated) and Ashley Gosselin-Ildari.

CHAPTER 1:

INTRODUCTION

Plesiadapiformes are a paraphyletic or polyphyletic taxon also referred to as "early primates" or "archaic primates" (e.g., Simons, 1964, 1967, 1972; Gingerich, 1975a, 1976; Szalay et al., 1987; Bloch et al., 2007). Plesiadapids (Trouessart, 1897) are an extinct, diverse group (Fig. 1.1) of "plesiadapiforms" that existed mainly in North America and Europe during the Paleogene (Gingerich, 1976). They are the focus of this study. Questionable records of the group's existence also come from Asia (Thewissen et al., 2001; Fu et al., 2002). Plesiadapids comprise one of the few mammalian groups from the Paleogene for which species-level evolution has been extensively documented by studies of large samples of dental and gnathic remains: they appear to have evolved rapidly (Gingerich, 1973, 1975a, b, 1976). The primary stratigraphic sections in which this pattern of evolution was established lie in several structural basins in the western interior of North America: the Clark's Fork Basin of northern Wyoming, the Crazy Mountains Basin of south-central Montana, the Wind River Basin of southwestern Wyoming, and the Bison Basin of central Wyoming. Specifically, the Clark's Fork Basin has sections that document the beginning and end of plesiadapid evolution, the Crazy Mountains Basin documents the beginning and middle portions, and the Bison and Wind River basins document only the middle portion.

During the Paleocene, there is much evidence for mammalian dispersal between Europe and North America (Savage and Russell, 1983; Tambareau et al., 1992). A diversity of European plesiadapids have been collected and described starting over 130 years ago (Gervais, 1877). Many of these European taxa have been proposed as sister taxa, subspecies, and/or ancestors and descendents of the North American taxa (Russell, 1964; Gingerich, 1973, 1975b, 1976; Rose, 1981). From the first appearance of plesiadapids in the fossil record until the youngest recorded occurrences, at least 28 species (including those from Europe, see Figure 1.1) have been recognized (Gingerich, 1975b, 1976; Rose, 1981; Hooker, 1994). In North America they range through the last seven million years of the Paleocene (Lofgren et al., 2004). There is one reported Eocene occurrence of *Plesiadapis dubius* (Rose and Bown, 1982); however, until further evidence of the family's persistence in North America is recovered, this record, which is based on a single tooth, must be considered tentative. However, in Europe the family definitely persisted into the early Eocene (e.g., Gingerich, 1973, 1975b, 1976; Hooker, 1994). The earliest known plesiadapid is *Pronothodectes matthewi* from Gidley Quarry of Montana (~63 Ma), while the latest occurrence is *Platychoerops daubrei* from Mutigny, France (~52.4 Ma) (Gingerich, 1976; see Gradstein et al. [2004] and Lofgren et al. [2004] for age information).

Plesiadapids have been known from skull material since 1935 (Simpson, 1935). Since then, these specimens have been studied with the idea that they might provide insight into the evolutionary origins of modern primates (or euprimates – Hoffstetter [1977]) (e.g., Russell, 1964; Gingerich, 1975a, 1976; MacPhee and Cartmill, 1986). As noted above, "plesiadapiforms" were traditionally viewed as a more primitive radiation of

primates, sharing many dental features with modern members of the group, but lacking some of the key skeletal features (Simpson, 1935; Gingerich, 1976). Since gradistic concepts of relationships have given way to cladistic ones, the key question regarding "plesiadapiform" relationships to modern primates is the following: *Do plesiadapiforms and Euprimates share a special relationship to the exclusion of any other extant or extinct order of mammals?* If the answer to this question is "yes," then morphological and reconstructed behavioral differences between plesiadapiforms and euprimates may illustrate an explicit sequence of adaptive changes, which equate to a description of "how" euprimates acquired their morphological and ecological specializations from their archaic "plesiadapiform" ancestors (Szalay and Dagosto, 1980, 1988; Cartmill, 1992; Bloch and Boyer, 2002; Bloch et al., 2007).

Among "plesiadapiforms," plesiadapids in particular have figured prominently in formulation of hypotheses regarding relationships of plesiadapiforms to euprimates. This is true primarily because plesiadapids were known from well-preserved skulls and skeletons long before the discovery of such remains for any non-plesiadapid plesiadapiform (Russell, 1964; Gingerich, 1971, 1975a; Szalay et al., 1975, 1987; MacPhee et al., 1983; Beard, 1990; Bloch and Boyer, 2002). As the number of plesiadapiforms known from non-dental remains has increased (Szalay, 1972; Kay et al., 1992; Bloch and Silcox, 2006), and the phylogenetic significance of this material has been evaluated (e.g., Bloch et al., 2007), it has been hypothesized that the Plesiadapidae are members of the Plesiadapoidea (Fig. 1.1), the sister group to Euprimates. The findings of these studies generate predictions regarding the primitive morphology and behavior of Plesiadapidae. Thus, further documentation of this group's evolution stands

to refine views of the evolutionary origin of Euprimates (Szalay, 1968; Szalay and Dagosto, 1980; Bloch and Boyer, 2003; Kirk et al., 2003). This additional documentation must begin with descriptions of new specimens of poorly represented species.

In this dissertation I aim to provide comprehensive descriptions and character analyses of newly discovered cranial and postcranial material referable to the Plesiadapidae, the core family of plesiadapiforms. I also address previous phylogenetic hypotheses for the Plesiadapidae and consider some functional morphological questions that have implications for the degree to which plesiadapids occupied a "primate-like" ecological niche.

Specifically, new information on plesiadapid crania and postcrania can help address the hypothesis that the specialized grasping hallux of Euprimates evolved in (and was inherited from) a "plesiadapiform" ancestor that lacked euprimate visual system features, such as a postorbital bar and convergent orbits on the cranium (Bloch and Boyer, 2002; Bloch et al., 2007; Sargis et al., 2007). If cladistic analyses incorporating new cranial and postcranial information on plesiadapids overturn the phylogenetic hypothesis that plesiadapids and carpolestids are sister taxa, and/or members of the sister taxon to euprimates (Bloch et al., 2007), this could show that characters relating to the hallucal grasp complex of the carpolestid plesiadapiform *Carpolestes simpsoni* (Bloch and Boyer, 2002) were not inherited from a common ancestor with Euprimates. This result, in turn, could have implications for theories on the original adaptive significance of euprimate features (e.g., Sussman, 1991; Cartmill, 1992; Bloch et al., 2007).

Different ideas regarding the adaptive significance of euprimate features have different predictions regarding the evolutionary sequence in which features of interest

were acquired. Specifically, the "angiosperm exploitation hypothesis" of R. Sussman (Sussman and Raven, 1978; Sussman, 1991) argues that features reflecting the ability to locomote in trees (like relatively long fingers and toes, and a divergent, opposable hallux with a nail) originally facilitated access to angiosperm resources (flowers, nectar, pollen, fruits, seeds, etc.) in a fine branch niche, making grasping features of primary importance. Sussman believed that teeth should and do show increasing specialization towards frugivory through early primate evolution, as elegantly argued by Szalay (1968). Visual system features are predicted to appear at the same time as or after grasping features, but there is no specific point in primate-euprimate evolution when visual system features are seen as integral or critical in Sussman's hypothesis. Instead, the visual system features are thought to be further improvements for a life spent in the trees searching out angiosperm products, and are described as an eventual consequence of coevolution between angiosperms, primates and other vertebrates that utilize angiosperm resources in an arboreal milieu (e.g., bats and various birds). The view of early primate-euprimate evolution presented by phylogenetic hypotheses that are supported by recent cladistic analyses corroborates the angiosperm exploitation hypothesis (Bloch et al. 2007), but refutes the "visual predation hypothesis" of Cartmill (1972). The visual predation hypothesis suggests that the synchronized evolution of euprimate pedal grasping and visual features allowed euprimates to visually locate and manually apprehend insects in the shrub-layer of forests at night. Decoupled evolution of grasping and visual features, and the precedence of grasping features in the course of evolution leading up to euprimates, is inconsistent with this hypothesis.

If a new phylogenetic hypothesis resulting from analyses incorporating information from new fossils of plesiadapids shows that the hallucal grasp complex of *Carpolestes simpsoni* (Bloch and Boyer, 2002) was not inherited from a common ancestor with Euprimates, this would re-open the possibility that euprimate pedal grasping and visual system features evolved as an integrated suite in the ancestral euprimate. Cartmill's visual predation hypothesis would thereby gain plausibility as an explanation for the adaptive significance of the evolution of these features.

Overview of Dissertation Chapters

Chapter 2 and 3 are devoted primarily to the documentation and description of two new plesiadapid skulls. Chapter 2 focuses first on cranial material of *Pronothodectes gaoi* (Fox, 1990), a member of the most basal genus of the Plesiadapidae (Gingerich, 1976). It then provides extensive documentation of previously studied cranial material for comparison.

Chapter 3 focuses on first cranial material of *Plesiadapis cookei*, the largest and one of the latest occurring of North American plesiadapids (Jepsen, 1930; Gingerich, 1976; Rose, 1981). It also provides extensive comparisons to the skull and dentition of the similarly-sized and penecontemporaneous *Plesiadapis tricuspidens* from France in order to address questions about relative body size and differential ecological specialization among these and other plesiadapids.

Chapter 4 documents and describes the postcranial skeleton associated with the new skull of *P. cookei* described in Chapter 3. The skeleton of *P. cookei* is the most completely known for a plesiadapiform: it provides the first knowledge of many elements

of the plesiadapiform skeleton. Extensive quantitative comparisons are provided to other plesiadapids, some non-plesiadapid plesiadapiforms, a few non-plesiadapiform Cretaceous and Paleocene eutherian mammals, and an extant sample consisting of various primates, treeshrews (Scandentia), the flying lemur *Cynocephalus* (Dermoptera), rodents, marsupials, and xenarthrans.

Chapter 5 presents a species level cladistic analysis and phylogenetic hypothesis for members of the Plesiadapidae. An hypothesis for the cranial and postcranial morphology of the "ancestral plesiadapid" is generated by optimizing character information gleaned from the previous three chapters onto the new species level tree. The character codings representing the ancestral plesiadapid are then used to reevaluate previously hypothesized relationships between plesiadapids and other euarchontan groups. The outcome of this last analysis will therefore test the hypothesis that euprimate pedal grasping features were inherited from a plesiadapiform ancestor, as described above.

Chapter 6 is an outline and summary of major conclusions.

Organization of Dissertation Chapters

In an effort to facilitate compartmentalization of this synthetic work for later publication, chapters 2-5 were written to stand as independent units. Therefore, each chapter has its own Abstract, Introduction, Abbreviations, Materials and/or Methods, Results, Discussion, Conclusions, Acknowledgments, and References sections. This explains why there is no Materials and Methods chapter for the dissertation as a whole. Furthermore, the figures and tables for each chapter are appended to the end of the

chapter text. Some redundancy has been avoided between chapters by referring certain discussions or explanations to the earlier chapters in which they were already covered. For instance, the Anatomical Terminology section of Chapter 3 simply refers the reader to that of Chapter 2.

REFERENCES

Beard, K.C., 1990. Gliding behavior and paleoecology of the alleged primate family Paromomyidae (Mammalia, Dermoptera). Nature 345, 340-341.

Bloch, J.I., Boyer, D.M., 2002. Grasping primate origins. Science 298, 1606-1610.

Bloch, J.I., Boyer, D.M., 2003. Response to comment on "Grasping Primate Origins". Science 300, 741c.

Bloch, J.I., Silcox, M.T., 2006. Cranial anatomy of the Paleocene plesiadapiform *Carpolestes simpsoni* (Mammalia, Primates) using ultra high-resolution X-ray computed tomography, and the relationships of plesiadapiforms to Euprimates. Journal of Human Evolution 50, 1-35.

Bloch, J.I., Silcox, M.T., Boyer, D.M., Sargis, E.J., 2007. New Paleocene skeletons and the relationship of plesiadapiforms to crown-clade primates. Proceedings of the National Academy of Sciences 104, 1159-1164.

Cartmill, M., 1972. Arboreal adaptations and the origin of the order Primates. In: Tuttle, R. (ed) The Functional and Evolutionary Biology of Primates. Aldine, Chicago, pp. 97-122.

Cartmill, M., 1992. New views on primate origins. Evolutionary Anthropology 1, 105-111.

Fox, R.C., 1990. *Pronothodectes gaoi* n. sp. from the late Paleocene of Alberta, Canada, and the early evolution of the Plesiadapidae (Mammalia, Primates). Journal of Paleontology 64, 637-647.

Fox, R.C., 1991. Systematic position of *Pronothodectes gaoi* Fox from the Paleocene of Alberta: reply. Journal of Paleontology 65, 700-701.

Fu, J.-F., Wang, J.-W., Tong, Y.-S., 2002. The new discovery of the Plesiadapiformes from the early Eocene of Wutu Basin, Shandong Province. Vertebrata PalAsiatica 40, 219-227.

Gervais, M.P., 1877. Enumération de quelques ossements d'animaux vertébrés, recueillis aux environs de Reims par M. Lemoine. Journal de Zoologie 6, 74-79.

Gingerich, P.D., 1971. Cranium of *Plesiadapis*. Nature 232, 566-&.

Gingerich, P.D., 1973. First record of the Paleocene primate *Chiromyoides* from North America. Nature 244, 517-518.

Gingerich, P.D., 1975a. Systematic position of *Plesiadapis*. Nature 253, 111-113.

Gingerich, P.D., 1975b. New North American Plesiadapidae (Mammalia, Primates) and a biostratigraphic zonation of the middle and upper Paleocene. University of Michigan Papers on Paleontology 24, 135-148.

Gingerich, P.D., 1976. Cranial anatomy and evolution of Early Tertiary Plesiadapidae (Mammalia, Primates). University of Michigan Papers on Paleontology 15, 1-141.

Gingerich, P.D., 1991. Systematic position of *Pronothodectes gaoi* Fox from the Paleocene of Alberta. Journal of Paleontology 65, 699.

Gradstein, F.M., Ogg, J.G., Smith, A.G., 2004. A Geologic Time Scale 2004. Cambridge University Press, Cambridge.

Hoffstetter, R., 1977. Phylogénie des primates. Confrontation des resultats obtenus par les diverses voies d'approche du probleme. Bulletins and Mémoires Société d'Anthropologie de Paris t.4, série XIII, 327-346.

Hooker, J.J., 1994. A new species of *Platychoerops* (Plesiadapiformes, Mammalia) from the latest Palaeocene of the Paris, London and Belgian basins. Geobios 27, 343-352.

Jepsen, G.L., 1930. Stratigraphy and paleontology of the Paleocene of northeastern Park County, Wyoming. Proceedings of the American Philosophical Society 69, 463-528.

Kay, R.F., Thewissen, J.G.M., Yoder, A.D., 1992. Cranial anatomy of *Ignacius graybullianus* and the affinities of the Plesiadapiformes. American Journal of Physical Anthropology 89, 477-498.

Kirk, E.C., Cartmill, M., Kay, R.F., Lemelin, P., 2003. Comment on "Grasping primate origins". Science 300, 741.

Lofgren, D.L., Lillegraven, J.A., Clemens, W.A., Gingerich, P.D., Williamson, T.E., 2004. Paleocene biochronology: the Puercan through Clarkforkian land mammal ages. In: Woodburne, M.O. (ed) Cenozoic Mammals of North America:

Geochronology and Biostratigraphy, 2nd edn. University of California Press, Berkeley, pp. 43-105

MacPhee, R.D.E., Cartmill, M., Gingerich, P.D., 1983. New Paleogene primate basicrania and the definition of the order Primates. Nature 301, 509-511.

MacPhee, R.D.E., Cartmill, M., 1986. Basicranial structures and primate systematics. Comparative Primate Biology, Volume 1: Systematics, Evolution, and Anatomy. Alan R. Liss, Inc., pp. 219-275.

Rose, K.D., 1981. The Clarkforkian land-mammal age and mammalian faunal composition across the Paleocene-Eocene boundary. University of Michigan Papers on Paleontology No 26, 197 pp.

Rose, K.D., Bown, T.M., 1982. New plesiadapiform primates from the Eocene of Wyoming and Montana. Journal of Vertebrate Paleontology 2, 63-69.

Russell, D.E., 1964. Les Mammifères Paléocènes d'Europe. Mémoires du Muséum National d'Histoire Naturelle, Série C 13, 1-324.

Sargis, E.J., Boyer, D.M., Bloch, J.I., Silcox, M.T., 2007. Evolution of pedal grasping in Primates. Journal of Human Evolution 53, 103-107.

Savage, D.E., Russell, D.E., 1983. Mammalian Paleofaunas of the World. Addison-Wesley Publishing Company, Reading, Massachusetts.

Simons, E.L., 1964. The early relatives of man. Scientific American 211, 51-62.

Simons, E.L., 1967. Fossil primates and the evolution of some primate locomotor systems. American Journal of Physical Anthropology 26, 241-254.

Simons, E.L., 1972. Primate Evolution, An Introduction to Man's Place in Nature. Macmillan, New York.

Simpson, G.G., 1935. The Tiffany fauna, upper Paleocene. II.-Structure and relationships of *Plesiadapis*. American Museum Novitates, 1-30.

Sussman, R.W., Raven, P.H., 1978. Pollination by lemurs and marsupials: an archaic coevolutionary system. Science 200, 731-736.

Sussman, R.W., 1991. Primate origins and the evolution of angiosperms. American Journal of Primatology 23, 209-223.

Szalay, F.S., 1968. The beginnings of primates. Evolution 22, 19-36.

Szalay, F.S., 1972. Cranial morphology of the Early Tertiary *Phenacolemur* and its bearing on primate phylogeny. American Journal of Physical Anthropology 36, 59-76.

Szalay, F.S., Tattersall, I., Decker, R.L., 1975. Phylogenetic relationships of *Plesiadapis* - postcranial evidence. Contributions to Primatology 5, 136-166.

Szalay, F.S., Dagosto, M., 1980. Locomotor adaptations as reflected on the humerus of Paleogene primates. Folia Primatologica 34, 1-45.

Szalay, F.S., Rosenberger, A.L., Dagosto, M., 1987. Diagnosis and differentiation of the order Primates. Yearbook of Physical Anthropology 30, 75-105.

Szalay, F.S., Dagosto, M., 1988. Evolution of hallucial grasping in the Primates. Journal of Human Evolution 17, 1-33.

Tambareau, Y., Russell, D.E., Sigogneau-Russell, D., Villatte, J., 1992. Decouverte de vertébrés dans le Paléocène de Campo (Pryenees aragonaises). Bulletin de la Societe d'Histoire Naturelle de Toulouse 128, 73-76.

Thewissen, J.G.M., Williams, E.M., Hussain, S.T., 2001. Eocene mammal faunas from northern Indo-Pakistan. Journal of Vertebrate Paleontology 21, 347-366.

Trouessart, E.L., 1897. Catalogues des Mammalium tam Viventium quam Fossilium. R. Friedlander und Sohn, Berlin.

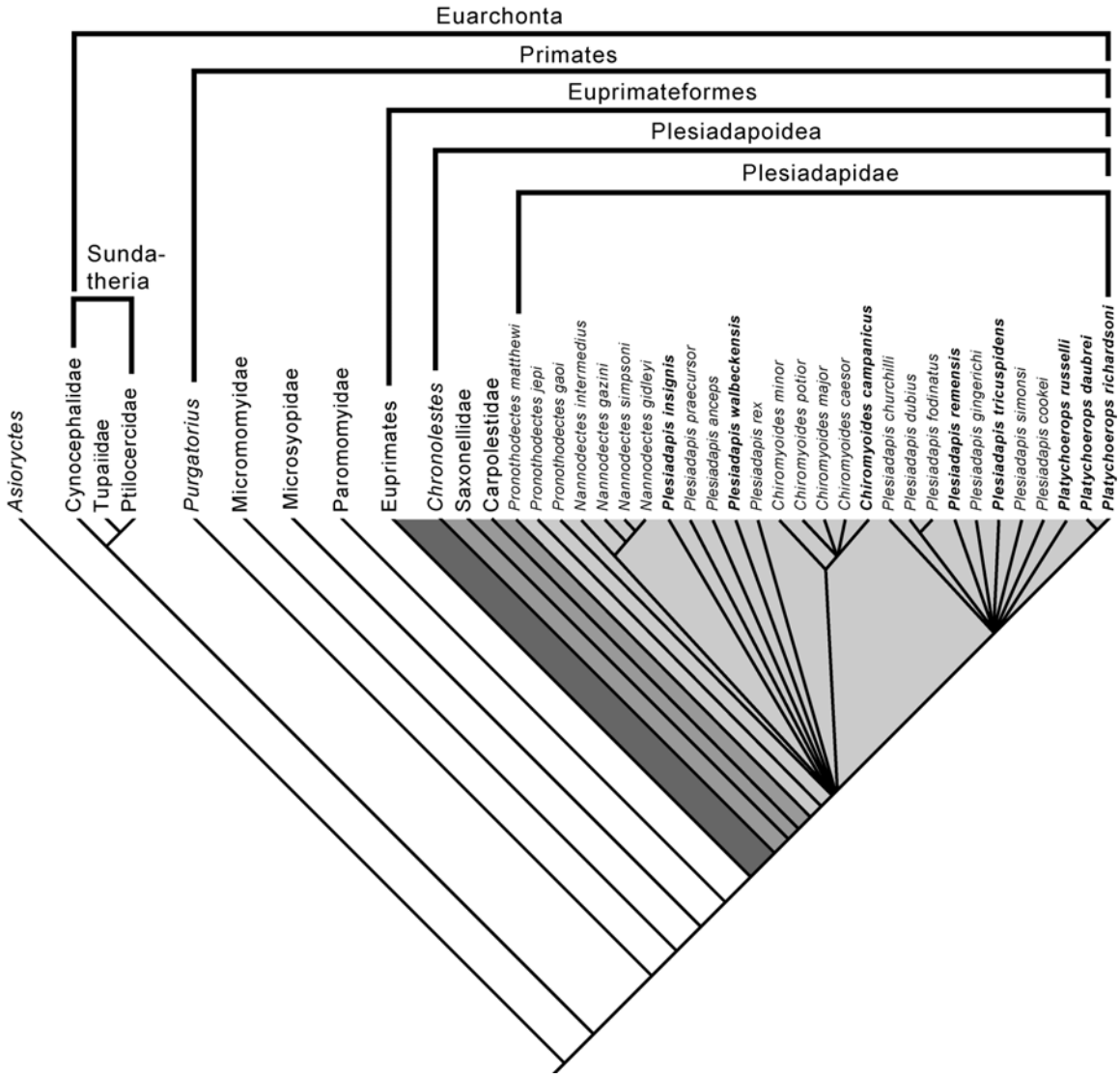

Figure 1.1. Phylogenetic relationships of Plesiadapidae and outgroups. Clade names and higher level topology follow Bloch et al. (2007). Topology of Plesiadapidae represents a summary of findings and views of Gingerich (1976, 1991) and Fox (1990, 1991). Bold names represent European species of Plesiadapidae. This figure is not meant to represent a phylogenetic hypothesis based on analysis of a particular matrix. It also does not represent an assumed phylogeny for the purpose of character analyses in this dissertation. Instead, this tree serves to summarize for the reader a working consensus from the published literature regarding plesiadapid relationships.

CHAPTER 2:
A REEVALUATION OF CRANIAL STRUCTURE IN PLESIADAPIDAE (PLESIADIFORMES: MAMMALIA) BASED ON NEW SKULL MATERIAL

ABSTRACT

Newly discovered skulls and petrosals attributed to a species of the most basal genus of Plesiadapidae, *Pronothodectes gaoi*, and a skull of *Nannodectes intermedius*, the geologically oldest known skull of a plesiadapid, are described comprehensively for the first time. Additionally, new observations and thorough photographic documentation of morphology are provided for the best preserved cranial specimen of *Nannodectes gidleyi*, and several specimens of *Plesiadapis tricuspidens*. These new specimens and observations will ultimately allow a more detailed and better supported reconstruction of the features characterizing the cranium of the ancestor of the Plesiadapidae, than was previously possible. All specimens observed have enlarged premaxillae that contact the frontals. However, in *P. tricuspidens* the premaxillae have a relatively larger contact with the frontals. As a consequence, the nasals of *P. tricuspidens* are exceptionally narrow at their caudal end. A reassessment of the evidence for bony contacts in the orbital mosaic reveals that existing specimens do not unambiguously support the previous conclusion that the maxilla and frontal had a sutural contact in this vicinity. A reassessment of the morphology of the orbitotemporal region of specimens of *P. tricuspidens* leads to the conclusion that it lacks foramen rotundum. All specimens except that representing *N. gidleyi* appear to have a laterally-positioned intratympanic, transpromontorial route for the internal carotid plexus. New evidence from the promontorium of the petrosal bone, its tympanic processes, and bones forming the auditory bullae of plesiadapids, rodents, treeshrews, and euprimates leads to the conclusion that the bony composition of the plesiadapid bulla is still ambiguous. However, previously undocumented similarities to the bullae of some euprimates suggest that the plesiadapid bulla is petrosally derived. *Pr. gaoi* and *N. intermedius* have a mediolaterally narrow external auditory meatus, whereas *P. tricuspidens* has a mediolaterally expanded, tube-like external auditory meatus. *Pr. gaoi* and *N. intermedius* appear to have proportionally smaller glenoid fossae than *P. tricuspidens* and *N. gidleyi*.

Previous perceptions of plesiadapid cranial morphology were based primarily on *P. tricuspidens*. Therefore the foregoing observations (as well as others) that illustrate *P. tricuspidens* to differ from most other plesiadapids and to exhibit different morphological features than previously supposed, may have implications for hypothesized relationships of plesiadapids to other plesiadapiforms and euarchontans.

INTRODUCTION

Plesiadapid cranial material has been previously described as sharing a number of features with crania of the Carpolestidae, the proposed sister taxon of the Plesiadapidae (Bloch and Silcox, 2006; Bloch et al., 2007). However, these taxa also exhibit a number of cranial morphological differences. Some of these differences appear to be the result of plesiadapid autapomorphies, while others appear to reflect carpolestid autapomorphies.

Features currently thought to be shared by and to reflect a close relationship between plesiadapids, carpolestids, and in some cases (features 1-2 below) anatomically modern primates (see Chapter 1: Fig. 1.1) (= Euprimates: Hoffstetter, 1977), include the following: (1) a petrosally derived tympanic bulla, (2) a posterior carotid foramen with a posteromedial position, (3) a separate foramen rotundum and superior orbital fissure, (4) orbital contact between the maxilla and frontal bones in the orbital cavity and (5) a nasal bone that becomes mediolaterally narrow at its caudal extent where it contacts the frontal bone (Bloch and Silcox, 2006; Bloch et al., 2007). On the other hand, some major cranial features of plesadapids that currently appear to separate them from the Carpolestidae include the following: (1) premaxillae that contact the frontal bones, (2) an external auditory meatus that is expanded into a tube-like form and (3) an internal carotid artery with non-functional stapedial, promontorial and main stem branches.

If the cladistic hypothesis that plesiadapids and carpolestids are sister taxa is correct, basal plesiadapids may lack some of the autapomorphies separating more derived members of the group from the Carpolestidae. Furthermore, basal plesiadapids should retain synapomorphies apparently shared by carpolestids and more derived plesiadapids.

Information on the cranium of basal plesiadapids is necessary to determine with more confidence whether the ancestral plesiadapid lacked or retained the apparent autapomorphies and synapomorphies of more derived members. I provide detailed descriptions of new plesiadapid cranial material, as well as new observations on, and comparisons among, all currently known plesiadapid crania. This information will ultimately allow a better-supported reconstruction of the ancestral form of the clade.

A specific major contribution of this work is the comprehensive description of the first cranial material of *Pronothodectes* based on specimens of *Pr. gaoi* (Fox, 1990a) from the middle part of the Paleocene of Alberta. These new cranial specimens are particularly important to reconstructing the ancestral pattern of the family because species of this genus, including *Pr. gaoi,* are dentally more primitive than all other plesiadapids in retaining a lateral lower incisor and a P_2 with "premolariform," rather than "peg-like," morphology (Gingerich, 1976; Fox, 1990a) (see Chapter 5).

Another important contribution of this work is the relatively large sample of petrosals available for examination in *Pr. gaoi* (n = 4) and *P. tricuspidens* (n = 11). Controversies in the literature (e.g., MacPhee et al. 1983 vs. Szalay et al., 1987) make it especially important to document morphological features in these bones and to establish constraints on the intraspecific variability in these features. Some of the disagreements regarding the anatomical significance of the morphological patterns of the petrosal bone can be distilled down to different interpretations of "reconstructed morphology" (e.g., Russell, 1964; MacPhee and Cartmill, 1986; Szalay et al., 1987; Bloch and Silcox, 2001) and differing inferences regarding species-level variability (MacPhee et al., 1983). A better understanding of the tympanic cavity is important for discussions of phylogenetic

relationships of the group, given the elevated significance assigned to this region of the basicranium by students of primate systematics (e.g., MacPhee, 1981; MacPhee et al., 1983; MacPhee and Cartmill, 1986; Bloch and Silcox, 2001).

In addition to providing additional descriptive information, I assess previous anatomical interpretations of the plesiadapid cranium using the new fossil and new comparative data. Specifically, I reevaluate the following features: (1) the position of the posterior carotid foramen, (2) the presence of an intratympanic route for the internal carotid plexus, (3) the presence of a foramen rotundum and (4) the bony composition of the auditory bulla. The position of the posterior carotid foramen has previously been tentatively considered as "posteromedial" (Bloch and Silcox, 2006), as mentioned above. Whether or not the internal carotid plexus had an intratympanic route has been considered ambiguous (MacPhee and Cartmill, 1986; Bloch and Silcox, 2001, 2006; Bloch et al., 2007). The foramen rotundum has been considered present in *Plesiadapis tricuspidens* by some (e.g., Russell, 1964; Bloch and Silcox, 2006) and absent by others (Kay et al., 1992). The bulla has likewise been considered petrosal by some (Russell, 1964; Gingerich, 1976; Bloch and Silcox, 2006) and non-petrosal by others (MacPhee et al., 1983; MacPhee and Cartmill, 1986; Kay et al., 1992; Beard, 1993). The same authors who consider the plesiadapid bulla as non-petrosal favor the hypothesis that euprimates are united by a common ancestor whose auditory bulla was comprised of only the petrosal, unlike that in any other studied modern mammalian group (e.g., MacPhee, 1981). A non-petrosal bulla has been documented in paromomyid plesiadapiforms (Bloch and Silcox, 2001), but claims (Kay et al., 1992) that the plesiadapid bulla is entotympanic remains unsubstantiated. The hypothesis that plesiadapids have a non-

petrosal bulla predicts that a suture delimiting the presence of two different bones was present at some point during the ontogeny of a given individual. If the bulla was not petrosally derived then it is possible that sutures, or some remnant of a mostly obliterated suture between the petrosal and the bulla, will eventually be preserved.

The position of the posterior carotid foramen, presence of an intratympanic route for the internal carotid plexus, and the presence of the foramen rotundum are addressed by assessment of morphology in new and existing specimens described here. The controversial suggestion that plesiadapids had a petrosal bulla (Russell, 1964; Gingerich, 1976; Bloch and Silcox, 2006) is addressed with these new fossils, new comparative data, and use of advanced visualization techniques such as high resolution x-ray computed tomography (HRxCT) and scanning electron microscopy (SEM). Specifically, I present new detailed photographic, HRxCT, and SEM data on the medial tympanic processes of new and existing plesiadapid specimens, various rodents (marmots – *Marmota*, chinchillas – *Lagostomus*, and kangaroo rats - *Dipodomys*), other plesiadapiforms (paromomyids) and euprimates (*Indri*). These data allow a more detailed assessment of the morphological evidence for bullar composition than was possible previously.

Anatomical terminology

The anatomical terminology employed in this study follows that of MacPhee (1981) with respect to anatomy of the tympanic region (i.e., structures of and surrounding the petrosal). Generally speaking, Miller's Anatomy of the Dog (Evans, 1993), Nomina Anatomica Veterinaria (1994) and Nomina Anatomica (1983) are followed with respect to the rest of the cranium. Wible and Gaudin (2004) and Wible (2008) provide glossaries

of terms, as well as lists of terms and synonyms that may be helpful in some cases. Table 2.1 is a list of numerical codes for relevant anatomical structures. Table 2.2 is a list of abbreviations for cranial bones and anatomical structures.

Institutional abbreviations

AMNH, American Museum of Natural History, New York; MaPhQ, Montauban Phosphorites du Quercy; MNHN, Muséum Nationale d'Histoire Naturelle, Paris; SBU, Stony Brook University; UALVP, University of Alberta Laboratory for Vertebrate Paleontology, Edmonton; UM, University of Michigan, Ann Arbor; UM, University of Michigan Museum of Paleontology, Ann Arbor; UMMZ, University of Michigan, Museum of Zoology, Ann Arbor; USNM, United States National Museum of Natural History, Smithsonian Institution, Washington; YPM-PU, Yale Peabody Museum-Princeton University collection, New Haven.

Generic abbreviations

I. - Ignacius

P. – Plesiadapis

Pr. – Pronothodectes

N. – Nannodectes

History of descriptive study of plesiadapid cranial material

Simpson (1935) provided the initial description of a plesiadapid skull and associated dentition (AMNH 17388), now attributed to *Nannodectes gidleyi* (Gingerich, 1976). The specimen came from the Mason Pocket locality in late Paleocene strata of the Nacimiento Formation, San Juan Basin, Colorado. The details Simpson provided on the cranial anatomy are brief. No figures were provided.

Russell (1959) provided a preliminary description of a more complete plesiadapid skull, *Plesiadapis tricuspidens* (MNHN CR 125), from the Berru locality near Reims in late Paleocene strata of the Paris Basin, France. This contribution included a labeled sketch of the skull in dorsal and ventral views, and corresponding photographs. As summarized by Gingerich (1976), Russell described the general form of the skull, interpreted it as preserving large premaxillae that contact the frontals, and otherwise focused on the basicranium. Russell (1959) stated that the skull preserves a posterior carotid canal, and that there are two subequal grooves on the promontorium for the promontory and stapedial arteries. He also stated that the bullae appeared to have been derived from the petrosal.

Simons (1960: fig. 1) reviewed the find of MNHN CR 125 and provided a reconstruction of the skull in lateral view. The caption states that there is "correction for distortion." Simons noted the lack of a postorbital bar and relatively large antemolar dentition as distinctive features of this Paleocene "primate," contrasting it with euprimates.

Russell (1964) provided the most comprehensive description of a plesiadapid skull (*P. tricuspidens*, based on MNHN CR 125, 126, 966, 965; 4306) as a follow-up to

his 1959 work. Figures 13-19 of Russell (1964) have been frequently relied upon as a reference for the cranial anatomy of *P. tricuspidens* (Gingerich, 1976; Bloch and Silcox, 2006). Russell (1964) was the only researcher to document the sutural and foraminal patterns in *P. tricuspidens* with original illustrations, although he provided no photographs. Due to the diagramatic form of the illustrations and controversy concerning sutural patters that followed, the lack of photographic evidence has become problematic. In fact, none of the cranial sutures, or foramina of the orbital region, have ever been adequately photographed. In Russell's (1964) figures 14 and 19, the orbitotemporal region is reconstructed as preserving a human- or tupaiid treeshrew-like pattern of foramina for cranial nerves with separate foramina for ophthalmic (t.d.r.) and maxillary (t.r.) branches of the trigeminal nerve. Although Russell also documented most major sutures in his figures 14 and 19, the alisphenoid/orbitosphenoid suture and the posterior termination of the orbitosphenoid/frontal suture were not illustrated, or discussed. Russell (1964) changed some of the interpretations he made in his original note in 1959. For instance, he reconsidered the stapedial artery to have been reduced relative to the promontorial branch, or absent.

Szalay (1971) concluded that the skull of *P. tricuspidens* had been incorrectly reconstructed in lateral view by Simons (1960) and Russell (1964), in which the tips of the upper and lower incisors were shown to meet one another while the cheek teeth were occluded. Szalay further suggested that the premaxillae did not contact the frontal and provided a photographic dorsal view of the skull (fig. 2) showing transverse cracks (as interpreted by other authors) in the premaxillae looking very much like symmetrical sutures, intersecting the nasals before reaching the maxillae.

Gingerich (1971) rebutted Szalay (1971), pointing out that Simons (1960) actually reconstructed the skull as Szalay (1971) claimed to have "re-reconstructed" it. Gingerich further suggested that Szalay (1971) had no new evidence to support his re-interpretation of the premaxilla as lacking frontal contact.

Szalay (1972) described a skull of a paromomyid plesiadapiform, *Phenacolemur jepseni* (AMNH 48005), and compared it to *P. tricuspidens* specimens MNHN CR 125 and MNHN CR 7377, as well as to skulls of extant and fossil euprimates. This represents the initial publication of the latter *P. tricuspidens* specimen. Although the photographs he provided of *P. tricuspidens* MNHN CR 125 are of high quality (Szalay, 1972: figs. 5, 6), they reveal little about the carotid plexus pathway. His descriptions, however, are consistent with those of Russell (1964). Szalay (1972: figs. 7-9) showed different stereophotographic views of MNHN CR 7377, an isolated squamosal glenoid, petrosal, and ectotympanic. A trough-like remnant of the carotid canal on this specimen is labeled with an arrow on figure 8, which effectively illustrates the carotid canal morphology and a groove extending anteriorly from it onto the promontorium.

Gingerich (1975) announced a new specimen of *P. tricuspidens* from Berru (the Pellouin skull). He provided a stereophotograph of its right ear (p.112, fig. 2) and suggested that its expanded external auditory meatus links it with tarsiiform euprimates.

Gingerich (1976) newly described a frontal fragment (YPM-PU 24618) from the Berru locality, and an edentulous splanchnocranium (YPM-PU 19642) of *P. anceps* from 7-up Butte, a late Paleocene locality in the Medicine Rocks area, Montana. The descriptions are brief and the section on cranial anatomy serves more as an addendum and review than as a comprehensive reassessment of basicranial evidence. Gingerich

(1976: Pl. 9b) noted that the ectotympanic bone of the basicranium has a "suspended ring" for attachment of the tympanic membrane that looks euprimate-like, which he illustrated with stereophotographs of the *P .tricuspidens* Pellouin skull. He identified a vidian foramen in the Pellouin skull, but did not illustrate this morphology. He confirmed Russell's previous suggestion that there is a laterally-positioned posterior carotid foramen and canal, noting their presence in the Pellouin skull. He provided the first and only photographic documentation of the course of the internal carotid plexus in *P. tricuspidens* with a close-up, annotated stereophotograph of the right petrosal (Gingerich, 1976: Pl. 9c). He provided additional evidence that a stapedial artery was absent by observing (but not clearly illustrating) that there exists a bony ridge on the promontorium ventral to the fenestra ovalis that would have blocked the course of the artery. He also provided an illustration of the *P. anceps* specimen, showing premaxillary/frontal contact (Gingerich, 1976: fig. 32), and overview stereophotographs of MNHN CR 125 (Gingerich, 1976: Pl. 8a-c), the Pellouin skull (Gingerich, 1976: Pl. 9a-c), and the frontal fragment from Berru (Gingerich, 1976: fig. 34). He used the reconstruction from Szalay (1971) as a basis for reconstruction of jaw musculature. Furthermore he used a lateral view of the brain "outline" based on Szalay's reconstruction along with a dorsal "outline" to estimate brain volume (Gingerich, 1976: fig. 35a). Figure 33 of Gingerich (1976) is a redrawing of part of figure 19 of Russell (1964) and represents the orbitotemporal region of *Plesiadapis*. It is labeled with equivalent but different terms. The sutural patterns depicted are similar to those in Russell's figure, but differ with respect to the relationship of the palatine/frontal suture to the postpalatine canal. Russell (1964) depicted the suture as entering the canal, while Gingerich showed the canal to be completely within the palatine. Finally, in plate

9c, Gingerich (1976) labeled a groove on the right promontorium of the Pellouin skull, which runs from posterolateral to anteromedial, as a "tympanic plexus groove." This groove is not visible on MNHN CR 125, and thus was not among those originally interpreted as a promontorial or internal carotid arterial route by Russell.

Gingerich et al. (1983) described a newly discovered crushed skull of *Nannodectes intermedius,* USNM 309902, from the Bangtail locality in south-central Montana. The description is brief, focusing on the teeth. The discussion focused on biostratigraphic implications of the specimen and the fauna with which it occurred. The authors interpreted USNM 309902 as having existed in the earliest Tiffanian (Ti) North American Land Mammal Age (NALMA). If this temporal attribution is correct, USNM 309902 is the geologically oldest known plesiadapid cranium. MacPhee et al. (1983) expanded on the description and discussion of the basicranium of this specimen, and re-analyzed the basicranium of *Nannodectes gidleyi,* AMNH 17388. They did not illustrate the actual specimens, but provided a schematic illustration of a generalized "plesiadapid" petrosal that shows unique morphologies of both specimens (MacPhee et al., 1983: fig. 1). There is an editorial mistake in the figure caption: two grooves are illustrated, "s1" and "s2." In the figure caption, the "s1" groove alone is said to characterize *N. intermedius,* while the "s2" groove alone is said to characterize *N. gidleyi*. However, inspection of the actual specimens indicates that the opposite is true (specimen numbers were switched in the figure caption). Nonetheless, their conclusions stand regarding the evidence these specimens provide of "variability" in expression of grooves on promontoria of plesiadapids. The "s1" groove was interpreted as a possible tympanic nerve route by MacPhee et al. (1983). It was noted that this is located in a much different

position from the tympanic plexus groove photographed by Gingerich (1976) for the Pellouin skull and represents a different structure (although both could certainly have held tympanic plexus fibers). The "s2" groove is not identified. The authors noted that it has a similar location to a canal previously identified as the internal carotid canal and illustrated by Russell (1964: fig. 15) in MNHN CR 125, and photographed and labeled by Gingerich (1976: Pl. 9c). They stated, however, that the groove does not connect to a foramen leading to extratympanic space, implying that it could not actually have held a functional internal carotid artery or nerve. They argued that this fact, combined with a lack of the "s2" groove on the other specimen, indicates that the internal carotid system is diminished in importance to the point that it was only sporadically retained in the adult plesiadapid specimens. MacPhee et al. (1983) also argued bullar composition cannot be determined in fossil taxa lacking a suture between the bulla-forming bone and promontorium of the petrosal (Russell, 1959, 1964; Gingerich, 1976) because only ontogenetic evidence can reveal whether the bulla started as an ossification separate from the petrosal bone.

MacPhee and Cartmill (1986) characterized plesiadapid basicranial anatomy according to previous publications. They provided an expanded argument against petrosal contribution of the auditory bulla based on further observations of the Pellouin skull (Gingerich, 1975; 1976). Specifically they pointed out that, although there is no visible suture between the petrosal bone and bulla medial to the promontorium, there is no suture between the ectoympanic and lateral aspect of the bulla either. This means that it is not clear whether the bulla is petrosal, entotympanic or ectotympanic in composition. It is important to note, however, that all of the specimens available to them lacked the

portion of the bulla medial to the annular component of the ectotympanic, where an ectotympanic suture is most likely to have been (given the results of more recent studies). Specifically, descriptions of paromomyid plesiadapiform basicrania (Kay et al., 1992; Bloch and Silcox, 2001) that do preserve the portion of the bulla medial to the annular component of the ectotympanic are interpreted as having an ectotympanic/entotympanic suture located in this portion. MacPhee and Cartmill (1986: fig. 17) also showed a radiograph of the Pellouin skull, which reveals the presence of extensive "cellules" inferred to communicate with the tympanic cavity. They suggested that presence of these "cellules," as a consequence of tympanic cavity pneumatic expansion, is further indication that previously noted (e.g., Gingerich, 1976) similarities between plesiadapids and modern lemuriforms are convergences. Finally, they documented a specific example of an animal convergent on plesiadapids and lemuriforms: the chinchillid *Lagostomus maximus* has a similarly constructed annular component to its external auditory meatus, and an obliterated suture between the ectotympanic bulla and pars cochlearis of the petrosal.

Szalay et al. (1987: figs. 1, 2) provided a detailed description, stereophotographs (the same as those provided by Szalay [1972: figs. 7-9]) and a reconstruction of MNHN CR 7377, a cranial fragment of *Plesiadapis tricuspidens*. They suggested that it represents a young individual because sutures between the squamosal and petrosal are "clearly visible," as well as sutures between the petrosal and the ectotympanic. The former are clearly illustrated. While the suture between the mastoid part (pars canalicularis) of the petrosal and the ectotympanic is visible, it is not clear whether these represent the "clearly visible" structures to which the authors refer. They pointed out

(and illustrated) additional features of *P. tricuspidens* that they argue are similarities with many modern primates. These include a carotid canal supported by a dome-like, ventrolaterally-projecting outgrowth from the petrosal that shields the cochlear fenestra (referred to as the "posterior septum" [ps] later on), and a ridge that projects from the roof of the tympanic cavity and extends posteromedially from the promontorium, holding the vestibular aqueduct.

Kay et al. (1992) described another (then) newly discovered paromomyid *Ignacius graybullianus* (USNM 421608) and compared its morphology to that of *P. tricuspidens*, among other taxa. They claimed to reinterpret the foramen rotundum identified by Russell (1964) in *P. tricuspidens* as a suboptic foramen (see Bloch and Silcox, 2006 and below, for more detailed discussion).

Bloch and Silcox (2001) described additional specimens of *Ignacius graybullianus* and redescribed USNM 421608. They compared these specimens to plesiadapids and specifically illustrated and discussed morphology of a previously unpublished specimen of *Plesiadapis cookei* (UM 87990). The morphology of the broken open tympanic cavity is shown in their figure 7. They noted (but the figure does not obviously show), a groove for an internal carotid arterial branch that clearly differs from the small criss-crossing grooves for the tympanic plexus (which *are* visible in their figure 7). They also showed that *P. cookei* is similar to *P. tricuspidens* in having bony struts connecting the annular part of the ectotympanic to the external auditory meatus. Bloch and Silcox (2001: 192) indicated that morphology relating to the carotid canal and posterior carotid foramen is poorly known in plesiadapids and is only preserved in the Pelluoin skull of *P. tricuspidens* among all known plesiadapid cranial specimens.

Bloch and Silcox (2006) described the skull of yet another plesiadapiform, *Carpolestes simpsoni*, based on a number of fragmentary specimens (UM 101963, UM 82670, UM 85177, UM 82688, UM 101923, UM 86273, USNM 482354). Again, comparisons were made with plesiadapids. Although no additional figures were included, they again discussed the controversy over the identification of foramina of *P. tricuspidens* specimens, initiated by Kay et al. (1992). They concluded that Kay et al. (1992) miscommunicated their disagreement with Russell (1964) and their reinterpretation of the morphology. The foramen Kay et al. (1992) reinterpreted as the suboptic foramen must actually correspond to what Russell (1964) identified as the "t.d.a," (= trou dechire anterieur: equivalent to the superior orbital fissure) based on their description of its location and morphology. This means they considered Russell's "t.r." (= trou rond: equivalent to the foramen rotundum) to actually correspond to a sphenorbital fissure. Bloch and Silcox (2006) then argued that Kay et al.'s (1992) reinterpretation is less plausible than Russell's because the medial walls of the orbits are more widely separated in *P. tricuspidens* than in treeshrews possessing suboptic foramina, and because Russell's "t.r." is too ventrally and posteriorly displaced to represent a sphenorbital fissure.

Finally, Gingerich and Gunnell (2005) described additional aspects of the skull of *Plesiadapis cookei* UM 87990. They stated that the skull, which is associated with both dentaries, is preserved in pieces, of which there is a palatal/splanchnocranial fragment, a neurocranial fragment with well-preserved auditory bullae ventrally, and a frontoparietal fragment. Their reconstruction postulates a total length of 90 mm and bizygomatic breadth of 58 mm. They considered the overall morphology as being similar to that of *P.*

tricuspidens. Gingerich and Gunnell (2005) also reconstructed the brain as being long and narrow, with large olfactory bulbs compared to modern primates. The rhinal fissure was identified and interpreted to indicate an unexpanded neopallium, suggesting neurological analogy with "olfactory reliant," sensory deprived "basal insectivores" such as *Tenrec*. The foramen magnum diameters were given as 8.5 by 6.0 mm. The volume of the brain was estimated at 5 cc, less than a third the estimate of 18.7 cc derived by Gingerich (1976) from double integration of pictures of skulls of *P. tricuspidens*. The authors state that 5 cc is a much more reliable estimate that is likely also to apply to *P. tricuspidens*.

MATERIALS AND METHODS

Material examined

All known specimens referable to the Plesiadapidae and representing a major portion of the cranium were examined in this study except for one specimen of *P. tricuspidens* that could not be located, MNHN CR 7377.

Previously unpublished or largely undescribed material studied includes three specimens referable to *Pronothodectes gaoi*: UALVP 46685, a crushed skull from DW-2, a "middle" late Paleocene (Ti3) locality in the Paskapoo Formation in central Alberta (Fox, 1990b); and UALVP 46687 and 49105, isolated basicranial fragments from the DW-2 and Joffre Bridge localities, respectively. Joffre Bridge is near DW-2 from the same strata and represents the same faunal zone.

Previously described specimens for which aspects of morphology are redescribed due to original errors or lack of detail in verbal or illustrative documentation include those referred to *Plesiadapis tricuspidens*, *Nannodectes intermedius* and *N. gidleyi*. Specimens of *P. tricuspidens* from the Berru locality of the Paris Basin assessed here include MNHN CR 125, 126, and 965, as well as the Pellouin skull. Additional specimens include isolated petrosals that represent *P. tricuspidens* (M. Godinot, pers.com.): MNHN BR 17414-19, 1371. The skull of *Nannodectes intermedius*, USNM 309902, from the Ti1-aged Bangtail locality in south-central Montana (Gingerich et al., 1983), is figured and discussed. Finally, I include images, description and analysis of *N. gidleyi* (AMNH 17388), the specimen originally described by Simpson (1935) and later considered by MacPhee et al. (1983).

Specimens included for direct comparison and contrast include those of the plesiadapiforms *Carpolestes simpsoni* (UM 101963 and USNM 482354), *Ignacius clarksforkensis* (UM 82616), and *Ignacius graybullianus* (USNM 421608 and USNM 482353); the fossil euprimates *Adapis parisiensis* (MaPhQ 33y) and *Leptadapis leenhardti* (YPM-PU 11481); and the extant rodents *Lagostomus maximus* (AMNH 41527, 41522), *Dipodomys heermani swarthi* (AMNH 124181, 39836, 121077), and *Sciurus carolinensis* (SBU MRd-12).

Methods of examination and documentation

Specimens were studied under a binocular light microscope. Sutures and cranial foramina were identified by comparison to extant and fossil skulls. Morphology was photo-documented using a Nikon Coolpix 4500 camera mounted on a copy stand or tripod. For more detailed morphology, I used a continuously-calibrated (for pixel scale) digital camera mounted on a steREO Discovery V12 Zeiss microscope with a 0.63x objective lens and 10x ocular lens, motorized focus and zoom, and capacity for reflected and transmitted illumination of objects in the object field (maximum = 36.5mm) via two Zeiss LCD 2500 light boxes. Measurements were taken from the resulting photographs (on structures such as cranial foramina) to the nearest hundredth of a millimeter using the measurement software Axiovision 4.4. In some cases, for specimens that could not be imaged with the Zeiss microscope, camera lucida drawings of minute morphological features were made and measured. Prior to photography for documentation purposes, specimens were whitened with ammonium chloride salt or magnesium powder to remove tonal contrasts due to the mottled coloration of the fossil or glare off the surface. After

whitening, dark and light areas on a specimen correspond predominantly to shadows and highlights, respectively, and reveal the specimen's shape more effectively. All externally visible morphological structures pertinent to description are labeled on the figures. Bones are identified with abbreviations (see Table 2.2). Other features are labeled with numbers (Table 2.1). Italicized numbers following figure citations in the description section correspond to labels on the morphology depicted in some or all of the cited figures.

High resolution x-ray computed tomography (HRxCT) data were acquired from the Center for Quantitative Imaging of Pennsylvania State University, the High-Resolution X-ray Computed Tomography Facility of the University of Texas at Austin, and the Center for Biotechnology of Stony Brook University on most specimens (data available upon request). These data were visualized with the software Amira 4.1.2-1 and Image J and assisted in description of internal morphology. HRxCT data were particularly important for verifying identifications of various foramina.

Measurements

Four measurements were taken on the petrosal bone (Table 2.3) and 61 measurements were taken on various aspects of the cranium (Table 2.4-5) using digital calipers, digital photographs, camera lucida drawings and skeletal reconstructions from scan imagery. These measurements were used to quantitatively compare specimens considered in this study.

Quantitative assessment of morphological differences among plesiadapids

A geometric mean was calculated from as many as 39 of the 61 basic measurements to reflect the overall skull size of each specimen (Table 2.4-5). Various size-standardized shape variables were calculated by taking the $\log_e$ ratio of particular measurements to a specimen's geometric mean or to another measurement for that specimen (Tables 2.4, 2.6).

Identification of plesiadapid tympanic cavity osteology and reconstruction of its soft anatomy

I use an extant phylogenetic bracket (Witmer, 1995) as provided by MacPhee (1981) to identify various osteological features and to reconstruct the soft anatomical correlates of grooves and foramina within the tympanic cavity of plesiadapids.

SYSTEMATIC PALEONTOLOGY

Class MAMMALIA

Order PRIMATES Linnaeus, 1758

Family PLESIADAPIDAE Trouessart, 1897

PRONOTHODECTES Gidley, 1923

PRONOTHODECTES GAOI Fox, 1990

Type

UALVP 31238, incomplete left dentary with P_{3-4}, M_{1-2}; alveoli for I_{1-2}, C, P_2.

Referred specimens

UALVP 46685, skull exhibiting postmortem deformation with right and left I^1, right I^2, right and left C, P^{2-4}, concealed left and right M^{1-3} (Figs. 2.1-5). UALVP 49105, isolated left petrosal and ectoympanic (Fig. 2.6). UALVP 46687, isolated right petrosal (Fig. 2.7).

Occurrence

UALVP 46685 and 46687 come from the DW-2 locality, thought to be middle Tiffanian in age (Ti3). UALVP 49105 comes from the Joffre Bridge locality, thought to be coeval with DW-2. Both localities located in strata of the Paskapoo Formation, which accumulated in the Alberta syncline of central Alberta (Fox, 1990b).

Description of new cranial material of *Pronothodectes gaoi*

UALVP 46685 is a highly deformed skull of *Pronothodectes gaoi*. Heavy wear on P^4 and a concealed M^{1-3} (revealed with HRxCT) demonstrate it to be an ontogenetically old individual. The alveolar processes of the maxillae have been rotated medially toward one another. The neurocranium has been rotated ventrally and folded anteriorly so that the right glenoid fossa actually faces dorsally (Fig. 2.1), while the basicranium has been translated anteriorly, ventral to the molar dentition, thereby concealing these teeth (Fig. 2.2). Finally, the convoluted specimen was flattened dorsoventrally. Due to this deformation, many sutures, foramina, and morphological details are obscured. Even so, the specimen provides a large amount of new information about cranial morphology in *Pronothodectes* that can be compared to that of other plesiadapids in order to assess patterns of change that may have characterized the family's evolutionary history.

Nasal.—The nasals contact only the premaxillae (Fig. 2.1: *1*) and frontals (Fig. 2.1: *2*). They have distinct sutures with the premaxillae but contact with the frontal is more difficult to discern due to crushing and missing bone. It is apparent that the nasals have a mediolateral width that is fairly constant from anterior to posterior (average unilateral width = 2.6 mm). They appear to have extended posteriorly to the level of P^{3-4}.

Premaxilla and Premaxillary Dentition.—Both premaxillae are preserved. The right side has suffered less damage than the left side (Figs. 2.1-3). The nasal (Fig. 2.1: *1*), maxillary (Fig. 2.1-3: *3*) and frontal (Fig. 2.1: *4*) sutures are visible. The suture with the nasal is straight and simple (Fig. 2.1: *1*). The suture with the right maxilla is observable just posterior to I^2 (Figs. 2.2, 3: *3*). It is convoluted, but runs dorsoventrally for ~3 mm

before meeting a large, anteroposteriorly running crack. Dorsal and posterior to the crack this suture is simpler, more like the suture with the nasal (Fig. 2.1B: *3*). As it is followed posteriorly, the suture extends medially and the premaxilla narrows (Fig. 2.1). The premaxillary/maxillary suture meets the frontal at a point slightly anterior to where the premaxillary/nasal suture meets the frontal. Thus the premaxillary/frontal suture, followed from lateral to medial, slopes posteriorly. The length of this suture is 4.36 mm. Whether the incisive foramen is contained completely within the premaxilla or at the juncture with the maxilla cannot be determined because of deformation in this region (Figs. 2.2, 3).

The premaxilla holds just two teeth, interpreted as I^{1-2} (Figs. 2.2, 3). These teeth have not been previously described for *Pr. gaoi*. I^1 is similar to that of other early plesiadapids. It has three main cusps: anterocone, laterocone and posterocone. There is slight development of a mediocone, in the form of a crest on the medial side of the crown. The tooth does not have a centroconule, as is characteristic of *Plesiadapis rex*, or a proliferation of cuspules on the lateral side of the tooth between the laterocone and posterocone as in *P. churchilli* (Gingerich, 1976). I^1 measures 4.03 mm in mesiodistal length, 2.94 mm in mediolateral width, 18.27 mm from the apex of the anterocone to the tip of the root, and 7.02 mm from the apex of the anterocone to the cervical margin of the crown. These dimensions are within the range seen for 62 central incisors of *P. rex* at Cedar Point Quarry (Gingerich, 1976). I^2 is a simple, caniniform tooth. It has a protocone, with a distinct postprotocrista extending between the apex of the cusp and the base of the crown on the distal side of the tooth. The crown is slightly compressed

buccolingually, measuring 1.90 mm in mesiodistal length and 1.49 mm in buccolingual width.

Lacrimal.—The dorsal half of the right lacrimal is preserved (Fig. 2.1). Remnants of the left element are difficult to discern, if present. The frontal (Fig. 2.1B, C: *5*) and part of the maxillary suture (Fig. 2.1B, C: *6*) of the right lacrimal are visible. The anterior margin is damaged such that the presence of a tubercle cannot be evaluated. The lacrimal contributed extensively to the orbital mosaic (Fig. 2.1B, C: *7*). It also formed the anteromedial part of the orbital rim. The lacrimal does not, however, appear to have extended outside of the orbit substantially: there was not a large facial process. The right lacrimal foramen (Fig. 2.1B, C: *8*) is quite large (~ 1.53 mm x 1.61 mm), appears to be located on the orbital rim and faces dorsolateroposteriorly (Fig. 2.1).

Maxilla and Maxillary Dentition.—The right and left maxillae are preserved with C, P^{2-4}, M^{1-3} on the right and left (Figs. 2.2, 3), although only C-P^4 are visible with the naked eye. The rostral parts of these bones are well preserved (Figs. 2.2, 3) but the orbital part is obliterated and the contribution of the maxillae to the orbital mosaic is unknowable (Figs. 2.2, 3).

The maxillae have been rotated medially through deformation so that the left and right tooth rows are at right angles to one another (Figs. 2.2, 3). Upper canines, premolars and molars have never before been described for *Pronothodectes gaoi*. Although it is not possible to give a very detailed description of P^4–M^3, their gross dimensions can be provided, as the teeth were extracted from the HRxCT image of the specimen (Fig. 2.2C).

The canine is a simple, single-rooted tooth with a slight "metacone" heel, distal to its main, paracone cusp. It measures 1.26 mm in length and 0.89 mm in buccolingual width. It is separated from I^2 by a substantial diastema of 2.46 mm. The P^2 follows the C by another diastema of 1.54 mm. It is also a simple tooth, but with two roots and comprised of a large paracone, a lingual swelling that could be called a "protocone lobe," and a distal swelling that represents a "metacone lobe." It measures 1.47 mm in mesiodistal length and 1.25 mm in buccolingual width. The P^3 follows P^2 directly. It is more complex, with three roots, paracone, possibly a metacone as well as parastyle and paraconule. It measures 1.79 mm in mesiodistal length and 2.23 mm in buccolingual width. P^4 follows P^3 directly. It is more complex yet, again with three roots, paracone, possibly a metacone, protocone, a parastyle and paraconule. It measures 2.02 mm in mesiodistal length and 3.09 mm in buccolingual width. There is uncertainty about the presence of a metacone on P^{3-4} because of extensive wear developed on these cusps. Diagnostic details of the molars are difficult to discern. HRxCT reconstructions suggest, however, that they lack mesostyles (Fig. 2.2C), as is true of other plesiadapids more primitive than *P. rex* (admittedly many *P. rex* individuals lack identifiable mesostyles). M^1 measures 2.82 mm in length and 4.06 mm in width. M^2 is 2.79 mm by 4.26 mm. M^3 is 2.60 mm by 3.93 mm. Fox (1991) noted that lower molars of *Pr. gaoi* described by Fox (1990a) are in the range of sizes exhibited by molars of *P. rex.* The dimensions of the upper molars of UALVP 46685 are in the low end or outside of the range of molar sizes known for *P. rex* from Cedar Point Quarry (Gingerich, 1976) and thus suggest that this is a small individual of *Pr. gaoi.* Alternatively, this specimen may indicate that larger samples of *Pr. gaoi* upper dentitions will demonstrate the species to be smaller, on

average, than *P. rex*. Repositioning cropped scan images of teeth allows an estimate of the length of the tooth row from P^2 to M^3 at 13.47 mm.

Frontal contact by the maxilla occurs between the premaxilla and lacrimal on the dorsum of the skull, measuring 3.77 mm in length on the left side (Fig. 2.1: *10*). Palatine contact (tranverse palatine suture) occurring on the palate is not visible (Fig. 2.2). Because the palate is visible anterior to P^4, it can be inferred that the palatine was restricted to a point posterior to this. It can also be inferred that the zygomatic process of the maxilla arose posterior to P^4. The presence of a mediolateral expansion on the ventral surface of the zygomatic bone (for attachment of the masseter muscle) suggests that the zygomatic process of the maxilla would have expressed a similar expansion (Fig. 2.1: *9*). The unilateral breadth of the palatal part of the right maxilla just posterior to I^2 is 3.39 mm. At the anterior margin of P^2 it measures 5.45 mm. These measurements thus reveal an anteriorly tapering snout. The infraorbital canal length cannot be determined due to crushing of the maxilla's posterior end, but the diameters of the left infraorbital foramen are measurable at 2.12 mm and 1.26 mm. The infraorbital foramen is situated above P^{2-3} (Figs. 2.2, 3: *11*).

Zygomatic.—As indicated above, a fragment of the right zygomatic is preserved (Fig. 2.1). None of the sutures are preserved (for the maxilla, lacrimal and squamosal). The maximum dorsoventral depth of the element is roughly 4 mm. The mediolateral expansion of the ventral surface of the zygomatic bone (for attachment of the masseter muscle) measures 1.29 mm (Fig. 2.1: *9*).

Frontal.—The frontals are visible on the dorsum of the skull; in this region the frontals contact the maxillae, nasals, and lacrimal (Fig. 2.1). Breakage makes the

existence and/or nature of contacts with the palatine, orbitosphenoid, alisphenoid, and parietal difficult to assess. The only dimension that can be meaningfully measured is the anteroposterior length of this element: along the metopic suture, the frontal measures 11.23 mm (Fig. 2.1: *12*). The anteriormost region of parietal contact is visible where the parietal on-lapped the frontal and left an impression (Fig. 2.1: *13*). The right frontal is well-enough preserved to exhibit a distinct ridge that runs from the anterolateral part of the bone, where it contacts the lacrimal, medially towards the metopic suture, meeting this suture at the posterior end of the bone, where it contacts the parietal (Fig. 2.1: *14*). This ridge, with its mirror on the opposite side, would have formed a distinct frontal "trigon." There is no sign of postorbital processes on these bones. HRxCT data reveal the frontal as a thin plate of bone anteriorly, and it shows that the bone thickens posteriorly and is densely trabeculated. No diploic cavities are identifiable. No ethmoid foramina are preserved.

Palatine.—The palatines are completely obscured and crushed, such that not even examination of HRxCT data illuminates their morphology.

Parietal.—The parietals are only slightly better preserved than the palatines, represented as a flat piece of bone visible on the ventral side of the skull (Fig. 2.2). Some discernable details of its sutural relationships to the frontal were described above.

Squamosal.—The right zygomatic process of the squamosal is preserved (Figs. 2.1, 2: *15*). The glenoid fossa is intact as well (Figs. 2.1, 2: *16*), although it is mainly obscured by other bone and matrix. The neurocranial portion of the squamosal is not recognizably preserved. No sutural contacts are preserved. The HRxCT image of the glenoid fossa and zygomatic process was digitally extracted (Fig. 2.2D, E). This image

reveals that 1) the postgenoid process is broken off and missing, 2) a postglenoid foramen is preserved and is located medial (not posterior) to the area from which the postglenoid process would have projected (Fig. 2.2D, E: *17*), and 3) there is a well-developed entoglenoid process medial to the postglenoid foramen (Fig. 2.2E: *18*). Furthermore the glenoid is revealed to be rather flat, and anteroposteriorly longer (6.96 mm) than mediolaterally wide (5.38 mm). The joint surface is deformed on its medial aspect where the right M^1 or M^2 crown is pressed into it. The entoglenoid process is quite large, projecting ventrally beyond the glenoid fossa by 1.79 mm. It is oriented longitudinally, at roughly 90 degrees from the hypothetical orientation of the intact postglenoid process, and slopes medially. The width of the zygomatic process of the squamosal at its base, where it meets the glenoid, is 1.76 mm (Fig. 2.2E: *19*). The length of the process, which appears to be mainly intact, is 4.95 mm. Its maximum depth is 3.77 mm.

Alisphenoid and basisphenoid.—Neither of these elements is recognizably preserved.

Petrosal.—The main structures in the basicranial region that are well preserved and can, therefore, be described in detail are the promontoria of the petrosals (Figs. 2.2-5). Two isolated petrosals of *Pr. gaoi* will also be described here (Figs. 2.6-7). Accordingly, several major points regarding the morphology will be addressed. First, the promontorium itself will be described (its shape and the presence, position, and relationships of any grooves and foramina). Next, the morphology of the bones surrounding the promontorium will be addressed, inasmuch as this morphology relates to anatomical interpretations of previously mentioned promontorial features. The form, number and position of bony processes extending from the promontorium will then be

outlined. This includes description of any bulla-forming bones and bony bulla-butressing septa extending from the promontorium. The description of the promontorium will be followed by comments on the pars canalicularis of the petrosal and finally the ectotympanic bone. Table 2.3 provides a summary of morphology exhibited/preserved by each specimen, including other plesiadapid taxa to be discussed later.

On UALVP 46685, crushing and shifting of the skull has obliterated most of the sutures between the petrosals and other elements (Fig. 2.2). The left petrosal is best exposed ventromedially (Figs. 2.2, 4). The pars cochlearis is visible as a fairly smooth, bulging piece of bone. It is marked by two major sets of grooves. One emerges from the posterolateral aspect, crosses the promontorium and disappears at the anteromedial aspect of the element. A groove with this particular course is recognizeable in most plesiadapid specimens (see below). It is termed the "*g3*" groove in further descriptions and discussions (Table 2.3; Fig. 2.4: *g3*). More specifically, this groove (1) stems from the area that is anterolateral to the oval window, (2) is often connected to the other set of grooves (termed "*g4*" here - see below) visible in this specimen and (3) leads towards a consistently present septum termed "*s2*" here (see below). Admittedly, to where this groove leads and how it terminates are unknown because this part of the course is not preserved in any plesiadapid specimen.

The other groove marks the medial side of the promontorium and has a ventrolateral course that brings it into close proximity with the posterolateral beginning of *g3*, although they do not visibly meet in this particular specimen. Many other plesiadapid specimens also frequently display sets of grooves with a course similar to that just described and are referred to as "*g4*" grooves from here on out (Fig. 2.4: *g4*). In

many cases the *g4* groove actually intersects the *g3* groove. The promontorium is flanked on its medial side by rostral and medial tympanic processes (Fig. 2.4: *20*), which are abruptly broken off at their roots. There are three visible ridge-like bony projections (or septa) that rise from the tympanic processes to buttress the ballooning pars cochlearis. The most anterior of these is termed the second septum here (Fig. 2.4: *s2*) because it is medial to the "first septum" (Fig. 2.4: *s1*), which is more laterally positioned and obscured by matrix in this particular specimen (but visible with HRxCT). Note that terminology employed here differs from similar terminology used by Russell (1964) for some of these septa. Russell (1964: p.94, fig. 15) uses uses "S1" for *s2*, and "S2" for *s1*. One characteristic of *g3*, introduced above, is that it leads to the ventral apex of, or to the medial side of *s2* (Fig. 2.4). The most posterior of the three visible septa houses the cochlear canaliculus (Fig. 2.4: *cc*), a tube that connects endocranial space above the inferior petrosal sinus to the spiral cochlea (MacPhee, 1981). In fairly complete specimens the ventral surface of this septum often is marked by a groove that ends medially and laterally in foramina (Fig. 2.4: *21, 22*). This feature is visible on the left side of UALVP 46685, where it appears as a groove on the septum for the *cc* that ends laterally at a foramen on the promontorium. This groove and foramen represent the tympanic canaliculus. Between the *s2* and the ridge over the cochlear canaliculus, is the third septum (Fig. 2.4: *s3*), which is oriented mediolaterally and is the smallest of the three. Posterolateral to the cochlear canaliculus, the remnants of yet another septum are visible on the right side of UALVP 46685. This is the "blister-like" sheet of bone (e.g., Szalay et al., 1987; also referred to as the "posterior septum" by MacPhee, 1981) that often stems from the promontorium medial to the fenestra cochleae and arches laterally

beneath it while also extending posteriorly to meet the posterior wall of the auditory bulla. The most significant aspect of this feature is that its ventral margin often marks the canal and/or course of the internal carotid plexus, which may include only nerves, but possibly also the internal carotid artery (Fig. 2.4: *ps*). Its presence and position demonstrate that the internal carotid plexus had an intratympanic, transpromontorial course (Fig. 2.4) and that it entered the tympanic cavity from a position posterior and slightly lateral to the promontorium, instead of medial to it.

Digital extraction of the left petrosal allows visualization of the oval window, also called the aperture for fenestra vestibuli (Fig. 2.4: *av*), which measures about 1.17 mm by 0.60 mm in its diameters. This leads into the spiral cochlea measuring 15.60 mm in maximum length, after completing two and a half turns. The aperture for the round window, or fenestra cochleae (*ac*) is not visible in this specimen. The primary facial foramen is visible anterolateral to the fenestra vestibuli (Fig. 2.4: *23*). It measures 1.07 mm by 0.44 mm. The *s1* is visible, assisting in identification of more easily observable morphology (e.g., *s2*) as described above.

The right promontorium is obscured everywhere except its medial side. The lateral, anterior, posterior and ventral aspects are mostly covered by a flattened plate of what appears to be bulla-forming bone and remnants of the ectotympanic (Figs. 2.1-3, 5: *24*). The *g4*, a variably present groove, *s2*, *s3*, and cochlear canaliculus can be seen on the exposed medial surface (Fig. 2.5). Furthermore, the broken edge of the medial tympanic process reveals that it was comprised of two bony laminae (Fig. 2.5: *25, 26*). This may indicate the presence of more than one bone (i.e., the bulla may not have been entirely or even partly petrosally derived). The presence of two distinct laminae

comprising this process is evident in other specimens as well (see below). HRxCT data does not further illuminate the possibility that the bulla was formed from a bone other than petrosal, because the two laminae are not differentiable with these data. HRxCT data does, however, allow visualization of *s1* and the fenestra vestibuli (Table 2.3; Fig. 2.5). The posterior septum is crushed mediolaterally, however, it is nearly complete anteroposteriorly, such that the minimum length of the carotid canal (formed in the ventral margin of the *ps*) can be estimated at ~1.5 mm.

UALVP 49105 is another petrosal of *Pr. gaoi* from the Joffre Bridge locality (Fig. 2.6). This petrosal is excellently preserved and not crushed or distorted. It includes much of the pars canalicularis, pars cochlearis, tympanic processes and some of the ectotympanic bone. It was initially identified on the basis of overall similarity to the petrosals in the skull of UALVP 46685 but also on a few discrete features that clearly identify it as a plesiadapiform including the posterior septum. The cochlea is about the same length as that of UALVP 46685, although the fenestra vestibuli is narrower, measuring only 1.03 mm in maximum diameter. The dimensions of the pars cochlearis are nearly identical to those in the skull, although the width is slightly greater. Clearly present is *g3*, recognizable by its relationship to *s2*, and its orientation and position on the promontorium (Fig. 2.6). However, *g3* in this specimen intersects another groove that approaches it from the medial side of the promonotorium, and connects it to the *g4* groove. The *g4* leads ventrolaterally from the vicinity of the foramen for the tympanic canaliculus (Fig. 2.6). The lateral side of this specimen is well preserved – unlike those of the skull. The fenestra vestibuli is visible here. Ventral to the fenestra vestibuli is the root of the posterior septum. The dorsolateral aspect of the posterior septum is marked

by a pair of parallel grooves (Fig. 2.6: *g1*), that lead out from the posterior carotid foramen (Fig. 2.6: *pcf*). These grooves lose definition where the posterior septum contacts the promontorium, but another groove becomes visible more anteriorly on the lateral aspect of the promontorium itself. This grooves wraps ventromedially around the promontorium and approaches the *s1* (Fig. 2.6: *g2*). This groove is present in many specimens, recognizeable by the relationships just described and is referred to as *g2*. It is also often present as a pair of parallel grooves, although not in UALVP 49105. A more dorsolaterally directed groove (Fig. 2.6: *g5*) that approaches the epitympanc crest, a ridge of bone that extends laterally from the promontorium, just anterior to the fenestra vestibuli (Fig. 2.6: *ec*). The *g5* groove tends to be more broadly excavated than the *g2* groove.

As implied in the discussion above, the remnants of *s1* and *s2* are preserved, as well as *s3*, cochlear canaliculus and posterior septum. Furthermore the posterior wall of the bulla is preserved where it contacts the posterior septum, and thus a fragment of the internal carotid canal is preserved. Although the ventral margin of the canal is broken off, its mediolateral diameter measures 0.29 mm (Fig. 2.6I). The medial tympanic process of UALVP 49105 is broken, but clearly shows a dorsal and ventral lamina of bone comprising it (Fig. 2.6: *25*-*26*). Again, because of the historical prediction that the plesiadapid bulla has an entotympanic element in it (e.g., MacPhee and Cartmill, 1986), it is tempting to conclude that these represent two distinct bones. As with the skull, HRxCT does not reveal differentiation between these two layers (Fig. 2.6B), even though this isolated specimen was scanned at a resolution five times higher than the skull (8 μm vs. 40 μm). The semicircular canals of the pars canalicularis surround a deeply excavated

subarcuate fossa. They are well preserved and measurements are recorded in Silcox et al. (in press). Although a fragment of ectotympanic (Fig. 2.6) is preserved, it is not enough to permit any significant description.

Finally a fourth petrosal, UALVP 46687 from the DW-2 locality, has most of the diagnostic morphology of the other three specimens, plus some additional features (Table 2.3; Fig. 2.7). Like UALVP 49105, the fenestra vestibuli and pars cochlearis are measureable and yield measurements similar to the other specimens. It preserves *g1-5*. It is also similar to UALVP 49105 in preserving a groove that arises on the medial aspect of the promontorium and intersects *g3*. *g1* is represented by two parallel grooves. Unlike, UALVP 49105, in the present specimen, *g2* is also represented by a set of two parallel grooves. It preserves a foramen related to the tympanic canaliculus. Unfortunately preservation of the septa is not as good as in other specimens: *s1* and *s3* are not visible. While posterior septum is preserved toward its anterior margin, the posterior wall of the bulla is crushed dorsally onto the roof of the tympanic cavity. Thus posterior septum is broken here and internal carotid canal is obliterated. Still, the piece of bullar posterior wall that has been pushed into the tympanic cavity is not too distorted. The posterior carotid foramen is visible (although not measureable) on this fragment (Fig. 2.7). The semicircular canals are preserved and their measurements are reported in Silcox et al. (in press).

Ectotympanic.—The external auditory meatus (*eam*) and crista tympanica (the raised ridge-like attachment point for the tympanic membrane that encircles the internal aspect of the *eam*) are preserved in UALVP 46685 on the right side. They are both likely to represent ectotympanic bone. The ectotympanic is thus visible on the dorsal view of

the skull (Fig. 2.1). The length of the *eam* from its anterolateralmost point to the crista tympanica is roughly 5.5 mm. The anteroposterior diameter is larger, 5.75 mm. Thus, although the ectotympanic is not ring-like, it is certainly not tubular. It is merely moderately laterally expanded. While the remains of the crista tympanica can be recognized as a raised, ring-like ridge on the internal surface of the ectotympanic, the ectotympanic does not preserve evidence of a distinct "annular component." Whether the ectotympanic formed a substantial component of the bullar walls and floor is not discernable from this specimen.

Occipital.—The basioccipital is preserved on the ventral surface of the skull between the two petrosals (Figs. 2.2, 3). It measures 8.46 mm in anteroposterior length. The anterior end, where it would have met the basisphenoid at the spheno-occipital synchondrosis, measures 3.25 mm in mediolateral width (Fig. 2.2: *27*). The anteroposterior midpoint is only 2.96 mm wide and the posterior end is 4.36 mm wide (Fig. 2.2). HRxCT reveals it to be a thin bone, but that may only mean that any dorsal thickness to the bone has been pulverized. The only clearly preserved remnants of the exoccipitals are the left occipital condyle (Figs. 2.2, 3: *28*) and the corresponding hypoglossal foramen (Figs. 2.2, 3: *29*). The root of the right occipital condyle is preserved, which is only informative inasmuch as it delineates the boundary of the foramen magnum (Figs. 2.2, 3: *30*). The occipital condyle measures 3.87 mm dorsoventrally by 2.47 mm mediolaterally. The hypoglossal foramen is located a short distance anterior to the condyle. It is 1.03 mm by 0.86 mm. The hypoglossal canal is split in two by a septum that is inset within it. The foramen magnum appears only slightly distorted; its mediolateral width measures about 7.4 mm. The exoccipital and

supraoccipital are likely fused to one another on the posterior aspect of the skull because no suture separating them is evident. The dorsoventral dimensions of the supraoccipital are intact, given that the base of the nuchal crest is preserved (Figs. 2.2, 3: *31*). The supraoccipital thus measures 8.30 mm dorsoventrally from the top of the foramen magnum to the top of the nuchal crest. The bone is concave in its dorsoventral profile, suggesting that the nuchal crest was prominent. Finally, the supraoccipital is marked by several small foramina.

REVISED DESCRIPTION OF OTHER NORTH AMERICAN PLESIADAPID CRANIA

Nannodectes intermedius USNM 309902

Despite having been figured in previous publications, most of the morphology present in this specimen remains inadequately illustrated and undescribed. Furthermore, some aspects of the petrosal description by MacPhee et al. (1983) are incorrect, due to what appears to have been an editorial mistake, as described above. In this section I revise and add to previous descriptions, assisted through HRxCT imagery.

Nasal.— Remnants of both the right and left nasals are preserved (Fig. 2.8). The tip of the left element measures 2.31 mm mediolaterally (Fig. 2.8: *32*). The anteroposterior length of the right counterpart measures 13.61 mm (Fig. 2.8: *33, 34*).

Premaxilla.— Right and left premaxillae are preserved, although the latter is extremely fragmentary (Fig. 2.8). The right side element has its dorsoventral depth (8.33 mm), palatal length (7.75 mm) and maxillary suture preserved (Fig. 2.8: *35*). The dorsal

margin clearly had a posteriorly projecting process that most likely contacted the frontal. No teeth remain in the right premaxilla, however, Gingerich et al. (1983: fig. 5) show that both I^1's and the right I^2 were preserved nearby.

Lacrimal.— A fragment of the lacrimal appears to be preserved (Fig. 2.8) but none of its sutures, the lacrimal foramen or the lacrimal tubercle are observable.

Maxilla.— The maxillae are preserved bilaterally. The anterior portion is broken on both sides so that the canine is missing. On the right side the P^{2-3} are missing. On the left all teeth are present (Fig. 2.8) and the P^2 to M^3 distance is 12.04 mm. On the left side, the roots of the posterior molars, including M^{2-3} are exposed in the orbit (Fig. 2.8: *36)*. None of the sutures of the maxilla are preserved except a small segment of the premaxillary suture on the right side (Fig. 2.8). The infraorbital foramen is preserved and measures 2.20 mm by 1.15 mm (Fig. 2.8: *37*).

Zygomatic.— A fragment of the left zygomatic bone is preserved (Fig. 2.8). It seems that most of its ventral anteroposterior length is present, measuring (9.70 mm); however the dorsal margin is broken, especially anteriorly, so that the maxillary contact is not visible.

Palatines, sphenoids, frontals and parietals.— These bones may be visible, but if so, they are too fragmentary to allow certain identification or meaningful description. A delicately preserved foramen that has been pushed into the palate through deformation may represent the optic foramen, because it is similar in proportional size and morphology to optic foramina of European plesiadapid specimens (Fig. 2.8: *38*).

Squamosal.— The right glenoid of the squamosal (Fig. 2.9: *39*) and its postglenoid process (Fig. 2.9: *40*) are nearly completely preserved. The glenoid is flat.

Its anteroposterior length is 4.49 mm, while its mediolateral width is 4.11 mm. Due to broken anterior and medial margins and a missing entoglenoid process, these values are likely to underestimate the dimensions of the pristine element. The postglenoid process projects straight ventrally by 1.43 mm. On the left side, some of the zygomatic process of the squamosal is preserved (Fig. 2.8), but not enough to warrant description.

Petrosal.— Both petrosals are preserved, including regions of pars cochlearis and canalicularis (Figs. 2.9-13). Remains of both ectotympanics and a substantial portion of the left auditory bulla also exist. The maximum diameter of the aperture for the fenestra vestibuli is 1.16-1.19 mm (left-right). The left spiral cochlea measures 14.5 mm in length (Fig. 2.9H) and completes 2.5 turns. The width of the pars cochlearis is 3.6-3.8 mm, while its dorsoventral depth as measured from the endocranial surface is 3.5-3.6 mm. The promontorium has only two visible grooves on its surface (Figs. 2.9-11). The identification of some of these requires consideration of how they relate to the preserved bony septa that buttress the promonotory. Four bony septa are preserved. The left promontorium visibly preserves the posterior septum (Figs. 2.10, 11) and the *s1* (Fig. 2.11A-C, C', E). HRxCT data shows that it additionally preserves the *s2*, and cochlear canaliculus, but no *s3*, arising from the medial tympanic process (Fig. 2.11E). This medial process appears to have a smooth, edge. It projects medially from the promontorium an average distance of 1.2 mm. The right promontorium preserves the cochlear canaliculus, but is broken on the medial side more anteriorly (Fig. 2.9).

The *g1* groove is present on the ventrolateral aspect of the promontorium. It actually grooves the ventral part of the posterior septum anteriorly; however, more posteriorly, it diverges to the lateral side of the posterior septum (Figs. 2.9-11). The *g1*

groove measures about 0.29 mm in diameter. This is the groove that MacPhee et al. (1983: fig. 1) labeled as "s2." In their figure caption they attribute this morphology to AMNH 17388, and describe USNM 309902 as possessing the morphology of the former specimen. MacPhee et al. (1983: 509) stated that this groove has a blind end, posteriorly against a "bridge of bone uniting the promontory to the posterior wall of the bulla." This description, however, did not reveal that the specimen is broken in some critical areas. How the bulla and promontory connected can actually only be inferred, because the whole bulla is shifted anteriorly and the posterior part of the bulla is broken out where the posterior carotid foramen would have been located (Figs. 2.9-13) on both ears. This is especially observable with the CT scan. The *g2* and *g5* grooves are not preserved and may or may not have been present. The *g4* groove may be present on the right ear where the medial side of the promontorium is best exposed. A groove running mediolateraly on the left promontorium appears to be the *g3* groove (Fig. 2.11: *g3*), because HRxCT data reveal that it leads towards the *s2*.

Both ears preserve the bone-enclosed facial nerve canals (Fig. 2.9: *41*). Semicircular canals are also preserved (Figs. 2.9, 11: *42*). Their diameters are provided in Silcox et al. (in press). The right ear preserves a large epitympanic recess (Fig. 2.9: *43*), a bone-enclosed chamber dorsolateral to the fenestra vestibuli and posterior to the epitympanic crest.

The left bulla, although shifted relative to the promontorium, is fairly undistorted (Figs. 2.10-13). As indicated above, the posterior wall of the bulla is missing, however, the limestone that infills it creates a natural cast, which allows visualization of its intact

form. The bulla measures 11.23 mm in anteroposterior length. There is no obvious suture with the ectotympanic (Figs. 2.10-12).

Ectotympanic.— The left ectoympanic is missing most of the *eam*. The crista tympanica and its concentric, inward projection are visible (Figs. 2.11, 12: *44*). On the right side, some of the *eam* is preserved (Fig. 2.9). It was 4.07 mm in mediolateral projection. Its anteroposterior width is not preserved well enough to allow measurement; however, it can at least be stated that the *eam* was not tubular. The crista tympanica is not as well preserved on this side (Fig. 2.9: *44*), but more of it is visible. The connection between the crista tympanica and the bulla is solid and marked by subtly raised ridges (Fig. 2.9: *45*), not prominent bony struts as in *P. tricuspidens*. The diameter of the crista tympanica is 5.3 mm (although it may be slightly distorted) and gives an indication of the tympanic membrane diameter. As with other plesiadapids there is no telling how much of the *eam* and bulla were comprised of ectotympanic.

Occipital.— The occipitals are fairly well preserved (Figs. 2.10, 11, 13). The basioccipital is a narrow element 7.22 mm in anteroposterior length and 2.21 mm in width at the spheno-occipital synchondrosis (Figs. 2.10, 11). At the anteroposterior midpoint the width is 2.04 mm. The width of the posterior margin cannot be measured reliably due to breakage. There is only faint development of a sagittally positioned longitudinal ridge on the element (Figs. 2.10, 11, 13: *46*). The lateral margins project ventrally and would have braced the edge of the bulla in the pristine specimen (Figs. 2.11, 13: *47*).

The preserved parts of the exoccipitals include the right occipital condyle (Figs. 2.10, 11, 13: *48*), foramen magnum diameter (Fig. 2.13: *49*), and jugular process (Fig.

2.13: *50*). The suture with the supraoccipital is difficult to locate due to fusion; however, it appears that the supraoccipital was very narrow ventrally and comprised only a narrow median segment of the foramen magnum's dorsal margin. The occipital condyle measures 2.83 mm in dorsoventral depth by 1.95 mm mediolaterally. The foramen magnum is 6.87 mm by 4.51 mm. The jugular process projects laterally by 1.30 mm. The bilateral distance between jugular processes can be reconstructed by measuring laterally from the midpoint of the foramen magnum. The value would have been roughly 12.2 mm. The contribution of the supra-exoccipital complex to the posterior margin of the skull is concave in dorsoventral profile due to posterior projection of the nuchal crest (Figs. 2.11, 13: *51*). The dorsoventral depth of the supraoccipital along the midline from the top of the foramen magnum to the top of the nuchal crest is 6.02 mm. The right lateral edge of this complex (Fig. 2.13: *52*) seems to correspond to the sutural margin with the pars canalicularis of the petrosal, which has been displaced. Thus the unilateral distance from the midline to the most lateral point on the right exoccipital is 8.71 mm.

Dentary.— The left dentary was also preserved with the skull. Some pieces of the ramus are visible underneath the zygomatic (Fig. 2.10). The dentary and mandibular dentition were described by Gingerich et al. (1983), but neither was figured. Thus, the mandibular teeth are shown here in various views (Fig. 2.14).

***Nannodectes gidleyi* AMNH 17388**

No aspect of this specimen has ever been illustrated except a schematic diagram in MacPhee et al. (1983). However, as indicated above, its morphology is incorrectly attributed to USNM 309902. Furthermore, both Simpson's (1935) and MacPhee et al.'s

(1983) descriptions are brief and contain inaccuracies and omissions. Simpson (1935:9) misinterpreted the exposed promontorium as a bulla that "is completely ossified, but is remarkably small and relatively little inflated."

Thus, much of the morphology of this specimen is illustrated and described for the first time here. This specimen could not be HRxCT-scanned because of an x-ray opaque naturally deposited/precipitated mineral infilling the petrosals. The skull is crushed flat and only the ventral aspect is visible (Figs. 2.15-16). The dorsal aspect is embedded in matrix and a composite, or plaster, that has been applied, apparently in order to stabilize the specimen. The skull is articulated with a cervical vertebral series. Lying parallel to the vertebral series is a clavicle. Just behind this accumulation is what appears to be part of a radius shaft.

Maxilla.— The nasals, premaxillae, and lacrimals are not visible. The maxillae are preserved bilaterally. Left P^3-M^3 and right M^{1-3} are present, still in their alveoli. One P^2 (probably left) is out of its alveolus and lying on the palate (Fig. 2.15). The length of the tooth row from P^2-M^3 is 14.00 mm (Fig. 2.15). The heavy wear on these teeth reveals that the animal was probably senescent. Neither element preserves any sutures except possibly the zygomatic contact on the right side. The zygomatic process of the maxilla arises at the level of M^2 (Fig. 2.15: *53*). The infraorbital foramen is visible on the right side at the level of P^3 (Fig. 2.15: *54*). Its dorsoventral depth is roughly 2.22 mm.

Zygomatic.— The right zygomatic bone is visible (Fig. 2.15) but fragmentary; no morphology of significance is apparent.

Palatine.— Fragments of both palatines are preserved (Fig. 2.15). The posterior end of the palatal part of the bone and the anterior bases of both pterygoid processes are

preserved (Fig. 2.15: *55*). In fact, the right pterygoid process is continuous with the basisphenoid (Fig. 2.15: *56*) and alisphenoid (Fig. 2.15: *57*) contributions to the process (see below). On the palate, the right palatine terminates at the choanae in a swollen rim of bone, also referred to as a postpalatine torus (Fig. 2.15: *58*). The outer (anterior) margin of the torus reaches the lateral margin of the pterygoid processes. Furthermore, the outer margin of the torus is angular, with the anterior part of it following a straight, transversely-to-slightly-posteriorly-running course (so that the right and left margins together form a "v" with its tip pointing posteriorly), and the lateral part following a straight, anteroposteriorly-running course (thus, together the lateral and anterior margins of the postpalatine torus would form an "m"). The inner margin of the torus, which forms the inferoposterior margin of the choanae, is biconcave, with a midline postpalatine spine present (Fig. 2.15: *59*), prior to shifting of the contralateral palatines. The level of the posterior termination to the palatal part of the palatine bone is ambiguous because the palatines have been thrust anteriorly and to the left.

Sphenoids.— The alisphenoid is visible as the right ectopterygoid process, while the basisphenoid is visible by its contribution to the right entopterygoid process (Fig. 2.15: *56, 57*).

Squamosal.— The right and left squamosals are preserved (Fig. 2.15). The right side is relatively complete and includes the glenoid (Fig. 2.15: *60*), postglenoid process (Fig. 2.15: *61*) and a fragment of zygomatic process (Fig. 2.15: *62*). The glenoid is flat with the condyle of the dentary still sitting in it. It measures 6.5 mm in anteroposterior length and 5.6 mm in mediolateral width. The postglenoid process is oriented transversly

and projects straight ventrally by 1.35 mm. It is lateral to the postglenoid foramen (Fig. 2.15: *63*).

Petrosal.— The pars cochlearis of both petrosals are preserved, as well as some of the septa and tympanic processes that attach to them (Figs. 2.15, 16). On the right side, a bit of the pars canalicularis is visible. The posterior septum is either broken, or differently configured than in other plesiadapid specimens, such that no evidence of the *g1* groove is present. Because the posterior septum actually appears fairly complete, it may be that the internal carotid plexus did not go through the middle ear, and took a different route in this taxon (see further discussion below). The lateral aspects of the promontoria are obscured so that the presence of the *g2* and *g5* grooves and anterior septum cannot be evaluated. The medial aspect on the right element preserves a groove that begins near the cochlear canaliculus and arches laterally to where the posterior septum meets the promontorium (i.e., where the *g1* groove would also normally reach the promontorium) (Fig. 2.16A-C). There is no evidence of a foramen located on the cochlear canaliculus and leading into the promontory on this side. The groove thus has the anatomical relationships of the *g4* groove of other specimens. This is the groove referred to by MacPhee et al. (1983) as the "s1" groove. They suggest it held fibers of the tympanic plexus of nerves. However, as noted above, this morphology is referred to USNM 309902 in their figure caption. The left side is differently configured. The groove and foramen relating to the tympanic canaliculus are present on the septum housing the cochlear canaliculus (Fig. 2.16A-C). However, the more ventromedial aspect of the promontorium is free of any marks. That is there is no groove that matches MacPhee et al.'s "s1" from the other side. Ventral to the fenestra vestibuli at the base of

the posterior septum, a deeply incised canal stems anterodorsally from an apparent foramen (Fig. 2.16C: *g4*). Both promontoria also have a groove that crosses from medial to lateral, approaching the *s2*. It thus appears to be the *g3* groove. However, the morphology of this groove on the left side looks suspiciously as though it could be due to postmortem damage (i.e., like a crack, the edges of which have become beveled by weathering).

Medial tympanic processes flare out from the medial side of both promontories. These processes measure 1.5-1.6 mm in width, on average. The stylomastoid foramina are preserved on both sides (Fig. 2.16: *64*) and circular. They measure roughly 0.80-0.90 mm in diameter. Interestingly, there is a foramen wedged medial to these facial nerve foramina, and lateral to the posterodorsal base of the posterior septum on both sides (Fig. 2.16B, C: *65*). This foramen appears to lead to a canal and may have transmitted the internal carotid plexus. If so, it means that the route of the internal carotid plexus has migrated dorsally, and slightly laterally from its position in other plesiadapids. The diameter of this possible posterior carotid foramen is about 0.29 mm, comparable to the posterior carotid foramen and internal carotid groove (*g1*) on other plesiadapids (Table 2.3).

Occipital.— The left occipital condyle and the jugular process are preserved (Fig. 2.15: *66, 67*). The dorsoventral height of the condyle is roughly 2.8 mm; the mediolateral width is 2.5 mm. The jugular process projects 2.64 mm laterally from the edge of the condyle. The mediolateral width of the foramen magnum (Fig. 2.15: *68*), although possibly slightly distorted owing to dorsoventral crushing, is 6.84 mm.

***Plesiadapis anceps* YPM-PU 19642**

The illustration of this specimen in Gingerich (1976) is adequate to show major morphological features; new illustrations are not necessary. Some details can be added to the description – mainly dimensions (see Tables 2.4-5). The nasals measure 21.84 mm in length, with anterior and posterior mediolateral widths that are equal (3.34 mm). At the anteroposterior midpoint, the bone is mediolaterally narrower (2.30 mm). The premaxilla/frontal suture measures 4.52 mm. The premaxilla is 9.51 mm in dorsoventral depth. The maxilla/frontal suture measures 4.6 mm. The entire anteroposterior length of the frontals is preserved as well as the anterior margin of the parietal/frontal suture. Thus, the length of the metopic suture can also be given at 13.08 mm.

REVISED DESCRIPTION OF FRENCH PLESIADAPID CRANIA

The remaining descriptions are of specimens and taxa that have been described in a comprehensive and detailed fashion previously. Detailed redescriptions (like those above) are thus unnecessary. However, questions have been raised about aspects of morphology in these specimens since their initial descriptions, as discussed in the introduction. Thus, I present new information (in the form of both observations and illustrations) on these specimens in the following sections. The new information is organized into three subsections for each specimen: one on cranial sutures, another on cranial foramina, and a final one on more general aspects of cranial morphology.

***Plesiadapis tricuspidens* MNHN CR 125**

Cranial sutures.— As indicated in the introduction, Russell (1964: figs. 13, 14, 19) provided reconstructions of the skull of *P. tricuspidens* showing cranial sutures, but did not provide photographic evidence for most of the drawings. Thus, images of major sutures are provided here (Figs. 2.17-20: *69-87*). In addition to sutures recognized by Russell, there seems to be evidence of an orbitosphenoid/frontal suture (Fig. 2.20: *87*); observation of MNHN CR 965 helps strengthen interpretation of the presence of this suture.

Cranial foramina.— Infraorbital foramina are well preserved in MNHN CR 125 (Fig. 2.19E: *88*). Foramen ovale is clearly present, contained within the alisphenoid (Fig. 2.20B, D: *89*). As indicated in the introduction, the presence of foramen rotundum in *P. tricuspidens* has been debated. The large foramen posterior to the optic foramen and dorsal to the split of the ecto- and entopterygoid crests (Fig. 2.20D: *90*) must be considered either the foramen rotundum (Russell, 1964) or the sphenorbital fissure (Kay et al., 1992), depending on whether another foramen (Fig. 2.20B, D, E: *91*) located directly posteroventral to the optic foramen (Fig. 2.20B, D, E: *92*) and best preserved in MNHN CR 965, is interpreted as the "t.d.a." (superior orbital fissure) or suboptic foramen (i.e., Russell, 1964; Gingerich, 1976; and Bloch and Silcox, 2006 considered it the former whereas Kay et al., 1992 considered it the latter). The logic of Kay et al. (1992) is as follows: if Russell (1964) was incorrect, and this smaller foramen is not the superior orbital fissure, then it did not transmit the ophthalmic division of the trigeminal nerve, and the more posterior foramen must have carried both the ophthalmic and

maxillary divisions. In this case, no foramen devoted solely to the maxillary division of the trigeminal would have existed, and thus a foramen rotundum did not exist.

My observations of the original material lead me to conclude that there is no foramen rotundum [i.e., what Russell called the "t.d.a." is in fact the suboptic foramen, as Kay et al. (1992) suggest]; however, the evidence for this conclusion must partly be gleaned from MNHN CR 965 and is discussed below. One point that can be made on MNHN CR 125, however, is that the "suboptic foramen" appears to be entirely within the orbitosphenoid, unlike the superior orbital fissure, which falls between the orbitosphenoid and alisphenoid. Notably, MNHN CR 125 has a different small foramen just posterior to the optic foramen and anterior to the "sphenorbital fissure." This small foramen could also plausibly be considered a superior orbital fissure because it appears to open anteriorly through the junction of the alisphenoid and orbitosphenoid (Fig. 2.20: *93*). However, this foramen is not bilaterally present and it is absent from MNHN CR 965, suggesting that it is simply another, variably present hole. It does, however, serve to reveal the alisphenoid/orbitosphenoid suture, which spans between said foramen (*93*) and the sphenorbital fissure (*90*).

Interpretations of foramina of the basicranium have also been contentious. As discussed in the introduction, Bloch and Silcox (2001) implied that this specimen was lacking evidence of a posterior carotid foramen. However, Figure 2.19B' shows the posterior carotid foramen perpendicular to its canal and illustrates its caliber and shape. There is no doubt regarding the interpretation of this feature given the consistency of its presence in other specimens of this species, as well as in other species (see above). The canal leading from the posterior carotid foramen through the base of the posterior septum

is roughly 2.8 mm long. Medial to the promontorium is a groove leading to a foramen that perforates the medial process of the bulla at its medial point of termination, and one that perforates the promontorium itself at its lateral point of termination. This feature has been interpreted as the vestibular aqueduct by Szalay et al. (1987) but it is clearly the tympanic canaliculus foramen and groove, as discussed for other specimens earlier (MacPhee, 1981) (Fig. 2.21C': *94-95*). This morphology is clearly present in most other plesiadapid specimens preserving the relevant anatomy, as discussed and illustrated above. The hypoglossal canal appears septate, and split into two foramina, as in *Pronothodectes.*

Morphology of cranial bones.– Some of the most critical information relating to the structure of the basicranium in this specimen has been lost: What remained of the medial process of the left petrosal when Gingerich (1976: Pl. 8c) photographed the specimen sometime prior to 1974 is now gone. However, a cast recently made from an old mold housed in the MNHN, retains the medial process. This cast also reveals that MNHN CR 125 was broken at the junction of medial tympanic process with pars cochlearis even before the medial process was lost (demonstrating that this specimen was never substantially better preserved than the Pellouin skull anyway).

The promontoria of MNHN CR 125 conform well to the description by Gingerich (1976). As noted above, however, neither the posterior carotid foramen nor the laterally positioned *g1* groove for the internal carotid plexus has been photographically illustrated previously. Figure 2.21B shows this morphology. Unlike other *P. tricuspidens* promontoria (see below) and unlike many other plesiadapid petrosals (see above),

MNHN CR 125 does not express the *g2-3* grooves. However, the *g4-5* grooves are present (Fig. 2.21).

***Plesiadapis tricuspidens* MNHN CR 965**

This specimen appears frustratingly incomplete on preliminary inspection, being represented by only sphenoids, palatine and parts of maxillae with teeth; however, it provides the most solid evidence available for deducing the pattern of cranial foramina in *P. tricuspidens*. In fact, reconstructions of cranial foraminal patterns by other authors have been based primarily on MNHN CR 965 (Russell, 1964; Kay et al., 1992). Little of the dorsal aspect of the orbitosphenoid or alisphenoid remains: only the ventral portions are intact, but this is helpful in some ways (Fig. 2.22).

Cranial sutures.— For the most part the sutural patterns in the orbitotemporal region depicted by Russell (1964: fig. 19) are based on this specimen and can easily be observed: they are illustrated here with photographs for the first time (Figs. 2.23, 24: *96-99*).

There are two particular sutures that were not previously discussed or illustrated by Russell (1964). The dorsal margin of the orbitosphenoid actually appears to be an intact sutural edge, and would represent the dorsal boundary with the frontal bone. This suture appears to be preserved in a consistent position in MNHN CR 125 as well (Figs. 2.23, 24A: *100*). Additionally, the alisphenoid/orbitosphenoid suture is evident (Fig. 2.24: *101*). It passes through, or just above, the sphenorbital fissure, such that the medial aspect of the foramen is probably formed of orbitosphenoid, while the lateral aspect is alisphenoid. On superficial inspection this boundary looks more like a crack, because it

is not convoluted like many other sutures; however, the contact between these particular bones frequently looks this way in various other taxa (e.g., tenrecs). Furthermore, two features (only one could be photo-documented) of this contact strongly suggest it is a suture: (1) the form of the discontinuity between the alisphenoid and orbitosphenoid is revealed by the absence (i.e., broken condition) of the orbitosphenoid in the region of interest. Instead of appearing "crack-like" and planar, the discontinuity is dished like a sutural contact (Fig. 2.24: *102*). (2) Even though the discontinuity is not convoluted like other sutures, it is still more complex than would be expected for a crack created by brittle deformation. Identification of this final suture helps interpret cranial foraminal patterns. Having recognized this suture on MNHN CR 965, it becomes apparent that it has a slightly different course than that preserved on the left side of MNHN CR 125 connecting foramina *90* and *93* (Fig. 2.20D'). The latter suture would likely have resulted in the orbitosphenoid forming most of the medial wall of the sphenorbital fissure.

Cranial foramina.— Foramina for the trigeminal nerve's mandibular division (Figs. 2.22, 25: *103*), for its combined maxillary and ophthalmic divisions (Figs. 2.22-25: *104*), and for the optic nerve (Figs. 2.22, 24-25: *105*) are clearly visible and traceable to endocranial space. There are a number of small foramina representing sinus drainage from the lateral aspects of the alisphenoid and the lateral aspect of the orbitosphenoid (Fig. 2.23, 24: *106*). These cannot be mistaken for cranial nerve foramina because they are not bilaterally present in some cases or do not lead to the endocranium in other cases. This is also true for the "suboptic foramen" located posteroventral to the optic foramen (Figs. 2.22, 24: *107*). It appears to lead into the trabecular space of the orbitosphenoid and probably communicates directly with the blood sinus foramina on the opposite side.

Bloch and Silcox (2006) argued that communicating suboptic foramina are not expected in a taxon with such broad interorbital spacing; however, despite broad interorbital spacing, the postorbital constriction of the neurocranium in *Plesiadapis* is extreme and results in a sphenoid region as narrow as that of many euprimates. It thus seems unlikely that previous interpretations of the suboptic foramen as the "t.d.a." are correct. It is acknowledged that there is some distortion, which prevents complete confidence in the interpretation: the left side of the orbitosphenoid has been displaced substantially. However, the right side is more intact and the remnants of the optic canal can be traced to the dorsal (endocranial) aspect of the orbitosphenoid (Fig. 2.23: *108*). There is no comparable canal that could represent the ophthalmic branch of the trigeminal running ventrolateral to this. Moreover, given the identification of the orbitosphenoid/alisphenoid suture above, Russell's (1964) "t.d.a." and ophthalmic canal would have run within the orbitosphenoid, which would be an unusual pattern for a eutherian mammal, as discussed above.

Morphology of cranial bones.—The only previously unmentioned aspect of this specimen is the existence of pneumatization of the alisphenoid (Figs. 2.22A, 2.23C, 2.25: *109*). This is consistent with observation by MacPhee and Cartmill (1986) that the Pellouin skull is enervated by empty "celluoles."

Plesiadapis tricuspidens **Pellouin skull**

Cranial sutures.— The Pellouin skull does not add an incredible amount of new information regarding position of cranial sutures. However, it does preserve perhaps the best example of a remnant of the palatine/alisphenoid suture (Figs. 2.26C-C', 2.29B-B':

110) and the only squamosal/alisphenoid suture (Fig. 2.26E-E': *111*). Furthermore, it increases confidence in descriptions based on other specimens by preserving similar sutural patterns. Specifically, there is a clear sutural surface for a large wing of premaxilla on the frontal (Fig. 2.27B-B': *112*). The frontal also preserves the sutural surface for the nasals, showing that the nasal was morphologically similar to MNHN CR 125 in this region (Fig. 2.27B-B': *113*).

In the palate, the transverse palatine suture is similar to that in other *P. tricuspidens* specimens (Fig. 2.26B-B': *114*) in its convoluted shape and in reaching the level of M^1. There appears to be a nearly obliterated palatine/frontal suture in the postpalatine canal. Unfortunately, neither the frontal/orbitosphenoid contact nor the alisphenoid/orbitosphenoid suture is visible.

On the dorsum of the skull, the frontal/parietal contact is visible at its anterior apex (Fig. 2.27D-D': *115*), but barely evident elsewhere. The parietal/squamosal contact is most distinct anteriorly (Fig. 2.27A, E-E': *116*) and broken in the region of squamosal foramina (Fig. 2.27E-E': *117*). Note that there are two squamosal foramina, one at the boundary between squamosal and parietal, and one completely within the squamosal (Fig. 2.27E-E'). An a suture between what appears to be parietal and occipital is visible along the nuchal crest (Fig. 2.27F-F': *118*). Sutures between the tubular external auditory meatus and postglenoid process anteriorly, and external auditory meatus and mastoid posteriorly, are clear (Fig. 2.26F-F': *119-120*). Regarding the ectotympanic bone, the tympanic annulus, holding the crista tympanica, projects well beyond the bony struts of the annular bridge and it even appears that there is a gap between the bridge and the

annulus suspended from it, but it is unclear whether this is a suture or due to breakage (Figs. 2.28B-B', 2.29C-C': *121*).

Cranial foramina.— The infraorbital foramen is well preserved and measures 2.34 mm by 1.79 mm. The palatine in the palate has three main foramina, unlike MNHN CR 125, which has four (as illustrated in Gingerich, 1976: Pl. 9a) (Fig. 2.26B-B': *122*). As indicated above, the postpalatine foramen is visible on the left side. The optic and "suboptic" foramina are obscured by crushing. However, the base of the "sphenorbital fissure" is visible in a way similar to that in MNHN CR 125 (Fig. 2.29B-B': *123*). Foramen ovale is visible, but barely so because it is obscured by matrix and broken (Fig. 2.29B-B': *124*). There is a foramen within the left scaphoid fossa (Fig. 2.26D-D': *125*), which may represent the vidian foramen. This appears to be that which Gingerich (1976) mentions (but did not illustrate).

Relating to the ear, a tubal canal is present on the right bulla (Fig. 2.29C-C': *126*). Regarding the promontoria of the pars cochlearis of the petrosal, both *ac*, but niether *av*, are visible. Arching over the *ac*, the posterior septum holds an actual carotid canal that is visible on both sides: the ventral half is sheared away on the left side, but the canal is intact on the right side and the posterior carotid foramen is both visible and measureable (0.31 mm on right side, 0.29 mm on left side) (Figs. 2.28, 29C-C': *127*). On the medial aspect of both promontoria, the opening of the tympanic canaliculus is present on the septum for the cochlear canaliculus (Fig. 2.28C", E: *128*). On the posterior side of the left caudal tympanic process of the petrosal (posterior wall of the bulla), the jugular foramen is clearly visible, formed between the bulla and the exoccipital, and measures roughly 2.13 mm in maximum diameter. As in MNHN CR 125, it is clearly divided into

two regions for the internal jugular vein laterally and cranial nerves IX-XI medially (Fig. 2.28C": *129*). The hypoglossal canal is also well preserved on the left side (Fig. 2.28C": *130*) and, as for MNHN CR 125, it is septated into two foramina. A small, laterally oriented foramen anterior to the *eam* is present.

Morphology of cranial bones.— The only region that requires additional description in light of new information on other plesiadapids is the pars cochlearis. As indicated above, the posterior septum with a carotid canal and *g1* groove is visible on the lateral aspect of the promontorium, as it is in other plesiadapids. No laterally coursing *g2* groove is visible on this specimen although, admittedly, this region is obscured, at least on the right side. Medial to the posterior septum the septum for the cochlear canaliculus is visible with the tympanic canaliculus foramen on it. Moving anteriorly from the cochlear canaliculus along the medial side of the bulla, there is no third septum, and thus the second septum is eventually encountered (Figs. 2.28, 29: *s2*). On both promontoria, a set of parallel grooves begins from the lateral side of the promontorium, near the posterior septum arches medially and anteriorly, approaching the second septum, and thereby reveals itself as the *g3* groove (Figs. 2.28, 29: *g3*). Arching ventrolaterally, away from the tympanic canaliculus, is the *g4* groove (Fig. 2.28: *g4*).

Neither promontorium is continuous with its medial tympanic process, due apparently to breakage. The breakage appears to have happened in the same way on both sides, with the pars cochlearis having been shifted ventrally away from the surrounding bulla (Fig. 2.28). Additionally, the caudal and rostral processes are broken on the right ear. On the left, the caudal process is intact, the medial process is broken even closer to

the pars cochlearis, and rostral processes, while broken, are more visible and intact than on the right side.

The broken edges of the bullar walls just ventral to the ectotympanic ring and medial to the pars cochlearis of the petrosal on the right side are clearly comprised of two layers of bone (Fig. 2.30E-G). Figure 2.30 also shows the double layer near the ectotympanic ring. The outer (more superficial) layer is generally thinner near the ectotympanic and of a deeper amber color than the deep layer. On the medial bullar wall, the superficial layer is thicker than the deep layer.

Morphology suggesting against a petrosal composition to the bulla (contrary to the evidence above – see discussion) is that the left ear has a distinct color change between the edge of the pars cochlearis and the posterior septum as well as between the pars cochlearis and the very base of the medial tympanic process. Associated with this color change is what also looks like a groove that begs interpretation as a sutural margin or bone boundary (Fig. 2.28E: *131*). However, closer inspection of this juncture reveals the presence of a thin crack at its posterior end that accentuates the distinction between these two regions of the petrosal.

***Plesiadapis tricuspidens* MNHN CR 126**

Cranial sutures.— This specimen shows convincing evidence of frontal/maxilla contact in the orbit. The sutures are generally sinuous (or convoluted) here. There are two anteroposteriorly running discontinuities along the medial orbital wall. The more dorsally positioned one is clearly a suture given its sinuous form (Fig. 2.31: *132*). It appears to separate the maxilla and frontal. The second discontinuity (Fig. 2.31: *133*),

ventral to the sinuous suture (*132*), may represent another suture although it has apparently always been interpreted as a crack due to its very straight contour. It would be easy to continue to discount this feature as a crack except for the presence of a similarly positioned ridge of bone on the maxilla of the Pellouin skull (Fig. 2.27A). If this straight "crack-like" feature is actually a suture, then it would seem to represent the palatine-maxilla suture, while *132* would represent the maxilla palatine suture.

While not easily visible on this specimen, it is still possible to tell that the palatine foramen is not completely formed by the palatine (as mentioned for MNHN CR 125 and MNHN CR 965 above) and that the frontal contributes to it (Fig. 2.31: *134*).

This is the only specimen to effectively illustrate the size, form and number of lacrimal foramina: there is a single large lacrimal foramen (Fig. 2.31: *135*) – an apparent second is formed by glue.

Morphology of cranial bones.— Measurements on the mediolateral breadth of the maxillae and medial-most point of frontal-lacrimal contact in this essentially undistorted specimen are similar to the same measurements in MNHN CR 125 (which is crushed dorsoventrally) suggesting it is also basically undistorted in the transverse plane. The posterolateral root of M^3 is exposed on the orbital surface of the maxilla, similar to the condition apparent in the Pellouin skull. The lacrimal foramen is located on the rostrum, just beyond the orbital rim. Furthermore, medial and dorsal to the lacrimal foramen the lacrimal bone bulges (Fig. 2.31E, F): this bulge appears to represent the lacrimal tubercle.

***Plesiadapis tricuspidens* MNHN BR 17414-19, 1371**

These specimens represent isolated petrosals from Berru identified by M. Godinot. In all cases I assessed the morphology independently and confirmed the attribution to *P. tricuspidens*. The specimens have been measured from HRxCT scans generated at Pennsylvania State University at a resolution of 0.0500 mm for pixel dimensions, and 0.0581 mm for slice spacing. MNHN BR 17418 preserves a stapes that has fallen into the cochlea. This element was digitally extracted, measured, and helps confirm that *P. tricuspidens* did not have a functional stapedial artery. The area of its obturator foramen is small relative to its footplate length, which makes it like modern primates that lack stapedial arteries (Coleman and Boyer, 2008; in prep.).

Table 2.3 is a codified description of these specimens and other petrosal specimens studied here. The presence/absence and measurements of various features is documented therein. None of these specimens reveals an apparent suture at the boundary between the medial tympanic process and the promontorium as in the case of the Pellouin skull.

SELECT QUANTITATIVE DIFFERENCES BETWEEN *P. TRICUSPIDENS* AND OTHER PLESIADAPIDS

As mentioned in the introduction, features thought to be distinctive for plesiadapids, as based on observations of *P. tricuspidens*, prior to this work, include a nasal bone that is narrow at its caudal extent; a premaxilla that has a broad contact with the frontal; and a tubular-shaped ectotympanic (e.g., Bloch et al., 2007). Table 2.5

provides measurements of these and other features. Table 2.6 provides natural log ratio variables quantifying their shape (see table 2.4 for descriptions of variables). Although sample sizes are too small for statistical confidence of any sort, it is interesting to note that *P. tricuspidens* has substantially proportionally narrower nasals (Table 2.6: N/GM), wider premaxillae (Table 2.6: N/Pmx, Pmx/GM), and a more tubular external auditory meatus (Table 2.6: EAM-S) than any of the other plesiadapids. Thus other plesiadapids are not *as distinctive* in these features as is *P. tricuspidens*. Another interesting difference between *P. tricuspidens* and other plesiadapids is its proportionally larger glenoid fossae (Table 2.6: Gld/GM). Finally, it appears that the largest plesiadapids (mainly *P. tricuspidens*) have the proportionally shortest cochleae (Table 2.6: Cl/GM), smallest petrosals (Table 2.6: Pcsa/GM) and smallest fenestra vestibulae (Table 2.6: ac/GM).

NEW EVIDENCE BEARING ON THE COMPOSITION OF THE PLESIADAPID BULLA

As mentioned in the introduction, the morphological prediction for a non-petrosal bulla is the presence of a suture separating the bulla from the pars cochlearis of the petrosal bone. However, whether and when this suture would have been obliterated by remodeling, and what the physical evidence for its presence should look like have not been outlined. A preliminary survey of mammals with basicranial forms similar to those of plesiadapids and basal euprimates includes several rodents, treeshrews, and two paromomyids. These taxa have large inflated bullar cavities with bony septa buttressing

the bulla. In *Sciurus carolinensis* and *Tupaia glis* the promontoria have modest medial and rostral tympanic processes. In *Sciurus,* the ectotympanic forms the bulla and septa, which contact the medial and rostral tympanic processes of the petrosal in an externally on-lapping, squamous suture. The overlap is extensive and can easily be visualized with HRxCT data (Fig. 2.32). In *Tupaia,* the condition is similar except that the bulla-forming bone is the entotympanic and the overlap is not so extensive, because the rostral and medial processes of its promonotorium are relatively smaller (MacPhee, 1981) (Fig. 2.33). In some rodents with this basic pattern (e.g., *Marmota*: Fig. 2.34), foramina for neurovasculature relating to the tympanic and internal carotid plexi can be observed to enter the tympanic cavity at the sutural boundary between the ectotympanic and petrosal on the medial aspect of the promontorium. Other rodents, specifically *Lagostomus* (Figs. 2.35, 36) and *Dipodomys,* fuse the suture between the ectotympanic and petrosal (and thus superficially appear to have a petrosal bulla), but still preserve evidence of this suture via the canals for tympanic plexus nerves that reach the middle ear cavity through this sutural conduit (Fig. 2.36). Thus, if plesiadapids have a non-petrosal bulla, one might expect the suture to be expressed as overlapping laminae of bones on the tympanic processes, as in *Sciurus* and *Tupaia,* or by the planar organization of canals for neurovasculature along a previously unfused suture.

Almost all the plesiadapid specimens that preserve part of the medial tympanic process show it to be comprised of two layers of bone. In fact, *Pronothodectes gaoi* (UALVP 49105) looks nearly identical to a *Sciurus carolinensis* ear that has been prepared in a way so as to mimic the inferred breakage on the fossil (Fig. 2.32). This fact, combined with the observation of what appears to be a suture on the medial aspect

of the promontorium of the Pellouin skull (Fig. 2.28), strongly suggest a suture in this vicinity. HRxCT scans of UALVP 49105 do not, however, strengthen the support for this interpretation because they do not reveal any separation between these bony layers, and furthermore, do not show any "planes of canals" along a possibly previously unfused boundary.

A further test of the significance of the apparent similarity in the medial tympanic process morphology between plesiadapids and mammals known to have non-petrosal bullae is to examine the cross-sectional morphology of more ventral and lateral components of the bullar wall. If plesiadapids do in fact have a bullar construction similar to that of *Sciurus*, for instance, then these more ventral regions of the bullar wall should be thin and comprised of a single lamina of bone as they are in *Sciurus*. This test is not possible in the UALVP specimens. However, it is possible in the Pellouin skull of *P. tricuspidens*.

The cross-sectional morphology of the more ventral and lateral parts of the bullar wall in the Pellouin skull exhibit two distinct layers. This is contrary to the prediction of the hypothesis that the two layers of bone on the medial tympanic process represent two different bones (Fig. 2.30). Furthermore, the broken open bulla in the otherwise intact skull of the euprimate *Adapis* looks extremely similar to the condition in *P. tricuspidens* in having two layers comprising the bulla (Fig. 2.30). Finally, the morphology of a petrosal specimen of the euprimate *Indri indri* contradicts the most straightforward interpretation of the significance of multiple bony layers on the medial process of the promontorium. *Indri* also exhibits the double layer morphology at the lateral margin of the medial process extending from the promontorium (Fig. 2.37).

Thus, despite the presence of suture-like morphologies on the medial tympanic process of plesiadapid specimens described here, there is still no solid morphological evidence for an entotympanic or ectotympanic bulla. There are, however, some surprisingly detailed similarities in bullar wall construction among existing plesiadapid specimens and some euprimates. In this context it is worth considering the morphology of various paromomyid plesiadapiforms, in which evidence for a suture (squamous) between promontorium and bulla is generally accepted (Bloch and Silcox, 2001). This suture is quite unique in that the hypothesized entotympanic has an edge that inserts dorsal to the medial tympanic process of the petrosal, opposite of the condition in treeshrews and rodents (as well as carnivorans [e.g., Vander Klaauw, 1931], pholidotans [Gaudin, 1999], and macroscelideans [Novacek, 1977; MacPhee, 1981]) (Fig. 2.38A-B').

Interestingly, there are several features of the paromomyid "medial tympanic process" which would seem to indicate that even the medial tympanic process is not petrosally-derived. Specifically, there are a series of distinct, ventrally raised ridges on the medial process, which continue laterally onto the promontorium and then stop abruptly along an anteroposteriorly running boundary (Fig. 2.38C-F:*bs*). This boundary appears to be a sutural edge: lateral to it, the ridges are nonexistent and the promontorium is smooth. Second, the dorsal surface of the promontorium seems to show the other side of this same suture (Fig. 2.38B: *bs?*). Finally, an HRxCT scan (8 μm resolution) of a juvenile individual of the paromomyid *Acidomomys hebeticus* (UM 108207) reveals that the bone forming the cochlea is distinct in its density and porosity from the bone forming the medial tympanic process as well as other contiguous regions (Fig. 2.39). The hazy boundary between bone forming the promontorium itself and its medial tympanic process

seen on the HRxCT scan is expressed as a distinctly visible discontinuiy on the medial aspect of the promontorium under a light microscope. However, the HRxCT image also shows that bones on either side of the apparent dorsal expression of this suture (*bs?*) are two separate processes of the same bone.

DISCUSSION

Presence and position of a posterior carotid foramen and canal

The evidence for an internal carotid plexus going through the middle ear has recently been considered limited (MacPhee et al., 1983; Bloch and Silcox, 2001, 2006). However, as shown in descriptions above, all specimens but one, that are preserved well enough, show a posterior carotid foramen, and/or the remnants of its canal on the posterior septum. In all of these specimens the posterior carotid foramen and/or the remnants of its canal show it to have had a posterolateral entrance into the tympanic cavity. This differs from the interpretation used by some recent authors (e.g., MacPhee et al., 1983; Silcox, 2001; Bloch and Silcox, 2006). On the other hand this finding agrees with Wible (1993), who considered both plesiadapids and paromomyids to exhibit a "posterolateral" entrance. The morphology of *Nannodectes gidleyi* AMNH 17388 is clearly different from that of other plesiadapid taxa preserving this region, in that the internal carotid plexus route, although still adjacent to the stylomastoid foramen, was not intratympanic. It seems likely that this difference is the result of a more dorsal location of the internal carotid plexus route. Even if this is incorrect, the earlier occurring more basal *N. intermedius* (Gingerich, 1976) has morphology like that of other plesiadapiforms

(Table 2.3) indicating that the morphology of *N. gidleyi* is derived, whatever the correct interpretation of it may be.

Reconstruction of soft anatomy in grooves on plesiadapid promontoria

Previous studies argued that apparent variable expression of grooves on the plesiadapid promontorium revealed them to be randomly reticulating rami of a tympanic plexus (MacPhee et al., 1983). The corollary to this argument, that there were no consistently present grooves, was taken as evidence that the internal carotid plexus did not consistently go through the middle ear cavity (MacPhee et al., 1983). However, the descriptions above demonstrate that there are at least five sets of grooves, identifiable through a set of anatomical relationships (Fig. 2.40). All of these grooves are not evident on every petrosal, however this seems more likely due to variable osteological expression of soft anatomical features and not to variable presence of neurovasculature. The logic behind this assumption will be discussed in more detail below.

It is important to first establish the identity of various septa in the plesidapid tympanic cavity, because various components of the neurovasculature in extant primates and treeshrews have specific relationships to these septa (MacPhee, 1981). The posterior septum and the septum of the cochlear canaliculus (Fig. 2.40) were identified earlier because their identification is more straightforward. I propose that the *s1* is equivalent to the anterior septum of MacPhee (1981). This is supported primarily by the observation that *s1* appears to be directly medial to the opening for the tubal canal (Fig. 2.40) (see also Russell, 1964). The anterior septum is present in various fossil euprimates (MacPhee and Cartmill, 1986) (Fig. 30), extant lemuroid (Fig. 2.37) and lorisoid

primates, as well as treeshrews and elephant shrews, according to MacPhee (1981). It has also been identified in *Ignacius graybullianus* (Bloch and Silcox, 2001) (Fig. 2.38).

Either the *s2* or *s3* is equivalent to the medial secondary septum of MacPhee (1981), while the other one cannot be analogized with morphology present in the sample of primates and treeshrews studied by him. The hypothesis that the *s2* is more nearly equivalent to the medial secondary septum is favored here as discussed below.

The *g1* groove is clearly related to the internal carotid plexus. This is supported by its anatomical relationships and its typical morphology. Specifically, it is located on the lateral aspect of the posterior septum and ventral apex of the pars cochlearis of the petrosal. It thus leads directly anterior from the internal carotid canal formed in the floor of the posterior septum. Furthermore, the fact that it often appears as a pair of grooves is consistent with a relationship to the internal carotid plexus, because the internal carotid plexus commonly exists as two major nerve bundles (e.g., MacPhee, 1981; Conroy and Wible, 1978; Wible, 1993).

The *g2* groove on the petrosal, which is usually present, is also interpreted as having held contents of the internal carotid plexus. This groove begins from where *g1* reaches the promontorium, and always approaches the lateral side of the anterior septum. MacPhee (1981) and other authors (e.g., Conroy and Wible, 1978) demonstrate that the internal carotid plexus follows the anterior septum (and thus leads towards the tubal canal) in various lemuroid euprimates, treeshrews and macroscelidean insectivores. My own observations reveal that the internal carotid plexus of *Capra* also leads towards the tubal canal. These anatomical associations and the fact that *g2* is sometimes present as a pair of parallel grooves strongly suggest that it relates to the internal carotid plexus.

The *g3* groove stems from an area on the promontorium that is slightly anteromedial to the oval window and leads to the medial side of the *s2* septum. Its course is thus more medially directed than that of the *g2* groove. It does not appear to be related to the internal carotid plexus because it approaches the *s2*, not the anterior septum, as in other mammals. It also seems unlikely to represent any other nerve bundle such as the lesser or greater petrosal nerves, because it is medial to the *g2* groove, which apparently represents the internal carotid plexus. MacPhee (1981) illustrates the lesser and greater petrosal nerves lateral to the internal carotid plexus route in euprimates, treeshrews and macroscelideans. Apparently in lemuroids, lorsoids and treeshrews of MacPhee (1981)'s sample a small vein follows the medial secondary septum. Thus, it seems most parsimonious to conclude that *s2* represents the equivalent of the medial secondary septum and *g3* primarily held a small vein. However, grooves connecting the *g3* and *g4* suggest that tympanic plexus fibers ran along the *g3* route as well.

The *g4* groove is often closely associated with the groove and foramen for the tympanic canaliculus. This is consistent with it representing branches of the tympanic nerve, as suggested by MacPhee et al. (1983) for *N. gidleyi* 17388. The majority of these nerves fibers appear to have reached the lateral side of the pars cochlearis using either an intrapetrous route on some ears, or subpetrous route on others, as indicated by the asymmetrical morphology of *N. gidleyi* AMNH 17388. On the right side of AMNH 17388 there is no evidence of a foramen located on the septum of the cochlear canaliculus, leading into the promontorium, but the *g4* groove appears well-developed, thus marking a subpetrous route for the tympanic nerve (MacPhee et al., 1983: fig. 1 "s1"). The left side is differently configured. The groove and foramen for the tympanic

canaliculus are present on the septum covering the cochlear canaliculus (Fig. 2.16A-C), but the more ventromedial aspect of the promontorium is free of any marks. Ventral to the fenestra vestibuli, at the base of the posterior septum, a deeply incised groove stems anterodorsally from an apparent foramen (Fig. 2.16C: *g4*). It seems likely that this represents the emergence of the tympanic nerve from an intra-petrous tympanic canaliculus route.

The *g5* groove is a trough-like groove that sometimes appears as an anterior continuation of *g1*. It is located dorsolateral to *g2*. It is quite broad and may represent the place of formation of the main part of the tympanic plexus. The deep petrosal nerve likely stemmed from this point to meet greater petrosal nerve, which seems to have emerged just lateral to this groove from the hiatus fallopi (Fig. 2.40).

As mentioned above, the morphological expression of some identified grooves is variable from specimen to specimen. It was argued that in the case of the morphology examined here, most of this variability is not likely to reflect variability in the presence of the soft anatomical structures these grooves are interpreted to have held. The logic behind this is demonstrated with an example: in *P. tricuspidens* (MNHN CR 125) the *g2* groove is absent. However, the carotid canal and *g1* groove are present. Thus, the internal carotid nerve and possibly an arterial remnant (see Chapter 5), clearly gained entrance to the tympanic cavity. The lack of a *g2* groove reflecting the "typical" course of the internal carotid plexus to the *s1* (MacPhee, 1981) is therefore not sufficient evidence to conclude that the internal carotid plexus did not have an intratympanic course. Given the absence of other "alternative" grooves that could plausibly represent the internal carotid plexus across the promontorium, the most conservative interpretation

is that the internal carotid plexus had the same course as in other plesiadapids in which the groove is visible. Variance in other structures such as the *g3* groove, may actually reflect real variability in soft anatomy, because it is interpreted to represent a vein. Generally speaking the observation of tympanic cavity morphological variability is important because it demonstrates that intraspecific variation must be carefully considered when interpreting detailed aspects of cranial morphology, just as it must when interpreting postcranial and dental characters.

Absence of the foramen rotundum in *Plesiadapis tricuspidens*

New observations of the specimens of interest show that Russell's (1964) "t.d.a." is clearly formed within the orbitosphenoid on MNHN CR 125 (Fig. 20B',20D': *91*). On MNHN CR 965 it appears to have been present only on the left side, and, as for MNHN CR 125, contained within the orbitosphenoid (Fig. 2.24C shows a ridge of the alisphenoid positioned where the posterior rim of the foramen should be, but this appears to be an artifact of breakage). Furthermore, in MNHN CR 965 it seems clear that this foramen simply did not connect to the endocranium through any sort of canal (Figs. 2.23, 25). What Russell (1964) identified as the foramen rotundum ("t.r.") appears to be formed at the boundary between the alisphenoid and orbitosphenoid, instead of within the alisphenoid. This interpretation is based on observation of an apparent suture that spans from this foramen (Fig. 2.20B', 20D': *90*) to a tiny foramen located ventral to the suboptic foramen (Fig. 2.20B', 20D': *93*) in MNHN CR 125. The question of why foramen *93* is not a candidate for a superior orbital fissure (t.d.a.) could be posed. I would argue that it is not the superior orbital fissure because (1) it is so miniscule and (2)

it is missing from the other side of MNHN CR 125 and as well as all other specimens. This suggests to me that it is not a major conduit for branches of CNs III-VI, as in other taxa with a superior orbital fissure. In MNHN CR 965, the location of the alisphenoid/orbitosphenoid suture is located more dorsally such that, given the breakage, it is possible that the orbitosphenoid did not reach the sphenorbital fissure in a significant way. These variations introduce some uncertainty to the interpretation. Even so, in light of the above observations, it seems that "suboptic foramen" is a better-supported designation for Russell's "t.d.a." and that Russell's "t.r." should be considered the sphenorbital fissure. This conclusion is illustrated in Figure 2.41.

Composition of bulla: sutural evidence on medial tympanic process

The total morphological pattern for the paromomyid ear suggests that its medial tympanic process is petrosally derived. Even if one accepts that there are two "types" of bone present in the paromomyid petrosal, as argued for *Acidomomys hebeticus* (Fig. 2.39) with bone relating to the medial tympanic process having apparently migrated down onto the promontorium to create a sutural effect, the fact that bone comprising this process also extends dorsal to much of the promontorium (onto the bone's endocranial surface) suggests that it is also a petrosally-derived bone: entotympanics and ectotympanics are not known to have endocranial expression in other taxa (MacPhee, 1981). Given the documented mode of development of entotympanic elements in treeshrews and various insectivorans (MacPhee, 1981), it is difficult to imagine how they ever could intervene between the petrosal and the endocranium. If two types of petrosally-derived bone are

similarly present in the euprimate *Indri* (Fig. 2.37), this could also explain the "bilaminar" appearance of its medial process.

Given the similarity between the medial tympanic processes of paromomyids, *Indri*, and plesiadapids, the more detailed interpretation of paromomyids can be applied to plesiadapids as well. Thus the apparent sutures relating to the medial tympanic process of some of the *Pronothodectes* specimens and the Pellouin skull likely were formed in a way similar to those of the *Ignacius* and *Acidomomys* specimens. That is, these sutures are likely to be so-called "petroso-petrosal" sutures that have been observed in *Tarsius* (MacPhee and Cartmill, 1986). It is explained that these sutures occur as a result of relatively rapid growth of the tympanic processes of the petrosal.

SUMMARY AND CONCLUSIONS

Description and analysis of new plesiadapid cranial specimens revealed the Plesiadapidae to be more diverse than previously recognized. Some features thought to be autapomorphic for the clade are revealed to be less developed in species other than *P. tricuspidens*. Specifically, the nasal bones are broader, the premaxillae are narrower and the external auditory meati are shorter in non-*P. tricuspidens* plesiadapids. Furthermore, previous conceptions of the clade's basicranial anatomy were revised. Contrary to some previous interpretations, there is strong morphological evidence that plesiadapids have a posterolaterally positioned posterior carotid foramen; a consistent intratympanic route for the internal carotid plexus; a combined superior orbital fissure and foramen rotundum (i.e., a sphenorbital fissure); and a petrosally derived auditory bulla. These new

observations and interpretations may bear on previously proposed phylogenetic relationships among plesiadapids, other plesiadapiforms and euprimates.

ACKNOWLEDGMENTS

I am particularly grateful to R. C. Fox and C. S. Scott for allowing me to lead the description and analysis of the UALVP *Pronothodectes gaoi* specimens. A. Walker and T. Ryan provided HRxCT scans of this specimen and others at the Center for Quantitative Imaging, Pennsylvania State University. M. Colbert and T. Rowe provided HRxCT scans of USNM 309902 at the High-Resolution X-ray CT Facility of the University of Texas at Austin. S. Judex and C. Rubin provided HRxCT scans at the Center for Biotechnology of the Department of Biomedical Engineering at Stony Brook University. M. Godinot, P. Tassy, and C. Sagne of MNHN, and M. Pellouin provided access to important comparative specimens of *Plesiadapis tricuspidens*. R. Emry of the USNM granted access to and study of USNM 309902, *Nannodectes intermedius*. M. Jin of the AMNH granted access to and study of AMNH 17388, *Nannodectes gidleyi*. M. Coleman provided measurements of cochlea length in Table 2.3. J. Scott of the University of Alberta, Department of Biological Sciences helped acquire scanning electron microscope images of UALVP 46685, 46687, and 49105. J. Wible of the Carnegie Museum of Natural History assisted in interpreting soft anatomical correlates of the osteology of the tympanic region. This research was further enhanced by discussions with J. Bloch, P. Gingerich, M. Godinot, J. Perry, M. Silcox, and many other researchers. D. Krause, M. O'Leary, J. Fleagle, W. Jungers, and P. Gingerich read and enhanced

previous manuscripts. This research was made possible by funding from a National Science Foundation grant to P. Gingerich and G. Gunnell (BCS-0129601), a National Science Foundation grant to D. Krause and J. Bloch (EAR-0308902), and a National Science Foundation Graduate Research Fellowship, an Evolving Earth Foundation grant, a National Science Foundation Doctoral Dissertation Improvement Grant (BCS-0622544), and an American Society of Mammalogists grant to D. Boyer.

REFERENCES

Beard, K.C., 1993. Phylogenetic systematics of the Primatomorpha, with special reference to Dermoptera. In: Szalay, F.S., McKenna, M.C., Novacek, M.J. (eds) Mammal Phylogeny: Placentals. Springer-Verlag, New York, pp. 129-150.

Bloch, J.I., Silcox, M.T., 2001. New basicrania of Paleocene-Eocene *Ignacius*: re-evaluation of the plesiadapiform-dermopteran link. American Journal of Physical Anthropology 116, 184-198.

Bloch, J.I., Silcox, M.T., 2006. Cranial anatomy of the Paleocene plesiadapiform *Carpolestes simpsoni* (Mammalia, Primates) using ultra high-resolution X-ray computed tomography, and the relationships of plesiadapiforms to Euprimates. Journal of Human Evolution 50, 1-35.

Bloch, J.I., Silcox, M.T., Boyer, D.M., Sargis, E.J., 2007. New Paleocene skeletons and the relationship of plesiadapiforms to crown-clade primates. Proceedings of the National Academy of Sciences 104, 1159-1164.

Coleman, M. N. and Boyer, D.M. 2008. A new line of evidence for investigating cerebral circulation patterns in fossils. Journal of Vertebrate Paleontology 28, 66A.

Conroy, G.C., Wible, J.R., 1978. Middle ear morphology of *Lemur variegatus*: Some implications for primate paleontology. Folia Primatologica 29, 81-85.

Evans, H.E., 1993. Miller's Anatomy of the Dog. W. B. Saunders, Philidelphia.

Fox, R.C., 1990a. *Pronothodectes gaoi* n. sp. from the late Paleocene of Alberta, Canada, and the early evolution of the Plesiadapidae (Mammalia, Primates). Journal of Paleontology 64, 637-647.

Fox, R.C., 1990b. The succession of Paleocene mammals in western Canada. Geological Society of America Special Paper 243, 51-70.

Fox, R.C., 1991. Systematic position of *Pronothodectes gaoi* Fox from the Paleocene of Alberta: reply. Journal of Paleontology 65, 700-701.

Gaudin, T.J., Wible, J.R., 1999. The entotympanic of pangolins and the phylogeny of Pholidota (Mammalia). Journal of Mammalian Evolution 6, 39-65.

Gidley, J.W., 1923. Paleocene primates of the Fort Union, with discussion of relationships of Eocene primates. Proceedings of the U S National Museum 63, 1-38.

Gingerich, P.D., 1971. Cranium of *Plesiadapis*. Nature 232, 566.

Gingerich, P. D., 1975. Systematic position of *Plesiadapis*. Nature 253, 111-113.

Gingerich, P.D., 1976. Cranial anatomy and evolution of Early Tertiary Plesiadapidae (Mammalia, Primates). University of Michigan Papers on Paleontology 15, 1-141.

Gingerich, P.D., Krause, D.W., Houde, P., 1983. A new earliest Tiffanian (Late Paleocene) mammalian fauna from Bangtail Plateau, western Crazy Mountain Basin, Montana. Journal of Paleontology 57, 957-970.

Gingerich, P.D., Gunnell, G.F., 2005. Brain of *Plesiadapis cookei* (Mammalia, Proprimates): surface morphology and encephalization compared to those of Primates and Dermoptera. University of Michigan Museum of Paleontology Contributions 31, 185-195.

Hoffstetter, R., 1977. Phylogénie des primates. Confrontation des resultats obtenus par les diverses voies d'approche du probleme. Bulletins and Mémoires Société d'Anthropologie de Paris t.4, série XIII, 327-346.

Kay, R.F., Thewissen, J.G.M., Yoder, A.D., 1992. Cranial anatomy of *Ignacius graybullianus* and the affinities of the Plesiadapiformes. American Journal of Physical Anthropology 89, 477-498.

Linnaeus, C., 1758. Systema naturae per regna tria natureae secundum classes, ordines genera, species cum characteribus, differentris, synonymis, locis, Editis decima, reformata edn. Laurentii Salvii, Stockholm.

MacPhee, R.D.E., 1981. Auditory Regions of Primates and Eutherian Insectivores: Morphology, Ontogeny, and Character Analysis. Contributions to Primatology 18, 1-282.

MacPhee, R.D.E., Cartmill, M., Gingerich, P.D., 1983. New Paleogene primate basicrania and the definition of the order Primates. Nature 301, 509-511.

MacPhee, R.D.E., Cartmill, M., 1986. Basicranial structures and primate systematics. Comparative Primate Biology, Volume 1: Systematics, Evolution, and Anatomy. Alan R. Liss, Inc., pp. 219-275.

Nomina Anatomica, 5th edition.1983. Williams & Wilkins, Baltimore.

Nomina Anatomica Veterinaria, 4th edition.1994. Adolf Holhauzen's Successors, Vienna

Novacek, M.J., 1977. Aspects of the problem of variation, origin and evolution of the eutherian auditory bulla. Mammal Review 7, 131-149.

Russell, D.E., 1959. Le crâne de *Plesiadapis.* Bulletin de la Société Géologique de France, pp. 312-314

Russell, D.E., 1964. Les Mammiferes Paléocènes D'Europe. Mémoires du Muséum National D'Histoire Naturelle, Série C 13, 1-324.

Silcox, M.T., 2001. A phylogenetic analysis of Plesiadapiformes and their relationship to Euprimates and other archontans. Ph.D., Johns Hopkins.

Silcox, M.T., Bloch, J.I., Boyer, D.M., Godinot, M., Ryan, T.M., Spoor, F., Walker, A. in press. The semicircular canal system in early primates, Journal of Human Evolution.

Simons, E.L., 1960. New fossil primates: a review of the past decade. American Scientist 48, 179-192.

Simpson, G.G., 1935. The Tiffany fauna, upper Paleocene. II.-Structure and relationships of *Plesiadapis*. American Museum Novitates, 1-30.

Szalay, F.S., 1971. Cranium of the Late Palaeocene primate *Plesiadapis tricuspidens*. Nature 230, 324-325.

Szalay, F.S., 1972. Cranial morphology of the Early Tertiary *Phenacolemur* and its bearing on primate phylogeny. American Journal of Physical Anthropology 36, 59-76.

Szalay, F.S., Rosenberger, A.L., Dagosto, M., 1987. Diagnosis and differentiation of the order Primates. Yearbook of Physical Anthropology 30, 75-105.

Trouessart, E.L., 1897. Catalogues des Mammalium tam Viventium quam Fossilium. R. Friedlander und Sohn, Berlin.

Van der Klaauw, C.J., 1931. The auditory bulla in some fossil mammals with a general introduction to this region of the skull. Bulletin of the American Museum of Natural History 62, 1-352.

Wible, J.R., 1993. Cranial circulation and relationships of the colugo *Cynocephalus* (Dermoptera, Mammalia). American Museum Novitates 3072, 1-27.

Wible, J.R., Gaudin, T.J., 2004. On the cranial anatomy of the yellow armadillo *Euphractus sexintus* (Dasypodidae, Xenarthra, Placentalia). Annals of the Carnegie Museum 73, 117-196.

Wible, J.R., 2008. On the cranial osteology of the hispaniolan solenodon *Solenodon paradoxurus* Brandt, 1833 (Mammalia, Lipotyphla, Solenodontidae). Annals of the Carnegie Museum 77, 321-402.

Witmer, L.M., 1995. The extant phylogenetic bracket and the importance of reconstructing soft tissues in fossils. In: Thomason, J.J. (ed) Functional Morphology in Vertebrate Paleontology. Cambridge University Press, Cambridge, pp. 19-33.

TABLES

Table 2.1. Numerical list of referenced anatomical features in selected cranial specimens of Plesiadapidae

UALVP 46685, 49105, 46687
1 – Nasal/premaxilla suture (Fig. 2.1)
2 – Nasal/frontal suture (Fig. 2.1)
3 – Premaxilla/maxillary suture (Figs. 2.1-3)
4 – Premaxilla/frontal suture (Fig. 2.1)
5 – Lacrimal/frontal suture (Fig. 2.1)
6 – Lacrimal/maxillary suture (Fig. 2.1)
7 – Lacrimal orbital process (Fig. 2.1)
8 – Lacrimal foramen (Fig. 2.1)
9 – Point on zygomatic where anteroposterior width was measured (Fig. 2.1)
10 – Maxilla/frontal suture (Fig. 2.1)
11 – Infraorbital foramen (Figs. 2.2, 4, 5)
12 – Metopic suture (Fig. 2.1)
13 – Frontal/parietal suture (Fig. 2.1)
14 – Frontal temporal ridge (Fig. 2.1)
15 – Zygomatic process of squamosal (Figs. 2.1, 2)
16 – Glenoid of squamosal (Figs. 2.1, 2)
17 – Postglenoid foramen (Fig. 2.2D)
18 – Entoglenoid process (Fig. 2.2E)
19 – Point on zygomatic process of squamosal where width was measured (Fig. 2.2D)
20 – Medial and rostral tympanic processes of petrosal (Figs. 2.4, 5)
21 – *tca* & *mca* foramen (Figs. 2.4, 6, 7)
22 – *tca* & *mca* groove (Figs. 2.4, 6)
23 – Primary facial foramen, facial canal and/or stylomastoid foramen (Figs. 2.4-6)
24 – Remnants of bulla (Figs. 2.1- 3, 5)
25 – Dorsal (petrosal?) layer of bone on medial process of petrosal (Figs. 2.4-6)
26 – Ventral (nonpetrosal?) layer of bone on medial process of petrosal (Figs. 2.4-6)
27 – Anterior end of basioccipital (Figs. 2.2, 3)
28 – Occipital condyle (Figs. 2.2, 3)
29 – Hypoglossal foramen (Figs. 2.2, 3)
30 – Foramen magnum (Figs. 2.2, 3)
31 – Nuchal crest (Figs. 2.2, 3)

USNM 309902
32 – Left nasal anterior end (Fig. 2.8)
33 – Right nasal anterior end (Fig. 2.8)
34 – Right nasal posterior end (Fig. 2.8)
35 – Right maxilla/premaxilla suture (Fig. 2.8)
36 – M^{2-3} roots exposed in orbit (Fig. 2.8)
37 – Infraorbital foramen (Fig. 2.8)
38 – Possible optic foramen (Fig. 2.8)

39 – Glenoid of squamosal (Fig. 2.9)
40 – Postglenoid process (Fig. 2.9)
41 – Facial canal (Fig. 2.9)
42 – Semicircular canal (Figs. 2.9, 11)
43 – Epitympanic recess (Fig. 2.9)
44 – Crista tympanica (Figs. 2.9, 12)
45 – Bony ridges of annular bridge (Fig. 2.9)
46 – Midline ridge of basioccipital (Figs. 2.10, 11, 13)
47 – Ventrally projecting lateral processes of basioccipital (Figs. 2.10, 11, 13)
48 – Right occipital condyle (Figs. 2.10, 11, 13)
49 – Foramen magnum (Figs. 2.10, 11, 13)
50 – Jugular process of exoccipital (Fig. 2.13)
51 – Nuchal crest (Figs. 2.11, 13)
52 – Exoccipital/petrosal suture (Fig. 2.13)

AMNH 17388
53 – Root of zygmatic process of maxilla (Fig. 2.15)
54 – Infraorbital foramen (Fig. 2.15)
55 – Pterygoid process of palatine (Fig. 2.15)
56 – Pterygoid process of basisphenoid (Fig. 2.15)
57 – Pterygoid process of alisphenoid (Fig. 2.15)
58 – Palatine postpalatine torus (Fig. 2.15)
59 – Postpalatine spine (Fig. 2.15)
60 – Glenoid of squamosal (Fig. 2.15)
61 – Postglenoid process (Fig. 2.15)
62 – Zygomatic process of squamosal (Fig. 2.15)
63 – Postglenoid foramen of squamosal (Fig. 2.15)
64 – Stylomastoid foramen (Figs. 2.15, 16)
65 – Possible posterior carotid foramen and *ic* canal (Figs. 2.15, 16)
66 – Occipital condyle (Fig. 2.15)
67 – Jugular process of exoccipital (Fig. 2.15)
68 – Foramen magnum (Fig. 2.15)

MNHN CR 125
69 – Nasal/premaxilla suture (Fig. 2.17)
70 – Nasal/frontal suture (Fig. 2.17)
71 – Maxilla/frontal suture (Fig. 2.17)
72 – Premaxilla/frontal suture (Fig. 2.17)
73 – Lacrimal/frontal suture (Fig. 2.17)
74 – Lacrimal/maxilla suture (Fig. 2.17)
75 – Lacrimal/zygomatic suture (Fig. 2.17)
76 – Parietal/frontal suture (Fig. 2.17)
77 – Parietal/squamosal suture (Fig. 2.17)
78 – Premaxilla/maxilla suture in palate (Fig. 2.17)
79 – Palatine/maxilla suture (Fig. 2.18)
80 – Palatine/sphenoid suture (Figs. 2.19, 20)

81 – Occipital/petrosal suture (Fig. 2.19)
82 – Petrosal/ectotympanic suture (Fig. 2.18)
83 – Ectotympanic/squamosal suture (Fig. 2.18)
84 – Parietal/frontal suture (Fig. 2.17)
85 – Maxilla/zygomatic suture (Figs. 2.17, 19)
86 – Alisphenoid/squamosal suture (Fig. 2.18)
87 – Dorsal orbitosphenoid/frontal suture (Fig. 2.20)
88 – Infraorbital foramen (Fig. 2.19)
89 – Foramen ovale (Fig. 2.20)
90 – Sphenorbital fissure (Fig. 2.20)
91 – Suboptic foramen (Fig. 2.20)
92 – Optic foramen (Fig. 2.20)
93 – Possible superior orbital fissure (Fig. 2.20)
94 – *tca* foramen (Fig. 2.21)
95 – *tca* groove (Fig. 2.21)

MNHN CR 965
96 – Palatine/frontal suture in the postpalatine canal (Fig. 2.23)
97 – Frontal/orbitosphenoid suture just anterior to the optic foramen (Figs. 2.23, 24)
98 – Orbitosphenoid/palatine contact running anteroposteriorly (Fig. 2.24)
99 – Palatine-alisphenoid suture (Fig. 2.24)
100 – Dorsal margin of orbitosphenoid (Figs. 2.23, 24)
101 – Alisphenoid/orbitosphenoid suture (Fig. 2.24)
102 – "Dished" surface on alisphenoid for broken out orbitosphenoid (Fig. 2.24)
103 – Foramen ovale (Figs. 2.22, 25)
104 – Sphenorbital fissure (Figs. 2.22-24, 25)
105 – Optic foramen (Figs. 2.22, 24, 25)
106 – Various foramina representing blood sinus drainage (Figs. 2.23, 24)
107 – Suboptic foramen (Figs. 2.22, 24)
108 – Remnants of optic canals on broken orbitosphenoid (Fig. 2.23)
109 – Basisphenoid sinus space (Figs. 2.22- 24, 25)

Pellouin Skull
110 – Palatine/alisphenoid suture (Figs. 2.26, 29)
111 – Squamosal/alisphenoid (Fig. 2.26)
112 – Premaxillary sutural surface of frontal (Fig. 2.27)
113 – Nasal sutural surface of frontal (Fig. 2.27)
114 – Palatine/maxilla suture on palate (Fig. 2.26)
115 – Frontal/parietal suture (Fig. 2.27)
116 – Parietal/squamosal suture (Fig. 2.27)
117 – Squamosal foramina (Fig. 2.27)
118 – ?Parietal/occipital suture (Fig. 2.27)
119 – Squamosal/tympanic suture (Fig. 2.26)
120 – Tympanic/petrosal suture (Fig. 2.26)
121 – Tympanic ring with annular bridge (Figs. 2.28, 29)
122 – Palatal palatine foramina (Fig. 2.26)

123 – Sphenorbital fissure (Fig. 2.29)
124 – Foramen ovale fragment (Fig. 2.29)
125 – Foramen in scaphoid fossa (Fig. 2.26)
126 – Tubal canal of right bulla (Fig. 2.29)
127 – Posterior carotid foramen and carotid canal (Figs. 2.28, 29)
128 – Foramen for *tca* (Fig. 2.28)
129 – Jugular foramen (Fig. 2.28)
130 – Hypoglossal foramen (Fig. 2.28)
131 – Possible suture along medial side of left promontorium (Fig. 2.29)

MNHN CR 126
132 – Frontal/maxilla suture in orbit (Fig. 2.31)
133 – Crack or maxilla/palatine suture? (Fig. 2.31; also labeled on Fig. 2.27)
134 – Region of palatine/frontal contact in postpalatine canal (broken) (Fig. 2.31)
135 – Lacrimal foramen (Fig. 2.31)
136 – Lacrimal/frontal suture (Fig. 2.31)
137 – Lacrimal/maxilla suture (Fig. 2.31)

Table 2.2. Abbreviations for cranial bones and osteological features.

Cranial bones

As – Alisphenoid
Bas – Basisphenoid
Boc – Basioccipital
Bul – Bulla forming bone
De – Dentary
Ect – Ectotympanic
Ent – Entotympanic
Eoc – Exoccipital
Fr – Frontal
Lc – Lacrimal
Mx – Maxilla
Ns – Nasal
Pa – Parietal
Pal – Palatine
Pmx – Premaxilla
Ptr – Petrosal
Os – Orbitosphenoid
Soc – Supraoccipital
Sq – Squamosal
Zy – Zygomatic bone

Osteological features

ac – aperture for cochlear fenestra
av – aperture for vestibular fenestra
bs – bullar suture (?)
cc – cochlear canaliculus (Visible as the most posterior "septum" on medial aspect of promontorium. Houses a canal that connects the spiral cochlea to endocranial space [see MacPhee, 1981]. HRxCT data were used in most cases to evaluate the presence of this feature.)
ccA – Broken open aperture of cochlear canaliculus
cf – carotid foramen
CN – cranial nerve
eam – external auditory meatus
ec – epitympanic crest
egp – entoglenoid process
fo – foramen/ina
fov – foramen ovale
g1 – a groove with a lateral route that likely holds the internal carotid plexus and possibly a remnant of the ica
g2 – a groove with a slightly more medial route that may hold internal carotid plexus fibers that approach the s1
g3 – a groove that leads to the s2, which likely contains contributions from the tympanic plexus, but primarily contains a small vein as in lemurs and treeshrews

g4 – a frequently present alternative or additional groove for tympanic plexus fibers to reach routes 1-3
g5 – frequently present groove that leads from a point ventral to the vestibular fenestra dorsolaterally, toward the epitympanic crest
hf – hiatus fallopii for greater petrosal nerve of CN VII
ips – inferior petrosal sinus
iof – infraorbital foramen
jf – jugular foramen for CN IX-XI
jp – jugular process of exoccipital
lf – lacrimal foramen
of – optic foramen
pcf - posterior carotid foramen (diameter). *In some cases this feature was not visible and had to be estimated from the width of the groove for the IC plexus on the petrosal. If measureable, the value is given after the condition symbol.
pgf – postglenoid foramen
pgp – postglenoid process
ppc – postpalatine canal
ppp – paroccipital process of petrosal. Also referred to as mastoid process. Serves as attachment point for posterior belly of digastric muscle.
ps – posterior septum (and internal carotid canal): laterally curving septum of bone that shields the fenestra cochlea dorsally and holds a canal that leads to the posterior carotid foramen ventrally
rtp – rostral tympanic process of petrosal bone
s1 – first (anterior) septum: Most lateral septum extending anteriorly from promontorium. Tubal canal forms between s1 and epitympanic crest.
s2 – second septum: Medial to s1, projects anteromedially from promontorium. g3 typically leads to the top ventral or medial aspect of this septum. *in one case of a *P. tricuspidens* specimen, the septum was not actually preserved, but surrounding morphology indicated to the author that it had originally been present.
s3 – third septum: projects medially between s2 and raised ridge of cochlear canaliculus, more posteriorly
sab – strut from annular part to bullar part
scc – semicircular canal
smf – stylomastoid foramen
sof – suboptic foramen
spf – sphenorbital fissure
tc – tubal canal
tca – tympanic canaliculus: Foramina and groove on or near ridge of cochlear canaliculus in tympanic cavity marking the entrance of the tympanic nerve from extracranial space, and the re-entrance of the nerve into the promontorium as it moves laterally to contribute to the tympanic plexus. Associated canals do not communicate with cochlea.
tng – tympanic nerve groove
vc – vidian canal?
zys – sutural surface for zygomatic on maxilla

Table 2.3a. Petrosal features of plesiadapid specimens. Column headings: av – fenestra vestibuli maximum diameter (**stapes foot plate maximum diameter is used as a substitute in some cases); cc, ps, g1-5, pcf, s1-3, tca – see Table 2.2; ccl – cochlear length (measurements courtesy of M. Coleman); lam – several specimens exhibit what appeared to be two laminae of bone comprising the remnant of the medial tympanic process (the dorsolateral edge of the bulla); pd – petrosal depth: height of pars cochlearis measured perpendicular to the plane of the endocranial surface of the element; pw – petrosal width: mediolateral thickness of petrosal as taken perpendicular to previous measurement. Information in Table 2.3 cells: a – morphology absent/different; n – morphology cannot be assessed because it is not preserved; nm – not measured or not measureable; p – morphology is present/preserved; pp – in the case of g1-4, indicates the presence of a set of parallel grooves are present in the appropriate position;? – relevant anatomy for gauging the anatomical condition is preserved, but obscured by other bone or matrix, or just difficult to interpret for some reason; *In some cases this feature was not visible and had to be estimated from the width of the groove for the internal carotid plexus on the petrosal. If measureable, the value is given after the condition symbol.

Taxon	**Spec**	***ccl***	***av***	***pd***	***pw***	***g1***	***g2***	***g3***	***g4***	***g5***
Pronothodectes gaoi	UALVP 46685 R	nm	1.21	4.55	3.45	?	?	?	p	?
Pronothodectes gaoi	UALVP 46685 L	15.60	1.17	4.68	3.48	?	?	p	p	?
Pronothodectes gaoi	UALVP 46687 R	nm	1.20	4.29	3.73	pp	pp	p	p	p
Pronothodectes gaoi	UALVP 49105 L	15.30	1.03	4.61	3.84	pp	p	p	p	p
Nannodectes intermedius	USNM 309902 R	14.50	1.16	3.54	3.55	p	?	a	p	?
Nannodectes intermedius	USNM 309902 L	nm	1.19	~3.6	~3.8	p	n	a	?	a
Nannodectes gidleyi	AMNH 17388 R	nm	nm	Nm	~3.5	n	?	a	p	?
Nannodectes gidleyi	AMNH 17388 L	nm	nm	Nm	~3.4	n	?	a	p	?
Plesiadapis tricuspidens	MNHN CR 125 R	nm	1.55*	Nm	4.47	p	a	a	p	p
Plesiadapis tricuspidens	MNHN CR 125 L	nm	nm	Nm	nm	?	a	a	p	p
Plesiadapis tricuspidens	Pellouin R	nm	nm	Nm	nm	?	a	pp	?	?
Plesiadapis tricuspidens	Pellouin L	nm	nm	Nm	4.31	p	a	pp	p	p
Plesiadapis tricuspidens	MNHN BR 1371	17.30	1.15	4.91	4.14	pp	p	pp	p	p
Plesiadapis tricuspidens	MNHN BR 17414	nm	nm	4.86	4.16	n	n	n	n	?
Plesiadapis tricuspidens	MNHN BR 17415	16.10	1.31	5.3	4.21	p	p	p	p	p
Plesiadapis tricuspidens	MNHN BR 17416	17.20	1.2	4.98	4.43	p	a	a	a	p
Plesiadapis tricuspidens	MNHN BR 17417	17.50	1.53	5.3	4.14	n	n	pp?	n	p
Plesiadapis tricuspidens	MNHN BR 17418	17.00	1.36	4.95	4.52	p	?	a	a	p
Plesiadapis tricuspidens	MNHN BR 17419	nm	nm	4.07	4.55	n	n	a	a	p
Plesiadapis cookei	UM 87990 R	21.03	1.32	~5.5	4.43	p	pp?	p	a	p
Carpolestes simpsoni	USNM 482354	8.64	nm	Nm	nm	p	?	?	?	?
Ignacius graybullianus	USNM 421608	nm	1.10*	3.28	3.04	p	n	n	n	?

Table 2.3b. Petrosal features of plesiadapid specimens

Taxon	**Spec**	***s1***	***s2***	***s3***	***tca***	***cc***	***ps***	***pcf***	***lam***	***bs***
Pronothodectes gaoi	UALVP 46685 R	p	p	p	?	p	p	n	p	a
Pronothodectes gaoi	UALVP 46685 L	p	p	p	p	p	p	p/nm	a	p?
Pronothodectes gaoi	UALVP 46687 R	n	n	n	p	?	p	p/nm	a	a
Pronothodectes gaoi	UALVP 49105 L	p	p	p	p	p	p	p/0.28	p	a
Nannodectes intermedius	USNM 309902 R	?	p	n	n	p	n	n	?	?
Nannodectes intermedius	USNM 309902 L	p	p	a	?	?	n	n/0.29*	?	a
Nannodectes gidleyi	AMNH 17388 R	?	p	a	p	p	?	n	?	a
Nannodectes gidleyi	AMNH 17388 L	?	p	a	p	p	?	n	?	a
Plesiadapis tricuspidens	MNHN CR 125 R	p	p	a	p	p	p	p/0.34	a	a
Plesiadapis tricuspidens	MNHN CR 125 L	p	p	a	p	p	p	n	a	a
Plesiadapis tricuspidens	Pellouin R	?	p	a	p	p	p	p/0.31	p	p?
Plesiadapis tricuspidens	Pellouin L	p	p	a	p	p	p	p/0.29	p	p?
Plesiadapis tricuspidens	MNHN BR 1371	p	p	a	n	p	n	n	n	n
Plesiadapis tricuspidens	MNHN BR 17414	n	?	n	n	p	n	n	n	n
Plesiadapis tricuspidens	MNHN BR 17415	p	p	a	?	p	n	n	p	a
Plesiadapis tricuspidens	MNHN BR 17416	p	p	a	n	p	n	n	p	a
Plesiadapis tricuspidens	MNHN BR 17417	n	p	?	n	p	n	n	p	a
Plesiadapis tricuspidens	MNHN BR 17418	p	p	p	?	p	n	n	p	a
Plesiadapis tricuspidens	MNHN BR 17419	p	p	n	?	p	n	n	p?	a
Plesiadapis cookei	UM 87990 R	p	p	a	p	p	n	n/0.40*	n	p?
Carpolestes simpsoni	USNM 482354	?	?	?	?	?	p	p/0.53	?	?
Ignacius graybullianus	USNM 421608	p	?	?	?	p	p	p/0.17	a	p?

Table 2.4. List of cranial measurements

Basic measurements (Table 2.5)

1 – Nasal: Maximum mediolateral width of anterior end
2 – Nasal: Maximum anteroposterior length
3 – Nasal: Maximum mediolateral width of posterior end (along frontal suture)
4 – Premaxilla: Maximum mediolateral width at anteroposterior level of juncture with maxilla
5 – Premaxilla: Distance to anterior margin of I^2, foramen measured from anterior margin of bone
6 – Premaxilla: Distance between I^1 and I^2 alveoli
7 – Premaxilla/frontal: length of suture on dorsum of skull
8 – Maxilla: Anteroposterior length in palate with measurement starting at anterior margin of suture with palatine
9 – Maxilla: Mediolateral width in palate at level of I^2 alveolus
10 – Maxilla: Mediolateral width in palate at anterior margin of P^2 or P^3 alveolus
11 – Maxilla: Length of tooth row from P^3 to M^3
12 – Maxilla: Distance between I^2 and P^3
13 – Maxilla/palatine: one half mediolateral width of palate at level of M^3
14 – Maxilla: Unilateral mediolateral width of maxilla at level of M^3, measurement starts at midline (not palatomaxillary suture) and ends at lateral edge of alveolar process
15 – Maxilla: maximum mediolateral width due to projection of maxillary zygomatic process
16 – Maxilla: on zygomatic process, anteroposterior distance of expansion of maxilla for attachment of masseter
17 – Maxilla/Zygomatic: Length of suture on anterior surface of maxilla
18 – Maxilla/Frontal: Length of suture on dorsum of skull
19 – Frontal: Maximum unilateral mediolateral width from metopic suture to most lateral point of contact with lacrimal and maxilla
20 – Frontal: Maximum anteroposterior length along midline from nasal contact to parietal contact
21 – Parietal: Unilateral mediolateral width at posterior contact with squamosal along nuchal crest
22 – Parietal: Length of sagittal crest
23 – Parietal: Maximum bilateral mediolateral width at postorbital constriction
24 – Squamosal: Mediolateral width of glenoid
25 – Squamosal: Anteroposterior length of glenoid, measured along medial margin, slightly obliquely going from postglenoid foramen to most anterior point on glenoid
26 – Squamosal: Dorsoventral projection of postglenid process
27 – Palatine: Anteroposterior length from anterior suture with maxilla to postpalatine torus
28 – Palatine: Unilateral mediolateral distance to outer margin of postpalatine torus
29 – Basioccipital: Bilateral mediolateral width at anteriormost point (spheno-occipital synchondrosis)

30 – Basioccipital: Maximum anteroposterior length
31 – Exoccipital: Bilateral mediolateral distance between hypoglossal foramina
32 – Exoccipital: Bilateral mediolateral width at posterior margin of skull (between tips of jugular processes)
33 – Exoccipital: Unilateral mediolateral distance from midline to outer margin of occipital condyle
34 – Exoccipital: Maximum mediolateral width of occipital condyle, measured laterally from lateral edge of foramen magnum
35 – Exoccipital: Dorsoventral height of occipital condyle, not including anteromedial projection of facet
36 – Zygomatic: Dorsoventral depth at lateral margin of excavation for orbits
37 – Zygomatic: Distance from anterior zygomatic/maxilla contact to lateral margin of excavation for orbits on zygomatic
38 – Orbits: Unilateral mediolateral distance between midline and lateral edge of excavation for orbit on zygomatic
39 – Basicranium: Distance from anterolateral margin of ectotympanic bone to stylomastoid foramen
40 – Exoccipital: Mediolateral width of foramen magnum
41 – External auditory meatus mediolateral length, measured from lateral tip to medial margin of annular component of ectotympanic bone.
42 – External auditory meatus anteroposterior length, measured posterior to potglenoid foramen.
43 – Total skull length
44 – Length from tip of maxillae to occipital condyle
GM – Geometric mean of all measurements except 7, 41, and 42 (number of measurements available for calculation)

Foramina and canal measurements (Table 2.5)
45 – Infraorbital foramen major diameter
46 – Infraorbital foramen minor diameter
47 – Optic foramen major diameter
48 – Optic foramen minor diameter
49 – Suboptic foramen major diameter
50 – Suboptic foramen minor diameter
51 – Sphenorbital fissure major diameter
52 – Sphenorbital fissure minor diameter
53 – Foramen ovale major diameter
54 – Foramen ovale minor diameter
55 – Hypoglossal foramen major diameter
56 – Hypoglossal foramen minor diameter
57 – Major diameter of MNHN CR 125 foramen *93*
58 – Postpalatine foramen major diameter
59 – Postpalatine foramen minor diameter
60 – Jugular foramen major diameter
61 – Length of internal carotid canal

Shape variables (Table 2.6)

ac/GM – Fenestra vestibuli relative length = ln[(Table 2.3a: *ac*)/GM]

Cl/GM – Cochlea relative length = ln[(Table 2.3a:*cl*)/GM]

EAM-S - External auditory meatus shape = ln(41/42)

Gld/GM – Glenoid relative size = ln(√(24*25)/GM)

N/Pmx – Nasal width relative to Premaxilla = ln(3/7)

N/GM – Nasal relative width = ln(3/GM)

Pcsa/GM – Petrosal relative cross-sectional area = ln[√(Table 2.3a: *pd* * *pw*)/GM]

Pmx/GM – Premaxilla relative width = ln(7/GM)

Table 2.5. Cranial measurements of Plesiadapidae (see Table 2.4 for descriptions)

Specimen	**MNHN CR 125**	**Pellouin skull**	**MNHN CR 965**	**UM 87990**	**UALVP 46685**	**AMNH 17388**	**USNM 309902**	**YPM-PU 19642**
Taxon	***Plesiadapis tricuspidens***	***Plesiadapis tricuspidens***	***Plesiadapis Tricuspidens***	***Plesiadapis cookei***	***Pronothodectes gaoi***	***Nannodectes Gidleyi***	***Nannodectes intermedius***	***Plesiadapis anceps***
Element	**Skull**	**skull**	**skull base**	**skull**	**skull**	**Skull**	**skull**	**rostrum**
Locality	**Berru**	**Berru**	**Berru**	**SC-117**	**DW-2**	**Mason Pocket**	**Bangtail**	**7-up Butte**
Measures								
1	4.30	-	-	4.84	2.67	-	2.31	3.34
2	30.69	-	-	31.35	18.4	-	13.61	21.84
3	1.51	2	-	4.57	2.6	-	2.31	3.34
4	7.68	-	-	8.61	-	-	-	-
5	16.25	-	-	15.93	6.52	-	-	-
6	5.50	-	-	3.87	2.66	-	-	-
7	9.60	-	-	-	4.36	-	-	4.52
8	35.78	30.36	-	29.37	-	-	-	-
9	4.44	5.75	-	5.53	3.39	-	-	-
10	6.89	8.02	-	7.71	5.45	-	-	-
11	21.16	20.8	-	22.16	12.36	12.4	10.55	-
12	15.14	12.37	-	14.04	6.73	-	-	-
13	6.66	6.84	6.54	6.8	-	-	-	-
14	13.89	13.26	10.82	15.12	-	-	-	-
15	27.99	24.76	-	26.1	-	-	-	-
16	3.79	3.47	-	2.33	1.29	1.44	-	-
17	15.01	17.7	-	18.44	-	-	-	-
18	8.38	-	-	8.84	3.77	-	-	4.6
19	14.15	-	-	15.11	.	-	-	10.2
20	20.68	19.69	-	21.02	11.23	-	-	13.08
21	10.09	8.63	-	10.82	-	-	-	-
22	41.88	38.52	-	41	-	-	-	-
23	11.31	10.85	-	11.66	-	-	-	-
24	13.54	14.02	-	10.12	5.38	5.6	4.11	-
25	13.98	13.52	-	11.52	6.96	6.5	4.49	-
26	4.01	4.54	-	3.69	-	1.35	1.43	-
27	13.83	11.16	12.93	12.57	-	-	-	-
28	4.26	3.74	4.33	4.45	-	3.1	-	-
29	6.37	6.94	-	-	3.25	-	2.21	-
30	14.82	14.4	-	14.42	8.46	-	7.22	-
31	10.94	10.54	-	10.59	-	-	-	-
32	24.97	25	-	26	-	17.4	12.2	-
33	8.3	8.5	-	8.6	6.17	5.92	5.39	-
34	4.39	4.05	-	4.38	2.46	2.5	1.95	-
35	6.48	5.06	-	5.36	3.87	2.8	2.8	-
36	8.97	9.78	-	7.86	3.99	-	-	-
37	16.69	-	-	16.55	-	-	-	-
38	27.21	-	-	24	-	-	-	-
39	11.95	12.45	-	10.8	-	-	-	-
40	8.95	6.88	-	8.71	7.4	6.84	6.87	-
41	11.60	11.50	-	4.80	5.75	-	-	-
42	6.80	6.60	-	12.00	5.50	-	4.07	-
43	106.36	-	-	87.74	-	-	-	-
44	89.27	80.27	-	78	-	-	-	-
GM	10.6 (39)	10.28 (30)	-	10.71 (39)	4.91 (21)	4.45 (11)	4.32 (14)	-

Table 2.5. continued

Specimen	**MNHN CR 125**	**Pellouin skull**	**MNHN CR 965**	**UM 87990**	**UALVP 46685**	**AMNH 17388**	**USNM 309902**	**YPM-PU 19642**
Taxon	***Plesiadapis tricuspidens***	***Plesiadapis tricuspidens***	***Plesiadapis Tricuspidens***	***Plesiadapis cookei***	***Pronothodectes gaoi***	***Nannodectes Gidleyi***	***Nannodectes intermedius***	***Plesiadapis anceps***
Element	**Skull**	**skull**	**skull base**	**skull**	**skull**	**Skull**	**skull**	**rostrum**
Locality	**Berru**	**Berru**	**Berru**	**SC-117**	**DW-2**	**Mason Pocket**	**Bangtail**	**7-up Butte**
Foramina								
45	2.8	2.34	-	2.73	2.12	2.22	2.2	-
46	1.3	1.79	-	1.52	1.26	-	1.15	-
47	1.36	-	1.21	-	-	-	-	-
48	0.84	-	1.02	-	-	-	-	-
49	1.45	-	1.64	-	-	-	-	-
50	1.17	-	~1.4	-	-	-	-	-
51	4.08		-	-	-	-	-	-
52	-	-	2.08	~2	-	-	-	-
53	2.61	-	3.12	-	-	-	-	-
54	1.49	-	1.42	-	-	-	-	-
55	1.52	~1.7	-	1.75	1.03	-	-	-
56	1.05	~1.4	-	1.6	0.86	-	-	-
57	0.72	-	-	-	-	-	-	-
58	2.53	-	2.97	-	-	-	-	-
59	1.81	-	-	-	-	-	-	-
60	2.38	-	-	2.86	-	-	-	-
61	2.8	2.7	-	-	~1.6	-	-	-

Table 2.6. Cranial shape variables of Plesiadapidae (see Table 2.4 for descriptions)

Specimen	**MNHN CR 125**	**Pellouin skull**	**MNHN CR 965**	**UM 87990**	**UALVP 46685**	**AMNH 17388**	**USNM 309902**	**YPM-PU 19642**
Taxon	***Plesiadapis tricuspidens***	***Plesiadapis tricuspidens***	***Plesiadapis Tricuspidens***	***Plesiadapis cookei***	***Pronothodectes gaoi***	***Nannodectes Gidleyi***	***Nannodectes intermedius***	***Plesiadapis anceps***
Element	**Skull**	**skull**	**skull base**	**skull**	**skull**	**Skull**	**skull**	**rostrum**
Locality	**Berru**	**Berru**	**Berru**	**SC-117**	**DW-2**	**Mason Pocket**	**Bangtail**	**7-up Butte**
N/GM	-1.95	-1.64	-	-0.85	-0.64	-	-0.63	-
N/Pmx	-1.85	-	-	-	-0.52	-	-	-0.30
Pmx/GM	-0.10	-	-	-	-0.12	-	-	-
EAM-S	1.04	1.08	-	0.92	0.04	-	-	-
Gld/GM	0.26	0.29	-	-0.50	0.22	-	-0.01	-
Cl/GM	0.47	-	-	0.67	1.16	-	1.21	-
Pcsa/GM	-0.84	-	-	-0.77	-0.19	-	-0.18	-
ac/GM	-2.09	-	-	-2.09	-1.45	-	-	-

APPENDIX TABLES

Appendix Table 2.1. Specimens scanned

taxon	specimen	kV	µA	x-y res	z spacing	number of slices	wedge	scanning location
Pronothodectes gaoi	UALVP 46685	150	325	43.9	49.1	861	rice	CQI PSU
Pronothodectes gaoi	UALVP 46687	150	325	40	49.1	123	rice	CQI PSU
Pronothodectes gaoi	UALVP 49105	150	325	40	49.1	246	rice	CQI PSU
Pronothodectes gaoi	UALVP 49105	55	145	6	6	207 (3)	air	SBU CBT
Nannodectes intermedius	USNM 309902	150	325	40	49.1	246	rice	CQI PSU
Nannodectes intermedius	USNM 309902	180	133	35.8	38.4	405	air	HRxCT UT
Plesiadapis tricuspidens	MNHN BR 1371	150	200	50	58.11	205	air	CQI PSU
Plesiadapis tricuspidens	MNHN BR 17414	150	200	50	58.11	205	air	CQI PSU
Plesiadapis tricuspidens	MNHN BR 17415	150	200	50	58.11	205	air	CQI PSU
Plesiadapis tricuspidens	MNHN BR 17416	150	200	50	58.11	205	air	CQI PSU
Plesiadapis tricuspidens	MNHN BR 17417	150	200	50	58.11	205	air	CQI PSU
Plesiadapis tricuspidens	MNHN BR 17418	150	200	50	58.11	205	air	CQI PSU
Plesiadapis tricuspidens	MNHN BR 17419	150	200	50	58.11	205	air	CQI PSU
Plesiadapis cookei	UM 87990	150	325	52.7	61.4	1435	water	CQI PSU
Ignacius graybullianus	USNM 482353	55	145	6	6	418 (1)	air	SBU CBT
Acidomomys hebeticus	UM 108207	55	145	6	6	426 (1)	water	SBU CBT
Sciurus caroliniensis	SBU MRd-12	55	145	8	8	213 (1)	air	SBU CBT
Lagostomus maximus	AMNH 41527	70	114	8	8	213 (1)	air	SBU CBT

CQI PSU – Center for Quantitative Imaging, Pennsylvania State University; HRxCT UT – High-Resolution X-ray CT Facility of the University of Texas at Austin; SBU CBT – Stony Brook University Center for Biotechnology.

Appendix Table 2.2. Index to anatomy visible on figures

Fig. 2.1 – 1, 2, 3, 4, 5, 6, 7, 8, 9, 10, 12, 13, 14, 15, 24. Ect, Fr, I^1 , Lc, Mx, Ns, Pmx, Sq, Zy
Fig. 2.2 – 3, 11, 15, 16, 17, 18, 19, 24, 27, 28, 29, ,30, 31, I^{1-2}, C^1, P^{2-4}, M^{1-3}, Boc, Mx, Pa, Pmx, Ptr, Soc, Sq
Fig. 2.3 – 3, 11, 24, 27, 28, 29, 30, 31, I^{1-2}, C^1, P^{2-4}, Boc, Mx, Pa, Pmx, Ptr, Soc, Sq
Fig. 2.4 – 20, 21, 22, 23, 24, av, cc, ccA, cs, g3-4, icp, pcf, Ptr, s1-3
Fig. 2.5 – 20, 23, 24, 25, 26, ac, av, bs, cc, fo, g3-4, Ptr, s1-3, scc
Fig. 2.6 – 20, 21, 22, 23, 25, 26, av, cc, ccA, cs, ec, Ect, g1-3, g5, hf?, pcf, ppp, s1-3
Fig. 2.7 – 20, 21, av, cs, g1-5, hf, pcf, ppp, Ptr
Fig. 2.8 – 32, 33, 34, 35, 36, 37, 38, De, I^1, Lc, Mx, r&l-Ns, r&l-Pmx, Sq, Zy
Fig. 2.9 – 39, 40, 41, 42, 43, 44, 45, ac, av, ccA, Ect, g1, Ptr, Sq
Fig. 2.10 – 44, 46, 47, 48,49, ac, av, Boc, Bul, ec, g1, Ptr, tt
Fig. 2.11 – 44, 47, 48, 49,51, ac, av, Boc, Bul, ccA, cs, ec, g1, g3, icp, Ptr, s1-2, Soc, tt
Fig. 2.12 – Bul, Ptr, 44
Fig. 2.13 – 46, 47, 48, 49, 50, 51, 52, Boc, Bul, Eoc, Ptr, Soc
Fig. 2.14 – I_1, C_1, P_{2-4}, $M_{1-3,}$ De
Fig. 2.15 – 53, 54, 55, 56, 57, 58, 59, 60, 61, 62, 63, 64, 65, 66, 67, 68, P^{2-4}, M^{1-3}, Eoc, Mx, Pal, ppp, Ptr, Sq, Zy
Fig. 2.16 – 64, 65, cc, g3-4, Ptr, s2, tca, tng
Fig. 2.17 – 69, 70, 71, 72, 73, 74, 75, 77, 84, fo, Fr, Lc, Mx, Ns, Soc, Sq, Zy
Fig. 2.18 – 79, 82, 83, 86, As, Boc, Ect, Eoc, fo, jf, M^3, Mx, Pal, pcf, Pmx, Ptr, Sq
Fig. 2.19 – 81, 85, 88, 89, Boc, Ect, Eoc, jp, Mx, Pa, pcf, Ptr, smf, Soc, Sq, Zy
Fig. 2.20 – 80, 87, 89, 90, 91, 92, 93, As, Bas, Fr, Os, Pa, Pal, Sq
Fig. 2.21 – 94, 95, Boc, cc, cs, Ect, Eoc, g4, g5, pgf, ptr, s1, s2, sab, Sq, tc, tng
Fig. 2.22 – M^2
Fig. 2.23 – 96, 97, 100, 104, 105, 106, 108, 109, As, Bas, Fr, Mx, Os, Pal, ppc
Fig. 2.24 – 96, 97, 98, 99, 100, 101, 102, 104, 105, 106, 107, As, Bas, Fr, Os, Pal, vc
Fig. 2.25 – 103, 104, 105, 108, 109, As, Bas, Os
Fig. 2.26 – 110, 111, 114, 119, 120, 122, 125, P^2-M^3, As, Bas, Boc, Bul, Ect, Fr, iof, jp, Mx, Pal, pgf, Ptr, Sq
Fig. 2.27 – 112, 113, 115, 116, 117, 118, 133, Fr, iof, Mx, Pa, Soc, Sq
Fig. 2.28 – 121, 127, 128, 129, 130, 131, ac, Bul, cc, cs, Ect, egp, Eoc, g1, g3, g4, g5, Ptr, s1, s2, smf, Sq
Fig. 2.29 – 110, 121, 123, 124, 126, 127, P^2-M^3, As, Bas, cc, cs, Bul, Ect, egp, Eoc, Fr, g3, iof, Mx, Pal, pgf, pgp, Ptr, s1, s2, Sq
Fig. 2.30 – none
Fig. 2.31 – 132, 133, 134, 135, 136, 137, P^3, M^3, Fr, iof, Lc, Mx, Mx?, Pal, ZyS
Fig. 2.32 – bs, Bul, eam, Ect, Ptr
Fig. 2.33 – bs, Boc, Bul, Ent, Ect, ips, pcf, rtp
Fig. 2.34 – bs, eam, Ect, Eoc, fo, icp?, jf, Ptr, Sq, tc, tca
Fig. 2.35 – 3, Bas, Boc, bs, ccA, Ect, Ptr, tc, tca
Fig. 2.36 – bs, Bul, Ect, Ptr, tca
Fig. 2.37 – icp, Ptr, s1, s2, tng?
Fig. 2.38 – ac, bs, cc, ccA, cs, ec, er, icp, Ptr, rtp, s1, s2, scc, tt

Fig. 2.39 – bs, Ptr, rtp, s1, s2
Fig. 2.40 – ac, av, cc, CN X, CN IX, eam, ec, er, icp, iof, jf, pcf, ps, s1-3, spf, tc, tca&mca, tt
Fig. 2.41 – As, fov, Fr, iof, Lc, lf, Mx, Mx?, of, Pa, Pal, ppc, sof, spf, Sq, vc?, zys

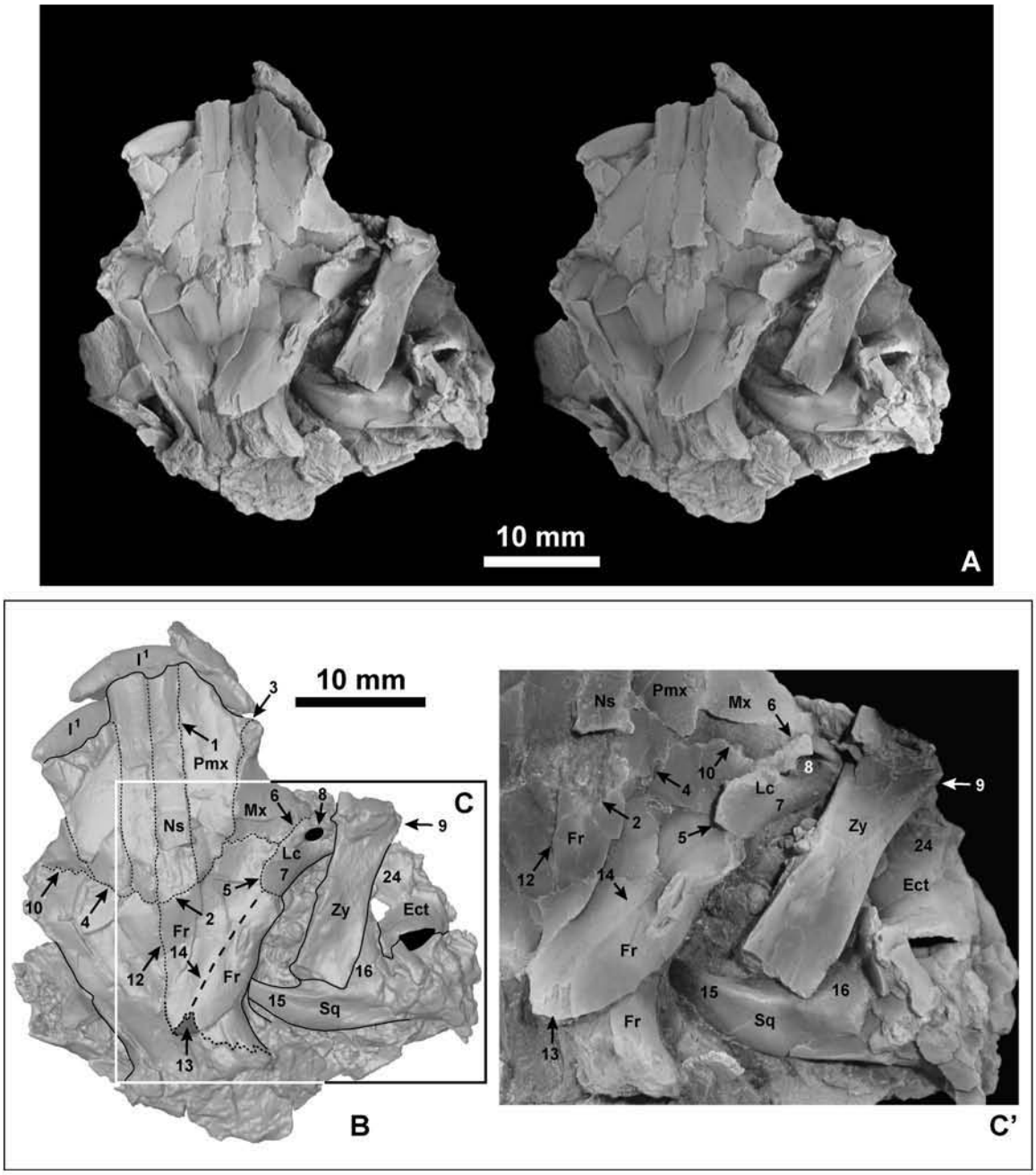
10 mm
A
10 mm
I1
I1
3
1
Pmx
Ns
Mx
6
8
9
C
Lc
7
24
Zy
Ect
10
4
5
2
Fr
14
12
Fr
16
15
Sq
13
B
Ns
Pmx
Mx
6
10
8
4
Lc
9
7
2
Zy
Fr
5
24
12
Ect
14
Fr
15
16
Fr
Sq
13
C'
Figure 2.1

Figure 2.1. UALVP 46685 *Pronothodectes gaoi*: A, stereophotographic dorsal view of skull. B, labeled HRxCT rendering of dorsal view. Fine black dashed lines indicate sutures. Coarse black dashed lines indicate position of frontal temporal lines. Solid lines indicate boundaries between major pieces of fossil. C, inset of orbital region. C', enlargement of C. Numbers and abbreviations: 1 – nasal/premaxilla suture, 2 – nasal/frontal suture, 3 – premaxilla/maxilla suture, 4 – premaxilla/frontal suture, 5 – lacrimal/frontal suture, 6 – lacrimal/maxillary suture, 7 – lacrimal orbital process, 8 – lacrimal foramen, 9 – point on zygomatic where anteroposterior width was measured, 10 – maxilla/frontal suture, 12 – metopic suture, 13 – frontal/parietal suture, 14 – frontal temporal ridge, 15 – zygomatic process of squamosal, 16 – glenoid of squamosal, 24 – remnants of bulla. Ect – ectotympanic; Fr – frontal; Lc – lacrimal; Mx – maxilla; Ns – nasal; Pmx – premaxilla; Sq – squamosal; Zy – zygomatic.

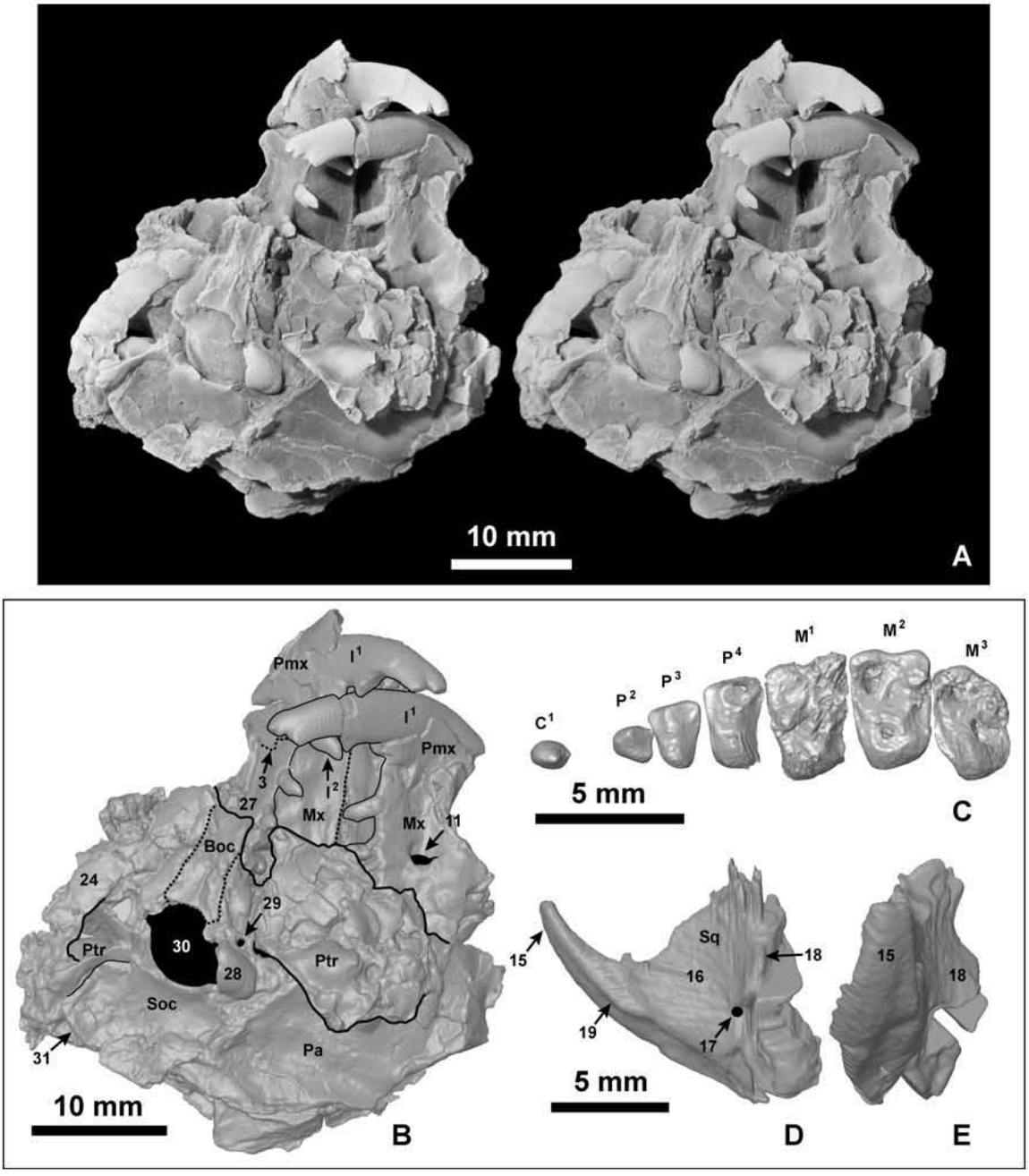
10 mm
A
Pmx
I1
I1
Pmx
3
I2
27
Mx
Mx
11
Boc
24
29
30
28
Ptr
Ptr
Soc
31
Pa
10 mm
B
C1
P2
P3
P4
M1
M2
M3
5 mm
C
15
Sq
18
16
19
17
5 mm
D
15
18
E
Figure 2.2

Figure 2.2. UALVP 46685 *Pronothodectes gaoi*: A, stereophotographic ventral view of skull. B, HRxCT rendering of ventral view. C, ventral close-up view of HRxCT rendering of dental arcade. D, ventral close-up view of HRxCT rendering of squamosal. E, lateral close-up view of HRxCT rendering of squamosal. Anterior to top for A, B, D; E. Fine dashed lines – sutures, fine and heavy solid lines – boundaries between different pieces of the fossil. Numbers and abbreviations: 3 – premaxilla/maxilla suture, 11 – infraorbital foramen, 15 – zygomatic process of squamosal, 16 – glenoid of squamosal, 17 – postglenoid foramen, 18 – entoglenoid process, 19 – point on zygomatic process of squamosal where width was measured, 24 – remnants of bulla, 27 – anterior end of basioccipital, 28 – occipital condyle, 29 – hypoglossal foramen, 30 – foramen magnum, 31 – nuchal crest. Boc – basoccipital; Mx – maxilla; Pa – parietal; Pmx – premaxilla; Ptr – petrosal; Soc – supraoccipital; Sq – squamosal.

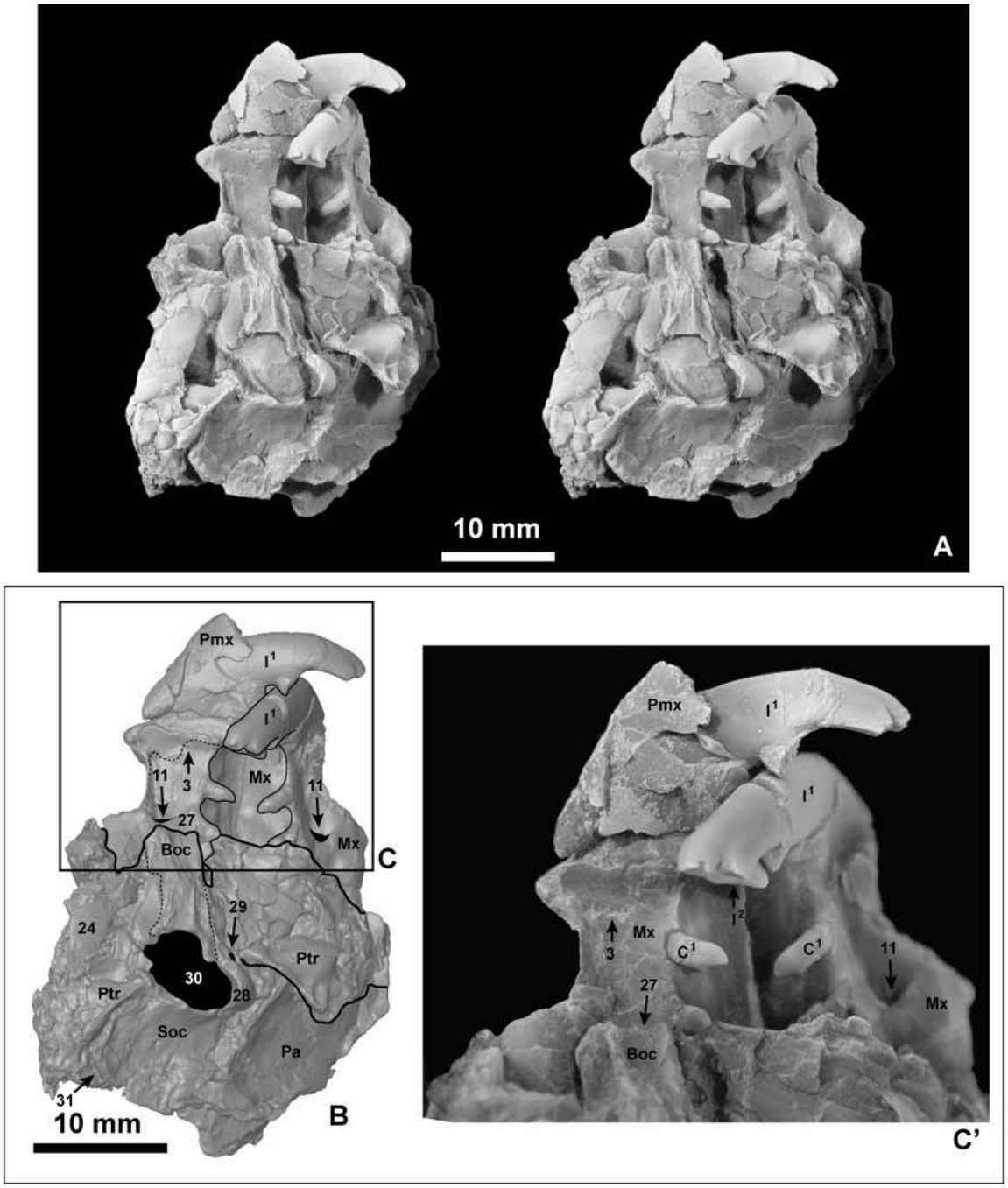
10 mm
A
Pmx
I1
I1
11
3
Mx
11
27
Mx
Boc
C
29
24
Ptr
30
Ptr
28
Soc
Pa
31
10 mm
B
Pmx
I1
I1
I2
Mx
3
C1
C1
11
27
Mx
Boc
C'

Figure 2.3

Figure 2.3. UALVP 46685 *Pronothodectes gaoi*: A, stereophotographic right lateral view of skull. B, HRxCT rendering of right lateral view. C, inset of rostrum. C', enlargement of C: Fine dashed lines – sutures, fine and heavy solid lines – boundaries between different pieces of the fossil. Numbers and abbreviations: 3 – premaxilla/maxilla suture, 11 – infraorbital foramen, 24 – remnants of bulla, 27 – anterior end of basioccipital, 28 – occipital condyle, 29 – hypoglossal foramen, 30 – foramen magnum, 31 – nuchal crest. Boc – basioccipital; Mx – maxilla; Pa – parietal; Pmx – premaxilla; Ptr – petrosal; Soc – supraoccipital; Sq – squamosal.

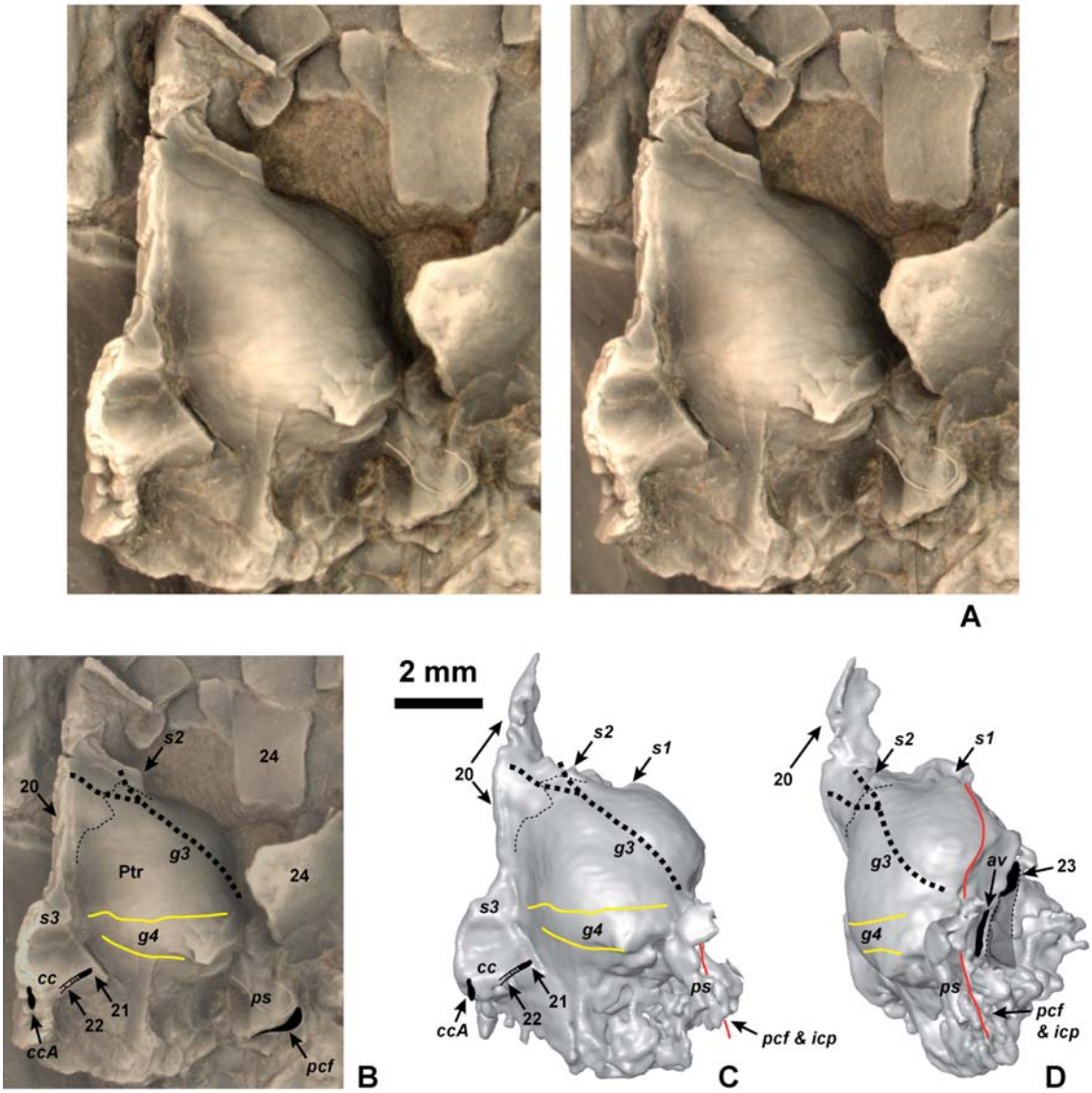
A
2 mm
s2
24
20
g3
Ptr
24
s3
g4
cc
21
22
ps
ccA
pcf
B
s2
s1
20
g3
s3
g4
cc
21
22
ps
ccA
pcf & icp
C
s2
s1
20
g3
av
23
g4
ps
pcf
& icp
D

Figure 2.4

Figure 2.4. UALVP 46685 *Pronothodectes gaoi*: A, stereophotographic ventral view of left promontorium. B, ventral view of left promontorium. C, HRxCT rendering of ventral view of left promontorium. Anterior to top in all parts. Fine dashed lines – sutures, thick dashed line – g3 groove, fine and heavy solid lines – boundaries between different pieces of fossil. Nerves reconstructed in yellow represent components of tympanic plexus. Neurovasculature reconstructed in red represents components of internal carotid plexus. D, HRxCT rendering of ventrolateral close-up of left promontorium. 2 mm scale applies to B-D. Numbers and abbreviations: 20 – medial and rostral tympanic processes of petrosal, 21 – tympanic and mastoid canaliculus foramen, 22 – tympanic and mastoid canaliculus groove, 23 – primary facial foramen, facial canal and/or stylomastoid foramen, 24 – remnants of bulla. av – aperture for fenestra vestibuli; cc - cochlear canaliculus; ccA – broken open aperture of cochlear canaliculus; ps – posterior septum (and internal carotid canal); g3 - groove that leads to s2 (for a small vein); g4 - groove for tympanic plexus fibers to reach routes g1-3; icp – internal carotid plexus; pcf – posterior carotid foramen; Ptr – petrosal; s1 – first (anterior) septum; s2 – second septum; s3 - third septum.

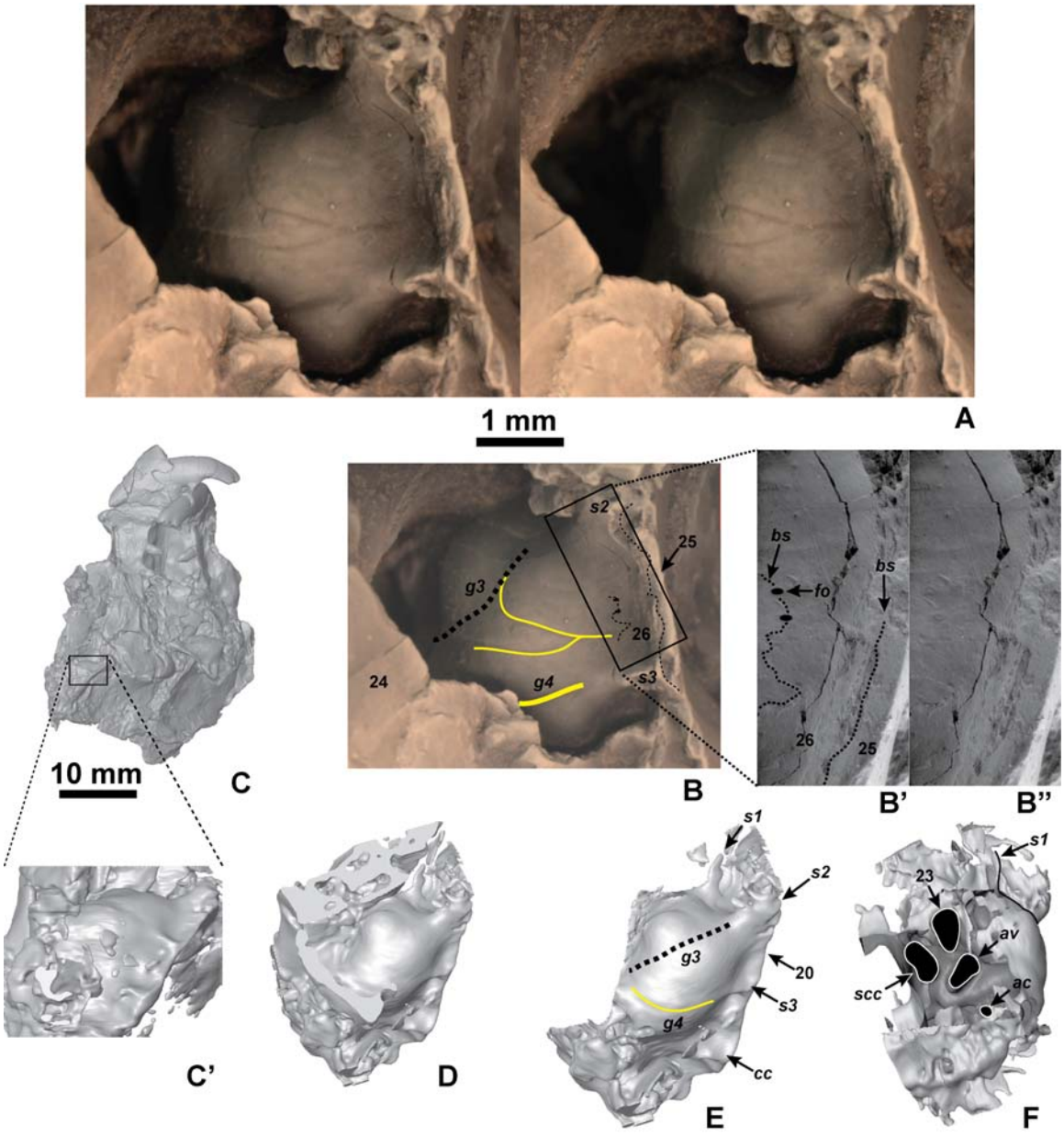

Figure 2.5

Figure 2.5. UALVP 46685 *Pronothodectes gaoi*: A, ventromedial close-up of right promontorium (1 mm scale). B, ventromedial close-up of right promontorium. B', ventromedial close-up of medial tympanic process. B'', ventromedial close-up of medial tympanic process, labels removed. C, HRxCT rendering of right lateral view of skull (10 mm scale). C', inset of promontorium in ventromedial view from C. D, image from C' rotated to ventral view. E, labeled image from D with obscuring morphology cropped away. F, labeled image from E rotated into lateral view, to reveal various foramina and cross-sectioned canals. Anterior to top in all parts. Nerves reconstructed in yellow represent components of tympanic plexus. Fine dashed lines – sutures, thick dashed lines – g3 groove, fine and heavy solid lines – boundaries between different pieces of fossil. Numbers and abbreviations: 20 – medial and rostral tympanic processes of petrosal, 23 – primary facial foramen, facial canal and/or stylomastoid foramen, 24 – remnants of bulla, 25 – dorsal (petrosal?) layer of bone on medial process of petrosal, 26 – ventral (nonpetrosal?) layer of bone on medial process of petrosal. ac – aperture of cochlear fenestra; av – aperture of fenestra vestibuli; bs – bullar suture; cc – cochlear canaliculus; fo – foramen (likely leads to canals that transmitted neurovasculature between tympanic cavity and jugular foramen); g3 (dashed because it is not well-defined) - groove that leads to s2 (for a small vein?); g4 - groove for tympanic plexus fibers to reach routes g1-3; icp – internal carotid plexus; pcf – posterior carotid foramen; Ptr – petrosal; s1 – first (anterior) septum; s2 – second septum; s3 - third septum; scc – semicircular canal.

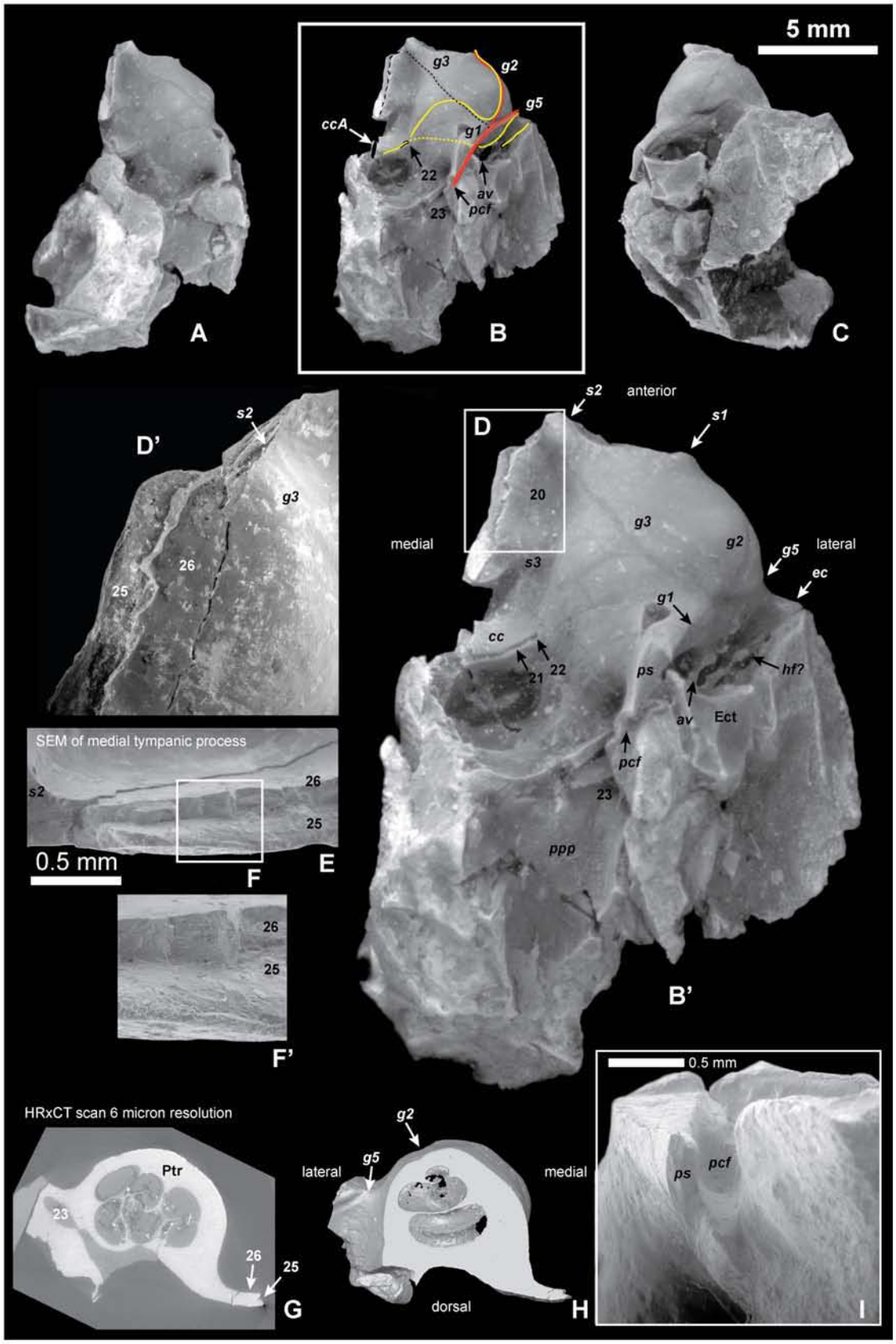
5 mm
A
B
C
g3
g2
g5
g1
ccA
22
av
pcf
23
D'
s2
g3
26
25
D
s2
anterior
s1
20
g3
medial
g2
g5
lateral
s3
ec
g1
cc
22
21
ps
hf?
av
Ect
pcf
23
ppp
B'
SEM of medial tympanic process
s2
26
25
0.5 mm
F
E
26
25
F'
HRxCT scan 6 micron resolution
Ptr
23
26
25
G
g2
lateral
g5
medial
dorsal
H
0.5 mm
ps
pcf
I
Figure 2.6

Figure 2.6. UALVP 49105 *Pronothodectes gaoi*: A, ventromedial view. B, ventral view. B', enlargement of ventral view. C, lateral view. D, inset of medial tympanic process in ventral view. D', enlargement of inset from D. E, Scanning Electron Microscopy (SEM) image, medial view of medial tympanic process. F, SEM inset of medial tympanic process in medial view. F', enlargement of inset from F. G, HRxCT slice showing that separation between the two laminae visible in B and D-F is not visible internally. H, rendering of HRxCT data. I, SEM of posterior view showing posterior carotid foramen. Anterior to top in A-D.' 5 mm scale applies to A-C. 0.5 mm scales apply to E and I. Nerves reconstructed in yellow represent components of tympanic plexus. Neurovasculature reconstructed in red represents components of internal carotid plexus. Coarse dashed line – boundary between laminae of medial tympanic process of petrosal, fine dashed line – g3 groove. Numbers and abbreviations: 20 – medial and rostral tympanic processes of petrosal, 21 – tympanic and mastoid canaliculus foramen, 22 – tympanic and mastoid canaliculus groove, 23 – primary facial foramen, facial canal and/or stylomastoid foramen, 25 – dorsal (petrosal?) layer of bone on medial process of petrosal, 26 – ventral (nonpetrosal?) layer of bone on medial process of petrosal. av – aperture of fenestra vestibuli; cc – cochlear canaliculus; ccA - broken open aperture of cochlear canaliculus; ps – posterior septum; ec – epitympanic crest; Ect – ectotympanic; g1 – groove for internal carotid plexus; g2 – groove for distal part of internal carotid plexus; g3 - groove that leads to s2 (for a small vein?); g5 – groove that leads toward epitympanic crest; hf? – hiatus fallopii; pcf – posterior carotid foramen; ppp – paroccipital process of petrosal; s1 – first (anterior) septum; s2 – second septum; s3 - third septum.

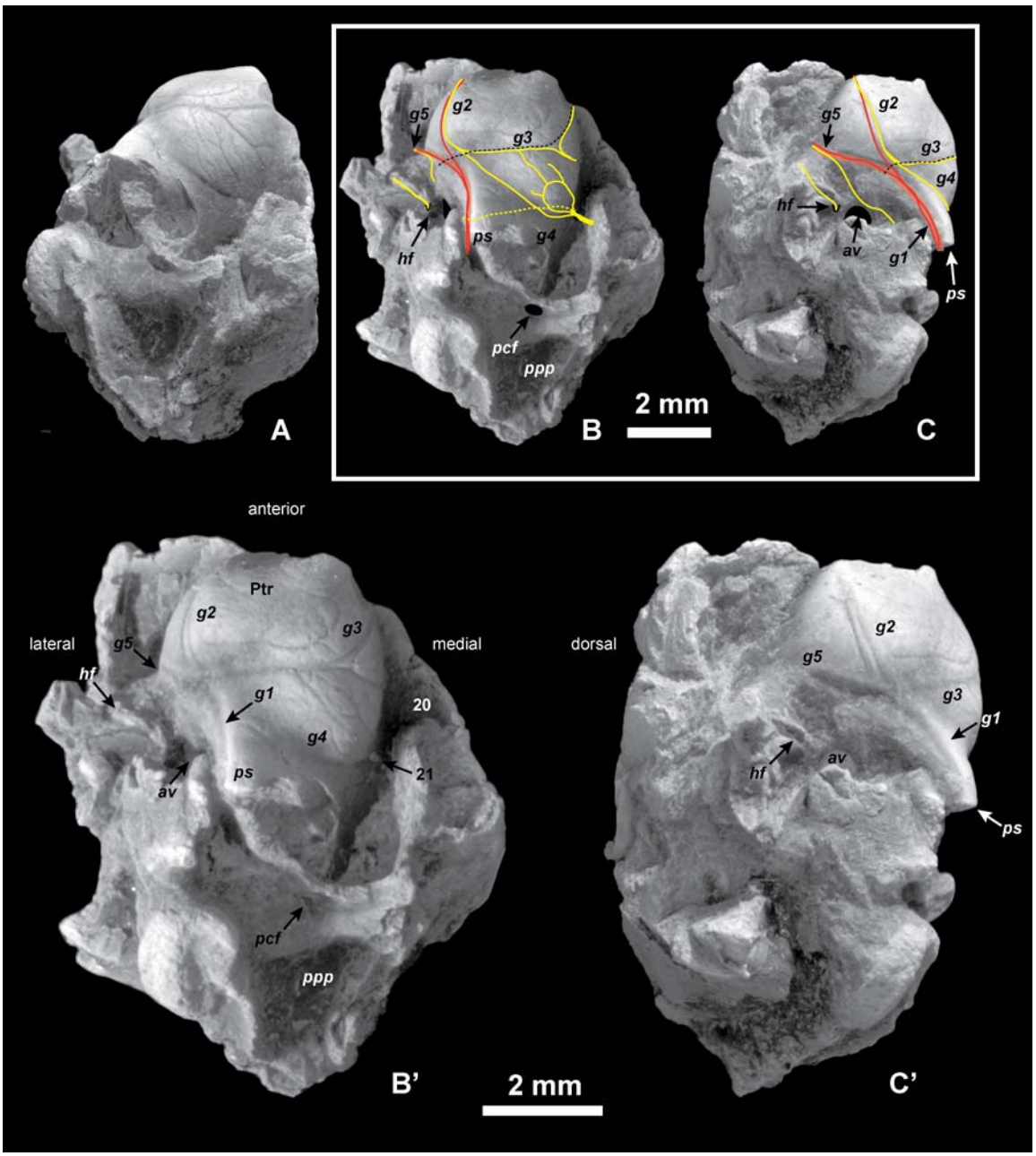
A
B
C
g5
g2
g3
g4
hf
ps
pcf
ppp
av
g1
2 mm
anterior
lateral
medial
dorsal
Ptr
20
21
B'
C'
2 mm
Figure 2.7

Figure 2.7. UALVP 46687 *Pronothodectes gaoi*: A, ventromedial view. B, ventral view. Note that unlabeled loop of nerves reconstructed here is not consistently visible in other specimens, but grooves labeled *g1-5* are consistently visible. B', enlarged ventral view of B with labels. C, lateral view. C', enlarged lateral view of C with labels. Nerves reconstructed in yellow represent components of tympanic plexus. Neurovasculature reconstructed in red represents components of internal carotid plexus. Anterior is towards the top in all parts. Fine dashed line – g3 groove. Numbers and abbreviations: 20 – medial and rostral tympanic processes of petrosal, 21 – tympanic and mastoid canaliculus foramen. av – aperture for fenestra vestibuli; ps – posterior septum; g1 – groove for internal carotid plexus; g2 – groove for distal part of internal carotid plexus; g3 - groove that leads to s2 (for a small vein?); g4 - groove for tympanic plexus fibers to reach routes g1-3; g5 – groove that leads toward epitympanic crest; hf – hiatus fallopii; pcf – posterior carotid foramen; ppp – paroccipital process of petrosal; Ptr – petrosal.

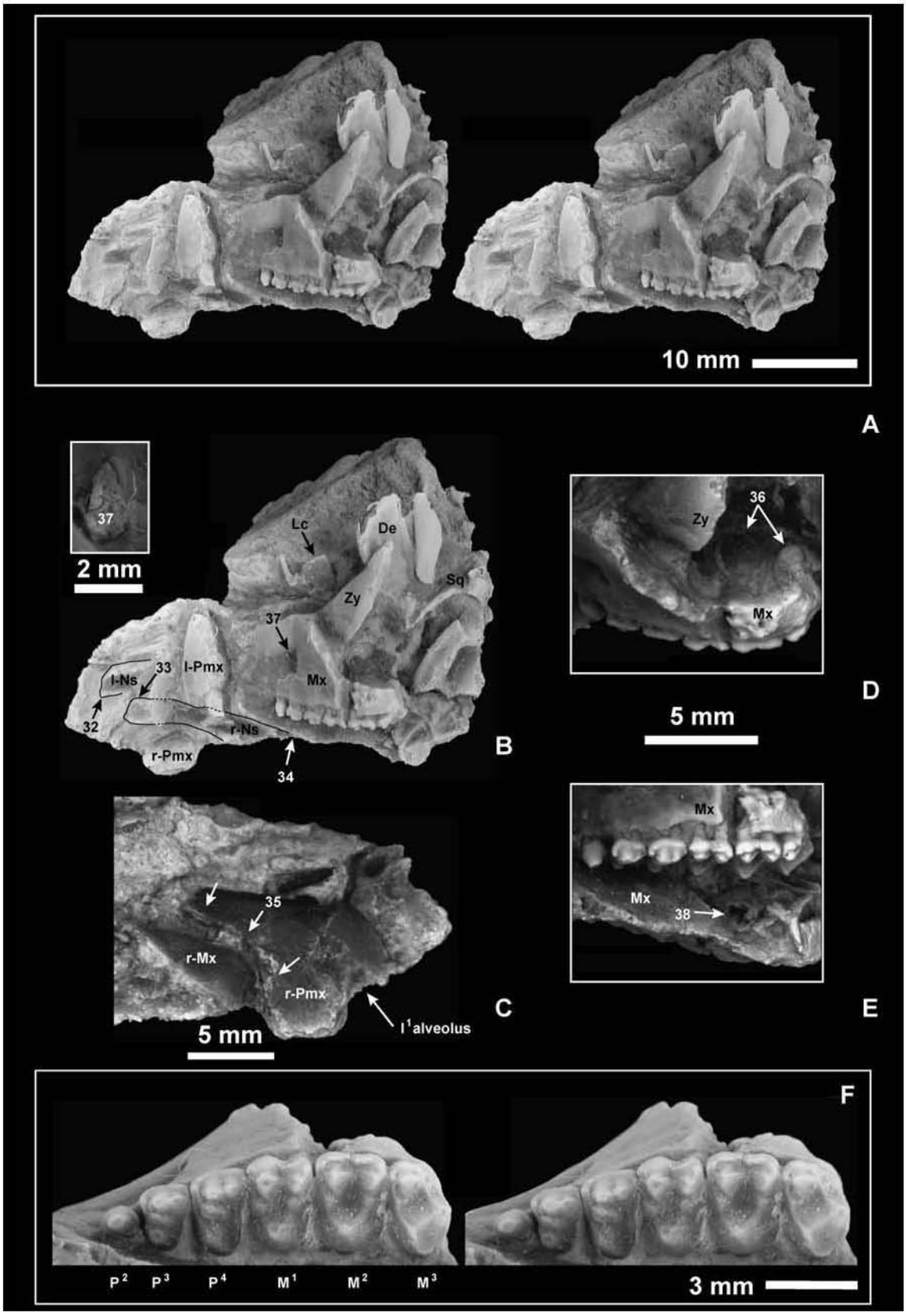
10 mm
A
37
2 mm
Lc
De
Sq
Zy
37
33
l-Ns
l-Pmx
Mx
32
r-Ns
r-Pmx
34
B
36
Zy
Mx
D
5 mm
Mx
35
r-Mx
38
Mx
r-Pmx
C
E
5 mm
l1 alveolus
F
P2 P3 P4 M1 M2 M3
3 mm

Figure 2.8.

Figure 2.8. USNM 309902 *Nannodectes intermedius*: A, stereophotographic left lateral view of rostrum. B, left lateral view of rostrum; also note inset of infraorbital foramen (*37*) in anterior view, with dorsal end up and medial on left. C, lateral view of right premaxilla. D, dorsolateral view of left maxilla showing molar roots. E, ventrolateral view of left maxilla showing foramina of questionable attribution. F, stereophotographic occlusal view of left maxillary dentition. Anterior to left in A, B, D, E; F. Anterior to right in C. Numbers and abbreviations: 32 – left nasal anterior end, 33 – right nasal anterior end, 34 – right nasal posterior end, 35 – right maxilla/premaxilla suture, 36 – M^{2-3} roots exposed in orbit, 37 – infraorbital foramen, 38 – possible optic foramen. De – dentary; Lc – lacrimal; Mx – maxilla; r&l-Ns – right and left nasals; r&l-Pmx – right and left premaxilla; Sq – squamosal; Zy – zygomatic.

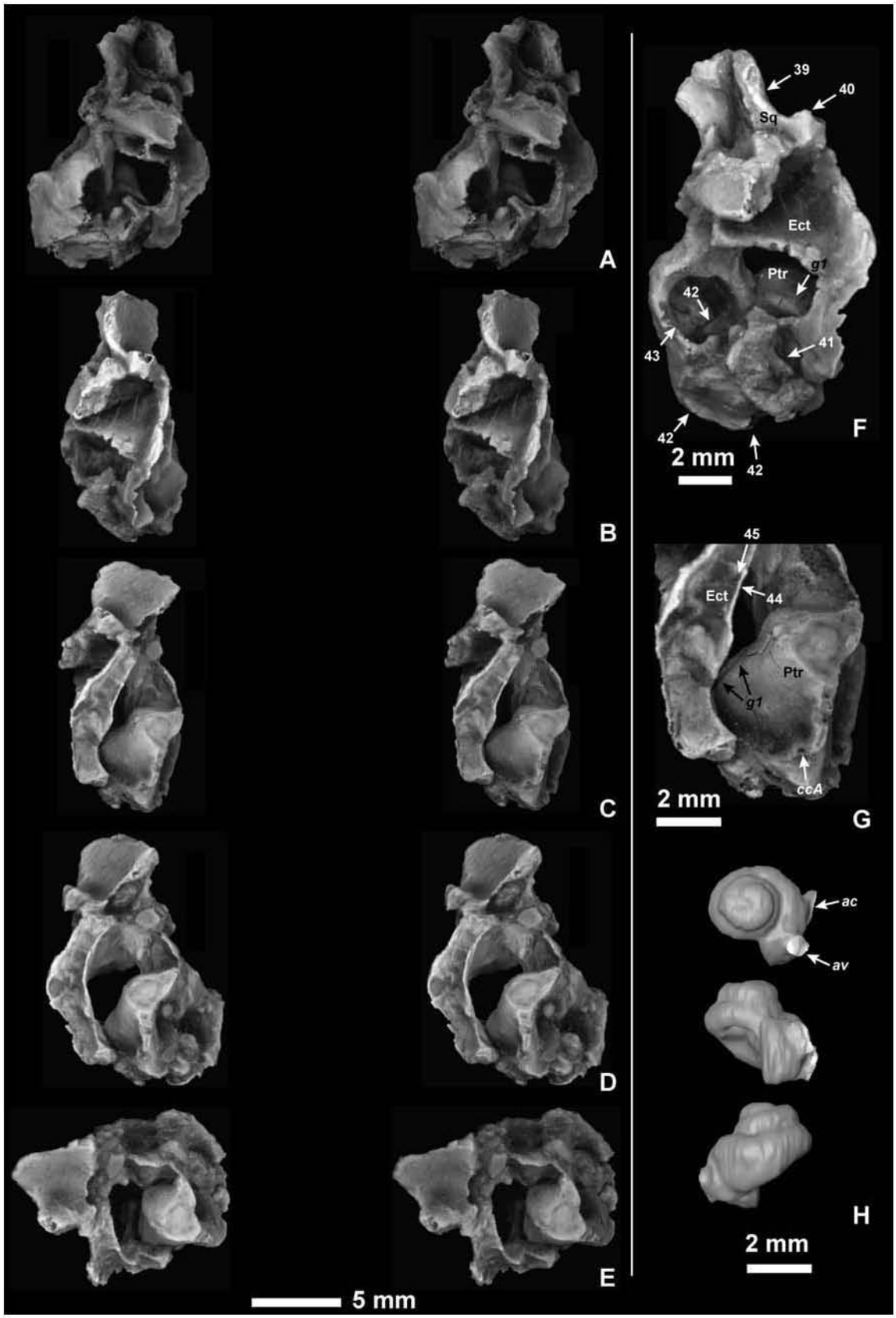
A
B
C
D
E
5 mm
39
40
Sq
Ect
Ptr
g1
42
43
41
42
42
2 mm
F
45
Ect
44
Ptr
g1
ccA
2 mm
G
ac
av
H
2 mm

Figure 2.9.

Figure 2.9. USNM 309902 *Nannodectes intermedius*: A-G, stereophotographic views of right petrosal and other basicranial fragments. A – lateral, B - ventral. C - ventromedial (because of deformation, the glenoid is seen in ventral view, revealing its mediolateral dimensions. D - medial. E - anterior. F - ventrolateral. G - ventromedial. H, three views (roughly lateral - top, dorsal and ventral – bottom) of cochlea extracted from HRxCT dataset. Anterior to top in A-D, F; G. Lateral to left in E. Numbers and abbreviations: 39 – glenoid of squamosal, 40 – postglenoid process, 41 – facial canal, 42 – semicircular canal, 43 – epitympanic recess, 44 – crista tympanica, 45 – bony ridges of annular bridge. ac – aperture of cochlear fenestra; av – aperture of fenestra vestibuli, ccA - broken open aperture of cochlear canaliculus; Ect – ectotympanic; g1 – groove for internal carotid plexus; Ptr – petrosal; Sq – squamosal.

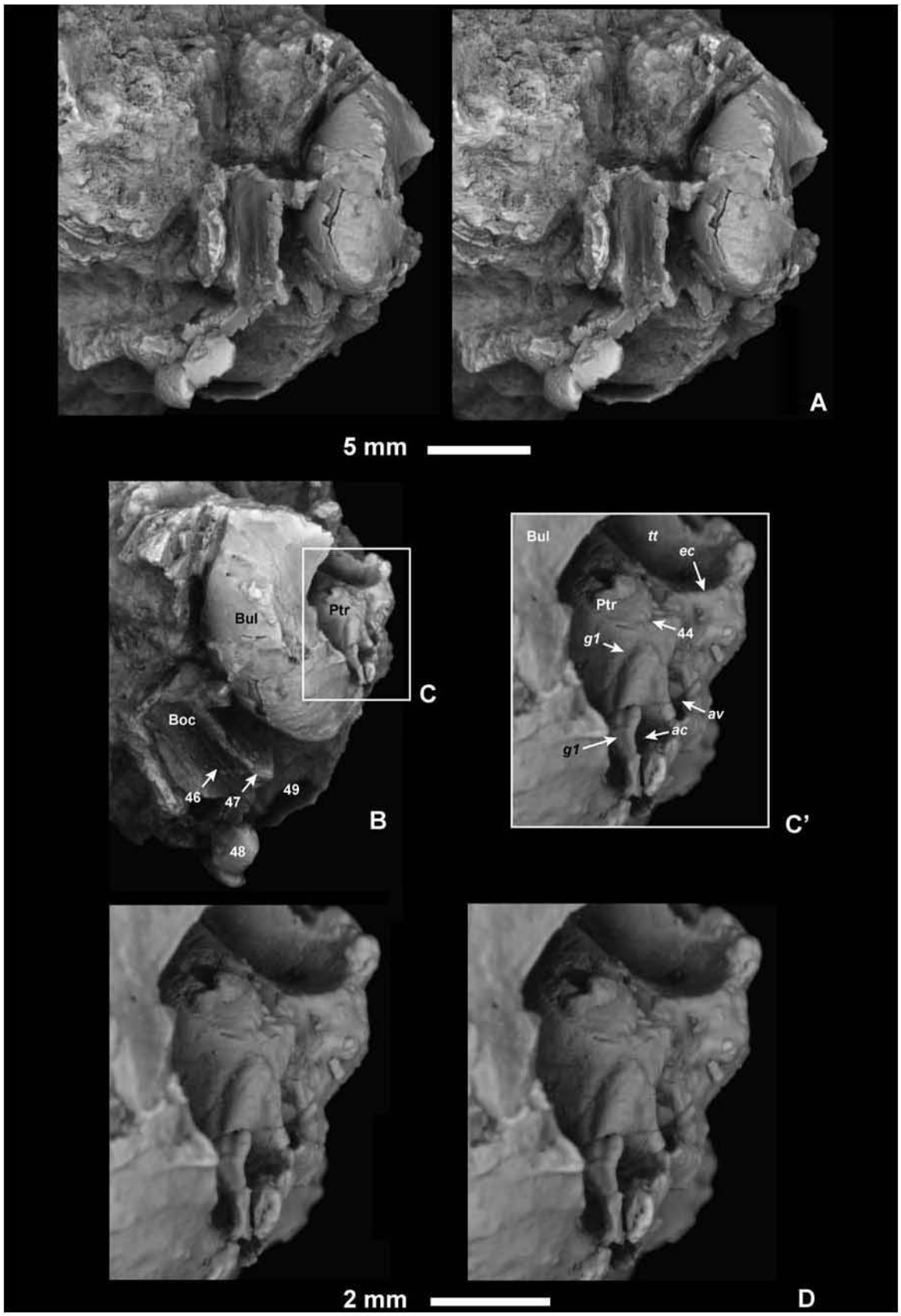

Figure 2.10.

Figure 2.10. USNM 309902 *Nannodectes intermedius*: A, stereophotographic ventral view of basicranial fragment. B, ventrolateral view of basicranial fragment with left auditory bulla intact. C, inset of left petrosal. C', enlargement of inset from C. D, stereophotographic ventrolateral view of left petrosal. Anterior to top in all parts. Numbers and abbreviations: 44 – crista tympanica, 46 – midline ridge of basioccipital, 47 – ventrally projecting lateral processes of basioccipital, 48 – right occipital condyle, 49 – foramen magnum. ac – aperture of cochlear fenestra; av – aperture of fenestra vestibuli; Boc – basioccipital; Bul – auditory bulla; ec – epitympanic crest; g1 – groove for internal carotid plexus; Ptr – petrosal; tt – tegmen tympani.

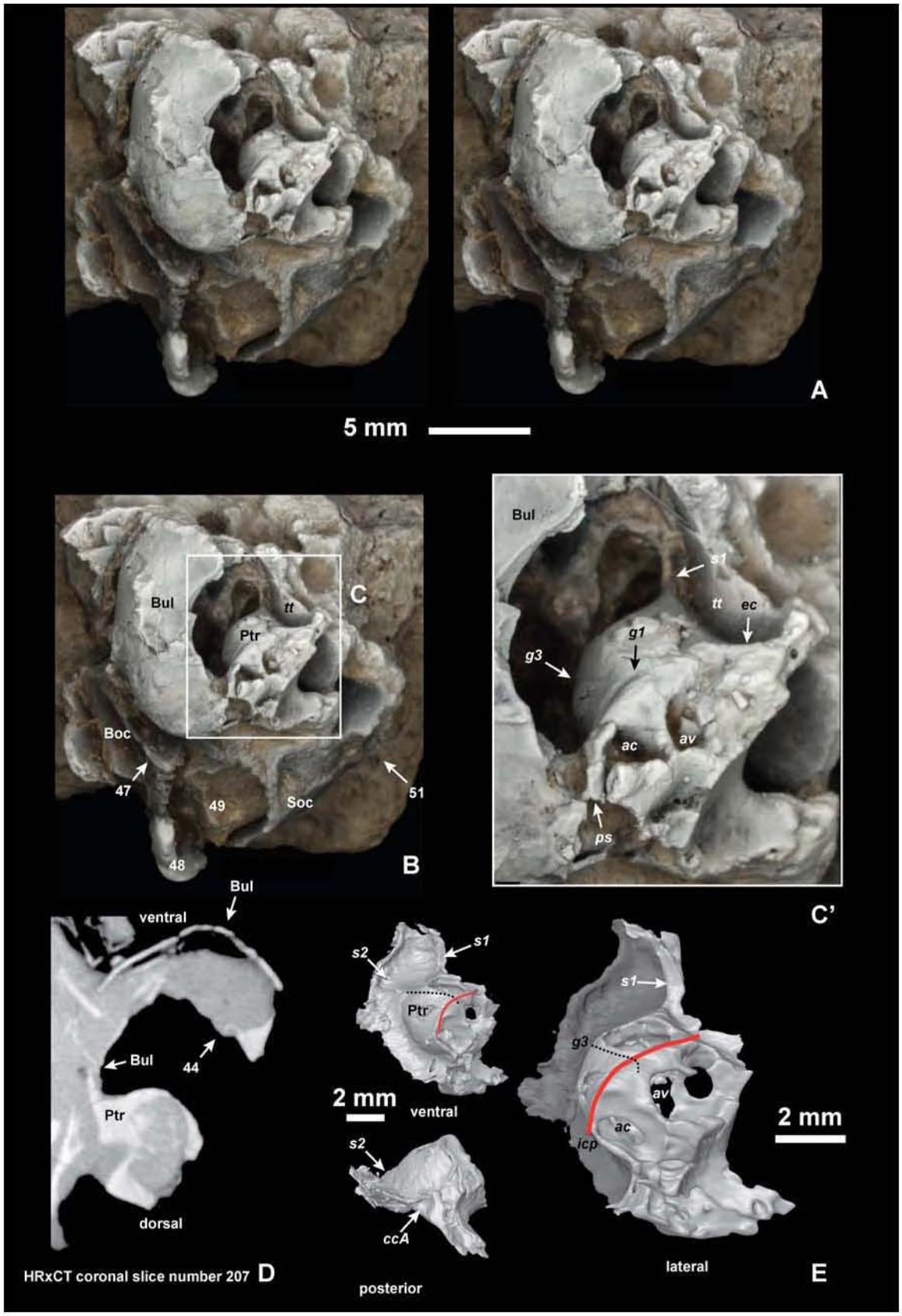
A
5 mm
Bul
tt
C
Ptr
Boc
47
49
Soc
51
48
B
Bul
s1
tt
ec
g1
g3
ac
av
ps
C'
Bul
ventral
Bul
44
Ptr
dorsal
HRxCT coronal slice number 207
D
s2
s1
Ptr
2 mm
ventral
s2
ccA
posterior
s1
g3
av
ac
icp
2 mm
lateral
E

Figure 2.11.

Figure 2.11. USNM 309902 *Nannodectes intermedius*: A, stereophotographic lateral view of left basicranial fragment. B, lateral basicranial fragment. C, inset of left petrosal. C', enlargement of inset C. D, HRxCT coronal slice number 207. E, three views of HRxCT renderings of left petrosal. Nerves reconstructed in yellow represent components of tympanic plexus. Neurovasculature reconstructed in red represents components of internal carotid plexus. Anterior to top in all parts. Fine dashed line – g3 groove. Numbers and abbreviations: 44 – crista tympanica, , 47 – ventrally projecting lateral processes of basioccipital, 48 – right occipital condyle, 49 – foramen magnum, 51 – nuchal crest. ac – aperture of cochlear fenestra; av – aperture of fenestra vestibuli; Boc – basioccipital; Bul – auditory bulla; ccA - broken open aperture of cochlear canaliculus; ps – posterior septum; ec – epitympanic crest; g1 – groove for internal carotid plexus; g3 - groove that leads to s2 (for a small vein?); Ptr – petrosal; s1 – first (anterior) septum; s2 – second septum; Soc – supraoccipital; tt – tegmen tympani.

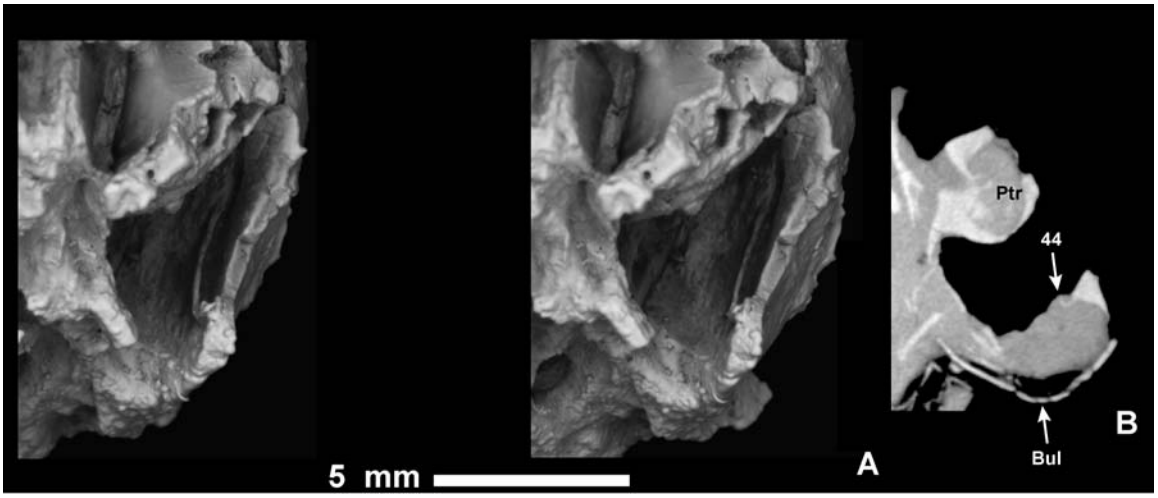

Figure 2.12. USNM 309902 *Nannodectes intermedius*: A, stereophotographic anterolateral view of left ear region. B, HRxCT coronal slice number 207. Lateral to right. Numbers and abbreviations: 44 – crista tympanica. Bul – auditory bulla ; Ptr – petrosal.

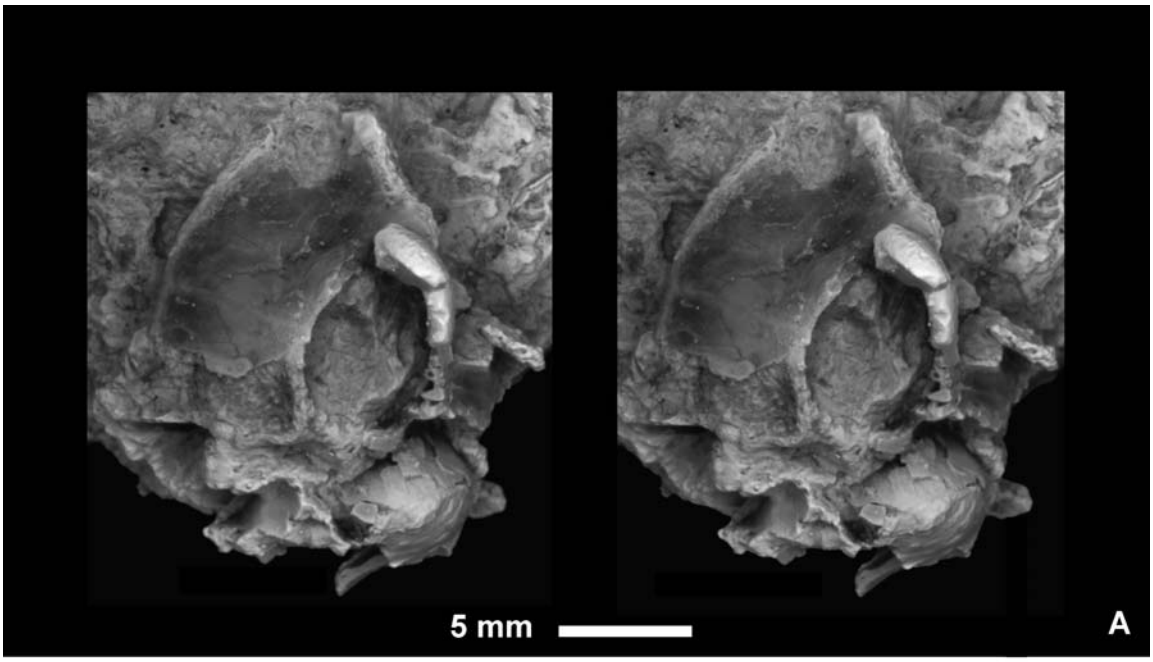

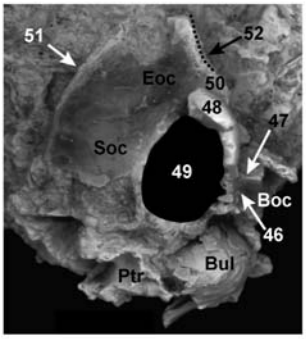

Figure 2.13. USNM 309902 *Nannodectes intermedius*: A, stereophotographic posterior view of basicranial fragment. B, labeled posterior view of basicranial fragment. Dorsal to left in A and B. Numbers and abbreviations: 46 – midline ridge of basioccipital, 47 – ventrally projecting lateral processes of basioccipital, 48 – right occipital condyle, 49 – foramen magnum, 50 – Jugular process of exoccipital, 51 – nuchal crest, 52 – exoccipital/petrosal suture. Boc – basioccipital; Bul – auditory bullal Eoc – exoccipital; Ptr – petrosal ; Soc – supraoccipital.

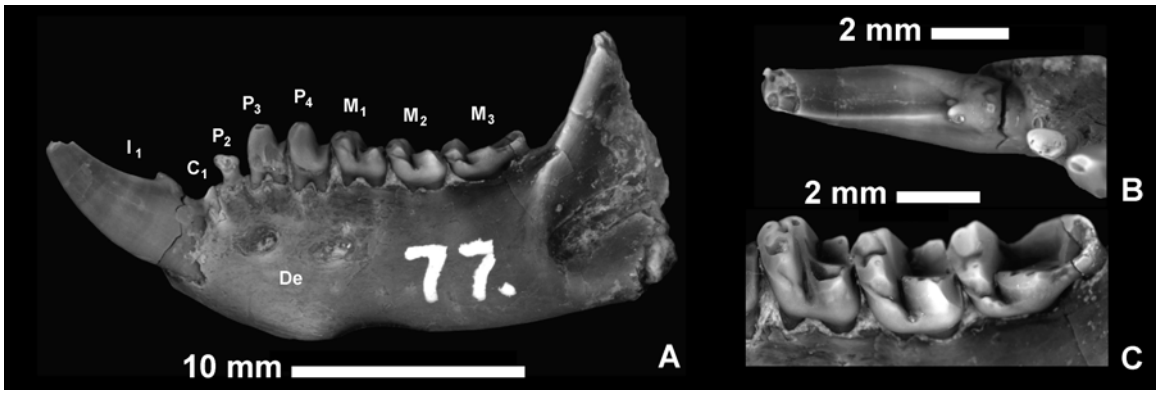

Figure 2.14. USNM 309902 *Nannodectes intermedius*: A, buccal view of left dentary. B, occlusal view of left anterior teeth. C, oblique bucco-occlusal view of left M^{1-3}. Abbreviation: De – dentary.

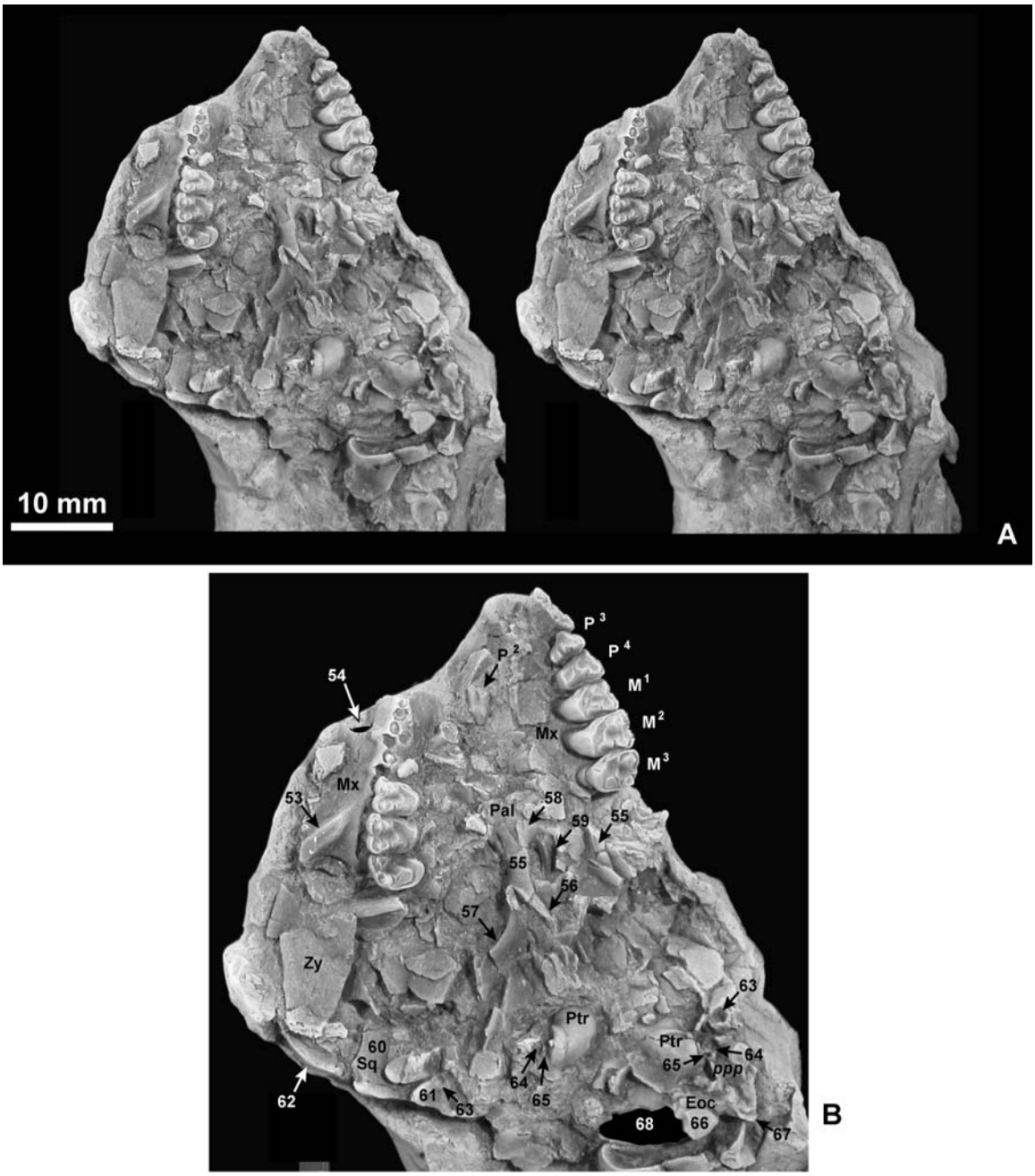

Figure 2.15. AMNH 17388 *Nannodectes gidleyi*: A, stereophotographic ventral view of skull. B, enlarged ventral view. Anterior to top in A and B. Numbers and abbreviations: 53 – root of zygmatic process of maxilla, 54 – infraorbital foramen, 55 – pterygoid process of palatine, 56 – pterygoid process of basisphenoid, 57 – pterygoid process of alisphenoid, 58 – palatine postpalatine torus, 59 – postpalatine spine, 60 – glenoid of squamosal, 61 – postglenoid process, 62 – zygomatic process of squamosal, 63 – postglenoid foramen of squamosal, 64 – stylomastoid foramen, 65 – possible posterior carotid foramen and internal carotid canal, 66 – occipital condyle, 67 – jugular process of exoccipital, 68 – foramen magnum. Eoc – exoccipital; Mx – maxilla; Pal – palatine; ppp – paroccipital process of petrosal; Ptr – petrosal; Sq – squamosal; Zy – zygomatic.

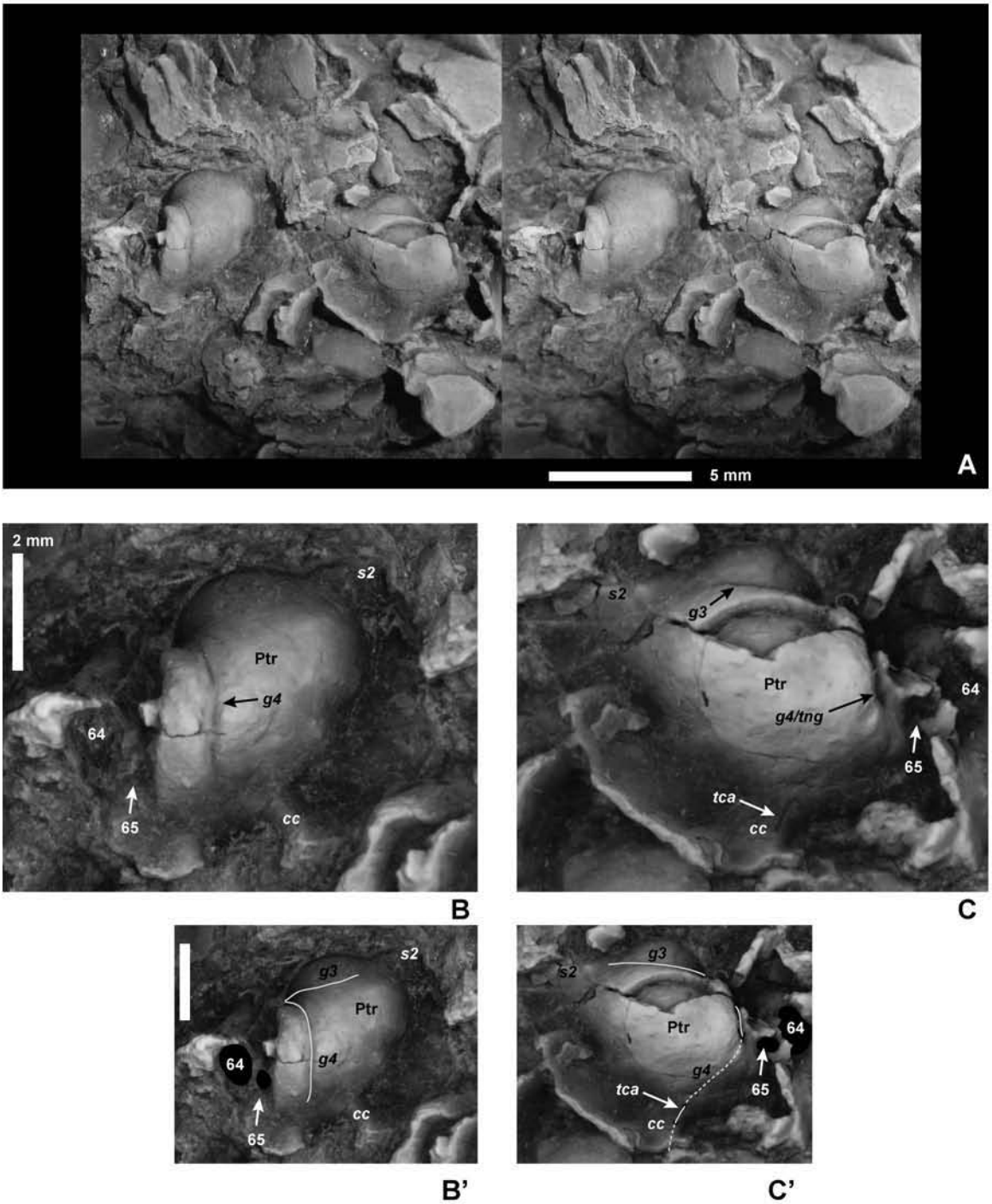
5 mm
A
2 mm
s2
Ptr
g4
64
65
cc
B
s2
g3
Ptr
64
g4/tng
65
tca
cc
C
s2
g3
Ptr
g4
64
65
tca
cc
B'
s2
g3
Ptr
64
g4
65
cc
C'

Figure 2.16

Figure 2.16. AMNH 17388 *Nannodectes gidleyi*: A, stereophotographic ventral view of basicranium. B, ventral view, with limited labeling, of right petrosal. B', ventral view, with interpretive labeling, of right petrosal. C, ventral view, with limited labeling, of left petrosal. C', ventral view, with interpretive labeling, of left petrosal. Anterior to top in all parts. Solid white lines represent course of nerves relating to tympanic plexus. Dashed white line represents nerve course passing through canal in promontorium. Numbers and abbreviations: 64 – stylomastoid foramen, 65 – possible posterior carotid foramen and internal carotid canal. cc – cochlear canaliculus; g3 - groove that leads to s2 (for a small vein?); g4 - groove for tympanic plexus fibers to reach routes g1-3; Ptr – petrosal; s2 – second septum; tca – tympanic canaliculus; tng – tympanic nerve groove.

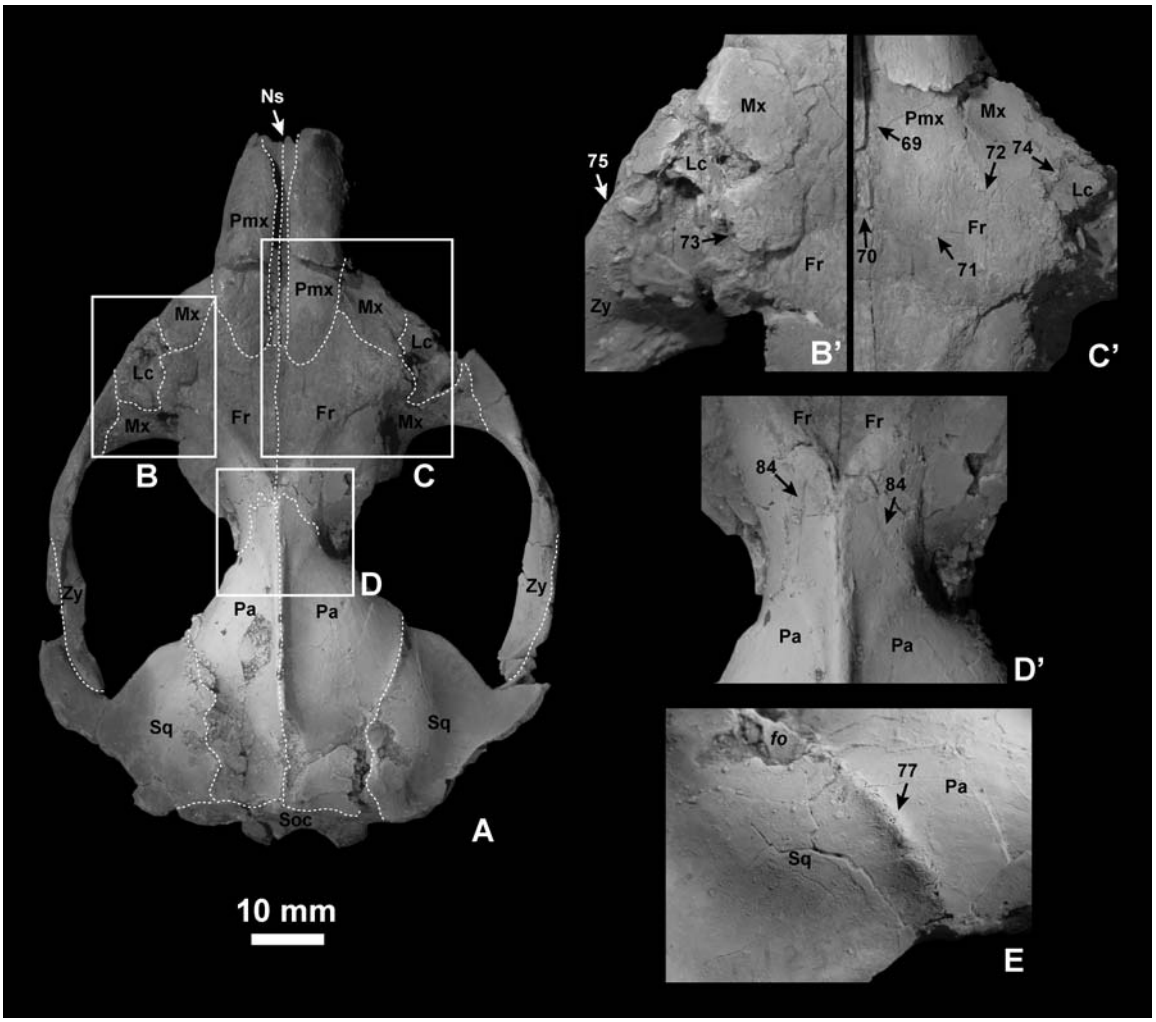

Figure 2.17. MNHN CR 125 *Plesiadapis tricuspidens*: A, dorsal view of skull. Sutures shown as white dashed lines. B, dorsal view, inset of left anterior orbit. B', enlargement of inset B. C, dorsal view, inset of right anterior orbit. C' enlargement of inset C. D' dorsal view, inset of orbitotemporal constriction. D', enlargement of inset D. E, lateral view of right neurocranium showing squamosal/parietal suture. Numbers and abbreviations: 69 – nasal/premaxilla suture, 70 – nasal/frontal suture, 71 – maxilla/frontal suture, 72 – premaxilla/frontal suture, 73 – lacrimal/frontal suture, 74 – lacrimal/maxilla suture, 75 – lacrimal/zygomatic suture, 77 – parietal/squamosal suture, 84 – parietal/frontal suture. fo – foramen; Fr – frontal; Lc – lacrimal; Mx – maxilla; Ns – nasal; Soc – supraoccipital; Sq – squamosal; Zy – zygomatic.

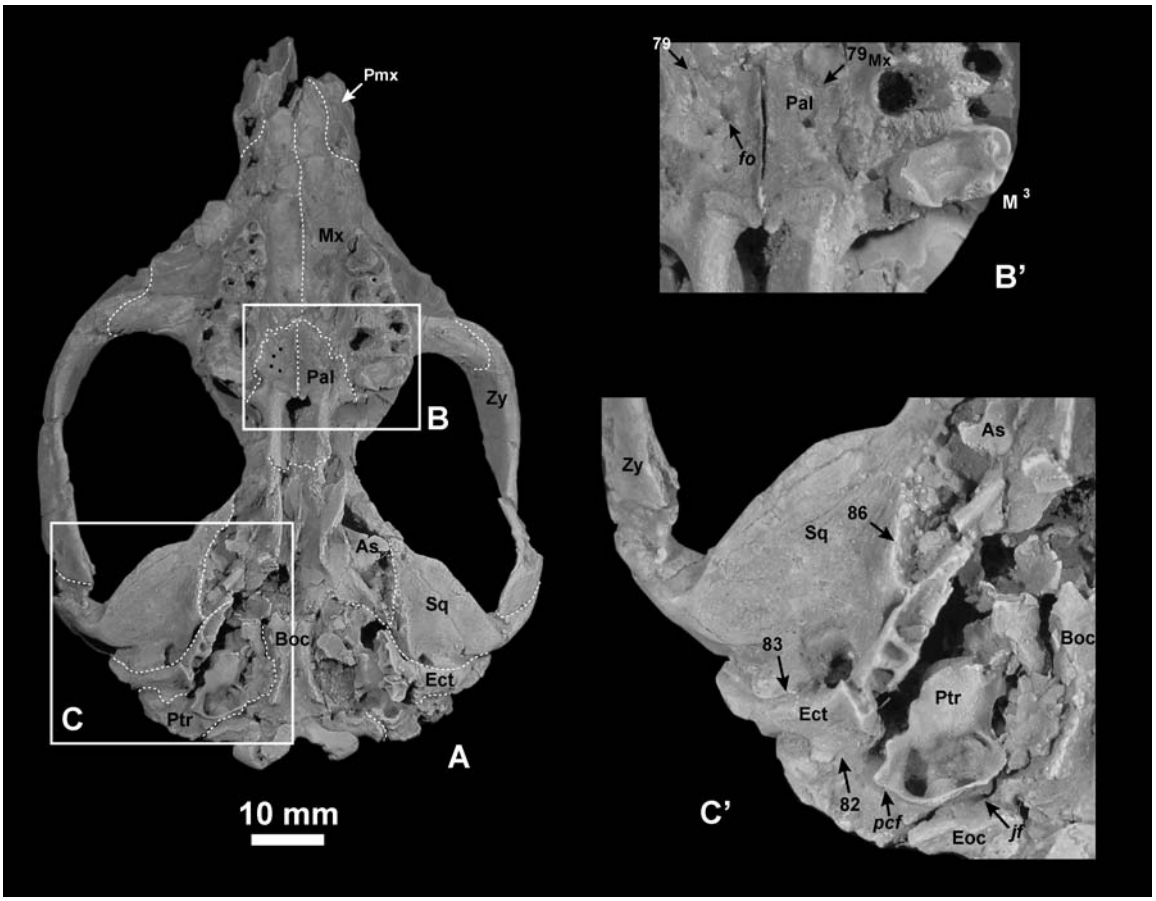

Figure 2.18. MNHN CR 125 *Plesiadapis tricuspidens*: A, ventral view of skull. Sutures shown as white dashed lines. B, ventral view, inset of posterior palate. B', enlargement of inset B. C, ventral view, inset of right baiscranium. C', enlargement of inset C. Numbers and abbreviations: 79 – palatine/maxilla suture, 82 – petrosal/ectotympanic suture, 83 – ectotympanic/squamosal suture, 86 – alisphenoid/squamosal suture. As – alisphenoid; Boc – basioccipital; Ect – ectotympanic; Eoc – exoccipital; fo – foramen; jf – jugular foramen; Mx – maxilla; Pal – palatine; pcf – posterior carotid foramen; Pmx – premaxilla; Ptr – petrosal; Sq – squamosal.

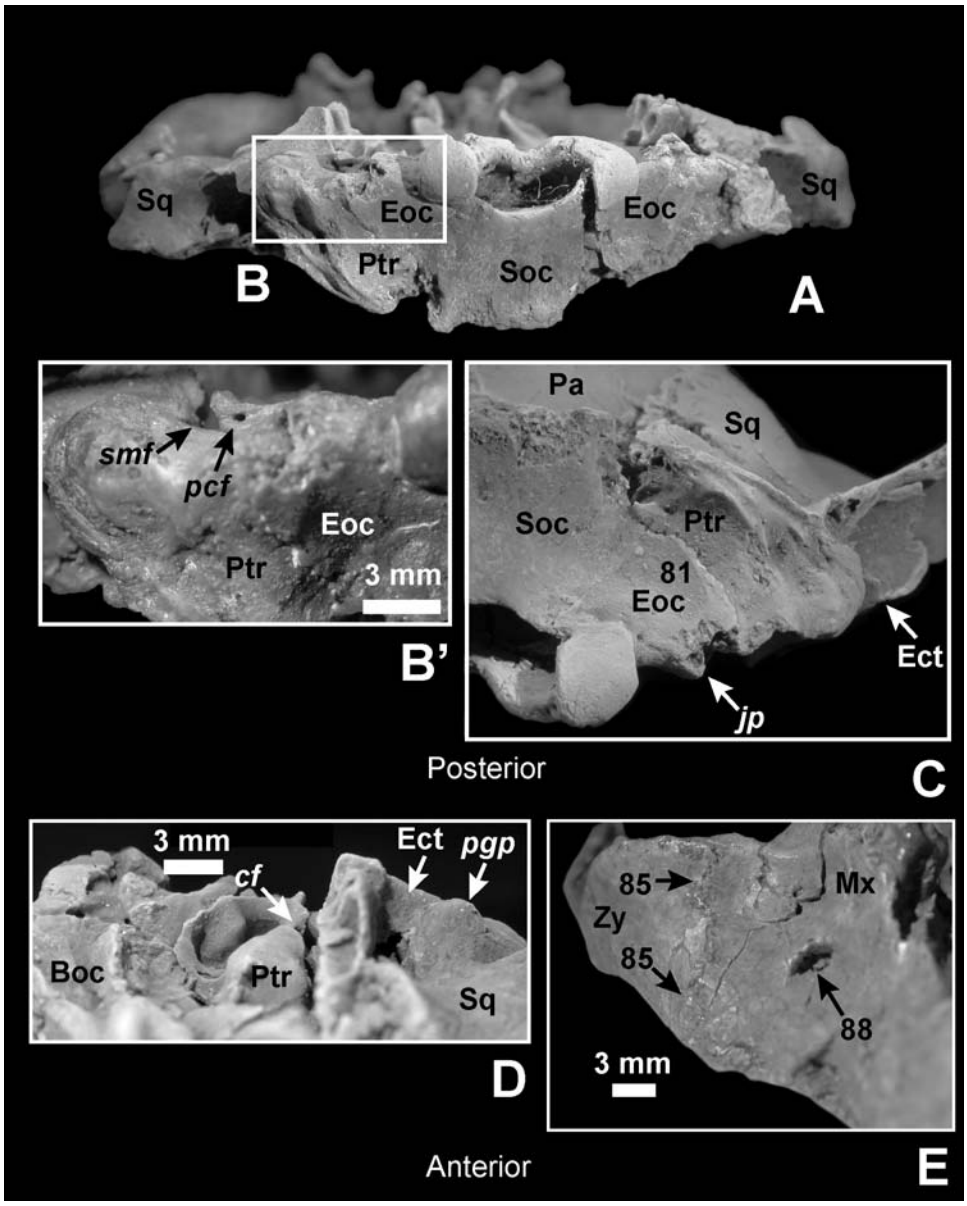

Figure 2.19. MNHN CR 125 *Plesiadapis tricuspidens*: A, posterior view of skull. B, posterior view, inset of right side. B', enlargement of inset B showing *pcf*. C, posterior view, close-up of right side, with dorsal surface facing up. D, anterior view of right petrosal, showing anterior end of carotid canal (*cf*). E, anterior view of right maxilla. Note that dorsal is up in C, but down in all other parts. Numbers and abbreviations: 81 – occipital/petrosal suture, 85 – maxilla/zygomatic suture, 88 – infraorbital foramen, 89 – foramen ovale. Boc – basioccipital; Ect – ectotympanic; Eoc – exoccipital; jp – jugular process of exocipital; Mx – maxilla; Pa – parietal; pcf – posterior carotid foramen; Ptr – petrosal; smf – stylomastoid foramen; Soc – supraoccipital; Sq – squamosal; Zy – zygomatic.

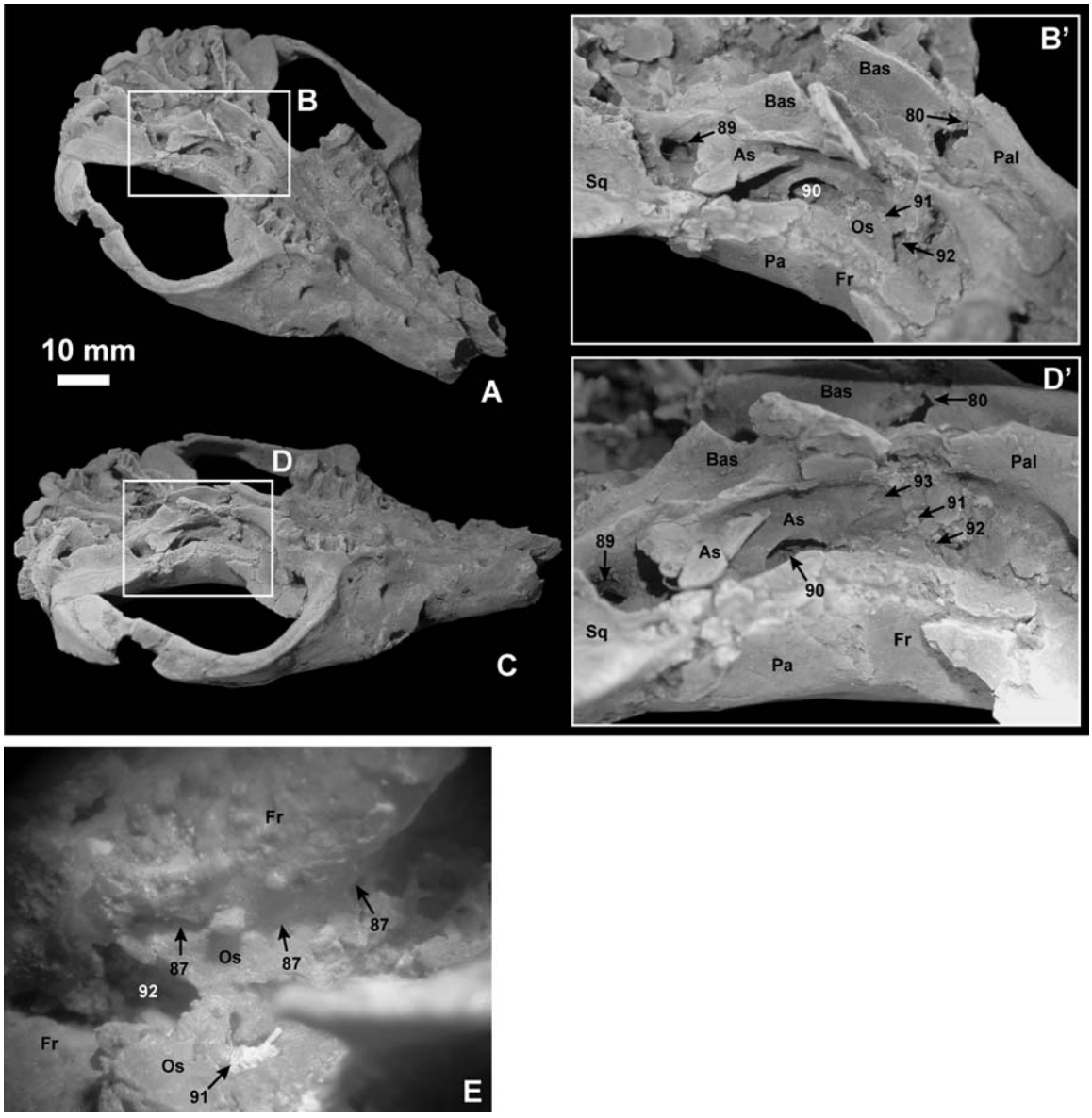

Figure 2.20. MNHN CR 125 *Plesiadapis tricuspidens*: A, anteroventrolateral view of skull. B, inset of orbitotemporal region. B', enlargement of inset B. C, ventrolateral view. D, inset of orbitotemporal region. D', enlargement of inset C. E, enlargement of frontal/orbitosphenoid contact. Note that in E, dorsal is up and ventral is down, which is opposite from the other images of the figure. Numbers and abbreviations: 80 – palatine/sphenoid suture, 87 – dorsal orbitosphenoid/frontal suture, 89 – foramen ovale, 90 – sphenorbital fissure, 91 – suboptic foramen, 92 – optic foramen, 93 – possible superior orbital fissure. As – alisphenoid; Bas – basisphenoid; Fr – frontal; Os – orbitosphenoid; Pa – parietal; Pal – palatine; Sq – squamosal.

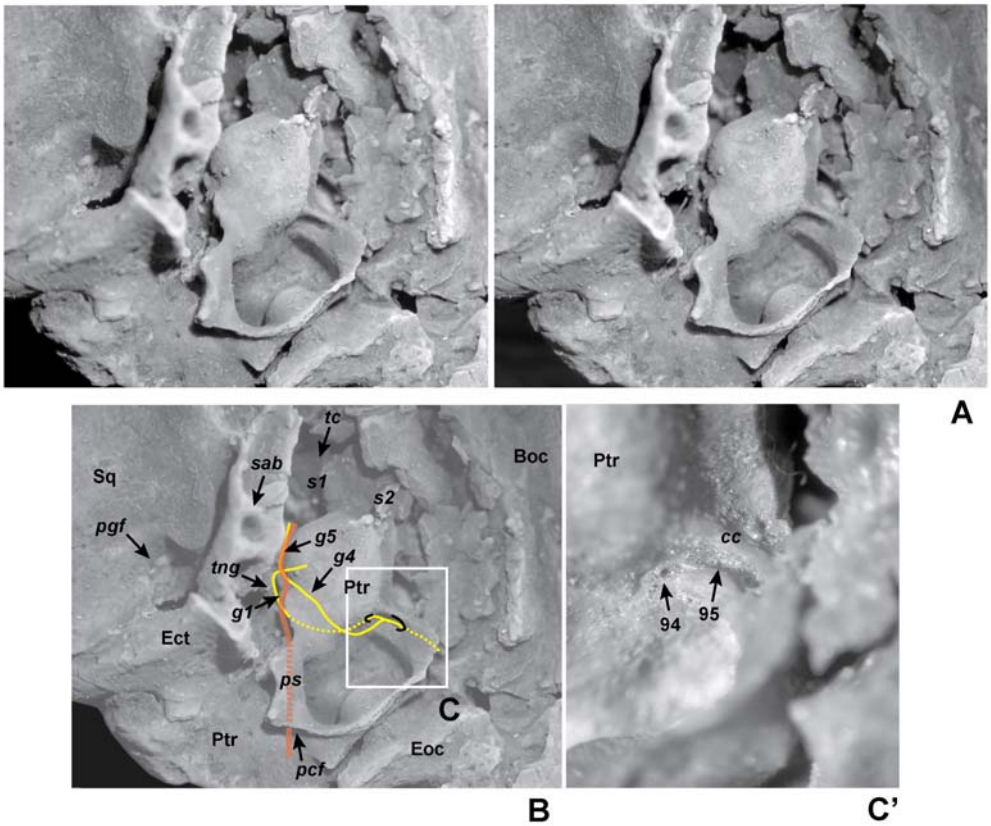

Figure 2.21. MNHN CR 125 *Plesiadapis tricuspidens*: A, stereophotographic ventral view of right promontorium. B, ventral view of right promontorium. C, ventral view of right promontorium inset of *tca* groove. C', enlargement of inset C showing groove and foramina relating to tympanic nerve (canal edges out of focus). Anterior to top. Nerves reconstructed in yellow represent components of tympanic plexus. Neurovasculature reconstructed in red represents components of the internal carotid plexus. Numbers and abbreviations: 94 – *tca* foramen, 95 – *tca* groove. Boc – basioccipital; cc – cochlear canaliculus; ps – posterior septum; Ect – ectotympanic; Eoc – exoccipital; g4 - groove for tympanic plexus fibers to reach routes g1-3; g5 – groove that leads toward epitympanic crest; pgf – postglenoid foramen; ptr – petrosal; s1 – first (anterior) septum; s2 – second septum; sab – strut from annular part to bullar part; Sq – squamosal; tc – tubal canal; tng – tympanic nerve groove.

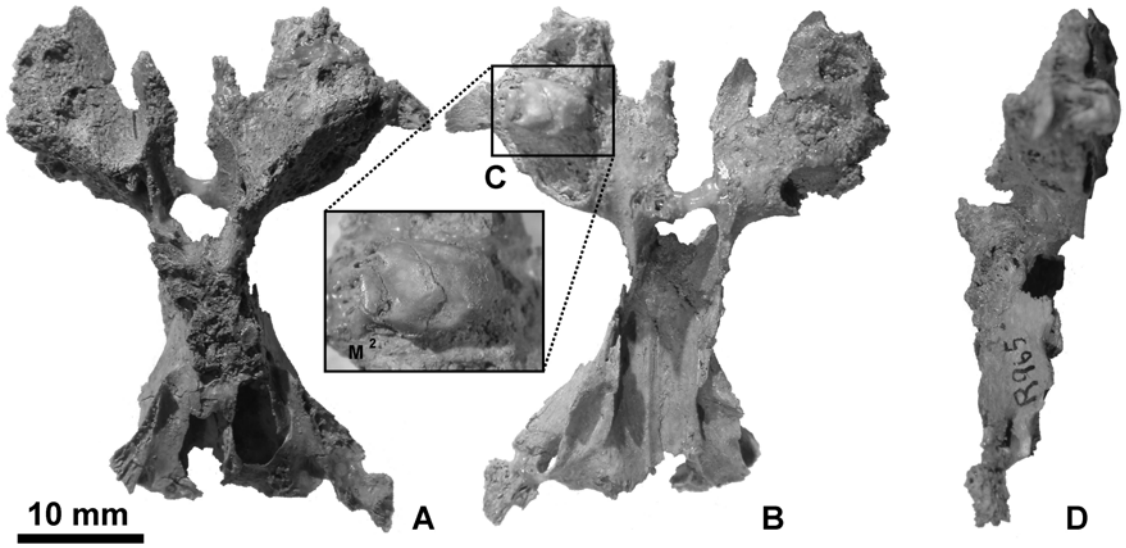

Figure 2.22. MNHN CR 965, *Plesiadapis tricuspidens*: A, dorsal view of cranial fragment. B, ventral view. C, ventral inset and enlargement of M^2. D, right lateral view. This specimen is revealed to be *P. tricuspidens* by size and morphology of M^2 as well as by details of cranial morphology.

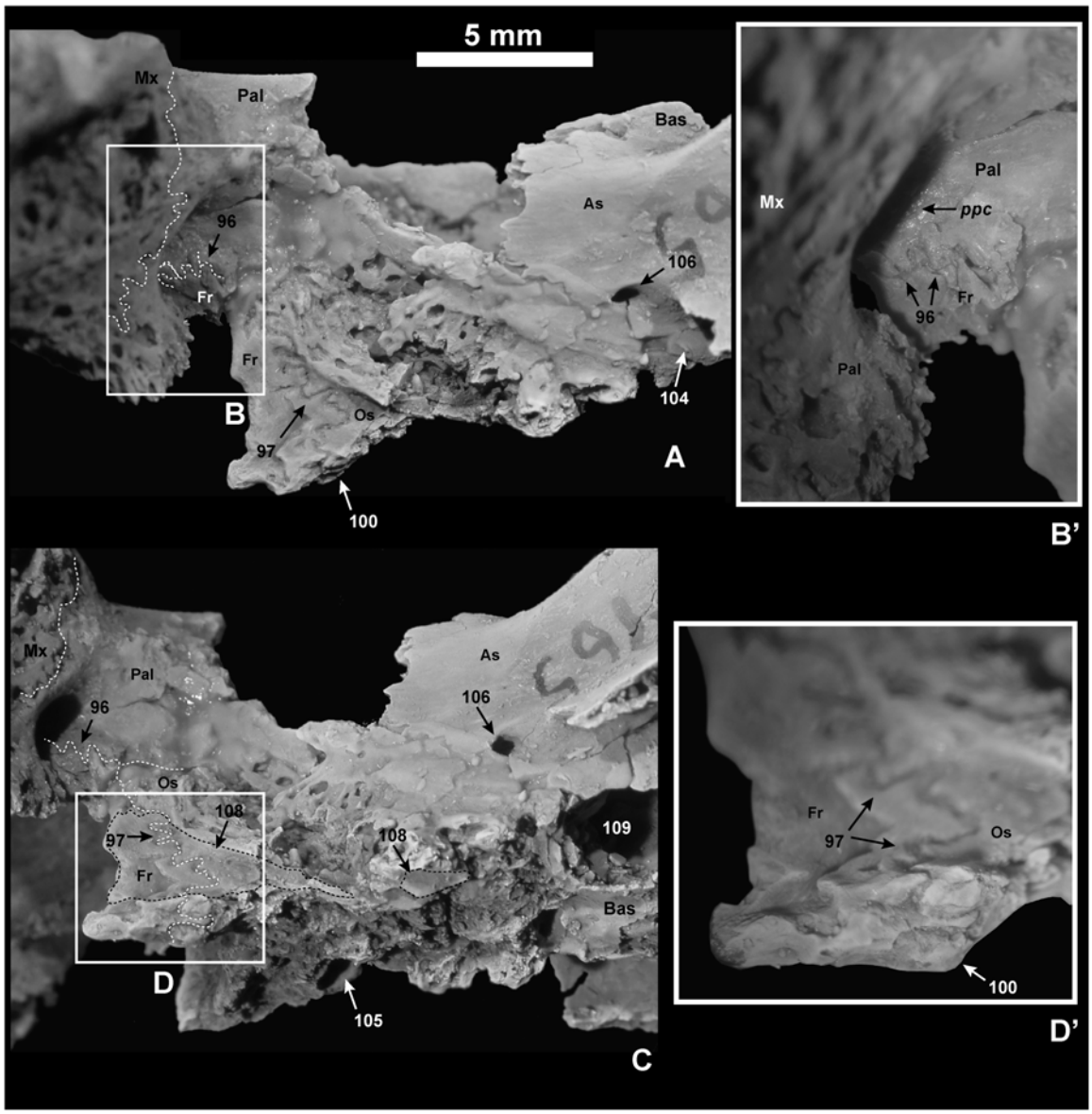
5 mm
Mx
Pal
Bas
As
96
106
Fr
Fr
B
104
Os
97
A
100
Mx
Pal
ppc
Fr
96
Pal
B'
Mx
Pal
96
As
106
Os
108
97
Fr
108
109
Bas
D
105
C
Fr
97
Os
100
D'
Figure 2.23

Figure 2.23. MNHN CR 965 *Plesiadapis tricuspidens*: A, right lateral view of orbitotemporal region. B, inset of right postpalatine foramen. B', enlargement of inset B. C, right dorsolateral view of orbitotemporal region. D, inset of frontal and orbitosphenoid fragment. D', enlargement of inset D. Sutures shown as white dashed lines. Anterior to left, dorsal down in all parts. Numbers and abbreviations: 96 – palatine/frontal suture in postpalatine canal, 97 – frontal/orbitosphenoid suture just anterior to optic foramen, 100 – dorsal margin of orbitosphenoid, 104 – sphenorbital fissure, 105 – optic foramen, 106 – various foramina representing blood sinus drainage, 108 – remnants of optic canals on broken orbitosphenoid (encompassed by black, dashed line and shaded lightly), 109 – basisphenoid sinus space. As – alisphenoid; Bas – basisphenoid; Fr – frontal; Mx – maxilla; Os – orbitosphenoid; Pal – palatine; ppc – postpalatine canal.

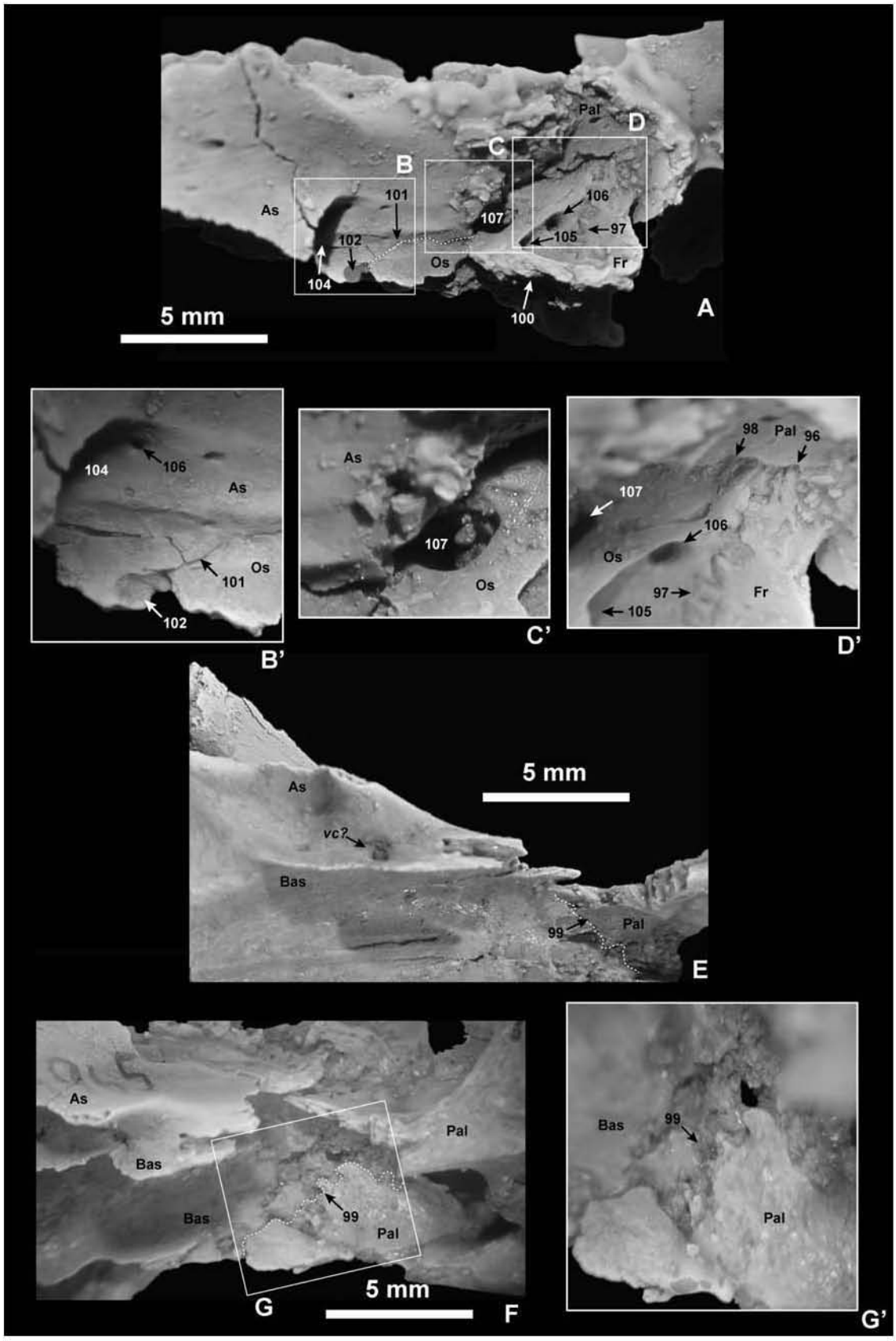
Pal
D
C
B
As
101
106
107
97
105
102
Os
Fr
104
100
A
5 mm
104
106
As
Os
101
102
B'
As
107
Os
C'
98
Pal
96
107
106
Os
97
Fr
105
D'
5 mm
As
vc?
Bas
99
Pal
E
As
Pal
Bas
Bas
99
Pal
5 mm
G
F
Bas
99
Pal
G'

Figure 2.24.

Figure 2.24. MNHN CR 965 *Plesiadapis tricuspidens*: A, left lateral view of orbitotemporal region (ventral up). B, inset of sphenorbital fissure and alisphenoid/orbitosphenoid suture. B', enlargement of inset B. C, inset of suboptic foramen. C', enlargement of inset C. D, inset of sphenoid/palatine and palatine/frontal sutures. D', enlargement of inset D. E, ventral view of right sphenoidal region. F, right ventrolateral view, orbitotemporal region. G, inset of sphenoid/palatine suture. G', enlargement of inset G. Sutures shown as white dashed lines. Anterior to right in all parts. Dorsal down in A-D.' Dorsal up in G and F. Numbers and abbreviations: 96 – palatine/frontal suture in postpalatine canal, 97 – frontal/orbitosphenoid suture just anterior to optic foramen, 98 – orbitosphenoid/palatine contact running anteroposteriorly, 99 – palatine/alisphenoid suture, 100 – dorsal margin of orbitosphenoid, 101 – alisphenoid/orbitosphenoid suture, 102 – "dished" surface on alisphenoid for broken out orbitosphenoid, 104 – sphenorbital fissure, 105 – optic foramen, 106 – various foramina representing blood sinus drainage, 107 – suboptic foramen. As – alisphenoid; Bas – basisphenoid; Fr – frontal; Os – orbitosphenoid; Pal – palatine; vc – vidian canal.

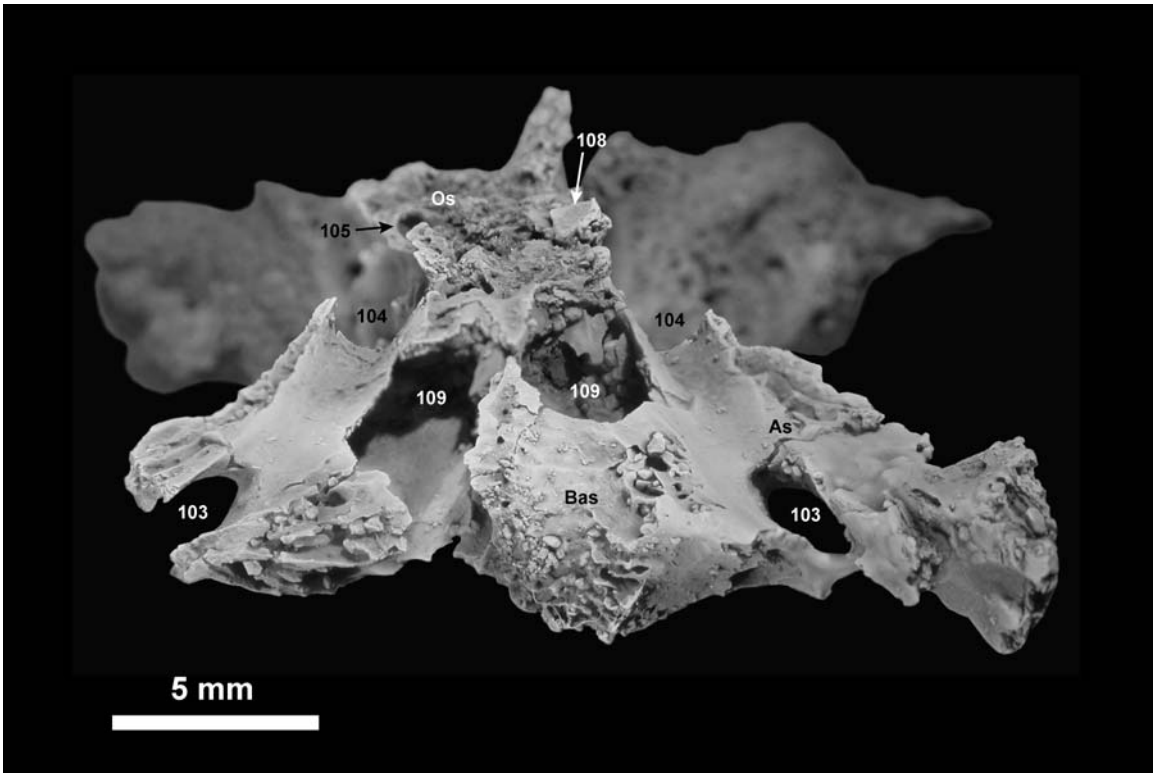

Figure 2.25

Figure 2.25. MNHN CR 965, *Plesiadapis tricuspidens*: Posterior view showing various foramina. Dorsal to top. Numbers and abbreviations: 103 – foramen ovale, 104 – sphenorbital fissure, 105 – optic foramen, 108 – remnants of optic canals on broken orbitosphenoid, 109 – basisphenoid sinus space. As – alisphenoid; Bas – basisphenoid; Os – orbitosphenoid.

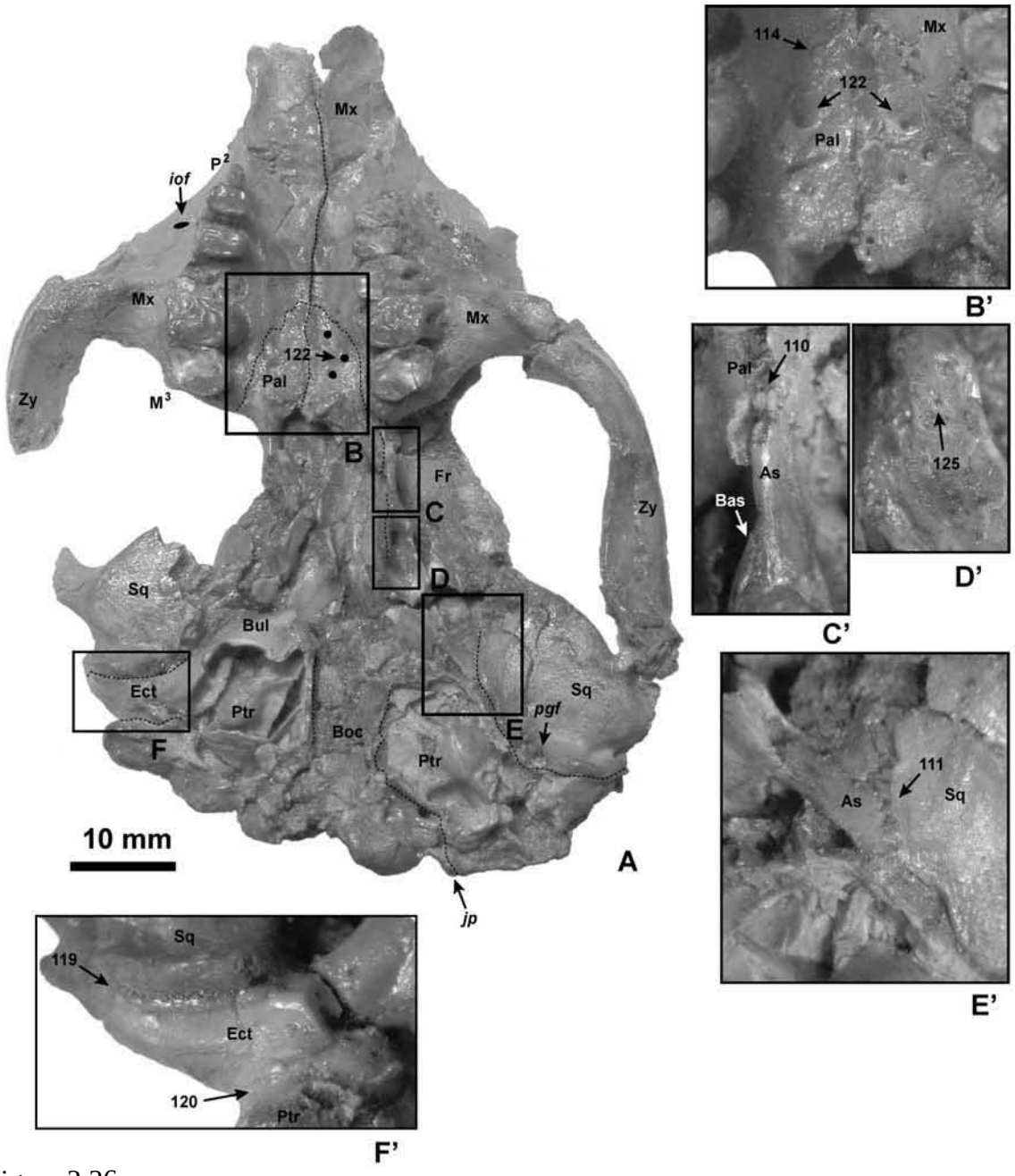
Mx
P2
iof
Mx
Mx
122
Pal
Zy
M3
B
Fr
C
Zy
D
Sq
Bul
Ect
Ptr
Boc
Sq
pgf
E
F
Ptr
10 mm
A
jp
Sq
119
Ect
120
Ptr
F'
114
Mx
122
Pal
B'
110
Pal
As
Bas
C'
125
D'
111
As
Sq
E'

Figure 2.26

Figure 2.26. Pellouin skull *Plesiadapis tricuspidens*: A, ventral view. B, inset of palate. B, labeled enlargement of inset B. C, inset of pterygoid process. C', enlargement of inset C. Note discontinuity between ento- and ectopterygoid processes, likely indicating basisphenoid/alisphenoid suture. D, inset of scaphoid fossa of pterygoid process. D', enlargement of inset D. E, inset of alisphenoid/squamosal suture. E', labeled enlargement of inset E. F, inset of posterolateral basicranium. F', enlargement of inset F. Sutures shown as black dashed lines. Numbers and abbreviations: 110 – palatine/alisphenoid suture, 111 – squamosal/alisphenoid suture, 114 – palatine/maxilla suture on palate, 119 – squamosal/tympanic suture, 120 – tympanic/petrosal suture, 122 – palatal palatine foramina, 125 – foramen in scaphoid fossa. As – alisphenoid; Bas – basisphenoid; Boc – basioccipital; Bul – auditory bulla; Ect – ectotympanic; Fr – frontal; iof – infraorbital foramen; jp – jugualr process of exoccipital; Mx – maxilla; Pal – palatine; pgf – postglenoid foramen; Ptr – petrosal; Sq – squamosal.

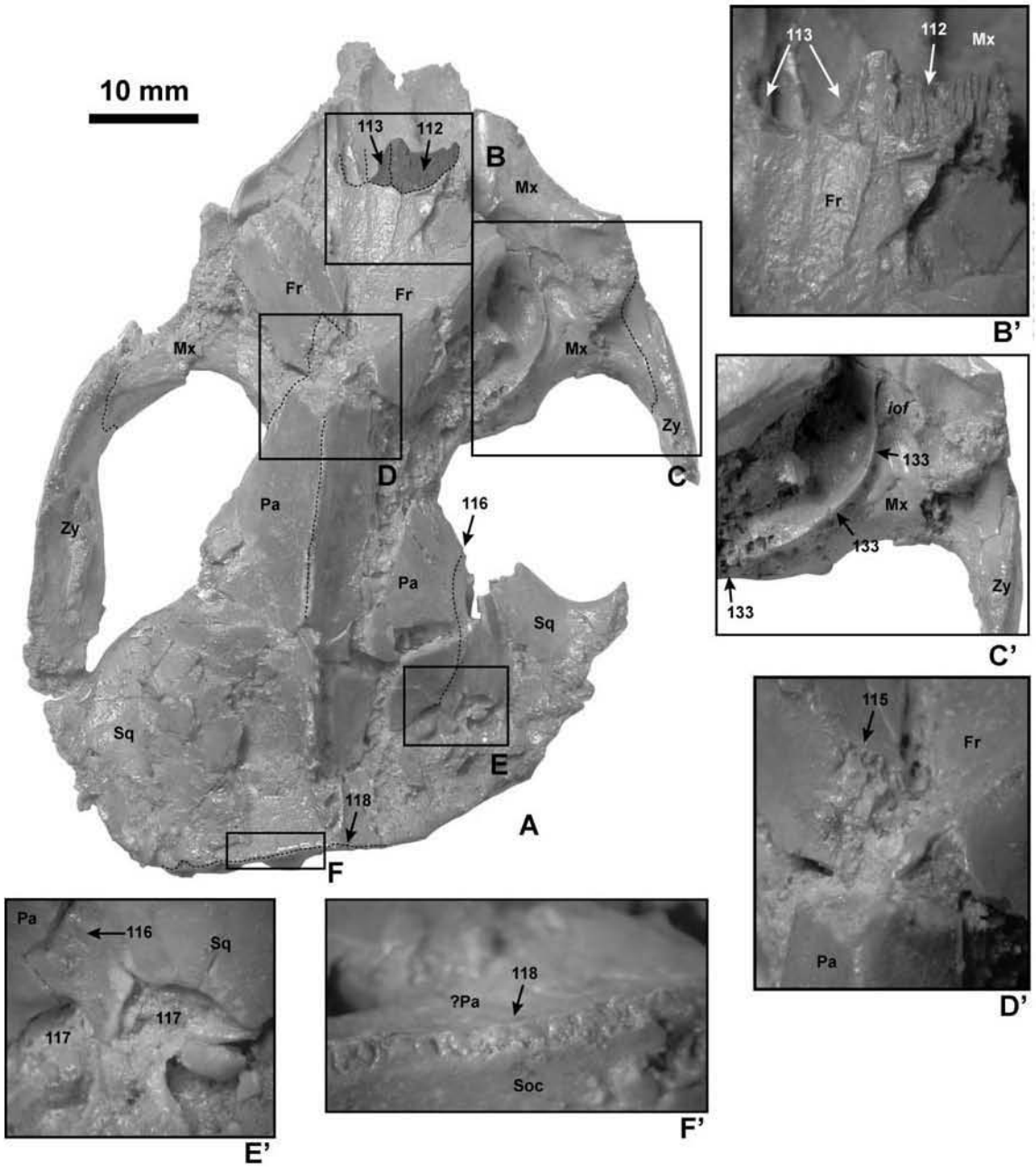
10 mm
113
112
B
Mx
Fr
Fr
Mx
Mx
Zy
D
C
Pa
116
Zy
Pa
Sq
Sq
E
118
A
F
Pa
116
Sq
117
117
E'
118
?Pa
Soc
F'
113
112
Mx
Fr
B'
iof
133
Mx
133
133
Zy
C'
115
Fr
Pa
D'

Figure 2.27

Figure 2.27. Pellouin skull *Plesiadapis tricuspidens*: A, dorsal view. B, inset of rostrum. B', enlargement of inset B. C, inset of dorsal aspect of maxilla. C', enlargement of inset C. D, inset of orbitotemporal region. D', enlargement of inset D. E, inset of lateral neurocranium. E' enlargement of inset E. F, inset of nuchal crest. F' enlargement of inset F. Sutures shown as black dashed lines. Numbers and abbreviations: 112 – premaxillary sutural surface of frontal. 113 – nasal sutural surface of frontal, 115 – frontal/parietal suture, 116 – parietal/squamosal suture, 117 – squamosal foramina, 118 – ?parietal/occipital suture, 133 – crack or maxilla/palatine suture? Fr – frontal; iof – infraorbital foramen; Mx – maxilla; Pa – parietal; Soc – supraoccipital; Sq – squamosal.

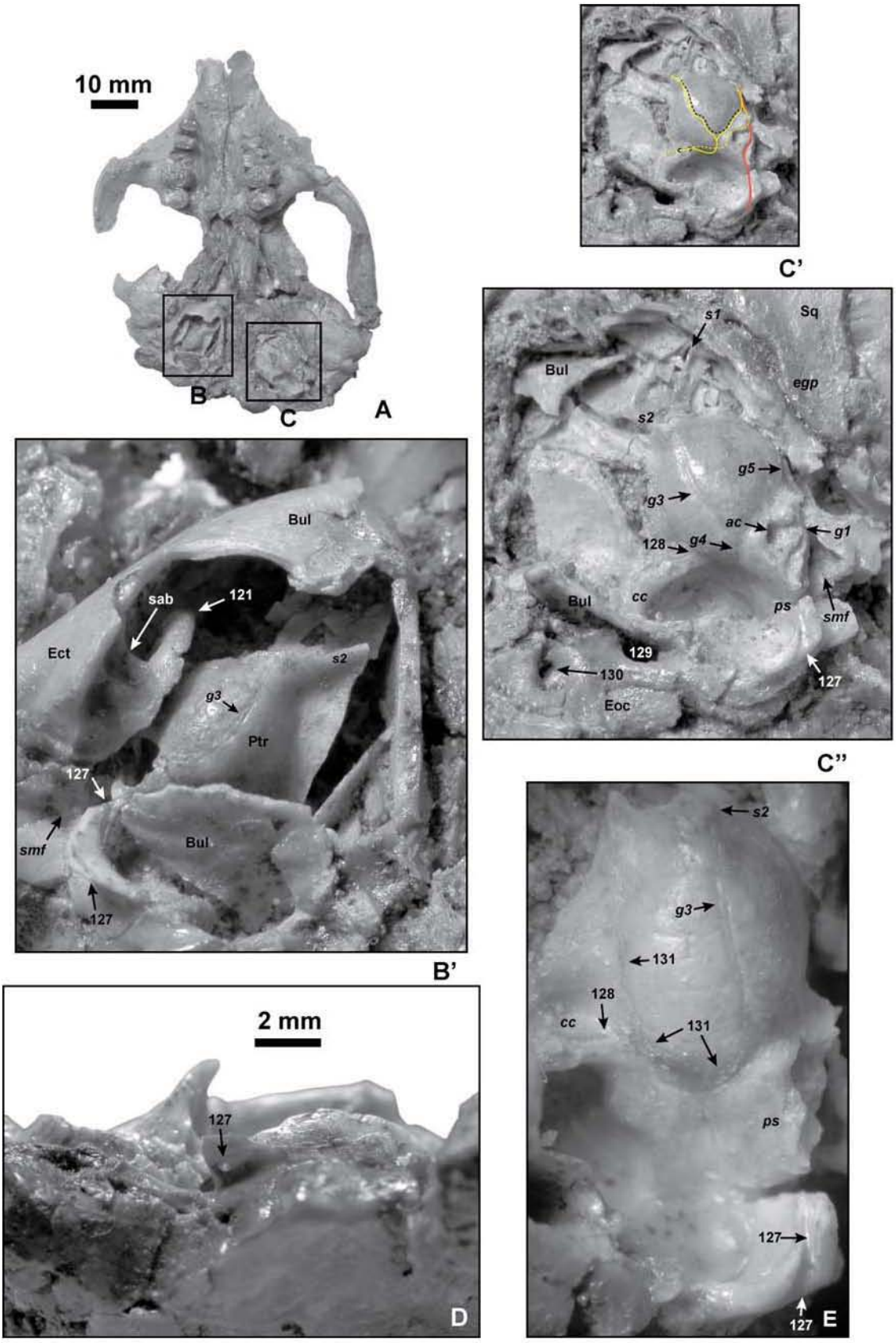
10 mm
A
B
C
C'
s1
Sq
Bul
egp
s2
g5
g3
ac
g1
128
g4
Bul
cc
ps
smf
129
130
127
Eoc
C''
Bul
sab
121
Ect
s2
g3
Ptr
127
smf
Bul
127
B'
2 mm
127
D
s2
g3
131
128
cc
131
ps
127
127
E

Figure 2.28

Figure 2.28. Pellouin skull *Plesiadapis tricuspidens*: A, ventral view. B, inset of right petrosal and bulla. B', labeled enlargement of inset B.C, inset of left petrosal and bullar fragments. C', enlargement of inset C with reconstructed vasculature. C'', labeled enlargement of inset C. D, posterior view of skull (ventral up) showing right posterior carotid foramen (*127*). E, labeled ventromedial view of left petrosal, showing grooves (*g3*), foramina (*127-128*), and apparent suture (*131*). Nerves reconstructed in yellow represent components of tympanic plexus. Neurovasculature reconstructed in red represents components of internal carotid plexus. Fine dashed line – g3 groove. Numbers and abbreviations: 121 – tympanic ring with annular bridge, 127 – posterior carotid foramen and carotid canal, 128 – foramen for tympanic and mastoid canaliculus, 129 – jugular foramen, 130 – hypoglossal foramen, 131 – possible suture along medial side of left promontorium. ac – aperture of cochlear fenestra; Bul – auditory bulla; cc – cochlear canaliculus; ps – posterior septum; Ect – ectotympanic; egp – entoglenoid process; Eoc – exoccipital; g1 – groove for internal carotid plexus; g3 - groove that leads to s2 (for a small vein?); g4 - groove for tympanic plexus fibers to reach routes g1-3; g5 – groove that leads toward epitympanic crest; Ptr – petrosal; s1 – first (anterior) septum; s2 – second septum; sab – strut connecting annular and bullar part of ectoympanic; smf – stylomstoid foramen; Sq – squamosal.

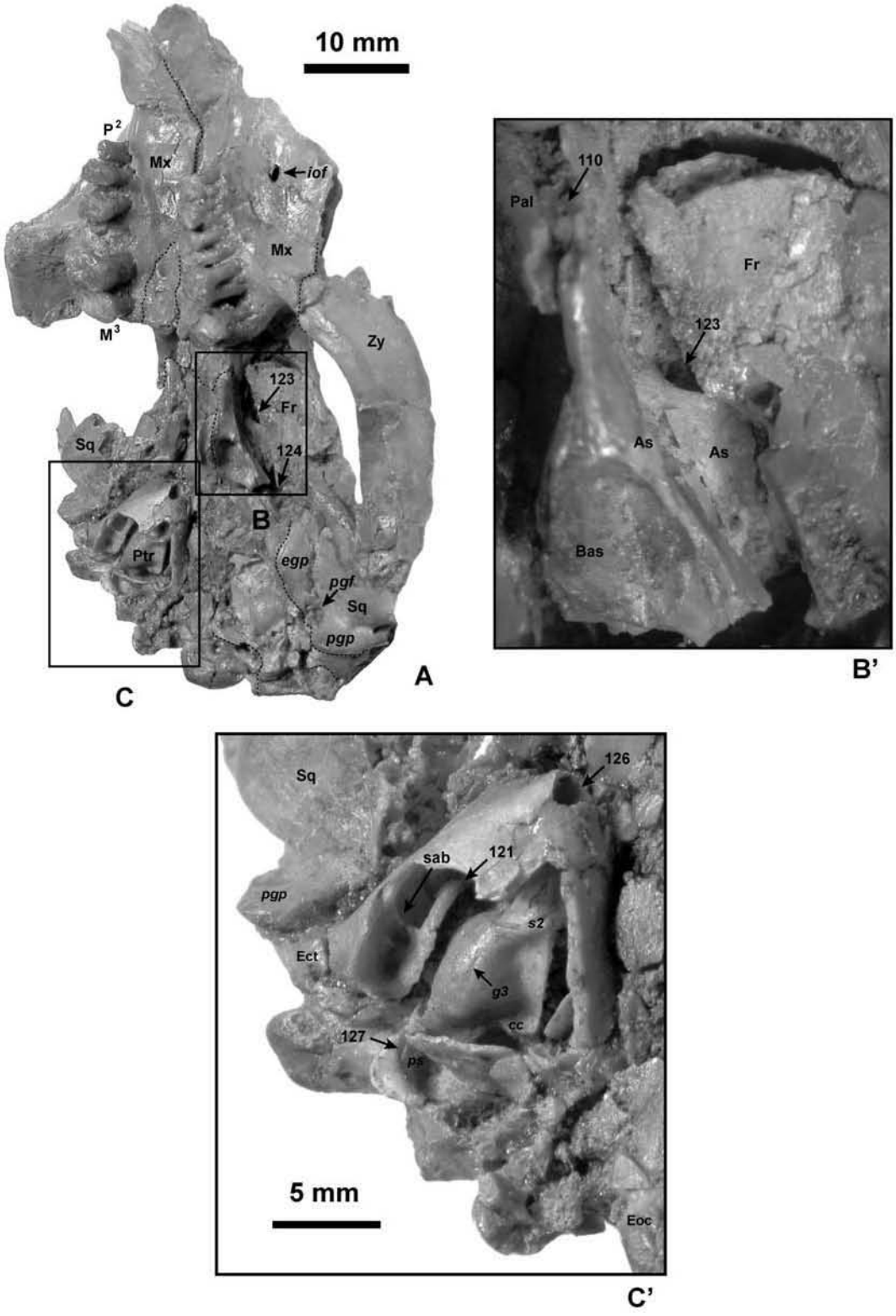
10 mm
P2
Mx
iof
Mx
M3
Zy
123
Fr
124
Sq
B
Ptr
egp
pgf
Sq
pgp
C
A
110
Pal
Fr
123
As
As
Bas
B'
126
Sq
sab
121
pgp
s2
Ect
g3
cc
127
ps
5 mm
Eoc
C'

Figure 2.29

Figure 2.29. Pellouin skull *Plesiadapis tricuspidens*: A, labeled left ventrolateral view. B, inset of left orbitotemporal region. B', enlargement of inset B showing sphenorbital fissure (*123*). Optic foramen is not visibly preserved. C, inset of right petrosal and bullar fragments. C', enlargement of inset C, showing tubal canal (*126*) opening. Numbers and abbreviations: 110 – palatine/alisphenoid suture, 121 – tympanic ring with annular bridge, 123 – sphenorbital fissure, 124 – foramen ovale fragment, 126 – tubal canal of right bulla, 127 – posterior carotid foramen and carotid canal. As – alisphenoid; Bas – basisphenoid; cc – cochlear canaliculus; ps – posterior septum; Bul – auditory bulla; Ect – ectotympanic; egp – entoglenoid process; Eoc – exoccipital; Fr – frontal; g3 - groove that leads to s2 (for a small vein?); iof – infraorbital foramen; Mx – maxilla; Pal – palatine; pgf – postglenoid foramen; pgp – postglenoid process; Ptr – petrosal; s1 – first (anterior) septum; s2 – second septum; sab – strut connecting annular to bullar part of ectotympanic; Sq – squamosal.

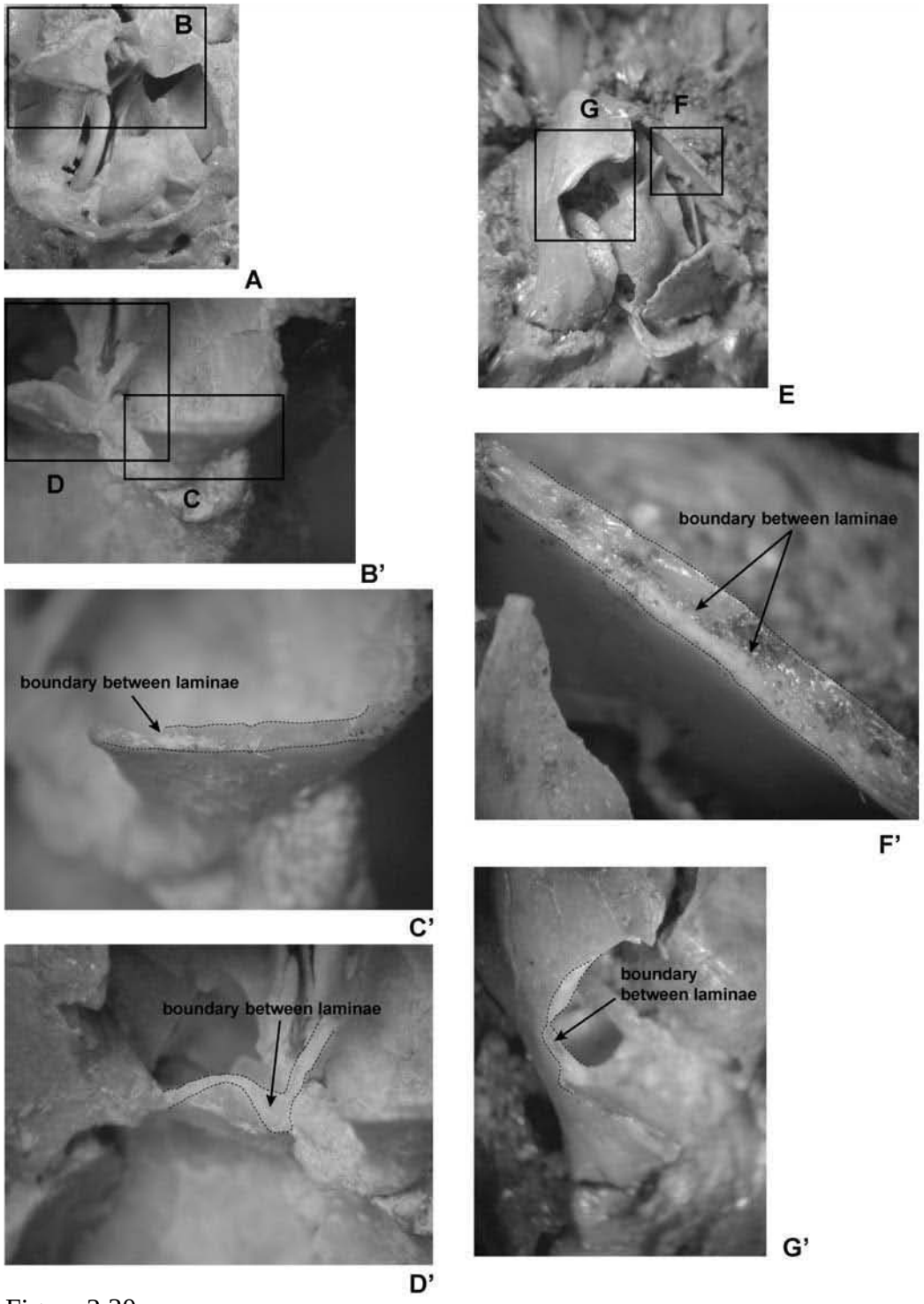
B
A
G
F
E
D
C
B'
boundary between laminae
F'
boundary between laminae
C'
boundary between laminae
boundary
between laminae
G'
D'

Figure 2.30

Figure 2.30. MaPhQ 33y *Adapis parisiensis* (A-D): A, ventral view of right petrosal and bulla (anterior up). B, inset of broken edges of bulla. B', enlargement of inset B, rotated 180 degrees in plane of page (anterior down). C, inset of lateral part of broken edge of bulla. C', enlargement of inset C – lateral flange of bulla showing double laminae. D, inset of more medial part of broken edges of bulla. D', enlargement of inset D – anterior part of bulla showing double laminae. Pellouin skull *Plesiadapis tricuspidens* (E-G): E, ventral view of right petrosal and bulla. F, inset of broken medial process. F', enlargement of inset F – medial flange of bulla showing double laminae. G, inset of broken lateral process. G', enlargement of inset G – lateral edge of bulla showing double laminae. Broken edges are highlighted with dashed lines. The two laminae illustrated to comprise the bony wall of the bulla may be derived from two, or more likely, a single cranial bone. The bulla is probably petrosal-derived in both taxa shown here.

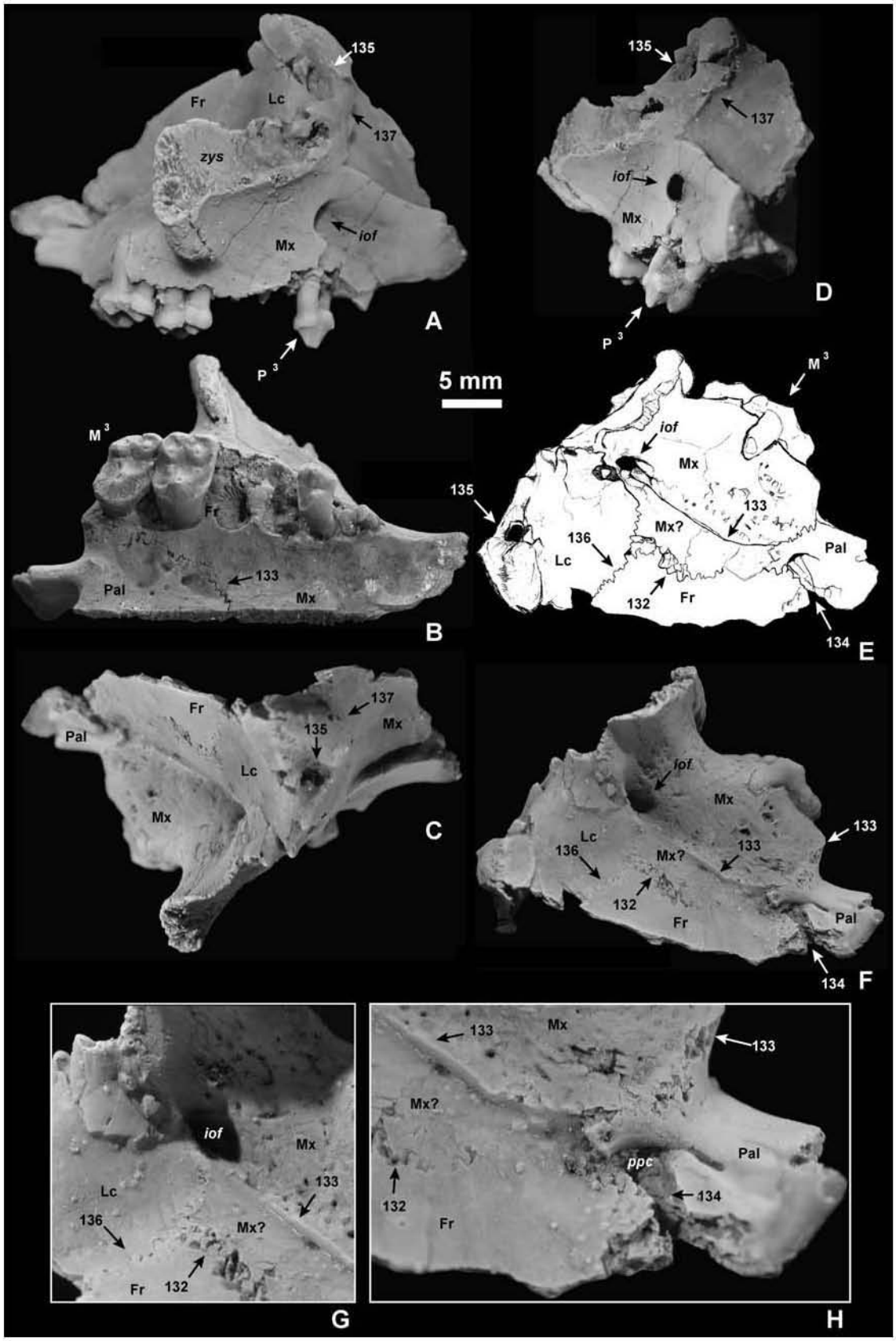
135
Fr
Lc
137
zys
Mx
iof
A
P 3
5 mm
M 3
Fr
Pal
133
Mx
B
135
137
iof
Mx
D
P 3
M 3
iof
Mx
135
133
Mx?
136
Lc
Pal
132
Fr
134
E
Fr
137
135
Mx
Pal
Lc
Mx
C
iof
Mx
133
Lc
136
133
Mx?
132
Fr
Pal
134
F
iof
Mx
133
Lc
136
Mx?
132
Fr
G
133
Mx
133
Mx?
Pal
ppc
132
134
Fr
H

Figure 2.31.

Figure 2.31. MNHN CR 126, *Plesiadapis tricuspidens*: A, lateral view of right cranial midface fragment. B, ventral view. C, dorsal view. D, anterior view. E, drawing of dorsolateral view. F, dorsolateral view. G, enlargement of anterior region from part F. H, enlargement of posterior region from part F. Note that bone labeled "Mx?" can only be considered as "maxilla" if (1) there is a suture spanning between *132* and *133* close to the *ppc*, and (2) the labeled, more anterior part of *133* actually represents a crack. A suture spanning *132* and *133* is not clearly visible. The existence of a ridge of bone on the Pellouin skull that would correspond to the anterior part of the maxillary process of *133* suggests that *133* may *not* be a crack in this region. If neither (1) or (2) are true then "Mx?" would actually correspond to the palatine. If only (1) is true then "Mx?" may represent an ethmoid os planum. Numbers and abbreviations: 132 – Frontal/maxilla suture in orbit, 133 – crack or maxilla/palatine suture?, 134 – region of palatine/frontal contact in postpalatine canal (broken), 135 – lacrimal foramen, 136 – lacrimal/frontal suture, 137 – lacrimal/maxilla suture. Fr – frontal; iof – infraorbital foramen; Lc – lacrimal; Mx – maxilla; Mx? – possible fragment of maxilla; Pal – palatine; zys – sutural surface on maxilla for zygomatic.

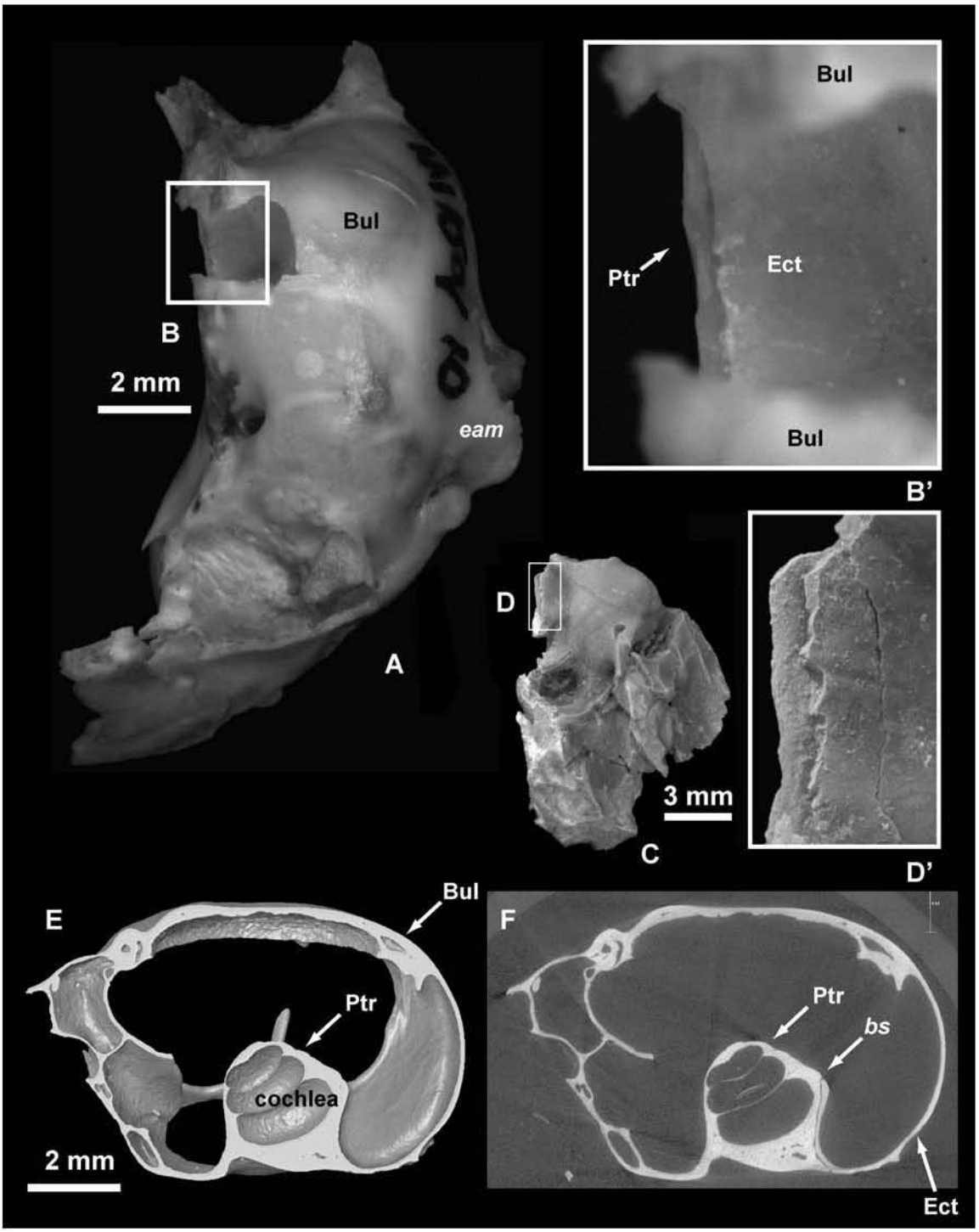
Bul
B
2 mm
eam
A
Bul
Ptr
Ect
Bul
B'
D
3 mm
C
D'
E
Bul
Ptr
cochlea
2 mm
F
Ptr
bs
Ect
Figure 2.32

Figure 2.32. SBU MRd-12 *Sciurus caroliniensis* (A-B', E-F): A, ventral view of left petrosal and ectotympanic bulla. B, ventral view, inset of medial region of bulla. B', enlargement of inset B. Note appearance of medial process of petrosal projecting beyond ventrally located, broken lamina of ectotympanic. UALVP 49105 *Pronothodectes gaoi* (C-D'): C, ventral view of left petrosal. D, ventral view, inset of medial tympanic process. D', enlargement of inset D. Note similarity of broken medial process to that in B'. E, anterior view, surface reconstruction of HRxCT data. F, anterior view of HRxCT slice. Anterior to top in A-D.' Lateral to left in E and F. Note that ectotympanic and petrosal boundary are clearly visible. Numbers and abbreviations: bs – bullar suture; Bul – auditory bulla; eam – external auditory meatus; Ect – ectotympanic; Ptr – petrosal.

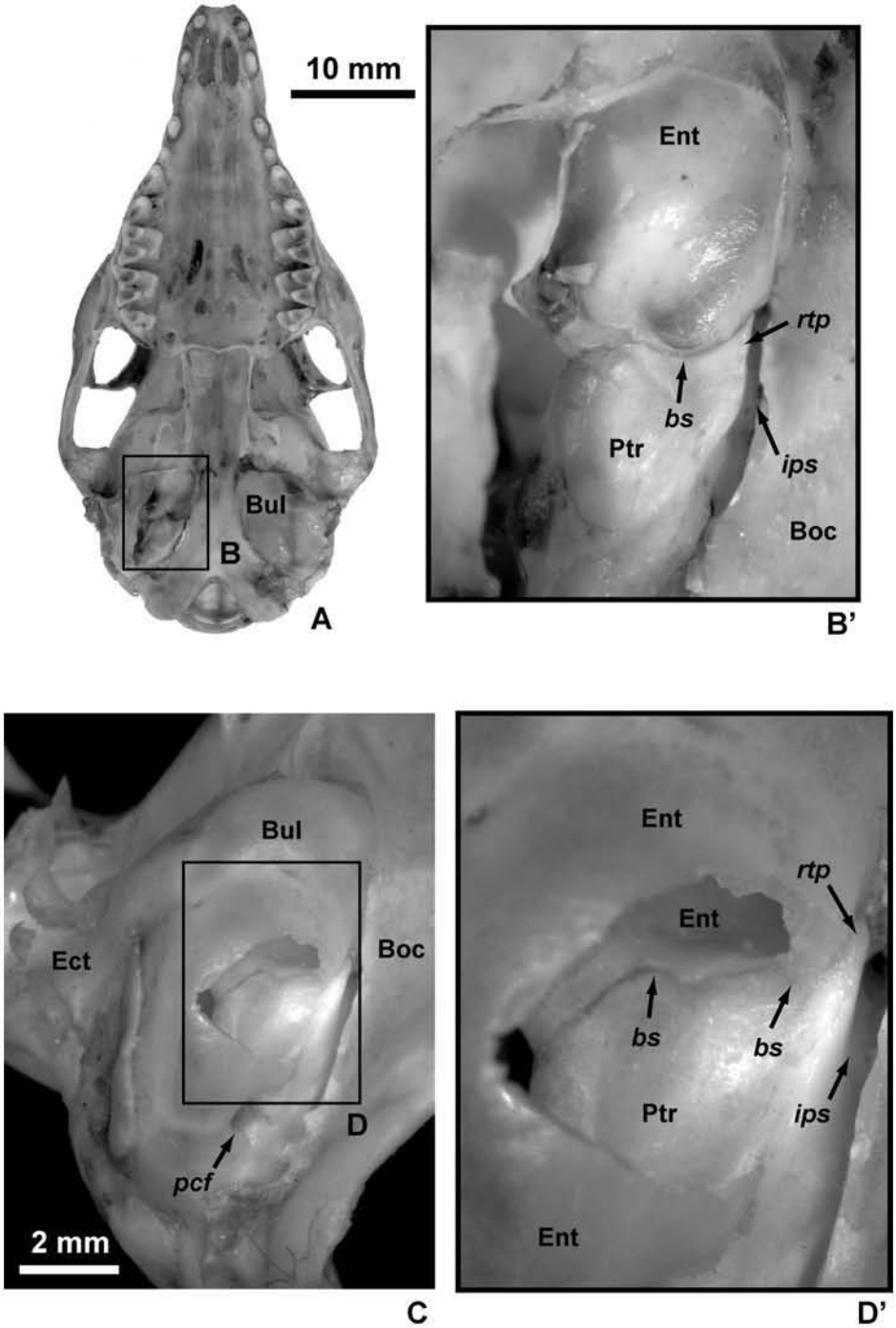
10 mm
Bul
B
A
Ent
rtp
bs
Ptr
ips
Boc
B'
Bul
Ect
Boc
D
pcf
2 mm
C
Ent
rtp
Ent
bs
bs
Ptr
ips
Ent
D'

Figure 2.33

Figure 2.33. UMMZ 58983 *Tupaia glis* (A, B, B'): A, ventral view of skull. B, inset of right basicranium. B', enlargement of inset B. SBU coll. *Tupaia glis* (C, D, D'): C, ventral view of right basicranium. D, inset of suture in right basicranium. D', enlargement of inset D. Note that ear morphology of this taxon is generally similar to that in *Sciurus* (Fig. 2.35). Medial process of petrosal is not well-developed, however, rostral process just anterior to where medial process would be located is present and dorsally buttresses lamina of entotympanic bone that lies ventral to it. Numbers and abbreviations: bs – bullar suture; Boc – basioccipital; Bul – auditory bulla; Ent – entotympanic; Ect – ectotympanic; ips – inferior petrosal sinus; pcf – posterior carotid foramen; rtp – rostral process of petrosal.

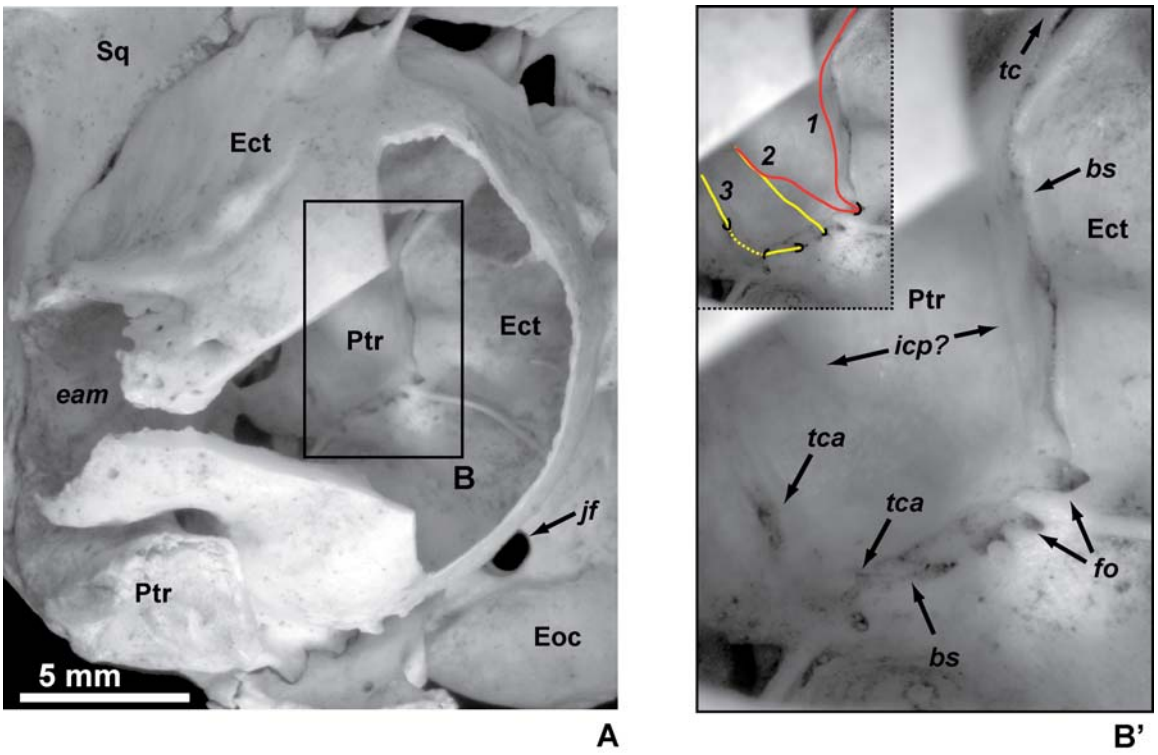
Sq
Ect
Ptr
Ect
eam
B
jf
Ptr
Eoc
5 mm
A
tc
1
2
3
bs
Ect
Ptr
icp?
tca
tca
fo
bs
B'

Figure 2.34

Figure 2.34. Boyer coll. *Marmota monax*: A, ventral view of right basicranium. B, inset of suture between petrosal and ectotympanic bones. B', enlargement of inset B, with reconstruction of neurovascular pathways. Anterior to top in all parts. *1* and *2* represent internal carotid plexus branches; *3* represents tympanic nerve. Stapedial artery is functional and enters bulla posteromedially. Given that this artery is only remnant of internal carotid system, it is likely that nerve plexus related to it also entered medially. Foramina apparent on medial side of promontorium lead to grooves that course laterally (*2*) and one that leads to *s2* (*1*). *s2* of *Marmota* is apparently not homologous to that in plesiadapids because in *Marmota* it leads to tubal canal (as *s1* does in plesiadapids and euprimates). The internal carotid plexus should send branches toward tubal canal. Thus the particular route of these grooves is another point supporting interpretation of them. Most posteriorly situated groove (*3*) likely relates to tympanic plexus as it leads from jugular foramen, courses laterally in groove that is sometimes shallowly floored by petrosal (and thus forms canal at these points) – probably going toward site of formation of tympanic plexus. Morphology relating to at least tympanic nerve of *Marmota* is thus similar to that in *Lagostomus* (see below), plesiadapids and even some euprimates (MacPhee, 1981). Numbers and abbreviations: bs – bullar suture; eam – external auditory meatus; Ect – ectotympanic, Eoc – exoccipital; fo – foramen; internal carotid plexus? – possible internal carotid plexus route; jf – jugular foramen; Ptr – petrosal; Sq – squamosal; tc – tubal canal; tca – tympanic canaliculus.

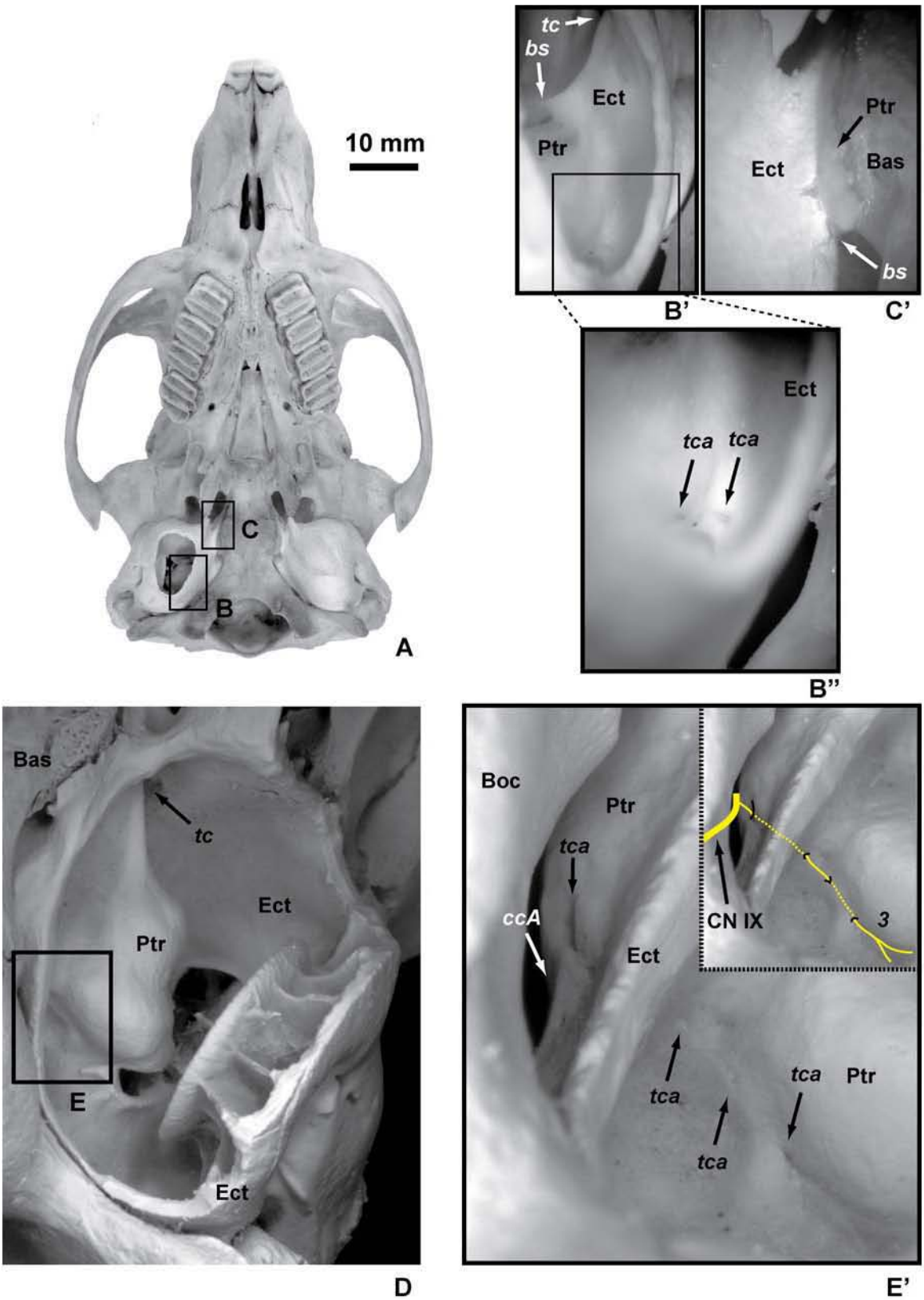
10 mm
C
B
A
tc
bs
Ect
Ptr
B'
Ptr
Ect
Bas
bs
C'
Ect
tca
tca
B''
Bas
tc
Ect
Ptr
E
Ect
D
Boc
Ptr
tca
ccA
CN IX
3
Ect
tca
tca
tca
Ptr
E'

Figure 2.35

Figure 2.35. UMMZ TS13 *Lagostomus maximus* (A-C): A, ventral view of skull. B, inset of right tympanic cavity. B', enlargement of inset B. B", enlargement of inset in B'. C, inset of anterior end of bulla. C' enlargement of inset C. There is distinct color difference visible near where petrosal/ectotympanic boundary must be in B', B" and C'. Note that in B" more medial (farther right) *tca* foramen represents opening of tympanic canaliculus into tympanic (bullar) cavity. *tca* foramen to left is beginning of shallow canal that represents continued lateral course of branches of tympanic nerve. AMNH 41522 *Lagostomus maximus* (D-E'): D, ventral view of left petrosal. Bulla has been cut away in this specimen. E, inset of medial aspect of promontorium. E', enlargement of inset E. Unlike *Marmota, Lagostomus* only has grooves on its promontorium relating back to tympanic canaliculus in wall of jugular foramen (internal carotid plexus apparently does not enter tympanic cavity from medial position in *Lagostomus*). In E' *tca* foramen farthest to left represents initial opening of tympanic canaliculus into bullar cavity. Next foramen to right represents beginning of canal for continued course of nerve, while that farthest to right represents end of this short, shallowly floored canal. Grooves and canals leading from here across promontorium appear similar to morphology in this region in plesiadapids and in *Marmota*. Numbers and abbreviations: Bas – basisphenoid ; Boc – basioccipital ; bs – bullar suture ; ccA – aperture for cochlear canaliculus ; Ect – ectotympanic ; Ptr – petrosal ; tc – tubal canal ; tca – tympanic canaliculus.

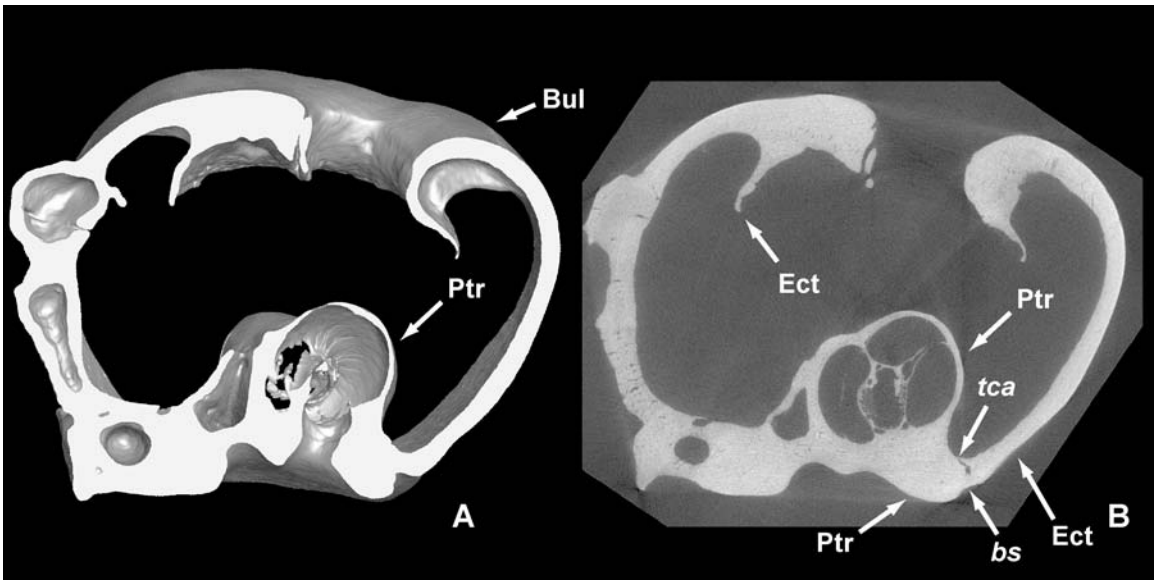

Figure 2.36

Figure 2.36. AMNH 41527 *Lagostomus maximus*: A, anterior view of left petrosal and ectotympanic, surface reconstruction of HRxCT data. B, anterior view of HRxCT slice. HRxCT imagery shows that, despite color difference visible at ectotympanic/petrosal boundary (Fig. 2.38B'-C'), there is no internally visible density difference or sutural surface. However, tympanic canaliculus can be traced through medial process and appears to follow ectotympanic/petrosal boundary. Numbers and abbreviations: bs – bullar suture; Bul – auditory bulla; Ect – ectotympanic; Ptr – petrosal; tca – tympanic canaliculus.

Figure 2.37

Figure 2.37. AMNH 185638 *Indri indri*: A, stereophotographic medial view of left petrosal with broken bulla and medial tympanic process. B, enlarged medial view. Anterior to bottom in both parts. Interestingly, broken medial process appears to be comprised of two bony lamina and looks just like broken medial process of taxa that have non-petrosal bulla, as well as that of plesiadapids (Figs. 2.35, 36). Euprimates, including *Indri*, have petrosal bulla, thus multiple laminae cannot be taken as evidence of multiple bones in this region. Numbers and abbreviations: icp – internal carotid plexus; Ptr – petrosal; s1 – first (anterior) septum: most lateral septum extending anteriorly from promontorium (tubal canal forms between s1 and epitympanic crest); s2 – second septum: forms medial to s1and projects anteromedially from promontorium (g3 typically leads to the ventral or medial aspect of this septum); tng? – tympanic nerve groove?

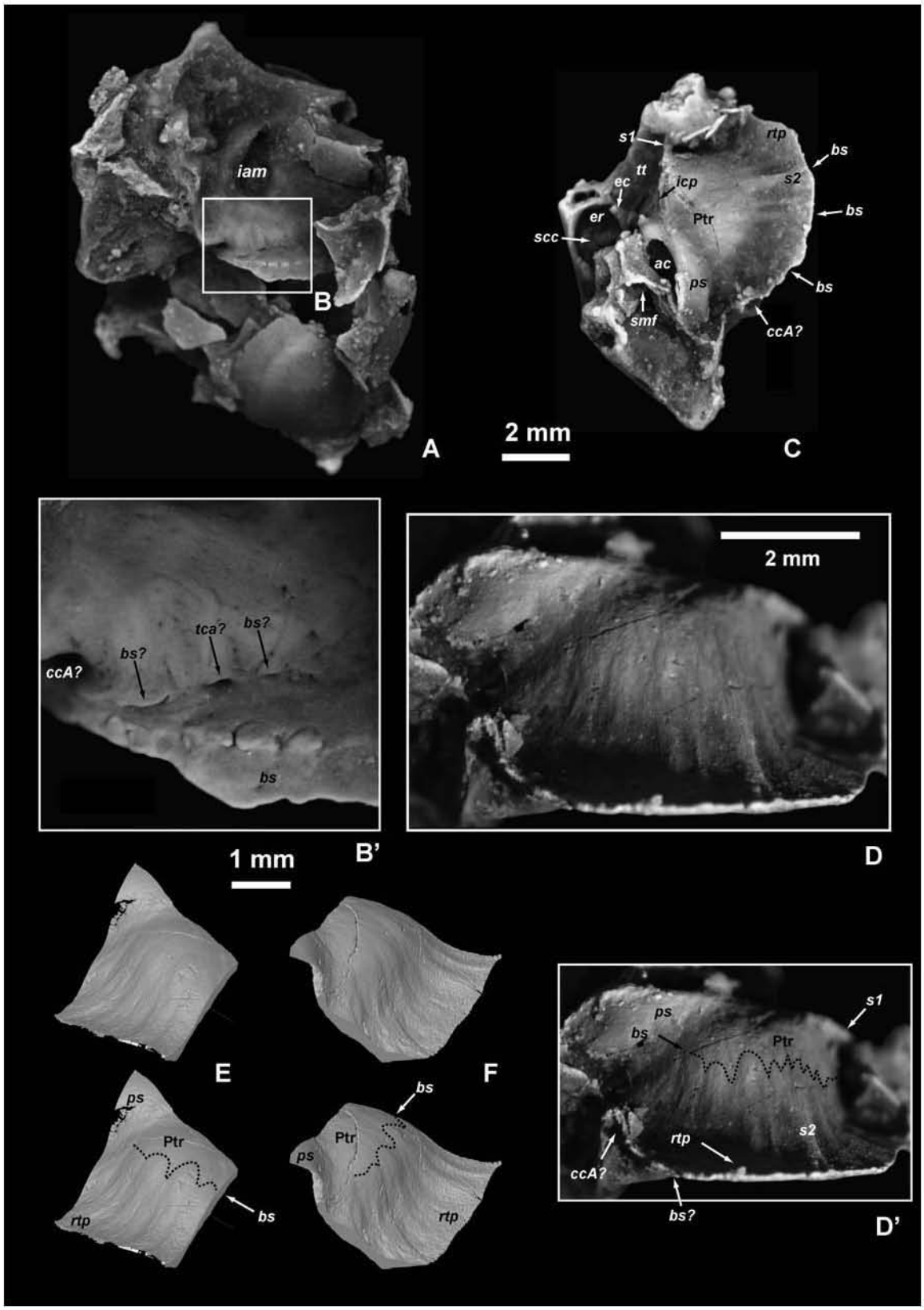
iam
B
A
2 mm
s1
rtp
bs
tt
ec
icp
s2
er
Ptr
bs
scc
ac
ps
bs
smf
ccA?
C
bs?
tca?
bs?
ccA?
bs
B'
1 mm
2 mm
D
E
F
ps
Ptr
rtp
bs
bs
Ptr
ps
rtp
ps
bs
s1
Ptr
s2
rtp
ccA?
bs?
D'

Figure 2.38

Figure 2.38. USNM 482353 *Ignacius clarkforkensis*: A, dorsal view of left ear region (anterior to right, lateral to top). B, inset of medial edge of medial tympanic process. B', enlargement of inset B. Note apparent sutural groove in addition to sutural surface for ectotympanic (as identified by Kay et al., 1992 and Bloch and Silcox, 2001). C, labeled ventral view of right ear (anterior to top). D, medial view of right ear. D', annotated medial view of right ear with dashed line highlighting fairly crisp, although subtle margin of ridges on medial process that may represent suture. E, anteromedial view of HRxCT reconstruction of right ear. F, posterior view of HRxCT reconstruction of right ear. Ventral to top in D-F. E and F illustrate course of boundary between medial tympanic process ridges and promontorium. Numbers and abbreviations: ac – aperture for cochlear fenestra, bs – bullar suture; cc – cochlear canaliculus; ccA – aperture for cochlear canaliculus; ps – posterior septum; ec – epitympanic crest; er – epitympanic recess; icp – internal carotid plexus; Ptr – petrosal; rtp – rostral tympanic process; s1 – first (anterior) septum (tubal canal forms between s1 and epitympanic crest); s2 – second septum forms medial to s1; scc – semicircular canal; tt – tegmen tympani.

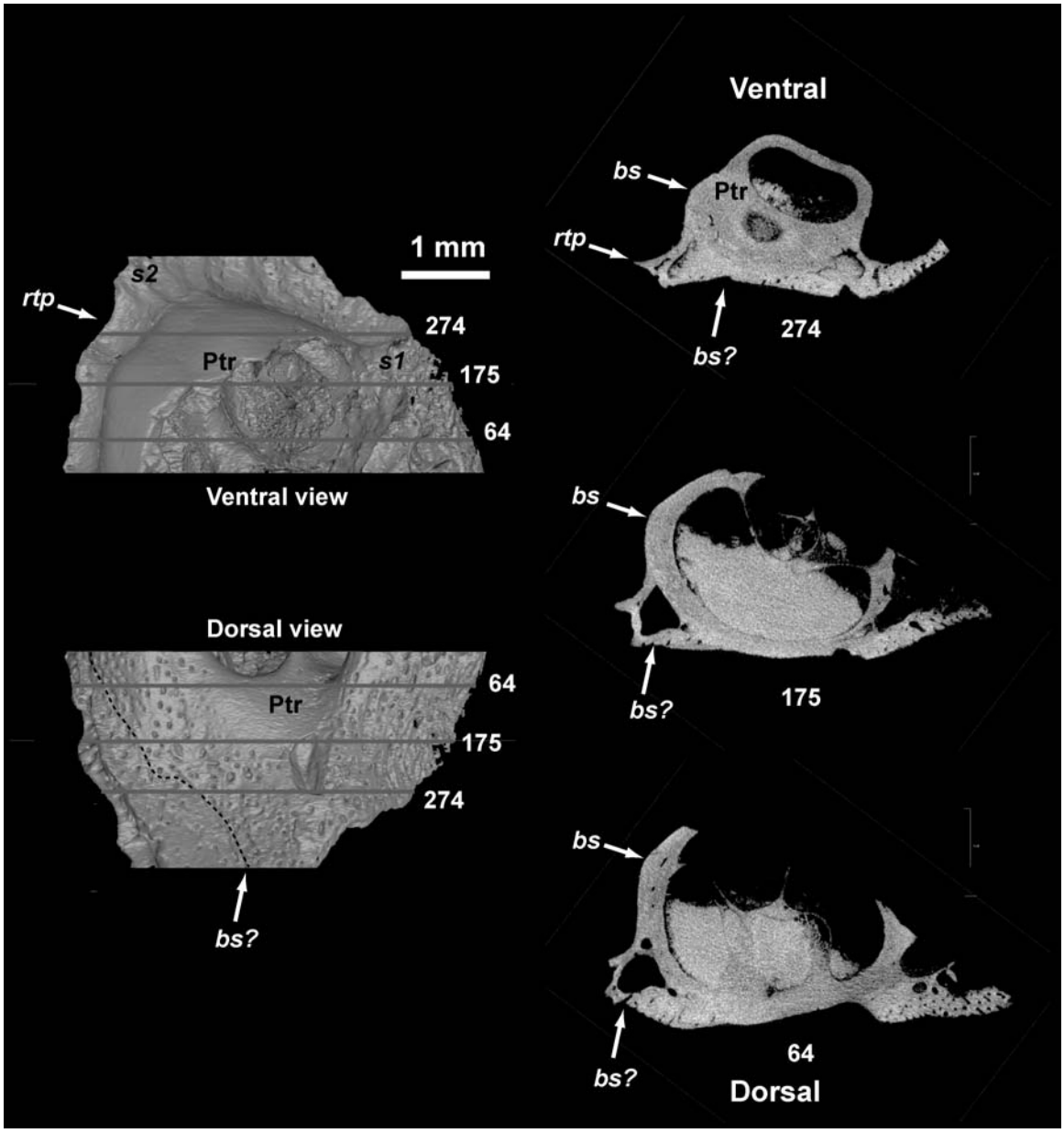
Ventral
bs
Ptr
rtp
274
bs?
1 mm
s2
rtp
274
Ptr
s1
175
64
Ventral view
bs
Dorsal view
64
Ptr
175
bs?
175
274
bs
bs?
64
bs?
Dorsal

Figure 2.39

Figure 2.39. UM 108207 *Acidomomys hebeticus*: Left promontorial fragment of petrosal HRxCT surface reconstructions and individual slices (64, 175, and 274 – slice numbers increase anteriorly). Medial is to left in all images. This individual is a juvenile with very porous bone, unshed deciduous teeth and unerupted adult teeth. These images were acquired to evaluate whether grooves illustrated for adult *Ignacius* specimen in Fig. 2.41B (*bs?*) and Fig. 2.41 D-F (*bs*) are in fact sutures. There is a density difference between dorsal region of bone and cochlea containing bone, specifically. Thus, structures illustrated for *Ignacius* in Fig. 2.41D-F appear to be sutural in that they are a meeting of two different types of bone, but that in Fig. 2.41B appears to be a meeting of two different outgrowths from same bone. The bone forming the medial process of the petrosal appears to extend over entire dorsal surface of bones housing cochlea in this specimen, and thus likely represents part of temporal bone (see text). Numbers and abbreviations: bs – bullar suture; Ptr – petrosal; rtp – rostral tympanic process; s1 – first (anterior) septum; s2 – second septum: forms medial to s1.

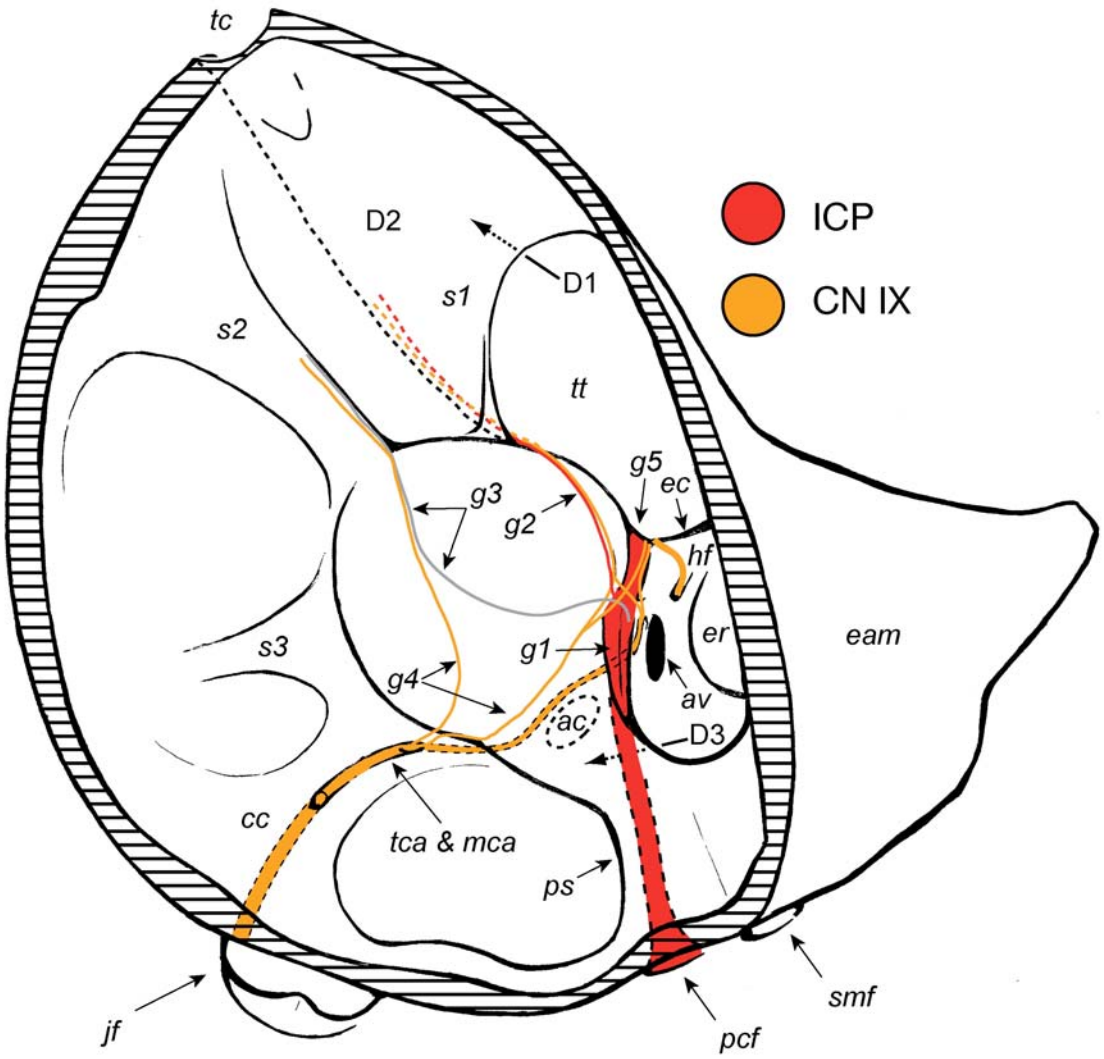
tc
D2
D1
s1
s2
tt
ICP
CN IX
g5
ec
g3
g2
hf
er
eam
s3
g1
g4
av
ac
D3
cc
tca & mca
ps
smf
jf
pcf

Figure 2.40

Figure 2.40. Reconstruction of plesiadapid ear based on all available specimens. Note that specimen of *P. tricuspidens* differ from this picture in having more tubular *eam*, and a more flaring annular component to ectotympanic. Furthermore only *Pr. gaoi* and a single specimen referable to *P. tricuspidens* appear to exhibit *s3*. The main source of confusion in how to interpret this anatomy in previous studies has stemmed from variable expression of variously and variably distributing branches of tympanic plexus (yellow) combined with small sample sizes (usually no more than one or two specimens) for each species. This drawing illustrates some of the likely variations represented in tympanic plexus distribution by different specimens. Major neurovascular routes formed by CN IX and internal carotid plexus include following: *g1*) lateral route that begins at posterior carotid foramen and proceeds through short canal to lateral aspect of promontorium – it likely held internal carotid plexus and possibly remnant of *ica*; *g2*) slightly more medial route that appears to stem anteriorly from *g1* and probably held internal carotid plexus fibers. This groove approaches *s1* and probably represents sympathetic fibers destined to join with cranial nerves after entering endocranial space through foramen lacerum, anterodorsal to opening of tubal canal; *g3*) route that leads to *s2*, which likely contains contributions from the tympanic plexus, but primarily holds a small vein (MacPhee, 1981); *g4*) frequently present alternative or additional route for tympanic plexus fibers to reach routes 1-3, and 5; *g5*) a groove that sometimes appears as an anterior continuation of *g1* and is dorsolateral to *g2*. It is quite broad and may represent place of formation of the main part of tympanic plexus. Deep petrosal nerve likely stemmed from this point to meet greater petrosal nerve, which seems to have emerged just lateral to this groove from hiatus fallopi. Numbers and abbreviations: ac – aperture for cochlear fenestra; av – aperture for fenestra vestibuli; cc – cochlear canaliculus; CN IX – ninth cranial neve (glossopharyngeal) nerve fibers; D1-3 – bullar cavity diverticula of MacPhee (1981); eam – external auditory meatus; ec – epitympanic crest; er – epitympanic recess; icp – internal carotid plexus; iof – infraorbital foramen; jf – jugular foramen; pcf – posterior carotid foramen; s1 – first (anterior) septum: (=S2 of Russell, 1964) most lateral septum extending anteriorly from promontorium (tubal canal forms lateral to s1; D1 and D2 are separated by s1); s2 – second septum (probably equivalent of medial secondary septum of MacPhee (1981): (=S1 of Russell, 1964) forms medial to s1 and projects anteromedially from promontorium (g3 typically leads to ventral or medial aspect of this septum); s3 – third septum: projects medially between s2 and raised ridge of cochlear canaliculus, more posteriorly; spf – sphenorbital fissure; tc – tubal canal; tca&mca – combined tympanic and mastoid canaliculus; tt – tegmen tympani.

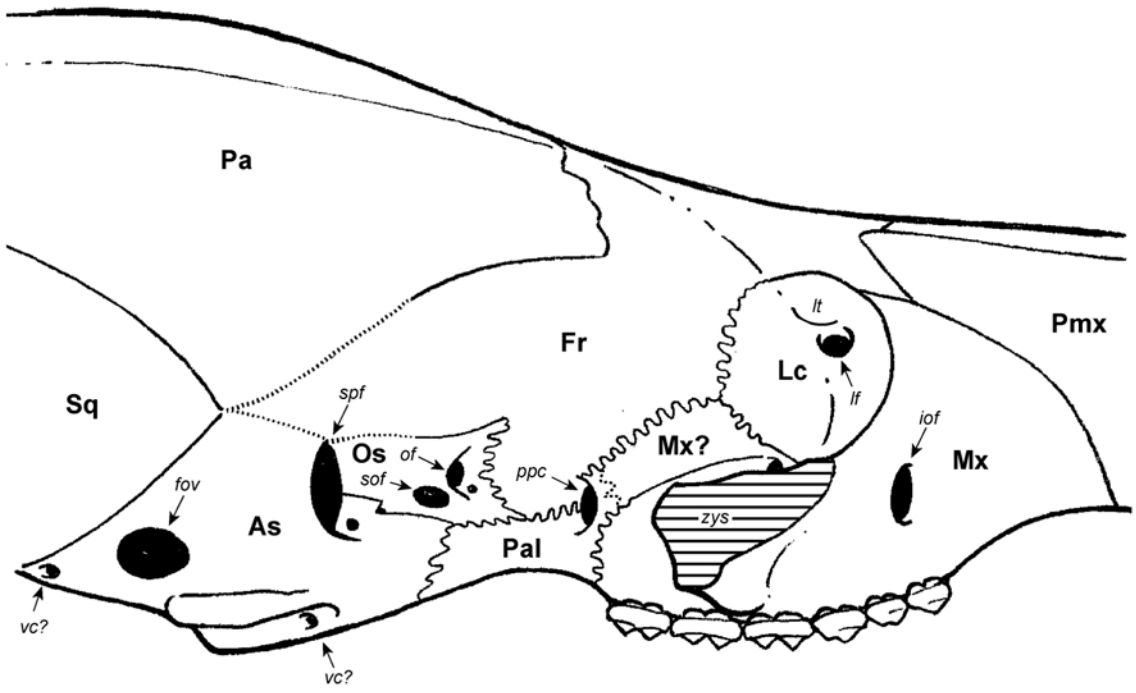

Figure 2.41. Plesiadapidae orbitotemporal suture/foramina reconstruction. Completely hypothetical sutures are shown as dotted lines. There seems to be some variability in position of alisphenoid/orbitosphenoid suture based on two specimens where it is interpreted as being partly preserved. Drawing represents what seems likely to be average position. In MNHN CR 125 it is more ventrally located than shown in photograph in Fig. 2.20D', while in MNHN CR 965 it is more dorsally located (Fig. 2.24A, C'). Style of illustration is based on that in Russell (1964: fig. 19) and Gingerich (1976: fig. 33). Numbers and abbreviations: As – alisphenoid; fov – foramen ovale; Fr – frontal; iof – infraorbital foramen; Lc – lacrimal; lf – lacrimal foramen; lt – lacrimal tubercle; Mx – maxilla; Mx? – possible fragment of maxilla; of – optic foramen; Pa – parietal; Pal – palatine; ppc – postpalatine canal; sof – suboptic foramen; spf – sphenorbital fissure; Sq – squamosal; vc? – possible entrance to vidian canal; zys – sutural surface on maxilla for zygomatic.

CHAPTER 3:
DESCRIPTION OF THE FIRST KNOWN CRANIUM OF *PLESIADAPIS COOKEI*, COMPARISON TO *P. TRICUSPIDENS*, AND CONSIDERATION OF SOME FUNCTIONAL ASPECTS OF DENTITION

ABSTRACT

I describe the first known skull of the plesiadapid *Plesiadapis cookei* UM 87990 from the middle Clarkforkian North American Land Mammal Age of the Clarks Fork Basin, Wyoming. This taxon has been described from its dentition as morphologically intermediate between the European taxa *Plesiadapis tricuspidens* and *Platychoerops russelli*, with which it existed penecontemporaneously. I compare skull morphology and aspects of the dentition of *P. cookei* with samples of *P. tricuspidens* and other plesiadapids. The cranium of *P. cookei* is very similar to that of *P. tricuspidens* in most respects and appears to have been of roughly the same size. However, the skull of *P. cookei* differs in (1) having larger teeth, (2) having a more molariform P_4, (3) lacking a P^2, (4) having broader nasal bones, (5) having smaller glenoid fossae, (6) possibly having a less expanded annular component to its ectotympanic bone, and (7) having a more posteriorly projecting nuchal crest. Features 3-7 make *P. cookei* more similar to earlier-occurring North American plesiadapids such as *Plesiadapis anceps, Nannodectes intermedius*, and *Pronothodectes gaoi*. The proportionally and absolutely larger teeth of *P. cookei*, compared to those of *P. tricuspidens*, are a curious distinctive feature. However, further consideration of other dental features, including orientation patch counts and relief index generated from scan data, suggests that large teeth in *P. cookei* reflect a specialized folivorous diet. Specifically, as compared to *P. tricuspidens*, *P. cookei* has a dentition with higher molar relief, greater molar complexity, more advanced molarization of premolars, and simpler central incisors. Therefore, despite being similar in their large body size, *P. cookei* in North America and *P. tricuspidens* in France probably inhabited different dietary niches.

INTRODUCTION

Among North American plesiadapids, one of the latest occurring and largest species is *Plesiadapis cookei* (Jepsen, 1930; Gingerich, 1976). The only known skull of *P. cookei* was discovered with an associated skeleton in late Paleocene strata of the Clarks Fork Basin in 1987 (Gunnell and Gingerich, 1987; Gingerich and Gunnell, 1992, 2005; Bloch and Silcox, 2001). The specimen has not yet received a thorough description or analysis despite the fact that the skull is arguably the most complete known for a North American plesiadapid. In some respects this new skull is even better preserved than the nearly complete skulls of *P. tricuspidens*, an apparently slightly smaller species (e.g., Fleagle, 1999) from the Paris Basin in France (Russell, 1964; Gingerich, 1976).

In light of its large body size, one might expect *P. cookei* to be evolutionarily derived in many respects compared to basal members of Plesiadapidae, which appear to be much smaller. However, the skull of *P. cookei* may still retain features that were present in the ancestral plesiadapid. Thus, a thorough understanding of the morphology of *P. cookei* is relevant to further assessing predictions generated by cladistic hypotheses that postulate plesiadapids as a sister group to carpolestids and as a close relative of anatomically modern primates (= Euprimates: Hoffstetter, 1977) (Bloch and Silcox, 2006; Bloch et al., 2007).

Another reason to study *P. cookei* relates to inferred environmental and ecological changes that bracket its existence in North America (e.g., Zachos et al., 2001). Understanding how this taxon differs morphologically from earlier (North American) and later (European) plesiadapids may reveal the nature of ecological differences among

these species. Changing ecological niches among plesiadapids through the late Paleocene are likely to track environmental changes experienced by these animals during this time period (Gingerich, 1976).

Gingerich (1976) argued that one of the most dramatic ecological/evolutionary transitions documented for plesiadapids occurred in a lineage leading from *P. tricuspidens* to *Platychoerops russelli* to *Platychoerops daubrei*. In this hypothesized lineage, the molar and incisor teeth exhibit a morphocline from bunodont and complex (respectively) in *P. tricuspidens* to selenodont and simple in *Pl. daubrei.* Gingerich (1976) suggested that this morphocline reflects an ecological/evolutionary transition from a generalized diet to a highly folivorous diet.

Gingerich (1976) also stated that *P. cookei* is dentally very similar to *Pl. russelli*. If *P. cookei* and *Pl. russelli* share a close phylogenetic relationship, their dental similarities may represent a commonly inherited trait, or one may have inherited its morphology more or less directly from the other. In the latter scenario, *P. cookei* could be a member of the *P. tricuspidens-Pl. russelli-Pl. daubrei* lineage and may represent a point on the morphocline described above. Alternatively, *P. cookei* and *Pl. russelli* may have each evolved separately from more bunodont forms like *P. tricuspidens* in response to similar ecological perturbations (e.g., changes in available food resources due to climate change). Either way the cranium and additional detailed aspects of the dentition of *P. cookei* might be expected to differ from those of *P. tricuspidens* in ways suggesting a more folivorous diet.

Major objectives

The current study provides the first thorough description and comparison of the skull of *Plesiadapis cookei* (UM 87990). As a result of this descriptive work, I address several persistent questions regarding the morphology of this specimen in greater detail than done in previous work. With regard to the composition of the auditory bulla, I assess whether morphology of the medial tympanic process of the promontorium suggests the presence of a suture. Additionally, I evaluate whether there is evidence for a suture between the lateral aspect of the bulla and the ectotympanic bone.

Following basic descriptions, I make focused comparisons of the *P. cookei* material to a sample of cranial specimens of *P. tricuspidens* and assess whether species-level size and shape differences exist. Using a set of measurements from Chapter 2, I make well-constrained estimates of relative skull sizes in *P. cookei* and *P. tricuspidens*, as well as other plesiadapids, to test the hypothesis that *P. cookei* is larger than *P. tricuspidens*. Finally, I test the hypothesis that *P. cookei* has a more specialized folivorous diet than *P. tricuspidens* through examination of a number of dental features. This analysis has implications for the hypothesis that *P. cookei* is plausibly reconstructed as a point along a morphocline reflecting a transition from more generalized to more specialized folivorous diets in plesiadapids (Gingerich, 1976).

Anatomical terminology

See Chapter 2. The same sources are referenced here as in the previous chapter.

Institutional abbreviations

AMNH, American Museum of Natural History, New York; MNHN, Muséum Nationale d'Histoire Naturelle, Paris; SBU – Stony Brook University; UALVP, University of Alberta, Laboratory for Vertebrate Paleontology; UM , University of Michigan Museum of Paleontology, Ann Arbor; USNM, United States National Museum of Natural History, Smithsonian, Washington D.C.; YPM-PU, Yale Peabody Museum – Princeton University collection, New Haven.

Generic abbreviations

I. - Ignacius

P. – Plesiadapis

Pl. - Platychoerops

Pr. – Pronothodectes

N. – Nannodectes

History of descriptive study of Plesiadapidae

Existing studies on crania of Plesiadapidae, including previous mention of the specimen described here, were summarized in Chapter 2. Furthermore, I provided additional descriptions and interpretations of plesiadapid cranial morphology based on new specimens of *Pronothodectes gaoi* and a re-examination of all existing plesiadapid cranial material. In the current study, I have followed interpretations given in Chapter 2 and refer to them frequently.

MATERIALS AND METHODS

Material examined

All known specimens referable to the Plesiadapidae and representing a major or critical portion of the cranium were examined in this study except for MNHN CR 7377, an isolated squamosal glenoid, petrosal, and ectotympanic of *Plesiadapis tricuspidens* from the Berru locality near Reims, France, which could not be located. Previously unpublished, or largely undescribed, specimens studied include all cranial material referable to a single specimen of *Plesiadapis cookei*. UM 87990, the primary focus of this report, is a skull and skeleton discovered in 1987 at University of Michigan locality SC-117 in strata of the Fort Union Formation, dated to the middle Clarkforkian (late Paleocene biochron Cf-2) in the Clarks Fork Basin, Wyoming. It was found preserved in a freshwater limestone nodule and was prepared using acid reduction techniques described in Bloch and Boyer (2001).

P. cookei is compared to other plesiadapids including *Pronothodectes gaoi* (UALVP 46685, 46687 and 49105), *Nannodectes intermedius* (USNM 309902), *N. gidleyi* (AMNH 17388), other species of *Plesiadapis*, mainly *P. tricuspidens* (MNHN CR 125, 126, 965, 4306; and the Pellouin skull), and the fragmentary, edentulous rostrum of *P. anceps* (YPM-PU 19642). Other specimens included for comparison are isolated petrosals of *P. tricuspidens* (MNHN BR 17414-19, 1371). For the most part, the comparative sample of plesiadapids utilized here represents the study sample of Chapter 2.

Methods of examination and documentation

Methods of microscopic examination, photographic documentation and measurement follow Chapter 2.

All externally visible morphological structures pertinent to the description are labeled on the figures. Bones are identified with abbreviations (see Table 3.2). Other features are labeled with numbers (Table 3.1). Italicized numbers following figure citations in the description section correspond to labels on the morphology depicted in some or all of the cited figures. Table 3.1 is a list of features corresponding to the labels in the figures.

High resolution x-ray computed tomography (HRxCT) data were acquired from Pennsylvania State University (data available upon request) for UM 87990. The original scan consisted of 1435 slices spaced at 0.0614 mm, each slice having a pixel resolution of 0.0527 mm. During the scan, the specimen was embedded in florist foam to hold it in place (see Appendix Table 2.1). Additionally, the florist foam was saturated with water, which constituted a wedge to help improve contrast between matrix and bone. These data were visualized with the software Amira 4.1.2-1 and Image J and assisted in description of internal morphology. HRxCT data was particularly important for verifying identifications of various foramina.

Measurements and analysis

Various measurements were taken using digital calipers, digital photographs, camera lucida drawings and bone reconstructions from scan imagery (Tables 2.3-5). Measurements of foramina are accurate to at least a twentieth of a millimeter. Other

cranial measurements are generally accurate to at least a tenth of a millimeter. These measurements were used to compare shape and size differences between *Plesiadapis cookei* (UM 87990) and other plesiadapids.

In order to assess possible dietary differences, digital surface models were created from HRxCT scans of teeth and analyzed. The data were processed according to methods in Boyer (2008) and Evans et al. (2007). Two analyses were undertaken using these images: (1) Two and three dimensional tooth crown surface area measurements from M_2's were used to calculate relief indices (Boyer, 2008); and (2) The software SurferManipulator (Evans et al., 2007) was used to calculate the complexity of the occlusal surface via a metric called an orientation patch count (OPC) (Evans et al. 2007) (Table 3.4). Relief indices and OPC's have higher values in taxa that include greater proportions of structural carbohydrate in their diets (Evans et al. 2007; Boyer, 2008). Thus these metrics provide a means for estimating dietary differences among plesiadapids.

SYSTEMATIC PALEONTOLOGY

Class MAMMALIA

Order PRIMATES Linnaeus, 1758

Family PLESIADAPIDAE Trouessart, 1897

PLESIADAPIS Gervais, 1877

PLESIADAPIS COOKEI Jepsen, 1930

Type

YPM PU 13292, associated right and left dentaries, right maxilla, one upper and one lower incisor from the little Sand Coulee area (Sec. 32, T 57 N, R 101 W, Park Co.), Big Horn Basin, Wyoming.

Referred specimen

UM 87990 (Figs. 3.1-12), skull with associated dentaries and postcranial skeleton preserved in a limestone nodule at Locality SC-117, Fort Union Formation, middle Clarkforkian (late Paleocene biochron CF-2), Clarks Fork Basin, Wyoming.

Description

The craniodental material of UM 87990 was preliminarily described by Gingerich and Gunnell (2005:187) as preserved in five pieces, of which there was said to be a "palatal/splanchnocranial piece, a neurocranial piece with well-preserved auditory bullae ventrally, a frontoparietal piece, and two dentaries". Since this description, additional preparation has been executed. The three skull pieces have been glued together. The

previous authors also do not mention a fragment of the squamosal and zygomatic sutured together, a left anterior premaxillary piece and a fragment of the right nuchal crest. The latter two elements are illustrated as isolated bones here. Furthermore, a fragment of the right zygomatic bone has been removed, but was temporarily reattached for photography. Finally the ventral part of the right ectotympanic bone was either intentionally or accidentally removed (Bloch and Silcox, 2001). The right ectotympanic has not been reattached because, when separated, the annular part of the ectotympanic and more of the promontorium can be viewed and studied than would otherwise be possible. Thus, the skull exists in five pieces; seven if both dentaries are counted. There appears to be a substantial amount of brittle deformation inflicted on the skull. The degree to which this distorts the true morphology was not determined previously, but is analyzed here (see Discussion and Conclusions). The specimen is interpreted to represent a young individual because, although the adult dentition was completely erupted, the teeth are almost completely unworn and most long bone epiphyses remained unfused to diaphyses.

Nasal.— The nasals have been shifted away from the bones they contacted; thus the shape of these bones is apparent, but not which bones they contacted (Fig. 3.1). Their mediolateral width is fairly constant from anterior to posterior (anterior unilateral width = 4.9 mm, posterior unilateral width = 4.5 mm), possibly with a slight midpoint constriction (Fig. 3.1). Due to breakage, shifting and crushing of bone, it is not possible to determine whether the nasals would have contacted the maxillae as well as the premaxillae (Fig. 3.1: *1*) and frontals (they do not contact the maxillae in other known plesiadapids). The nasals appear to have extended posteriorly to the level of M^1, but this is at least partly an artifact of the skull's deformation.

Premaxilla and premaxillary dentition.— The anterior part of the right premaxilla is preserved (Fig. 3.2). The nasal, maxillary, and symphyseal premaxillary sutures are visible. The nasal suture is straight and simple (Figs. 3.1, 2: *1*). The right maxillary suture is observable just posterior to I^2 (Fig. 3.2: *2*). The suture is not convoluted and runs dorsoventrally before starting to curve posteriorly. A strip of bone exists along this sutural edge, which obtains an anteroposterior width of up to about 2 mm and appears to have received the maxilla on its lateral side. A higher magnification view of this surface reveals anteroposteriorly directed grooves and ridges, marking the early stages of what would likely have become pronounced "inter-locking" of bones along the maxillary/premaxillary suture in an older individual (Fig. 3.2B: inset). Whether the incisive foramen is contained completely within the premaxilla or at the juncture with the maxilla cannot be determined because of some breakage in this region (Fig. 3.2, 5). Even so, the symphyseal surface for the right premaxilla is present (Fig. 3.2: *3*), as well as some surface for palatal contact with the maxilla (Fig. 3.2: *2*). The premaxilla has alveoli for just two teeth, interpreted as I^1 and I^2, the latter of which is preserved in place (Fig. 3.2). The I^1 is not preserved; however, this tooth is known for the species (see below). The right I^2 is a simple, caniniform tooth. It has a paracone, with a distinct, postprotocrista extending between the apex of the cusp and the base of the crown on the distal side of the tooth. The crown is slightly compressed buccolingually relative to its mesiodistal dimensions. I^2 measures 4.12 mm in mesiodistal length and 2.95 mm in mediolateral width.

Lacrimal.— Due to crushing, the lacrimals have been almost completely destroyed. The rostrum has been shifted posteriorly and the anterolateral margins of the

frontal have been pushed laterally and ventrally into the orbit, shearing and crushing the lacrimals in consequence. On the left side, a small segment of the lacrimal, as well as the frontal and zygomatic sutures, are visible within the orbit (Figs. 3.1: *4*, *5*; Fig. 3.4: *4*). These visible bits of suture at least allow confident conclusion that the facial process of the lacrimal was not very anteriorly extensive.

Maxilla and maxillary dentition.— The right and left maxillae are preserved with P^4, M^{1-2} on both sides, P^3 on the right side, and both sets of alveoli for M^3 (Figs. 3.1, 3-7). This specimen is the first to demonstrate the lack of the upper canine and P^2 in *P. cookei*. The teeth are well-preserved with almost no wear, as expected for a young individual (Figs. 3.3-5). The anterior margin for contact with the premaxilla is preserved; thus the measured length of the diastema between I^2 and P^3 of roughly 14 mm can be stated with confidence. The rostral parts of the maxillae, as well as their zygomatic, palatal and alveolar processes are well-preserved (Figs. 3.1-3). The orbital part is crushed (Fig. 3.4). Thus, the contributions of the maxillae to the orbital mosaics are poorly delimited (Fig. 3.4). Frontal contact occurs in an interval between the nasal (or premaxilla?) and lacrimal on the dorsum of the skull, measuring 8.9 mm on the left side (Fig. 3.1: *6*).

Palatine contact of the maxilla occurred on the palate at the level of M^1 via a slightly convoluted suture (Fig. 3.5: *7*). The palatal part of the maxilla was measured from its contact with the palatine at the M^1 level to the most anterior point. The overall length of the maxilla in the palate is thus 30.2 mm. In ventral view, on the left side, a notch can be seen separating the M^3 alveolar process from the pterygoid process of the palatine (Fig. 3.5: *8*). The palatine/maxilla contact continues from its apex, medial to M^1, to run posteriorly through the lateral side of this notch, which held the lesser palatine

nerve and vessels in life (Fig. 3.5: *9*). If M^3 had been preserved, the length of the tooth row from P^3 to M^3 would have measured about 23 mm. Some of the M^3 alveoli may have breached the dorsal surface of the alveolar process of the maxilla, and thus communicated with the orbital cavity (Figs. 3.1, 3, 5: *10*). Specifically, on the left side, it appears that one or both buccal roots communicated, but the lingual root did not (Figs. 3.1, 5). On the right side the buccal roots did not breach the maxilla's dorsal surface, but the lingual root did (Fig. 3.3). This variable pattern may indicate that any apparent dorsal communications between the M^3 alveoli and the orbit in this specimen are actually the result of postmortem breakage.

The alveolar processes have been rotated and translated medially so that the left and right tooth rows are slightly angled toward one another (Fig. 3.6B) and the original inter-tooth row distance has been constricted. The unilateral breadth of the palate, as preserved, measures 5.5 mm at the level of I^2, 7.7 mm at the anterior margin of P^2, and 13.6 mm at the level of M^3. These first two measurements reveal an anteriorly tapering snout. The unilateral width of the maxilla, as measured from the sagittal plane with the alveolar process included, is 15.1 mm but the zygomatic process projects laterally another 11 mm. The right infraorbital foramen, situated just anterior to P^3, is 2.73 mm high and 1.52 mm wide (Figs. 3.3, 5, 6: *11*). The left infraorbital foramen is visible damaged.

Zygomatic.— The zygomatics are fairly well-preserved, although the left element is more complete. The left sutural contact with the lacrimal and maxilla measures 18.4 mm (Figs. 3.1, 4-6: *12*). This contact is straight and slopes laterally and posteriorly from its most anterodorsal point (Figs. 3.1, 4-6: *12*). The dorsoventral depth of the element decreases steadily laterally and posteriorly. At the lateral edge of the orbital excavation

(Figs. 3.1, 4-6: *13*), the zygomatic is 7.9 mm deep. There is no evidence of a postorbital process in this vicinity. The ventral surface of the anterior end of the zygomatic is expanded transversely for attachment of the superficial masseter (Fig. 3.5: *14*) (as is the zygomatic process of the maxilla at its suture with the zygomatic). This expansion measures 2.38 mm. The total anteroposterior length of the element along its ventral margin is 24.9 mm. The posterior end has a fragment of the zygomatic process of the squamosal still attached to it. The suture between these two elements measures at least 14.2 mm.

Frontal.— The frontals are visible on the dorsum of the skull; in this region the frontals clearly contact the maxillae and lacrimals (Fig. 3.1: *4*, *6*). The contact between the premaxillae (if any) and nasals are obscured by breakage. Furthermore, breakage makes the existence and/or nature of contacts with the palatine, orbitosphenoid, alisphenoid, and parietal difficult to assess. A metopic suture is prominent (Fig. 3.1, 6: *15*) and extends from the anterior end of the frontals to the parietals. Noting some breakage in the region of nasal contact, the anteroposterior length of the frontal is 21 mm and the unilateral width, from the metopic suture to the lacrimal suture, is roughly 15.3 mm. The frontals exhibit distinct ridges (temporal crests) that run medially from the anterolateral part of the bones, where they contact the lacrimals, toward the metopic suture. The temporal crests meet the metopic suture at the posterior end of the frontals, where they contact the parietals (Fig. 3.1: *16*). Thus, they would have formed a distinct "trigon" on the forehead. There is no sign of postorbital processes on these bones. HRxCT data reveal the frontal as a thin plate of bone anteriorly and show that the bone thickens posteriorly and is densely trabeculated. No major diploic cavities are

identifiable. No ethmoid foramina could be identified. At the parietal's most anterior point of contact with the frontal, it reaches a few millimeters beyond the apex of the converging temporal crests, to the point of maximum mediolateral constriction of the orbitotemporal region (Fig. 3.1, 4: *17*). This suture is difficult to see with the naked eye or light microscopy; however, HRxCT imagery reveals its position and form more distinctly. The parietal onlapped the frontal (Fig. 3.7: *18*). Thus, although much of the neurocranium has an "outer shell" of parietal, the frontal extends quite far posteriorly. Most likely, the frontal forms at least the anterior part of the endocranial surface, the topology of which reflects that of the brain, mainly the olfactory bulbs (Fig. 3.5: *19*). In fact, the posterior part of the frontal has its endocranial surface and the endocranial expression of its suture with the parietal exposed (Fig. 3.5: *20*). This region is described by Gingerich and Gunnell (2005).

Palatine.— The palatal processes of the palatines are visible and well preserved (Fig. 3.5). The base of the left pterygoid process is preserved (Fig. 3.5: *21*). More of the posterior parts also may be present, but shifted dorsally and posteriorly into the neurocranium (Fig. 3.5). On the palate, the palatines terminate at the choanae in a swollen rim of bone, also referred to as a postpalatine torus (Fig. 3.5: *22*). The outer margin of the torus reaches the lateral margin of the pterygoid processes. Furthermore, the outer margin of the torus is sharply angled, with the anterior part of it following a straight, transversely-running course, and the lateral parts following a straight, anteroposteriorly-running course. Prior to shifting of the contralateral palatines the inner margin of the horizontal process of the palatine, which forms the direct boundary to the choanae, would have been biconcave with a postpalatine spine present (Fig. 3.5: *23*). This

posterior termination of the palatal part of the palatine bone is at the level of the posterior margin of M^3.

Parietal.— Much of what can be said about the parietals has been described in the context of the frontal. The sutures with the alisphenoid and squamosal are obscured by breakage. The right and left elements meet along a straight sagittal suture to form a single sagittal crest (Figs. 3.1, 4, 6-8, 10: *24*). They appear to end short of the nuchal crests (e.g., Fig. 3.8: *25*), such that a different bone forms the posterior margin of the dorsal aspect of the skull (Fig. 3.8: *26*). However the identity of the particular bone that forms this last segment is not obvious (see below). It appears that the parietals were free of foramina for ramus temporalis branches of the stapedial artery or emissarial venae commitantes; however, this assessment lacks confidence because the elements have suffered so much breakage. The length of the sagittal crest is roughly 41 mm (this measurement includes the fragment shown in Fig. 3.8, which is not attached to the specimen in other figures).

Squamosal.— The left glenoid fossa and part of the right glenoid fossa are intact (Figs. 3.4, 5: *27*). Fragments of the contribution to the neurocranial portion are preserved, but their sutural contacts are obscured through crushing. Although looking at physical specimens hints that meaningful morphology of the alisphenoid or petrosal contact might be preserved, HRxCT data shows the internal morphology to be shifted, sheared, and crushed in these regions. The left postglenoid process (Figs. 3.4, 5: *28*) is oriented transversely and is situated lateral to the postglenoid foramen (Fig. 3.5: *29*). It projects straight ventrally by about 3.7 mm and is separated from the glenoid by a shallow, transversely running trough on the joint surface (Fig. 3.4: *28*). The entoglenoid

process is quite large, projecting ventrally beyond the glenoid fossa by 2.5 mm (Figs. 3.4, 5: *30*). It is oriented longitudinally at roughly 90 degrees from the orientation of the postglenoid process, and slopes medially. The glenoid is rather flat and anteroposteriorly longer (11.52 mm) than mediolaterally wide (10.12 mm). HRxCT imagery seems to reveal a sinus space within the squamosal medial to the anterior half of the left glenoid. A sinus that balloons out into the endocranial space would have reduced the endocranial volume as compared to a case in which such sinuses were lacking.

Sphenoids.— Fragments of the alisphenoid and basisphenoid are preserved, but shifted into the endocranium (Figs. 3.5, 7: *31*-*32*). The boundary between the two bones is not discernable; however, the bases of the entopterygoid (basisphenoid) and ectopterygoid (alisphenoid) processes are visible. HRxCT imagery reveals a cylindrical trough (most clearly on the left side) on the endocranial surface above the pterygoid processes that would have held the ophthalmic and/or the maxillary divisions of CN V (trigeminal nerve) (Fig. 3.7: *33*). The trough appears mainly undistorted for a short distance and has a diameter measuring 1.90 to 2.10 mm in this interval. At the convergence of the pterygoid crests is a canal that may represent the former location of the vidian nerve (Fig. 3.7: *34*). The foramina connecting this canal to extracranial space are minute and asymmetrical. The interpretation of their function is thus tentative. More posteriorly, HRxCT imagery of the fragmented remains of the basisphenoid suggest the presence of large sphenoidal sinus spaces, but the fossil is extremely battered in this region and this interpretation is tentative.

Petrosal.— The pars cochlearis of both petrosals is preserved, but the left element is obscured underneath a crushed bulla (Fig. 3.5: *35*). The pars canalicularis (Fig 5: *36*)

is better preserved on the left side than the right side, and the description of its morphology is therefore based on the left. The maximum diameter of the aperture for the fenestra vestibuli, or "oval window," is 1.32 mm (Fig. 3.9: *av*). The spiral cochlea measures 21.03 mm in length. The width of the pars cochlearis of the right side is 4.43 mm, while its dorsoventral depth, as measured from the endocranial surface, is about 5.5 mm. The ventral surface of the pars cochlearis (the promontorium) is criss-crossed by grooves of varying diameter (Fig. 3.9). Several bony ridges (or septa) extend out from the promontorium at varying angles, some of which are only apparent with HRxCT. Ventral to the fenestra vestibuli on the lateral aspect of the promontorium is a large groove, measuring 0.40 mm in diameter (Fig. 3.9: *g1*). This groove is directed anterodorsally. It is the *g1* groove (Fig. 2.40). At its posteriormost point, it is associated with the posterior septum (MacPhee, 1981), which covers the aperture for the fenestra cochleae, or "round window," (Fig. 3.9: *ac*) and contains the internal carotid canal in its ventral margin (Fig. 3.9: *ps*). The anterodorsal continuation of *g1* onto the promontorium appears equivalent to what has been termed *g5* for other plesiadapids (Fig. 2.40; Fig. 3.9: *g5*). There are other grooves on the lateral aspect of the promontorium. One seems to run from medial to lateral starting from the lateral side of the anterior apex of the posterior septum where it arises from the promontorium (Fig. 3.9: *tng*). As this groove emerges from the fossula for the fenestra cochleae, formed by the posterior septum its canal deepens and runs vaguely parallel and laterodorsal to *g1*. After moving a short distance anteriorly on the petrosal, it dives under a bridge of bone and thus becomes a short canal. The canal ends and the groove resumes for a short distance before becoming shallow and disappearing just anterior and ventral to the anterior apex of the fenestra

vestibuli. This groove's point of origination in the posterior septum-formed fossula of the fenestra cochleae is close to a foramen for an intrapetrous canal. The intrapetrous canal leads medially to a foramen on the medial side of the promontorium where it obtains the distinctive morphology relating to the tympanic canaliculus (Fig. 3.9: *tca*). Another groove courses more ventromedially than *g5* from near the anterolateral margin of posterior septum (Fig. 3.9: *g2*). This second groove represents *g2* (Fig. 2.40). It approaches a septum that only is visible with HRxCT imagery. This septum is the most anterior and lateral of those preserved on the specimen. It appears equivalent to the *s1* (Fig. 2.40) and MacPhee's (1981) anterior septum, which marks the course of the main bundle of neurovasculature of the internal carotid plexus as the contents approach the foramen lacerum to gain entrance to the endocranium. Another groove is present that is medial to, but also vaguely parallel to the *g2* groove (Fig. 3.9: *g2*). Traced anteriorly or posteriorly, this groove can be seen to converge toward the *g2* groove. Consequently, it stems from the lateral aspect of the promontorium near the point where the internal carotid plexus enters the tympanic cavity and then leads toward the anterior septum. Thus, this more medially positioned groove also is likely to have transmitted to the internal carotid plexus, especially considering the fact that the internal carotid plexus frequently consists of two nerve bundles (MacPhee, 1981). Yet another groove crosses the promontorium at a right angle to the two *g2* grooves (Fig. 3.9: *g3*). This groove starts from near to where the tympanic nerve groove ends on the lateral side of the promontorium. Then the groove traverses to the medial side of the remnant of a second bony ridge, or septum, that extends anteromedially from the promontorium (Fig. 3.9: *s2* -

this septum is located medial to the anterior septum). A groove appears to represent *g3* (Fig. 2.40).

The lateral walls of the auditory bulla (Figs. 3.5, 9: *37*) have been crushed concentrically toward the promontorium such that septa and tympanic processes have been crushed and obscured to some degree. For instance, the posterior septum is broken and the posterior wall of the bulla is destroyed such that no posterior carotid foramen is visible. On the medial side, the ridge above the cochlear canaliculus (Fig. 3.9: *cc*) is just barely visible. The cochlear canaliculus itself is visible with HRxCT. Additionally, as mentioned earlier, the groove and foramen that typically sit on the ventral aspect of this ridge, which appear to relate to the tympanic nerve, are visible. Running anteriorly and posteriorly from the foramen of tympanic canaliculus is a distinct foramina-enervated groove (Fig. 3.9: *bs*).

A fragment of the pars canalicularis is preserved on the left side. It is relatively short anteroposteriorly. There is a deep groove that abuts the jugular process of the exoccipital and appears to lead to the stylomastoid foramen; it may also represent the digastric fossa (Fig. 3.5: *38*). Lateral to this is a prominent tubercle that probably buttressed the posterior aspect of the ectotympanic tube and is probably best referred to as a mastoid process (Fig. 3.5: *39*). If the pars canalicularis of the petrosal had any posterior exposure in the pristine skull, it is not apparent from the fossil (Fig. 3.10).

Ectotympanic.— What seems likely to be the ectotympanic bone is preserved bilaterally (Fig. 3.5). Although the right side is fragmentary, it exposes morphology not visible on the left (Fig. 3.11). The left reveals that the external auditory meatus is narrow compared to its mediolateral length and it can thus be described as “tubular” (Figs. 3.4, 5,

9: *40*). The right side reveals an annular (ring-like) projection of bone at the medial base of the external auditory meatus "tube" for attachment of the tympanic membrane (crista tympanica) (Figs. 3.9, 11: *41*). The crista tympanica essentially marks the end of the external auditory meatus. The external auditory meatus-forming tube of bone extends roughly 12 mm laterally from what remains of the crista tympanica on the left side. The diameter of the tube flares somewhat as it approaches its medial base. Prior to this flaring, directly posterior to the postglenoid foramen, its diameter is about 4.8 mm. The annular component of the ectotympanic is solidly connected to the outer tube by a series of bony struts (Fig. 3.11: *42*). There is no visible suturing or gaps between the annular component and outer tubular component [i.e., there is no "recessus dehiscensce" (Bloch and Silcox, 2001)]. The annular component does not flare substantially beyond the struts of the annular bridge. However, at least some bone has been lost from this margin because an intact crista tympanica is typically marked by a concentric projection of bone toward the middle of the external auditory meatus (i.e., there is a "lip" on the annular component – see morphology of *N. intermedius* USNM 309902 Fig. 2.11D, 2.12). What remains of the annular component of the external auditory meatus in UM 87990 lacks a concentrically projecting lip.

Whether the ectotympanic is limited to the lateral part of the skull and bullar cavity or comprised most or all of the bulla is unknown due to breakage and the lack of any informative sutural margins (Fig. 3.5).

Occipital.— The occipitals are fairly well preserved. The basioccipital is crushed dorsally into the endocranium, but its dimensions can be measured (Fig. 3.5). Its anteroposterior length measures 14.4 mm. Mediolaterally, the anterior end is 4.7 mm and

the midpoint is slightly narrower, roughly 4.4 mm. The posterior width cannot be measured due to breakage. The bone is marked by a longitudinal ridge along its midline (Fig. 3.5: *43*). The pre-distortion dorsoventral thickness of the bone is difficult to estimate.

The exoccipitals are quite well preserved, retaining both occipital condyles (Fig. 3.4, 5, 10: *44*), the left hypoglossal foramen (Fig. 3.5: *4*5), the posterior margins of both posterior lacerate foramina (or jugular foramina) (Fig. 3.5: *46*), both jugular processes (Figs. 3.5, 10: *47*), and the majority of their contribution to the posterior surface of the skull (Fig. 3.10). The suture, or contact, with the basioccipital is completely obscured. Each condyle is 5.1 mm high and 4.5 mm wide. The hypoglossal foramen is 1.75 mm by 1.60 mm and has two smaller foramina inset within it. The left jugular foramen is preserved more completely and is 2.9 mm in maximum diameter. The jugular processes do not project posteriorly beyond the condyles, as they sometimes do in other taxa. The processes project lateral to the edge of the condyles by 2.4 mm on both sides. The foramen magnum appears undistorted and is 6.4 mm high and 9.1 mm wide (Fig. 3.10: *48*). The dorsal rim of the foramen magnum is comprised mainly of right and left exoccipitals. The two bones almost meet in the midline and may have actually touched in the pristine skull (Fig 10: *49*). Given that the exoccipitals and supraoccipital appear generally undistorted overall, the mediolateral diameter of the back of the skull between posteriormost projections of the exoccipital jugular process can be measured at 21.7 mm.

The supraoccipital is fragmentary (Figs. 3.10, 13) and is preserved on the posterior sides of the nuchal crests. This bone was thin and overlay the exoccipital (Figs. 3.5, 10, 13: *50*). The region of contact between the missing pieces of supraoccipital can

be seen as a wedge-shaped, rugose depression on the exoccipitals (Fig. 3.10: *51*). The apex of this "wedge" points ventrally and would have reached the middle of the dorsal rim of the foramen magnum. The back of the skull is concave in dorsoventral profile, due to strong development of the nuchal crest (Figs. 3.4, 8). The height of the supraoccipital from the top of the foramen magnum to the top of the nuchal crest is at least 9.9 mm. As discussed above, the identity of bone forming the inner core and dorsal/anterior surface of the nuchal crest is not clear. The bone appears to be the exoccipital, but could also include an interparietal element.

Dentary.— The dentaries are well-preserved (Fig. 3.12). The right side retains all tooth positions. The teeth are diagnostically indistinguishable from other referred *P. cookei* specimens. The P_4 for the species has previously been described as being simple with only a protoconid and hypoconid (Gingerich, 1976; Rose, 1981). However, this specimen, and others in which this tooth is unworn, demonstrate that the P_4 of *P. cookei* possesses an entoconid and a talonid basin. Furthermore, the protoconid comprises the distal margin of a trigonid basin formed by an encircling crest (Figs. 3.12, 13) with an incipient paraconid in its mesial aspect. This morphology is actually reminiscent of that in *Platychoerops* from the Eocene of Europe (Fig. 3.13).

COMPARISONS

Position of internal carotid groove

P. cookei is similar to many other plesiadapids in having a laterally positioned carotid groove (*g1*) with a diameter in the range of 0.30 to 0.40 mm (Table 2.3). This

morphology, as well as the presence of *g2* grooves, demonstrates an intratympanic route for the internal carotid plexus of *P. cookei*.

Grooves on the promontorium

Compared to other plesiadapids the *g2* grooves diverge from the *g1* groove unusually far proximally (Fig. 3.9): they are already distinct on the posterior septum, rather than forming farther cranially, on the promontorium. The divergence of the two *g2* grooves from one another on the promontorium is also unusual, and is not observed in any other plesiadapid specimens described in the Chapter 2. It is unknown whether this unusual morphology is a characteristic of *P. cookei* or whether it represents intraspecific variability in the course of nerves in this area (and therefore represents a pattern that could just as easily appear in an individual of another species such as *Pronothodectes gaoi*).

Composition of bulla: sutural evidence on medial tympanic process

The medial tympanic process of *P. cookei* is unique among the comparative sample of plesiadapids in exhibiting a "suture-like" line of foramina (Fig. 3.9D). Comparative rodent specimens of *Marmota* and *Lagostomus* (Chapter 2) show neurovasculature invading the middle ear cavity at the petrosal/ectotympanic boundary, creating a line of foramina at the sutural boundary. This extant morphological pattern makes it tempting to interpret the line of foramina in *P. cookei* as the remnant of a suture as well. This may or may not be correct: HRxCT data does not provide any more insights, as the boundary between the pars cochlearis of the petrosal and its medial

process appears as solid bone. Admittedly, the resolution of the scan may simply be too coarse to allow visualization of such a suture. Even if there is no evidence of such a feature at any resolution, the foramina could still represent a suture that is almost completely fused through internal remodeling. For instance, the tympanic canaliculus foramen is among the many other tiny foramina that form this boundary. If the entrance point for these nerves corresponds to the boundary between bulla-forming bone and a separate petrosal, then the morphological pattern would be extremely similar to that of the extant rodents *Marmota* (Fig. 2.34) and especially *Lagostomus* (Figs. 2.35, 36). However, these nerves are perfectly capable of obtaining access to the intratympanic cavity via "intrapetrous" canals, as discussed by MacPhee (1981) for *Microcebus*, and in specimens of *Eulemur* (SBU efr-3562: pers. observ.). Given observations on *Indri* and paromomyid plesiadapiforms (Figs. 2.37-39), the line of foramina cannot be regarded as evidence of a non-petrosal bulla even if it is a suture or boundary between different bony laminae. It is perhaps also relevant to note that UM 87990 was apparently ontogenetically younger than other specimens whose skulls were discussed in Chapter 2 (as reflected by its pristine teeth), and is the only one to exhibit this line of foramina.

Consideration of the ectoympanic bulla of rodents such as *Marmota* and *Lagostomus* raises the question of the medial extent of ectotympanic-derived bone in *P. cookei*. No visible suture exists anywhere on the bulla or external auditory meatus delimiting the boundary between ectotympanic from bulla-forming bone. Nor is such morphology convincingly well preserved in other plesiadapids or plesiadapiforms (see Chapter 2).

Major cranial differences between *Plesiadapis cookei* and *P. tricuspidens*

The crania of *P. cookei* and *P. tricuspidens* are not highly divergent. In fact, they are uniquely similar among known plesiadapid skulls in their laterally expanded, tubular external auditory meati, and in the minimal exposure of the molar roots on the dorsal surface of their maxillae. On the other hand, *P. cookei* differs distinctly from *P. tricuspidens* in having proportionally broader nasals (Table 2.6: N/GM), and a proportionally smaller glenoid fossa (Table 2.6: Gld/GM). Additionally, *P. cookei* appears to differ from *P. tricuspidens* in having an ectotympanic ring that does not flare beyond its attachment to the bullar part of the ectotympanic as substantially, and possibly in having a more posteriorly projecting nuchal crest. Interestingly, the features separating *P. cookei* from *P. tricuspidens*, also separate smaller North American plesiadapids from *P. tricuspidens*, including *P. anceps, N. intermedius, N. gidleyi*, and *Pr. gaoi* (see Chapter 2). Some previously undocumented dental differences between *P.cookei* and *P. tricuspidens* are also revealed by UM 87990: unlike *P. tricuspidens*, *P. cookei* lacks a P^2 and a has more molariform P_4.

IMPLICATIONS OF CRANIODENTAL MATERIAL FOR BODY SIZE IN PLESIADAPIDAE

Though it is clear that both *P. cookei* and *P. tricuspidens* were absolutely large among plesiadapids generally, the comparison of body size in these species has remained ambiguous. *P. cookei* has molar teeth with occlusal areas that are 140% (M^1), 127% (M^2) and 119% (M^3) larger than those of *P. tricuspidens* [data from Gingerich (1976: table A-

16) for *P. tricuspidens* and Rose (1981: table 14) for *P. cookei*]. These data lead to the hypothesis that *P. cookei* was a bigger animal than *P. tricuspidens* (Gingerich et al., 1982; Fleagle, 1999). However, side-by-side comparison of the UM 87990 cranium and MNHN CR 125 (or the Pellouin skull) in dorsal or ventral view shows that the *P. tricuspidens* specimens dwarf *P. cookei*, the opposite of what tooth size differences would lead one to predict. Close inspection reveals that this contradiction is mainly due to differential patterns of deformation among the different skulls. Whereas UM 87990 is compressed anteroposteriorly and mediolaterally so that it is now smaller in these dimensions than it was in life, the *P. tricuspidens* specimens are compressed dorsoventrally, so that they probably still retain their transverse plane dimensions. The degree to which size differences have been accentuated is revealed by a series of 39 measurements on individual cranial bones (Table 2.5: Table 3.3). This exercise shows that the skulls of *P. cookei* and *P. tricuspidens* are almost identical in the size of almost every feature measured except for the glenoid fossae, which are distinctly larger in the two *P. tricuspidens* specimens. Specifically, measurements from all regions of the *P. cookei* skull (UM 87990) are, on average, 99% the size of those of both skulls of *P. tricuspidens* (MNHN CR 125 and the Pellouin skull). The value "99%" is literally the antilogged average of 39 natural log ratios of *P. cookei* to *P. tricuspidens* cranial measurements. In other words, it is an average of 39 direct comparisons. A less direct comparison using a geometric mean of these 39 measurements yields a slightly different but comparable result. The geometric mean of the *P. cookei* measurements is 10.7, while that of MNHN CR 125 is 10.6, suggesting that, instead, the *P. tricuspidens* skull is 99% the size of that of *P. cookei*. Comparisons between *P. cookei* and a sample of *P.*

tricuspidens postcrania in the Chapter 4 illustrate that the two taxa are also nearly identical in their long bone diameters. The fact that so many skeletal elements suggest equivalent sizes for these two taxa is taken as strong evidence that *P. cookei* and *P. tricuspidens* are of equivalent size, despite differences in tooth sizes.

In contrast, the *P. cookei* skull is much larger than known skulls of other plesiadapid taxa. Using the direct comparisons method, it is 154% the size of that of *Plesiadapis anceps* (YPM-PU 19642), 170% the size of *Nannodectes gidleyi* (AMNH 17388), 176% the size of *Pronothodectes gaoi* (UALVP 46685), and 210% the size of *Nannodectes intermedius* (USNM 309902) (Table 3.3).

The accuracy of these estimates for smaller plesiadapids can be checked by comparison to measurements of the skull, teeth and skeleton of *P. insignis* (Gingerich, 1976). Gingerich measured the skull length of *P. insignis* at 50 mm (Gingerich, 1976: p.35, table 6). The measurements of its teeth are in the range of those of *N. intermedius.* (Gingerich 1976: compare p.35, table 5 with p.105, table A-3) Furthermore, its postcrania are nearly identical in their lengths to those known of *N. intermedius* (see Chapter 5). I would thus predict the skull length of *N. intermedius* to be the same as that of *P. insignis.* In fact, dividing the estimated length of *P. cookei*'s skull by 210% (=105.8 mm/2.10) gives an estimated length of 50.4 mm for *N. intermedius*.

DENTAL FUNCTIONAL MORPHOLOGY OF *P. COOKEI* AND *P. TRICUSPIDENS*

The fact that tooth size differences appear to exist between *P. cookei* and *P. tricuspidens* without body size differences is unusual, because teeth are usually highly correlated with body size among mammals (e.g., Gingerich et al., 1982). It is at least possible that previously hypothesized differences in dietary preference (Gingerich, 1976) explain the tooth size differences. Specifically, larger teeth in *P. cookei* could reflect a more folivorous diet, as do relatively large teeth in extant primates (Kay, 1975). Such a dietary difference is consistent with the specific suggestion of Gingerich (1976): that *P. cookei* had a more specialized folivorous diet than did *P. tricuspidens*, based principally on incisor and upper fourth premolar morphology. The folivory hypothesis can be tested further by analyzing the dentition in more detail to see if there are other differences separating *P. cookei* and *P. tricuspidens* that would either support or refute this hypothesis.

Relief index and selenodonty

Boyer (2008) has shown that, across broad phylogenetic sample sets, taxa that eat more leaves and less fruit have lower second molars with significantly greater relief than those of more generalized or fruit-eating taxa (where "relief" is the log ratio of the surface area of the tooth crown to the area of the crown's projection into a two dimensional occlusal plane). Teeth with higher relief indices in these comparisons can be qualitatively described as more "cresty," or more selenodont. ANOVA comparing relief

indices of a sample of M_2's of *P. cookei*, *P. tricuspidens*, and *Pl. daubrei* shows significant among-taxon variance (df = 2, F = 26.6, P<<0.001). Further, "Tukey's Honestly Significantly Different (HSD)" pairwise comparisons show *P. cookei* to have significantly higher relief than *P. tricuspidens* (P<<0.001), and moderately, but significantly lower relief than *Pl. daubrei* (P = 0.014) (Table 3.4; Fig. 3.14). A detailed qualitative comparison of morphology in M_2's between the taxa reveals that the greater relief is likely accomplished by three features typically associated with greater reliance on leaves (Fig. 3.13). *P. cookei* has a more distolingually expanded entoconid, a more buccolingually expanded (or a more "open") trigonid, and a more distolingually-postioned metaconid (as compared to the protoconid). All of these differences should increase the shearing area present on *P. cookei*'s molars compared to those of *P. tricuspidens*. Interestingly, *Platychoerops* differs from *P. tricuspidens* in some of these same respects (and much more drastically so) and is more similar to *P. cookei*.

Orientation Patch Count and complexity

Evans et al. (2007) have shown that rodents and carnivorans with similar diets are similar in a metric that reflects the "complexity" of the occlusal surface of the entire cheek tooth row. When this metric, the "Orientation Patch Count," is calculated on the same samples of M_2's that were used in the relief index calculation, a nearly identical pattern emerges with all taxa being significantly different according to ANOVA (df = 2, F = 22.4, P<<0.001) and Tukey's HSD pairwise comparisons (Table 3.4; Fig. 3.14). *Pl. daubrei* has higher complexity than *P. cookei*, (P<0.01) and *P. cookei* has higher complexity than *P. tricuspidens* (P = 0.03).

Lower premolar molarization

As indicated in the description, *P. cookei* has a more molarized P_4 than previously described, which is substantially more molariform than the condition seen in *P. tricuspidens* (Fig. 3.13D-F). Molarization of premolars is a known correlate of specialization for a more folivorous diet among extant taxa (Gingerich, 1976; Van Valen, 1982; Jernvall et al., 2008). In fact, a molariform P_4 is one of the features cited as reflecting a leafy diet for *Pl. daubrei* (Gingerich, 1976). As noted above, the molarization of P_4 seems likely to have initiated and progressed in the same way in the lineages leading to *P. cookei* and *Pl. daubrei*.

Incisor simplification

Jepsen (1930) recognized that the lower incisors of *P. cookei* and *Pl. daubrei* are similar in lacking a margoconid (Fig. 3.12). However, this is also true of *P. tricuspidens*. The shared feature of "margoconid absense" by the three taxa has thus been taken as evidence of a close relationship. Gingerich (1976) noted additional similarities between the upper incisors of *P. cookei*, *Pl. russelli*, and *Pl. daubrei*. His points are reiterated here: *P. cookei* is uniquely similar to *Pl. russelli* and *Pl. daubrei*, to the exclusion of *P. tricuspidens* in its upper central incisor morphology. Specifically, the posteroconid is often (but not always) very reduced in *P. cookei*, and the apical morphology is much simplified compared to that of *P. tricuspidens*. Whereas *P. tricuspidens* has a large anterocone and laterocone, and retains a distinctive mediocone and centroconule, *P. cookei* has a reduced anterocone and laterocone, and lacks the mediocone and

centroconule. The differences in prominence and/or presence of cusps on central upper incisors between *P. cookei* and *P. tricuspidens* are markedly evident in a qualitative side-by-side comparison of the two taxa. In Figure 3.15, the central incisors of the two taxa are shown at the same scale. Despite the fact that the shaft of I^1 is much larger in *P.cookei*, the anterocone, laterocone, and posterocone of this specimen are the same size or smaller than those in the otherwise much smaller specimen of a *P. tricuspidens* central incisor from Berru, France.

DISCUSSION AND CONCLUSIONS

The fact that the cranium of *P. cookei* is similar to that of *P. tricuspidens* in a number of respects, including absolute size, is consistent with the hypothesis of Gingerich (1976) that these two taxa are more closely related to one another than to the other plesiadapids whose crania are described in Chapter 2. However, it is interesting that *P. cookei* still retains a number of similarities to other North American species that are lacking in *P. tricuspidens.*

The dietarily significant morphological differences separating *P. cookei* and *P. tricuspidens* support the hypothesis that *P. cookei* can represent a point along a morphocline leading from *P. tricuspidens* to *Pl. russelli* (Fig. 3.16), as does the temporal range of *P. cookei*, which is intermediate between the two other taxa (Hooker and Millbank, 2001). These two pieces of evidence are also consistent with the hypothesis that *P. cookei* is a member of the phylogenetic lineage linking *P. tricuspidens* and *Pl. russelli*.

SUMMARY AND CONCLUSION

The skull of *Plesiadapis cookei* exhibits a laterally positioned internal carotid plexus groove like other plesiadapids. It lacks distinctive sutures delimiting the auditory bulla from either the ecotympanic or the petrosal bone. Furthermore, *P. cookei* exhibits a number of similarities to North American plesiadapids, not shared by *P. tricuspidens*, and several similarities to *P. tricuspidens* not shared by other North American plesiadapids. While *P. cookei* appears to have been the same size as *P. tricuspidens*, based on overall cranial measurements, its teeth are bigger. Larger teeth and a number of other dental features in *P. cookei* suggest that it had a more specialized folivorous diet than did *P. tricuspidens*. An inferred specialized folivorous diet in *P. cookei* makes it similar to *Platychoerops*, whose species have previously been hypothesized to be descendents of *P. tricuspidens*.

The cladistic relationships of *P. cookei*, *P. tricuspidens* and *Platychoerops* should be reanalyzed to determine whether the morphological features of *P. cookei* are 1) convergent similarities to *Platycheorops* evolved for a similarly folivorous diet, 2) features inherited from a common ancestor with *Pl. russelli*, the plesiadapid with which it shares the most dental similiarities (Jepsen, 1930; Gingerich, 1976), or 3) a reflection of it being a member of a lineage (and a point along a morphocline) leading from *P. tricuspidens* to *Pl. daubrei* (Gingerich, 1976). Such an analysis is presented in Chapter 5.

ACKNOWLEDGEMENTS

I am grateful to P. Gingerich, G. Gunnell, and J. Bloch for the opportunity to lead the study and description of UM 87990. P. Gingerich and W. Sanders facilitated and oversaw the production and provision of high quality casts of this specimen. A. Walker and T. Ryan provided HRxCT scans of this specimen and others at the Center for Quantitative Imaging, Pennsylvania State University. S. Judex and C. Rubin provided HRxCT scans at the Center for Biotechnology of the Department of Biomedical Engineering at Stony Brook University. M. Godinot, P. Tassy and C. Sagne of MNHN, and M. Pellouin provided access to important comparative specimens of *Plesiadapis tricuspidens* and *Platychoerops*. This research was enhanced by discussions with J. Bloch, P. Gingerich, M. Godinot, J. Perry, M. Silcox, R. Secord and many other researchers. D. Krause, M. O'Leary, J. Fleagle, W. Jungers, and P. Gingerich read and enhanced previous manuscripts. It was made possible by funding from a National Science Foundation grant to P. Gingerich and G. Gunnell (BCS-0129601), a National Science Foundation grant to D. Krause and J. Bloch (EAR-0308902), and a National Science Foundation Graduate Research Fellowship, an Evolving Earth Foundation grant, a National Science Foundation Doctoral Dissertation Improvement Grant (BCS-0622544), and an American Society of Mammalogists grant to D. Boyer.

REFERENCES

Bloch, J.I., Boyer, D.M., 2001. Taphonomy of small mammals in freshwater limestones from the Paleocene of the Clarks Fork Basin. In: Gingerich, P.D. (ed) Paleocene-Eocene stratigraphy and biotic change in the Bighorn and Clarks Fork basins, Wyoming. University of Michigan Papers on Paleontology 33, 185-198.

Bloch, J.I., Silcox, M.T., 2001. New basicrania of Paleocene-Eocene *Ignacius*: re-evaluation of the plesiadapiform-dermopteran link. American Journal of Physical Anthropology 116, 184-198.

Bloch, J.I., Silcox, M.T., 2006. Cranial anatomy of the Paleocene plesiadapiform *Carpolestes simpsoni* (Mammalia, Primates) using ultra high-resolution X-ray computed tomography, and the relationships of plesiadapiforms to Euprimates. Journal of Human Evolution 50, 1-35.

Bloch, J.I., Silcox, M.T., Boyer, D.M., Sargis, E.J., 2007. New Paleocene skeletons and the relationship of plesiadapiforms to crown-clade primates. Proceedings of the National Academy of Sciences 104, 1159-1164.

Boyer, D.M., 2008. Relief index of second mandibular molars is a correlate of diet in Primates and other euarchontan mammals. Journal of Human Evolution 55, 1118-1137.

Evans, A.R., Wilson, G.P., Fortelius, M., Jernvall, J., 2007. High-level similarity of dentitions in carnivorans and rodents. Nature 445, 78-81.

Fleagle, J.G., 1999. Primate Adaptation and Evolution. Academic Press, New York.

Gervais, M.P., 1877. Enumération de quelques ossements d'animaux vertébrés, recueillis aux environs de Reims par M. Lemoine. Journal de Zoologie 6, 74-79.

Gingerich, P.D., 1976. Cranial anatomy and evolution of Early Tertiary Plesiadapidae (Mammalia, Primates). University of Michigan Papers on Paleontology 15, 1-141.

Gingerich, P.D., Smith, B.H., Rosenberg, K., 1982. Allometric scaling in the dentition of primates and prediction of body weight from tooth size in fossils. American Journal of Physical Anthropology 58, 81-100.

Gingerich, P.D., Gunnell, G.F., 1992. A new skeleton of *Plesiadapis cookei*. The Display Case University of Michigan 6, 1, 3.

Gingerich, P.D., Gunnell, G.F., 2005. Brain of *Plesiadapis cookei* (Mammalia, Proprimates): surface morphology and encephalization compared to those of Primates and Dermoptera. University of Michigan Museum of Paleontology Contributions 31, 185-195.

Gunnell, G.F., Gingerich, P.D., 1987. Skull and partial skeleton of *Plesiadapis cookei* from the Clarks Fork Basin, Wyoming. American Journal of Physical Anthropology 72, 206a.

Hoffstetter, R., 1977. Phylogénie des primates. Confrontation des resultats obtenus par les diverses voies d'approche du probleme. Bulletins and Mémoires Société d'Anthropologie de Paris t.4, série XIII, 327-346.

Hooker, J.J., Millbank, C., 2001. A Cernaysian mammal from the Upnor Formation (Late Palaeocene, Herne Bay, UK) and its implications for correlation. Proceedings of the Geologists' Association 112, 331-338.

Jepsen, G.L., 1930. Stratigraphy and paleontology of the Paleocene of northeastern Park County, Wyoming. Proceedings of the American Philosophical Society 69, 463-528.

Jernvall, J., Gilbert, C.C., Wright, P.C., 2008. Peculiar tooth homologies of the greater bamboo lemur (*Prolemur = Hapalemur simus*): When is a paracone not a paracone? In: Fleagle, J.G., Gilbert, C.C. (eds) Elwyn Simons: A Search for Origins. Springer, New York, pp. 335–342.

Kay, R.F., 1975. The functional adaptations of primate molar teeth. American Journal of Physical Anthropology 43, 195-216.

Linnaeus, C., 1758. Systema naturae per regna tria natureae secundum classes, ordines genera, species cum characteribus, differentris, synonymis, locis, Editis decima, reformata edn. Laurentii Salvii, Stockholm.

MacPhee, R.D.E., 1981. Auditory Regions of Primates and Eutherian Insectivores: Morphology, Ontogeny, and Character Analysis. Contributions to Primatology 18, 1-282.

Rose, K.D., 1981. The Clarkforkian land-mammal age and mammalian faunal composition across the Paleocene-Eocene boundary. University of Michigan Papers on Paleontology 26, 1-189.

Trouessart, E.L., 1897. Catalogues des Mammalium tam Viventium quam Fossilium. R. Friedlander und Sohn, Berlin.

Van Valen, L.M., 1982. Homology and causes. Journal of Morphology 173, 305-312.

Zachos, J., Pagani, M., Sloan, L., Thomas, E., Billups, K., 2001. Trends, rhythms, and aberrations in global climate 65 Ma to present. Science 292, 686-693.

TABLES

Table 3.1. List of anatomical features

1 – Premaxilla/nasal suture (Figs. 3.1, 2, 4, 5, 6)
2 – Premaxilla/maxillary suture (Figs. 3.1, 2, 4, 5, 6)
3 – Premaxillary symphysis (Figs. 3.1, 2)
4 – Lacrimal/frontal suture in orbit (Figs. 3.1, 4)
5 – Lacrimal/zygomatic suture in orbit (Fig. 3.1)
6 – Maxilla/frontal suture on forehead (Fig. 3.1)
7 – Maxilla/palatine suture at level of M^1 in palate (Fig. 3.5)
8 – Notch between pterygoid process of palatine and M^3 alveolus marking lesser palatine nerve route (Fig. 3.5)
9 – Maxilla/palatine suture at level of M^3 in palate (Fig. 3.5)
10 – Dorsal communication of M^3 alveolus with orbital cavity (Figs. 3.1, 3, 5)
11 – Infraorbital foramen (Figs. 3.3, 4, 5, 6)
12 – Zygomatic/maxillary suture (Figs. 3.1, 4, 5, 6)
13 – Edge of orbital excavation on zygomatic bone (Figs. 3.1, 4, 5, 6)
14 – Expansion of ventral surface of zygomatic for masseter attachment (Fig. 3.5)
15 – Metopic suture (Figs. 3.1, 6, 7)
16 – Ridges of frontal trigon (Figs. 3.1, 6)
17 – Frontal/parietal suture, most anterior part (Figs. 3.1, 4, 6)
18 – Cross-sectional view of frontal parietal contact (Fig. 3.7)
19 – Endocranial surface of frontal, depressions for olfactory bulbs (Fig. 3.5)
20 – Frontal/parietal suture on endocranial surface (Fig. 3.5)
21 – Base of left pterygoid process of palatine (Fig. 3.5)
22 – Postpalatine torus (Fig. 3.5)
23 – Postpalatine spine (Fig. 3.5)
24 – Sagittal crest (Figs. 3.1, 4, 6, 7, 8, 10)
25 – Nuchal crest (Figs. 3.1, 4, 8, 10)
26 – Parietal/?interparietal suture on dorsum of skull (Fig. 3.8)
27 – Glenoid fossa (Figs. 3.4, 5)
28 – Postglenoid process (Figs. 3.4, 5)
29 – Postglenoid foramen (Figs. 3.5)
30 – Entoglenoid process (Figs. 3.4, 5)
31 – Basisphenoid entopterygoid process (Figs. 3.5, 7)
32 – Alisphenoid ectopterygoid process (Figs. 3.5, 7)
33 – Canal leading to sphenorbital fissure (Fig. 3.7)
34 – Possible vidian canal (Fig. 3.7)
35 – Pars cochlearis of petrosal (Figs. 3.5, 9)
36 – Pars canalicularis of petrosal (Fig. 3.5)
37 – Tympanic processes of auditory bulla (Figs. 3.5, 9)
38 – Digastric fossa, stylomastoid foramen area (?) (Figs. 3.4, 5)
39 – Paroccipital process (mastoid process) of petrosal (Figs. 3.4, 5, 10)
40 – Tubular external auditory meatus (Figs. 3.4, 5, 9, 10, 11)
41 – Crista tympanica (Figs. 3.9, 11)

42 – Bony struts supporting crista tympanica (Fig. 3.11)
43 – Sagittal ridge of bone on basioccipital (Fig. 3.5)
44 – Occipital condyles (Figs. 3.4, 5, 10)
45 – Hypoglossal foramen (Fig. 3.5)
46 – Jugular foramen (Fig. 3.5)
47 – Jugular processes (Figs. 3.5, 10)
48 – Foramen magnum (Fig. 3.10)
49 – Sagittal contact between right and left exoccipitals (Figs. 3.5, 10)
50 – Sutural contact between remnants of supraoccipital and exoccipital (Fig. 3.10)
51 – Wedge-shaped depression on exoccipitals, where supraoccipital is lost (Fig. 3.10)

Table 3.2. Anatomical abbreviations

Cranial bones

Boc – Basioccipital
Bul – Bulla forming bone
De – Dentary
Eoc – Exoccipital
Ect – Ectotympanic
Fr – Frontal
Lc – Lacrimal
Mx – Maxilla
Ns – Nasal
Pa – Parietal
Pal – Palatine
Pmx – Premaxilla
Ptr – Petrosal
Soc – Supraoccipital
Sq – Squamosal
Zy – Zygomatic

Miscellaneous osteological feature

av – aperture for vestibular fenestra
ac – aperture for cochlear fenestra
bs – bullar suture (?)
cc – cochlear canaliculus: Visible as the most posterior "septum" on medial aspect of promontorium. Houses a canal that connects the spiral cochlea to endocranial space (see MacPhee, 1981). HRxCT data was used in most cases to evaluate the presence of this feature.
ec – epitympanic crest
eam – external auditory meatus
g1 – a groove with a lateral route that likely holds the internal carotid plexus and possibly a remnant of the internal carotid artery
g2 – a groove with a slightly more medial route that may hold internal carotid plexus fibers that approach the s1
g3 – a groove that leads to the s2, which likely contains contributions from the tympanic plexus, but is probably mainly responsible for transmitting a small vein (MacPhee, 1981)
g4 – a frequently present alternative or additional groove for tympanic plexus fibers to reach routes 1-3
g5 – frequently present groove that leads from a point ventral to the fenestra vestibuli dorsolaterally, toward the epitympanic crest
ica – internal carotid artery
icp – internal carotid (neurovascular) plexus
pcf – posterior carotid foramen

ps – posterior septum (and internal carotid canal): laterally curving septum of bone that shields the fenestra cochlea dorsally and holds a canal that leads to the posterior carotid foramen ventrally

s1 – first (anterior) septum: most lateral septum extending anteriorly from promontorium (tubal canal forms between *s1* and epitympanic crest)

s2 – second (medial secondary) septum: forms medial to s1, projects anteromedially from promontorium. *g3* typically leads to the ventral or medial aspect of this septum

s3 – third septum: Projects medially between *s2* and raised ridge of cochlear canaliculus, more posteriorly

tca – tympanic canaliculus: Foramina and groove on or near ridge of cochlear canaliculus in tympanic cavity marking the entrance of the tympanic nerve from extracranial space, and the re-entrance of the nerve into the promontorium as it moves laterally to contribute to the tympanic plexus. Associated canals do not communicate with cochlea.

Table 3.3. Size comparison among plesiadapid skulls

Specimen **Taxon**	**USNM 309902** ***Nannodectes intermedius***	**UALVP 46685** ***Pronothodectes gaoi***	**AMNH 17388** ***Nannodectes gidleyi***	**YPM-PU 19642** ***Plesiadapis anceps***	**MNHN CR 965** ***Plesiadapis tricuspidens***	**Pellouin Skull** ***Plesiadapis tricuspidens***	**MNHN CR 125** ***Plesiadapis tricuspidens***	**UM 87990** ***Plesiadapis cookei***
mean CR 125 %	202 (14)	174 (21)	187 (11)	121 (6)	108 (4)	99.5 (30)	100 (39)	100.5 (39)
Cranial estimate[a]	50.7 mm	61.1 mm	56.9 mm	87.9 mm	98.5 mm	106.9 mm	106.3 mm	105.8 mm
mean UM 87990%	210 (14)	173 (21)	170 (11)	153 (6)	110 (4)	99.4 (30)	99.5 (39)	100 (39)
Cranial estimate[b]	50.4 mm	61.2 mm	62.3 mm	69.2 mm	96.2 mm	106.5 mm	106.3 mm	105.8 mm

[a]Cranial estimates based on a measured length of 106.36 mm for MNHN CR 125.
[b]Cranial estimates based on a estimated length of 105.83 mm for UM 87990.

Table 3.4. Tooth measurements of Plesiadapidae and Paramyidae.[a] Abbreviations: BH – Buckman Hollow, Cf – Clarkforkian, CPQ – Cedar Point Quarry, DQ – Divide Q, E – Europe, ECM – Eagle Coal Mine, GGS – George Gaylord Simpson locality, GQ – Gidley Q, MP – Mammalian Palaeogene reference levels, NA – North America, PQ – Princeton Q, PE – Palaeogene European biozones, SC – Sand Coulee, To – Torrejonian, Ti – Tiffanian, RBQ – Rock Bench Q, WN – Who Nose? Q

Specimen	Species	Ctnt	Locality	Relative age	absolut age	2d area	3d area	RFI	OPC
YPM-PU 17787	*Plesiadapis churchilli*	NA	SDQ	Ti-4	58.1	8.72	31.26	0.493	62
UM 108786	*Plesiadapis churchilli*	NA	DQ	Ti-4	58.1	9.33	33.98	0.460	61
UM 108748	*Plesiadapis churchilli*	NA	DQ	Ti-4	58.1	10.73	33.41	0.482	72
Mean	***Plesiadapis churchilli***					**9.59**	**32.88**	**0.478**	**64.79**
UM 80720	*Plesiadapis cookei*	NA	SC-19	Cf-2	56.4	29.39	78.05	0.488	64
UM 82364	*Plesiadapis cookei*	NA	SC-19	Cf-2	56.4	25.72	71.79	0.513	67
UM 65050	*Plesiadapis cookei*	NA	SC-20	Cf-2	56.4	26.20	71.59	0.503	67
UM 69913	*Plesiadapis cookei*	NA	SC-136	Cf-2	56.4	32.49	94.08	0.532	63
UM 65720	*Plesiadapis cookei*	NA	SC-62	Cf-2	56.4	27.73	75.46	0.501	62
UM 71764	*Plesiadapis cookei*	NA	SC-62	Cf-2	56.4	32.01	85.59	0.492	67
UM 79636	*Plesiadapis cookei*	NA	SC-116	Cf-2	56.4	25.04	67.03	0.492	60
UM 69995	*Plesiadapis cookei*	NA	SC-220	Cf-2	56.4	27.68	75.76	0.503	61
UM 87990	*Plesiadapis cookei*	NA	SC-117	Cf-2	56.4	23.38	61.26	0.482	53
UM 8801	*Plesiadapis cookei*	NA		Cf-2	56.4	29.79	78.26	0.483	68
Mean	***Plesiadapis cookei***					**27.94**	**75.89**	**0.499**	**63.25**
UM 68741	*Plesiadapis gingerichi*	NA	SC-179	Cf-1	56.8	18.67	47.77	0.469	69
YPM-PU 17814	*Plesiadapis simonsi*	NA	s24, 55N 97W	Ti-5b	57.2	16.18	42.54	0.483	77
UM 108451	*Plesiadapis simonsi*	NA	SC-389	Ti5b	57.2	16.27	41.88	0.473	65
Mean	***Plesiadapis simonsi***					**16.22**	**42.21**	**0.478**	**71**
UM 68027	*Plesiadapis dubius*	NA	SC-156	Cf-2	56.4	8.39	22.26	0.488	56
UM 67244	*Plesiadapis dubius*	NA	SC-143	Cf-2	56.4	10.77	23.89	0.508	69
UM 87211	*Plesiadapis dubius*	NA	FG-100	Cf-2	56.4	8.49	22.63	0.477	70
UM 63733	*Plesiadapis dubius*	NA	SC-143	Cf-2	56.4	10.06	18.98	0.487	52
UM 71332	*Plesiadapis dubius*	NA	BH	Cf-1	56.8	6.68	17.62	0.485	64
UM 77285	*Plesiadapis dubius*	NA	FG-41	Cf-1	56.8	9.65	18.48	0.481	59
UM 68357	*Plesiadapis dubius*	NA	BH	Cf-1	56.8	12.75	26.32	0.481	65
UM 109907	*Plesiadapis dubius*	NA	SC-389	Ti-5b	57.2	13.55	23.79	0.515	58
Mean	***Plesiadapis dubius***					**10.04**	**21.74**	**0.490**	**61.56**
UM 109996	*Plesiadapis fodinatus*	NA	SC-389	Ti-5b	57.2	8.65	23.97	0.455	61
UM 109581	*Plesiadapis fodinatus*	NA	SC-389	Ti-5b	57.2	7.17	24.10	0.507	63
UM 109521	*Plesiadapis fodinatus*	NA	SC-389	Ti-5b	57.2	7.07	27.29	0.471	67
YPM-PU 13941	*Plesiadapis fodinatus*	NA	PQ	Ti-5a	57.6	10.18	27.61	0.499	63
YPM-PU 14032	*Plesiadapis fodinatus*	NA	PQ	Ti-5a	57.6	11.67	25.48	0.508	67
YPM-PU 13975	*Plesiadapis fodinatus*	NA	PQ	Ti-5a	57.6	8.74	31.15	0.528	60
YPM-PU 17601	*Plesiadapis fodinatus*	NA	PQ	Ti-5a	57.6	10.64	28.64	0.489	62
Mean	***Plesiadapis fodinatus***					**9.16**	**26.89**	**0.494**	**63.21**
UM 870065	*Plesiadapis rex*	NA	GGS 13	Ti-3	59.2	9.60	25.33	0.485	68
GGS-13, 2002 spec.	*Plesiadapis rex*	NA	GGS 13	Ti-3	59.2	8.31	22.08	0.488	52
UM 900317	*Plesiadapis rex*	NA	GGS 13	Ti-3	59.2	10.03	26.17	0.479	68
UM 900312	*Plesiadapis rex*	NA	GGS 13	Ti-3	59.2	9.65	24.01	0.456	57
UM 880149	*Plesiadapis rex*	NA	GGS 13	Ti-3	59.2	9.57	24.81	0.476	62
UM 870063	*Plesiadapis rex*	NA	GGS 13	Ti-3	59.2	10.34	24.72	0.436	50
UM 870061	*Plesiadapis rex*	NA	GGS 13	Ti-3	59.2	11.60	30.01	0.475	66
UM 880566	*Plesiadapis rex*	NA	GGS 13	Ti-3	59.2	9.51	23.88	0.460	60
UM L13-2	*Plesiadapis rex*	NA	GGS 13	Ti-3	59.2	10.10	25.22	0.458	53
YPM-PU 20059	*Plesiadapis rex*	NA	CPQ	Ti-3	59.2	10.07	25.76	0.470	67
YPM-PU 20058	*Plesiadapis rex*	NA	CPQ	Ti-3	59.2	9.56	24.43	0.469	67
YPM-PU 21289	*Plesiadapis rex*	NA	CPQ	Ti-3	59.2	9.45	22.91	0.443	58
Mean	***Plesiadapis rex***					**9.82**	**24.94**	**0.466**	**60.54**
UALVP 43232	*Pronothodectes matthewi*	NA	WN	To-2	63.1	4.48	11.47	0.470	62
UALVP 43276	*Pronothodectes matthewi*	NA	WN	To-2	63.1	4.05	11.01	0.500	51
AMNH 35469	*Pronothodectes matthewi*	NA	GQ	To-2	63.1	4.62	11.94	0.474	57
AMNH 35462	*Pronothodectes matthewi*	NA	GQ	To-2	63.1	5.13	13.53	0.485	60
AMNH 35467	*Pronothodectes matthewi*	NA	GQ	To-2	63.1	4.62	12.10	0.482	56
UALVP 43231	*Pronothodectes matthewi*	NA	WN	To-2	63.1	3.53	8.60	0.445	58
UALVP no num 1	*Pronothodectes matthewi*	NA	WN	To-2	63.1	5.11	13.43	0.483	63
UALVP 43279	*Pronothodectes matthewi*	NA	WN	To-2	63.1	4.76	12.67	0.490	62
UALVP 43275	*Pronothodectes matthewi*	NA	WN	To-2	63.1	4.73	12.15	0.472	56
YPM-PU 17454	*Pronothodectes jepi*	NA	RBQ	To-2	63.1	6.15	16.26	0.486	70
YPM-PU 17436	*Pronothodectes jepi*	NA	RBQ	To-2	63.1	4.67	11.86	0.466	52
YPM-PU 14783	*Pronothodectes jepi*	NA	RBQ	To-2	63.1	6.00	15.51	0.475	57
Mean	***Pronothodectes***					**4.82**	**12.54**	**0.477**	**58.61**

Table 3.4 continued. European plesiadapids.

Specimen	Species	Ctnt	Locality	Relative age	absolut age	2d area	3d area	RFI	OPC
MNHN BR-71-l	*Chiromyoides campanicus*	E	Berru	MP6-7(PE 1)	57.2	7.25	16.54	0.412	55
MNHN BR 13925	*Chiromyoides campanicus*	E	Berru	MP6-7(PE 1)	57.2	8.15	17.75	0.389	62
MNHN-R 859	*Chiromyoides campanicus*	E	Berru?	MP6-7(PE 1)	57.2	7.90	16.99	0.383	55
UM SC-243	*Chiromyoides sp.*	NA	SC-243	Ti-4	58.1	6.52	14.94	0.415	59
Mean	***Chiromyoides***					**7.46**	**16.56**	**0.400**	**57.63**
MNHN AV 5762	*Platychoerops daubrei*	E	Avernay	MP 9 (PE V)	52.0	22.68	62.10	0.504	84
MNHN AL(j)	*Platychoerops daubrei*	E	Avernay	MP 9 (PE V)	52.0	20.67	60.43	0.536	70
MNHN MU 5578	*Platychoerops daubrei*	E	Mutigny	MP 8 (PE III)	54.8	15.57	42.56	0.503	68
MNHN MU 5939	*Platychoerops daubrei*	E	Mutigny	MP 8 (PE III)	54.8	19.58	56.28	0.528	76
MNHN MU 5560	*Platychoerops daubrei*	E	Mutigny	MP 8 (PE III)	54.8	22.74	70.12	0.563	76
MNHN MU 6184	*Platychoerops daubrei*	E	Mutigny	MP 8 (PE III)	54.8	18.72	50.95	0.501	72
MNHN MU 6275	*Platychoerops daubrei*	E	Mutigny	MP 8 (PE III)	54.8	18.22	49.61	0.501	70
MNHN MU 12302	*Platychoerops daubrei*	E	Mutigny	MP 8 (PE III)	54.8	20.99	62.82	0.548	70
MNHN MU 12301	*Platychoerops daubrei*	E	Mutigny	MP 8 (PE III)	54.8	18.70	55.22	0.541	71
Mean	***Platychoerops daubrei***					**19.76**	**56.68**	**0.525**	**73.08**
MNHN BR 12493	*Plesiadapis tricuspidens*	E	Berru	MP6-7 (PE 1)	57.2	16.80	42.95	0.469	60
MNHN BR NN4a	*Plesiadapis tricuspidens*	E	Berru	MP6-7 (PE 1)	57.2	17.42	43.79	0.461	55
MNHN BR NN4c	*Plesiadapis tricuspidens*	E	Berru	MP6-7 (PE 1)	57.2	18.82	48.28	0.471	59
MNHN BR-L-51	*Plesiadapis tricuspidens*	E	Berru	MP6-7 (PE 1)	57.2	22.97	59.73	0.478	62
MNHN CR 14363	*Plesiadapis tricuspidens*	E	Berru	MP6-7 (PE 1)	57.2	16.23	40.68	0.459	61
MNHN BR NN2a	*Plesiadapis tricuspidens*	E	Berru	MP6-7 (PE 1)	57.2	18.72	47.65	0.467	51
MNHN BR NN2b	*Plesiadapis tricuspidens*	E	Berru	MP6-7 (PE 1)	57.2	16.81	40.93	0.445	61
MNHN BR NN2d	*Plesiadapis tricuspidens*	E	Berru	MP6-7 (PE 1)	57.2	15.25	36.99	0.443	46
Mean	***Plesiadapis tricuspidens***					**17.88**	**45.12**	**0.462**	**56.86**

Table 3.4 continued. Clarkforkian rodents.

Specimen	Species	Ctnt	Locality	Relative age	absolut age	2d area	3d area	RFI	OPC
UM 77755	*Acritoparamys atwateri*	NA	SC-188	Cf-2	56.8	4.46	10.86	0.445	50
UM 77719	*Microparamys cheradius*	NA	SC-188	Cf-2	56.8	2.35	5.42	0.419	69
UM 77752	*Acritoparamys atavus*	NA	SC-188	Cf-2	56.8	2.20	5.56	0.462	57
UM 75443	*Acritoparamys atavus*	NA	SC-188	Cf-2	56.8	5.63	13.52	0.438	63
UM 77771	*Reithroparamys* sp. indet.	NA	SC-188	Cf-2	56.8	7.05	17.91	0.466	64
UM 71177	*Acritoparamys atwateri*	NA	SC-74	Cf-2	56.8	4.79	12.26	0.470	57
YPM-PU 14200	*Acritoparamys atavus*	NA	ECM	Cf-3	56.8	2.79	6.96	0.456	67
UM 69871	*Acritoparamys atavus*	NA	SC-214	Cf-3	56.8	2.36	5.97	0.467	68
UM 71173	*Acritoparamys atavus*	NA	SC-74	Cf-3	56.8	2.27	6.03	0.474	64
UM 77834	*Paramys taurus*	NA	SC-48	Cf-3	56.8	6.64	16.49	0.455	59
Mean	**Paramyidae**					**4.05**	**10.10**	**0.455**	**61.78**

a – gray cells show data used in analyses of this study

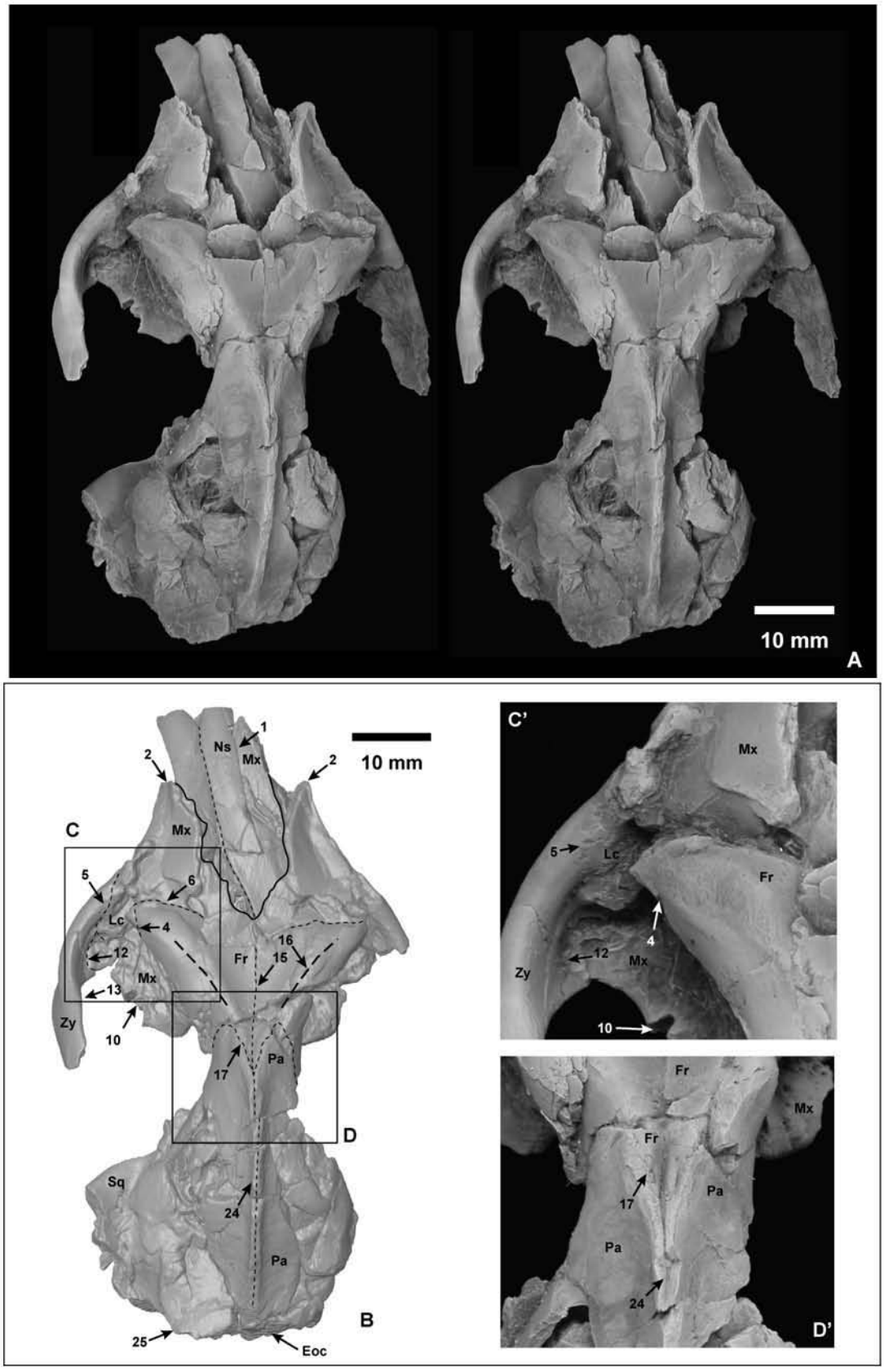
10 mm
A
Ns
Mx
1
2
2
10 mm
C
Mx
5
6
Lc
4
12
Mx
13
Zy
10
Fr
16
15
17
Pa
D
Sq
24
Pa
25
Eoc
B
C'
Mx
5
Lc
Fr
4
12
Mx
Zy
10
Fr
Mx
Fr
17
Pa
Pa
24
D'

Figure 3.1

Figure 3.1. Cranium of *Plesiadapis cookei* (UM 87990). A, stereophotographic dorsal view. B, HRxCT dorsal view reconstruction shown without parallax. C, inset of anteromedial wall of orbit. C', enlargement of inset C. D, inset of orbitotemporal region. D', enlargement of inset D. Fine dashed lines represent sutures, coarse dashed lines represent temporal crests, and solid lines indicate major discontinuities on the specimen's surface. Numbers and abbreviations: 1 – premaxilla/nasal suture, 2 – premaxilla/maxillary suture, 4 – lacrimal/frontal suture in orbit, 5 – lacrimal/zygomatic suture in orbit, 6 – maxilla/frontal suture on forehead, 10 – dorsal communication of M^3 alveolus with orbital cavity, 12 – zygomatic/maxillary suture, 13 – edge of orbital excavation on zygomatic bone, 15 – metopic suture, 16 – ridges of frontal trigon, 17 – frontal/parietal suture, most anterior part, 24 – sagittal crest, 25 – nuchal crest; Eoc – exocipital; Fr – frontal; Lc – lacrimal; Mx – maxilla; Ns – nasal; Pa – parietal; Sq – squamosal; Zy – zygomatic.

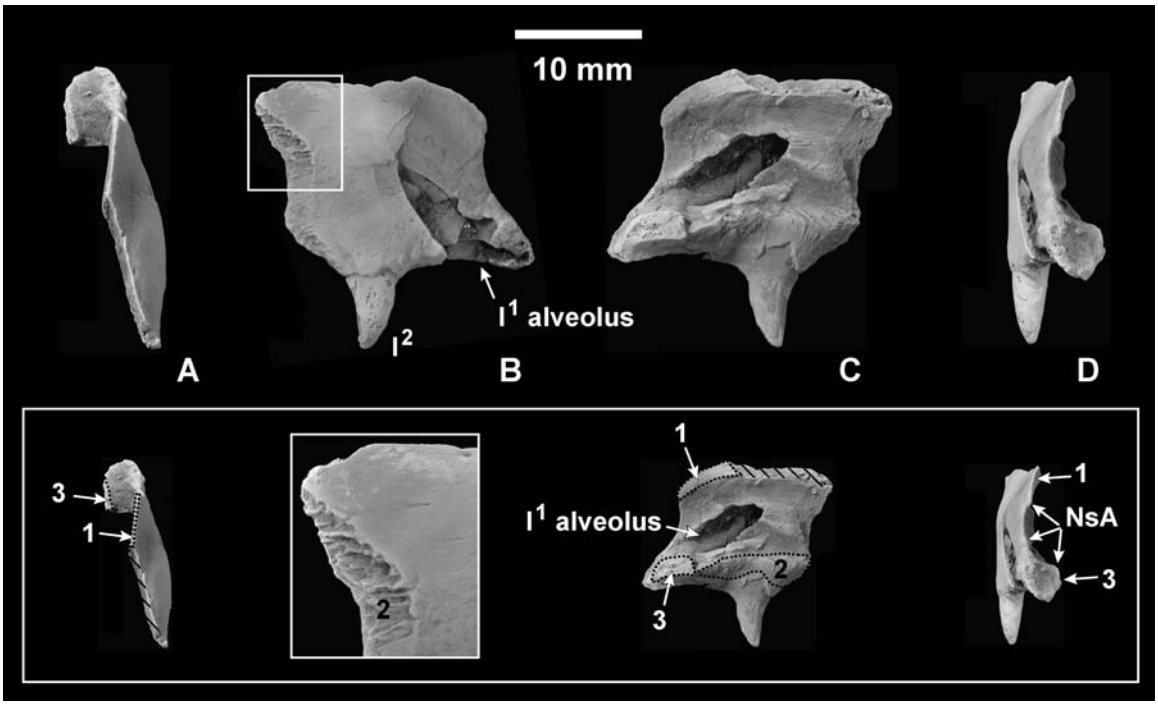

Figure 3.2. Right premaxilla of *Plesiadapis cookei* (UM 87990) in A, dorsal (anterior to top); B, lateral (anterior to right); C, medial (anterior to left); and D, anterior views (dorsal to top) with corresponding labeled or enlarged photographs at bottom. Hatching indicates broken surfaces. Dashed lines encircle sutural surfaces. Numbers and abbreviations: 1– premaxilla/nasal suture, 2 – premaxilla/maxillary suture, 3 – premaxillary symphysis; NsA – Nasal aperture.

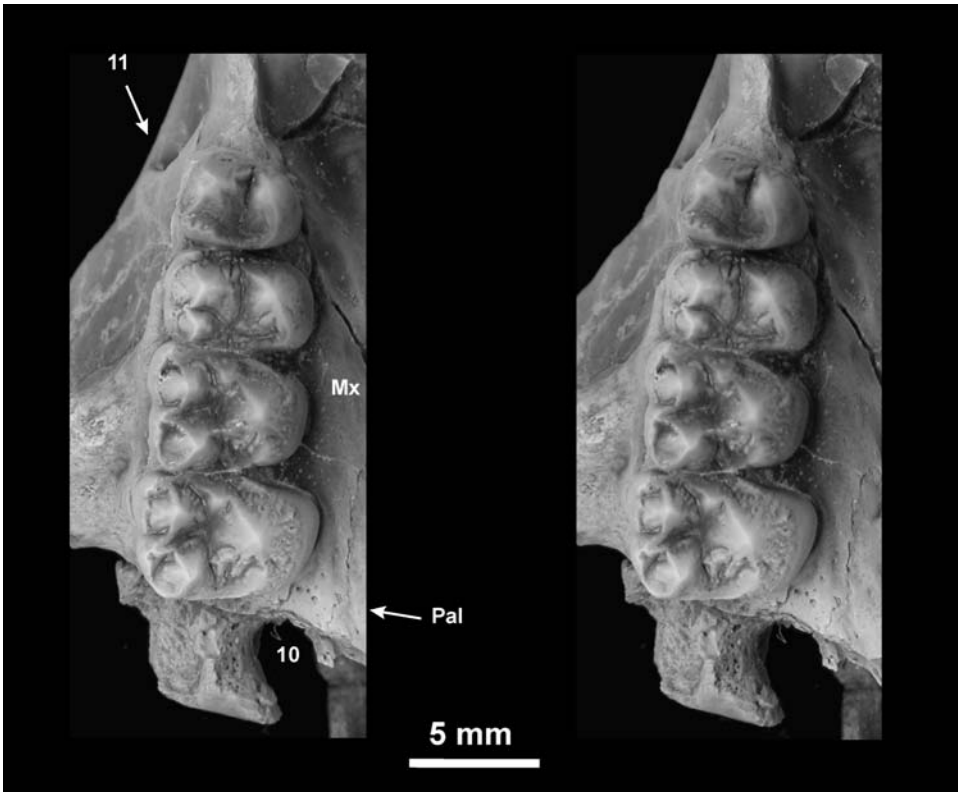

Figure 3.3. Right maxillary teeth (P^3-M^2) of *Plesiadapis cookei* (UM 87990) in stereophotographic occlusal view. Note absence of P^2, lack of paraconule on $P^{3,4}$, and dilambdodont morphology of molars sporting mesostyles. These features form a diagnostic suite for *Plesiadapis cookei*. Numbers and abbreviations: 10 – dorsal communication of M^3 alveolus with orbital cavity, 11 – infraorbital foramen; Mx – maxilla; Pal – palatine.

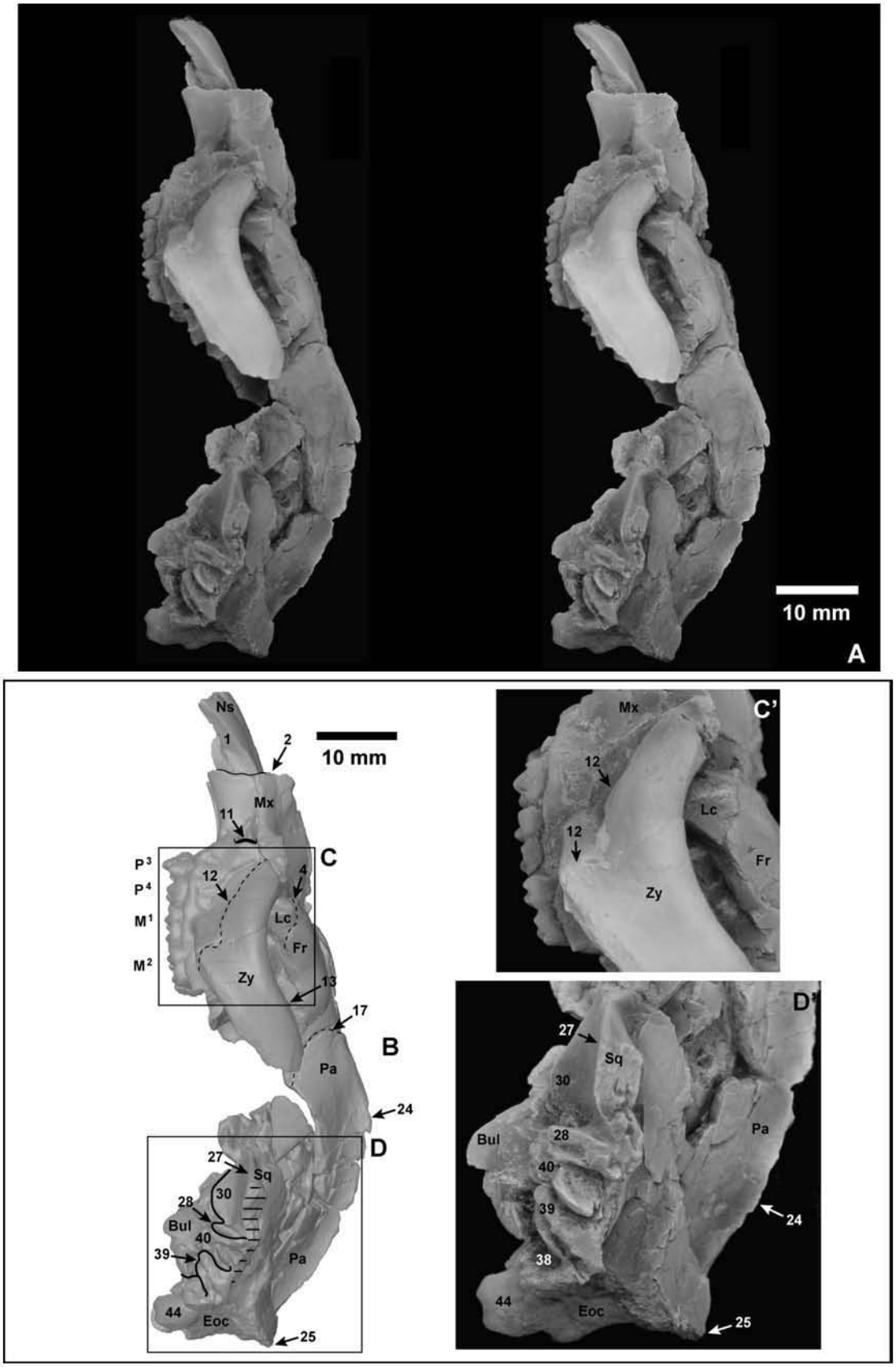
10 mm
A
Ns
1
2
10 mm
Mx
11
C
P3
P4
M1
M2
12
4
Lc
Fr
Zy
13
17
B
Pa
24
D
27
Sq
30
28
Bul
40
39
Pa
44
Eoc
25
C'
Mx
12
Lc
12
Fr
Zy
D'
27
Sq
30
Bul
28
Pa
40
39
24
38
44
Eoc
25

Figure 3.4.

Figure 3.4. Cranium of *Plesiadapis cookei* (UM 87990). A, stereophotographic left lateral view. B, HRxCT left lateral view reconstruction shown without parallax. C, inset of lateral splanchnocranium. C', enlargement of inset C. D, inset of basicranium. D', enlargement of inset D. Hatches indicate broken surfaces. Fine dashed lines represent sutures and solid lines indicate major discontinuities on the specimen's surface. Numbers and abbreviations: 1– premaxilla/nasal suture, 2 – premaxilla/maxillary suture, 4 – lacrimal/frontal suture in orbit, 11 – infraorbital foramen, 12 – zygomatic/maxillary suture, 13 – edge of orbital excavation on zygomatic bone, 17 – frontal/parietal suture, most anterior part, 24 – sagittal crest, 25 – nuchal crest, 27 – glenoid fossa, 28 – postglenoid process, 30 – entoglenoid process, 38 – digastric fossa, stylomastoid foramen area (?), 39 – paroccipital process (mastoid process) of petrosal, 40 – tubular external auditory meatus, 44 – occipital condyle; Bul – auditory bulla; Eoc – exoccipital; Fr – frontal; Lc – lacrimal; Mx – maxilla; Ns – nasal; Pa – parietal; Sq – squamosal; Zy – zygomatic.

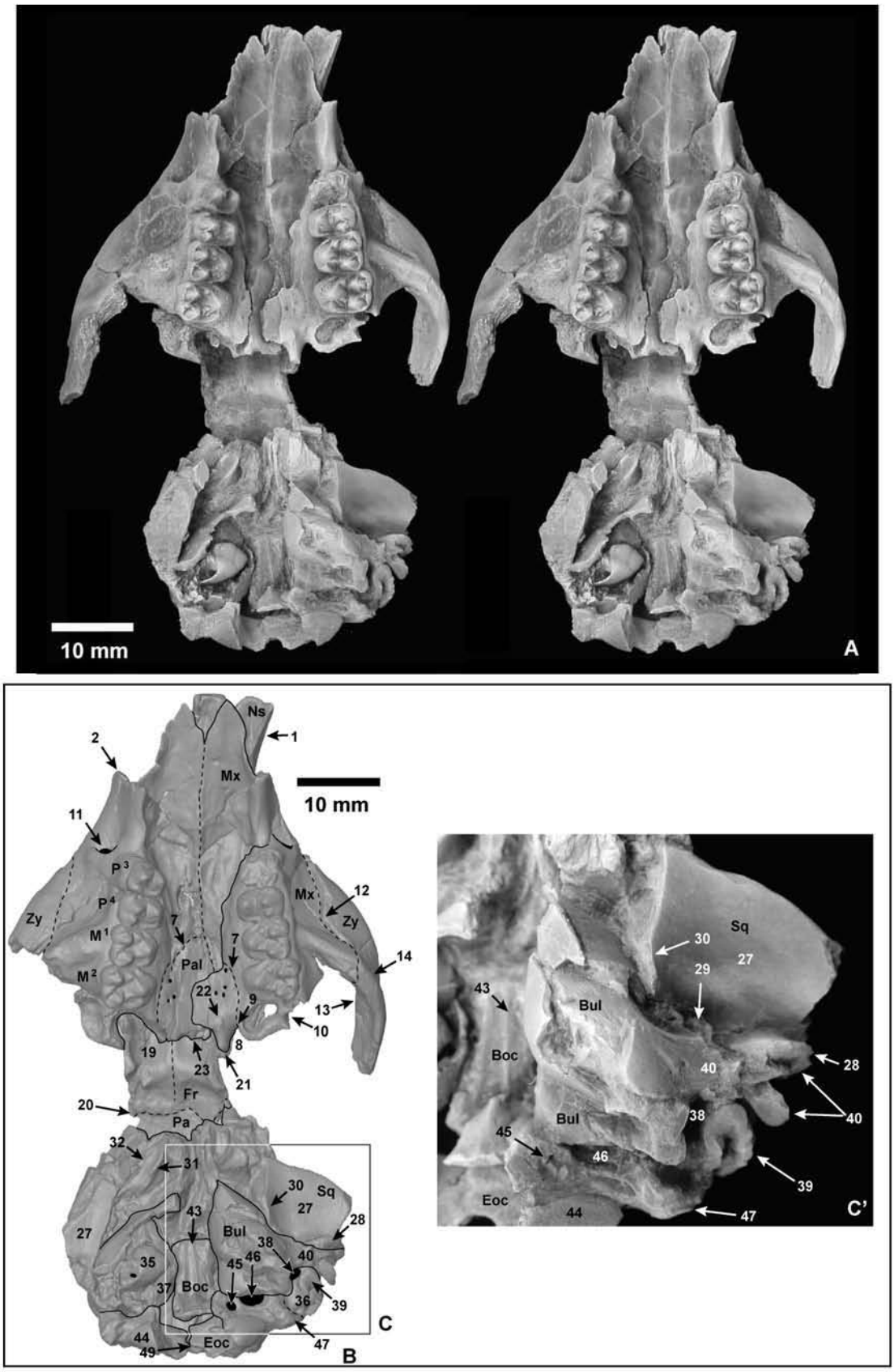
10 mm
A
Ns
1
2
Mx
10 mm
11
P3
P4
M1
M2
Zy
7
Pal
22
9
13
10
12
14
8
19
23
21
Fr
20
Pa
32
31
30
Sq
27
43
Bul
28
38
40
45
46
35
37
Boc
36
39
44
49
Eoc
47
B
C
C'
29
Bul
Boc
40
38
45
46
Eoc
44
47
39

Figure 3.5.

Figure 3.5. Cranium of *Plesiadapis cookei* (UM 87990). A, stereophotographic ventral view. B, HRxCT ventral view reconstruction shown without parallax. C, inset of left glenoid and bulla. C', enlargement of inset C. Fine dashed lines represent sutures and solid lines indicate major discontinuities on the specimen's surface. Numbers and abbreviations: 1 – premaxilla/nasal suture, 2 – premaxilla/maxillary suture, 7 – maxilla/palatine suture at level of M^1 in palate, 8 – notch between pterygoid process of palatine and M^3 alveolus marking lesser palatine nerve route, 9 – maxilla/palatine suture at level of M^3 in palate, 10 – dorsal communication of M^3 alveolus with orbital cavity, 11 – infraorbital foramen, 12 – zygomatic/maxillary suture, 13 – edge of orbital excavation on zygomatic bone, 14 – expansion of ventral surface of zygomatic for masseter attachment, 19 – endocranial surface of frontal, depressions for olfactory bulbs, 20 – frontal/parietal suture on endocranial surface, 21 – base of left pterygoid process of palatine, 22 – postpalatine torus, 23 – postpalatine spine, 27 – glenoid fossa, 28 – postglenoid process, 29 – postglenoid foramen, 30 – entoglenoid process, 31 – basisphenoid entopterygoid process, 32 – alisphenoid ectopterygoid process, 35 – pars cochlearis of petrosal, 36 – pars canalicularis of petrosal, 37 – tympanic processes of auditory bulla, 38 – digastric fossa, stylomastoid foramen area (?), 39 – paroccipital process (mastoid process) of petrosal, 40 – tubular external auditory meatus, 43 – sagittal ridge of bone on basioccipital, 44 – occipital condyles, 45 – hypoglossal foramen, 46 – jugular foramen, 47 – jugular processes, 49 – sagittal contact between right and left exoccipitals; Boc – basioccipital; Bul – auditory bulla, Eoc – Exoccipital; Fr – frontal; Mx – maxilla; Ns – nasal; Pa – parietal; Sq – squamosal; Zy – zygomatic.

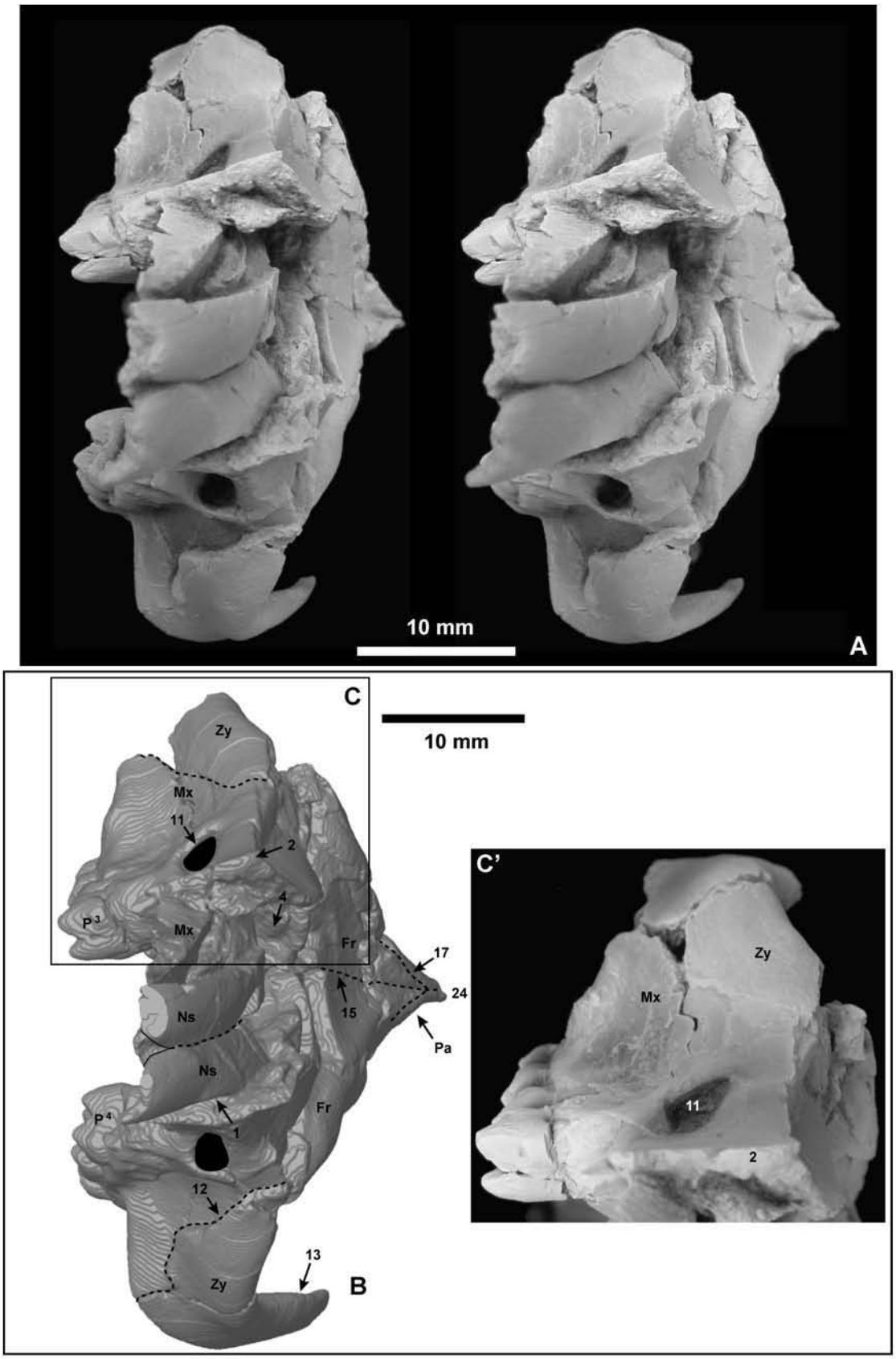
10 mm
A
C
10 mm
Zy
Mx
11
2
4
P3
Mx
Fr
17
24
15
Pa
Ns
Ns
P4
1
Fr
12
13
Zy
B
C'
Zy
Mx
11
2

Figure 3.6.

Figure 3.6. Cranium of *Plesiadapis cookei* (UM 87990). A, stereophotographic anterior view. B, HRxCT anterior view reconstruction shown without parallax. C, inset of right splanchnocranium. C', enlargement of inset C. Fine dashed lines represent sutures and solid lines indicate major discontinuities on the specimen's surface. Numbers and abbreviations: 1 – premaxilla/nasal suture, 2 – premaxilla/maxillary suture, 11 – infraorbital foramen, 12 – zygomatic/maxillary suture, 13 – edge of orbital excavation on zygomatic bone, 15 – metopic suture, 16 – ridges of frontal trigon, 17 – frontal/parietal suture, most anterior part, 24 – sagittal crest; Fr – frontal; Mx – maxilla; Ns – nasal; Pa – parietal; Zy – zygomatic.

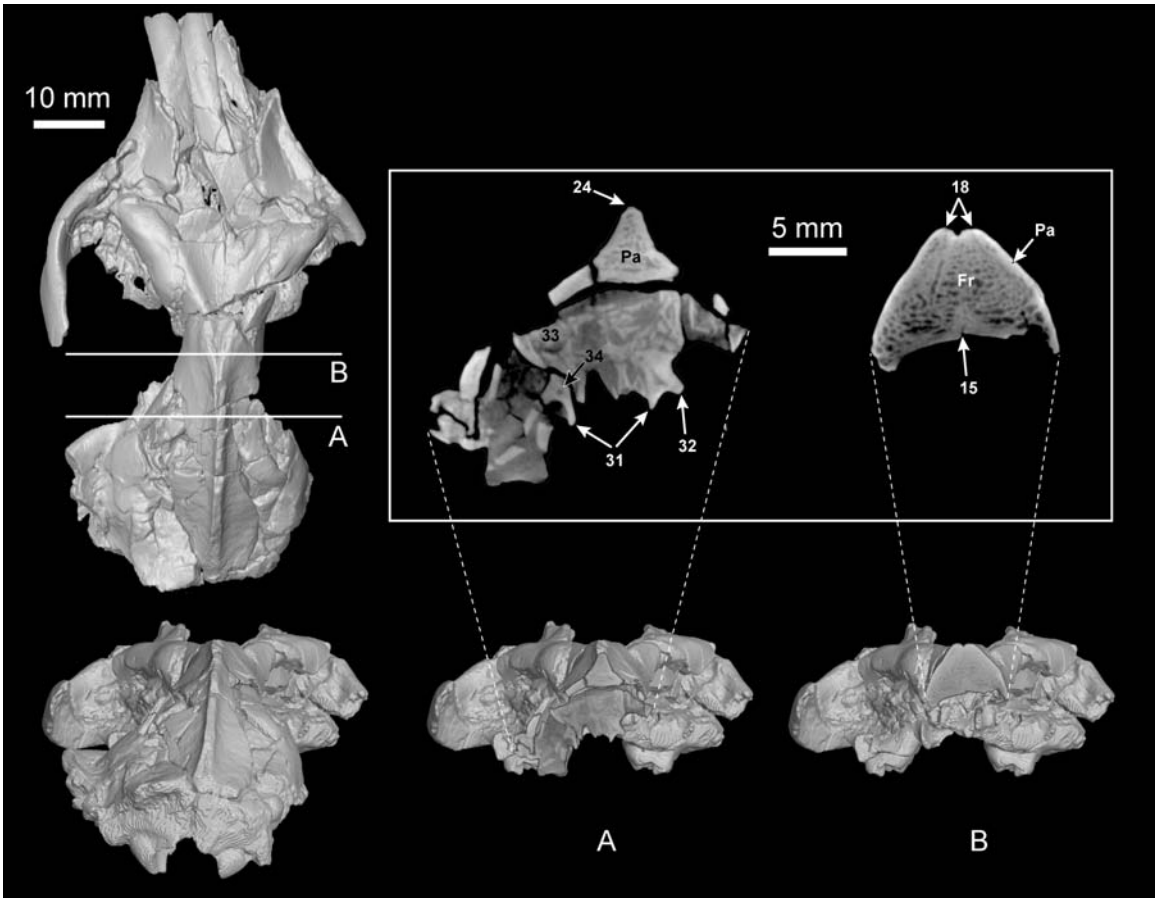

Figure 3.7. Cranium of *Plesiadapis cookei* (UM 87990) – internal information revealed by HRxCT data. Top left – cranium reconstruction in dorsal view (perpendicular to slice orientation, showing position of cross-sections in A and B. Bottom left – cranium rotated into posterodorsal view. A, Skull reconstruction in posterodorsal view with bone posterior to first cross section level removed. Enlargement of this cross section shows sphenoids that have been crushed into the cranium. B, Skull reconstruction in posterodorsal view with bone posterior to second cross section level removed. Enlargement of this cross section through orbitotemporal region, close to point of maximum orbitotemporal constriction, shows onlapping suture of parietal on frontal. Numbers and abbreviations: 15 – metopic suture, 18 – cross-sectional view of frontal/parietal contact, 24 – sagittal crest, 31 – basisphenoid entopterygoid process, 32 – alisphenoid ectopterygoid process, 33 – canal leading to sphenorbital fissure, 34 – possible vidian canal; Fr – frontal; Pa – parietal.

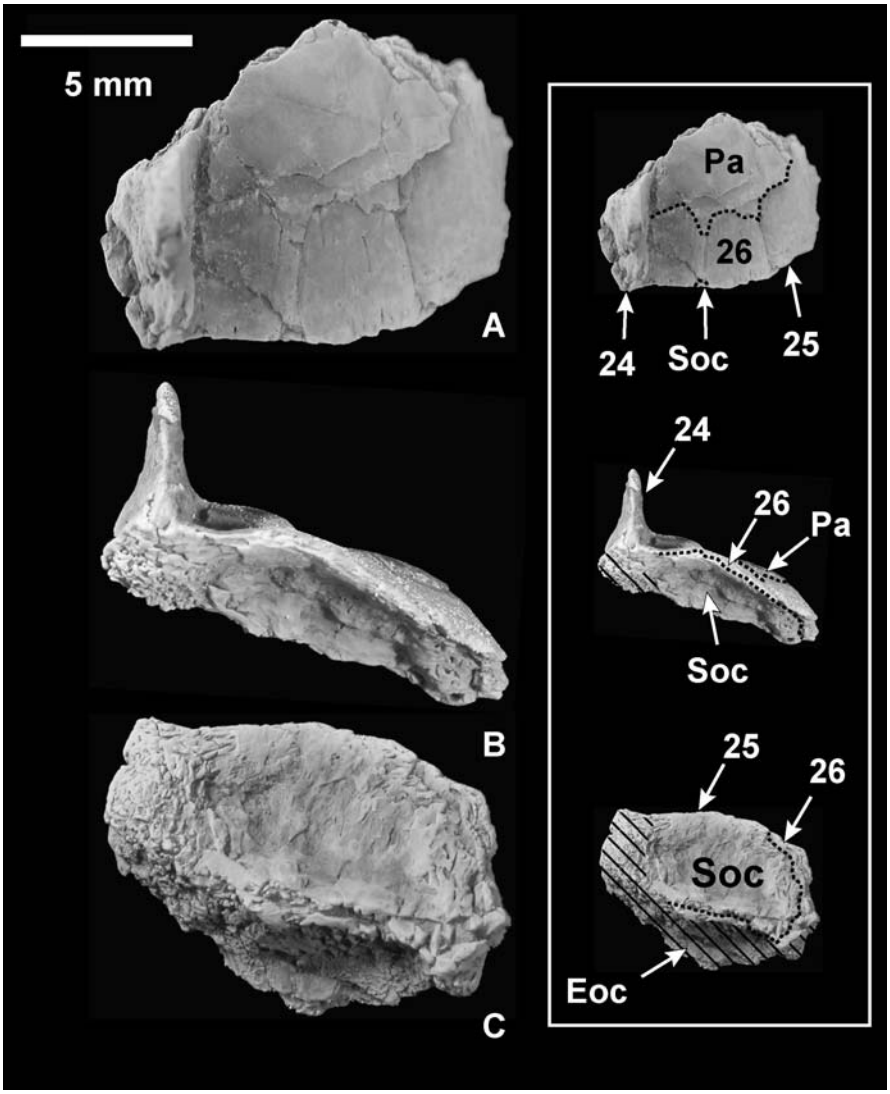

Figure 3.8. Fragment from right nuchal crest of *Plesiadapis cookei* (UM 87990) in A, dorsal (anterior to top); B, posterior (dorsal to top), and C, ventral views (anterior to bottom) with corresponding labeled photographs on right. Fine dashed lines represent sutures and hatched areas indicate broken surfaces. Numbers and abbreviations: 24 – sagittal crest, 25 – nuchal crest, 26 – parietal/?interparietal suture on dorsum of skull; Eoc – exocipital; Pa – parietal; Soc – supraoccipital.

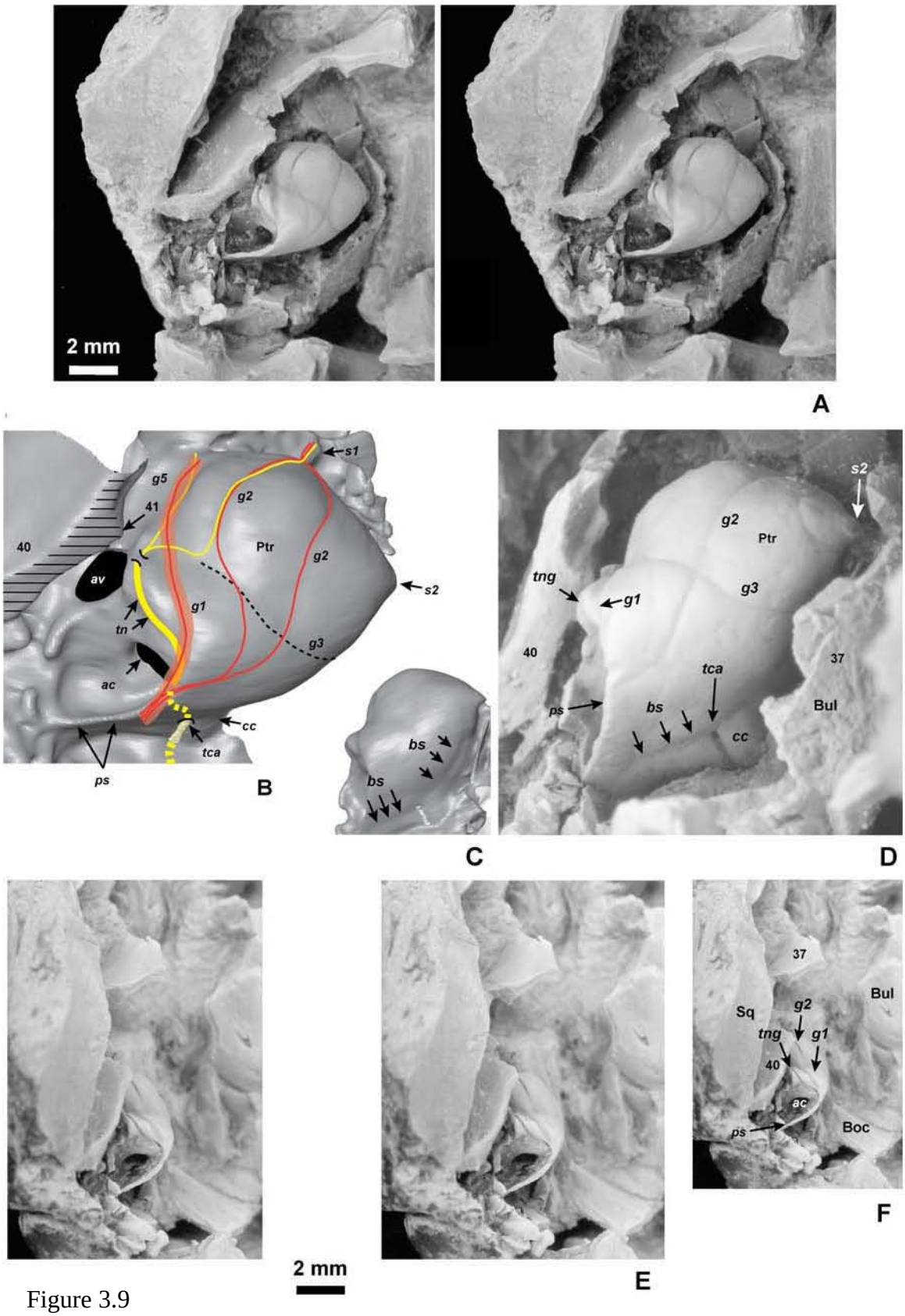
2 mm
A
s1
g5
41
g2
Ptr
g2
40
av
s2
g1
tn
g3
ac
cc
tca
ps
B
bs
bs
C
s2
g2
Ptr
tng
g1
g3
40
37
tca
ps
bs
Bul
cc
D
2 mm
E
37
Bul
Sq
g2
tng
g1
40
ac
ps
Boc
F

Figure 3.9

Figure 3.9. Right promontorium of *Plesiadapis cookei* (UM 87990): A, stereophotographic ventral view. B, HRxCT ventral view reconstruction shown without parallax. C, HRxCT ventromedial view reconstruction – fragment of tympanic process (*37*) has been digitally removed to show continuation of foramina lined groove that may represent a suture. D, close-up of promontorium in same view as part C. E, stereophotographic lateral view (ventral to right, anterior to top). F, same view as E. Hatches indicate broken surfaces, thick red line represents main course of internal carotid plexus while thin red lines represent branches stemming from the internal carotid plexus. Yellow lines represent components of the tympanic plexus. Fine dashed line – g3 groove. Numbers and abbreviations: 37 – tympanic processes of auditory bulla, 40 – tubular external auditory meatus, 41 – crista tympanica; Boc – basioccipital; Bul – auditory bulla; Eoc – exoccipital; Ptr – petrosal; Sq – squamosal; ac – aperture for cochlear fenestra; av – aperture for fenestra vestibuli; bs – bullar suture; cc – cochlear canaliculus; g1 – groove with lateral route that likely holds internal carotid plexus and possibly remnant of internal carotid artery; g2 – groove with slightly more medial route that may hold internal carotid plexus fibers that approach s1; g3 – groove that leads to s2, which likely contains contributions from tympanic plexus, but was mainly responsible for transmitting a small vein; g4 – frequently present alternative or additional groove for tympanic plexus fibers to reach routes 1-3; g5 – frequently present groove that leads from point ventral to vestibular fenestra dorsolaterally, toward epitympanic crest; ps – posterior septum; s1 – first (anterior) septum: most lateral septum extending anteriorly from promontorium (tubal canal forms between s1 and epitympanic crest); s2 – second septum: forms medial to s1, projects anteromedially from promontorium., tca – tympanic canaliculus; tng – tympanic nerve groove.

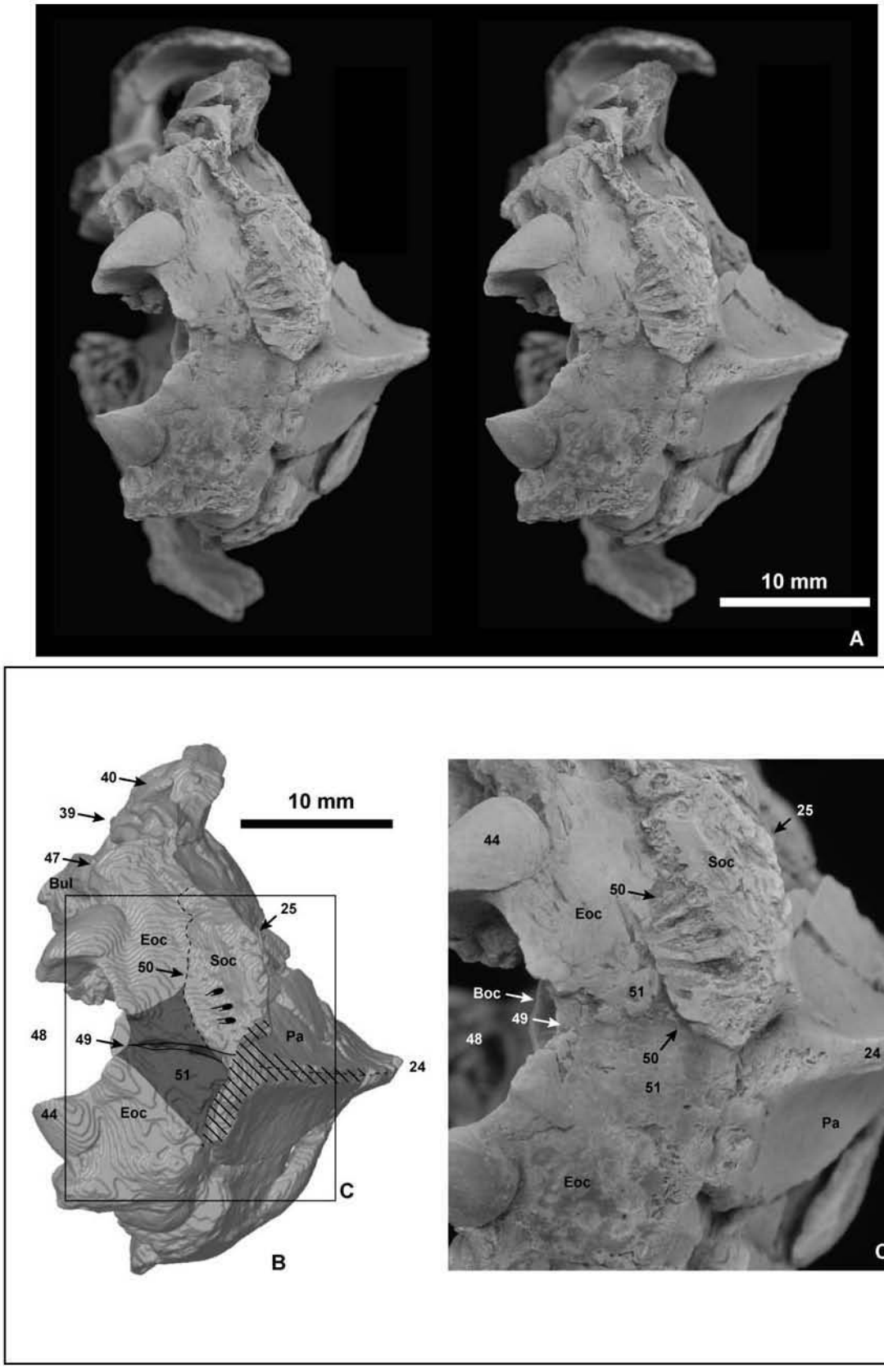
10 mm
A
40
39
47
Bul
10 mm
25
Eoc
50
Soc
48
49
Pa
24
51
44
Eoc
C
B
25
44
Soc
50
Eoc
Boc
51
49
48
50
24
51
Pa
Eoc
C

Figure 3.10

Figure 3.10. Cranium of *Plesiadapis cookei* (UM 87990). A, stereophotographic posterior view. B, HRxCT posterior view reconstruction shown without parallax. C, close-up of posterior view. Dashed lines represent sutures, hatched areas represent broken surfaces, and area in solid gray represents former site of supraoccipital bone. Numbers and abbreviations: 24 – sagittal crest, 25 – nuchal crest, 39 – paroccipital process (mastoid process) of petrosal, 40 – tubular external auditory meatus, 44 – occipital condyle, 47 – jugular process, 48 – foramen magnum, 49 – sagittal contact between right and left exoccipitals; 50 – sutural contact between remnants of supraoccipital and exoccipital; 51 – wedge-shaped depression on exoccipitals, where supraoccipital is lost; Boc – basioccipital; Eoc – exoccipital; Pa – parietal; Soc – supraoccipital.

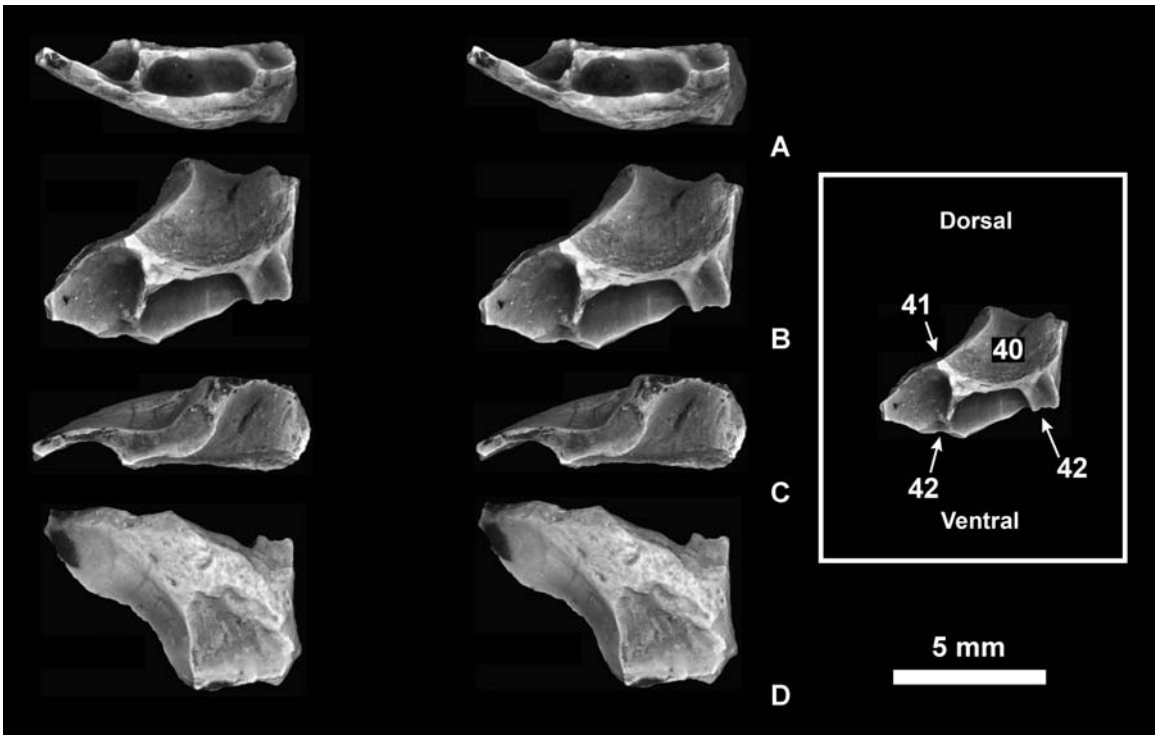

Figure 3.11. Right ectotympanic fragment of *Plesiadapis cookei* (UM 87990) in stereophotographic A, ventral (medial to top); B, medial (dorsal to top - labeled view to right); C, dorsal (medial to bottom); and D, lateral views (dorsal to bottom). Numbers and abbreviations: 40 – tubular external auditory meatus, 41 – crista tympanica, 42– bony struts supporting crista tympanica.

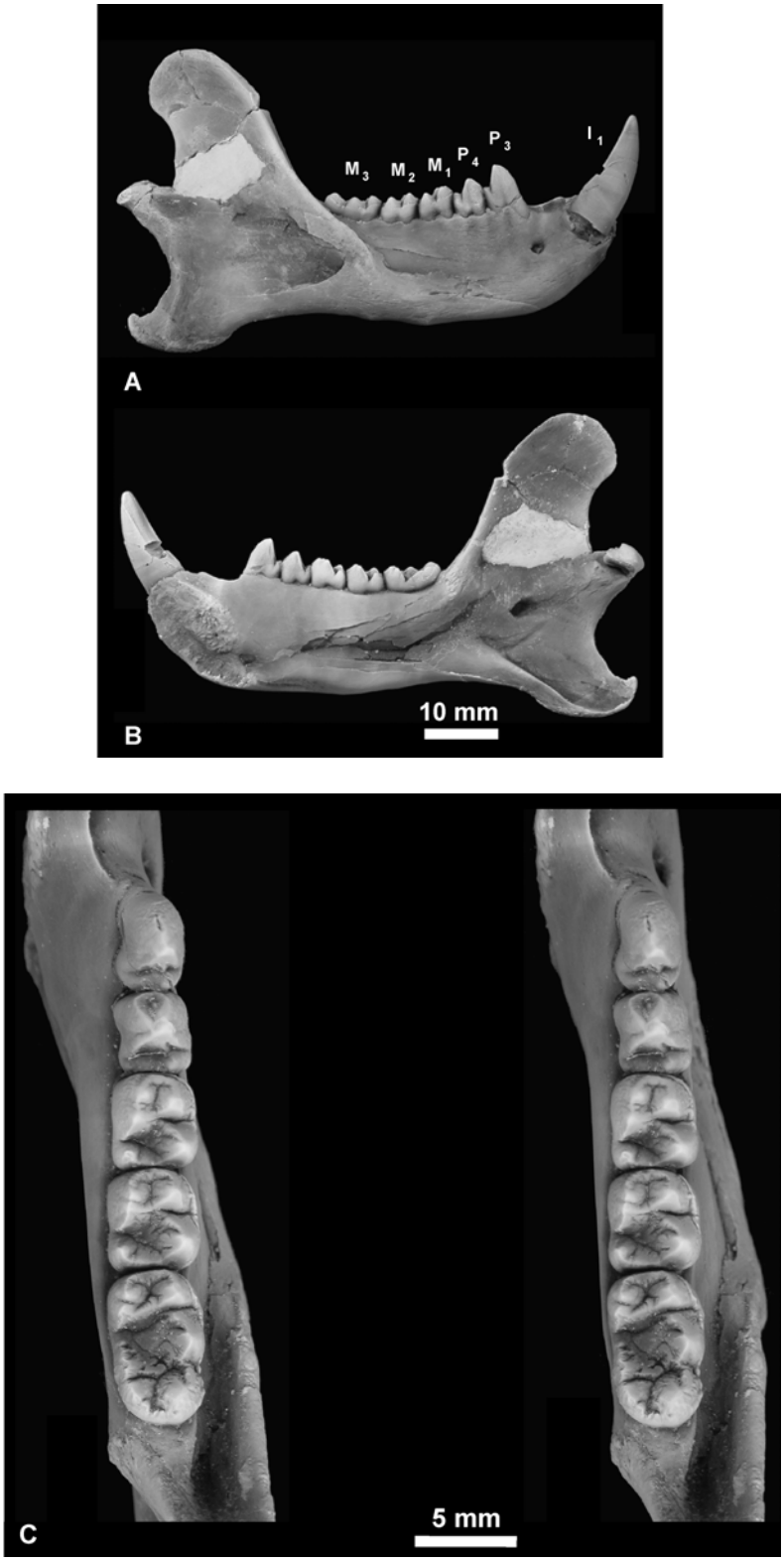

Figure 3.12. Right dentary of *Plesiadapis cookei* (UM 87990) in A, buccal; B, lingual; and C, stereophotograph occlusal views. On A and B, note lack of margoconid on I_1. On C, note trigonid basin of P_4.

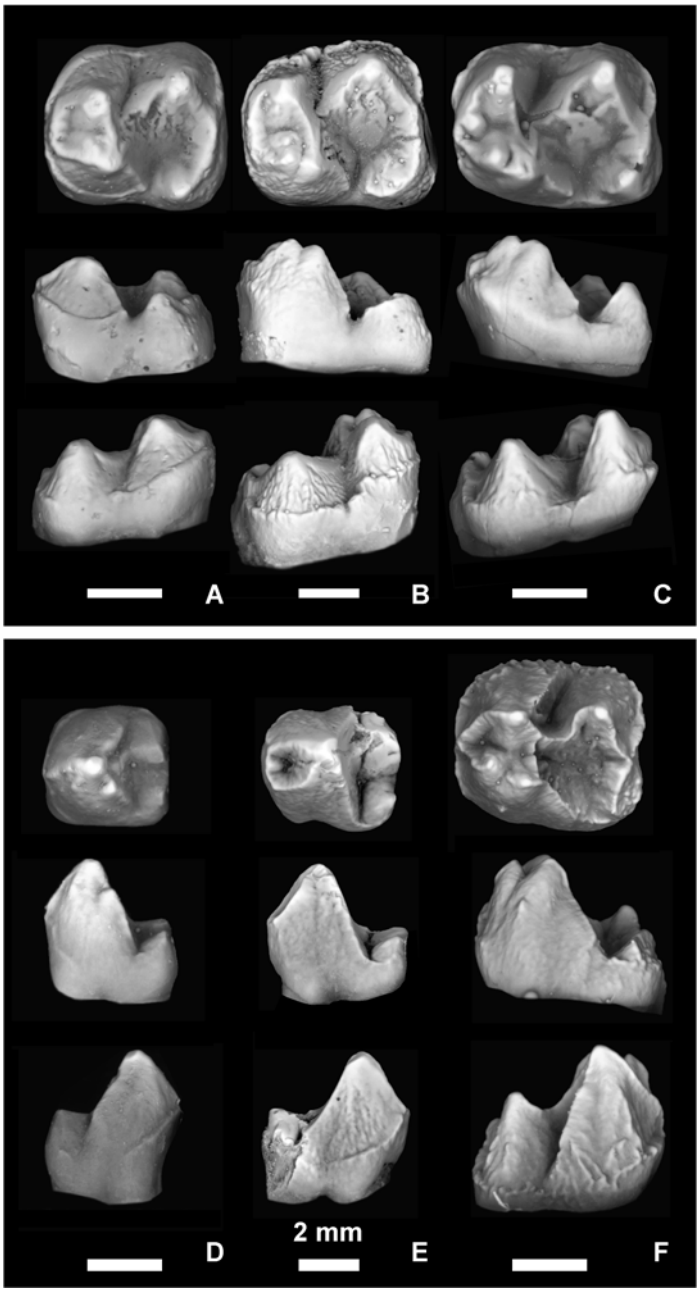

Figure 3.13. Lower teeth of selected Plesiadapidae. Top, M_2s, and bottom, P_4s, of A, D, *Plesiadapis rex* (unnumbered specimen from MNHN Berru collection, MNHN R129); B, E, *Plesiadapis cookei* (UM 66719, UM 69265), and C, F, *Platychoerops daubrei* (MNHN AL 5164, MNHN AL-j) in occlusal, lingual and buccal views (top to bottom within each frame). Molars are scaled to buccolingual width of talonid. Premolars are scaled to molar of the same taxon. Note that the M_2s of *P. cookei* and *Pl. daubrei* are relatively longer than those of *P. rex*, have relatively more buccolingually expanded trigonids, and larger, better-developed entoconids. Note that P_4s of all three taxa are virtually unworn, but only that of *P. rex* lacks a trigonid basin, even though it has metaconid. Furthermore, the P_4 of *P. cookei* has the beginnings of a paraconid and a fairly distinct entoconid, visible in occlusal view. All scales represent 2 mm.

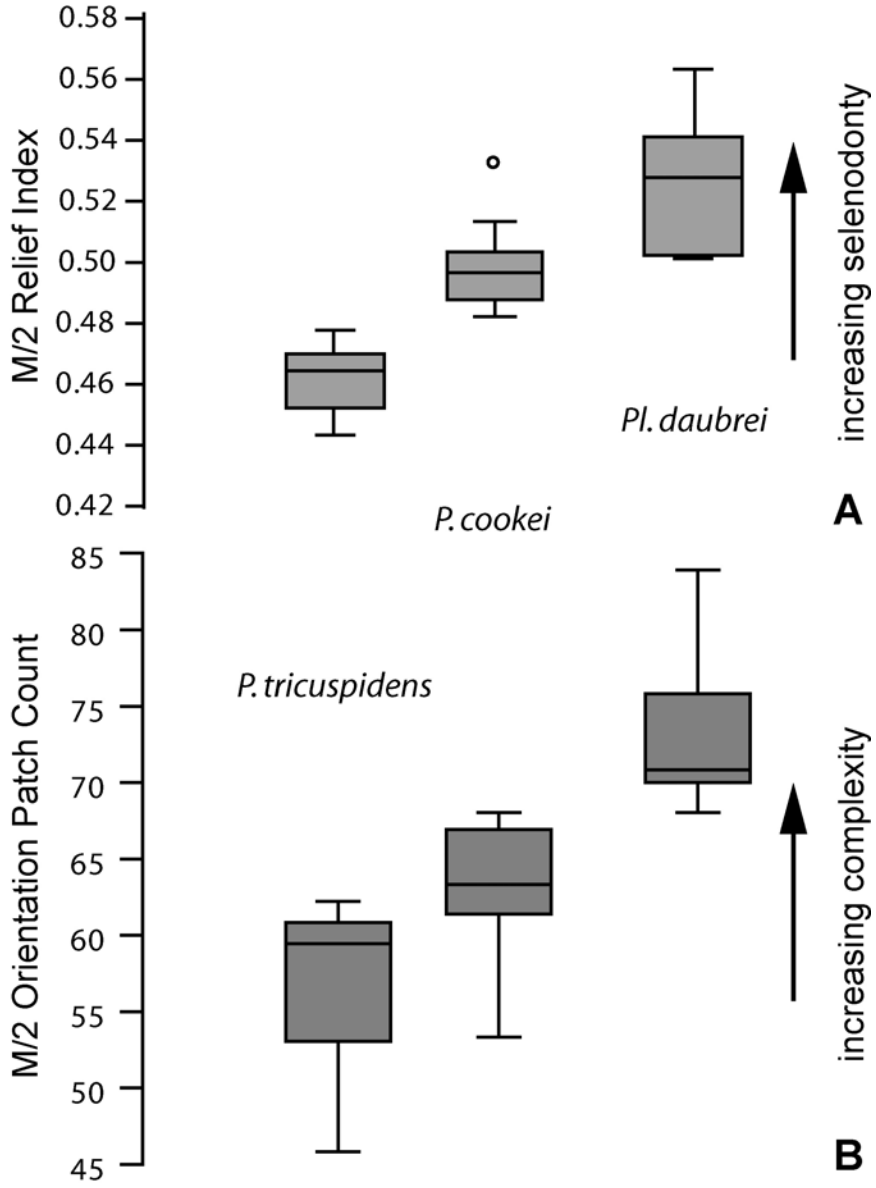

Figure 3.14. A, Plot of relief index of M_2 of *Plesiadapis tricuspidens*, *Plesiadapis cookei*, and *Platychoerops daubrei*. Relief index is the natural logarithm of the ratio of the square root of three dimensional crown area to the square root of two dimensional crown area. Measurements were generated from digital images of teeth acquired as described in Boyer (in press). The higher the relief index, the more "selenodont" the tooth, and the more specialized toward leaves the diet is likely to have been. B, Plot of orientation patch count (OPC) of M_2 of the same three plesiadapid species. A higher OPC corresponds to a more complex tooth occlusal surface, and a greater reliance on leaves in the diet (Evans et al., 2007). Boxes encompass 50% of the data. Whiskers encompass the rest, not counting major outliers. The horizontal line in the box represents the median for the distribution. ANOVA followed by Tukey's HSD tests show that these three plesiadapids have distinctly different degrees of molar relief and complexity.

Figure 3.15. I^1s of *Plesiadapis cookei* (UM 66725 – top row) and *P. tricuspidens* (unnumbered specimen from MNHN Berru collection – bottom row) in A, anterior; B, posterior; C, lateral; and D, medial views. Note that despite being smaller overall, *P. tricuspidens* has a posterocone that is larger, and an anterocone and laterocone that are the same size as those in *P. cookei*. Furthermore, *P.cookei* lacks the mediocone and centrocone crest of *P. tricuspidens.* The small cusps and simplified form of the *P. cookei* I^1 make it very similar to that of *Platychoerops.*

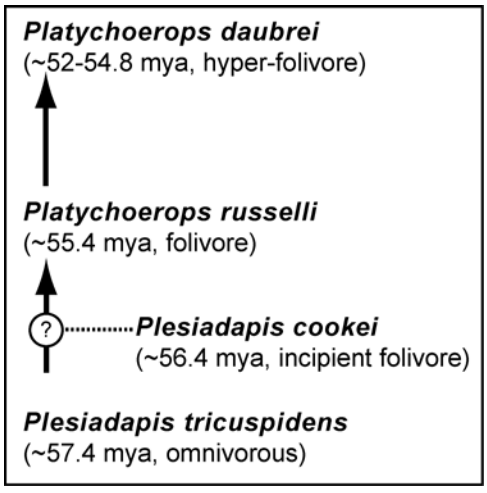

Figure 3.16. Ancestor-descendent lineage starting with *Plesiadapis tricuspidens,* ending with *Platychoerops daubrei*, and possibly including *Plesiadapis cookei*.

CHAPTER 4:
THE FIRST KNOWN SKELETON OF *PLESIADAPIS COOKEI* AND BASIC FEATURES OF THE SKELETON OF PLESIADAPIDAE

ABSTRACT

The only evidence for the existence of most Paleocene mammals consists of the remains of their dentitions. Paleocene primates are no exception, with only a handful of non-dental specimens in existence. I describe the most completely known skeleton of a Paleocene primate, *Plesiadapis cookei* UM 87990, from the middle Clarkforkian North American Land Mammal Age of the Clarks Fork Basin, Wyoming. Previously described partial skeletons and postcranial material attributed to other plesiadapid species, particularly that of *P. tricuspidens* from France, are compared to the skeleton of *P. cookei*. HRxCT data of bones are used to reconstruct articulated fore- and hind limb complexes more completely than previously possible. I evaluate functional implications of the skeleton and CT reconstructions, including the implications for the hypothesis that *P. cookei* utilized suspensory postures more than other plesiadapids.

The skeletal morphology of *P. cookei* is similar to what is known of other non-carpolestid plesiadapiforms in many respects. The forelimb is interpreted to have exhibited a habitually flexed elbow, a physiologically abducted forearm, and a partly supinated manus. Examination of articular surfaces and HRxCT reconstructions of the articulated hand and wrist indicate a habitually dorsiflexed manus that was capable of more extensive dorsiflexion than palmarflexion. This is consistent with a capacity for pronograde or orthograde quadrupedal locomotion. It is not a specialization for suspensory postures. Furthermore, the articulated wrist indicates a mobile pollical metacarpal, contrary to previous assessments. New information on metacarpal associations indicates that the phalanges are significantly longer relative to the metacarpus than previously thought. Regarding the hind limb, plantarflexion of the astragalotibial joint results in conjunct inversion and medial rotation of the foot by almost 90°. Furthermore, the foot was capable of an additional 90° of inversion-eversion and 45° of conjunct plantarflexion-dorsiflexion at the astragalocalcaneal joint. The nature of the mobility at the hip, knee and foot together would have facilitated clinging and climbing on relatively large tree trunks. The vertebral column exhibits proportions similar to those of callitrichid primates and phalangerid marsupials. The neck is relatively short, the thorax is slightly longer than the lumbus, and the tail is elongate. The position of the anticlinal vertebra near the end of the thoracic region suggests that *P. cookei* could use a bounding gait. Various other features suggest the use of orthograde postures. Findings that suggest arboreality and specialization for vertical postures are in agreement with previous conclusions based on studies of other plesiadapids and other regions of the postcranium of *P. cookei*. However, further unambiguous support for the suggestion that *P. cookei* relied on suspensory postures was not discovered.

INTRODUCTION

Among North American plesiadapids (Fig. 1.1), one of the latest occurring and largest species is *Plesiadapis cookei* (Jepsen, 1930; Gingerich, 1976). The only known skull and skeleton of *P. cookei*, UM 87990, was discovered in late Paleocene strata of the Clarks Fork Basin in 1987 (Gunnell and Gingerich, 1987; Gingerich and Gunnell, 1992; Gingerich and Gunnell, 2005). The specimen has not yet received a thorough description or analysis despite the fact that it is arguably the most completely preserved skeleton of a plesiadapiform yet recovered (Bloch and Boyer, 2007).

The relative completeness of the skeleton allows for documentation of inter- and intra-limb skeletal element proportions, and assessment of likely habitual configurations and ranges of mobility of the major joints of the limbs. Estimates of the latter two parameters have never been made for the radiocarpal and mid-carpal joints.

An initial obstacle to study of this fossil was its preservation in a freshwater limestone nodule along with an individual of *Uintacyon*, a similarly sized apparently arboreal carnivoran (Carnivora, Miacidae): this made the process of preparation and documentation difficult. The skeletons were prepared using acid reduction techniques described in Bloch and Boyer (2001). Detailed records of skeletal associations were not kept and there is thus substantial confusion as to which postcranial elements were originally components of *P. cookei* and which belong to *Uintacyon*. This uncertainty is becoming increasingly minor due to recent description of plesiadapiform specimens with documented skeletal-dental associations (e.g., Beard, 1989; Bloch et al., 2007). Some elements are easily identified as belonging to *P. cookei*, because they are well known

among plesiadapiforms (e.g., Szalay et al., 1975); however, the more rarely preserved elements included in UM 87990 must be considered as only tentatively attributed to *P. cookei*. These include metapodials II-V, some of the carpals, tarsals, vertebrae and ribs. In the descriptive and/or comparative sections of this work I make comparative arguments for attribution (or rejection) of these elements to *P. cookei*.

Major objectives

The current study provides the first thorough description and comparison of the skeleton of *Plesiadapis cookei* (UM 87990). My primary aim is to provide high quality imagery and extensive measurements documenting the skeleton's form and mechanically significant features such as patterns of articulation and consequent joint mobility. I will also address a few persistent questions regarding morphology in this specimen in greater detail than in previous work (e.g., Bloch and Boyer, 2007).

Anatomical terminology

The anatomical terminology employed in this study follows Szalay and Dagosto (1980), the Nomina Anatomica (1983), Beard (1989), "Miller's Anatomy of the Dog" (Evans, 1993), and the Nomina Anatomica Veterinaria (1994) for different regions of the skeleton. I generally follow Beard (1989) and Szalay and Dagosto (1980) for descriptions of forelimb anatomy. However, I deviate from Beard in applying the directional terms "radial" and "ulnar" to the radius, whereas he only used it for the carpal bones. Beard chose to use a human anatomical reference for the radius, but this creates a confusing situation for *Plesiadapis* because the most natural position for the radius

appears to be a pronated one. This problem is compounded in discussions of articulations of the radius with the humerus and ulna. Even disregarding the problem of establishing the anterior surface of the radius, using "mediolateral" terminology is confusing because the axis of the radius shaft exhibits torsion (see *Radius description*). Therefore, the mediolateral axis of the proximal end nearly corresponds to the dorsopalmar axis of the distal end.

Human/primate carpal terminology is used because of the relevance of plesiadapiforms to studies by anthropologists. Furthermore, use of this terminology follows previous treatments of the Plesiadapidae (Beard, 1993a).

The terms "superior" and "inferior" are considered equivalent to "cranial" and "caudal" for the clavicle, scapula, innominate, and sacrum in contrast to what is generally considered appropriate for anatomy of quadrupedal animals (Nomina Anatomica Veterinaria, 1994). This is done to permit use of detailed anatomical references such as "supraspinus fossa," "infraglenoid tuberosity," and "anterior superior iliac spine" (Nomina Anatomica, 1983). Furthermore, use of this terminology follows that in recent treatments of other euarchontan mammals (e.g., Sargis, 2002a, b). In discussions of cervical, trunk, and sacral vertebrae, "craniocaudal" terminology is used as specified in the Nomina Anatomica Verterinaria (1994) and as done in recent treatments of other euarchontan mammals (Sargis, 2001). However, for caudal vertebrae, I deviate from this format in order to avoid confusing references to "caudal caudal vertebrae." Instead, I use "proximodistal" terminology here.

Institutional and collections abbreviations

AMNH, American Museum of Natural History, New York; HTB, Cleveland Museum of Natural History, Hamann-Todd non-human primate osteological collection, Cleveland; L.Q., Les Quesnoy Quarry; MNHN, Muséum Nationale d'Histoire Naturelle, Paris; SMM, Science Museum of Minnesota, St. Paul; SBU, Stony Brook University, Stony Brook; UALVP, University of Alberta Laboratory for Vertebrate Paleontology, Edmonton; UM, University of Michigan Museum of Paleontology, Ann Arbor; UMMZ, University of Michigan Museum of Zoology, Ann Arbor; USNM, United States National Museum of Natural History, Smithsonian Institution, Washington D.C.; VPL/JU/NKIM – Vertebrate Paleontology Laboratory, University of Jammu, Jammu Tawi, India; YPM-PU, Yale Peabody Museum-Princeton University collection, New Haven.

Generic abbreviations

P. - Plesiadapis

Pr. – Pronothodectes

Pl. – Platychoerops

N. – Nannodectes

Other abbreviations

AcD - acetabulum (of innominate) anteroposterior depth (Sargis, 2002b: measurement 5)

AcL - acetabulum (of innominate) superoinferior length (Sargis, 2002b: measurement 4)

AcV - anticlinal vertebral position: first thoracic = 1, last lumbar = number of thoracic vertebrae + number of lumbar vertebrae

AD - acromion (of scapula) superoinferior depth measured from superior tip of acromion to scapular spine, perpendicular to scapular spine

AFD - auricular facet (of sacrum) maximum anteroposterior depth

AFL - auricular facet (of sacrum) maximum superoinferior length

AfW - accessory facet (of hamate) radioulnar width

AL - acromion (of scapula) mediolateral length

AP - projection of acromion (of scapula) lateral to glenoid fossa, measured perpendicular to inferior half of glenoid fossa

APL - accessory process (of thoracic and lumbar vertebrae) length: measured from apex of notch between postzygapophysis and accessory process to tip of accessory process

Atd - autopod (1=hand, 2=foot)

BSV - base shape variable = ln(PED/PEW)

Br-I - brachial index = 100*(radius-Le/humerus-Le)

C-L - length of cervical region of vertebral column

C%l - length of cervical region as percentage of trunk (thoracic + lumbar region) length

Ca-L - length of first 10 caudal vertebrae

Ca# - number of caudal vertebrae

Ca%l - length of first 10 caudal vertebrae as percentage of trunk length (thoracic + lumbar region)

CaH - capitulum (of humerus) height (Sargis, 2002a: measurement 13)

caIW - caudal interfacet mediolateral width (of atlas): measured between lateral edges of axis facets

CaL - capitulum (of humerus) anteroposterior length (Szalay and Dagosto, 1980: CL)

CaW - capitulum (of humerus) mediolateral width (Szalay and Dagosto, 1980: CW; Sargis 2002a: measurement 11)

CfA - calcaneum facet (of cuboid) angle with respect to metatarsal facet of cuboid

CfD - capitate facet (of hamate) dorsoventral depth

CH - dorsoventral height of vertebral canal

CL - coracoid (of scapula) mediolateral length

Cr-I - crural index = 100*(tibia-Le/femur-Le)

crIW - cranial interfacet mediolateral width (of atlas): measured between lateral edges of occipital facets on lateral masses of atlas

CW - mediolateral width of vertebral canal

DAL - distal articular surface (of fibula) anteroposterior length (Sargis, 2002b: measurement 43)

DCL - deltopectoral crest (of humerus) proximodistal length (Sargis 2002a: measurement 17)

dCW - dorsal vertebral canal (of atlas) mediolateral width – measured dorsal to articular facets for occiput and axis

DL - dorsal side craniocaudal length (of posterior arch of atlas)

DED - distal end dorsoventral or anteroposterior depth of various elements (unless otherwise specified in table footnotes) (Sargis, 2002a: measurements 32) (Sargis, 2002b: measurement 45)

DEV - distal end variable = DEW/DED

DEW- distal end mediolateral or radioulnar width (unless otherwise specified in table footnotes) (Sargis, 2002a: measurements 16, 31) (Sargis, 2002b: measurement 19, 36)

DFT - distance to flexor tubercle distal margin (from proximal end of distal phalanx)

DpV- diaphragmatic vertebral position in thoracic region of vertebral column

EEC - entepicondyle (of humerus) mediolateral width

ETH - extensor tubercle (of distal phalanx) height dorsal to proximal articular surface

FHL - femoral head proximodistal length (Sargis, 2002b: measurement 10)

FHW- femoral head mediolateral width (Sargis, 2002b: measurement 11)

FTH - flexor tubercle height ventral to proximal articular surface (distal phalanx)

FTW - flexor tubercle (of distal phalanx) mediolateral width

GD - glenoid (of scapula) superoinferior depth (Sargis, 2002a: measurement 3)

GM - geometric mean

GTL - greater trochanter (of femur) proximodistal length (Sargis, 2002b: measurement 12)

GW - glenoid (of scapula) anteroposterior width (Sargis, 2002a: measurement 4)

HfD - hamate facet (of triquetrum) dorsoventral depth

Hf-I - humerofemoral index = 100*(humerus-Le/femur-Le)

HfW - hamate facet (of triquetrum) radioulnar width

HMD - head (of femur) maximum anteroposterior thickness, measured parallel to plane of rim of femoral head epiphysis

HMW- head (of femur) maximum mediolateral width, measured parallel to plane of rim of femoral head epiphysis

HSV - head shape variable = ln(DEW/DED)

HShV- head-shaft shape variable = ln[Le/√(HMW*HMD)]

ICW - intercondylar notch (of femur) mediolateral width (Sargis, 2002b: measurement 26)

IL - ilium superoinferior length (Sargis, 2002b: measurement 2)

InD - ilium neck (between acetabulum and posterior inferior iliac spine) anteroposterior thickness

Int-L - intermembral index = 100*[(humerus-Le + radius-Le)/(femur-Le + tibia-Le)]

InW - ilium neck (between acetabulum and posterior inferior iliac spine) mediolateral width

IsD - ischium anteroposterior depth (Sargis, 2002b: measurement 8)

IsL - ischium superoinferior length (Sargis, 2002b: measurement 7)

IspL - ischial spine (of ischium) distance inferior to inferior margin of acetabulum

IspV - ischial spine (of ischium) position variable = AcL/IspL

IW - ilium width (Sargis, 2002b: measurement 3)

L - left

L# - number of lumbar vertebrae, using rib definition

L%l - length of lumbar region as percentage of trunk (thoracic + lumbar region) length

LCD - lateral condyle (of femur) anteroposterior depth (Sargis, 2002b: measurement 21)

LCL - lateral condyle (of femur or tibia) proximodistal length (Sargis, 2002b: measurements 25 and 30)

LCW - lateral condyle (of femur or tibia) mediolateral width (Sargis, 2002b: measurements 23 and 32)

LD - lateral deviation (of mediolateral axis on distal humerus) of coronal plane in degrees

Le - maximum length (Sargis, 2002a: measurements 5, 18, 26; Sargis, 2002b: measurements 1, 9, 29, 42)

L-L - lumbar region (rib-less vertebrae of trunk) length

LML - lamina (of vertebrae) craniocaudal length

LSH - lunate surface (of scaphoid) proximodistal length, perpendicular to LSL

LSL - lunate surface (of scaphoid) maximum dorsoventral length

LTL - lesser trochanter (of femur) mediolateral length (Sargis, 2002b: measurement 13)

LTP - lesser trochanter (of femur) proximodistal position (Sargis, 2002b: measurement 27)

LTPV - lesser trochanter (of femur) position variable = ln(Le/LTP)

Ltr-I - limb-trunk index = 100*([(humerus-Le + radius-Le + femur-Le + tibia-Le)/2]/trunk-L)

MC - metacarpal

MCD - medial condyle (of femur) anteroposterior depth (Sargis, 2002b: measurement 20)

MCL - medial condyle (of femur or tibia) proximodistal length (Sargis, 2002b: measurements 24 and 31)

MCW - medial condyle (of femur or tibia) mediolateral width (Sargis, 2002b: measurement 22 and 33)

MH - maximum dorsoventral height (of atlas)

MML - medial malleolus proximodistal length (Sargis, 2002b: measurement 37)

MMW - medial malleolus mediolateral width (Sargis, 2002b: measurement 38)

MSD - mid-shaft dorsoventral or anteroposterior depth (unless otherwise specified in table footnotes) (Sargis, 2002b: measurement 16)

MSW -mid-shaft mediolateral or radioulnar width (unless otherwise specified in table footnotes) (Sargis, 2002a: measurement 8; Sargis, 2002b: measurement 15)

MT - metatarsal

MW - maximum mediolateral width (of atlas)

NcD - notch (of ulna) dorsoventral depth (Sargis, 2002a: measurement 24)

NcL - notch (of ulna) proximodistal length (Sargis, 2002a: measurement 25)

NkL - neck (of rib) length: measured between lateral edge of tubercle and lateral edge of head.

NL - neck (of radius) proximodistal length (Sargis, 2002a: measurement 27)

nm - not measured

nn - no (catalogue) number

NSV - notch (of ulna) shape variable = $\ln[L/\sqrt{(PNW*NcL)}]$

OL - olecranon process (of ulna) proximodistal length (Sargis, 2002a: measurement 19)

PAW - proximal articular surface (of humerus) mediolateral width (Sargis, 2002a: measurement 6)

PCW - proximal carpal articular facet (of hamate) radioulnar width

PCD - proximal carpal articular facet (of hamate) dorsoventral depth

PCV - proximal carpal articular facet (of hamate) shape variable = PCW/PCD

PD - pubis dorsoventral depth (Sargis, 2002b: measurement 6)

PED - proximal end dorsoventral or anteroposterior depth (unless otherwise specified in table footnotes) (Sargis, 2002a: measurements 7, 33; Sargis, 2002b: measurement 35, 44)

PEW - proximal end mediolateral or radioulnar width (unless otherwise specified in table footnotes) (Sargis, 2002a: measurement 28; Sargis, 2002b: measurement 34)

PfD - pisiform facet (of triquetrum) dorsoventral depth

PfW - pisiform facet (of triquetrum) radioulnar width

PGL - patellar groove (of femur) proximodistal length (Sargis, 2002b: measurement 17)

PgV - peroneous longus tendon groove (of cuboid) variable = PtgW/GM

PGW - patellar groove (of femur) mediolateral width (Sargis, 2002b: measurement 18)

PNW - proximal end of notch (of ulna) mediolateral width

PtgW - peroneous longus tendon groove (of cuboid) proximodistal width

PTW - proximal end of trochlea (of ulna) mediolateral width (Sargis, 2002a: measurement 20)

R - right side

RFL - radial facet (of ulna) proximodistal length (Sargis, 2002a: measurement 21)

RFV - radial facet (of ulna) variable = ln(RFL/RFW)

RFW - radial facet (of ulna) mediolateral width (Sargis, 2002a: measurement 22)

RRL - radial head rim proximodistal length (Sargis, 2002a: measurement 29)

RSD - radial surface (of scaphoid) maximum dorsoventral depth

RSV - radial head size variable = ln[L/√(PEW*PED)]

RSW - radial surface (of scaphoid) maximum mediolateral width

Rt-I - radiotibial index = 100*(radius-Le/tibia-Le)

Ry - ray (as in “digit ray”)

S-L - sacrum length

S# - number of sacral vertebrae

S%l - length of sacral region as percentage of trunk (thoracic + lumbar region) length

ScT - scaphoid tubercle proximodistal length

SL - scapula length measured along inferior margin of scapular blade between inferior angle and inferior border of glenoid fossa (Sargis, 2002a: measurement 1)

SND - superoinferior thickness of scapula measured just medial to glenoid and coracoid at deepest point of scapular notch

SPL - spinous process length measured parallel to process on ventral edge (if angled) starting from lamina

SSV - shaft shape variable = ln[Length/√(MSW*MSD)]

StL - styloid process (of ulna and radius) proximodistal length (Sargis, 2002a: measurements 23 and 30)

T-L - length of thoracic region (rib-bearing vertebrae)

T%l - length of thoracic region (rib-bearing vertebrae) as percentage of trunk (thoracic + lumbar region) length

TAD - tibial astragalar articular surface anteroposterior depth (Sargis, 2002b: measurement 40)

TAW - tibial astraglar articular surface mediolateral width (Sargis, 2002b: measurement 39)

TbCL - tibial crest proximodistal length (Sargis, 2002b: measurement 41)

TH - trochlea (of humerus) proximodistal height (Szalay and Dagosto, 1980: TH; Sargis, 2002a: measurement 12)

Th# - number of thoracic vertebrae (rib-bearing vertebrae)

TL - trochlea (of humerus) anteroposterior length (Szalay and Dagosto, 1980: TL; Sargis 2002a: measurement 14)

TPL - transverse process of vertebrae length: for atlas and other cervical vertebrae measured from edge of vertebral artery foramen (foramen transversarium), for other vertebrae measured from lateral edge of vertebral body

TrL - triquetrum proximodistal length

Trl-V - triquetrum proximodistal length variable = TrL/GM

TrW - triquetrum maximum radioulnar width

TTL - third trochanter (of femur) mediolateral length (Sargis, 2002b: measurement 14)

TTP - third trochanter (of femur) proximodistal position (Sargis, 2002b: measurement 28)

TW - trochlea (of humerus) mediolateral width (Szalay and Dagosto, 1980: TW; Sargis, 2002a: measurement 10)

UfD - ulnar facet (of triquetrum) depth

UfW - ulnar facet (of triquetrum) width

vCW - ventral vertebral canal mediolateral width (of atlas) measured between articular facets for occiput and axis

VL - ventral side, craniocaudal length (of anterior arch of atlas)

History of descriptive study of the plesiadapid postcranium

Plesiadapidae is known from an extensive sample of postcranial specimens that has been building for over a century. The following is a summary of the previous studies of plesiadapid postcranial fossils and a listing of the specimens figured and described in each study. This section also serves to document the comparative sample employed to assist in the description and comparative analysis of *Plesiadapis cookei* based on UM 87990.

Lemoine (1893) was the first to figure and mention elements of a plesiadapid skeleton (attributable to *P. tricuspidens*) from near the village of Cernay-Les-Reims, France. He noted the presence of prominent flexor sheath ridges on the proximal phalanges.

Gregory (1920: p. 70 and Pl. XXVII) illustrated and discussed a humerus (AMNH 17379) now attributed to *Nannodectes gidleyi* Gingerich 1976 in his monographic treatment of *Notharctus*. Gregory considered this specimen to fit a "tupaioid" morphological pattern and referred to it as "*Nothodectes.*" "*Nothodectes*" was later synonymized with *Plesiadapis gidleyi* (Simpson, 1935), which was later transferred by Gingerich (1976) to the genus *Nannodectes*.

Teilhard de Chardin (1922: Pl. 1:33) figured a distal humerus belonging to *P. remensis* from Cernay-Les-Reims and commented on the habitus of plesiadapids, describing them as "sciuroid" in their ecology.

The specimen described by Gregory (1920) is part of a larger accumulation of associated craniodental and postcranial remains originally discovered by Walter Granger in 1916 at the "Mason Pocket locality" of the Nacimiento Formation, San Juan Basin,

southern Colorado. This locality is placed in the Tiffanian (Ti) 4 biozone (Gingerich, 1976; Lofgren et al., 2004). Simpson (1935) was the first to thoroughly describe the bones from the Mason Pocket locality attributed by him to "*P. gidleyi*." Specifically, he indicated that AMNH 17379 included an atlas, other fragmentary cervical vertebrae, two thoracic vertebrae, six lumbar vertebrae, ribs, the sacrum, and two anterior caudal vertebrae. Some of these bones were illustrated (Simpson, 1935: p. 13, fig. 6). He described and illustrated the left scapula, right humerus, ulna, and radius (p. 14, fig. 7), a metacarpal and proximal phalanx (p. 15, fig. 8), right proximal femur, left calcaneum, right astragalus, and left tibia (p. 19, fig. 11). He attributed another specimen, AMNH 17409, from this locality to "*P. gidleyi*" as well. This specimen includes a right innominate (p. 17, fig. 9) and a left distal femur (p. 19, fig. 10). He also described the existence of many isolated intermediate phalanges, although he was not convinced that these belonged to *N. gidleyi* and did not figure them. Based on the morphology preserved in AMNH 17379 and 17409, Simpson concluded that *N. gidleyi* was likely closer to "lemurids" than "tupaiids" but that *N. gidleyi* must have been derived for an ecological niche very different from that of lemurid, or notharctine, euprimates. All of the bones described by Simpson and many more associated with the skeleton were observed and measured during the course of this study.

Russell (1964) made a major contribution to knowledge of plesiadapid postcranial anatomy by publishing the results of his efforts at Mouras (Berru) Quarry, near the village of Cernay-Les-Reims. He provided a long list of elements recognized by him as pertaining to *P. tricuspidens* (Russell, 1964: p. 289-293). Some of these were indicated as being associated with single individuals. He did not, however, provide descriptions or

illustrations of this material, except for the claws. He compared the claws to those of the flying lemur, *Cynocephalus*, noting that they were similar in being mediolaterally narrow and dorsoventrally deep. The task of describing the rest of the material was left to later researchers. Simons (1964: p. 56, fig. 3) was the first to figure and discuss some of this new material. It is difficult to assess which particular specimens the illustrations in Simons (1964) were based on, because they have been reconstructed to varying degrees. However, some of the lower limb bones appear to correspond to MNHN R 408 (a complete femur) and MNHN R 410 (a fragmentary tibia), considered by Russell (1964) to be components of the same individual. It is important to note that MNHN R 410 lacks both its proximal and distal ends. Simons considered *Plesiadapis* to have been a treeshrew or tree squirrel-like arborealist, and reiterated Russell's observation regarding similarity between the claws of *Plesiadapis* and *Cynocephalus*.

Russell (1967) studied a slab-preserved specimen of Piton's (1940) *Menatotherium insigne* from the Menat Basin in central France, and recognized its dentition as pertaining to *Plesiadapis insignis*. This unnumbered specimen and another lacking a skull, housed at the MNHN, allowed future researchers to estimate limb lengths and indices for *P. insignis* (see below). The small size of *P. insignis*, its similarity to early-occurring North American forms of *Plesiadapis*, and contextual information from the deposits that yielded the specimen, suggested to Gingerich (1976) and others that this specimen was probably contemporaneous with Tiffanian 1 index taxon *Plesiadapis praecursor*, making it the oldest known postcranial remains of a plesiadapid at the time (older than that from Cernay and the Mason Pocket). I was able to observe the type

specimen with skull at the MNHN, but could not locate the referred specimen and was not able to see the counter slab to the type, which is housed at a separate museum.

Napier and Walker (1967) commented on the locomotion of plesiadapids based on what had so far been illustrated. They suggested that plesiadapids were treeshrew or tree squirrel-like in their locomotion.

Szalay (1972: p. 34) calculated brachial (93), crural (93), and intermembral (81) indices from figures provided in Simons (1964) of the Cernay material. However, it should be noted that the full length of the tibia is not actually known for *P. tricuspidens*, and thus the crural and intermembral indices are inferences. My own calculations, using the femur (MNHN R 408) and fragmentary tibial shaft (MNHN R 410), yield a crural index of about 92-93.

Szalay and Decker (1974: figs. 3-5, 8-12) described and illustrated an astragalus (AMNH 89533) and calcaneum (AMNH 89534) of *Plesiadapis* cf. *P. gidleyi* from the early late Paleocene Saddle Locality. The Saddle locality was later determined to preserve *P. anceps* and *N. gazini* (Gingerich, 1976) and it therefore seems that these tarsal specimens should now be referred to one of these two taxa. The authors also illustrated an astragalus (no number provided) and a calcaneum MNHN R 611 of *P. tricuspidens*. I was able to identify the astragalus figured in this paper when I visited the MNHN. It was not, however, associated with a number. Szalay and Decker's figure 6 reveals what appears to be the number "47" written on the specimen. These numbers have since been worn away. Russell (1964, p. 291) listed "MNHN R 5347" as an astragalus of *P. tricuspidens*. This fact appears to solve the mystery of the specimen's identification. Szalay and Decker (1974) indicated that the articulation between the

astragalus and calcaneum was highly mobile and would permit a substantial degree of inversion and eversion, as required in an arboreal setting where substrates may occur at random orientations and descent of large tree trunks is often necessary, requiring hind foot reversal. The mid-tarsal joint was also identified as a point of axial mobility and mobility in plantar- and dorsiflexion.

Szalay et al. (1975) were the first to provide substantial descriptions, figures, and analysis for *P. tricuspidens* material from the Cernay collection listed by Russell (1964). They also figured (p. 140, fig. 1) additional vertebral specimens of *N. gidleyi* (AMNH 17379), beyond those illustrated by Simpson (1935); however, these illustrations are not faithful to the actual preserved morphology and instead represent reconstructions of hypothetical complete, undistorted elements. They considered the anatomy of the vertebrae to be lacking the appropriate comparative context and thus uninformative for phylogenetic or functional considerations. They figured several humeri including MNHN BR-3-L (p. 141, fig. 2; p. 143, fig. 4) and a reconstruction based on MNHN BR-3-L, and BR-4-L (p.144, fig. 5). Szalay et al. also considered morphology of *N. gidleyi* and *P. walbeckensis* in their discussions of humeral morphology. They concluded that the spherical, rather than cylindrical capitulum rendered *Plesiadapis* and euprimates unusually similar. Otherwise, they noted that the plesiadapid humeri were more similar to those of arctocyonids than to those of Paleocene "insectivorans." They figured ulnae on pages 141-142 (figs. 2, 3). No numbers were given but I have determined that the four ulnae in these figures, from left to right in their figure, correspond to MNHN BR-7-L, MNHN R 452, MNHN R 1521, and MNHN R 443. Szalay et al. also illustrated a reconstruction of a complete (minus the styloid process) and undistorted ulna based on

MNHN R 546 (p. 146, fig. 6). They agreed with Simpson's (1935) assessment that *Plesiadapis* and *Notharctus* have similar ulnae. They noted specifically that the two are united in the shallowness of the trochlear notch, proximal bowing of the shaft and a relatively small olecranon process. They figured a radius, MNHN R 550 (p. 143, fig. 4), and considered it especially primate-like in the oval form of its proximal articular surface. They figured two distal phalanges (p. 148, fig. 7) unnumbered at the time, but revealed by later researchers as pertaining to MNHN R 5313 and MNHN R 613 (Beard, 1989, p. 132). The authors noted what is apparent from the figure (that the bones are claws) and did not add any information to Russell's (1964) assessment. They mentioned abundant preserved cheiridial elements from Cernay among the material that Russell (1964) attributed to *Plesiadapis*, but called into question their association because of the abundance of similarly-sized arctocyonids from the locality. Szalay et al. (1975) figured an innominate, MNHN CR 448 (p. 149, fig. 8), and a partial reconstruction of the innominate based on MNHN CR 448, CR 409 and CR 413 (p. 149, fig. 9). They considered the morphology of innominates of *N. gidleyi* (AMNH 17409) and *P. walbeckensis* (no numbers given) as well, and concluded that the plesiadapid innominate is generally "primitive." In fact, they considered *Tupaia* to have a more primate-like innominate than plesiadapids. Szalay et al., however, suggested that a proportionally large acetabulum is a special similarity between plesiadapids and euprimates. The femur was described based on MNHN BR-15-L, MNHN BR-16-L, MNHN CR 408, MNHN CR 438, MNHN CR 444, MNHN CR 450 and "an additional half dozen fragmentary bones" (Szalay et al., 1975: p. 151). They figured MNHN R 444, MNHN R 450 (p. 152, fig. 10), and a reconstruction based on all considered specimens (p. 153, fig. 11). Their

discussion of the femur indicates that it is fundamentally different from that of fossil notharctine euprimates. However, they pointed out that some features distinguishing plesiadapids from these adapiforms unite them with lorisines. Some of the distinct features of the plesiadapid femur, mentioned by Szalay et al., include the low angle between the femoral neck and shaft, the distinct constriction of the femoral neck relative to the femoral head, a large medially projecting lesser trochanter, a distally positioned third trochanter, and an anteroposteriorly shallow patellar groove. They noted the existence of the tibia (MNHN CR 410) and fibula figured by Simons (1940), and suggested that they are too fragmentary for meaningful description: they considered Simpson's description of the tibia of *N. gidleyi* as adequate. Elements of the ankle joint were mentioned again; the authors referenced Szalay and Decker (1974). Specifically, they figured an astragalus based on MNHN R 610 (p. 155, fig. 12) and a calcaneum based on MNHN R 611 (p.156, fig. 13). They listed what they considered to be four derived primate characters of the astragalus and calcaneum including a pronounced groove for the tendon of flexor digitorum fibularis on the plantar side of the calcaneal sustentaculum, an astragalus with a continuous navicular and sustentacular facet, a proximodistally long tibial trochlea and a "helical-shape" to the posterior astragalocalcaneal articulation. They also provided tables (p. 158, table I; p. 160, table II) that compare these tarsal bones more systematically and thoroughly among what they consider to be condylarth, palaeoryctoid, primate, and adapid "morphotypes." They concluded with a functional assessment, suggesting that the forearm was habitually flexed and axially mobile and that the "upper hindlimb" had a capacity for powerful extension, but a lack of leaping adaptations. They reiterated functional inferences from

Szalay and Decker (1974) regarding the ankle joint. All of the material mentioned in Szalay et al. (1975) was observed, photographed, and measured in the course of the current work.

Gingerich (1976) contributed to knowledge on the plesiadapid postcranium by providing photographs and measurements of limb bones of the specimen of *P. insignis* from Menat (p. 35, table 6; p. 84, fig. 36 and table 12; pls. 11-12). Furthermore, he mentioned the existence of a distal humerus of *Platychoerops* (UCMP 103829). He remeasured the postcranial elements of *P. tricuspidens* depicted in Simons (1964) and came up with a slightly different set of brachial (95), crural (100), and intermembral (88) indices than given by Szalay (1972). However, as mentioned above, the length of the tibia of *P. tricuspidens* is not actually known. He reported the same set of indices for *P. insignis* as 86, 91, and 72, respectively. Gingerich was the first to extensively compare plesiadapids to sciurid rodents, the lack of which he regarded as a shortcoming of previous treatments by Gregory (1920), Simpson (1935) and Szalay et al. (1975). He concluded that the limb proportions were similar to those of terrestrial sciurids and *Marmota*. Furthermore, he interpreted the robustness of the limbs as more consistent with a terrestrial, rather than arboreal, habitus. His interpretation of the evidence from the humerus, ulna, and radius of *N. gidleyi* (AMNH 17379) added support to this conclusion. Specifically, the large teres major tuberosity on the humerus was noted to be consistent with a digging habitus. Furthermore, Gingerich saw the morphology of the ulna and radius as having the capacity for only limited pronation and supination. He noted that the distal humeri of *Plesiadapis* (as figured by Teilhard de Chardin, 1922) and *Platychoerops* (UCMP 103829) differ from that of *N. gidleyi* in having more expanded

supinator crests. He also noted that the shallow olecranon fossa of the humerus of these larger forms would have prevented full extension of the elbow, consistent with Szalay et al.'s (1975) view.

Gingerich (1976) reviewed the literature discussing the life habits of *Plesiadapis* including assessments by Teilhard de Chardin (1922, see above]. Russell (1962) suggested that plesiadapids were likely capable of climbing trees when in danger, but that they were predominantly terrestrial. Simons (1967) and Van Valen (1971) considered it likely that at least some species, if not all known species, were terrestrial. However, these assessments were not based on detailed examinations of the postcranium. Gingerich concluded that the available evidence supported a terrestrial reconstruction for known plesiadapids. He acknowledged that there could have been, and probably were, more arboreally adapted plesiadapiforms, which may even have included some species of plesiadapids. However, his case for terrestriality as the modal substrate preference among plesiadapids is a compelling one. I was able to directly observe the newly mentioned *Platychoerops* humerus (UCMP 103829). I also observed some of the *P. insignis* material directly at the MNHN; however, I studied *P. insignis* using Gingerich's (1976) photographs.

Szalay and Drawhorn (1980) further discussed the diagnostic and functional features of archontan (treeshrew, dermopteran, chiropteran, euprimate, and plesiadapiform) astragali and calcanea. They figured several plesiadapids. These include an unnumbered YPM astragalus of *P. rex* (p. 145, fig. 6. IIIA-E). Later Beard (1989) figured and discussed YPM-PU 23977, which probably represents the same specimen. They provided the first detailed figures of the astragalus and calcaneum of AMNH

17379, still attributed by them to "*P. gidleyi*" (p. 152, fig. 9. III.A-E, IV.A-E). This same figure also includes the astragalus and calcaneum of the primitive arboreal treeshrew *Ptilocercus lowii*. The intent of the figure design is not explicitly stated, but presumably it is meant to illustrate two different taxa, which come close to Szalay's view of the "archontan morphotype." Szalay and Drawhorn also illustrated tarsals of *P. tricuspidens* (MNHN R 610-611: p. 159, fig. 11. III.A-E, IV.A-E) next to tarsals of *Cynocephalus volans*. Why Szalay and Drawhorn chose to re-illustrate the calcaneum MNHN R 611 (see above), but not the astragalus MNHN R 5347, is not stated. There do appear to be differences between MNHN R 610 and MNHN R5347 (see below), but Szalay did not mention any of these or what they might mean. Furthermore, I could not find a reference to Szalay and Drawhorn's figure 11 in their text, but presumably the intent of the figure was to illustrate similarity between *Plesiadapis* and *Cynocephalus*. Szalay and Drawhorn (1980) argued that *Cynocephalus* has mobility in its ankle joint to an extreme that is only of use in arboreal settings.

Szalay and Dagosto (1980) provided a more detailed functional assessment of the plesiadapid and plesiadapiform distal humerus than previously given. The work is elegant in its assessment of functional properties using qualitative comparative morphology combined with quantitative comparisons. These authors provided the first illustrations of a humerus of *P. walbeckensis* (the existence of which was first mentioned in Szalay et al., 1975) from the Walbeck fissure fillings (p. 10, fig. 3). Walbeck is roughly correlative with Ti2-3 (Gingerich, 1976; Gradstein et al., 2004). The authors do not provide a catalogue number for the specimen. Szalay and Dagosto (1980) described a second "archontan" from the Mason Pocket locality (AMNH 89519) but then suggested

that it may not even be an archontan. The authors reiterated their view that the spherical capitulum on the humerus of plesiadapids and euprimates may link the two groups both behaviorally and phylogenetically. They further described the ulnar trochlea of the humerus as possessing a lateral ridge and suggested that this ridge is homologous to the central keel of euprimate humeri. Szalay and Dagosto (1980) directly commented on Gingerich's (1976) conclusions concerning plesiadapid terrestriality and stated that the features he identified as linking plesiadapids and marmots are primitive features found in most "unspecialized" Paleocene mammals. They further disagreed with Gingerich's assessment of specific aspects of the morphology: Szalay and Dagosto regarded the capitulum and radial head of plesiadapid humeri as significantly more spherical and rounded (respectively) than those of marmots. They argued that the arboreal rodent *Ratufa*, while generally similar to a marmot, is a better analogue for *Plesidapis* because of its more spherical capitulum and more rounded radial head. Szalay and Dagosto (1980) additionally presented the hypothesis that plesiadapiforms could be viewed as claw-climbing arborealists and analogized them with modern callitrichid euprimates. I have not been able to directly observe any of the specimens newly illustrated in this work.

Gunnell and Gingerich (1987) published an abstract on a new specimen of *P. cookei*, the same specimen as that which I describe in detail here (UM 87990). They suggested that it was adapted to a claw-climbing, arboreal lifestyle.

Szalay and Dagosto (1988) described entocuneiforms and first metatarsals of archontans and euprimates and discussed the evolution of euprimate pedal grasping. They figured the first know entocuneiforms for plesiadapids including an isolated

specimen from the Bison Basin Saddle locality (AMNH 92011: p. 9, fig. 6), which they identified on the basis of its similarity to craniodentally associated elements from the Berru locality, one of which was also figured (p. 10, fig. 7). The authors did not provide a number for the Berru specimen, but Beard (1989) later recognized it as pertaining to MNHN R 416. Szalay and Dagosto considered the distinctive features of the entocuneiform to be its large plantar-projecting process and a facet for MT I that is mediolaterally broad, relatively flat, and saddle-shaped. They viewed the bone as morphologically similar to that of the extant primitive treeshrew *Ptilocercus lowii*. Because *Ptilocercus* is capable of grasping with a divergent hallux that exhibits mobility at the metatarsal-entocuneiform joint, Szalay and Dagosto suggested that the same activities could be inferred for plesiadapids. However, no first metatarsals had yet been described for any plesiadapids.

Gunnell (1989: p. 41-48) discussed the astragalus, calcaneum, and cuboid of *Plesiadapis*. His figures 16 and 17 (p. 45) compare the astragalus and calcaneum to that of *Marmota*. Gunnell acknowledged that the astragalus and calcaneum indicate a high degree of mobility, as argued by Szalay and Decker (1974). However, he brought up the terrestriality hypothesis of (Gingerich, 1976) and noted that mobility of the ankle does not necessarily argue for an arboreal habitus, as indicated by the mobile foot of terrestrial *Marmota* and as convincingly argued by Jenkins (1974). However, he stated that an on-going study by him and Gingerich indicated an arboreal habitus for the skeleton of *P. cookei*.

Beard (1989) brought studies of plesiadapiform postcranial anatomy several steps forward with an excellent dissertation, wherein he described and illustrated previously

unstudied material. Specifically, he described and figured a skeleton of *Nannodectes intermedius* (USNM 442229: p. 20-89, figs. 1-16) including the following bones: left scapula, right humerus, right ulna, left radius, right scaphoid, right lunate, left pisifom, right capitate, both hamates, left MC I, right MC II, right MC III, four proximal manual phalanges, four intermediate manual phalanges, several distal manual phalanges, left tibia, left cuboid, left hallucal metatarsal, four non-hallucal metatarsal fragments and two pedal intermediate and two pedal distal phalanges. All of this material plus additional elements associated with this specimen (but not described by Beard) were observed, measured, and in some cases HRxCT-scanned in the course of this study. Furthermore, Beard described isolated elements from Cedar Point Quarry attributed to *P. rex* (p. 89-101, figs. 17, 18) including YPM-PU 23976, a proximal humeral fragment (not figured); YPM-PU 23975, a distal tibial fragment; YPM-PU 23977 and UM 94816, right and left astragali, respectively. Of these bones, I was only able to directly study UM 94816.

Beard (1989) additionally described a number of previously unstudied bones of *P. tricuspidens*, relying on Russell's (1964) documentation of their association to a partial skeleton mentioned above (p. 101-132, figs. 19-21). The bones newly described by Beard included the following: MNHN R 415, a right cuboid; MNHN R 416, a left entocuneiform; MNHN R 5295, a right MT III; MNHN R 5296, a pedal intemediate phalanx; MNHN R 5297, a manual proximal phalanx; MNHN R 5298, a left MT IV; MNHN R 5300, a right MT III; MNHN 5301 and 5303, manual proximal phalanges; MNHN R 5305, a left MC II; MNHN R 5306, a distal epiphysis of a right MT I; MNHN R 5309, a pedal distal phalanx; MNHN R 5310, a fragment of a pedal distal phalanx; MNHN R 5312, a manual intermediate phalanx; MNHN R 5313, a pedal distal phalanx;

MNHN 5315, a pollical proximal phalanx; MNHN R 5317, a fragment of a pedal distal phalanx; MNHN R 5318, a left mesocuneiform; MNHN R 5319, a right capitate; MNHN R 5330, a right triquetrum; and MNHN R 5321, a left hamate.

Additional elements of *P. tricuspidens* described by Beard include MNHN R 5372, a right navicular and a proximal phalanx; MNHN R 5373, a right MC II; MNHN R 5342, 5355, 5365, and 5371, manual proximal phalanges; MNHN R 5352, a manual intermediate phalanx and distal phalanx; MNHN R 5360, 5366, and 5369, manual intermediate phalanges; MNHN R 5361, a manual distal phalanx; MNHN R 5331 and 5359, left and right entocuneiforms; MNHN R 5340, 5350, 5353, and 5358, metacarpal fragments; MNHN R 5323, a right MT IV; MNHN R 5325, a left MT II; MNHN R 5326, a left MT IV, MNHN R 5336, a distal metatarsal fragment; MNHN R 5337, a proximal left MT II fragment; MNHN R 5345 and 5351, both proximal right MT II fragments; MNHN R 5368, a proximal left MT II fragment; MNHN R 5370, a distal metatarsal fragment; MNHN R 503, 5328, and 5329, pedal proximal phalanges; MNHN R 5324, 5330, 5341, 5346, and 5363, pedal intemediate phalanges; and MNHN R 589, 612, 613, 5344, 5377, 5379, and 5381, pedal distal phalanges. Out of this impressive list of bones included in his descriptions, Beard illustrated MNHN R 5320 (right triquetrum, p. 106, fig. 19), MNHN R 5319 (right capitate, p. 109, fig. 20), and MNHN R 5321 (left hamate, p. 111, fig. 21).

I was able to directly observe, photograph, and measure extensively many of the elements of *P. tricuspidens* in the course of this study. However, I did not do this for the proximal phalanx of MNHN R 5372, the intermediate phalanx of MNHN R 5352, mesocuneifom (MNHN R 5318), right capitate (MNHN R 5319), left hamate (MNHN R

5321), some metapodials (MNHN R 5298, 5300, 5325, 5326, 5335-37, 5340, 5345, 5351, 5358, 5368, and 5370), some proximal phalanges (MNHN R 5301, 5328, 5329, 5342, 5355, 5365, and 5371), some intermediate phalanges (MNHN R 5312 and 5366), some distal phalanges (MNHN R 5310, 5312, 5317, 5377, and 5381), and the distal epiphysis of MT I (MNHN R 5306).

Beard's work documented some important morphological patterns that enhance the description and analysis of *P. cookei*. According to Beard, associations documented for the elements of *N. intermedius*, by Dr. P. Houde, who originally discovered and prepared the specimen, indicate that the pedal phalanges are longer and more robust than the manual phalanges. This was later found to be true of micromomyid (Bloch and Boyer, 2007) and paromomyid plesiadapifoms (Boyer and Bloch, 2008), although not for carpolestid plesiadapiforms (Kirk et al., 2008). *N. intermedius* includes the first described carpal bones for a plesiadapid, including the only described scaphoid for a plesiadapiform. Its MT I, MC I, and "pollical" proximal phalanx were also the first described. Furthermore, Beard's comparisons of carpals between *N. intermedius* and *P. tricuspidens* revealed that they are nearly identical in structure. The above information has been used by Bloch and Boyer (2007) and Boyer and Bloch (2008) to help confirm identity of elements in accumulations of semi-articulated to merely dentally-associated plesiadapiform bones.

Beard's (1989) comparative observations strongly emphasize similarities to the extant dermopteran *Cynocephalus*. His structural and functional analyses demonstrated that plesiadapiforms did indeed have a capacity for axial rotation of the forearm. This information, plus the documentation of a robust, divergent pollex (e.g., p. 420, table 6; p.

457) and hallux, suggested to Beard that plesiadapids were arborealists. He contrasted some of their forearm and phalangeal characters with those of extant dermopterans and extinct paromomyid plesiadapiforms, inferring that plesiadapids "spent most of their time in above branch arboreal postures" (p. 458).

Beard later published some of his dissertation findings. Figure 1 in Beard (1990) shows the articulated metacarpals of digits I-III of *N. intermedius* USNM 442229. Godinot and Beard (1991) presented extensive descriptions and comparisons of fossil primate hands. In it they figured (p. 311, fig. 1; p. 313, fig. 2) a composite digit ray of *P. tricuspidens* using MNHN R 5305 (MC II or MC V – the authors appear to have disagreed on the designation), MNHN R 5303 (proximal phalanx), MNHN R 5341 (intermediate phalanx) and MNHN R 5361 (distal phalanx). They interpreted the metacarpophalangeal joint as having a capacity for extreme dorsiflexion, the proximal interphalangeal joint as having greater capacity in palmarflexion and limited dorsiflexion, and the distal interphalangeal joint as having a neutral range of flexibility. They suggested that the large flexor tubercle on the distal phalanx indicates a robust tendon of flexor digitorum profundus. Godinot and Beard also noted that relatively dorsoventrally deep phalanges would have resisted forces imposed by powerful contraction of this muscle. Thus they concluded that *P. tricuspidens* could have forcefully driven its claws into substrates such as tree branches and clung to them. They compared the morphology of *P. tricuspidens* to that of *Daubentonia*, and they compared what they viewed as likely habitual digital postures for *P. tricuspidens* to those used by lorisines in pronograde and orthograde postures on various substrates.

Gingerich and Gunnell (1992) published a photograph of the skeleton of *P. cookei* (UM 87990) being formally described in this study, mounted in a life-like posture to highlight its incorporation into the Hall of Evolution of the University of Michigan's Exhibit Museum. It was mounted clinging to a vertical tree trunk to illustrate the interpretation of it presented by these authors in abstract form in 1987.

Beard (1993a) presented results of a cladistic analysis of Archonta including various plesiadapifoms. The analysis recovered plesiadapiforms as stem dermopterans. More specifically, plesiadapids formed the outgroup to a clade he called "Eudermoptera" (=Paromomyidae + Cynocephalidae). He compared and contrasted previously described morphology of plesiadapids to that of other plesiadapiforms and archontans. One synapomorphy of the clades supported by his analyses was his interpretation of carpal configuration based on the morphology of the bones of *N. intermedius* (USNM 442229) (p. 137, fig. 10.8). He suggested that both *N. intermedius* and dermopterans had a triquetrum that contacted the scaphoid *and* lunate on its radial surface (see Sargis [2004] for a more thorough critique of Beard [1993a]).

Runestad and Ruff (1995) tested the hypothesis of Gingerich (1976) that the "robustness" of plesiadapids limbs was evidence of terrestriality in this group, and the hypothesis of Beard (1993b) that paromomyid plesiadapiforms were gliders. They did this by regressing limb lengths against limb cross-sectional areas for comparative samples of extant gliding, nongliding arboreal, and nongliding terrestrial/fossorial rodents, and marsupials. They found that gliders had the longest limb bones relative to the cross-sectional areas of their limb bones and that nongliding terrestrialists had the relatively shortest limb bones (= the most robust limbs). They analyzed previously

described plesiadapid bones including those of *P. tricuspidens* (MNHN BR-3-L, MNHN R 450, MNHN BR-16-L and MNHN R 444), *N. intermedius* (USNM 442229), and *N. gidleyi* (AMNH 17379). They found that these taxa had limbs that were shorter than those of extant gliders, arboreal nongliders and paromomyids, but similar in proportional length to those of terrestrial sciurids. Although the authors did not discuss the significance of this finding, the results support the view of Gingerich (1976).

Hamrick (2001) plotted third digit ray proportions (metacarpal, proximal phalanx and intermediate phalanx) of archontan mammals on ternary diagrams (a graph with three axes where each axis represents the length of one of the bones of a digit ray in the form of its percentage of the entire digit ray length). He included measurements from undescribed bones of *P. cookei* (UM 87990) and found them to plot with scandentians and to be separated from those of modern primates. He argued that euprimate manual digit proportions were a "novel" innovation associated with the evolutionary origin and subsequent adaptive radiation of the clade.

Bloch and Boyer (2002) added to Hamrick's (2001) ternary diagram by plotting digits of *P. cookei* and other plesiadapiforms (although they do not indicate which particular specimens were plotted). They also provided the first figure (p. 1609, fig. 5B) of a digit ray based on bones of *P. cookei* (UM 87990). They showed that non-plesiadapid plesiadapiforms plot with euprimates and suggested that *P. cookei* is derived in having scandentian-like proportions. Thus, they disagreed with Hamrick's (2001) suggestion that euprimates were characterized by a change in finger proportions compared to plesiadapiforms. Instead, they concluded that long fingers, and the manual

prehensility they provide, is an innovation of the ancestor of a clade comprised of euprimates and plesiadapiforms (but probably excluding dermopterans and treeshrews).

Youlatos and Godinot (2004) quantitatively compared the morphology of *P. tricuspidens* and *P*. n. sp. material from Berru and the early Eocene Le Quesnoy locality, respectively, to that of a sample of extant terrestrial and arboreal rodents. Much of the material listed in their table 1 (p. 105) has been figured or mentioned elsewhere (not including the list from Russell, 1964) including ulnae (MNHN R 546 and MNHN R 443), radii (MNHN R 550), femora (MNHN BR-16-L, MNHN R 408, MNHN R 444) and ungual phalanges (MNHN R 5361, MNHN R 5381, MNHN R 5309). Additionally they analyzed for the first time several new ulnae (MNHN R 411 and MNHN R 615), radii (MNHN R 553 and MNHN R 597), a femur (MNHN R 407), and claws (MNHN R 612-613). They also included newly recognized uncatalogued specimens of radii and ungual phalanges. The authors listed "MNHN R 542" as a proximal ulna. I could not find this specimen when I visited the MNHN. I did, however, find a proximal ulna with the number MNHN R 452 and presume that this is the specimen to which the authors intended to refer. Russell does not list MNHN R 542 as an element of *Plesiadapis.* According to Russell (1964: p. 309), "MNHN R 542" is a partial humerus of *Pleursapidotherium aumonieri*. Youlatos and Godinot also listed "MNHN R 2527," which I could not locate and Russell did not list. Another problem appears to be their listing of "MNHN R 5370" as a claw; Russell (1964) listed this bone as a metapodial and Beard (1989) confirmed his identification. Youlatos and Godinot also listed "MNHN R 549" as a claw. Again, I could not locate this element and Russell did not list it as an ungual. Instead, Russell (1964: p. 309) listed MNHN R 549 under *Pleuraspidotherium*

and identified it as a fragmentary ulna. It seems likely that the specimen to which they referred as "MNHN R 549" actually corresponds to MNHN R 5*8*9, listed by Russell (1964: p. 291) as a distal phalanx and described in more detail by Beard (1989). Despite problems with specimen numbers, I have little doubt that these authors correctly identified bones of *P. tricuspidens* for their study. Using multivariate methods, they convincingly demonstrated that *P. tricuspidens* is more similar to the arboreal squirrels in their sample than to the terrestrial ones. They analogized the lifestyle of *P. tricuspidens* with that of the extant tree squirrel *Ratufa* (as suggested by Szalay and Dagosto, 1980). Unlike Runestad and Ruff's (1995) study, Youlatos and Godinot's (2004) measurements did not incorporate information on the "robustness" of the limbs, which certainly partly explains why their results contrast with those of the earlier publication.

Bloch and Boyer (2007) discussed morphological and functional features of the plesiadapid postcranium. They referred to new observations of "a skeleton of *Plesiadapis cookei*… in the process of being described." (p. 562). A layout of this skeleton in anatomical position was provided (p. 545, fig. 3D). This is the same skeleton, UM 87990, as that referred to by Gunnell and Gingerich (1987), Gunnell (1989), Gingerich and Gunnell (1992), Hamrick (2001) and Bloch and Boyer (2002), and which is described in detail in this chapter. Bloch and Boyer (2007) stated that *P. cookei* differs from other plesiadapids in morphology of the scapula, humerus, claws, and digital proportions. They suggested that these differences reflect a greater tendency toward suspensory postures in *P. cookei*.

Bloch et al. (2007) reiterated the points made by Bloch and Boyer (2007) and presented the results of a cladistic analysis that included plesiadapids and other

euarchontans (Fig. 1.1). Their analysis recovered a clade composed of plesiadapids and carpolestid plesiadapiforms. Saxonellids and *Chronolestes* formed outgroups to this clade. They called this clade plus its outgroups "Plesiadapoidea." The analysis recovered Euprimates as the sister taxon to Plesiadapoidea. They suggested that specialized grasping of carpolestids was primitive for the Plesiadapoidea, and a synapomorphy of Euprimateformes (Plesiadapoidea + Euprimates), again implying that the incipient grasping and short fingers of plesiadapids are derived.

Boyer and Bloch (2008) presented length measurements for individual elements of *N. gidleyi* (MC III, two proximal phalanges and three intermediate phalanges – AMNH 17379), *N. intermedius* (MC III, six proximal phalanges and four intermediate phalanges – USNM 442229), and *P. cookei* (MC II, MC III, both MT IIIs, six proximal phalanges and five intermediate phalanges – UM 87990). They also presented cross-sectional area measurements for the intermediate phalanges of these specimens (p. 239-240, Table 11.1). The authors plotted other measurements of the intermediate phalanges of these plesiadapids in figures 11.11 (p.248) and 11.12 (p. 249). They figured the first photograph of an intermediate phalanx of *P. cookei* (p. 249, fig. 11.12) and the first illustrations of its distal ulna and radius (p. 256, fig. 11.19). Furthermore, they plotted measurements of vertebrae of *N. intermedius* (USNM 442229) (p. 262, fig. 11.25) and indices from limb measurements of *P. cookei* (UM 87990) (p. 265, fig. 11.27). They stated that the brachial index of *P. cookei* is 101 and that the intermembral index is 89, but did not give the crural index. These values differ from those given by Gingerich (1976) for *P. tricuspidens*, indicating a proportionally longer forearm in *P.cookei*. Generally, the data they presented and their interpretations are supportive of previous

suggestions that plesiadapids were arboreal, and that *P. cookei* may have had more suspensory/antipronograde tendencies than other plesiadapids.

Finally, Kirk et al. (2008) presented an analysis of digit proportions using ternary diagrams, as done by Hamrick (2001) and Bloch and Boyer (2002). However, Kirk et al.'s comparative sample was much larger than those of earlier publications. They included data for the same plesiadapiform specimens studied by Boyer and Bloch (2008). They confirmed that some plesiadapids and other plesiadapiforms had euprimate-like hand proportions, but suggested that *P. cookei* had proportions indicative of a terrestrial lifestyle. They further showed that many clades of mammals (carnivorans, rodents and marsupials) have arboreal members with euprimate-like intrinsic hand proportions, as does the scandentian *Ptilocercus lowii*. Their main conclusions were that euprimates are not unique among mammals in their long fingers and that plesiadapiforms and euprimates are not even unique among the clade Euarchonta in their hand proportions due to the primate-like proportions exhibited by *Ptilocercus*.

MATERIALS AND METHODS

Materials examined

UM 87990, the primary focus of this report, is the postcranial skeleton of *Plesiadapis cookei* discovered in 1987 at University of Michigan locality SC-117 in strata of the Fort Union Formation, dated to the middle Clarkforkian (late Paleocene biochron Cf-2) in the Clarks Fork Basin. The vast majority of postcranial specimens referred to the Plesiadapidae and representing a major or critical portion of an element were examined

for comparison. These include isolated specimens referred to *Pronothodectes gaoi* from the Paskapoo Formation of Alberta; a skeleton of *Nannodectes intermedius* (USNM 442229, USNM 309900, USNM 399898) from the Bangtail locality of Montana; a skeleton of *N. gidleyi* (AMNH 17388, AMNH 17379, and AMNH 17409) from the Mason Pocket locality of Colorado; and various specimens of other species of *Plesiadapis,* including *P. rex* from Cedar Point Quarry, Wyoming; *P. churchilli* from Wannagan Creek, North Dakota and Divide Quarry Wyoming; and *P. tricuspidens* from the Berru locality of Cernay-Les-Reims, France (see tables for specimen numbers). These comparisons serve the usual role of highlighting probable species and generic-level differences but they also help in determining whether various elements included in UM 87990 can be plausibly attributed to *P. cookei*. Qualitative and quantitative comparisons to various extant taxa are also made. Extant specimen numbers are given in the text of the Results sections and in the tables.

Methods of examination and documentation

UM 87990 was examined visually and by using medical grade computed tomography (CT) and high resolution x-ray computed tomography (HRxCT) data. Morphology was photo-documented using a Canon SLR digital camera mounted on a copy stand. Prior to photography, the specimens were whitened with magnesium powder or ammonium chloride to remove tonal contrasts due to mottled coloration or glare.

CT and HRxCT data were acquired from Stony Brook University facilities for UM 87990. The medical scanner was used for larger bones, while a μCT40 machine was used for hand and foot bones (see Appendix Tables 4.1-4 for list of elements scanned,

and scanning resolution – these data are available upon request). These data were visualized with the software Amira 4.1.2-1, Aviso 5.0, and Image J and were critical for determining and illustrating patterns of articulation between carpal, tarsal, and metapodial bones. They were also useful for estimating joint positions and ranges of joint motion.

Measurements and analysis

Various measurements were taken (1) on physical specimens and casts using digital calipers, (2) on photographs using the software Sigma Scan Pro 5.0, or (3) on surfaces created from HRxCT scan images using the software Amira 4.1.2-1 and Aviso 5.0. These measurements are presented in tables organized by bone or region of a bone. Along with raw measurements, various natural logarithm shape ratios are often presented. The names of these measurements and ratios are abbreviated in table headings. These abbreviations and the measurements they represent are defined in the abbreviations section above. Measurements recorded here are used to assist in descriptions of the shapes of bones and to compare shape and size differences among bones of *Plesiadapis cookei* (UM 87990) and those of other taxa. In addition to providing a set of "new" measurements, all measurents used and defined by Sargis (2002a, b) and Szalay and Dagosto (1980) are recorded here. Some or all of their data are incorporated into analyses. Various analyses were undertaken using the programs SPSS 11.0 and PAST.

Univariate comparisons.—Measurements and shape indices of *P. cookei* are compared to those of samples of *P. tricuspidens* and other plesiadapids using students t-test (Sokal and Rohlf, 1997). These analyses assume UM 87990 represents the mean for *P. cookei*, and determine the probability that distributions of measurements for other

plesiadapid samples have the same mean. When linear or area measurements are compared among taxa, the values were first natural-log transformed. This was done because variance in measurements of biological populations is typically only meaningful in proportion to the average value of the measurements for that population. A distributional result of this fact is that populations of biological measurements are theoretically (even if sometimes statistically imperceptibly) right skewed (Sokal and Rohlf, 1997; Gingerich, 2000). Logarithms express metrical data in terms of proportions and thereby provide a data format that can be analyzed to meaningfully address biological questions. For instance, the observation that an elephant population has absolutely greater variance in body mass than a mouse population is not very informative. However, finding a difference in variance in logarithms of body mass would deserve further consideration.

Multivariate comparisons.—Principal coordinates (PC) analyses of Euclidean distance matrices are used to compare various sets of measurements of *P. cookei* to those of samples of extant and fossil taxa. Specifically, PC analyses are undertaken on variables sampling aspects of the skeleton in six different ways including variables sampling (1) the distal end of the humerus, (2) metacarpals, (3) astragalus, (4) calcaneum, (5) aspects of the vertebral column, and (6) combinations of long bone and body segment lengths. Size-standardized variables were created for these analyses by dividing each measurement for a given specimen by the geometric mean of all, or a subset, of the linear measurements for that specimen. This method of size-standardization has been shown to be successful by numerous researchers (e.g., Mosimann and Malley, 1979, Jungers et al., 1995; Hamrick et al., 1999). Any measurements that could conceivably have values of

zero or less were excluded from geometric mean calculations (e.g., the distance that the greater trochanter of the femur projects proximal to the femoral head could easily be positive, zero or negative in a taxon of *any* absolute size). Particular variable sets used to create geometric means are cited in relevant table legends below. The resulting geometric mean ratios were then natural-log transformed. Whether it is necessary to use logarithms of ratios is debated (e.g., Jungers et al., 1995). I chose to do so here based on the fact that it frequently improves normality of distributions of ratios (Sokal and Rohlf, 1997). Furthermore my own experimentation with different data formats lead me to use logs rather than raw ratios. For instance, a version of the analysis of humeral variables performed on un-logged ratios captured less variance, and captured it less evenly in the first two coordinates, than the logged version of the same data (see additional discussion in Chapter 5).

Body mass estimation.—Body mass is estimated for *P. cookei* and other plesiadapids using six limb bone lengths and six diameters. Two different sets of regressions are used: Gingerich (1990) generated regressions from data of Alexander et al. (1979). This dataset samples a phylogenetically diverse array from shrews to elephants. An unpublished dataset of primates from the UMMZ collection is used to generate a parallel set of regressions. The results of these two sets of regressions are presented and compared.

Intrinsic hand proportions.—A reconsideration of digit proportions of *P. cookei* using methods and the comparative data set of Kirk et al. (2008) is undertaken.

Organization of results

Each bone is discussed in its own Results section. Each of these sections has as many as three subsections: description, function, and comparisons. The first of these subsections is always the description. Descriptions include minimal comparative and soft anatomical references.

Subsections assessing functional features of each bone and comparing *P. cookei* to other extant and fossil taxa (mainly other plesiadapids) often follow each description. Following the results sections focusing on specific bones, results of comparative analyses that integrate the morphology and measurements from many regions of the skeletons are presented (i.e., those analyses that cannot logically be included under the heading of a particular bone or set of bones).

SYSTEMATIC PALEONTOLOGY

Class MAMMALIA

Order PRIMATES Linnaeus, 1758

Family PLESIADAPIDAE Trouessart, 1897

PLESIADAPIS Gervais, 1877

PLESIADAPIS COOKEI Jepsen, 1930

Type

YPM PU 13292, associated right and left dentaries, right maxilla, one upper and one lower incisor from the little Sand Coulee area (Sec. 32, T 57 N, R 101 W, Park Co.), Big Horn Basin, Wyoming.

Referred specimen

UM 87990, skull with associated dentaries and postcranial skeleton (Figs. 4.1-3; 5-16; 19-30; 33; 36-45; 48-49; 51-52) preserved in a limestone nodule at Locality SC-117, Fort Union Formation, middle Clarkforkian (late Paleocene biochron CF-2), Clarks Fork Basin, Wyoming.

Ontogenetic state of UM 87990

The adult dentition is completely erupted; however, the teeth are almost completely unworn and most long bone epiphyses remain unfused to diaphyses. This appears to be a fairly typical preservational state in which to find plesiadapiform specimens. For example, skeletons of *Carpolestes simpsoni* (UM 101963) described by

Bloch and Boyer (2002) and *N. intermedius* (USNM 309902 and USNM 442229) also have adult dentitions but unfused epiphyses. Many of the postcranial specimens attributed to *P. tricuspidens* from the Berru locality in France also lack fully fused epiphyses. Specimens of the paromomyid *Acidomomys hebeticus* (Bloch et al., 2002; Boyer and Bloch, 2008) lack a fully adult dentition. The morphological condition of postcrania associated with these subadult *A. hebeticus* specimens differs markedly from those of the former specimens with fully adult dentitions, and that of *P. tricuspidens.* Furthermore, *A. hebeticus* specimens differ similarly from postcrania of a more mature paromomyid specimen of *Ignacius clarkforkensis* (UM 108210) with slightly worn adult teeth (Boyer and Bloch, 2008). Known specimens with fully adult dentitions, like UM 87990, are therefore interpreted to represent fully-grown or nearly fully-grown individuals, despite persistence of some epiphyseal sutures. It is possible that some epiphyses remained unfused for much of these animals' natural lifetimes, as is the case for mice and other rodents (e.g., Roach et al. 2003).

Clavicle

Description.—The right and part of the left clavicle are preserved (Fig. 4.1A). No clavicle has been previously described for a plesiadapid. However, a skull and partial skeleton of *N.gidleyi* (AMNH 17388) preserves parts of right and left clavicles, and thus allows confirmation that the clavicles described here do in fact belong to *P. cookei*. The bone has a strong inferior convexity to its shaft. The medial articular surface for the sternum is roughened and triangular in shape, possibly because it is poorly preserved. The lateral articular facet for the acromion process of the scapula is narrowly elliptical

(6.8 mm by 3.5 mm). The shaft of the clavicle is expanded superoinferiorly, and is quite unusual in this respect. At the mediolateral midshaft, it measures 4.9 mm in superoinferior length by 2.9 mm in anteroposterior depth. The medial third of the inferior surface of the bone is marked by a prominent crest. The bone is marked by substantial depressions superior to the crest on both anterior and posterior surfaces. On the posterior surface, this depression continues as a groove to the medial edge of the lateral third of the bone. The lateral side of the clavicle lacks such prominent crests; however, the bone surrounding the acromial articular surface is raised and roughened. This roughened area extends about a quarter of the clavicle's length medially on the superior surface, and nearly half the clavicle's length on the inferior surface.

Function.—The great superoinferior length of the bone suggests ample room for attachment of muscles and ligaments of the pectoral girdle. Specifically, the inferior flange on the medial side probably served to increase the insertion area of the clavicular head of pectoralis major on its anterior surface. On the posterior surface, the most lateral part of the groove above the inferior flange probably served as the attachment site of the subclavius muscle. The roughened areas on the lateral aspect of the bone undoubtedly refect the attachment points of the trapezius muscle (superiorly) and the deltoid muscle (inferiorly).

Comparisons.—Comparing the clavicle of *P. cookei* to that preserved for *N. gidleyi* AMNH 17388 reveals general similarity, even with regard to the unusual cross-sectional proportions (Table 4.1). This is different from, for instance, humans and treeshrews, which have clavicles with rod-like shafts. If the unusual morphology of the

clavicle reflects some basic aspect of locomotion, posture, or feeding in *P. cookei*, then these behaviors were most likely shared by *N. gidleyi*.

Scapula

Description.—The right scapula of *P. cookei* is the most completely known for a plesiadapid (Fig. 4.1B; Table 4.2). All that is missing is the inferior margin of the spine (possibly including a metacromion process), most of the coracoid process, the part of the scapular blade that held the supraspinous fossa, and part of the infrapinous fossa. The glenoid is shallowly concave and mediolaterally narrower than it is superoinferiorly long. The glenoid faces laterally relative to the blade. The coracoid process projects anteriorly. It is marked by two tuberosities, one on its superior surface and the other laterally, just superior to the glenoid fossa. The acromion is mediolaterally narrow and superoinferiorly elongate. It projects nearly parallel to the scapular spine, and extends laterally beyond the glenoid fossa. It reaches superiorly to the level of the coracoid process. The superolateral tip of the acromion is slightly swollen and smooth, representing the articular surface for the clavicle. Medial and inferior to the clavicular articular surface, the bone becomes raised and rugose. If there had been a metacromion process, it would normally have extended inferiorly, inferomedial to this rugosity; however, the bone is broken here. The inferior margin of the scapular blade is oriented at an obtuse angle of ~125° to the glenoid fossa. The inferior margin of the blade, just medial to the glenoid, is fractured and its morphology is somewhat obscured. However, a distinct pit is visible on the anteroinferior surface that likely represents what is often referred to as an “infraglenoid” tuberosity (the attachment point of the long head of the

triceps brachii muscle). About three-quarters of the distance from the glenoid fossa to the inferior angle of the scapula, the inferior border curves anteriorly and an inferoposteriorly-facing surface is developed above the inferior margin. The superior edge of this inferoposteriorly facing surface meets the inferior margin of the infraspinous fossa. This surface extends down to the inferior angle, and appears to represent the attachment site of the teres major muscle (George, 1977). The inferior angle itself is blunt and anteroposteriorly thick. More superiorly, what remains of the scapular blade (the part representing the fragmentary infraspinus fossa) is deeply concave posteriorly.

Function.—The glenoid's narrow, shallowly concave surface suggests that its articulation with a much larger, convex humeral head resulted in a mobile shoulder joint (see below). However, mobility in abduction may have been limited by the acromion process because it extends so far laterally.

Comparison.—Comparison of the scapula of *P. cookei* to that of other plesidapids does not reveal much, due to the fragmentary nature of the other specimens. The acromion process of *N. intermedius* USNM 442229, however, differs from that of *P. cookei* in that the acromion projects superiorly and is therefore oriented almost perpendicular to the scapular spine, instead of parallel to it, as in *P. cookei*. As a result, the acromion also differs in not extending laterally beyond the glenoid in *N. intermedius*. It seems that the shoulder of *N. intermedius* should be more mobile in abduction than that of *P. cookei*. Interestingly, comparing the scapulae of these plesiadapids to that of *Tupaia glis*, reveals that *P. cookei* and *Tupaia* are more similar to each other than either is to *N. intermedius*. This includes aspects of the morphology of the acromion as well as the blade.

Humerus

Description.—The right and left humeri of *P. cookei* are preserved (Fig. 4.2). The left side is in much better condition. Both have had segments of their shafts reconstructed with paste epoxy. The left humerus also has some epoxy in a broken part of the medial keel of its trochlea. The proximal epiphyses remain unfused in both elements.

The greater and lesser tuberosities are well developed. The greater tuberosity is positioned more superiorly than the lesser tuberosity, but neither extends superior to the top of the humeral head, which is hemispherical. The greater tuberosity has a distinct depression on its superior surface (probably for the supraspinatus muscle) and another depression on its posterolateral surface (probably for the infrapspinatus muscle). The greater tuberosity is continuous with the deltopectoral crest, which projects anterolaterally from the humeral shaft and reaches its apex at ~40% of the shaft length. The lesser tuberosity projects medially. Distally, the lesser tuberosity is continuous with the medial border of the humeral shaft, which swells into the teres major tubercle. This tubercle is large and covers the proximodistal middle portion of the shaft. The supinator crest begins to flare laterally and posteriorly at the proximal edge of the distal third of the shaft. It ends at the lateral epicondyle.

The distal end can be separated into the medial and lateral epicondyles, the articular surfaces for the radius (capitulum) and ulna (trochlea), and the fossae bounding these articular surfaces both anteriorly and posteriorly. The lateral epicondyle does not extend appreciably lateral to the capitulum, it is marked by a shallow depression for a radial collateral ligament. The medial epicondyle (entepicondyle), on the other hand,

projects medially to a substantial degree and its medial surface, which probably formed an attachment point for digital flexors, is oriented mediodistally. Spanning between the medial epicondyle and the shaft (more proximally) is a strut that encloses a large, elliptical entepicondylar foramen. The capitulum is separated from the trochlea by a deep constriction of the articular surface, often referred to as the "zona conoidea." The capitulum appears "sub-spherical" as a result of (1) constriction of the zona conoidea and (2) having a radius of curvature that first increases and then decreases lateral to the zona conoidea. The lateral edge of the capitulum is marked by a proximodistally running groove, but the articular surface extends laterally beyond this groove: this articular region, lateral to the capitulum is referred to as the lateral flange (e.g., Beard, 1989). The surface of the capitulum faces proximally, anteriorly, and distally but does not continue onto the posterior surface of the bone. The anterior surface of the humerus, just proximal to the capitulum, is excavated to form a substantial supracapitular fossa. The humeral trochlea is mediolaterally narrower than the capitulum. Its radius of curvature increases medially from the zona conoidea until its medial margin, or "keel" (Szalay and Dagosto, 1980; Beard, 1989), is reached. The posterior and anterior aspects of the trochlea are roughly equal in the degree to which they are developed. Superior to the trochlea on the posterior side of the humerus is a noticeable, but fairly shallow olecranon fossa. Medial to the trochlea on the posterior surface of the medial epicondyle is a dorsoepitrochlear fossa, for attachment of the ulnar collateral ligament. The rotational axis for the ulna and radius on the distal articular surfaces, as well as the mediolateral axis of the entire distal end of the humerus, is rotated lateral to the proximal end by ~30º. Thus, the medial

epicondyle actually projects somewhat anteriorly, and the "anterior" surface of the distal humerus faces somewhat laterally.

Function.—The humeral head, with its low but large tuberosities, suggests that the shoulder was mobile. The large deltopectoral crest suggests the ability for powerful adduction and extension of the humerus, as does the large, distally-positioned teres major tuberosity (e.g., Gingerich, 1976). The flaring supinator crest provides ample area for origins of the brachialis muscle anteriorly and the triceps posteriorly. The posterior arc of the supinator crest gave the muscles that attached to it (extensor carpi radialis and brachioradialis) a point of origination situated posterior to the brachial-antebrachial joint. This would have given these muscles the mechanical capacity to "hyper-flex" the forearm, beyond a position in which the arm and forearm axes were parallel (or fully flexed). The deep supracapitular fossa is consistent with this capacity because it provides a depression for the radial head to move into as the forearm is "hyper-flexed," and allows a more acute angle to be formed between the arm than if it were not present. The sub-spherical shape of the capitulum suggests that the radius could rotate around its proximodistal axis and contribute to supination and pronation of the hand. The capacity for axial mobility in the forearm partly explains the pronounced medial epicondyle: the large size and medial projection of the epicondyle increased the area of attachment and leverage for the major pronators of the forearm that arose from it. The conical shape of the ulna trochlea suggests that this joint was capable of flexion and extension only. The relatively shallow olecranon fossa and posterior restriction of the capitulum suggest that fully extended forearm postures were unstable or impossible. Lateral rotation of the

distal end implies that the forearms were typically somewhat abducted during pronograde postures (Fig. 4.3).

Comparison.—A dataset from Szalay and Dagosto (1980) was modified to compare the distal end of the humerus of *P. cookei* to those of other plesiadapids and mammals (mainly other euarchontans) (Table 4.3C, Fig. 4.4). Six size-standardized variables were analyzed with principal coordinates analysis (PCA). *P. cookei* is revealed to be most similar in its joint morphology to that of other plesiadapids, as well as adapid and omomyid euprimates. On the other hand, primitive eutherian mammals and non-primate euarchontans are well-separated from *P. cookei*.

Comparing *P. cookei* only to other plesiadapids in a more focused, if qualitative fashion, reveals it to differ from smaller forms including *Pr. gaoi, N. intermedius*, and *N. gidleyi* in having much greater lateral deviation of its distal end (Table 4.3A: LD). *P. tricuspidens, P. remensis*, and *Pl. daubrei* appear to have the distal end of the humerus oriented like that of *P. cookei*. While all known plesiadapids have a prominent medial keel on the ulnar trochlea of the humerus, *P. cookei* differs from *Pr. gaoi, P. rex, P. tricuspidens* and *Pl. daubrei* in lacking a lateral keel on its trochlea. This feature is present in many euprimates, but is also found in the primitive arboreal treeshrew *Ptilocercus lowii*. In taxa possessing a lateral keel, the trochlea is more easily distinguished from the zona conoidea lateral to it. The specimens of *Nannodectes* are like *P. cookei* in lacking the lateral keel. *P. cookei* further differs from *P. rex* alone in the presence of a dorsoepitrochlear fossa (it is retained in all other plesiadapid specimens). Finally, *P. cookei* appears to differ from at least *P. tricuspidens* in having a more gracile humerus (Table 4.3A: note higher SSV). Furthermore, while the left humerus of *P.*

cookei is absolutely longer than any complete elements known for *P. tricuspidens*, almost all of the fragmentary humeri of *P. tricuspidens* have greater midshaft diameters than those of *P. cookei*, further implying that the humerus is a more gracile bone in UM 87990 than in any known individual of *P. tricuspidens.*

Radius

Description.—The left radius and the distal epiphysis of the right radius are preserved. However, the two elements have been adhered to one another with paste epoxy as if they originally belonged to the same bone (Fig. 4.5A). A medical CT scan image was manipulated to estimate the morphology of the actual element. The diaphysis was separated from the surface reconstruction, inverted and repositioned on the epiphysis (Fig. 4.6). In the following description, the terms "ulnar" and "radial" are used in place of lateral and medial. The "ulnar side" of the radius is that which contacts the ulna at the distal radioulnar joint, and to which the interosseous membrane attaches. The radial side is the opposite side (i.e., the side that the pollex is on; also equivalent to the pre-axial side).

Overall, the radius is a slender element with a slight dorsoulnar convexity to its shaft. The radioulnar axis of the distal end is rotated dorsoulnarly by ~40° relative to the proximal end (radial head). That is, when the proximal end of the radius is articulated with the humerus in a fully pronated position, the manus would have been supinated by ~40° (full supination is equal to 180°) (e.g., Fig. 4.3). Furthermore, the manipulated CT image reveals that the distal articular surface faced ventrally and ulnarly.

The central fossa of the radial head for articulation with the humeral capitulum is spherically concave. However, the proximal end of the radius (radial head) appears oval, or even slightly rectangular in proximal view: the head is mediolaterally wider than dorsoventrally deep (Table 4.4A: BSV). This is due to the fact that the spherical depression of the central fossa is flanked radially by a broad "lateral lip." At this point, it is convenient to note that the terminology of Beard (1989) is followed in this section even though it is somewhat confusing, because it allows for detailed descriptions of morphology. The "lateral lip" of the radial head typically articulates with the zona conoidea, which is on the medial side of the capitulum. In terms of radioulnar directions, the "lateral lip" is on the radial side of the radial head. Opposite the lateral lip, on the ulnar side of the bone, the radial head is rimmed by a proximally projecting crescentic ridge that would have articulated with the lateral flange of the capitulum during pronated forearm postures: it is referred to as the "medial crescent" by Beard (1989). The ventral and ulnar aspects of the radial head exhibit an articular surface for the ulna, referred to as the "rim of the radial head." Distal to the radial head rim, the circumference of the bone decreases (the radial neck) before the cross-section increases abruptly on the ventral surface at the tuberosity for biceps brachii. Farther distally the shaft cross-section becomes more elliptical with the major axis oriented almost dorsoventrally. The dorsal margin of this elliptical shaft is continuous with the radial side of the bone, while the ventral side corresponds to the ulnar side. The peak of the dorsal arch of the shaft is marked by a tuberosity for the pronator teres muscle. This point is located at about two-thirds the length of the shaft from the proximal end. Starting from the ulnar side of the proximal end, a crest crosses the dorsal margin of the shaft to meet the pronator teres

tuberosity. This crest probably delimits the radial edge of the compartment for the digital extensor musculature. The ulnar margin of the shaft of the radus develops a distinct crest for the interosseous membrance toward its distal end. The shaft swells abruptly to accommodate the distal articular surface. The dorsoradial margin of the distal epiphysis is marked by three tuberosities that formed the bony boundaries of the three extensor tendon compartments that cross the proximal carpal joint. From radial to ulnar these tuberosities correspond to the styloid process, Lister's tubercle, and a frequently present but unnamed tubercle (Stern, 1988). The first extensor compartment would have been located radial and ventral to the styloid process. The distal articular surface itself is triangular in distal view. The radial margin forms a vertex of the triangle, while the ulnar surface is the opposing base of the triangle. The distal articular surface is marked by a faint dorsoventral ridge reflecting the respective positions of the scaphoid and lunate on either side of it. Ulnar to the lunate area, the articular surface extends on to the radial shaft for contact with the ulna.

Function.—The spherical depression of the central fossa of the radial head suggests that the radius was axially mobile, as does the corresponding morphology of the humeral capitulum. A distally positioned, dorsally elevated pronator teres muscle attachment would provide a large area and lever arm for this muscle to resist substrate reaction forces causing supination, whereas the supinator muscle, attaching along the ulnar margin of the pronator teres attachment, could resist the opposite motion. Together, these muscles, as well as biceps brachii and some of the muscles originating from the supinator crest, could stabilize or rotate the humeroradial joint. The shallow distal articular surface suggests a mobile radiocarpal joint. The orientation of the joint surface

suggests a ventriflexed, abducted proximal carpal row. The pronounced tubercles delimiting the extensor compartments are consistent with a mobile wrist joint in which extreme hand postures (primarily extremes of dorsiflexion and abduction) could have caused the extensor tendons to strain their boundaries if not reinforced by bony buttresses.

Comparison.—Compared to that of other plesiadapids, the radius of *P. cookei* is not remarkable. The radial head is essentially the same shape as it is in the other taxa for which it is known (Table 4.4A). The distal end is also similar among all taxa for which it sufficiently known, although it is too fragmentary in both *Nannodectes* specimens to be confident in this assessment. The distal end appears to be physiologically supinated (i.e., to exhibit torsion) relative to the proximal end to a similar degree in *N. intermedius* and *P. tricuspidens*. The pronator teres tuberosity is equally noticeable in *N. intermedius*, the only other specimen for which it is preserved. Two points of interesting variation include the following: (1) *P. cookei* has a more gracile radial shaft than those of *P. tricuspidens* and *N. intermedius* (Table 4.4A: SSV) and (2) *N. intermedius* has a larger radial head for its shaft length (Table 4.4A: HLV) as compared to either *P. cookei* or *P. tricuspidens*.

Ulna

Description.—A nearly complete left and a proximal fragment of the right ulnae are preserved. Unfortunately, a segment of the shaft of the left side is missing, and the exact length is unknowable, although it can be estimated using the left radius. This was done during preparation of the skeleton and the missing segment of the ulna has been reconstructed with paste epoxy (Fig. 4.5B). Neither side preserves enough of the

olecranon process to estimate its total length. Thus, the total length given in Table 4.5A is likely an underestimate.

Overall, the ulna is a gracile, rod-like element. The proximal end has a pronounced posterior (or ventral) convexity to it. This shape is accentuated by the slight dorsal cant of the olecranon process and the distal end bends ventrally, creating an anterior convexity in this region. The element thus appears "s-shaped" in lateral profile. However, the distal curvature may be an artifact of the reconstruction of the shaft in this region to some degree. The shaft is mediolaterally narrower than dorsoventrally deep for most of its length. The trochlear notch for articulation of the ulna is saddle-shaped, being anteriorly concave proximodistally, and convex mediolaterally. Viewed dorsally, the proximal and distal margins of the trochlear notch obliquely intersect the proximodistal axis of the ulna (i.e., the medial sides of the proximal and distal margins are situated more proximally than the lateral sides). The facet for the radial head is located lateral to and is confluent with the trochlear notch. It is pyriform (pear-shaped) in profile, with the apex of the "pear" pointing proximally. It extends distally beyond the distal margin of the trochlear notch. The radial facet is fairly flat, but it is gently saddle-shaped in the same way as the trochlear notch. Its surface is dorsolaterally oriented.

Ventral to the trochlear notch, on the medial side of the ulna, is a deep groove that appears to have extended some distance proximally onto the olecranon. This groove continues distally for approximately half the length of the shaft. Distal to the trochlear notch, this same groove is accentuated by a ridge that extends distally from the notch, dorsal to the groove for ~1 cm. Dorsolateral to this ridge is a flattened, anteriorly-facing surface that probably received the brachialis muscle insertion. Ventral to the trochlear

notch and radial facet on the lateral side, there is not such a pronounced depression as on the opposite side. However, there is a sharp, faint groove caused by a narrow lip that protrudes from the posterior surface of the ulna. Farther distally, the lateral aspect of the shaft obtains a more distinctive, yet still shallow, depression. Toward the distal end of the bone the shaft develops two diverging dorsal ridges. The lateral one approaches the distal radial facet, while the other passes medial to it before meeting up with a surface that is contiguous with the radial facet and the carpal facet more distally. The more lateral of the two ridges appears to be the interosseous crest, while the medial one probably represents the medial edge of the area of origination for the pronator quadratus muscle (George, 1977).

The distal end is marked by a dorsodistally-facing, convex facet for the distal radius and the lunate (see below). Distal to this, the styloid process sports a convex, dorsodistomedially facing facet for the triquetrum and pisiform of the proximal carpal row.

Function.—The ulnar trochlea complements the morphology of the radius and humerus in the rather flat form and lateral orientation of its radial facet, which would have permitted the head of the radius to rotate on it. A dorsally projecting olecranon process suggests habitually flexed forearms and may even have limited the capacity for full extension, depending on the undistorted size of the olecranon process (Szalay et al., 1975). The only notable muscle scars are the groove on the medial surface of the proximal end, which likely provided a large area for insertion of the flexor carpi ulnaris muscle (George, 1977) and the ridge denoting the edge of the attachment for what was probably a well-developed pronator quadratus muscle (George, 1977). The presence of a

distinct, convex distal radial facet reinforces the inference that there was substantial axial mobility in the radius with respect to the ulna. Its location on the dorsal aspect of the ulna is consistent with morphology of the radius, suggesting that the wrist was maintained in a semi-supinated orientation most of the time.

Comparison.—In general, the ulna of *P. cookei* does not differ appreciably from those of other plesiadapids. None of the shape indices in Table 4.6A reveal any quantified differences. Qualitatively comparing more subtle aspects of the morphology, it can be stated that the ulna of *P. cookei* seems to be unique in the shallowness of the longitudinal groove marking the lateral side of its shaft for origination of extensor musculature. The ulna of *P. cookei* also appears more gracile than those of other plesiadapids; however, as mentioned, this is not borne out by any measurements (e.g., Table 4.5A: NSV and SSV).

Scaphoid

Description.—The right scaphoid is preserved (Table 4.6; Fig. 4.7A). It was originally identified by comparisons to the scaphoid of *N. intermedius* USNM 442229 (Beard, 1993a) and a scaphoid dentally associated to the paromomyid *Acidomomys hebeticus* (Boyer and Bloch, 2008). Aside from being "boat-shaped," as the etymology of the bone's name suggests, with a convex proximal articular surface forming the "hull of the boat" and the concave distal articular surface forming the "boat's interior," the scaphoid of *P. cookei* could also be described as "barbell-shaped" because the ventral tubercle is quite large and distinct from the articular surface for the radius. On the proximal surface, the radius facet is triangular to pyriform in outline (Figs. 4.7A, 4.8: *5*),

with a vertex of the triangle (or the apex of the pear) pointing radially. The radius facet meets the lunate facet (Figs. 4.7A, 4.8: *3*) at its ulnar margin and the two surfaces form an angle of ~90º with one another here. In ulnar view, parallel to the surface of the lunate facet, the lunate facet meets the facet for the distal carpals at its distal margin (Figs. 4.7A, 4.8: *2*), and these two surfaces form an angle of around 100º. It is also apparent in ulnar view that the distal carpal articular surface of the scaphoid is not entirely parallel to the radius facet. In fact, the average tangent of the concave distal articular surface differs from that of the proximal radius surface by ~45°, such that these surfaces deviate in their orientation, from proximal or distal, to somewhat dorsal with respect to one another.

In distal view, the distal articular surface is triangular in outline; its radial apex reaches the radiodistal tip of the scaphoid tubercle and continues onto it. Dorsal to the distal carpal surface is a flat, distally facing shelf (Fig. 4.7A, 4.8: *1*) that may have articulated with bones of the distal carpal row during extremely dorsiflexed postures of the mid-carpal joint. The smooth, articular bone of the radial margin of the distal carpal articular surface continues proximally onto the radial and ventral aspects of the scaphoid tubercle (Figs. 4.7A, 4.8). A prepollex or radial sesamoid (Haines, 1955) may have articulated here. Radioventral to the lunate surface another tuberosity is formed. This bump is thus located ulnar to the scaphoid tubercle. A distinct groove, which likely transmitted tendons of the flexor compartment (e.g., flexor pollicis longus), is present between the two tuberosities.

Function.—The most salient functional features of the scaphoid are its dorsally inclined distal articular surface for the capitate, centrale and probably hamate (in certain postures), the shelf-like surface on its dorsal aspect (that probably reflects hyperextended

of the midcarpal joint), and its prominent tubercle, the large size of which could have helped increase the volume of the carpal tunnel.

Comparison.—The scaphoid of *P. cookei* is nearly identical to that of *N. intermedius* (Fig. 4.8). This is significant because Beard (1993a) interpreted *N. intermedius* as having a facet for the lunate on its "distal surface" as well as a facet for the triquetrum on its lateral surface. This interpretation is fundamentally incorrect, as implied by the description above and as illustrated in Figure. 4.8. The interpretation used here is supported by a number of other lines of evidence that will be presented throughout subsequent descriptions and comparisons. Beard's interpretation was initially plausible because (1) the *N. intermedius* scaphoid is incompletely preserved, allowing for more speculation about the missing morphology; (2) the morphology of the bone he incorrectly identified as the lunate fit his expectations of what it should be under his interpretation of the scaphoid morphology, and (3) the complete carpus was not available to allow an assessment of whether this interpretation could "work" in an articulated specimen.

Lunate

Description.—The lunate is typical in its form. That is, from radial or ulnar view it appears as a "crescent moon," with a convex proximal end and a concave distal end for the distal carpal row (Figs. 4.7B, 4.9A). Its maximum dorsoventral depth is 5.1 mm, while its mediolateral width is 2.3 mm. From dorsal view it appears wedge-shaped because the scaphoid facet is shorter (1.8 mm) than the ulnar side (2.5 mm). Therefore, when articulated with the scaphoid, its distal surface faces slightly radially: together the combined distal surface of the lunate and scaphoid form a "cupped" surface for the distal

carpals (Figs. 4.7B, 4.9A: *2*). Additionally, the shelf-like distally facing facet on the scaphoid continues ulnarly with morphology of the lunate (Figs. 4.7B, 4.9A: *4*). The radius articular surface of the lunate is also visible in dorsal view (Figs. 4.7B, 4.9A: *6*). It arcs from the radiodistal edge of the lunate, down to the lunate's proximoulnar margin, where it contacts the dorsal edge of a small, ulnar facing facet for the distal part of the distal radial facet of the ulna (Figs. 4.7B, 4.9A: *3*). This facet for the ulna can be seen more clearly from ulnar view. This view also shows that the lunate is mainly non-articular on the ulnar side. Its proximal surface has the facet for the ulna. Distal to this there is a non-articular gap, and farther distal still there is a strip-like facet for the triquetrum, which faces laterodistally (Fig. 4.7B, 4.9A: *1*).

Function.—The morphology of the lunate, like that of the scaphoid, suggests a habitually dorsiflexed carpus, and the capacity for a large amount of dorsiflexion.

Comparison.—Comparing the lunate described here to that described for *N. intermedius* by Beard (1989) (Fig. 4.9A, C), one must conclude that the two bones are very different. This is surprising given (1) the similarity of the scaphoids of these two taxa (Fig. 4.8) and (2) the good fit between the scaphoid and the lunate described here. These two facts begin to suggest that the bone described as the lunate in *N. intermedius* is probably incorrectly identified as such, or incorrectly attributed to *N. intermedius*. Two observations support the former hypothesis. A bone with nearly identical morphology was prepared while preserving its association with an intermediate phalanx of USNM 442229 (Fig. 4.9D), strongly suggesting the bone identified by Beard as the lunate does in fact belong to *N. intermedius*. However, if this bone is actually the lunate, then the newly identified element and the originally described one should represent opposite sides

(there is no evidence for more than one individual having been preserved with USNM 442229). However, they appear to be from the same side (Fig. 4.9C, D). Only the sesamoid bones exist in multiple on a single side of the hand or foot and have morphology similar to these mystery bones. Direct comparison to pedal sesamoids of *Sciurus carolinensis* SBU MRd-10 (Fig. 4.9B) confirms the true identity of Beard's (1989) lunate as a sesamoid. When the lunate of *N. intermedius* is finally recovered, it will likely be similar to that described here for *P. cookei*.

Triquetrum

Description.—Both triquetra are preserved (Table 4.7; Fig. 4.7C). They are subrectangular in dorsal view due to proximodistal dimensions that are narrow compared to their radioulnar dimensions. They are squarish-to-oval in proximal and distal views. The proximal end is completely covered by articular surface. Dorsal and ventral facets are separated by radioulnarly oriented ridge. The dorsal facet articulates with the distal facet of the ulnar styloid process. The ventral facet articulates with the pisiform. Both facets are dorsoventrally concave. The ulna facet is additionally radioulnarly concave. In other words, this surface is spherically depressed. The pisiform facet is additionally radioulnarly convex. Thus the pisiform facet is saddle-shaped. The ulnar, dorsal and ventral surfaces of the bone are non-articular. The radial surface articulates with lunate. This articular surface is proximodistally flat, but dorsoventrally convex. The facet is oriented at a right angle to the proximal facet for the ulna. Thus, when the medial facet of triquetrum is articulated with its facet on the lunate, the bone's true mediolateral axis is revealed to be oblique to that being used for descriptive purposes (Figs. 4.7C, 4.8) by

~45°. The distal facet thus faces obliquely toward the radial direction. The triquetrum completes a deeply cupped mid-carpal joint, in which sits the hamate, capitate and centrale. Aside from its radial orientation, the distal facet (for the hamate) is characterized by being shallowly, spherically concave and equal in its radioulnar and dorsoventral dimensions. Ventral to this facet, still on the distal surface of triquetrum, is a nutrient foramen. Ventral and lateral to the foramen is a tubercle that supports the pisiform facet on its proximal surface.

Function.—The small size and narrow proportions of the triquetrum suggest a hand that was habitually abducted toward the ulna (Godinot and Beard, 1991).

Comparison.—The only other plesiadapid for which the triquetrum is known is *P. tricuspidens*. The two taxa are fairly similar in the morphology of their triquetra. *P. tricuspidens* differs in having a proximodistally proportionally thicker element (Table 4.7: TrL-V), suggesting its hands may have exhibited less ulnar deviation than those of *P. cookei*. Furthermore, *P. tricuspidens* has a much large tubercle on its ventroulnar aspect. Finally, *P. tricuspidens* differs in exhibiting a nutrient foramen on its proximal aspect (lateral to the pisiform facet) as well as on its distal aspect. Whether these types of differences are also found at the intraspecific level is unknown. However, as the right and left triquetra of *P. cookei* are identical, it can at least be said that these differences are beyond what is expected for intraindividual variation.

Pisiform

Description.—The right pisiform is preserved (Fig. 4.7D). The element is quite large but confidently attributed to *P. cookei*: its articular surface for the triquetrum

matches the opposing facet on the triquetrum described above. Furthermore, it is nearly identical to the pisiform described for *N. intermedius* (Beard, 1989) although much larger (Table 4.8). When articulated with the rest of the proximal carpal row, the pisiform tubercle projects roughly parallel to the proximal radius articular surface of the other carpals (Fig. 4.10) and at almost 90° to the scaphoid tubercle (i.e, if the pisiform is considered to project ventrally, then the scaphoid tubercle can be described as projecting distally). The triquetrum facet is reciprocally saddle-shaped compared to its corresponding facet on the triquetrum. This facet is dorsally and slightly distally oriented. The ulna facet is pyriform and gently concave. It is proximally and slightly dorsally oriented. The pisiform has a distinct shaft that is narrower than the proximal end. The distal end for attachment of the flexor carpi ulnaris, hypothenar muscles and pisohamate ligament (Haines, 1955; George, 1977) is swollen proximodistally relative to the shaft.

Function.—A pisiform that projects at 90° from the scaphoid tubercle suggests a habitually dorsiflexed hand and possibly pronograde postures (Fig. 4.10). The large size of the pisiform suggests a capacity for powerful ventriflexion (using flexor carpi ulnaris) from an initially dorsiflexed posture, and is also suggestive of pronograde postures.

Comparison.—P. cookei is nearly identical to *N. intermedius* in its pisiform morphology. The only notable difference is a shorter shaft relative to facet size and shaft diameter in *N. intermedius* (Table 4.8: BSV and SSV). If these animals utilized similar postures and behaviors in life, a larger pisiform might have been required to maintain equivalent abilities in ventriflexion in the absolutely larger animal (*P. cookei*) because it would have had a proportionally greater mass.

Trapezium

Description.—The left trapezium is preserved (Figs. 4.11A, 4.12). This bone is not known for any other plesiadapid, or plesiadapiform for that matter. It is identifiable as the trapezium mainly by its ability to articulate with the proximal articular surface of the first metacarpal (MC I). The facet of MC I is "kidney bean"-shaped in distal view (Fig. 4.11A; 4.12A: *2*). It measures 3.73 mm by 1.91 mm. Its surface area is 5.6 mm^2. In ulnar and radial view, the the outline of the trapezium is trapezoidal. This is due to dimensions that differ from the dorsal side of the bone (1.97 mm) to the ventral side (3.00 mm). The ulnar surface has a proximal facet for the trapezium (Fig. 4.12A: *3*) that slopes distally toward the dorsal side. The proximodistal axis of the trapezium deviates from the plane of the trapezoid facet by ~45° toward radial.

Function and comparison.—When the trapezium is articulated with the scaphoid and trapezoid (Fig. 4.12), the MC I facet of the trapezium faces radially and ventrally compared to the MC II facet of the trapezoid. This suggests the presence of a divergent pollex. Furthermore, the MC I facet is broadly separated from the MC II facet when the two bones are articulated, indicating that MC I and MC II would not have contacted one another in the articulated hand (Figs. 4.10-12). Beard (1989) recognized that *N. intermedius* had a widely divergent pollex. However, he considered MC I and II of *N. intermedius* to have had a relatively immobile contact with one another, based on study of the metacarpals alone. This interpretation now seems unlikely given overall similarity between *P. cookei* and *N. intermedius* elements. The convex, slightly incongruent articulation between trapezoid and trapezium suggests the presence of substantial

mobility at the trapezoid-trapezium-scaphoid joints, meaning MC I could have moved quite extensively relative to the other metacarpals. This is similar to the mobility in many euprimate pollices (Napier, 1961). It differs in detail, however, in that hand types defined by Napier (1961) as "opposable," obtain their mobility at the carpometacarpal joint, not at an intercarpal joint(s). The carpometacarpal joint of the first digit in *P. cookei* does not appear highly mobile due to the very close fit between the opposing facets of MC I and the trapezium.

Trapezoid

Description.—The right and left trapezoids are preserved (Fig. 4.11B, 12). Like the trapezium, it is the only example of this bone known for any plesiadapiform. The distal articular facet is rectangular in distal view and measures 4.13 mm by 2.15 mm. Its surface area is 8.2 mm^2. It is gently saddle-shaped, with a concave dorsoventral profile and convex radioulnar profile. In radial or ulnar view it is true to its name-sake in having a trapezoidal outline, with a narrower proximal end than distal end. The radial surface articulates with the trapezium. This surface is also saddle-shaped with a concave dorsoventral profile and a convex proximodistal profile. The ulnar surface for articulation with either the capitate or the centrale (or both?) is helical at its distal end, such that toward its dorsal margin it forms an obtuse angle with the second metacarpal facet, while ventrally this facet is at an acute angle to the metacarpal facet. The proximodistal length of the bone is 2.4 mm. Only the dorsal surface of the trapezoid is largely non-articular.

Function.—The saddle-shaped facets for the trapezium and MC II suggest that both of these bones were mobile with respect to the trapezoid.

Hamate

Description.—The left hamate is preserved. In dorsal view it is the shape of a right triangle with the distal and radial surfaces forming legs of the "triangle," and the ulnar surface forming the hypotenuse (Table 4.9; Figs. 4.11C, 13). The distal surface for the fourth and fifth metacarpals is dorsoventrally concave. It has a surface area of 10.7 mm. In distal view the distal articular surface is "trapezoid" shaped: the dorsal margin is radioulnarly wider than the ventral margin. The maximum radioulnar width of the dorsal margin of the distal surface is slightly narrower than the dorsoventral depth of the distal surface. The ulnar surface is gently convex and articulated with both the triquetrum (distally) and lunate (proximally), and possibly even the capitate in some postures (proximally and radially), although there is no clear demarcation between regions touched by one bone versus the other. The distal margin of the triquetrum facet has a lip protruding beyond it, which would have served to limit radial translation of the hamate with respect to the triquetrum. The radial surface of the hamate (for articulation of the capitate) is proximodistally concave. Toward its proximal base, the radial surface is dorsoventrally convex. This convexity appears to be the boundary between the capitate facet, which occupies the more ventral part of the radial side, and an accessory facet dorsal to it that faces slightly dorsad (Fig. 4.13B: *5*). The proximal surface has a narrow facet that extends onto the ventral surface and appears to have received the scaphoid in certain postures (Fig. 4.13B: *3*). On either side of the ventral expression of the scaphoid facet, nutrient foramina separate it from the other ulnar and radial surface facets.

Function.—The three proximal carpal articular surfaces of the hamate suggest it to have been a highly mobile bone (along with the rest of the distal carpal row) that was capable of taking on many different positions and articular configurations with respect to the rest of the carpus.

Comparison.—Compared to the hamates known for *P. tricuspidens* and *N. intermedius,* that of *P. cookei* differs in several respects. The radioulnar width of the distal end in the hamate of *P. cookei* is narrower relative to its dorsoventral depth (Table 4.9: DEV). The capitate articular surface is concave instead of flat. Finally, the proximal margin has a more distinctive facet for the scaphoid than seen in either *N. intermedius* or *P. tricuspidens* (Fig. 4.13B: *3*). The greater development of the proximal scaphoid facet may suggest more frequent reliance on adducted hand postures, because in order for this facet to contact the scaphoid solidly the hamate must be adducted with respect to it. Although the differences between *P. cookei* and the other plesidapids do not seem great, they are not trivial either. In the absence of better cranial-postcranial associations for the hamate of UM 87990, it is at least possible that these differences indicate that this bone does not actually belong to *P. cookei*.

Metacarpals

There are two different MC II-V morphs that occur with the specimen (set 1 - Fig. 4.14; sets 1-2 – Fig. 4.15; set 2 - Fig. 4.16; Tables. 4.10-12). The two sets are of similar size and morphology. It is difficult to determine which elements belong to which set and further which belong to *P. cookei*. Comparisons to other better-associated plesiadapid

skeletal material are made in the final metacarpals subsection to determine which elements form a set and which belong to *P. cookei*.

Pollical metacarpal description.—Both pollical metacarpals are preserved (Figs. 4.14A, 15). They are unambiguously identified as such by their similarity to the previously described pollical metacarpals of *N. intermedius* USNM 442229 and *N. gidleyi* AMNH 17379 (Beard, 1989, 1990) (Table 4.10; Fig. 4.17). The proximal end is marked primarily by a dorso-ulnarly facing facet for the trapezium. The facet is convex in longest dimension and slightly concave in its narrowest direction. These two curvatures constitute a saddle-shaped surface. The proximal end of the bone is much greater in its mediolateral dimensions than it is in its dorsoventral dimensions. This is due mainly to a pronounced, radially projecting tuberosity. The ulnar side of the bone presents a flattened area that is smooth and looks like an articular facet. Beard (1989) interpreted this feature on *Nannodectes* as a point of contact between MC I and MC II; however, these bones do not seem to have actually contacted one another (see trapezium and trapezoid sections above). The shaft is absolutely short compared to the other metacarpals (Table 4.10). It is also more robust, with a greater cross-sectional area for its length (Table 4.10: SSV). The cross-sectional shape of the shaft is more elliptical than that of the other metacarpals. The distal end has three ridges, or keels. The radial side keel is more proximally restricted than the median and ulnar-side keel, constributing to a distal profile that is asymmetrical in the greater slope of the radial side. The distal articular surface is centered over the median and ulnar keels. It extends onto the dorsal side of the distal end where it is hemispherically convex. Beard (1989) previously described the plesiadapid MC I as having lateral torsion of the distal end. This is true for

the bone presently being described: the long axis of the proximal facet represents the dorsoventral axis of the articulated hand in certain trapezium postures (see above). In a metacarpal with no torsion, the dorsopalmar axis of the shaft and distal end is aligned with the dorsoventral axis of the proximal facet. However, the dorsoventral axis of MC I is laterally rotated some 45° from the dorsoventral axis. The bone is oriented according to the distal end anatomical planes in Figure 4.14A and 4.15. Thus the existence of this torsion can be appreciated by asymmetrical positioning of the proximal end facet in dorsal view of the bone in Figure 4.14A.

Pollical metacarpal function.—Beard (1989) estimated MC I of *N. intermedius* to diverge from the second metacarpal by 73°. This is in the range of euprimates with specialized grasping capacities. He also suggested that there was limited mobility at the carpo-metacarpal joint due to what he interpreted as a facet between MC I and MC II. He considered these features and torsion of the metacarpal shaft to have enabled advanced "pseudo-opposability" of MC I (Napier, 1961). As mentioned (see trapezium and trapezid sections above), I disagree with this assessment based on my interpretation of the relationship between the trapezium and trapezoid, and my interpretation of the mobility at trapezium-trapezoid-scaphoid joints of *P. cookei*. While I agree that MC I was divergent, I estimate the divergence to have been only ~24°, which indicates little about the degree of grasping specialization.

The large radial tuberosity of the proximal end of *P. cookei*'s MC I seems likely to have received the tendon of the abductor pollicis longus muscle, a ventroflexor of the wrist and abductor of the wrist and pollex.

Metacarpal II description.—MC II of set 1 (Figs. 4.14B, 15) is represented by the complete left side element and a fragment of the proximal end of the right side. The left side has a straight shaft that becomes progressively mediolaterally wider from its proximal end to its distal end. This is especially noticeable just beyond the proximal articular surface, because the girth of the shaft increases abruptly here. The proximal articular surface for the trapezoid slopes so that its ulnar edge projects farther proximally than its radial edge. The articular surface for the trapezoid also faces slightly dorsally relative to the metacarpal shaft orientation. The trapezoid facet is saddle-shaped and has a surface area of 7.7 mm^2. The ulnar side of the proximal end facet is separated into ventral and dorsal regions. Both regions probably articulated with both MC III (distally) and the capitate (proximally). The strip of articular surface connecting the dorsal and ventral facets articulated with the capitate. The radial side of the proximal end appears to be devoid of articular facets. Both the radial and ulnar sides of the proximal end are flat without any substantial convexity or concavity. In ventral view, the distal end has three prominent keels: two lateral and one median. The radial side of the distal end profile slopes away from its distal apex more gradually than the ulnar side. In dorsal and lateral view, it can be seen that the distal articular surface extends onto the dorsal side of the element and is hemispherically convex. This hemispherical articular surface is laterally flanked by deep pits (for collateral ligaments). The proximolateral margins of the pits are formed by large tuberosities.

MC II of set 2 (Fig. 4.16A) is similar to MC II of set 1, just described, but they clearly come from two different individuals (both are left side elements) and two different species. Major differences that distinguish the two include the following: (1)

the “set 2” MC II is a larger, more gracile bone (Table 4.10); (2) the trapezoid facet has a larger surface area of 9.5 mm^2; (3) there appear to be facets on the radial side of the proximal end, possibly for MC I and/or the trapezium; (4) the dorsoventral depth of the “set 2” MC II head is absolutely and proportionally larger than than that of the “set 1” MC II (Table 4.10); (5) the “set 2” MC II shaft is bowed laterally and does not increase in width from proximal to distal so continuously or dramatically; (6) the proximal end trapezium facet also does not face dorsally to any substantial degree.

Metacarpal III description.—MC III of set 1 (Figs. 4.14C, 15) is represented by the complete right side element and a fragment of the proximal end of the left side. MC III of set 1 is similar to MC II of set 1 in many respects. Points of similarity include the flatness of the radial and ulnar side facets on the proximal end and the overall morphology of the distal end. The two differ in other aspects of proximal end morphology and shaft length (MC III is longer). The ulnar side of the proximal end of MC III does not project so far proximally relative to the radial side as it does in the “set 1” MC II. There two radial side facets on the proximal end, a dorsal one and ventral one. The dorsal one is larger than the ventral one. The dorsal radial side facet in turn is smaller than the ulnar facet on the “set 1” MC II with which it likely articulates. However, the distal margins of the corresponding facets on MC III and MC II match. The smaller ventrally-located facet on MC III probably articulated with the ventral facet on the ulnar side of MC II. The ulnar side of MC III has a dorsal facet and ventral facet that match those of the “set 1” MC IV. Unlike MC II, the proximal end of MC III is mediolaterally wider than the shaft. Specifically, the dorsal radial-side proximal facet projects laterally farther then the shaft just distal to it, while the dorsal ulnar-side facet is

flush with the shaft distal to it. The proximal end of the capitate facet has a surface area of 7.1 mm^2.

The "set 2" MC III, as for MC II's, is similar to the "set 1" MC III (Figs. 4.15, 16B). It differs in being a larger and more gracile element, and in having an absolutely and proportionally deeper distal end (Table 4.10). The proximal end also differs in having its radial side facet flush with, instead of flaring beyond, the shaft distal to it. The proximal end capitate facet of the "set 2" MC III has a surface area of 8.45 mm^2.

Metacarpal IV description.—MC IV of set 1 (Figs. 4.14D, 15) is fragmentary and missing its distal end. The proximal end facet for the hamate, like the carpal facets on MC II and III, projects farther proximally on its ulnar side. MC IV differs from MC II's and is similar to MC III's in having a proximal end that is mediolaterally wider than the the shaft just distal to it. However, it is more like the "set 2" MC III in having the radial side proximal facet flush with the shaft beyond it, while the ulnar side proximal facet is more flaring. On the other hand, the "set 1" MC IV differs from MC III's and is actually similar to the "set 1" MC II in having a carpal facet that faces dorsally relative to its shaft. The radial side proximal facets match the corresponding ulnar side facets on the "set 1" MC III perfectly, indicating that the two bones articulated. The ulnar side of the proximal end of MC IV is concave, unlike those of MC II's and III's, which are flat. Furthermore the ulnar facet is not differentiated as distinctly into dorsal and ventral regions. The dorsal part of the ulnar side facet is elliptical in outline, similar to the dorsal proximal facets on other metacarpals, but the ventral extension of this facet is proximodistally proportionally thicker than in the other metacarpals. Finally, MC IV

differs from MC II and III in having a shaft that bows slightly ulnarly instead of radially. The proximal end hamate facet of MC IV has a surface area of 6.81 mm^2.

The "set 2" MC IV is represented by complete right and left side elements (Fig. 4.16C). They are essentially similar to the "set 1" MC IV morphologically but differ in being slightly larger. The proximal end hamate facet of the "set 2" MC IV has a surface area of 8.49 mm^2. The bone is similar to the other "set 2" metacarpals in having a dorsoventrally deep distal end. It differs from the "set 2" MC III in being slightly longer. Addtionally the mediolateral asymmetry of the head is mirrored compared to MC II and III's of both sets (i.e., the ulnar side of the distal end is more gradually sloping than the radial side).

Metacarpal V description.—The "set 1" MC V is similar to the other set 1 metacarpals in the proportional dorsoventral depth of its distal end (Fig. 4.14E; Table 4.12). It is further similar to other described metacarpals (of both sets) in most aspects of the distal end morphology (i.e., spherical shape of the dorsal aspect of the distal articular facet, presence of pits for collateral ligaments with tuberosities flanking these pits). While identification of the other metacarpal positions is relatively straightforward, bones with morphology nearly identical to that described here as MC V have been previously described as MC II by Beard (1989, 1990) and Godinot and Beard (1991) for both *N. intermedius* and *P. tricuspidens*. Some history of study and comparative evidence must be reviewed briefly to support the different interpretation used here.

Debate over the attribution of this bone was discussed in Godinot and Beard (1991). The authors indicate that one of them originally identified MNHN R 5305 as a MC V. Accordingly, this fossil was compared to MC V of *Daubentonia* in their figure 1.

However, they indicate that Beard's work on *N. intermedius* revealed MNHN R 5305 to be a MC II. The most straightforward evidence contradicting Beard (1989, 1990) and Godinot and Beard's (1991) final interpretation is the description and illustrated documentation of metacarpal articulations preserved in a skeleton of the micromomyid plesiadapiform *Dryomomys szalayi* in Bloch and Boyer (2007). The metacarpal irrefutably identified as MC V of *D. szalayi* based on these preserved articulations is illustrated in Boyer and Bloch (2008: p. 253, fig. 11.15). It is nearly identical to the bones identified as MC II's previously.

The "set 1" MC V (Fig. 4.14E) proximal end is distinct in having a hamate facet that is dorsoventrally convex with a large amount of its surface facing dorsally relative to the shaft. The hamate facet has a surface area of 6 mm^2. The radial side facet of the proximal end faces slightly proximally as it arcs from the dorsal aspect of the bone to the ventral aspect. Taken as a whole, this arcing, proximally-facing facet is slightly convex. This convexity matches the concavity on the ulnar facet of MC IV. The ulnar side of MC V does not appear to have any distinctive facets, although Beard (1989, 1990) described and illustrated it as having an articulation with MC III in *N. intermedius* USNM 442229. The "set 1" MC V shaft narrows distal to the facets of the proximal end and then broadens dramatically as it approaches the distal end. More specifically, this MC V is distinctive among other metacarpals and the "set 2" MC V in that the ulnar margin of the distal end of the shaft flares much more than the radial margin. The asymmetry of the head of MC V is similar to that of MC IV in being opposite from the asymmetry of MC II's and III's. The asymmetry of the head of MC V differs from that in MC IV in being

even more pronounced. The distal end of MC V shows torsion relative to the proximal end so that its ventral surface faces slightly radially.

The "set 2" MC V is represented by the complete right side element and the proximal end of the left (Fig. 4.15; Fig. 4.16D). It is similar to the "set 1" MC V. The two bones differ in that the "set 2" MC V is longer and more gracile, it has a larger surface area for the hamate (7.5 mm^2), it does not show the dramatic ulnar flaring of the distal part of the shaft; and does not show the extreme asymmetry in the distal end profile.

Assessment of metacarpal association and attribution.—Comparative specimens allow a formulation of a hypothesis on which particular metacarpals of UM 87990 comprise a set belonging to the same animal and further, which set belongs to *P. cookei*. Specifically, comparative specimens utilized include MC I, III, and V of *N. intermedius*; MC I and III of *N. gidleyi*; MC III-V of *P. tricuspidens*; and MC I, III, and IV of *P*. n. sp. [new species of *Plesiadapis* from the Le Quesnoy locality discussed by Youlatos and Godinot (2004), currently being prepared for formal diagnosis by M. Godinot]. The starting point for this analysis was assessment of which of the two MC V morphs is most likely to represent that of *P. cookei*. Principal coordinates analysis of size standardized measurements (Table 4.11; Fig. 4.17) reveals that the "set 1" morph is much more similar to the three MC V's of *P. tricuspidens* than is the "set 2" morph. This result allows confident attribution of the set 1 MC V to *P. cookei*. Next, two pieces of information suggest that MC III of "set 1" is more likely to be that of *P. cookei* than the "set 2" morph. First, the ratio of *P. tricuspidens'* MC III (MNHN R 5295) to its MC V (average of MNHN R 5305 and a second unnumbered specimen) is 1.31. This value is closer to

that between the "set 1" MC III and "set 1" MC V metacarpals of UM 87990 (1.27), than between the "set 2" MC III and the "set 1" MC V (1.47). The ratio between the two bones in *N. intermedius* USNM 442229 is slightly higher than that for *P. tricuspidens* (1.39). Secondly, the shape of the metacarpal heads differs between MC III's of "set 1" and "set 2" (Table 4.10, Fig. 4.18). The heads are relatively shallower in the dorsoventral direction in the "set 1" morph. This is also a similarity to *P. tricuspidens* from Berru. If the attribution of the "set 1" MC III to *P. cookei* is accepted, then MC IV from set 1 must also belong due to the similar sizes and the good fit between the corresponding articular surfaces of the two bones. Likewise, a good fit between MC II, III, and IV of "set 2" suggest that they are all from the same animal, which was not *P. cookei* (Fig. 4.15). MC II of "set 1" can be attributed to *P. cookei* on the basis of its small size compared to MC II of "set 2", and the shape of its head. Another point supporting the attribution of MC II, III, and V "set 1" metacarpals to *P. cookei* is the fact that they are more robust than the corresponding "set 2" metacarpals (see "SSV" of Table 4.10 – a larger value indicates a more gracile element). This greater robusticity of the "set 1" metacarpals makes them similar to those of *P.tricuspidens* and *P*. n. sp. from France. On the other hand the gracility of the "set 2" metacarpals III and V makes them similar to those of *N. intermedius* and *N. gidleyi*. However, this cannot be taken as evidence that the "set 2" metacarpals belonged to *P. cookei*, because MC I of *N. intermedius* is more gracile than MC I's of *P. cookei* and *P*. n. sp. Therefore, it is expected that the lateral metacarpals of *N. intermedius* should also be more gracile than those of *P. cookei*, not equally gracile. Finally, comparing the surface areas of the distal carpal surfaces to those of the proximal articular surfaces of the metacarpals reveals that there is a much better correspondence

between the distal carpals and the "set 1" metacarpals than between the distal carpals and the "set 2" metacarpals (Table 4.12).

Metacarpus function.—The wedge-shaped proximal ends of MC II-IV articulate to produce a pronounced transverse metacarpal arch (Fig. 4.15B). Napier (1961) explained that this gives the hands the capacity for convergence (i.e., when the proximal interphalangeal joints flex, the finger tips converge on each other), which enhances grasping ability. The extensive dorsally-facing part of the distal articular surfaces indicates the capacity for stabile "hyper-dorsiflexed" finger postures as are used in pronograde and orthograde quadrupedal locomotion (Jenkins, 1974).

Proximal phalanges

Proximal phalanx of first digit description.—Three elements referable to this bone are preserved. These include proximal bases of what appear to be both hallucal proximal phalanges (Fig. 4.19), and a third fragmentary base and shaft of the left pollical proximal phalanx. The elements are too fragmentary for meaningful quantification of their morphology, although a few measurements are given in Table 4.13. The bones are recognizable as such by comparison to previously identified first digit proximal phalanges of *P. tricuspidens* and *N. intermedius* (Beard, 1989). Hallucal and pollical elements are distinguished here for the first time based on the much larger size of the hallucal elements. The proximal end of this bone is distinct among the proximal phalanx sample in the asymmetry of tubercles that laterally flank and extend ventral to the proximal articular surface. The medial side tubercle is blunt and proximally restricted, while the lateral side tubercle is pointed and proximally extended beyond its partner (Fig.

4.19). The shaft of the pollical element is also distinct among the proximal phalanges of the sample in being strongly dorsally curved, in having a more triangular cross-section and a more dramatic difference between the proximal and distal end shaft diameters.

Proximal phalanx of first digit function.—The projecting lateral process of the proximal end may have served to increase the attachment area and mechanical advantage for intrinsic flexor and adductor musculature of the hand.

Proximal phalanx of first digit comparison.—The proximal phalanx of the first digit is preserved for *P. tricuspidens, N. intermedius* and *N. gidleyi* (Table 4.13). The right and left elements of *N. intermedius* and *P. tricuspidens* are almost identical in their proportions. However, that of *N. gidleyi*, while fitting the description of this element generally and being roughly the same length as that of *N. intermedius*, is much more gracile (SSV = 1.57 vs. 1.79, respectively: in *P. tricuspidens* SSV = 1.60 – see Table 4.13). The *N. gidleyi* element also has smaller proximal and distal ends than those of *N. intermedius*. The more robust versions of these bones seem likely to represent pedal elements.

Lateral proximal phalanges description.—The other 11 proximal phalanges of the skeleton are fairly similar to each other in most respects (Figs. 4.19, 20). The morphological differences that do exist may reflect differences between manual and pedal elements. Specifically, two of the complete phalanges are distinctly shorter than the remaining four (Table 4.13). Previous postcranial associations for *P. tricuspidens*, *N. intermedius* (Beard, 1989) and other plesiadapiforms (Bloch and Boyer, 2007; Boyer and Bloch, 2008) suggest that the manual phalanges are shorter than the pedal elements. These two shorter phalanges additionally appear to be more dorsoventrally curved, to

have stouter shaft diameters for their length, and to have absolutely and proportionally shallower dorsoventral dimensions of the proximal and distal ends. Natural logarithm shape ratios constructed to quantify these differences show that among the *P. cookei* sample, as well as among other plesiadapids, the manual proximal phalanges are probably more robust (have a greater SSV: Table 4.13). However, the dorsoventral dimensions of the proximal and distal ends to not appear to consistently differentiate proximal phalanges into manual and pedal groups (BSV and HSV: Table 4.13).

In general all proximal phalanges have a proximal articular surface that is spherically concave. Relative to the shaft, the proximal articular surface faces proximally and slightly dorsally. A pair of tubercles laterally flanks the proximal articular surface and extends proximoventrally. These tubercles are usually asymmetrical with one being larger, blunter, and extending farther proximally than the other. Distal to the proximal end, the shaft narrows mediolaterally to near its midpoint, before widening slightly just proximal to the distal articular surface. The dorsoventral dimensions of the shaft tend to decrease continuously from the proximal to distal end. Oftentimes the shaft curves away from the side with the larger proximal tubercle. The ventral surface of the shaft is usually marked by prominent flexor sheath ridges. Although these ridges are impressive in covering almost the entire length of the shaft, they are subtle in their ventral projection. Their presence is more distinctly highlighted by the groove formed where they meet the ventral surface of the shaft (Figs. 4.19, 20). The distal articular surface is distinctive in the presence of two longitudinal grooves separating three trochleae, as can be seen in ventral and distal views of these bones. The lateral trochleae are mediolaterally narrower than the median one. They also tend to have a larger radius of curvature. One of the

lateral trochleae is usually larger, or projects farther distally than the other. Typically this larger trochlea is on the opposite side of that sporting the larger, blunt proximal tubercle. As can be seen in lateral and dorsal views, the distal articular surface has its largest radius of curvature on its ventral aspect, a narrower one distally, and almost no expression of the distal articular surface on its dorsal aspect. The lateral aspects of the distal end are pitted for collateral ligaments.

Lateral proximal phalanx function.—The shape of the proximal articular surface of the proximal phalanx and its orientation with respect to the shaft, combined with articulating metacarpals in which the distal articular surfaces are spherical and oriented dorsally, suggest a metacarpophalangeal joint that was (1) mobile in abduction-adduction, axial rotation, and flexion-extension; and (2) was most stable in a dorsiflexed position, where the greatest overlap in corresponding joint surface area is formed. The orientation of the distal articular surface of the proximal phalanx, its differential radius of curvature, and the presence of extensive flexor sheath ridges suggest habitual ventroflexion of the proximal interphalangeal joints.

Lateral proximal phalanges comparions.—Compared to other plesiadapids, *P. cookei* cannot be demonstrated to differ strongly in any easily quantifiable fashion. Smaller *Nannodectes* species seem to exhibit less pronounced lateral trochleae on the distal articular surfaces and to have proportionally slightly wider shafts. Some of the proximal phalanges from the French Berru locality have prominent ventrally projecting flexor sheath ridges (e.g., MNHN R 503; MNHN unnumbered Divers coll. specimen: see Table 4.13). Although they are identified as plesidapids, this noted morphologic

difference makes them more like known paromomyid plesiadapiforms (Beard, 1989; Boyer and Bloch, 2008). Thus, their attribution to *Plesiadapis* is questionable.

Intermediate phalanges

Description.—Seven intermediate phalanges are included in UM 87990 (Table 4.14; Fig. 4.21). Four of these are complete. As for the lateral proximal phalanges, these elements are all generally similar except with regard to a few features that may reflect differences between bones of the hand and foot. Previous studies (Beard, 1989; Bloch and Boyer, 2007; Boyer and Bloch, 2008) have suggested that the manual elements are shorter. Although only one of the intermediate phalanges identified as a manual element can be measured for its total length (Fig. 4.21, Table 4.14), three others are complete enough to reveal that they would have been much shorter than three others identified as pedal elements. These shorter elements, identified as belonging to the hand, also appear to be smaller midshaft dimensions and to have proximal ends that are proportionally smaller in their dorsventral dimensions. Natural logarithm shape ratios constructed to quantify these differences show that among the *P. cookei* sample, as well as among other plesiadapids, the manual intermediate phalanges are probably more robust and may have slightly shallower dorsoventral dimensions of the proximal end (have a greater SSV, and lower BSV, respectively: Table 4.14). However, the dorsoventral dimensions of the proximal and distal ends do not appear to consistently differentiate proximal phalanges into manual and pedal groups (BSV and HSV: Table 4.14).

In general, the intermediate phalanges have a cylindrically concave proximal articular surface. It is often marked by three longitudinal grooves that fit the three

trochleae of the proximal phalanges. The dorsal and ventral margins extend proximally roughly equal distances, relative to the proximodistal axis of the shaft. However, the ventral margin is usually slightly more proximally projecting, which makes the proximal articular surface face slightly dorsally, relative to the shaft axis. The proximal end is usually slightly greater in its dorsoventral depth than its proximodistal width, with a couple of exceptions for certain manual elements. The ventral surface is marked by prominent tubercles that project ventrally. These appear to be either the flexor sheath tubercles or insertion points for the flexor digitorum superficialis tendons. Beyond the proximal end, the shaft shape is similar to that of proximal phalanges, narrowing in its mediolateral dimension until roughly the proximodistal midpoint of the shaft, and narrowing in its dorsoventral dimension for the entire length of the shaft. For much of the shaft length, the dorsoventral dimension is greater than the mediolateral dimension. The shafts are essentially straight, except for the three longest (probably pedal) elements, which show the slightest amount of dorsal convexity (Boyer and Bloch, 2008). The distal ends of the intermediate phalanges have a single groove down the center of their distal articular surface, rather than two grooves, as in the case of proximal phalanges. In lateral profile it can be seen that distal articular surface has a fairly constant radius of curvature and ~180° of arc to it, although one phalanx (Fig. 4.21G) appears to have well over 180°. Furthermore, in dorsal and lateral view it can be seen that the articular surfaces have a greater amount of ventral-facing area than dorsal-facing area, although they are not as retricted in the amount of dorsal area as the proximal phalanx distal articlar facets.

Function.—The dorsoventrally deep shafts of the intermediate phalanges suggest that they were resistant to parasagittal stresses experienced due to body weight during

antipronograde clinging postures, or due solely to the force of contraction of the digital flexor muscles. The form and orientation of the distal articular surface suggests that the distal phalanges would have had a large range of flexibility and could have attained substantially dorsiflexed configurations (unlike the intermediate phalanx at the proximal interphalangeal joint). However, when joint surfaces are maximally overlapped, the distal phalanx is strongly ventriflexed (Godinot and Beard, 1991).

Comparison.—Compared to other plesiadapids, the intermediate phalanges of *P. cookei* differ most substantially in their proximal end dimensions (Table 4.14: BSV). The dorsoventral depth of this region is greater relative to its mediolateral width than for most other plesiadapids and many arboreal mammals (Boyer and Bloch, 2008). One exception is *P*. n. sp. from the earliest Eocene Le Quesnoy locality in France. It is similar to *P. cookei* in this regard. An ANOVA of on BSV (proximal end dorsoventral depth over mediolateral width) for *P. cookei, Nannodeces, P. tricuspidens* and *P*. n. sp. shows significant among group variance ($df=3$, $F=38.64$, $P<<0.001$). *P. cookei* and *P*. n. sp. do not differ from one another ($P=0.06$), but both differ significantly from *P. tricuspidens* ($P=0.03$, $P<0.001$) and *Nannodectes* ($P<0.001$, $P<0.001$), which are both lower. Furthermore, *P. tricuspidens* differs significantly from *Nannodectes* ($P<0.001$), which is the lowest in BSV. In other words, *Nannodectes* has dorsoventrally shallow phalanges compared to *P. tricuspidens*. *P. tricuspidens* has shallow phalanges compared to *P. cookei* and *P*. n. sp. Boyer and Bloch (2008) showed extant taxa that use their phalanges for antipronograde, or suspensory activities (including *Cynocephalus, Daubentonia*, bats, and sloths) to share this feature with *P. cookei* and *P*. n. sp.

Distal phalanges

Description.—There are ten distal phalanges preserved, only three of which are virtually complete (Fig. 4.22, Table 4.15). These elements are all quite similar to each other. There is no morphological basis to sort manual and pedal claws. There are, however, two phalanges in the sample (Fig. 4.22A, D) that appear similar to one another and different from the others. They have a mediolaterally wider flexor tubercle that also has two processes that project proximally from the lateral aspects of its proximal margin. If there is any significance to this distinctive morphology, it may be that these two phalanges represent first digits.

The distal phalanges can be described as relatively large, "hook-like" claws with narrow shafts and pronounced flexor tubercles. More specifically, the proximal articular surface is much taller dorsoventrally than it is mediolaterally wide. It is marked by a central ridge, which meets the central grooves of the corresponding distal facet on the intermediate phalanges. Dorsal to the proximal articular surface is a vertically expanded area for insertion of the extensor tendon (the extensor tubercle). Ventral to the proximal articular surface is another larger vertically expanded area, possibly for contact with a distal sesamoid. Distal to this, on the ventral surface of the claw, are two nutrient foramina – spaced side by side with a thin rod of bone separating them. Distal to these foramina is the flexor tubercle. The flexor tubercle is usually slightly longer proximodistally than mediolaterally wide. Its mediolateral width is typically greater than that of the claw shaft to which it attaches. The ventral surface of the flexor tubercle is typically separated proximodistally into three regions. The most proximal part is flat to slightly convex, is continuous with the rod-like bony process separating the nutrient

foramina, and faces slightly proximally. The middle part of the flexor tubercle can be further subdivided into right and left pits. These pits are ventrally facing, to slightly proximally facing. They presumably represent the actual attachment points for the flexor digitorum longus tendon. Finally, the third, distal part of the flexor tubercle is strongly convex. The proximal end of the third part faces ventrally while the distal part faces distally. Distal to the flexor tubercle the ventral margin of the claw shaft first arches dorsally and then arches strongly ventrally. The tip of the claw shaft is usually more ventrally situated than the ventral margin of the flexor tubercle. The dorsal surface of the claw, as viewed laterally, is slightly concave between the extensor tubercle and the main shaft. Otherwise, the shaft is smoothly convex for its entire length. The proportionally great lengths of the claw shafts obscure the fact that they are also quite dorsoventrally deep. This point is best appreciated by looking at the claw in dorsal or ventral view, so that the claw's mediolateral narrowness can be seen.

Function.—The proportionally large dorsoventral depth of the intermediate phalanges is taken to an extreme in the distal phalanges: it can be inferred that these elements were also robust to parasagittal bending moments. The strongly curved claw shafts, and large distally positioned extensor tubercles suggest a capacity for strongly clinging or grappling to/on substrates. A more in-depth study of the functional significance of plesiadapiform claws is underway (Maiolino and Boyer, 2008).

Comparison.—Compared to other plesiadapids (Table 4.15: see CSV), *P.cookei* has on average the proportionally narrowest (or deepest) claws. ANOVA of specimens, grouped by taxon, in the available sample show significant among taxon variance (df=4, F=5.858, P=0.0013). However, values of *P. cookei* overlap extensively with those of *P.*

tricuspidens, *P*. n. sp. and *N. intermedius* specimens. A post-hoc test [Tukey's honestly significant differences (HSD)] of means shows that they are not significantly different. If larger samples, or samples in which digit positions could be more carefully standardized, were to show *P. cookei* to have significantly narrower claws than other plesiadapids, this would be consistent with the previous interpretation that it was more committed to an arboreal way of life than these other plesiadapids (Bloch and Boyer, 2007). On the other hand the claws of *P. churchilli* are significantly wider than those of *P. cookei* and *N. intermedius* (P=0.0003 and P=0.01, respectively). The one claw of *Pr. gaoi* is also relatively wide, like those of *P. churchilli*, and looks more like those of scansorial or terrestrial animals.

Innominate

Description.—Both innominates are preserved with UM 87990 (Table 4.16; Fig. 4.23). Both are fragmentary and distorted in different ways, but consideration of both sides allows a view of the complete element. The ilium is the longest of the three bones comprising the innominate. It forms the superior margin of the acetabulum and then tapers in its cross-sectional dimensions superiorly. The posterior margin begins to flare as the posterior inferior iliac spine is reached. This is also the beginning of a roughened facet for the ala of the sacrum, the auricular facet. The anterior surface also flares slightly as the auricular facet is approached, but there is no distinct spine associated with its beginning. A sharp crest runs superoinferiorly between the posterior and anterior surfaces of the ilial shaft. The crest starts at the anterior inferior iliac spine (a small raised roughened area, just superior to the acetabulum) and runs to the anterior superior iliac

spine at the superior tip of the iliac blade. This crest thus separates the gluteal surface of the iliac crest (posteriorly) from the iliacus surface (George, 1977). Starting at the posterior inferior iliac spine the gluteal surface becomes anteroposteriorly wider as it is followed to the superior margin of the blade, while the iliacus surface actually narrows slightly.

The lunate facet of the acetabulum is typical in its form with a gap that opens anteroinferiorly toward the obturator foramen. The sutures between the different bones of the innominate are barely visible, but it can be seen that the ischium forms the longest arc of the lunate facet (~10.5 mm), the ilium continues the facet for a slightly shorter distance (~9.7 mm), and the pubis has the shortest contribution (~6.1 mm). The acetabulum appears to have fairly shallow margins. Cranial (or superior) buttressing of the acetabulum is evident. The anteroposterior dimension of the acetabulum is roughly equal to its superoinferior dimension. Therefore the acetabulum has a circular, rather than elliptical outline.

The superior pubic ramus forms an angle of ~150º with the ilium. Its anterior margin is slightly convex at the level of the acetabulum. At the apex of this convexity, the ramus flares mediolaterally, creating a broad attachment area for the pectineus muscle that is ~13 mm long, or a little less than two-thirds the total length of the superior pubic ramus. A ridge projects anteriorly from the inferior margin of the pubic portion of the acetabulum and then arcs inferiorly to follow the pubic ramus. The external surface of the ramus is concave posterior to this ridge. This ridge forms a rim to a depression encircling the obturator foramen. The obturator externus muscle likely occupied this depression.

Because of the large angle formed between the ilium and pubic ramus, the pubic symphysis ends up forming quite far posteriorly and is quite short superoinferiorly. It is situated ~6 mm inferior to the level the ischial spine. The superior pubic ramus is wider anteromedially than posterolaterally: its inferior border (that forming the edge of the obturator foramen) diverges from the superior border dramatically and reaches the level of the inferior margin of the pubic symphysis. The segment of pubis (or ischium) just inferior to the pubic symphysis is the narrowest segment of the bone rimming the obturator foramen.

The ischial ramus is fairly straight. It is just a little over half the length of the ilium. It posterior surface is convex until the ischial spine is reached just ~2 mm below the inferior margin of the acetabulum. The posterior surface is then concave until it peaks at the ischial tuberosity. The tuberosity is narrow mediolaterally. The ridge forming the edge of obturator externus muscle attachment area crosses from the inferior margin of the ischial tuberosity to the anterior margin of the ischial ramus.

Function.—The narrow ilium suggests relatively small gluteal musculature and limited capacity for forceful extension of the thigh using these muscles (George, 1977; Sargis, 2002b). A distinct depression for the obturator externus muscle (an external rotator) and a robust attachment area for pectineus (an internal rotator) may indicate that rotational movements were important components of locomotor behaviors. This is further suggested by the position of the ischial spine, which forms a trochlea for the obturator internus muscle: it is very close to the acetabulum (~2 mm inferior to it). Thus the major effect of its contraction would be lateral rotation and abduction of the thigh. When the spine is more inferiorly positioned, the muscle can have more of an effect in flexion of

the thigh (Gambaryan, 1974). The hamstrings were probably not well developed, as surmised from the narrow dimensions of the ischial tuberosity. Furthermore the fact that the ischium does not display any retroflexion suggests vertical leaping was not used (Fleagle and Anapol, 1992). Finally, the inferior position and narrow dimensions of the pubic symphysis are not typical of highly active, hind limb driven animals (Boyer and Bloch, 2008). The cranial buttressing of the acetabulum may indicate the use of orthograde postures in which body weight was directed through the cranial part of the lunate facet, as suggested by other authors (Beard, 1989).

Comparison.—The innominate of *P. cookei* does not appear to differ drastically from that of other plesiadapids for which it is known. These specimens are not very complete. However, a couple of points can be made from the available material. The known innominate fragments of *P. tricuspidens* are larger than those of *P. cookei* (Table 4.16). This is interesting considering that most of the known forelimb elements are roughly the same size in the two species, with *P. cookei* usually exhibiting greater proximodistal lengths. The acetabula of all specimens show some cranial buttressing. The acetabula of *N. gidleyi* appear to be more elliptical and less circular in outline (although they exhibit damage that makes them techniquely unmeasurable) than those of *P. tricuspidens* and *P. cookei*. Another point of interest is the much farther distal positioning of the ischial spine in three innominates of *N. gidleyi*, relative to the acetabular dimensions (Table 4.16: IspV). Thus, in these smaller forms, the obturator internus muscle had a greater component of force inferiorly directed and this muscle could therefore contribute to flexion of the limb more than it could in the larger taxa.

Femur

Description.—Both femora of UM 87990 are preserved (Fig. 4.24; Table 4.17A-C). The left element is in better condition. The right element is missing the apophysis of the greater trochanter, has a noticeably displaced proximal epiphysis, and has a crushed distal shaft segment.

The femur is slender and straight with a slightly anteriorly convex bend to its shaft. The femoral head is globular. Its articular surface has a narrow extension that covers the posterior aspect of the ridge connecting the head to the greater trochanter. The fovea capitis femoris is positioned close to the inferior rim of the epiphysis and slightly posterior of medial. The femoral head sits on a femoral neck that projects at ~145° from the femoral shaft.

The greater trochanter extends to the proximal level of the femoral head. It is canted slightly anteriorly. A deep trochanteric fossa is present on its posterior surface. The distolateral edge of the fossa meets a faint ridge that arcs medially across the posterior surface of the femur to meet the lesser trochanter; this ridge is the intertochanteric crest. The lesser trochanter is positioned quite far distally, such that the femoral shaft becomes noticeably constricted distal to the head and greater trochanter, but proximal to the lesser and third trochanters. The lesser trochanter projects medially and somewhat proximally, at an angle paralleling the femoral neck. It is relatively large and projects medially beyond the femoral head on the left side. The third trochanter is comparatively small in its lateral projection. It is positioned slightly farther distally than the lesser trochanter. It sports a laterally facing rugosity for the gluteus superficialis muscle (George, 1977; Sargis 2002b).

The femoral shaft is smooth, lacking any expression of the linea aspera, and is mediolaterally wider than anteroposteriorly deep. The distal epiphyseal suture is distinctly visible. The shaft lacks any significant torsion and the condyles face posterodistally relative to the proximal end, instead of laterodistally or mediodistally. The patellar groove is shallow, and is only slightly proximodistally longer than it is mediolaterally wide, giving it a "squarish" appearance in anterior view. The medial margin of the patellar groove projects anteriorly to a greater extent than the lateral margin. In addition, most aspects of the distal end's medial side are slightly absolutely larger than those of the lateral side; specifically, the medial condyle is proximodistally longer and mediolaterally wider than the lateral condyle. The medial and lateral epicondyles sport notable pits for the collateral ligaments. Additionally the lateral epicondyle has a pit that is more crescentic in form, and positioned below the collateral ligament pit, probably for origin of the popliteus muscle.

Function.—From a functional perspective, the femur of *P.cookei* matches the functional signal inferred from the innominate. The femur appears specialized for behaviors that emphasize medial and lateral rotation of the bone, rather than flexion and extension of it. For instance, due to the shape of the femoral head and the asymmetry introduced by the positioning of the fovea capitis femoris, the articulated surfaces of the femur and acetabulum correspond most closely when the femur is flexed, abducted and laterally rotated. The motions that maintain the closest fit between the joints are adduction and abduction and medial and lateral rotation. Furthermore, abduction from a flexed, medially rotated position engages the lateral extension of the femoral condyle with the inferior aspect of the lunate facet (Fig. 4.25: position 4). From this position no

more abduction could have really occured, but lateral rotation, followed by extension, allowed the condyles to shift farther caudally. Relatively small greater and third trochanters, and a medially projecting (rather than posteriorly projecting) lesser trochanter are further indicative that the femur was not flexed and extended forcefully using the gluteal musculature (Sargis, 2002b). However, the expansive trochanteric fossa and expanded area distal to the intertrochanteric crest for the obturators and quadratus femoris, respectively, would have given the limb a capacity for powerful abduction and lateral rotation of a flexed, adducted thigh. The large, medially projecting lesser trochanter would have provided a large lever arm for the iliopsoas muscle: from a somewhat extended, abducted, medially rotated posture, iliopsoas would also have served to flex, adduct, and laterally rotate the femur. The proximally restricted patellar groove and distally extensive condyles suggest that full extension of the knee was infrequent or impossible, and that a flexed knee was a habitual posture. Relatively shallow femoral condyles suggest extension of the knee was not particularly forceful (Beard, 1989; Sargis, 2002b) when it occurred. The pattern of buttressing of the patellar groove margins are consistent with a posture wherein the femur was habitually flexed and abducted, and the knees were flexed (Boyer and Bloch, 2008).

Comparison.—The femur of plesiadapids does not exhibit a drastic amount of variation in the species for which it is known. Most aspects of the description given for *P. cookei* apply equally to *P. tricuspidens*, *N. gidleyi* and a newly recognized specimen of *N. intermedius* (Table 4.17A-C). The description of the femoral head of *P. cookei* differs from that given by Beard (1989) for other plesiadapids. He characterized the plesadapid femoral head as being spherical, having a centrally placed fovea capitis femoris, and as

lacking a lateral extension of its articular facet. He made this point in order to contrast plesiadapids with non-plesiadapid plesiadapiforms (Beard, 1989: fig. 76). While I agree that plesiadapids differ from non-plesiadapids to a degree, based on my observations of the entire collection of *P. tricuspidens* in Paris and *N. gidleyi*, almost all appear to exhibit the three features they were said to lack. Plesiadapids appear to differ from non-plesiadapids in having a slightly less posteriorly positioned fovea capitis femoris and in having a smaller lateral articular surface extension. It is important to make this clear because of the functional implications for these features, as discussed above. Because of the large sample of *P. tricuspidens* from France, an assessment of shape variation can be done with the potential for statistical confidence. Using t-tests on data from Table 4.17C, it can be shown that the femur of *P. cookei* differs from all relatively complete femora from the Berru locality in France in being longer (ln[Le]: $t = -5.98$, $P = 0.0003$), more gracile (SSV: $t = -7.06$, $P = 0.0001$), having a *proportionally* smaller femoral head (HShV:$t = -13.25$, $P<<0.0001$) and a more proximally positioned lesser trochanter (LTPV:$t = -6.46$, $P = 0.0004$). However, *P. cookei* is no different from *P. tricuspidens* in mid-shaft cross-sectional area of its femur (ln[MSW*MSD]: $t = -0.49$, $P = 0.63$), the area of the femoral head (ln[HMW*HMD]: $t = -0.066$, $P = 0.95$), or the absolute proximodistal position of its lesser trochanter (ln[LTP]: $t = 0.97$, $P = 0.355$). Thus, it is only the absolutely increased length of the femoral shaft distal to the lesser trochanter that makes *P. cookei* and *P. tricuspidens* different in femoral size and shape.

Tibia

Description.—Both tibiae are preserved. The right element is in much better condition; both epiphyses and the shaft are complete (Fig. 4.26; Table 4.18A-B). The bone is narrow and rod-like, and lacks a prounced cnemial crest. The shaft has a pronounced sigmoid curvature to its shaft: the proximal half is medially bowed while the distal end curves laterally. The proximal end is wider than it is deep. The medial condyle is smaller than the lateral condyle and more distally positioned. The condyles face proximally with respect to the proximal segment of the shaft. However, due to the sharp lateral curvature in the first part of the shaft, the condyles face laterally by 25° or so with respect to the more distal segment of the shaft. Both condyles are shallowly concave. They are separated by an intercondylar eminience on which the lateral intercondylar tubercle projects farther proximally. The medial condyle appears to have a deeper concavity, as a result of its more distal position with respect to the lateral condyle and the intercondylar eminence. The intercondylar eminence is truncated in its posterior projection such that there is an intercondylar notch between the posterior margins of the condyles for the posterior cruciate ligament. The proximodistal thickeness of the medial condyle is less than that of the lateral condyle due to buttressing of the lateral condyle for articulation with the fibula on its distal aspect. The anterior surface of the proximal end is marked by a distinct, shallow groove for attachment of the patellar tendon. This groove is located ~2 mm below the proximal lip of the tibial plateau, and forms a convex arc that is ~5 mm long. The tibial tuberosity is located just distal to this but is barely visible.

The anteromedial side of the tibial shaft is convex due to the curvature of the shaft. It is also relatively rugose. This rugosity extends for a little over half the length of the shaft. The lateral and posterior surfaces of the shaft are strongly concave, extending about a third of the way distally down the shaft. They are separated by a sharp ridge that would have held the interosseous membrane. Most of the distal two-thirds of the shaft is subcircular in cross-section, with the anteroposterior dimension being slightly greater. Just proximal to the distal articular surface the shaft cross-section becomes more triangular because of an anterolaterally projecting crest. Slightly posterior to this crest the interosseous crest gains prominence again. Thus, the distal end of the shaft has a distinct lateral surface formed between these two crests. The surface is slightly concave and would have articulated with the fibula. It is usually referred to as the fibular notch. The surface of the fibular notch is relatively rugose.

The distal articular surface for the astragalus is flat and slants to face lateral from distal by ~20°. It also faces posterior of distal by somewhat less than 20°. The anteroposterior length of the astragalar facet is greater than its mediolateral width. The medial malleolus projects beyond the distal articular surface by ~2 mm. Its lateral surface forms an obtuse angle with the distal articular surface. The medial malleolus is quite long anteroposteriorly (5 mm), or about half the anteroposterior length of the entire facet, even if short proximodistally. In distal view, it is clear that the anteroposterior axis (formed where the malleolus and distal articular surface meet) exhibits medial torsion relative to the proximal end of the tibia. The lateral surface of the medial malleolus is also distinctive in being laterally convex, possibly indicating that it met a concave surface

on the astragalus. In anterior view the medial malleolus appears to have a “sharp” tip. This is due to the presence of two prominent depressions on its distomedial surface.

Function.—Most features of the tibia suggest against leaping or cursorial locomotion, including the relatively anteroposteriorly shallow tibial plateau, a concave lateral tibial condyle, the absence of a prominent cnemial crest, a proximally situated groove for the patellar tendon, and an ungrooved astragalar articular surface (Boyer and Bloch, 2008).

The relative sizes of the tibial and femoral condyles have implications for mobility at the knee (Sargis, 2002b). The ratio between the lengths of the medial femoral and tibial condyles is 0.9 while that between the lateral condyles is 0.75. A lateral tibial condyle that is *enlarged* and a corresponding lateral femoral condyle that is *reduced*, compared to one another or the medial condyles, suggests that the capacity of the tibia to axially rotate on the femur was enhanced, with the medial condyle serving as the axis of rotation, and translation occurring between the lateral condyles. On the femur, the relatively large pit for the popliteus tendon may indicate that this muscle had an important role in causing or maintaining a certain degree of medial rotation. The dramatic concavity of the posterior surface of the proximal tibial shaft may indicate a robust tibialis posterior muscle or flexor digitorum tibialis. The former of these muscles is a plantar flexor and invertor, while the latter is typically the most important muscle for flexing the digits during powerful grasping in certain primates (Boyer et al., 2007). The concavity of the lateral surface would have held part of the attachment of tibialis anterior, a dorsiflexor and pedal invertor, but this surface is not unusual in its proportional size or morphology. The distal end of the tibial shaft is notable in the roughened surface of the

fibular notch and the strong crest forming the anterior border of the fibular notch. These features suggest a syndesmosis with the fibula and an especially robust anterior tibiofibular ligament. The distal articular surface is notable in its flat articular surface for the astragalus and the convex lateral surface of the medial malleolus. These features suggest that, the astragalus may have been able to pivot medially and laterally on the tibia, with its medial surface sliding around the convex lateral surface of the medial malleolus. This motion would result in abduction and adduction of the foot relative to the tibia. The distomedial pits of the medial malleolus reflect a robust deltoid ligament that attached the tibia to the navicular, astragalus, and calcaneum, thus helping to maintain the integrity and stability of this joint.

Comparison.—The tibia is a rare element in the French collections of *P. tricuspidens*. Why this should be the case is unclear. Regardless, only one specimen is available for comparison from this assemblage (MNHN R 218); it represents only the proximal end but still preserves significant morphology. Both species of *Nannodectes*, however, preserve tibiae. All specimens are basically similar. Because the *Nannodectes* specimens also preserve distal femora, the proportions of the femoral and tibial condyles can be compared among them. In *N. intermedius* the medial condyles are available only. The ratio between its femoral and tibial condyle lengths is 0.89. In *N. gidleyi* both sets of condyles are present: the medial condyles form a ratio of 0.97, while the lateral ones give 0.82. Thus the pattern is the same as for *P. cookei*, in suggesting a looser fit between the lateral condyles than the medial ones. However, the slightly "tighter" fit between both medial and lateral condyles of *N. gidleyi* may suggest a less axially mobile knee joint, and possibly a greater degree of agile pronograde locomotion. An additional difference

between *N. gidleyi* and other plesiadapids — a convex, rather than concave lateral condyle, as seen in tree squirrels and treeshrews — is also consistent with agile pronograde locomotion.

Fibula

Description.—The fibula is known from fewer plesiadapid specimens even than the tibia. However, both right and left fragmentary fibulae are preserved with UM 87990 (Figs. 4.27, 28; Table 4.19). The right side has an undistorted complete diaphysis, the left is broken, and shifted (this seems to be postmortem breakage). The epiphyses are missing from both elements. The proximal end of the shaft, where the epiphysis would have sutured, is expanded anteromedially to posterolaterally, but is narrow in the perpendicular direction. Thus the proximal shaft can be described as "blade-like." Approximately 2 mm distal to the proximal end, the shaft depth narrows to about two-thirds its proximal end depth. Farther distally, the shaft continues to narrow gradually until just prior to reaching the distal end, where it flares out in all directions and develops an anteromedially oriented rugosity, which would have contacted the fibular notch of the tibia, just posterior to the tibia's crest for the anterior tibiofibular ligament. The anteromedial "edge" of the "blade" of the fibula's proximal end is concave, while the posterior posterolateral margin is convex. The proximal end of the anterolateral surface has a proximodistally oriented crest toward the anterior margin that separates this bone into a smaller, more anteriorly-facing surface and a posterior more laterally-facing surface. The more anterior surface is that typically referred to as the anterior surface with medial and lateral lips (Stern, 1988), while the larger, more posterior surface is equivalent

to the peroneal surface. The peroneal surface is slightly concave at the proximal end, but becomes convex farther distally. The posteromedial surface is marked by a sharp, posteromedially projecting crest that separates this surface into anterior and posterior regions of roughly equal anteroposterior dimensions. The surface posterolateral to this crest is that typically referred to as the posterior, or "flexor surface," whereas the more anteromedial one is that referred to as the medial or "tibialis posterior surface " (Stern, 1988). Followed distally, the crest separates these two surfaces arcs anteriorly, converging on another crest, the interosseous crest, which has its proximal origin from the medial lip of the "anterior" surface.

Function.—A striking feature of the fibula is the blade-like crest projecting posterolaterally from the proximal end. This crest extends the posterior or "flexor surface" of the fibula proximally, far beyond its limit in humans, for instance. This crest would greatly augment the area of origin for both the flexor digitorum fibularis muscle on the posteromedial side of the crest and the peroneus longus muscle on the opposite side (anterolateral). Thus, functions associated with these muscles, such as forceful flexion of the digits and eversion of the foot, may have been enhanced. The rugose tuberosity for the fibular notch on the medial aspect of the distal end suggests a strong tibiofibular syndesmosis, and thus limited mobility between the tibia and fibula.

Comparison.—I was unable to locate the only other plesiadapid fibula specimen available for comparison (a distal end of *P. tricuspidens* MNHN BR-11-L: Beard, 1989). Beard only mentions the presence of a distal articular surface for the tibia being present, and suggests a synovial joint existed, instead of a syndesmosis. Thus either these two taxa had vastly different distal fibulae, or our interpretations differ markedly.

Astragalus

Description.—UM 87990 preserves a complete right and fragmentary left astragalus (Fig. 4.29A; Table 4.20A-C). The astragalus of plesiadapids is relatively well known (Szalay and Decker, 1974). Most descriptive features of these published specimens also apply to the astragalus of *P. cookei*.

The most distinctive feature of the right astragalus is its mediolateral asymmetry. On the astragalar body, the dorsal facet for the tibia (the lateral tibial facet) slopes steeply medially. This occurs because the fibular facet (which meets the lateral margin of the lateral tibial facet) is much deeper dorsoventrally (4.9 mm) than the dorsoventrally oriented facet for the medial malleolus (medial tibial facet: 3.4 mm). As a further result of this asymmetry, the angle between the facets of the lateral side of the lateral tibial facet is slightly acute (84°), while the medial one is obtuse (115°).

The lateral and medial margins of the lateral tibial facet are farthest apart distally and converge proximally, so that the facet is triangular. It forms an arc of ~90° and is shallowly grooved distally. The medial edge of the lateral tibial facet extends onto the neck of the astragalus. The medial and lateral margins of the lateral tibial facet also curve in the transverse plane so that they are laterally convex. The lateral convexity of the facet margins results in the medial tibial facet being concave, matching the convex surface of the medial malleolus of the tibia (see above).

The medial tibial facet is triangular, with one of the apices of the triangle meeting the distal edge of the lateral tibial facet. Its dorsal and ventral margins thus diverge proximally and the whole surface curves ventrally in the sagittal plane. Thus the facet

could even be described as having the shape of a paisley motif. The surface supporting the fibular facet is square to rectangular in shape. The articular area itself is restricted to the dorsal half of this surface. This facet also has a paisley shape; however it is more like the lateral tibial facet in having the largest girth distally, and margins that converge proximally. Ventral to the facet itself is a divot for the astragalofibular ligament. The apex of the triangular surface of the fibular facet stops short of the proximal margin of the lateral tibial facet, after the two facets diverge around a prominent superior astragalar foramen.

On the proximal surface of the astragalus, plantar to the superior astragalar foramen, the area between the two facets increases and develops into an expansive concavity. This concavity leads to the flexor fibularis groove on the plantar side of the astragalus. In plantar view the surface of this groove is triangular, with a proximodistally oriented medial margin formed by the edge of the medial tibial facet, and a more obliquely running lateral facet formed by the proximal margin of the posterior astragalocalcaneal (ectal) facet.

Lateral to the flexor fibularis groove, the ectal facet is rectangular, with its narrow dimension oriented mediolaterally. It is saddle-shaped with a proximodistal concavity and mediolateral convexity. The first curvature of the saddle is more pronounced than the second and forms an arc of ~45°. The lateral margin of the ectal facet meets the surface for the fibular facet at an angle of just over 90°. The axis of the ectal facet diverges from that of the lateral tibial facet by ~20°, such that the latter is oriented more medially. At the mediodistal margin of the contact between the ectal facet and the flexoris fibularis groove is a deep sulcus separating this structure from the middle astragalocalcaneal

(sustentacular) facet. This sulcus leads medially to the inferior astragalar foramen (which leads to the superior astragalar foramen).

Medial to the inferior astragalar foramen is the proximal extension of the sustentacular facet, the medial edge of which meets the medial tibial facet. This facet is proximally concave, where it occupies the sulcus beneath a platform holding the flexor fibularis groove. Followed distally it becomes convex as it also diverges slightly laterally, wrapping around the neck of the astragalus. Because this "strip-like" facet wraps obliquely around the "cylindrical" neck of the astragalus, it is often referred to as "helical" in its shape (Szalay and Decker, 1974). Distally it meets the facets for the spring ligament and navicular bone.

In dorsal view the neck of the astragalus is oriented at an angle with respect to the body, such that it projects medially. Distal to the neck is the head, which is occupied by the distal end of the sustentacular facet, the spring ligament facets and the navicular facets mentioned above on its posterolateral, posteromedial, and distal surface, respectively. In dorsal view, the head is much wider than the neck. The medial and lateral edges of its navicular facet appear to flare dorsally and proximally with respect to the middle part of the facet. Thus, in distal view, the facet appears reniform. The lateral side of the navicular facet faces distally with respect to the proximodistal axis of the lateral tibial facet. The mediolateral long axis of this side of the facet is parallel to the plane of the lateral tibial facet of the astragalus. The medial part of the navicular facet (the other half of the "kidney bean") faces mediodistally, and its mediolateral long axis is oriented dorsomedial to plantolateral with respect to the lateral tibial facet.

Function.—The functional features of the astragalus have been discussed at length for plesiadapids and plesiadapiforms (Szalay and Decker, 1974; Szalay, 1984). A few observations and interpretations can, however be added here. Beard (1989) speculated on the degree and nature of mobility between the astraglus and tibia but the occurrence of these elements from a single individual allows a better constrained assessment of mobility here. It can be demonstrated by manipulation of the astragalus and tibia that at full dorsiflexion of the tibia on the astragalus, the head and neck of the astagalus project anteriorly and form an angle of slightly less than 90° with the shaft of the tibia. When the astragalus is plantarflexed by rotating it through the full 90° of arc formed on the lateral tibial facet, there are two other conjunct motions that occur because of the slanting surface of the lateral tibial facet, and laterally concave surface of the medial tibial facet (Fig. 4.30): (1) the astragalus inverts (rotates laterally on its proximodistal axis) by a full 90°. (2) The distal end of the astragalus rotates medially (around a dorsoplantar axis) by a full 90°. The angle between the astraglar neck and body changes by somewhat less than 90°. Thus the act of "plantar-flexion" of the astragalus on the tibia, results in relatively litte true plantar flexion (see discussion below for the broader significance of these features for positional behaviors).

Comparison.—To compare *P. cookei* to other plesiadapids and other mammals, 18 linear and six angular measurements were taken on the astragalus (Table 4.20A-D; Figs. 4.31, 32). The linear measurements were standardized against absolute size in the usual way (see Materials and Methods) using a geometric mean of all 18 linear measurements. The angular measurements are reported in degrees, but were analyzed in radians.

Principal coordinates analysis of the Euclidean distance matrix reveals all available plesiadapid astragali to be basically similar to each other. The astragali of two extant euprimates, a dermopteran, a treeshrew, a fossil adapiform, and *Deccanolestes* (a fossil, possible euarchontan from India) plot in different parts of the principal coordinates space (Fig. 4.32), and do not overlap with region occupied by the plesiadapids. It is interesting to note that astragali of *Cynocephalus volans*, *Loris tardigradus*, and the adapiform are morphologically closer to each other and those of plesidapids than they are to astragali of the other euprimate *(Galago moholi*) or *Tupaia glis.* This is apparent visually and also by taking into consideration the minimum spanning tree between data points. Considered feature by feature, the morphospace proximity makes some sense (e.g., *L. tardigradus*, *C. volans*, and the adapiform have a laterally curved medial tibial facet and an elliptical, rather than circular shape to its astragalar head, like those of plesiadapids but unlike those of *G. moholi* or *T. glis*), and it may further support the interpretation of plesiadapiforms by Beard (1989) as being slow, cautious arborealists.

The astragalus of *P. cookei* differs from those of other plesiadapids in at least two notable ways. First, it has a more proximodistally expanded proximal end to its medial tibial facet. In fact this expansion almost appears pathological because, as a consequence, the concave part of the sustentacular facet into which the sustentaculum of the calcaneus must insert for articulation has been narrowed substantially. The concavity is actually too narrow for the calcaneal element to fit into it easily and flushly contact the astragalar surface. The increase in the proximodistal depth of the medial tibial articular surface and consequent narrowing of the concavity of the proximal part of the sustentacular facet appears to also be correlated with proximoventral expansion of the

flexor fibularis groove surface. Expansion of the flexor fibularis groove surface could conceivably have been the progressive result of high stresses on this surface caused by the flexor fibularis tendons that run under it. Second, and less likely as a result of pathology, the astragalar neck is proportionally longer compared to the astragalar body in *P. cookei* as compared to other plesiadapids.

Calcaneum

Description.—UM 87990 preserves a complete right and fragmentary left calcaneum (Fig. 4.29B; Table 4.21A-C). Plesiadapid calcanea are relatively well known (Szalay and Decker, 1974). Most descriptive features applying to these published specimens also apply to the calcaneum of *P. cookei*.

The most distinctive feature of the calcaneum of *P. cookei* is the large peroneal tuberosity on the lateral side, which covers 40% of the proximodistal length of the bone. Because of its great length, it arises from the tuber proximal to the distal end of the ectal facet; however, it does not project distally beyond the calcaneocuboid facet. The dorsoplantar depth is also relatively large. The lateral surface of the tubercle is marked by a deep groove that crosses it obliquely from dorsoproximal to plantodistal.

The calcaneal tuber and posterior calcaneoastragalar (ectal) facet represent a bit less than two-thirds the length of the bone. The tuber is deep dorsoventrally relative to its proximodistal length. The proximal end is mediolaterally wider than the shaft of the tuber distal to it. The medial side of the tuber projects more strongly medially than the lateral side projects laterally. The ectal facet is shaped like a segment of a cone with its tip truncated. The axis of ectal facet points almost medially relative to the proximodistal

axis of the calcaneum, but deviates distally by ~15°. A small fibular facet is located lateral to the ectal facet and faces laterally.

The middle and anterior calcaneoastragalar facets (proximal and distal sustentacular) are located mediodistal to the ectal facet and separated from it by a non-articular sulcus. The proximal sustentacular facet is shallowly cylindrically concave with an axis paralleling that of the ectal facet. The surfaces of the ectal facet and proximal sustentacular facet are *not* parallel but rather deviate from parallel by ~30° (i.e., they form an angle of ~150° with one another). Distally, the distal sustentacular facet is fairly flat and is continuous with the proximal one. Its entire surface is rotated medially with respect to the proximal sustentacular facet, so that it is comes close to paralleling the surface of the ectal facet. Given the change in sustentacular facet surface angle from proximal to distal, this facet can be described as helical in form, like its convex counterpart on the astragalus.

The proximal end of the proximal sustentacular facet is confluent with a facet that covers the proximal side of the sustentaculum. This flat, square facet is the "sustentaculum tali" that would normally contact the proximal extension of the sustentacular facet of the astragalus in other plesiadapids, although it cannot do so in UM 87990 (see above).

The calcaneocuboid facet is saddle-shaped in UM 87990, being strongly concave mediolaterally, and slightly convex dorsoventrally due to a subtle pit in the facet on its plantar aspect, just dorsal to the anterior plantar tuberosity (see Beard, 1989). The calcaneocuboid is oriented oblique to the long axis of the calcaneum, and faces 15° or 20° medially. The main notable features of the plantar surface are (1) the anterior plantar

tubercle, which is centrally located but flares medially, and (2) the deep groove running medial to the anterior plantar tubercle on the plantar surface of the sustentaculum.

Function.—Functional features of the plesiadapid calcaneum have been discussed at length by other authors (Szalay and Decker, 1974). The most important feature cited is the helical form of the astragalocalcaneal facets, which allows the astragalus to rotate the dorsal surface of its distal end to face medially at the same time as it moves proximally on the calcaneum, resulting in inversion of the mediolateral axis of the lower ankle joint and the entire foot (Fig. 4.33). New functional statements are best made in a comparative context.

Comparison.—In order to gauge the overall similarity between different plesiadapids and a few select non-plesiadapid mammals (see Table 4.21A-C), a principal coordinate analysis was run on 19 linear size-standardized and six angular measurements (Fig. 4.34). The resulting pattern (Fig. 4.35) is similar to that for the astragalus. All plesiadapids cluster together, while the non-plesiadapids are at opposite ends of the principal coordinates space, except for *Cynocephalus volans*, which is very close to the plesiadapid space. Among the plesiadapids sampled, *N. gidleyi*, followed by *P. cookei*, are the most different from *P. tricuspidens* and *P. churchilli*.

Three features that make *P. cookei* unique among plesiadapids suggest an increased capacity for, and control of, inversion and eversion movements at the lower ankle joint: (1) a proportionally longer astragalar neck and calcaneal head (NV: Table 4.20A; DV: Table 4.21A), (2) a larger angular difference between the proximal and distal parts of its calcaneal sustentacular facet, and (3) the longest calcaneum ectal facet length and arc length (Cc-08: Table 4.21A), but an astragalar ectal facet length that is average

among the *P. tricuspidens* sample (Ast-10: Table 4.20A). Features 1and 2 indicate that the helical sustentacular facets are proportionally longer and that their surfaces encompass a larger arc. Thus, a greater amount of inversion-eversion rotation was possible. Feature 3 suggests that the calcaneal ectal facet was proportionally larger compared to the astragalar ectal facet in *P. cookei* than it was in *P. tricuspidens*, at least. This greater offset would allow the astragalus ectal facet to have rotated through a larger arc on the calcaneum ectal facet, which would have been necessary to accommodate more extensively rotating helical sustentacular facets.

Other differences between *P. cookei* and other plesiadapids concern morphology relating to muscles that control inversion-eversion. The peroneal tuberosity and groove for the peroneous longus tendon crossing it are larger and deeper, respectively, in *P. cookei* than in *P. tricuspidens,* suggesting a stronger peroneous longus muscle, the main function of which is to evert the foot (Boyer et al., 2007). Likewise, the groove on the plantar aspect of the calcaneum for the flexor fibularis (and tibialis posterior and flexor tibialis) tendon(s) is broader and better defined in *P. cookei* than in *P. tricuspidens*, suggesting that these muscles, responsible for both plantarflexion and inversion were better developed. Another difference between *P. cookei* and other plesiadapids is the degree to which the plantar pit of the calcaneocuboid joint is developed. This pit is said to control the movement of the cuboid and allows it to rotate more effectively on the calcaneum (Beard, 1989), as it does during inversion and eversion movements.

Cuboid

Description.—The right cuboid is preserved in UM 87990 (Table 4.22; Figs. 4.36A, 4.37). It is a rectangular, cube-shaped bone. The majority of the proximal end for articulation with the calcaneum is flat, with a slight convexity. It faces ~58° lateral from proximal, relative to the distal facet, but has a dorsoventral axis that parallels the distal facet's axis. The medial side of the proximal articular surface curves slightly distally. This medial portion thus faces medially. In the closest packed position between the calcaneum and cuboid, this medially-facing area does not contact the calcaneum but forms a continuation of the calcaneum's distal sustentacular facet and would have contacted the astragalus. However, this change of surface orientation creates a strong convexity at the proximal peak of the bone and marks the point of contact with the plantar pit of the calcaneum (see above).

There is a medially-facing facet for the navicular on the medial side of the bone. It is distal to and confluent with the proximal articular facet. Distal to and confluent with the navicular facet, there is a convex facet for the ectocuneiform. The tangent of its surface faces distomedially, and slightly dorsally. Distal to the ectocuneiform facet is a recessed non-articular area, leading up to the distal end of the bone. The dorsal surface of the cuboid is proximodistally concave and non-articular. In anterior view, the lateral surface is marked by a blunt, tubercle-like projection. This tubercle can be followed to the posterior surface where it serves to form the proximal boundary to a deep, broad mediolaterally-running groove for the peroneus longus muscle tendon. This groove has a greater girth medially than laterally. The distal articular surface is triangular in distal view. The facet has anterolateral, medial and posterior surfaces. The medial surface,

which abuts the ectocuneiform, is notched. The medial two-thirds of the distal surface itself is shallowly dorsoventrally concave, for MT IV; the lateral third, where MT V fits, is shallowly convex.

Function.—The orientation of the proximal and distal facets indicate habitual abduction of the foot with respect to the proximal tarsus: the cuboid facet on the calcaneum is medially rotated by ~15°, but subtracting the ~60° angle between the proximal and distal cuboid facets reveals that the metatarsal facet would have faced 45° laterally with respect to the axis of the calcanaeum. Manipulation of the articulated calcaneum and cuboid reveal that they do not rotate very extensively, contrary to Szalay and Decker (1974) and Beard's (1989) description of the nature of movements at this joint in other plesiadapids and plesiadapiforms. There is much more mobility in abduction and adduction of the cuboid on the calcaneum, thereby reducing or increasing the 45° of abduction that occurs in the closest packed position. It is interesting to note that, in an inverted foot position, mobility in abduction-adduction of the foot translates to plantarflexion-dorsiflexion relative to the more proximal limb elements (e.g., tibia proximodistal axis).

Comparison.—Compared to other plesiadapids, *P .cookei* differs in having a proportionally broader peroneus longus groove (PgV: Table 4.22). This supports functional inferences regarding morphological differences between the upper ankle bones of *P. cookei* and other plesiadapids (see above). That is, a larger peroneous longus tendon groove may equate to more forceful control over eversion of the foot.

Ectocuneiform

Description.—A left ectocuneiform is preserved (Figs. 4.36B, 4.37). No other plesiadapids have an ectocuneiform preserved; thus it cannot be confirmed with comparative information that this bone is correctly identified as belonging to *P. cookei*. However, it seems to fit with the cuboid, which clearly belongs to *P. cookei* based on comparative information (see above). Furthermore, it is quite similar to the ectocuneiform of another plesiadapiform, *Ignacius clarkforkensis* (Boyer and Bloch, 2008). Thus, it is tentatively attributed to *P. cookei*.

It is square in lateral or medial view and mediolaterally narrow (2.9 mm) compared to its dorsoplantar (4.8 mm) and proximodistal (4.7 mm) dimensions. It is dorsoventrally wedged, with it dorsal surface mediolateraly wider than its ventral surface. Its proximal surface is concave and slopes medially relative to its proximodistal axis, while its distal surface is slightly concave and faces directly distal. The proximal surface is notched on its medial side, while the distal surface has a shallow notch on its lateral side. The dorsal surface is smooth and non-articular. The plantar surface is notched for the continued course of the peroneus longus tendon. The dorsolateral corner of the proximal end has a proximolaterally facing surface that would have contacted the distal tip of the anterodistomedially-facing surface of the medial side of the cuboid. The plantoproximal corner of the lateral side has a tiny facet that would have contacted a corresponding facet on the cuboid (Fig. 4.37). Distal to these two points for the cuboid is a concave articular area that seems to fit the distal region of the medial articular surface of the cuboid. However, in order to approximate these facets, the distal metatarsal surface of the ectocuneiform must be inset proximally to the metatarsal facet of the

cuboid. The medial side of the bone has distinctive articular facets along the dorsal and proximal margins (for the mesocuneiform), and along its distal margin (for MT II).

Function.—The presence of an MT II facet indicates that the tarso-metatarsal joint of MT III was distally positioned relative to that for MT II. Thus the foot would not have been as mobile as in *Cynocephalus* and other taxa wherein tarso-metatarsal joints II-V occur in a single plane perpendicular to the proximodistal axis of the foot. The lack of ectocuneiforms of other plesidapids and the similarity of the UM 87990 ectocuneiform to that known for other plesidapiforms obviates the utility of addtional comparative statements at this time.

Mesocuneiform

Description.—The right mesocuneiform is preserved (Figs. 4.36C, 4.37). It is slightly smaller than the ectocuneiform and triangular in dorsal view. In lateral view it is trapezoidal, with smaller dorsoplantar dimensions proximally (4.0 mm) than distally (5.0 mm). The proximal articular surface faces laterally, toward the ectocuneiform, relative to the proximodistal axis of the bone, while the distal end faces distally. As with the ectocuneiform, the mesocuneiform is wedge-shaped with a mediolaterally broader dorsal surface than plantar surface. The lateral surface for articulation with the ectocuneiform is flat, while the medial surface for articulation with the entocuneiform is concave. The bone is quite short proximodistally: the length of its lateral side is only 2.8 mm. Thus, when articulated with the ectocuneiform, its distal metatarsal facet was inset proximally compared to that of the ectocuneiform (and also compared to the entocuneiform – as based on entocuneiforms known for other plesiadapids – see Szalay and Dagosto, 1988).

Metatarsals

Hallucal metatarsal description.—The right hallucal metatarsal (MT 1), like the pollical metacarpal, is a robust bone (Figs. 4.38A, 4.39; Table 4.23). The proximal articular surface for the entocuneiform faces proximally. The entocuneiform facet is dorsoplantarly convex and mediolaterally concave, thus giving the joint a distinct saddle shape. This facet is roughly equal in its mediolateral and dorsoventral dimensions. The facet is flanked by proximoventrally projecting tubercles on its lateral and medial sides. The lateral side tubercle is the peroneal tubercle that received the tendon of peroneous longus. The medial side tubercle is larger than the peroneal tubercle. The shaft narrows distal to the proximal end. Near the midpoint of the shaft, the cross-sectional shape is roughly circular. The shaft expands mediolaterally as the distal articular surface is approached from the midpoint. The ventromedial aspect of the shaft is marked by a strong, longitudinally running groove. The articular surface of the distal end is similar to that of the pollical metacarpal in having three keels, in the asymmetry of its profile, in the form of its articulation with the hallucal proximal phalanx, and in the ratio of its mediolateral width to dorsoventral depth (see Tables 4.10, 23). Furthermore, the hallucal metatarsal is similar to the pollical metacarpal in the torsion formed between the dorsoventral axis of its proximal end and the dorsoplantar axis of the distal end. The main differences between these two bones are that the hallucal metatarsal is larger, more gracile, and has a proximal facet that is mediolaterally broader and which faces more proximally and less dorsally.

Hallucal metatarsal function.—The large size of the medial side proximal tubercle, relative to the lateral side peroneal tubercle, may indicate the presence of a large tibialis anterior tendon, a dorsiflexor and invertor of the foot. The strong groove on the medial side of the shaft may have received fibers of an opponens hallucis muscle (Straus, 1930; George, 1977). The saddle-shaped facet for the entocuneiform, the lateral torsion of the distal end relative to the proximal end, and the evidence for the presence of a muscle that could pull the hallux more fully into opposition are consistent with previous interpretations that the hallux was specialized for grasping in a way essentially similar to that of euprimates and the treeshrew *Ptilocercus* (Szalay and Dagosto, 1988; Sargis et al., 2007).

Metatarsal II description.—There are two bones that appear to represent MT II (Figs. 4.38B-C, 4.39; Table 4.23): a right element that preserves everything but the proximal end and a left element that is only the proximal end. It is not certain that these both represent the same taxon, however no information contradicts this possibility and they are treated as belonging to *P. cookei*. Some of the justification for identifying this bone as MT II, specifically, must be done in a comparative context that considers all preserved metatarsals together. The results of these analyses are presented below.

As for MC II, the lateral margin of the proximal articular surface (for the mesocuneiform) projects slightly farther proximally than the medial aspect. This proximal facet is slightly convex, but basically flat, and articulates well with the mesocuneiform. The medial side of the proximal end has two facets: a dorsally located one and a ventral one. The dorsal facet faces dorsomedially, and the ventral one faces ventromedially. Taken as a whole, these two facets form a convex surface for

articulation with the entocuneiform. The lateral side has a flat, parasagittally oriented articular surface, which additionally faces slightly distally. The borders of facets here are not distinctly delimited. However, this surface would have contacted the distal end of the medial aspect of the ectocuneiform proximally, and the medial side of MT III distally.

The shaft of MT II shaft becomes progressively mediolaterally wider from its proximal end to its distal end. The distal end is bowed away from the more lateral digits and toward MT I. The distal articular surface is similar to those of the metacarpals. It differs in being larger and in having a smaller dorsoplantar depth for its mediolateral breadth (a lower HSV). The head is asymmetrical, with a more gradually sloping medial aspect to the distal profile (as for MC II and III). Although it is fragmentary, enough is preserved to determine that it would have been longer than any of the metacarpals of set 1, and about the same length as the "set 2" MC III and IV.

Metatarsal III description.—MT III is represented by the complete right side element and by the proximal half of the left side element. It is quite different from MT II in that it is longer and more gracile, its proximal end is more asymmetrical, and its distal end is narrower (Figs. 4.38D, 4.39; Table 4.23). The lateral side of the proximal articular surface of MT III (for the ectocuneiform) projects farther proximally than the medial side. The articular surfaces on the medial and lateral aspects of the proximal end of the bone have nonarticular gaps that separate each side into dorsal and ventral articular regions. These nonarticular "gaps" appear as notches on the lateral and medial sides of the bone in proximal view. The medial side of the proximal articular surface has a dorsally positioned, distal extension onto the medial side of the shaft, representing a point of articulation with MT II. The medial side of the proximal end also has a ventrally

positioned, proximodistally narrow facet for MT II. The lateral side of the proximal end has two distinctly developed facets for MT IV. The more dorsal of these faces ventrodistally, while the more ventral one faces slightly dorsally. Together these facets form a concave surface that cups the medial side of MT IV. The shaft of MT III is straight, changing little in its cross-sectional dimensions along its length. The distal end is similar to that of MT II, except that it is absolutely mediolaterally narrower and dorsoplantarly shallower, but proportionally dorsoventrally deeper (i.e., it has a lower HSV – see Table 4.23).

Metatarsal IV description.—MT IV is the only metatarsal position represented by two morphs. The "set 1" morph (Figs. 4.38E, 4.39) is a right side element that is similar in length to MT III and has a similar distal end morphology. Furthermore, the right side MT III and MT IV articulate smoothly. On the other hand, the "set 2" morph (Fig. 4.40A) is a left side element that is longer than MT III and the right side MT IV. The distal end morphology is difficult to assess due to breakage but it appears to have been absolutely and proportionally mediolaterally wider with more prominent tubercles flanking collateral ligament pits.

The proximal end of the "set 1" MT IV is in some ways similar to that of MT III. The lateral side of the proximal articular surface (for the cuboid) projects farther proximally than the medial side. The medial side of the proximal articular surface of the "set 1" MT IV has a dorsally positioned distal extension onto the medial side of the bone. However, this extension is much greater in MT IV than in MT III. This difference represents the existence of a much more extensive articulation between MT III and IV than between MT II and III. There is a non-articular gap separating the dorsally located

medial side facet on MT IV from a ventrally placed one. As for dorsal facets, the ventrally placed facet is larger than the corresponding medial side facet on MT III. The lateral side of the proximal end of MT IV differs from that of MT III in having a continuous concave articular surface for the more lateral metatarsal (MT V) with no nonarticular gaps separating it into dorsal and ventral regions.

In most respects the proximal end of the "set 2" MT IV is similar to that of the "set 1" element. However, it is diagnostically different in the morphology of the medial side, dorsal facet for MT III. Specifically, this facet is larger and strongly concave in the "set 2" MT IV (instead of slightly convex). As a result of these differences in articular surface morphology, the "set 2" MT IV, which is a left side element, will not articulate securely with the left side MT III.

Metatarsal V description.—Only a proximal fragment of the right MT V is preserved (Fig. 4.40B). It is identifiable as MT V by its large peroneal tuberosity. However, it clearly did not belong to *P. cookei*, as revealed by MT V's preserved with two other plesiadapid skeletons (Table 4.23). Although not described by Beard (1989), a proximal base and distal shaft of an MT V of *Nannodectes intermedius* USNM 442229 are preserved. A specimen of cf. *P. churchilli* (SMM P77.33.517) from Wannagan Creek in North Dakota also preserves this element (Fig. 4.39B, C). The plesiadapid MT V is revealed to be treeshrew or dermopteran-like by these specimens. The UM 87990 MT V does not fit this pattern and does not even articulate well with the "set 1" MT IV. Presumably, it articulates with the "set 2" MT IV better, however the MT V facet on MT IV is too broken to assess this possibility.

Assessment of metatarsal association and attribution.—As discussed in the descriptions, all but a left MT IV and a right MT V appear to belong to *P. cookei*. This interpretation is not as thoroughly supported as those for the metacarpals mainly because (1) there are fewer and less complete metatarsals than metacarpals in UM 87990 and (2) there are fewer complete comparative metatarsal specimens available. The most speculative of the attributions for the metatarsals described above is that of MT II, given its fragmentary nature and unusual morphology (compared to MT III and IV). However, this attribution is actually supported by comparisons to *N. intermedius* material. Measurements of proximal and distal fragments of MT I-V preserved with *N. intermedius* USNM 442229 show that its MT II is similar to the element identified as such for UM 87990 in being more robust than MT III and IV (Table 4.23). An additional similarity between MT II of USNM 442229 and UM 87990 is that both have a distal end that is proportionally dorsoventrally shallower than those of the other metatarsals. These same proportional features also appear to characterize the MT II of *Dryomomys szalayi* UM 41870, although quantitative data are not available for comparison at this time (Boyer and Bloch, 2008). The identification of *P. cookei's* MT III and IV is supported by the similarity of the proximal ends of these bones to those of MT III and IV of USNM 442229. Dentally-associated skeletal remains of cf. *P. churchilli* (SMM P77.33.517) from Wannagan Creek of North Dakota also include fairly complete proximal ends of MT III and IV. Again, these are nearly identical to those of *N. intermedius* and *P. cookei*. As discussed above, the same *P. churchilli* specimen also includes a nearly complete MT V. A composite plesiadapid foot can thus be assembled (Figs. 4.33, 39C) using information from these three specimens along with information from the tarsals.

Vertebral column

Vertebral column description.—Much of the vertebral column is preserved but, for the most part, positional information was not recorded as it was prepared. Thus, assignments of vertebrae to various positions of the cervical, thoracic, lumbar and caudal regions are based on specific morphological features and assumed morphological and metrical trends. For instance, the sixth cervical vertebra is identified based on the presence of a hypertrophied anterior tubercle. As another example, the first thoracic vertebra is identified as such because it has a body with a shallower dorsoventral depth than any other preserved thoracic vertebrae. There are bound to be mistakes in this seriation. Hopefully, more complete specimens and better comparative data will illuminate such misidentifications.

Due to the column being preserved in disarticulation near the skeleton of *Uintacyon*, it is possible that some vertebrae may not actually belong to *P. cookei*; however, a good number of vertebrae in the skeleton of *Uintacyon* remain associated with its skull, which is still partly embedded in limestone. Furthermore, *N. gidleyi* and *N. intermedius* preserve vertebrae from all regions of the column. These other plesiadapid bones help in confirming the identity of vertebrae from UM 87990 as belonging to *P. cookei*. Still, it would not be surprising if some vertebrae of *Uintacyon* were mistakenly attributed to *P. cookei*; however, this is most likely to be true for the more distal caudal vertebral positions.

Because the vertebral column was not preserved in articulation, and because there are definitely some vertebrae missing, it is not clear exactly how many vertebrae would

have been present in the complete column. From a small dataset in Table 4.24, it can be seen that standard numbers of vertebrae among a few scansorial sciurids, generalized euprimates, scandentians, and some marsupials are seven cervical, 12 thoracic, seven lumbar, three sacral and 25 caudal vertebrae. However, there is a bit of variation in the number of thoracic, lumbar, and sacral vertebrae, and a lot of variation in the number of caudals. UM 87990 preserves five cervical (Fig. 4.41), 12 thoracic (Fig. 4.42), and six lumbar vertebrae (Fig. 4.43). For descriptive and comparative purposes, I reconstruct the plesiadapid vertebral column as having seven cervical, 13 thoracic and seven lumbar vertebrae (Table 4.24). The sacrum is complete with three vertebrae (Fig. 4.44). There is no way to generate a constrained estimate of the number of caudal vertebrae from the comparative data. However, there are 17 preserved caudal vertebrae and at least three specific anterior positions are missing (Fig. 4.45). There were thus at least 20 caudal vertebrae.

Vertebral column comparisons.—Comparisons of *P. cookei's* vertebral column to those of other taxa were made using four different principal coordinate analyses on Euclidean distance matrices relating cases in the sample (Fig. 4.46). Variables for these analyses were calculated from craniocaudal length measurements of the vertebrae and vertebral column. More specifically, as discussed in the Methods section, "size free" shape variables were created as natural log ratios of each measurement to the geometric mean of all measurements included for a specimen in a given analysis. The first analysis (Fig. 4.46A) uses measurements and/or estimates (in the case of some incomplete fossil specimens) of five vertebral segment lengths from Table 4.24. The second (Fig. 4.46B) uses all available vertebrae lengths in the column of *P. cookei* up to Ca10 (31

measurements, see caption of Fig. 4.46 for a specific listing). The next analysis (Fig. 4.46C) uses a subsample of 14 of these measurements (see caption of Fig. 4.46 for a specific listing), allowing inclusion of *N. intermedius* (USNM 442229) elements. The final analysis (Fig. 4.46D) uses a different subset of 14 of the 31 measurements from Figure 4.46B (see caption of Fig. 4.46 for a specific listing), allowing the inclusion of *N. gidleyi* (AMNH 17379) elements. In the first three analyses (Fig. 4.46A-C), a fairly consistent pattern results, despite different variable sets: euprimates of the sample are fairly similar to each other, with *Tarsius* forming an outlier. Plesiadapids and plesiadapiforms are similar to each other, and typically plot just outside of the euprimate distribution, closer to the phalangerid opposum *Trichosurus* and the two rodents of the sample. Generally, the first coordinate seems to be driven by measurements relating to tail length, while the second appears to relate to neck length. Thus, with a relatively long neck and short tail, *Cynocephalus* is in its own region of each morphospace. Figure 4.46D only includes one measurement reflecting tail length (length of Ca1). This does not appear to be enough information to capture the informative aspects of variance in tail length of the sample. Thus the distribution here is quite different. Still, it shows plesiadapids to be closer in form to various euprimates, rodents and oppossums than to *Cynocephalus* or *Tupaia*.

Atlas

Description.—The atlas is well preserved (Fig. 4.41). The right transverse process is broken lateral to the canal for the vertebral artery. The posterior arch is craniocaudally shortest at the midline and becomes longer, or more expanded, laterally; however, its

shortest part is still longer than the most expanded part of the anterior arch, its mediolateral midpoint (Fig. 4.41; Table 4.25). The posterior arch has a small tubercle for attachment of the rectus capitis posterior minor muscle. The foramen for entrance of the vertebral artery is located between the lateral aspect of the axis facet and the posterior arch. This foramen leads to a canal that pierces the atlas from ventral to dorsal, lateral to the vertebral foramen (for the spinal cord). At the beginning of its course, the canal has an opening on the ventrolateral aspect of the atlas. The canal then traverses medially and cranially though the posterior arch of the atlas to open within the vertebral canal just above the occipital articular facets of the lateral masses of the atlas. The middle part of the vertebral artery canal has another opening on the dorsolateral surface of the posterior arch.

Comparison.—Not much can be said of the functional significance of the atlantal morphology outside of a comparative context. With regard to the atlas, *P. cookei* is similar to *N. gidleyi*, *N. intermedius*, tupaiids and *Sciurus* in most respects. *P. cookei's* atlas differs from these taxa in having an anterior arch that is more craniocaudally expanded compared to the posterior arch. This makes it slightly more similar to the condition in *Ptilocercus*, dermopterans and chiropterans (Sargis, 2001). Sargis (2001) suggested that a more expanded atlas in *Ptilocercus*, as compared to that of *Tupaia*, correlates with reduced neck mobility in the former taxon.

Axis

Description.—The axis is fragmentary (Fig. 4.41B; Table 26), missing the cranial and caudal tips of its spinous process, the posterior zygapophyses, the tips of the

transverse processes, and the posterior centrum epiphysis. The body is also severely crushed. It seems likely that the element would have exhibited a cranial projection to its spinous process prior to breakage. A substantial portion of the spinous process's caudal projection is intact. The dorsal edge of the spinous process is preserved near the craniocaudal midpoint. The foramina transversaria are preserved, as are the roots of the transverse processes, which form the lateral edges of said foramina. The odontoid process is preserved. It has craniolaterally facing depressions for the alar ligaments. As is often the case, the axis is the longest of the cervical vertebrae, even without accounting for what is likely to have been a significant amount of craniocaudal crushing, the loss of the caudal centrum epiphyis, or the length of the odontoid process (Table 4.26).

Comparison.—In most preserved features, the axis of *P. cookei* is similar to that of *N. intermedius*. One notable difference is that *N. intermedius* has a proportionally larger vertebral canal. However, this is true throughout the vertebral column and also distinguishes vertebrae of *N. gidleyi* from those of *P. cookei*. It is likely an allometric effect of absolute size differences between the three plesiadapids.

Other cervical vertebrae

Description.—Three other cervical (C) vertebrae are preserved. One is identified as C3 (Fig. 4.41C), although it could also represent C4. It is not C5 or C7 because it does not articulate well with C6. It is almost perfectly preserved. The lamina of the vertebra is craniocaudally expanded, relative to its mediolateral width: this is one reason it is assigned to C3 rather than C4. The spinous process appears to have been weakly developed. The prezygapophyses are oriented dorsally whereas the postzygapophyses

face ventrally. The centrum is rectangular with a distinct midline ventral ridge. Its cranial facet faces cranially and is angled slightly ventrally. Within the vertebral canal, the dorsal surface of the centrum is marked by two foramina. The transverse processes are long and narrow, projecting inferolaterally.

Another cervical vertebra is represented by the centrum alone (Fig. 4.41D). It is considered to be C4, even though it cannot be articulated with C3, due to the missing caudal C3 epiphysis. There is slight mismatch between the caudal epiphysis of "C4" and C6, which is taken as additional evidence that it is correctly identified as C4. The C4 centrum is even more "rectangular" than that of C3, because the dorsal and ventral surfaces are parallel to one another, and there is no midline ridge on the ventral surface. Like C3, there are two foramina on the dorsal surface. The cranial centrum facet faces slightly ventrally, like that of C3. The caudal facet faces slightly dorsally; however it has a dorsal lip, which makes the surface cylindrically concave.

The last preserved cervical vertebra is identified as C6, mainly due to the presence of broken roots of hypertrophied anterior tubercles, as typically characterize this position (Fig. 4.41E). The left half of the pedicle and lamina are also broken away, as are the tips of the transverse processes. The prezygapophyses are oriented slightly more medially than the dorsally facing facets of C3, while the postzygapophyseal facets are oriented slightly more laterally than the ventrally facing facets of C3. The foramina transversaria are preserved. The centrum is basically identical in shape and morphology to that of C4.

Comparison.—Again, a comparative context is needed to comment on functionally salient features of the cervical vertebrae. C3, C4 and C6 in *P. cookei* have morphology similar to that preserved in *N. gidleyi* and *N. intermedius,* although these

taxa appear to have slightly more prominent ventral midline ridges on their vertebrae. Plesiadapids are also morphologically similar to *Ptilocercus* and arboreal tree squirrels in (1) having vertebral bodies of the cervical vertebrae that are mediolaterally wide relative to their craniocaudal length and (2) lacking pronounced spinous processes. On the other hand, *Tupaia* and terrestrial rodents (e.g., *Rattus*) have mediolaterally narrower vertebral bodies and more pronounced spinous processes. These differences have been related to contrasts in head mobility among various taxa (Argot, 2002). The tupaiid-like form is thought to retain greater mediolateral mobility due to the presence of a narrower body. *Cynocephalus* is an interesting case because it has cervical centra that are similar to those of plesiadapids in most respects, but it has prominent spinous processes on all of its cervical vertebrae, unlike plesiadapids (Stafford, 1999).

Table 4.24 gives neck length as a proportion of trunk length. *P. cookei* is similar to most of the relatively small scansorial-to-arboreal taxa in its proportional neck length. *Cynocephalus* and *Tarsius* have much longer necks. As stated above, principal coordinate analyses also appear to differentiate these two taxa on the basis of their long necks. Stafford (1999) presents data showing *Cynocephalus*, bats and sloths to have exceptionally long necks among arboreal to scansorial mammals.

Thoracic vertebrae

Description.—All but one (12 out of 13) of the thoracic (T) vertebrae appear to be preserved (Fig. 4.42). The missing position is the diaphragmatic vertebra, which should have dorsolaterally angled prezygapophyseal facets, like the vertebrae more cranial to it, and dorsomedially facing postzygapophyseal facets, like the vertebrae more caudal to it,

including the lumbar, sacral and proximal part of the caudal region. Generally speaking, vertebrae described in this section were identified as being part of the thoracic region by the presence of rib facets on the body or transverse processes and in some cases by the orientation of the zygapophyseal facets. The craniocaudal position of a given thoracic vertebra, other than whether it comes before or after the diaphragmatic position is difficult to determine due to extensive postmortem deformation that prevents assessments through articulation or detailed measurements. Often centrum length, height or overall size increases progressively from anterior to posterior. The first thoracic vertebra (Fig. 4.42A) is craniocaudally shorter than the others, but there is no pattern of increase in the remaining prediaphragmatic vertebrae (Table 4.27; Fig. 4.42B-I). This is demonstrated beyond any doubt by the only two vertebrae preserved in articulation (Fig. 4.42E), in which the more cranial one is slightly, but definitely, longer. However, the two postdiaphragmatic thoracic vertebrae (Fig. 4.42J-K) are longer than the ten vertebrae cranial to them. The first three thoracic vertebrae exhibit dorsoventrally shallow cranial and caudal centrum facets, while T4-T10 are deeper, with no discernable pattern of increase or decrease. T12 cannot be measured cranially and T13 cannot be measured caudally, but together they are the deepest caudally and deepest cranially (respectively) in the thoracic region. Centrum mediolateral widths are even less tractable. T1 is wider cranially than all vertebrae that follow until T13. Caudally it is the widest of the thoracic region. Of the vertebrae with preserved transverse processes, the most caudal ones are mediolaterally narrower than the more anterior ones (i.e., Fig. 4.42E vs. 4.42H-I). Of those with intact laminae and spinous processes, the more posterior postions have more vertically oriented processes. The prediaphragmatic spinous processes are all longer

dorsoventrally than craniocaudally. The thoracic vertebrae have zygapophyses with rounded margins, although T12 appears to have postzygapophyses that are slightly more angular, or square. The postzygapophyses of T13 are too broken for meaningful comment. The postdiaphragmatic spinous process of T12 is broken, but was probably vertically oriented, revealing it as the anticlinal vertebra. The T13 process is badly broken, but its caudal and dorsocaudal margins are intact, revealing that it was cranially oriented and most likely shorter dorsoventrally than craniocaudally long. The two postdiaphragmatic vertebrae preserve the roots of large accessory processes (anapophyses).

Comparison.—To have 13 thoracic vertebrae is slightly above average among small generalized, terrestrial to arboreal mammals (Table 4.24). It is the same number seen in tupaiid treeshrews (13), but one less than in *Ptilocercus* and *Cynocephalus* (14) (Sargis, 2001). It is generally thought that a longer thorax represents an emphasis on stabilization rather than mobility (Sargis, 2001). The presence of an anticlinal vertebra within the thoracic region, and large anapophyses, indicates that this region had pronounced mobility in dorsiflexion and extension, but was restricted in axial rotation or medial flexion. Animals that sometimes use a bounding, asymmetrical gait, and which therefore do not require dorsostability, are charactized by such features (e.g., *Sciurus*, treeshrews, many arboreal quadrupedal primates). Apes, humans, lorises, sloths, *Cynocephalus* and some opossums lack a thoracic anticlinal vertebra, and do not engage in quadrupedal bounding gaits (Boyer and Bloch, 2008). The thoracic region of *P. cookei* therefore indicates that it was *not* restricted to slow, cautious locomotion.

There are at least two basic differences between thoracic vertebrae of *P. cookei* and those of *N. gidleyi* and *N. intermedius*. As mentioned previously, the vertebral canals are proportionally larger in the smaller taxa. Additionally, the spinous processes of at least *N. intermedius* are craniocaudally narrower for their proximodistal lengths compared to those of *P. cookei*. The lack of a pronounced serial increase in vertebral centrum dimensions really only contrasts *P. cookei* from *Eulemur* and *Tupaia* among members of the available sample. Overall, *P. cookei* appears most similar to the scansorial phalangerid marsupial *Trichosurus vulpecula* in the number of thoracic vertebrae (13), the position of its anticlinal vertebra (Table 4.24), and in patterns of change in height and length of thoracic vertebral centra.

Lumbar vertebrae

Description.—Six lumbar (L) vertebrae are preserved (Fig. 4.43). It appears that at least one is missing based on lack of precise articulation and drastic size difference between what appear to be L1 and L3 of the preserved series (Table 4.27; Fig. 4.43A, B). The lumbar vertebral centra increase in all dimensions sequentially from cranial to caudal. The spinous processes appear to become longer dorsoventrally and narrower craniocaudally from cranial to caudal. The transverse processes are small, arise from the vertebral body, and are cranially positioned on L1 and L3. On the remaining lumbar vertebrae, the transverse processes are larger, arise from the base of the pedicle, and are positioned at the craniocaudal midpoint of each element. All transverse processes project cranioventrally to some degree. The accessory processes are largest on L1 and appear to decrease sequentially, although breakage makes it difficult to be certain of this trend.

The zygapophyses increase in size between L1 and L3, but appear of roughly equivalent size on L3 to L7. The prezygapophyses face dorsomedially and are concave. The postzygapophyses face the opposite direction, and are slightly convex. They are distinctly squared in outline.

Comparison.—Functional trends of the thoracic region are continued into the lumbus. Orientation of spinous processes, zygapophyses and large anapophyses suggest mobility in dorsiflexion and ventriflexion near the end of the thoracic region, as exhibited by *Tupaia*, for example (Jenkins, 1974). Prominent mammillary processes and prezygapophyses, and large, ventrally projecting transverse processes correlate with the use of a bounding gait (Boyer and Bloch, 2008), presumably because such morphology provides room for epaxial musculature, creating the capacity for powerful extension (and possibly also flexion) of the spine. Proportionally speaking, *P. cookei* has relatively small prezygapophyses and mammillary processes. Likewise, craniocaudally wide spinous processes typically characterize taxa with more rigid backs that do not engage in agile bounding and scampering (Sargis, 2001; Boyer and Bloch, 2008). Furthermore, taxa that rely on a bounding gait increase the length of the lumbus relative to the thorax (Sargis, 2001; Shapiro and Simons, 2002). The lumbar region of *P. cookei* is estimated to have been 81% the length of the thoracic region. This contrasts with agile scansorial treeshrews in which the lumbar region is 94% the length of the thoracic region (Table 4.24).

Compared to smaller plesiadapids, *P. cookei* is similar in its lumbar vertebral morphology. The major differences are proportionally larger vertebral foramina and narrower spinous processes in the smaller taxa. The lumbar spinous process proportions

of *N. intermedius* suggest that it utilized an agile bounding gait like tree squirrels and tupaiid treeshrews (Boyer and Bloch, 2008). Ptilocercid treeshrews are similar to *P. cookei* in having craniocaudally expanded lumbar spinous processes, while those of tupaiid treeshrews are narrower and more similar to those of *Nannodectes* (Sargis, 2001). *Cynocephalus* has broad spinous processes like *P. cookei*. *Cynocephalus* differs from all of the taxa mentioned in having caudally projecting lumbar spinous processes (Boyer and Bloch, 2008).

Sacrum

Description.—The sacrum is crushed, and missing one of its prezygapophyses and the tips of its spinous processes as a result (Tables 4.28, 29; Fig. 4.44). It is comprised of three vertebrae. The costal processes of the first two vertebrae are fully committed to forming the auricular facets for the innominates. The costal processes of the third vertebra are fused to those of the second. Individual costal processes are separated by spinal nerve foramina. Each vertebra exhibits separate spinous processes. Although the spinous processes are broken, enough remains to say that the first process was superiorly (cranially) oriented and was the largest of the three. The second spinous process was probably the smallest, although it also appears to be the most fragmentary. The third process is slightly smaller than the first and is oriented vertically. The laminae of the three vertebrae are separated by "interzygapophyseal intervertebral gaps" that communicate with the vertebral canal. The form of the prezygapophysis of the first sacral vertebra is similar to those of the caudal lumbar vertebrae. The postzygapophysis of the third sacral vertebra is similar to, although smaller than, those of the caudal lumbar

vertebrae. It is also similar to that of the most proximal of the preserved caudal vertebrae (see below).

Comparison.—The orientation and large size of the spinous process of the first sacral vertebra is similar to that of the caudal lumbar vertebrae. This suggests that the sacrum was integrated into the relatively rigid segment formed superiorly (cranially) by the caudal lumbar vertebrae. In highly agile taxa such as treeshrews, *Sciurus* and richochetal rodents (Gambaryan, 1974), the spinous process of the first sacral vertebra is often reduced. This morphology is associated with a relatively large range of flexibility at the lumbosacral joint, important for agile locomotor behaviors. The presence of a large first sacral spinous process thus indicates less flexibility and less agile locomotion. However, there is some evidence that the reduction of this process only correlates with agility in taxa that mainly use pronograde postures: a brief survey of taxa that frequently use orthograde postures reveals them to have a large, cranially oriented first sacral spinous process, even including those that also exhibit agile (e.g., *Callithrix*) or acrobatic (e.g., *Galago*) locomotor behaviors. Given independent evidence suggesting a somewhat agile locomotor repertoire in *P. cookei* (e.g., position of the anticlinal vertebra), the sacral spinous process size and orientation may be an indicator of substantial reliance on orthograde postures.

The sacra of *N. intermedius* and *N. gidleyi* are virtually identical to that of *P. cookei* in the morphological features mentioned above. The paromomyid plesiadapiform *Ignacius clarkforkensis* differs in having a reduced first spinous process (Boyer and Bloch, 2008). All treeshrews exhibit the reduced condition (Sargis, 2001). *Cynocephalus* exhibits the plesiadapid condition.

Caudal vertebrae

Description.—There are 17 caudal (Ca) vertebrae attributed to UM 87990 (Fig. 4.45; Table 4.30). The most proximal position preserved (Fig. 4.45A) has a complete vertebral canal, pre- and postzygapophyses, posteriorly projecting transverse processes, and the broken base of a spinous process. The centrum is missing but it would have been relatively craniocaudally short and mediolaterally wide. Typically there are three proximal caudal vertebrae with these basic proportions, as there are in the most completely known plesiadapiform tail of *Ignacius clarkforkensis* (Boyer and Bloch, 2008). The next most proximal caudal vertebra still retains a complete vertebral canal, but it is substantially more elongate than the first (but shorter and less elongate than the next in the series). This appears to be either Ca4 or Ca5 (Fig. 4.45B). The following vertebra appears to be Ca6 (Fig. 4.45C). It is much longer than the first two. It has an incomplete vertebral canal (the laminae do not meet in the sagittal plane). The pre- and post zygapophyses did not directly articulate with those of more proximal and distal vertebrae, respectively. There is a set of cranioventrally projecting transverse processes and a set of caudoventrally projecting processes. The vertebra identified as Ca7 is very similar to Ca6. It differs in being absolutely longer, proportionally narrower, and in having absolutely and proportionally smaller transverse processes. From Ca8-Ca12 (Fig. 4.45E-I) the vertebrae are identified on the basis of increasing length and/or decreasing prominence of zygapophyses and transverse processes. The centrum diameters of these vertebrae do not appear to vary drastically or systematically through this region. Ca11 and Ca12 (Fig. 4.45H, I) are extremely similar to one another and it is possible that their

identifications have been reversed. If not, Ca12 is the longest preserved caudal vertebra. Distal to Ca12 (Fig. 4.45J-Q) the vertebrae are identified on the basis of decreasing centrum length, width and height (Table 4.30).

Comparison.—The caudal vertebrae of *P. cookei* reveal it to have had a relatively long tail (Table 4.24, 30; Figs. 4.46, 47). A proportionally long tail is a feature of arboreal specialists. Stafford (1999) showed that *Ptilocercus lowii* has a significantly proportionally longer tail than more scansorial-to-terrestrial scandentians; he also documented that *Ratufa,* the arboreally committed tree squirrel, has a longer tail than more versatile sciurid rodents. Boyer and Bloch (2008) showed a sample of quadrupedal arboreal primates to have longer tails than some rodents and tupaiids. Looking at the first ten caudal vertebrae, the tail of *P. cookei* is proportionally longer (standardized against trunk length) than that of *Tupaia* and *Sciurus,* and similar to those of many euprimates (Table 4.24). It is also similar in proportional length to that of *Cynocephalus*; however, considering the whole tail (instead of just the first ten vertebrae) reveals *Cynocephalus* to actually have a short tail (Stafford, 1999; Boyer and Bloch, 2008). This is due to an abrupt and drastic serial decrease in vertebral length after Ca10 in *Cynocephalus* and a reduced number of caudal vertebrae (Table 4.24; Fig. 4.47). These features do not characterize the tail of *P. cookei,* which has a more typical gradual decrease in vertebral length through the tail (Fig. 4.47), and at least three more vertebrae than the tail of *Cynocephalus.*

N. intermedius preserves Ca6 and Ca7, which appear virtually identical to those of *P. cookei. N. gidleyi* preserves two of the first three caudals, which also appear similar to that preserved in *P. cookei*.

Manubrium and Sternebrae

Description.—The manubrium and six sternebrae are preserved (Fig. 4.48; Table 4.31). None of these elements are known for any other plesiadapiforms. The manubrium is longer than any of the sternebrae (Table 4.31). The right costal process is broken but the left one is intact. Its lateral edge received the first rib. On its craniodorsal aspect a slight depression for the clavicle articulation is observable. The cranial margin of the manubrium is convex. The dorsal surface is flat. The ventral surface is marked by a strong midline keel. The keel is narrowest at its root. Thus, a transverse cross-section through the manubrium reveals it to be in the shape of an "I-beam."

The articular surface for the first sternebra is oriented somewhat ventrally. Thus, when articulated, the manubrium and first sternebra form an obtuse ventral angle. The sternebrae are blocky bones and are all fairly similar to each other. The first is strongly keeled, while the keel becomes increasingly muted on more caudal positions. The last sternebra differs from the others in having a caudal end that is rounded instead of flat, and in having a longitudinal groove on its dorsal surface.

Comparison.—The manubrium of *P. cookei* appears more similar to that of *Tupaia glis* than to those of many euprimates in having a stronger keel and in forming a strong angle with the first sternebra.

Ribs

Description.—Twelve rib fragments are attributed to UM 87990 (Fig. 4.49; Table 4.32). Six appear to be left side elements. One or two of the floating ribs (T10-13) are

preserved. The ribs are slender and most exhibit a crest along their caudal borders. This crest is most expansive near the rib angles and becomes less pronounced farther ventrally. On the medial surface of these crests is a groove for the intercostal neurovasculature.

Comparison.—The ribs compare best to those of tupaiid treeshrews and other plesiadapiforms (Boyer and Bloch, 2008) among euarchontan mammals. Ptilocercid treeshrews, dermopterans, and many euprimates have ribs that are much more craniocaudally expanded (Sargis, 2001) than those of *P. cookei*. *N. gidleyi* preserves rib fragments showing it to be similar to *P. cookei* in this regard (Table 4.32).

Body proportions in *P. cookei* and other plesiadapids

A set of seven body segment lengths were analyzed with three separate principal coordinate analyses of the Euclidean distance matrices relating cases in the sample (measurements include: Trk-L, H-L, R-L, MC III-L, F-L, T-L, and MT III-L – see Tables 4.33-35; Fig. 4.50). As discussed in the Methods section, the variables used to create the distance matrices are log ratios of each measurement to the geometric mean of all measurements for a specimen in a given analysis. The first analysis does not include metapodial length data (MC III-L and MT III-L were removed from all calculations), and can therefore include measurements of the skeleton of *P. insignis*, on which MT III-L is unmeasurable (Gingerich, 1976) (Fig. 4.50A). It shows *P. insignis* to plot by itself, closest to terrestrial and scansorial rodents and *Tupaia glis*. *P. cookei* plots nearby, but is in the middle of a distribution including various arboreal taxa. Other plesiadapiforms, *Ignacius* and *Carpolestes* plot even farther from *P. insignis*. *Cynocephalus volans* plots far from all of these taxa.

A second analysis includes all seven measurements (Fig. 4.50B). *P. insignis* is not included because metapodial data are not available for it. The positions of the included plesiadapiforms are similar to what they are in the previous analysis: they plot close to each other, are surrounded by arboreal taxa, and are not particularly close to other euarchontans, *Tupaia* or *Cynocephalus*.

The third analysis includes all of the measurements of the second analysis except for trunk length (Trk-L was removed from all calculations) (Fig. 4.50C). This allows the inclusion of a larger, more diverse taxon sample. The positions of the plesiadapiform taxa are similar to what they are in the other two analyses. Interestingly the primitive, arboreal treeshrew, *Ptilocercus lowii*, plots close to the plesiadapiforms. Measurements representing a composite micromomyid plesiadapiform were included and show it to plot close to *Carpolestes* and *P. cookei*. Interestingly cercopithecid euprimates plot in the same part of the morphospace as some of these plesiadapiforms. Unlike other extant taxa in this region of the morphospace, the sampled cercopithecids (Table 4.35) are relatively terrestrially adapted among euprimates.

Comparing limb indices of *P. cookei* to those of other plesiadapids reveals that it has a short trunk (Table 4.34: Tr-I) compared to its limb lengths, a long radius and femur compared to its humerus length (Table 4.34: Br-I and Hf-I), a tibia that is short compared to the radius but long compared to the femur (Table 4.34: Rt-I and Cr-I), and a forelimb that is long compared to the hind limb (Table 4.34:Int-I). One exception here is that *P. insignis* has an even longer femur relative to its humeral length. Most of these metrics cannot be evaluated in *P. tricuspidens* because no tibial lengths are available (thus previous calculations of intermembral index are estimates: e.g., Gingerich, 1976).

Carpolestes simpsoni (UM 101963) and micromomyid plesiadapiforms have even longer radii relative to the humerus than does *P. cookei*. *C. simpsoni* has a shorter humerus relative to the femur, while micromomids have a longer humerus relative to the femur. *Ignacius* (UM 82616 and UM 108210) and micromomyids have longer tibiae relative to the femur, and *Ignacius* has longer limbs relative to its vertebral column. *Ignacius* has a relatively shorter radius compared to the humerus and tibia and it has a shorter forelimb compared to the hind limb. Micromomyids, on the other hand, have a longer radius relative to the tibia and a longer forelimb relative to the hind limb compared to *P. cookei*.

Body mass estimation in *P. cookei* and other plesiadapids

Gingerich and Gunnell (2005) recently estimated body mass for UM 87990 using data from Alexander et al. (1979) and methods of Gingerich (1990). The same methods are utilized here. Additionally a different dataset of extant primates from the UMMZ collection is used to estimate plesiadapid body masses. Average values of long bone dimensions needed for body mass estimation in each taxon are given in Table 4.36. Regression parameters are given in Table 4.37A, B. Body mass estimates are given in Tables 4.38A-C.

As demonstrated in other publications (e.g., Gingerich and Gunnell, 2005), there is a large amount of variance in body mass estimates for a single taxon. The relative magnitude of this variance is quantified with coefficients of variation for estimates based on long bone lengths, long bone diameters, and all dimensions in Table 4.38C. Comparison of estimates based on Gingerich's (1990) dataset and those based on the

unpublished primate dataset reveal some interesting differences. Length-based estimates are consistently larger than diameter-based estimates using Gingerich's data. The reverse is true using the primate-only sample. Compared to other plesiadapids, *P. cookei* is estimated to be about the same size as *P. tricuspidens*, but much larger than other plesiadapids. Cranial-based estimates of size differences between *P. cookei* and other plesiadapids (Chapter 2) can be compared to those from the postcranium by assuming an isometric relationship between skull size and body mass or by using a regression based on an extant sample. Both methods are used here. Silcox et al. (in press) present body mass regressions based on extant primates, which I use here with plesiadapid cranial length estimates from chapter 2 (see Table 4.38C).

Generally speaking, the skull-based comparisons suggest that the differences between *P. cookei* and other smaller plesiadapids were greater than the differences based on the postcranium-based comparisons (Table 4.38C). However, the skull and postcranial lengths of *P. cookei* and *P. tricuspidens* are consistent in suggesting that these taxa were the same size. On the other hand, postcranial diameters suggest a substantially larger body mass for *P. tricuspidens*.

Digit proportions in *P. cookei* and other plesiadapids

Kirk et al. (2008) commented on the functional implications of intrinsic hand proportions in plesiadapiforms. Specifically, they looked at the phalangeal index, the ratio of the sum of the lengths of the intermediate and proximal phalanges to the length of the metacarpal of the third digit ray. They found plesiadapids to be diverse in their hand proportions. *N. intermedius* and *N. gidleyi* have fingers that are ~130% the length of the

third metacarpal, similar to arboreal animals in their comparative sample. *P. cookei* was estimated to have fingers only 108% the length of its third metacarpal. This value is most similar to that of terrestrial sciurids. However, they used the "set 2" MC III in their calculations. Detailed morphological and quantitative comparisons to bones of *P. tricuspidens* and other plesiadapids (see above) indicate that the "set 1" third metacarpal is more likely to have actually belonged to *P. cookei*. Calculating phalangeal index for *P. cookei* with data presented above using the method of Kirk et al. (2008) reveals the fingers to be 130% the length of the "set 1" metacarpal. This is nearly identical to the values calculated by Kirk et al. (2008) for the two *Nannodectes* individuals.

Kirk et al. (2008) did not calculate the phalangeal index for *P. tricuspidens*, *P.* n. sp., or *P. insignis*. The phalangeal indices for these taxa, however, can be calculated. Finger bones are identified using the autopodal attributions of Beard (1989) for MNHN specimens of *P. tricuspidens* (reflected in Tables 4.13, 14), and by attributing the shorter phalanges of the *P.* n. sp. sample to the manus. The bones of *P. insignis* remain in articulation and no speculation about their original positions is required (Gingerich, 1976: p.141, Pl. 12). *P. tricuspidens* appears to have had fingers that are 111% the length of MC III, *P.* n. sp. had fingers that are 128% the length of MC III, and *P. insignis* had a third finger that is 140% the length of its MC III.

DISCUSSION AND CONCLUSIONS

Morphology of *P. cookei*

The skeleton of *P. cookei* UM 87990 is significant in that it provides a more complete view of several regions of the anatomy than previously available for any plesiadapid. Bones preserved in UM 87990 that were previously unknown for any species of *Plesiadapis* include the pollical metacarpal, scaphoid, lunate, pisiform, trapezoid, trapezium, ectocuneiform, hallucal metatarsal and much of the vertebral column. Bones previously only known from fragmentary elements for *Plesiadapis* include the innominate and tibia. The new morphology has allowed some significant progress in understanding the articular relationships of wrist bones, metacarpals, and metatarsals. It must be acknowledged, however, that due to problems with associations and the persistent lack of an actual complete wrist of a single individual there is still a large amount of uncertainty regarding the reconstructions of the wrist and hand presented in the descriptions.

Phylogenetic significance.—Several new observations with possible phylogenetic significance came to light. These will be discussed in detail with regard to specific character matrices in Chapter 5.

A reconstruction of the wrist showing that the lunate intervened between the scaphoid and triquetrum refutes the reconstruction by Beard (1989, 1993a) who suggested that the scaphoid and triquetrum articulated with one another. However, Stafford and Thorington (1998) have already showed that, if plesiadapiforms were in fact characterized by the configuration proposed by Beard (1989, 1993a), this would be an

autapomorphy, because it appears that the lunate ossification center in *Cynocephalus* intervenes between the triquetrum and scaphoid before fusing to the scaphoid. From a phenetic perspective, the fact that plesiadapids have humeri that are morphologically more similar to those of primates than to those of other euarchontans could reflect a special relationship of plesiadapids (and other plesiadapiforms) to euprimates. However, this signal is not paralleled by similar analyses of the morphology of the astragalus, calcaneum, vertebrae, or body segments.

Functional significance.—The opportunity to consider the functional significance of mobility at several joints of the limbs at a time is a major benefit provided by such a complete skeleton of a single individual. Analyses presented in the Results section reveal that *P. cookei* probably utilized postures in which the arm was typically extended or flexed in the sagittal plane to some degree, but not substantially abducted or laterally rotated (i.e., the distal end of the humerus pointed caudally or ventrally, but not substantially laterally). As discerned in previous studies of *P. tricuspidens* (Szalay et al., 1975), it seems that the elbow was typically flexed from a fully extended posture by around 90º or more. The forearm would have been abducted by ~30º, relative to the anteroposterior axis of the humerus. The manus was typically partly supinated and slightly dorsiflexed, although it had the capacity for a large range of dorsiflexion. The mechanical capacity for such a large range of dorsiflexion of the hand (and digits) is most likely important for pronograde quadrupedalism, and possibly descents of large diameter vertical substrates (Jenkins, 1974).

A typical hind limb posture would have been characterized by a femur that was abducted, flexed, and laterally rotated relative to the innominate. The knee would have

been flexed, and the leg slightly abducted. The foot would have been dorsiflexed and slightly inverted with the capacity for a large range of inversion.

Abducted limbs result in a posture with sprawled hands and feet. Such a posture would have made *P. cookei* adept at navigating relatively large diameter substrates. A physiologically supinated hand and inverted foot would have accommodated cylindrical substrates well (i.e., tree trunks and branches). Jenkins (1974) presents data on *Tupaia glis* showing it to adopt such supinated hand and inverted foot postures during quadrupedal locomotion on relatively narrow branches.

The nature of mobility, in the hind limb especially, would have been useful in ascending vertical substrates, because the hind limb has much of its mobility concentrated in an anterposteriorly extending plane with a mediolateral, rather than dorsoventral orientation. Thus, extension of the hind limb would not tend to push the body farther away from the substrate. The femur of *Plesiadapis* extends and flexes in the transverse plane. Because the knee would have been laterally rotated during much of the support phase of locomotion, flexion and extension of the knee also occurred mainly in a transverse plane. Finally, as explained in the Results section, although flexion and extension of the astragalotibial joint is limited, abduction-adduction movements and inversion-eversion movements are emphasized. It is important to keep the body close to the substrate during vertical climbing because the moment created by gravity on body mass with respect to a vertical substrate increases when the center of mass moves away from the substrate.

To be clear, what suggests orthograde postures and locomotion in *Plesiadapis* is the *unusual degree* to which its limbs appear to have been sprawled. For instance,

Jenkins (1974) found that *Tupaia glis* utilizes sprawled limb postures and relies on abduction-adduction (instead of flexion and extension) movements in its hind limbs to a significant degree: *Tupaia glis* is a pronograde scansorialist, not an orthograde arborealist. However, the hind limb of *Tupaia* does not resemble that of *P. cookei* very much in features that would seem to have promoted transverse plane mobility in *P. cookei*. Furthermore, the hind limb postures that Jenkins (1974) illustrates for *Tupaia* still show the femur to be more sagittally oriented and mobile than suggested in the reconstructions presented above for *P. cookei*. The hind limb of the treeshrew *Ptilocercus* does resemble that of *P. cookei* in many respects (Sargis, 2002b). *Ptilocercus* is arboreally committed, engaging in vertical clinging and climbing behaviors (Le Gros Clark, 1926). So it seems reasonable to conclude that *Ptilocercus* limits its movements to a transverse plane even more than does *Tupaia* (although no data are available), that this helps *Ptilocercus* locomote in arboreal settings, and that *P. cookei* moved more like *Ptilocercus* than *Tupaia*.

The reduced ability for plantarflexion in plesiadapids relative to treeshrews and many primates (see above) begs the question of how vertical descent postures could have been accomplished in plesiadapiforms. In fact, Beard (1989) suggested plesiadapiforms were not effective at descending vertical supports, and suggested gliding behaviors might have represented an alternative means of descending from tree canopies. However, assembling the hind limb of *P. cookei* with an abducted, extended femur, a knee flexed at 90º, an astragalotibial joint plantarflexed by 90º, and a fully inverted astragalocalcalcaneal joint (Fig. 4.51) shows an approximation of a limb posture that could be used for vertical descents. It should be noted that further inversion of the foot

could be accomplished by rotating the transverse tarsal joints and metatarsals, but just exactly how and how much these bones should be moved with respect to each other is difficult to constrain. It is interesting to compare the posture of *P. cookei* depicted in Figure 4.51 to the cineradiography-based drawing of hind foot reversal in *Tupaia* in Jenkins (1974: p.102, fig. 6) because it shows the postures to be similar except for the increased degree of abduction in the hind limb of *P. cookei.*

The major features differentiating *P. cookei* from other plesiadapids are its more gracile limb bones, in some cases proportionally longer limb bones, and its proportionally narrower intermediate phalanges (Boyer and Bloch, 2008). Additionally, *P. cookei* has features of the ankle that appear to give it more mobility than the ankle of other plesiadapids. The metacarpals of *P. cookei* and *P. tricuspidens* appear to be more robust than those of *Nannodectes*, although not proportionally shorter compared to the phalanges (see below). Finally, the vertebrae of *P. cookei* differ from those of *Nannodectes* in having features that suggest the vertebral column was more rigid and "stabile." Overall, these unique features of *P. cookei* may correspond to a lifestyle that was more committed to arboreal settings and possibly orthograde postures.

However, it has also been previously stated that *P. cookei* was not only an arborealist but had morphology suggesting "suspensory tendencies" (Bloch and Boyer, 2007; Boyer and Bloch, 2008). These authors specifically mentioned features of the scapula, humerus, intermediate phalanges and claws. The differences between the scapulae of *P. cookei* and *N. intermedius* actually are consistent with a *less* mobile shoulder in *P. cookei* and do not clearly support the case of a suspensory habitus in *P. cookei*. While there are some differences between the humerus of *P. cookei* and those of

Nannodectes and other plesiadapids, these were not quantified here and are not strongly suggestive of suspensory postures anyhow. In fact, some of the humeral morphology that *was* quantified shows all plesiadapids to be similar in morphology of the distal humerus. A smaller amount of lateral torsion in the humeral shaft of small-bodied plesiadapids as compared to large-bodied ones is the opposite from what is predicted for a suspensory habit in large plesiadapids: suspensory primates and xenarthrans are characterized by medial torsion, if any. On the other hand, the intermediate phalanges of *P. cookei* are distinctly different from those of *P. tricuspidens* and *Nannodectes* in ways that could suggest a suspensory habit. These intermediate phalanx features of *P. cookei* are also found in *Cynocephalus*, bats, and sloths (Boyer and Bloch, 2008). However, *Daubentonia* also exhibits intermediate phalanges with extraordinarily mediolaterally narrow proximal ends, like *P.cookei* and suspensory taxa (Boyer and Bloch, 2008). Although the Aye aye is adept in quadrumanus suspensory locomotion (pers. observ.), it is not a "suspensory animal" in the manner of a sloth or dermopteran. Finally, the claws of *P. cookei*, while being slightly narrower than those of smaller-bodied plesiadapids and being more hook-like in having a longer shaft, are overall very similar to the claws of other plesiadapids. The features that do differentiate the claws of *P. cookei* from those of smaller plesiadapids could easily be related to allometric trends in phalanges with the "same" functional capacity, although this remains to be demonstrated.

Postcranial proportions

The position of plesiadapids and other plesiadapiforms in the principal coordinates plots based on body segment length data is consistent with the suggestion

that plesiadapiforms are “callitrichid-like” or “squirrel-like” arborealists (Bloch and Boyer, 2007; Boyer and Bloch, 2008). This is true with the exception of *P. insignis*, which appears to have been most similar to terrestrial or scansorial taxa, as suggested by Gingerich (1976). It must, however, be acknowledged that the variance in body segment proportions of the comparative sample does not necessarily correspond to “behavioral groups.” This is revealed by the position of more terrestrially adapted cercopithecoid euprimates, which plot in the midst of more arboreal taxa in Figure 4.50C. Even so, suspensory taxa (including *Cynocephalus volans*, sloths and apes) plot close to each other in a region not overlapping the position of *P. cookei*. This could be considered more evidence against the suggestion of Bloch and Boyer (2007) and Boyer and Bloch (2008) that *P. cookei* had “suspensory tendencies.” In this regard, limb proportions are consistent with evidence from vertebral proportions and analysis of joint mobility. That is, the vertebral column exhibits a short neck and a long tail – features not typical of suspensory taxa (Stafford, 1999). Consideration of joint mobility suggests sprawled limbs and dorsiflexed hands and feet (see above), quite the opposite of the medially approximated limbs and ventriflexed hands and feet expected for suspensory animals.

More phylogenetically focused comparisons of body segment lengths could be interpreted as supporting the hypothesis of suspensory tendencies for *P. cookei*. Suspensory taxa are characterized by higher brachial and intermembral indices than quadrupedal arboreal taxa, for instance (Boyer and Bloch, 2008). *P. cookei* has a greater brachial index and intermembral index than other plesiadapids. Furthermore, the longer, more gracile humerus and femur of *P. cookei*, as compared to those of *P. tricuspidens*,

are consistent with more frequent use of antipronograde postures in *P. cookei* (Jungers, 1985).

Digit proportions

Newly determined digit proportions of *P. cookei* are actually consistent with much of the rest of the morphology in suggesting arboreal habits, contrary to Kirk et al.'s (2008) conclusion. The relatively short fingers of *P. tricuspidens* are, however, surprising. This result may be an artifact of misassignment of some of the finger bones to the foot in the MNHN sample. That is, the intermediate phalanges assigned to the hand by Beard (1989) may represent only the shortest digits of the hand, while some of the longer manual phalanges, and specifically those of the third digit, may be misidentified as pedal elements. Some of the incomplete phalanges assigned to *P. cookei*'s hand (Fig. 4.21C, D) would have been close to the length of the only phalanges assigned to the hand of *P. tricuspidens* [for instance, Boyer and Bloch (2008) provide an estimated length for the intermediate phalanx of UM 87990 depicted in Fig. 4.21A of 10.3 mm], but these are not relevant to calculations of phalangeal index because the phalanges of the third digit are usually close to the longest (or *the* longest) of the hand, not the shortest. The best evidence for this interpretation is that from the articulated specimen of *P. insignis*. The lengths of bones of its third digit ray give a phalangeal index of 140 (third metacarpal = 11.7 mm; third proximal manual phalanx = 8.6 mm; fourth intermediate manual phalanx = 7.8 mm). However, if phalanges from the fifth digit ray (fifth proximal manual phalanx = 7.5 mm; fifth intermediate manual phalanx = 5.6 mm) are used with the third metacarpal to calculate the phalangeal index, a value of 112 results, nearly identical to the

value for *P. tricuspidens.* In summary, it seems likely that *P. tricuspidens* (like *P. cookei, P. insignis,* and *Nannodectes*) will be revealed to have phalangeal indices of around 130-140 when more confidently identified digit rays are available. This is less than that of most arboreal euprimates, but much higher than that of many terrestrial mammals (Kirk et al., 2008). If, on the other hand, it turns out that *P. tricuspidens* truly does have such short fingers, then this information appears to contradict much other information from the skeleton suggesting arboreal habits (Youlatos and Godinot, 2004). It should, however, be noted that it *would be* consistent with the absolutely thicker and proportionally shorter limbs of *P. tricuspidens* as compared to those of *P. cookei* and extant arboreal mammals (Runestad and Ruff, 1995).

Body mass estimates

Differences in results of the two sets of postcranial regressions used to generate body mass estimates are interesting because they suggest that *P. cookei* has exceptionally relatively long limbs among mammals (based on the Gingerich [1990] equations), but relatively short limbs compared with extant primates (based on the unpublished extant primate sample). The absolute body mass estimates generated by both sets of postcranial regressions are of some interest because they sample the skeleton so broadly and show such congruence that they may actually be fairly accurate. That is, *P. cookei* probably weighed somewhere between 1-3 kg, but not as much as the 5 kg suggested by a regression from Silcox et al. (in press) based on skull length of extant primates.

Proportional differences in body mass between *P. cookei* and other plesiadapids as suggested by the postcranium are much smaller than estimates of proportional

differences generated from information on skull length. The postcranium suggests that *P. cookei* is at most five times the mass of the smallest plesiadapid *N. intermedius*, while the skulls suggest that it was 10 or 16 times the mass. The contradiction between skull and postcranial estimates most likely indicates that there is *not* an isometric relationship between skull length and body mass among plesiadapids. Further, the negatively allometric relationship of the Silcox et al. (in press) regression is an even less accurate representation of the relationship between plesiadapid head length and body mass. Instead, it seems that there is a positive allometric relationship between body mass and head length among plesiadapids. That is, head length increases at a faster rate with increasing body mass than predicted by isometry.

The fact that *P. cookei* and *P. tricuspidens* are estimated to have had a similar body mass based on limb lengths and diameters is taken as further evidence that the absolute difference in tooth size between these two taxa is due to different ecological niches (see Chapter 3). A head that is relatively large compared to the body may promote interspecific variance in tooth size that is not correlated to differences in body size.

SUMMARY

While the skeleton of *P. cookei* provides new insight into plesiadapiform morphology and behavior, many of the observations presented here still have no statistical basis and some of the comparative methods used to identify ambiguously associated elements are speculative. Therefore, it is likely that some of the information presented here is wrong, and that some of the conclusions based on it are misguided.

Thus, it is imperative that more skeletal materal for *Plesiadapis* be recovered and described. Likewise, more information on other plesiadapiforms and larger, more diverse comparative samples should be assembled and analyzed. Uncertainty acknowledged, it can be said that appendicular postcranial morphology of *P. cookei* is pervasively suggestive of a committed arboreal lifestyle, although "sloth-like" suspensory postures were probably used infrequently, if ever. A natural and possibly frequently used posture is illustrated in Figure 6.1. The axial skeleton does not contradict an arboreal habitus, although it was unlike that of many suspensory animals.

ACKNOWLEDGMENTS

I am grateful to P. Gingerich, G. Gunnell, and J. Bloch for the opportunity to lead the study and description of UM 87990. P. Gingerich and W. Sanders facilitated and oversaw the production and provision of high quality casts of this specimen. S. Judex and C. Rubin provided HRxCT scans at the Center for Biotechnology of the Department of Biomedical Engineering at Stony Brook University. J. Groenke, J. Georgi and staff of the CT lab at Stony Brook University provided medical grade CT scans of the skeleton of UM 87990. J. Sertich of Stony Brook University provided access to a camera. S. Maiolino of Stony Brook University provided measurements on distal phalanges. M. Godinot, P. Tassy and C. Sagne of MNHN, and M. Pellouin provided access to important comparative specimens of *Plesiadapis tricuspidens* and *Plesiadapis* n. sp. S. Chester, C. Gilbert and E. Sargis of Yale University helped with access to comparative specimens. This research was enhanced by discussions with J. Bloch, P. Gingerich, M. Godinot, J.

Perry, M. Silcox, R. Secord and many other researchers. It was made possible by funding from a National Science Foundation grant to P. Gingerich and G. Gunnell (BCS-0129601), a National Science Foundation grant to D. Krause and J. Bloch (EAR-0308902), and a National Science Foundation Graduate Research Fellowship, an Evolving Earth Foundation grant, a National Science Foundation Doctoral Dissertation Improvement Grant (BCS-0622544), and an American Society of Mammalogists grant to D. Boyer.

REFERENCES

Alexander, R.M., Jayes, A.S., Maloiy, G.M.O., Wathuta, E.M., 1979. Allometry of limb bones of mammals from shrews (*Sorex*) to elephant (*Loxodonta*). Journal of Zoology, London 189, 305-314.

Argot, C., 2002. Functional-adaptive analysis of the hindlimb anatomy of extant marsupials and the paleobiology of the Paleocene marsupials *Mayulestes ferox* and *Pucadelphys andinus*. Journal of Morphology 253, 76-108.

Beard, K.C., 1989. Postcranial anatomy, locomotor adaptations, and palaeoecology of Early Cenozoic Plesiadapidae, Paromomyidae, and Micromomyidae (Eutheria, Dermoptera). Ph.D. Dissertation, Johns Hopkins University.

Beard, K.C., 1990. Gliding behavior and paleoecology of the alleged primate family Paromomyidae (Mammalia, Dermoptera). Nature 345, 340-341.

Beard, K.C., 1993a. Phylogenetic systematics of the Primatomorpha, with special reference to Dermoptera. In: Szalay, F.S., McKenna, M.C., Novacek, M.J. (eds) Mammal Phylogeny: Placentals. Springer-Verlag, New York, pp. 129-150.

Beard, K.C., 1993b. Origin and evolution of gliding in Early Cenozoic Dermoptera (Mammalia, Primatopmorpha). In: MacPhee, R.D.E. (ed) Primates and Their Relatives in Phylogenetic Perspective. Plenum Press, New York, pp. 63-90.

Bloch, J.I., Boyer, D.M., 2001. Taphonomy of small mammals in freshwater limestones from the Paleocene of the Clarks Fork Basin. In: Gingerich, P.D. (ed) Paleocene-Eocene stratigraphy and biotic change in the Bighorn and Clarks Fork basins, Wyoming, University of Michigan Papers on Paleontology, pp. 185-198.

Bloch, J.I., Boyer, D.M., 2002. Grasping primate origins. Science 298, 1606-1610.

Bloch, J.I., Boyer, D.M., 2007. New skeletons of Paleocene-Eocene Plesiadapiformes: a diversity of arboreal positional behaviors in early primates. In: Dagosto, M., Ravosa, M.J. (eds) Primate Origins: Adaptations and Evolution. Plenum Press, New York, pp. 535-582.

Bloch, J.I., Silcox, M.T., Boyer, D.M., Sargis, E.J., 2007. New Paleocene skeletons and the relationship of plesiadapiforms to crown-clade primates. Proceedings of the National Academy of Sciences 104, 1159-1164.

Boyer, D.M., Patel, B.A., Larson, S.G., Stern, J.T.J., 2007. Telemetered electromyography of peroneus longus in *Varecia variegata* and *Eulemur*

rubriventer: implications for the functional significance of a large peroneal process. Journal of Human Evolution 53, 119-134.

Boyer, D.M., Bloch, J.I., 2008. Evaluating the mitten-gliding hypothesis for Paromomyidae and Micromomyidae (Mammalia, "Plesiadapiformes") using comparative functional morphology of new Paleogene skeletons. In: Sargis, E.J., Dagosto, M. (eds) Mammalian Evolutionary Morphology: A Tribute to Frederick S. Szalay. Kluwer, New York, pp. 233-284.

Evans, H.E., 1993. Miller's Anatomy of the Dog. W. B. Saunders, Philadelphia.

Fleagle, J.G., Anapol, F.C., 1992. The indriid ischium and the hominid hip. Journal of Human Evolution 22, 285-305.

Gambaryan, P.P., 1974. How Mammals Run. Wiley, New York.

George, R.M., 1977. The limb musculature of the Tupaiidae. Primates 18, 1-34.

Gervais, M.P., 1877. Enumération de quelques ossements d'animaux vertébrés, recueillis aux environs de Reims par M. Lemoine. Journal de Zoologie 6, 74-79.

Gingerich, P.D., 1976. Cranial anatomy and evolution of Early Tertiary Plesiadapidae (Mammalia, Primates). University of Michigan Papers on Paleontology 15, 1-141.

Gingerich, P.D., 1990. Prediction of body mass in mammalian species from long bone lengths and diameters. Contributions from the Museum of Paleontology 28, 79-92.

Gingerich, P.D., 2000. Arithmetic or geometric normality of biological variation: an empirical test of theory. Journal of Theoretical Biology 204, 201-221.

Gingerich, P.D., Gunnell, G.F., 1992. A new skeleton of *Plesiadapis cookei*. The Display Case University of Michigan 6, 1, 3.

Gingerich, P.D., Gunnell, G.F., 2005. Brain of *Plesiadapis cookei* (Mammalia, Proprimates): surface morphology and encephalization compared to those of Primates and Dermoptera. University of Michigan Museum of Paleontology Contributions 31, 185-195.

Godinot, M., Beard, K.C., 1991. Fossil primate hands: a review and an evolutionary inquiry emphasizing early forms. Human Evolution 6, 307-354.

Gradstein, F.M., Ogg, J.G., Smith, A.G., 2004. A Geologic Time Scale 2004. Cambridge University Press, Cambridge.

Gregory, W.K., 1920. On the structure and relations of *Notharctus*, an American Eocene primate. Memoires of the American Museum of Natural History 3, 45-243.

Gunnell, G.F., Gingerich, P.D., 1987. Skull and partial skeleton of *Plesiadapis cookei* from the Clarks Fork Basin, Wyoming. American Journal of Physical Anthropology 72, 206a.

Gunnell, G.F., 1989. Evolutionary history of Microsyopoidea (Mammalia, ?Primates) and the relationship between Plesiadapiformes and Primates. University of Michigan, Papers on Paleontology 27, 1-157.

Haines, R.W., 1955. The anatomy of the hand of certain insectivores. Proceedings of the Zoological Society of London 125, 761-776.

Hamrick, M.W., Rosenman, B.A., Brush, J.A., 1999. Phalangeal morphology of the Paromomyidae (?Primates, Plesiadapiformes): The evidence for gliding behavior reconsidered. American Journal of Physical Anthropology 109, 397-413.

Hamrick, M.W., 2001. Primate origins: evolutionary change in digit ray patterning and segmentation. Journal of Human Evolution 40, 339-351.

Jenkins, F.A., 1974. Tree shrew locomotion and the origins of primate arborealism. In: Jenkins, F.A. (ed) Primate Locomotion. Academic Press, New York, pp. 85-115.

Jepsen, G.L., 1930. Stratigraphy and paleontology of the Paleocene of northeastern Park County, Wyoming. Proceedings of the American Philosophical Society 69, 463-528.

Jungers, W.L., 1985. Body size and scaling of limb proportions in primates. In: Jungers, W.L. (ed) Size and Scaling in Primate Biology. Plenum Publishing Corporation, New York, pp. 345-381.

Jungers, W.L., Falsetti, A.B., Wall, C.E., 1995. Shape, relative size, and size-adjustments in morphometrics. Yearbook of Physical Anthropology 38, 137-161.

Kirk, E.C., Lemelin, P., Hamrick, M.W., Boyer, D.M., Bloch, J.I., 2008. Intrinsic hand proportions of euarchontans and other mammals: implications for the locomotor behavior of plesiadapiforms. Journal of Human Evolution 55, 278-299.

Le Gros Clark, W.E., 1926. On the anatomy of the pen-tailed tree-shrew. Proceedings of the Zoological Society of London 1926, 1179-1309.

Lemoine, V., 1893. Etude sur les os du pied des mammifères de la faume cernaysienne et sur quelques pieces osseuses nouvelles de cet horizon paléontologique. Bulletin de la Societe Géologique de France (3eme ser) 21, 353-368.

Linnaeus, C., 1758. Systema naturae per regna tria natureae secundum classes, ordines genera, species cum characteribus, differentris, synonymis, locis, Editis decima, reformata edn. Laurentii Salvii, Stockholm.

Lofgren, D.L., Lillegraven, J.A., Clemens, W.A., Gingerich, P.D., Williamson, T.E., 2004. Paleocene biochronology: the Puercan through Clarkforkian land mammal ages. In: Woodburne, M.O. (ed) Cenozoic Mammals of North America: Geochronology and Biostratigraphy, 2nd edn. University of California Press, Berkeley, pp. 43-105.

Maiolino, S.A., Boyer, D.M., 2007. Evidence from claw morphology for a diversity of positional behaviors in plesiadapid “plesiadapiforms.” Journal of Vertebrate Paleontology 27, 111A.

Mosimann, J.E., Malley, J.D., 1979. Size and shape variables. In: Orloci, L., Rao, C.R., Stiteler, W.M. (eds) Multivariate Methods in Ecological Work. International Cooperative, Fairland, pp. 175-189.

Napier, J.R., 1961. Prehensility and opposability in the hands of primates. Symposia of the Zoological Society of London 5, 115-132.

Napier, J.R., Walker, A.C., 1967. Vertical clinging and leaping - a newly recognized category of locomotor behavior of primates. Folia Primatologica 6, 204-219.

Nomina Anatomica, 1983. 5th edition. Williams & Wilkins, Baltimore.

Nomina Anatomica Veterinaria, 4th edition.1994. Adolf Holhauzen's Successors, Vienna

Piton, L.-E., 1940. Paléontologie du gisement éocène de Menat (Puy-de-Dôme) (Flore et Faune). Vallier, Clermont-Ferrand, 301p.

Roach, H.I., Mehta, G., Oreffo, R.O.C., Clarke, M.P., Cooper, C., 2003. Temporal analysis of rat growth plates: cessation of growth with age despite presence of a physis. Journal of Histochemistry and Cytochemistry 51, 373-383.

Runestad, J.A., Ruff, C.B., 1995. Structural adaptations for gliding in mammals with implications for locomotor behavior in paromomyids. American Journal of Physical Anthropology 98, 101-119.

Russell, D.E., 1962. Essai de reconstitution de la vie Paléocène au Mont de Berru. Bulletin du Muséum National d'Histoire Naturelle 34, 101-106.

Russell, D.E., 1964. Les Mammiferes Paléocènes D'Europe. Mémoires du Muséum National D'Histoire Naturelle, Série C 13, 1-324.

Russell, D.E., 1967. Sur *Menatotherium* et l'age Paléocène du gisement de Menat (Puy-de-Dôme). Problèms Actuels de Paléontologie, College International de Centre National de Recherche Scientifique, Paris 163, 483-490.

Sargis, E.J., 2001. A preliminary qualitative analysis of the axial skeleton of tupaiids (Mammalia, Scandentia): functional morphology and phylogenetic implications. Journal of Zoology 253, 473-483.

Sargis, E.J., 2002a. Functional morphology of the forelimb of tupaiids (Mammalia, Scandentia) and its phylogenetic implications. Journal of Morphology 253, 10-42.

Sargis, E.J., 2002b. Functional morphology of the hindlimb of tupaiids (Mammalia, Scandentia) and its phylogenetic implications. Journal of Morphology 254, 149-185.

Sargis, E.J., 2004. The postcranial morphology of *Ptilocercus lowii* (Scandentia, Tupaiidae): An analysis of primatomorphan and volitantian characters. Journal of Mammalian Evolution 9, 137-160.

Sargis, E.J., Boyer, D.M., Bloch, J.I., Silcox, M.T., 2007. Evolution of pedal grasping in Primates. Journal of Human Evolution 53, 103-107.

Shapiro, L.J., Simons, C.V.M., 2002. Functional aspects of strepsirrhine lumbar vertebral bodies and spinous processes. Journal of Human Evolution 42, 753-783.

Silcox, M.T., Bloch, J.I., Boyer, D.M., Godinot, M., Ryan, T.M., Spoor, F., Walker, A., in press. The semicircular canal system in early primates. Journal of Human Evolution.

Simons, E.L., 1964. The early relatives of man. Scientific American 211, 51-62.

Simons, E.L., 1967. Fossil primates and the evolution of some primate locomotor systems. American Journal of Physical Anthropology 26, 241-254.

Simpson, G.G., 1935. The Tiffany fauna, Upper Paleocene. II.-Structure and relationships of *Plesiadapis*. American Museum Novitates 816, 1-30.

Sokal, R.R., Rohlf, J.F., 1997. Biometry, The Principles and Practice of Statistics in Biological Research. W. H. Freeman and Company, New York.

Stafford, B.J., Thorington, R.W.J., 1998. Carpal development and morphology in archontan mammals. Journal of Morphology 235, 135-155.

Stafford, B.J., 1999. Taxonomy and Ecological Morphology of the Flying Lemurs (Dermoptera, Cynocephalidae). Doctor of Philosophy, City University of New York.

Stern, J.T.,Jr., 1988. Essentials of Gross Anatomy. F. A. Davis, Philadelphia.

Straus, W.L., Jr., 1930. The foot musculature of the highland gorilla (*Gorilla beringei*). Quarterly Review of Biology 5, 261-317.

Szalay, F.S., 1972. Paleobiology of the earliest primates. In: Tuttle, R.H. (ed) Functional and Evolutionary Biology of Primates. Aldine, Chicago, pp. 3-35.

Szalay, F.S., Decker, R.L., 1974. Origins, evolution and functon of the tarsus in Late Cretaceous Eutheria and Paleocene primates. In: Jenkins, F.A. (ed) Primate Locomotion. Academic Press, New York, pp. 223-259.

Szalay, F.S., Tattersall, I., Decker, R.L., 1975. Phylogenetic relationships of *Plesiadapis* - postcranial evidence. Contributions to Primatology 5, 136-166.

Szalay, F.S., Dagosto, M., 1980. Locomotor adaptations as reflected on the humerus of Paleogene primates. Folia Primatologica 34, 1-45.

Szalay, F.S., Drawhorn, G., 1980. Evolution and diversification of the Archonta in an arboreal milieu. In: Luckett, W.P. (ed) Comparative Biology and Evolutionary Relationships of Tree Shrews. Plenum Press, New York, pp. 133-169.

Szalay, F.S., 1984. Arboreality: is it homologous in metatherian and eutherian mammals? In: Hecht, M.K., Wallace, B., Prance, G.T. (eds) Evolutionary Biology, Vol 18. Plenum, New York, pp. 215-258.

Szalay, F.S., Dagosto, M., 1988. Evolution of hallucial grasping in the Primates. Journal of Human Evolution 17, 1-33.

Teilhard de Chardin, P., 1922. Les mammifères de l'éocène inférieur francais et leurs gisements. Annales de Paléontologie 11, 9-116.

Trouessart, E.L., 1897. Catalogues des Mammalium tam Viventium quam Fossilium. R. Friedlander und Sohn, Berlin.

Van Valen, L., 1971. Adaptive zones and the orders of mammals. Evolution 25, 420-428.

Youlatos, D., Godinot, M., 2004. Locomotor adaptations of *Plesiadapis tricuspidens* and *Plesiadapis* n. sp. (Mammalia, Plesiadapiformes) as reflected in selected parts of the postcranium. Journal of Anthropological Sciences 82, 103-118.

TABLES

Table 4.1. Measurements of plesiadapid clavicles.

Taxon	Specimen	Le	PEW[a]	PED	MSW	MSD	DEW	DED
P. cookei	UM 87990	32.50	3.60	4.30	2.90	4.90	3.50	6.80
N. gidleyi	AMNH 17388	17.09	--	1.62	--	2.44	--	3.45

a - W = anteroposterior; D = superoinferior

Table 4.2. Measurements of plesiadapid scapulae.

Taxon	Specimen	SL(1)[a]	GW(4)	GD(3)	SND	CL	AD	AP	AL
P. cookei	UM 87990	49.00	7.70	10.70	11.70	3.90	11.10	5.80	4.50
N. inermedius	USNM 442229	--	3.42	5.10	5.03	2.17	4.73	0.00	3.31
N. gidleyi	AMNH 12379	--	4.13	--	6.05	--	--	--	--
cf. *P. churchilli*	SMM P77.33.517	--	4.61	7.69	--	--	--	--	--

a – numbers in parentheses correspond to measurement numbers in Sargis (2002a)

Table 4.3A. Measurements of the proximal ends and shafts of plesiadapiform humeri.

Taxon	Specimen	LD	Le(5)[a]	PEW	PED(7)	PAW(6)	MSW(8)	MSD	DCL(17)	SSV
P. cookei	UM87990 (L)	32	75.24	13.90	10.80	10.50	7.85	6.73	29.70	2.34
P. cookei	UM87990 (R)	--	--	13.60	10.80	10.40	6.60	6.98	--	--
P. tricuspidens	MNHN BR 14522	--	--	--	--	--	7.10	7.69	--	--
P. tricuspidens	MNHN BR-03-L	34	70.40	13.43	11.45	9.91	8.96	8.02	30.25	2.12
P. tricuspidens	MNHN BR 12591	27	--	--	--	--	7.73	7.88	--	--
P. tricuspidens	MNHN BR 12590	29	--	--	--	--	8.09	7.05	--	--
P. tricuspidens	MNHN BR 12585	--	--	--	--	--	8.60	7.36	--	--
P. tricuspidens	MNHN R 405	55*	--	--	--	--	7.61	7.60	--	--
P. tricuspidens	Berru (Mr Malfait)	34	--	--	--	--	--	8.99	--	--
P. tricuspidens	MNHN BR-04-L(a)	27	--	--	--	--	7.77	7.61	--	--
P. tricuspidens	MNHN BR-04-L(b)	37	71.93	12.04	10.50	9.61	8.58	7.66	26.78	2.18
P. tricuspidens	MNHN R 492	31	--	--	--	--	7.90	8.33		--
P. tricuspidens	MNHN R 442	22	--	--	--	--	7.60	6.96	--	--
P. tricuspidens	MNHN R 591	40	69.03	12.09	10.22	9.64	7.71	7.20	24.72	2.23
P. tricuspidens	MNHN R 148	23	--	--	--	--	7.91	7.11	--	--
cf. *P. remensis*	MNHN CR 208	23	--	--	--	--	--	--	--	--
cf. *Pl. daubrei*	UCMP 102829	28	--	--	--	--	8.59	--	--	--
P. rex	UM 64588	19	--	--	--	--	4.06	3.75	--	--
N. intermedius	USNM 42229	15	--	--	--	--	3.41	3.28	--	--
N. gidleyi	AMNH 17379	13	--	--	--	--	3.74	--	--	--
cf. *Pr. gaoi*	UALVP 49114	16	--	--	--	--	4.96	4.89	--	--
"Nothodectes"	AMNH 17379	19	38.71	7.98	5.45	~5.5	3.76	3.65	15.31	2.35
C. simpsoni	UM 101963	8	21.27	4.22	3.73	3.31	2.10	2.22	8.76	2.29

a – numbers in parentheses correspond to measurement codes of Sargis (2002a)

*probably distorted

Table 4.3B. Measurements of the distal ends of plesiadapiform humeri.

Taxon	Specimen	DEW(16)[a]	CaH(13)	TW(10)	TH(12)	CaW[b](11)	TL(14)	CaL	EEC	GM[c]
P. cookei	UM87990 (L)	22.80	6.40	5.84	4.33	8.75	6.63	6.35	8.05	6.49
P. cookei	UM87990 (R)	22.25	--	5.80	--	8.52	7.20	6.30	--	--
P. tricuspidens	MNHN BR 14522	18.25	5.54	4.65	3.99	6.51	5.59	4.16	6.00	5.06
P. tricuspidens	MNHN BR-03-L	20.35	5.52	4.60	3.16	8.16	7.09	4.85	7.68	5.61
P. tricuspidens	MNHN BR 12591	20.49	6.39	5.77	4.55	8.42	6.44	4.59	6.09	5.84
P. tricuspidens	MNHN BR 12590	--	5.63	4.53	3.87	8.66	6.56	4.88	--	--
P. tricuspidens	MNHN BR 12585	--	6.34	--	--	7.89	--	4.50	--	--
P. tricuspidens	MNHN R 405	23.75	5.67	6.65	5.40	9.47	7.19	4.47	7.22	6.55
P. tricuspidens	Berru (Mr Malfait)	20.38	5.69	6.03	4.94	7.68	6.70	4.14	6.65	5.90
P. tricuspidens	MNHN BR-04-L(a)	20.40	5.97	5.53	3.71	7.63	5.92	4.40	7.11	5.54
P. tricuspidens	MNHN BR-04-L(b)	19.29	--	6.40	4.20	--	7.07	--	6.13	--
P. tricuspidens	MNHN R 492	23.25	6.19	6.01	5.16	8.23	6.85	4.16	8.17	6.24
P. tricuspidens	MNHN R 442	20.71	5.76	5.39	4.26	8.51	--	4.36	6.28	--
P. tricuspidens	MNHN R 591	--	--	5.57	3.45	--	6.31	--	8.11	--
P. tricuspidens	MNHN R 148	--	--	5.22	3.57	--	6.47	--	7.01	--
cf. *P. remensis*	MNHN CR 208	16.74	5.02	4.17	3.73	7.03	5.81	3.42	5.80	4.82
cf. *Pl. daubrei*	UCMP 102829	22.92	6.55	6.51	5.06	8.87	6.81	6.13	7.84	6.76
P. rex	UM 64588	12.10	3.14	2.90	2.20	5.05	3.59	3.45	3.84	3.40
N. intermedius	USNM 442229	10.70	2.45	2.96	1.58	3.89	3.51	2.80	3.25	2.89
N. gidleyi	AMNH 17379	11.95	2.80	2.71	2.11	4.57	--	--	4.17	--
cf. *Pr. gaoi*	UALVP 49114	14.52	3.90	3.80	3.01	5.40	4.10	3.90	5.09	4.14
"Nothodectes"	AMNH 17379	11.21	3.25	3.30	2.97	3.95	3.84	3.42	3.80	3.53
C. simpsoni	UM 101963	7.23	1.69	1.55	1.09	2.60	1.88	1.34	3.12	1.80

a - numbers in parentheses correspond to measurement codes of Sargis (2002a)
b – capitulum width measurements include the width of the lateral flange
c - Geometric mean is based on TW, TH, CaW, TL, CaL, and EEC only.

Table 4.3C. Comparative shape variables of the distal humerus.

Code	Taxon	Specimen	TW-sv[a]	TH-sv	CaW-sv	TL-sv	CaL-sv	EEC-sv
1	*Protungulatum donnae*	UM 1836	0.682	1.072	1.332	1.235	0.682	1.218
2	Actocyonid	USNM 9999	0.591	0.769	1.694	1.192	0.858	1.270
3	*Mason Pocket*	AMNH 89519	1.077	0.529	1.485	1.123	0.928	1.133
4	*P. walbeckensis*	Walbeck	0.905	0.825	1.544	0.945	0.932	0.985
5	*Saxonellla creparturae*	Walbeck	1.058	0.698	1.407	0.872	0.872	1.267
6	*Adapis parisiensis*	Basel QW 1481	0.969	0.729	1.466	1.098	1.115	0.789
7	*A. parisiensis*	Basel QW 1482	0.935	0.740	1.510	1.013	1.032	0.915
8	*A. parisiensis*	AMNH81001	1.017	0.760	1.441	1.027	1.214	0.721
9	*Leptadapis magnus*	Basel QD 663	0.999	0.782	1.499	0.910	0.930	1.009
10	*L. magnus*	Basel QD 664	0.960	0.842	1.591	1.037	1.037	0.724
11	*L. magnus*	Basel QD 681	1.019	0.654	1.548	1.000	0.971	1.000
12	*Smilodectes gracilis*	AMNH11484	0.871	0.924	1.581	0.888	0.897	0.986
13	Omomyid Bridger Basin	AMNH29126	1.195	0.577	1.573	1.016	0.876	1.035
14	Omomyid Bitter Creek	AMNH113301	0.982	0.609	1.217	1.152	0.974	1.225
15	Microchoerine Omomyid 1	Basel QD 328	1.098	0.795	1.230	1.041	0.909	0.984
16	Microchoerine Omomyid 2	Basel QJ 620	1.227	0.879	1.359	1.011	1.044	0.646
17	Microchoerine Omomyid 3	Basel QV 18	1.140	0.803	1.243	0.984	0.984	0.907
18	Microchoerine Omomyid 4	Basel QK 989	1.030	0.850	1.417	0.876	0.850	1.082
19	*Ptilcercus lowii*	Sargis 2002a[b]	0.947	0.920	1.012	0.953	0.960	1.240
20	*Tupaia minor*	Sargis 2002a[b]	0.735	0.956	1.121	1.222	1.026	1.013
21	*Tupaia glis*	Sargis 2002a[b]	0.732	1.048	1.081	1.242	1.034	0.939
22	cf. *Pr.gaoi*	UALVP 49114	0.918	0.727	1.305	0.991	0.943	1.229
23	*P. rex*	UM 64588	0.855	0.646	1.487	1.057	1.017	1.131
24	*P. cookei*	UM 87990 (L)	0.899	0.667	1.347	1.021	0.978	1.240
25	*Deccanolestes*	unpublished	0.658	0.969	1.250	1.102	0.928	1.229
26	*Cynocephalus*	UF5969	0.718	0.973	1.257	1.265	1.055	0.854
27	*N. intermedius*	USNM 442229	1.025	0.547	1.346	1.215	0.969	1.124
28	*Nothodectes*	AMNH 17379	0.935	0.842	1.119	1.088	0.969	1.077
29	cf. *Pl. daubrei*	UCMP 102829	0.963	0.748	1.312	1.007	0.907	1.159
30	*P. tricuspidens*	MNHN BR 14522	0.919	0.788	1.286	1.104	0.821	1.185
31	*P. tricuspidens*	MNHN BR-03-L	0.819	0.563	1.454	1.263	0.863	1.368
32	*P. tricuspidens*	MNHN BR 12591	0.987	0.779	1.441	1.102	0.786	1.043
33	*P. tricuspidens*	MNHN R 405	1.016	0.824	1.446	1.098	0.682	1.103
34	*P. tricuspidens*	Berru (Mr Malfait)	1.022	0.837	1.302	1.135	0.702	1.127
35	*P. tricuspidens*	MNHN BR-04-L(a)	0.998	0.670	1.376	1.068	0.794	1.282
36	*P. tricuspidens*	MNHN R 492	0.962	0.826	1.318	1.097	0.665	1.308
37	cf. *P. remensis*	MNHN CR 208	0.865	0.774	1.457	1.204	0.708	1.202
38	*C. simpsoni*	UM 101963	0.858	0.603	1.441	1.041	0.743	1.731

a-variables represent the natural log of each raw variable from Table 4.3B divided by the geometric mean in that table

b-CaL was not available for these specimens and was approximated with CaH

Table 4.4A. Measurements of the proximal ends and shafts of plesiadapid radii.

Taxon	Specimen	PEW(28)[a]	PED(33)	NL(27)	RRL(29)	Le(26)	MSD	MSW	BSV	SSV	RSV
P. cookei	UM 87990	8.60	6.73	10.10	3.56	76.30	3.56	5.62	0.25	2.84	2.31
N. intermedius	USNM 442229	4.05	3.10	4.45	1.90	32.84	1.82	2.69	0.27	2.70	2.23
N. gidleyi	AMNH 17379	4.45	3.59	4.80	1.92	--	1.91	2.69	0.21	--	--
Pr. gaoi	UALVP 49124 (DB 031)	4.89	3.77	5.74	2.87	--	--	--	0.26	--	--
P. tricuspidens	MNHN R 550	8.11	6.26	9.36	3.39	70.10	3.77	6.02	0.26	2.69	2.29
P. tricuspidens	MNHN BR 11399	7.51	5.50	9.70	3.33	--	--	--	0.31	--	--
P. tricuspidens	MNHN BR 5440	7.35	6.17	8.37	3.11	--	--	--	0.18	--	--
P. tricuspidens	MNHN R 597	7.55	6.22	8.70	3.23	--	--	--	0.19	--	--

a – numbers in parentheses correspond to measurement numbers in Sargis (2002a)

Table 4.4B. Measurements of the distal ends of plesiadapid radii.

Taxon	Specimen	DEW(31) [a]	DED(32)	StL(30)
P. cookei	UM 87990	9.09	6.82	1.57
N. intermedius	USNM 442229	~3.6	3.07	--
N. gidleyi	AMNH 17379	4.48	3.70	--
Pr. gaoi	UALVP 49124 (DB 031)	--	--	--
P. tricuspidens	MNHN R 550	8.69	6.27	0.99
P. tricuspidens	MNHN BR 11399	--	--	--
P. tricuspidens	MNHN BR 5440	--	--	--
P. tricuspidens	MNHN R 597	--	--	--

a – numbers in parentheses correspond to measurement numbers in Sargis (2002a)

Table 4.5A. Measurements and shape variables of plesiadapid ulnae.

Taxon	Specimen	Le(18)[a]	PTW(20)	RFL(21)	RFW(22)	NcL(25)	MSW	MSD	RFV	NSV	SSV
P. cookei	UM 87990 (L)	88.30	5.74	5.58	4.69	8.43	3.30	5.85	0.17	2.54	3.00
P. cookei	UM 87990 (R)	--	5.60	5.39	5.08	7.70	--	--	0.06	--	--
P. tricuspidens	MNHN BR-07-L	--	5.09	4.82	4.57	6.77	3.20	5.89	0.05	--	--
P. tricuspidens	MNHN BR 70713*	--	5.09	5.41	4.51	6.01	2.66	5.19	0.18	--	--
P. tricuspidens	MNHN R 411	--	5.43	5.94	5.49	8.34	3.11	6.61	0.08	--	--
P. tricuspidens	MNHN R 546	85.08	5.90	5.73	5.46	8.26	3.57	5.67	0.05	2.50	2.94
P. tricuspidens	MNHN R 443	--	5.81	5.42	4.78	7.78	3.39	6.46	0.12	--	--
P. tricuspidens	MNHN R 452	--	4.90	4.90	4.72	7.07	--	--	0.04	--	--
P. tricuspidens	MNHN R 1521*	--	4.28	4.60	4.27	6.88	2.35	4.41	0.08	--	--
P. tricuspidens	MNHN R 5196	--	4.61	4.40	4.19	6.80	--	--	0.05	--	--
P. tricuspidens	MNHN nn*	--	3.69	4.11	3.84	5.24	--	4.69	0.07	--	--
P. rex	UM 64588	--	3.00	2.87	2.54	4.30	1.49	3.35	0.12	--	--
N. intermedius	USNM 442229	41.20	2.72	2.30	2.06	3.74	1.30	2.94	0.11	2.56	3.05
N. gidleyi	AMNH 117379	--	3.22	2.80	2.31	4.96	1.49	3.16	0.19	--	--

a – numbers in parentheses correspond to measurement numbers in Sargis (2002a)

Table 4.5B. Measurements of plesiadapid ulnae.

Taxon	Specimen	OL(19)[a]	StL(23)	NcD(24)
P. cookei	UM 87990 (L)	--	2.80	3.80
P. cookei	UM 87990 (R)	--	--	3.30
P. tricuspidens	MNHN BR-07-L	7.32	--	2.48
P. tricuspidens	MNHN BR 70713*	--	--	1.88
P. tricuspidens	MNHN R 411	--		2.47
P. tricuspidens	MNHN R 546	9.87	--	3.17
P. tricuspidens	MNHN R 443	--	--	2.54
P. tricuspidens	MNHN R 452	7.77	--	2.11
P. tricuspidens	MNHN R 1521*	--	--	1.67
P. tricuspidens	MNHN R 5196	--	--	--
P. tricuspidens	MNHN nn*	--	--	1.41
P. rex	UM 64588	6.16	--	1.94
N. intermedius	USNM 442229	5.13	1.21	1.60
N. gidleyi	AMNH 117379	4.54	--	1.74

a – numbers in parentheses correspond to measurement numbers in Sargis (2002a)

Table 4.6. Measurements of plesiadapid scaphoids.

Taxon	Specimen	Le[a]	LSL	LSH	RSW	RSD	TL
P. cookei	UM 87990	9.78	4.03	1.42	5.62	4.1	5.03
N. intermedius	USNM 442229	4.21	1.72	0.72	2.44	1.65	1.9

a – the maximum length formed between the medial and lateral margins of the bone

Table 4.7. Measurements of plesiadapid triquetra.

Taxon	Specimen	TrW	TrL	PfW	PrfD	PufD	UfW	UfD	HfW	HfD	GM[a]	TrL-V
P. cookei	UM 87990	5.43	2.17	4.01	1.72	1.93	3.15	2.24	2.83	3.17	2.85	0.76
P. tricuspidens	MNHN R 5320	6.07	2.85	4.00	1.11	1.90	2.74	2.01*	3.06	2.90	2.99	0.95

a-geometric mean of all measurements
*broken facet, measurement may be inaccurate

Table 4.8. Measurements of plesiadapid pisiforms.

Taxon	Specimen	Le	PEW	TfW	TrfD	TufD	UfD	MSW	MSD	DEW	DED	SSV	BSV
P. cookei	UM 87990	8.87	2.80	3.23	1.78	1.95	2.41	1.89	2.21	2.96	4.22	1.47	1.28
N. intermedius	USNM 442229	3.60	1.52	1.54	0.72	1.11	1.17	1.16	0.84	1.26	1.61	1.29	1.11

Table 4.9. Measurements of plesiadapid hamates.

Taxon	Specimen	Le[a]	DEW	DED	PCW	PCD	CfD	AfW	DEV	PCV
P. cookei	UM 87990 (L)	3.3	3.92	3.42	4.15	2.52	2.07	1.38	1.15	1.65
P. tricuspidens	MNHN R 5321 (L)	3.46	3.84	3.22	3.57	2.15	2.06	nm	1.19	1.66
N. intermedius	USNM 442229	1.93	2.26	1.54	2.29	1.4	1.4	0.57	1.47	1.64
N. intermedius	USNM 442229 (L)	1.97	2.24	1.43	2.35	1.38	1.23	0.55	1.57	1.70

a – proximodistal length measured on radial side of bone

Table 4.10. Measurements and shape variables of plesiadapid metacarpals.

Taxon	Specimen	Bone	Le	PEW	PED	MSW	MSD	DEW	DED	GM[a]	HSV	SSV
P. cookei	UM 87990 set 1	L MC I	11.40	4.80	3.10	2.50	1.80	3.40	3.00	3.60	0.125	1.68
N. intermedius	USNM 442229	R MC I	6.64	2.54	1.61	1.27	1.03	1.84	1.71	1.96	0.073	1.76
N. gidleyi	AMNH 17379	L MC I	6.92	2.89	1.57	1.54	1.08	2.13	2.02	2.17	0.053	1.68
P. n. sp.	MNHN nn	L MC I	11.70	4.30	3.20	2.80	1.80	3.30	nm	nm	nm	1.65
P. cookei	UM 87990 set 1	L MC II	17.00	2.70	4.00	2.50	2.20	3.90	3.50	3.90	0.108	1.98
P. cookei	UM 87990 set 2	L MC II	18.90	2.90	4.20	2.70	2.30	4.30	4.20	4.27	0.024	2.03
P. cookei	UM 87990 set 1	R MC III	20.00	3.00	4.00	2.20	2.20	4.00	3.50	4.00	0.134	2.21
P. cookei	UM 87990 set 2	L MC III	23.20	2.70	4.40	2.30	2.10	4.20	4.00	4.18	0.049	2.36
N. intermedius	USNM 442229	R MC III	11.51	1.33	--	1.09	1.05	2.09	--	--	--	2.38
N. gidleyi	AMNH 17379	L MC III	12.02	1.61	1.88	1.13	1.02	2.14	1.63	2.04	0.272	2.42
P. tricuspidens	MNHN R 5295	R MC III	21.10	2.70	4.10	2.50	2.30	4.40	3.70	4.17	0.173	2.17
P. n. sp.	MNHN nn	L MC III	18.50	2.40	nm	2.20	1.90	3.50	nm	nm	nm	2.20
P. n. sp.	MNHN nn	L MC III	19.20	nm	nm	2.40	2.00	nm	nm	nm	nm	2.17
P. n. sp.	MNHN nn	L MC III	21.50	nm	nm	2.60	2.40	nm	nm	nm	nm	2.15
P. insignis	MNHN Menat	R MC III	11.7	--	--	--	--	--	--	--	--	--
P. cookei	UM 87990 set 1	R MC IV	23.80	3.10	4.40	2.40	2.10	4.30	4.10	4.34	0.048	2.36
P. cookei	UM 87990 set 2	L MC IV	23.70	3.00	4.20	2.30	2.10	4.20	4.00	4.23	0.049	2.38
P. cookei	UM 87990 set 1	R MC IV	--	2.80	4.00	2.20	2.20	--	--	--	--	--
P. tricuspidens	MNHN R 5364	R MC IV	24.70	3.20	3.80	2.70	2.40	4.50	3.50	4.37	0.251	2.27
P. n. sp.	NMHN nn	L MC IV	18.60	2.50	nm	2.00	1.60	3.40	nm	nm	nm	2.34
P. cookei	UM 87990 set 1	R MC V	15.80	3.30	3.00	2.40	2.10	3.90	3.30	3.74	0.167	1.95
P. cookei	UM 87990 set 2	R MC V	17.80	3.30	3.20	1.80	2.30	4.00	3.50	3.77	0.134	2.17
N. intermedius	USNM 442229	L MC V	8.78	1.91	1.69	1.00	0.94	2.02	1.77	1.92	0.132	2.20
P. tricuspidens	MNHN R 5305	R MC V	15.15	3.30	2.90	2.40	2.00	4.30	3.40	3.74	0.235	1.93
P. tricuspidens	MNHN R 5373	L MC V	13.00	3.30	2.70	2.20	1.80	3.60	2.80	3.34	0.251	1.88
P. tricuspidens	MNHN nn	L MC V	15.20	3.40	2.90	2.10	1.80	3.80	3.10	3.52	0.204	2.06
P. insignis	MNHN Menat	R MC V	9.7	--	--	--	--	--	--	--	--	--

a-geometric mean of Le, PEW, PED, MSW, MSD, DEW, and DED

Table 4.11. Shape variables of plesiadapid metacarpals.

Taxon	Specimen	Bone	V-Le[a]	V-PEW	V-PED	V-MSW	V-MSD	V-DEW	V-DED
P. cookei	UM 87990 set 1	L MC I	1.154	0.289	-0.149	-0.364	-0.692	-0.056	-0.181
N. intermedius	USNM 442229	R MC I	1.219	0.258	-0.198	-0.435	-0.644	-0.064	-0.137
N. gidleyi	AMNH 17379	L MC I	1.161	0.288	-0.322	-0.342	-0.697	-0.017	-0.070
P. cookei	UM 87990 set 1	L MC II	1.472	-0.368	0.025	-0.445	-0.573	-0.001	-0.109
P. cookei	UM 87990 set 2	L MC II	1.488	-0.387	-0.016	-0.458	-0.618	0.007	-0.016
P. cookei	UM 87990 set 1	R MC III	1.611	-0.287	0.001	-0.597	-0.597	0.001	-0.132
P. cookei	UM 87990 set 2	L MC III	1.713	-0.437	0.051	-0.598	-0.689	0.004	-0.044
N. gidleyi	AMNH 17379	L MC III	1.774	-0.236	-0.081	-0.590	-0.692	0.049	-0.224
P. tricuspidens	MNHN R 5295	R MC III	1.622	-0.434	-0.017	-0.511	-0.595	0.054	-0.119
P. cookei	UM 87990 set 2	R MC IV	1.703	-0.336	0.015	-0.592	-0.725	-0.008	-0.056
P. cookei	UM 87990 set 2	L MC IV	1.723	-0.344	-0.007	-0.609	-0.700	-0.007	-0.056
P. tricuspidens	MNHN R 5364	R MC IV	1.731	-0.313	-0.141	-0.483	-0.600	0.028	-0.223
P. cookei	UM 87990 set 1	R MC V	1.442	-0.124	-0.219	-0.442	-0.576	0.043	-0.124
P. cookei	UM 87990 set 2	R MC V	1.551	-0.134	-0.165	-0.740	-0.495	0.058	-0.075
N. intermedius	USNM 442229	L MC V	1.522	-0.004	-0.126	-0.651	-0.713	0.052	-0.080
P. tricuspidens	MNHN R 5305	R MC V	1.400	-0.124	-0.254	-0.443	-0.625	0.140	-0.094
P. tricuspidens	MNHN R 5373	L MC V	1.359	-0.012	-0.212	-0.417	-0.618	0.075	-0.176
P. tricuspidens	NMHN nn	L MC V	1.463	-0.034	-0.193	-0.516	-0.670	0.077	-0.127

a-natural log ratios of each variable from Table 4.10 (the name of which is given in the suffix the new variable name) to the geometric means from 4.10. For example V-Le = Ln(Le/GM)

Table 4.12. Comparisons of plesiadapid metacarpal-carpal articular areas.

Ry	Set 1 area	Set 2 area	Carpal area
MC II	7.70	9.50	8.20[a]
MC III	7.10	8.50	~6[b]
MC IV	6.80	8.50	10.72 [c]
MC V	6.00	7.50	

a – trapezoid distal facet area
b – reconstructed capitate distal facet area
c – hamate distal facet area.

Table 4.13. Measurements of plesiadapid proximal phalanges.

Taxon	Specimen	Atd/Ry	Le	PEW	PED	MSW	MSD	DEW	DED	BSV	HSV	SSV
P. cookei	UM 87990 (Fig. 4.19A)	2/1	--	--	4.00	--	--	--	--	--	--	--
P. cookei	UM 87990 (Fig. 4.19B)	2/1	--	4.20	4.16	--	--	--	--	-0.01	--	--
P. cookei	UM 87990 (Fig. 4.19C)	2?/?	--	--	4.23	--	2.80	--	--	--	--	--
P. cookei	UM 87990 (Fig. 4.19D)	2?/?	--	4.69	3.90	2.17	2.85	--	--	-0.18	--	--
P. cookei	UM 87990 (Fig. 4.19E)	1?/?	--	--	--	--	--	3.36	2.37	--	--	--
P. cookei	UM 87990 (Fig. 4.19F)	2?/?	--	--	--	--	--	3.15	2.72	--	--	--
P. cookei	UM 87990 (Fig. 4.19G)	2?/?	--	--	--	--	--	--	2.81	--	--	--
P. cookei	UM 87990 (Fig. 4.20A)	1?/?	12.76	4.09	3.24	2.26	2.31	3.21	2.41	-0.23	0.29	1.72
P. cookei	UM 87990 (Fig. 4.20B)	1?/?	15.52	4.54	3.47	2.22	2.58	3.65	2.53	-0.27	0.37	1.87
P. cookei	UM 87990 (Fig. 4.20C)	2?/?	15.23	4.52	4.11	2.33	2.87	3.47	2.84	-0.09	0.20	1.77
P. cookei	UM 87990 (Fig. 4.20D)	2?/?	17.28	4.67	3.89	2.48	2.78	3.67	2.94	-0.18	0.22	1.88
P. cookei	UM 87990 (Fig. 4.20E)	2?/?	17.28	4.68	3.9	2.37	2.95	3.66	2.97	-0.18	0.21	1.88
P. cookei	UM 87990 (Fig. 4.20F)	2?/?	17.67	4.76	4.49	2.47	2.87	3.87	2.76	-0.06	0.34	1.89
?P .tricuspidens	MNHN R 503	2?/?	17.32	4.90	3.68	3.45	2.91	3.61	2.56	-0.29	0.34	1.70
P .tricuspidens	MNHN Divers Coll. nn	1?/?	14.25	4.71	3.54	3.27	2.74	3.45	2.71	-0.29	0.24	1.56
P .tricuspidens	MNHN R 5303	1/?	14.17	4.57	3.37	2.65	2.25	3.58	2.61	-0.30	0.31	1.76
P .tricuspidens	MNHN R 5297	1/?	15.63	4.86	4.18	3.03	2.60	3.67	3.05	-0.15	0.18	1.72
P .tricuspidens	MNHN BR 14538	1?/1	12.87	4.40	3.72	2.38	2.58	3.01	2.66	-0.17	0.12	1.65
P .tricuspidens	MNHN R 5315	2?/1	12.41	4.81	4.18	2.42	2.58	3.47	3.12	-0.14	0.10	1.60
P .tricuspidens	Pell. Coll (CM 091)	2?/?	16.97	4.57	3.51	2.73	2.56	3.31	2.33	-0.26	0.35	1.86
P .tricuspidens	Pell. Coll. Nn	1?/?	14.23	4.54	3.73	2.79	2.51	3.23	2.43	-0.19	0.29	1.68
P. n. sp.	NMHN nn	?/?	16.05	nm	nm	2.75	2.37	3.41	2.48	nm	0.32	1.84
P. n. sp.	NMHN nn	?/?	--	nm	nm	2.88	2.6	3.55	2.68	nm	0.28	--
P. n. sp.	NMHN nn	?/?	--	nm	nm	2.6	2.55	3.43	2.79	nm	0.21	--
P. n. sp.	NMHN nn	?/?	13.84	nm	nm	2.56	2.34	3.16	2.35	nm	0.30	1.73
P. n. sp.	NMHN nn	?/?	15.39	nm	nm	2.53	2.22	3.22	2.42	nm	0.29	1.87
P. n. sp.	NMHN nn	?/?	14.07	nm	nm	2.58	2.2	2.84	2.04	nm	0.33	1.78
P. n. sp.	NMHN nn	?/?	14.71	nm	nm	2.36	1.98	3.14	2.23	nm	0.34	1.92
P. n. sp.	NMHN nn	?/?	14.69	nm	nm	2.07	1.73	2.67	2.03	nm	0.27	2.05
P. n. sp.	NMHN nn	?/1	12.53	nm	nm	4.49	3.43	1.96	2.42	nm	-0.21	1.16
P.insignis	MNHN Menat specimen	1/3	8.6	--	--	--	--	--	--	--	--	--
P.insignis	MNHN Menat specimen	1/5	7.5	--	--	--	--	--	--	--	--	--
P.insignis	MNHN Menat specimen	2/3	9.7	--	--	--	--	--	--	--	--	--
P.insignis	MNHN Menat specimen	2/4	9.9	--	--	--	--	--	--	--	--	--
P.insignis	MNHN Menat specimen	2/5	9.2	--	--	--	--	--	--	--	--	--
N. intermedius	USNM 442229 (143a)*	1?/?	7.76	2.43	1.96	1.38	1.22	1.95	1.19	-0.21	0.49	1.79
N. intermedius	USNM 442229 (143b)*	2?/?	8.21	2.43	1.96	1.30	1.29	1.88	1.20	-0.21	0.45	1.85
N. intermedius	USNM 442229 (143c)*	2?/?	8.73	2.40	1.81	1.30	1.20	1.83	1.26	-0.29	0.37	1.95
N. intermedius	USNM 442229 (143d)*	2?/1	6.79	2.38	--	1.40	1.46	1.74	1.43	--	0.20	1.56
N. intermedius	USNM 442229a	2?/1	6.79	2.47	2.20	1.47	1.33	1.92	1.32	-0.11	0.37	1.58
N. intermedius	USNM 442229b	2?/?	9.21	2.58	2.16	1.43	1.38	1.87	1.18	-0.18	0.46	1.88
N. gidleyi	AMNH 17379	1/?	9.20	2.46	2.13	1.48	1.36	1.82	1.34	-0.15	0.30	1.87
N. gidleyi	AMNH 17379	1?/?	8.56	2.68	2.06	1.56	1.33	2.08	1.39	-0.27	0.41	1.78
N. gidleyi	AMNH 17379	?/1	6.24	2.04	1.63	0.98	1.12	1.53	1.31	-0.22	0.16	1.79

*numbers in parentheses following USNM 442229 correspond to unique identifiers of the particular element (i.e., unofficial “sub-specimen” numbers) assigned by P. Houde during preparation of the specimen

Table 4.14. Measurements of plesiadapid intermediate phalanges.

Taxon	Specimen	Atd/Ry	Le	PEW	PED	MSW	MSD	DEW	DED	BSV	HSV	SSV
P. cookei	UM 87990 (Fig. 4.21A)	1?/?	--	3.65	4.06	1.73	2.93	--	--	0.11	--	--
P. cookei	UM 87990 (Fig. 4.21B)	1?/?	12.05	3.93	4.03	1.70	2.81	3.02	3.27	0.03	-0.08	1.71
P. cookei	UM 87990 (Fig. 4.21C)	1?/?	--	3.4	3.43	1.70	2.36	--	--	0.01	--	--
P. cookei	UM 87990 (Fig. 4.21D)	1?/?	--	3.45	3.53	1.69	2.54	--	--	0.02	--	--
P. cookei	UM 87990 (Fig. 4.21E)	2?/?	13.56	3.88	3.95	1.94	2.56	3.1	3.17	0.02	-0.02	1.81
P. cookei	UM 87990 (Fig. 4.21F)	2?/?	13.24	3.86	4.16	1.82	2.95	2.89	3.2	0.07	-0.10	1.74
P. cookei	UM 87990 (Fig. 4.21G)	2?/?	13.25	3.85	4.18	1.85	2.83	3.06	3.45	0.08	-0.12	1.76
P. tricuspidens	MNHN R 5296	2/?	13.88	4.17	3.85	2.10	2.82	2.87	3.49	-0.08	-0.20	1.74
P. tricuspidens	MNHN BR nn	2?/?	12.26	3.68	3.30	1.95	2.23	2.50	3.09	-0.11	-0.21	1.77
P. tricuspidens	MNHN BR 14536	2?/?	11.04	3.81	3.67	1.89	2.14	2.68	3.03	-0.04	-0.12	1.70
P. tricuspidens	MNHN CR nn	2?/?	12.56	3.38	3.62	1.95	2.38	2.47	3.07	0.07	-0.22	1.76
P. tricuspidens	MNHN R 5363	2/?	12.90	4.08	4.03	2.04	2.84	3.12	3.45	-0.01	-0.10	1.68
P. tricuspidens	MNHN R 5324	2/?	11.91	3.87	3.89	2.00	2.58	2.72	3.23	0.01	-0.17	1.66
P. tricuspidens	MNHN R 5341	2/?	11.10	3.70	3.41	1.49	2.08	2.44	3.01	-0.08	-0.21	1.84
P. tricuspidens	MNHN R 5360	1/?	9.08	3.32	3.10	1.59	1.99	2.18	2.64	-0.07	-0.19	1.63
P. tricuspidens	MNHN R 5330	2/?	12.28	3.19	3.19	1.79	2.20	2.45	2.72	0.00	-0.10	1.82
P. tricuspidens	MNHN R 5346	2/?	12.53	3.79	3.83	2.02	2.51	2.62	3.18	0.01	-0.19	1.72
P. tricuspidens	MNHN R 5342	1/?	9.64	3.14	3.24	1.87	2.32	2.41	2.85	0.03	-0.17	1.53
P. tricuspidens	MNHN R 5369	1/?	9.50	3.33	3.21	1.92	2.21	2.40	2.75	-0.04	-0.14	1.53
P. tricuspidens	Pellouin Coll. nn	1?/?	9.29	3.34	3.26	1.76	1.97	2.51	2.89	-0.03	-0.14	1.61
P. n. sp.	MNHN nn	?/?	12.39	3.67	3.9	1.72	2.54	nm	nm	0.06	nm	1.78
P. n. sp.	MNHN nn	?/?	11.59	3.65	4.14	2.05	2.78	nm	nm	0.13	nm	1.58
P. n. sp.	MNHN nn	?/?	11.42	3.29	3.85	1.88	2.47	nm	nm	0.16	nm	1.67
P. n. sp.	MNHN nn	?/?	12.07	3.08	3.59	1.8	2.55	nm	nm	0.15	nm	1.73
P. n. sp.	MNHN nn	?/?	11.37	3.46	3.89	2.1	2.68	nm	nm	0.12	nm	1.57
P. n. sp.	MNHN nn	?/?	11.04	3.68	3.88	1.92	2.7	nm	nm	0.05	nm	1.58
P. n. sp.	MNHN nn	?/?	12.19	3.38	4	2.28	2.84	nm	nm	0.17	nm	1.57
P. n. sp.	MNHN nn	?/?	11.46	3.91	4.25	2.32	2.98	nm	nm	0.08	nm	1.47
cf *P. churchilli*	SMM P77.33.517	1?/?	8.40	2.48	2.15	1.27	1.31	1.70	1.87	-0.14	-0.10	1.87
P. insignis	MNHN Menat specimen	1/4	7.8	--	--	--	--	--	--	--	--	--
P. insignis	MNHN Menat specimen	1/5	5.6	--	--	--	--	--	--	--	--	--
N. intermedius	USNM 442229 (142)*	1/?	6.56	2.18	1.92	1.08	1.31	1.46	1.54	-0.13	-0.06	1.71
N. intermedius	USNM 442229	2/?	7.28	2.14	1.76	1.04	1.20	1.31	1.59	-0.19	-0.19	1.88
N. intermedius	USNM 442229 (140)*	2/?	6.97	2.14	1.72	0.97	1.18	1.31	1.65	-0.22	-0.23	1.87
N. intermedius	USNM 442229 (141)*	2/?	7.02	2.11	1.76	1.04	1.33	1.35	1.71	-0.18	-0.24	1.79
N. gidleyi	AMNH 17379	1?/?	6.95	2.10	1.73	1.00	1.06	1.43	1.63	-0.20	-0.13	1.91
N. gidleyi	AMNH 17379	1?/?	7.10	2.28	1.92	0.99	1.14	1.39	1.73	-0.17	-0.22	1.90
N. gidleyi	AMNH 17379	2?/?	8.27	2.35	2.31	1.06	1.46	1.51	1.74	-0.02	-0.14	1.89

*numbers in parentheses following USNM 442229 correspond to unique identifiers of the particular element (i.e., unofficial “sub-specimen” numbers) assigned by P. Houde during preparation of the specimen

Table 4.15. Measurements of plesiadapid distal phalanges.

Taxon	Specimen	Le	DFT	PEW	PED[a]	ETH	FTW	FTH	MSW	MSD	CSV
P. cookei	UM 87990 (Fig. 4.22A)	--	4.81	3.11	3.5	0.8	2.32	2.55	1.31	3.93	1.10
P. cookei	UM 87990 (Fig. 4.22B)	~12	--	--	3.94	0.83	--	--	1.65	4.47	1.00
P. cookei	UM 87990 (Fig. 4.22C)	--	4.45	2.91	4.17	0.69	2.22	2.30	1.29	4.14	1.17
P. cookei	UM 87990 (Fig. 4.22D)	--	4.84	2.94	3.64	0.92	2.83	2.34	1.39	4.31	1.13
P. cookei	UM 87990 (Fig. 4.22E)	--	--	--	--	1.03	--	--	1.62	~4.5	1.02
P. cookei	UM 87990 (Fig. 4.22F)	12.50	4.82	3.02	3.76	0.74	1.85	2.79	1.54	4.66	1.11
P. cookei	UM 87990 (Fig. 4.22G)	13.81	4.85	3.25	3.95	0.74	2.28	2.60	1.59	4.50	1.04
P. cookei	UM 87990 (Fig. 4.22H)	--	4.78	3.09	3.77	0.79	2.27	2.98	1.68	4.47	0.98
P. cookei	UM 87990 (Fig. 4.22I)	--	4.76	2.91	--	--	2.15	~2.4	--	--	--
P. cookei	UM 87990 (Fig. 4.22J)	--	4.77	3.14	3.96	1.11	2.28	2.73	--	--	--
P. tricuspidens	Berru, Divers (A)	--	5.07	2.81	3.64	0.85	1.89	3.18	1.55	4.48	1.06
P. tricuspidens	Berru, Divers (B)	--	--	2.27	--	--	1.74	--	--	--	--
P. tricuspidens	MNHN R 5344	--		3.05	--	--	2.57	--		--	--
P. tricuspidens	MNHN R 539	--	6.53	2.84	3.28	0.76	2.01	2.99	1.59	3.77	0.86
P. tricuspidens	MNHN R 5379	--	--	1.93	--	--	1.74	--	--	--	--
P. tricuspidens	MNHN R 613	11.95	4.82	3.19	3.87	0.78	2.44	2.94	1.45	3.60	0.91
P. tricuspidens	MNHN R 612	--	4.67	2.76	3.10	0.88	2.46	2.85	1.41	3.85	1.00
P. tricuspidens	MNHN R 5361	--	3.53	2.13	3.03	0.66	1.99	2.07	1.09	2.86	0.97
P. tricuspidens	MNHN R 5309	--	4.88	3.46	3.87	0.72	2.61	2.36	1.47	3.38	0.83
P. tricuspidens	MNHN R 5313	--	--	3.24	--	--	2.35	--	--	--	--
P. tricuspidens	Berru, Pellouin (CM 091)	12.86	4.33	2.94	4.19	0.59	1.83	2.98	1.51	4.29	1.04
P. n. sp.	LQ. 1	11.28	4.60	3.08	3.38	0.66	2.82	2.78	1.54	3.48	0.81
P. n. sp.	LQ. 2	--	4.09	2.16	3.46	0.76	1.60	2.18	1.45	4.07	1.03
P. n. sp.	LQ. 3	--	4.27	2.92	3.16	0.81	2.06	3.32	1.45	3.89	0.98
P. n. sp.	LQ. 4	10.55	4.08	2.53	3.50	0.64	2.35	2.81	1.49	3.57	0.88
P. n. sp.	LQ. 5	9.68	4.06	2.73	3.21	0.57	2.25	2.57	1.29	3.45	0.98
P. n. sp.	LQ. 6	--	--	2.81	--	--	2.39	--	--	--	--
P. n. sp.	LQ. 7	--	4.09	2.50	3.30	0.32	1.41	2.27	1.53	3.79	0.90
P. n. sp.	LQ. 8	--	4.17	2.14	2.80	0.51	1.79	2.30	1.31	3.37	0.95
P. n. sp.	LQ. 9	--	4.14	2.71	2.86	0.50	2.31	2.46	1.23	3.10	0.92
P. n. sp.	LQ. 10	9.66	3.76	2.64	3.18	0.65	2.03	2.52	1.23	3.50	1.05
P. n. sp.	LQ. 11	--	4.47	2.60	3.29	0.58	1.77	2.58	1.37	3.56	0.95
P. n. sp.	LQ. 12	--	4.42	2.26	3.01	0.88	1.87	2.68	1.41	3.78	0.99
P. n. sp.	LQ. 13	--	3.64	2.17	3.23	0.60	1.32	2.43	1.30	3.38	0.96
cf. *P. churchilli*	SMM P77.33.517 (A)	--	--	1.84	--	--	1.48	--	--	--	--
cf. *P. churchilli*	SMM P77.33.517 (B)	--	3.02	1.91	2.03	0.67	1.57	1.28	0.96	2.54	0.98
cf. *P. churchilli*	SMM P77.33.517 (C)	--	2.95	1.85	2.21	0.49	1.45	1.45	1.08	2.40	0.80
cf. *P. churchilli*	SMM P77.33.517 (D)	7.06	2.91	2.05	2.15	0.55	1.42	1.43	1.10	2.28	0.73
N. intermedius	USNM 442229 (142)*	5.22	2.30	1.39	1.67	0.36	0.95	1.23	0.66	1.76	0.99
N. intermedius	USNM 442229 (assoc2)*	5.41	1.77	1.35	1.78	0.41	0.97	0.96	0.71	1.88	0.98
N. intermedius	USNM-442229 (141)*	4.53	2.02	1.43	1.61	0.39	0.93	1.19	0.69	1.80	0.96
N. intermedius	USNM 442229 (A)*	--	2.16	1.47	1.79	0.35	1.09	1.01	0.65	2.01	1.13
N. intermedius	USNM 442229 (C)*	--	2.18	1.39	1.71	0.47	1.28	1.20	0.74	1.90	0.95
Pr. gaoi	UALVP 49110	~6.7	2.80	1.52	1.99	0.31	1.30	1.21	0.89	2.16	0.89

a – only includes articular area

*numbers in parentheses following USNM 442229 correspond to unique identifiers of the particular element (i.e., unofficial "sub-specimen" numbers) assigned by P. Houde during preparation of the specimen

Table 4.16. Measurements of plesiadapid innominates.

Taxon	Specimen	Le(1)[a]	IL(2)	IW(3)	AcL(4)	AcD(5)	PD(6)	IsL(7)	IsD(8)	IspL	InD	InW	IspV
P. cookei	UM 87990 (R)	73.77	41.51	10.34	11.16	11.77	24.60	19.89	13.54	3.46	7.17	4.85	0.31
P. cookei	UM 87990 (L)	72.50	38.90	7.95*	10.92	--	--	19.90	13.33	3.90	7.00	4.94	0.36
P. tricuspidens	MNHN R 448	--	--	--	13.46	12.34	--	21.90	--	3.73	8.59	6.20	0.28
P. tricuspidens	MNHN R 409	--	--	10.87	--	--	--	--	--	--	7.12	7.03	--
P. tricuspidens	MNHN R 413	--	--	12.79	--	--	--	--	--	--	9.27	8.18	--
P. tricuspidens	Pell. Coll. Nn	--	--	--	--	--	--	18.47	--	4.54	--	--	--
N. gidleyi	AMNH 17409	--	--	--	7.35	--	--	13.99	--	3.32	3.85	3.57	0.45
N. gidleyi	AMNH 17379	--	--	4.57	6.88	--	--	--	--	3.58	3.67	3.57	0.52
N. gidleyi	AMNH 17379	--	--	4.57	6.52	--	--	--	--	3.82	3.27	3.02	0.59

a – numbers in parentheses correspond to measurement numbers in Sargis (2002b)

Table 4.17A. Measurements of the proximal ends of plesiadapid femora.

Taxon	Specimen	FHL(10)[a]	FHW(11)	GTL(12)	LTL(13)	TTL(14)	TTP(28)
P. cookei	UM 87990 (R)	9.40	8.99	--	8.30	1.73	23.50
P. cookei	UM 87990 (L)	8.77	8.67	2.78	8.90	1.95	24.97
P. tricuspidens	MNHN BR 14523	7.88	7.57	--	8.29	2.18	20.39
P. tricuspidens	MNHN BR-15-L	7.84	8.42	2.34	8.19	1.99	23.48
P. tricuspidens	MNHN Br-13-L	--	--	--	8.57	2.03	--
P. tricuspidens	MNHN BR 13856	8.89	8.77	5.04	8.61	1.75	23.40
P. tricuspidens	MNHN BR 11865	8.19	7.79	3.16	7.68	1.36	22.00
P. tricuspidens	MNHN BR 11866	8.58	8.52	--	9.32	2.23	23.31
P. tricuspidens	MNHN BR 12569	--	--	--	8.08	1.82	--
P. tricuspidens	MNHN BR-12-L	--	--	--	7.70	1.31	--
P. tricuspidens	MNHN BR-16-L	8.56	10.15	3.62	10.06	2.34	25.78
P. tricuspidens	MNHN R 444	8.89	9.17	2.69	8.62	2.73	23.61
P. tricuspidens	MNHN R 450	7.78	7.38	2.22	8.28	1.41	23.40
P. tricuspidens	MNHN R 445	--	--	--	--	1.74	--
P. tricuspidens	MNHN R 440	8.23	8.95	--	9.12	2.83	24.05
P. tricuspidens	MNHN R 438	8.71	8.37	--	5.91	2.22	21.60
P. tricuspidens	MNHN R 446	8.55	8.78	2.79	9.36	1.91	26.32
P. tricuspidens	MNHN R 408	9.00	9.31	3.93	9.93	1.50	24.04
P. tricuspidens	MNHN R 407	--	--	--	--	--	--
P. tricuspidens	MNHN BR 5454	6.62	7.62	2.13	--	--	--
P. tricuspidens	MNHN R 523	--	7.68	7.65	3.30	1.57	20.73
P. tricuspidens	MNHN R 578	--	--	--	8.87	1.45	--
P. churchilli	P78.14.93	5.67	6.10	2.11	5.99	1.59	17.60
N. gidleyi	AMNH 17379	5.13	5.34	2.57	6.06	1.27	14.73
N. gidleyi	AMNH 17409	--	--	--	--	--	--
N. intermedius	USNM 309895	--	--	--	--	--	--

a – numbers in parentheses correspond to measurement numbers in Sargis (2002b)

Table 4.17B. Measurements of the distal ends of plesiadapid femora.

Taxon	Specimen	PGL(17) [a]	PGW(18)	DEW(19)	MCD(20)	LCD(21)	MCW(22)	LCW(23)	MCL(24)	LCL(25)	ICW(26)
P. cookei	UM 87990	9.22	5.73	15.60	11.83	10.87	5.37	4.84	7.55	7.26	4.48
P. cookei	UM 87990 (L)	8.59	6.09	15.23	12.02	10.67	4.93	4.01	7.72	7.23	4.62
P. tricuspidens	MNHN BR 14523	--	--	13.57	--	--	--	4.85	6.54	6.82	3.62
P. tricuspidens	MNHN BR-15-L	9.23	5.96	14.47	11.68	10.28	4.92	4.84	7.41	7.08	3.60
P. tricuspidens	MNHN Br-13-L	9.36	5.87	15.20	11.73	10.88	5.17	5.16	8.01	7.21	3.33
P. tricuspidens	MNHN BR 13856	9.32	6.49	15.68	12.02	10.32	5.68	5.29	7.61	7.08	3.09
P. tricuspidens	MNHN BR 11865	--	--	--	--	--	--	--	--	--	--
P. tricuspidens	MNHN BR 11866	--	--	--	--	--	--	--	--	--	--
P. tricuspidens	MNHN BR 12569	10.22	6.8	15.08	12.39	11.68	5.66	5.39	8.72	8.23	3.36
P. tricuspidens	MNHN BR-12-L	--	--	--	--	--	--	--	--	--	--
P. tricuspidens	MNHN BR-16-L	10.7	6.62	16.44	13.04	12.04	5.64	5.62	8.60	7.86	3.87
P. tricuspidens	MNHN R 444	8.7	5.48	13.86	11.20	10.69	4.74	4.56	7.50	6.96	3.34
P. tricuspidens	MNHN R 450	7.72	5.41	12.96	10.44	--	3.92	3.79	7.13	6.34	3.57
P. tricuspidens	MNHN R 445	--	--	--	--	--	--	--	--	--	--
P. tricuspidens	MNHN R 440	--	--	--	--	--	--	--	--	--	--
P. tricuspidens	MNHN R 438	--	7.33	15.14	--	--	5.36	5.30	--	7.11	3.46
P. tricuspidens	MNHN R 446	10.51	7.21	15.49	12.54	11.34	5.85	5.11	8.13	6.99	3.01
P. tricuspidens	MNHN R 408	9.81	7.01	15.74	11.20	--	5.28	5.08	7.63	7.24	3.80
P. tricuspidens	MNHN R 407	10.01	8.08	16.75	12.82	11.75	5.80	5.50	8.45	7.68	4.26
P. tricuspidens	MNHN BR 5454	--	--	--	--	--	--	--	--	--	--
P. tricuspidens	MNHN R 523	--	--	--	--	--	--	--	--	--	--
P. tricuspidens	MNHN R 578	--	--	--	--	--	--	--	--	--	--
P. churchilli	P78.14.93	--	--	--	--	--	--	--	--	--	--
N. gidleyi	AMNH 17379	--	--	--	--	--	--	--	--	--	--
N. gidleyi	AMNH 17409	4.70	3.77	8.51	7.54	6.37	2.83	2.80	4.72	4.11	2.05
N. intermedius	USNM 309895	5.10	3.68	8.38	6.57	6.50	2.80	2.96	4.34	nm	1.89

a – numbers in parentheses correspond to measurement numbers in Sargis (2002b)

Table 4.17C. Measurements and shape variables of plesiadapid femora.

Taxon	Specimen	Le(9) [a]	MSW(15)	MSD(16)	LTP(27)	HMW	HMD	SSV	HShV	LTPV
P. cookei	UM 87990 (R)	85.70	7.21	6.69	17.66	9.49	9.10	2.51	2.22	1.58
P. cookei	UM 87990 (L)	87.50	7.20	6.36	18.01	9.47	9.37	2.56	2.23	1.58
P. tricuspidens	MNHN BR 14523	69.81	6.35	5.74	15.35	8.28	8.11	2.45	2.14	1.51
P. tricuspidens	MNHN BR-15-L	74.65	7.95	6.19	18.84	9.05	9.28	2.36	2.10	1.38
P. tricuspidens	MNHN Br-13-L	--	7.62	6.06	--	--	--	--	--	--
P. tricuspidens	MNHN BR 13856	77.18	8.00	7.36	17.93	9.18	9.63	2.31	2.11	1.46
P. tricuspidens	MNHN BR 11865	--	7.03	5.62	18.02	8.45	8.49	--	--	--
P. tricuspidens	MNHN BR 11866	--	7.27	Nm	18.95	9.96	10.33	--	--	--
P. tricuspidens	MNHN BR 12569	--	7.77	6.24	--	--	--	--	--	--
P. tricuspidens	MNHN BR-12-L	--	6.48	5.41	--	--	--	--	--	--
P. tricuspidens	MNHN BR-16-L	84.30	8.18	7.01	20.74	10.49	10.18	2.41	2.10	1.40
P. tricuspidens	MNHN R 444	74.70	7.71	6.01	17.48	9.69	9.34	2.40	2.06	1.45
P. tricuspidens	MNHN R 450	71.46	6.53	5.39	18.70	8.88	9.35	2.49	2.06	1.34
P. tricuspidens	MNHN R 445	--	7.32	6.69	--	--	--	--	--	--
P. tricuspidens	MNHN R 440	--	6.99	6.23	18.79	9.41	9.56	--	--	--
P. tricuspidens	MNHN R 438	75.89	7.56	6.04	17.20	--	9.92	2.42	--	--
P. tricuspidens	MNHN R 446	81.44	8.20	6.44	18.77	10.08	10.39	2.42	2.07	1.47
P. tricuspidens	MNHN R 408	80.44	7.66	6.46	17.86	9.71	9.98	2.44	2.10	1.50
P. tricuspidens	MNHN R 407	--	8.12	6.51	--	--	--	--	--	--
P. tricuspidens	MNHN BR 5454	--	--	--	--	8.45	8.35	--	--	--
P. tricuspidens	MNHN R 523	--	--	--	--	8.34	--	--	--	--
P. tricuspidens	MNHN R 578	--	--	--	--	--	--	--	--	--
P. churchilli	P78.14.93	--	5.20	4.94	12.75	6.30	6.50	--	--	--
N. gidleyi	AMNH 17379	--	--	--	10.96	5.82	6.09	--	--	--
N. gidleyi	AMNH 17409	--	4.26	4.22	--	--	--	--	--	--
N. intermedius	USNM 309895	--	3.98	3.69	--	--	--	--	--	--

a – numbers in parentheses correspond to measurement numbers in Sargis (2002b)

Table 4.18A. Measurements of the length and proximal ends of plesiadapid tibiae.

Taxon	Specimen	Le(29)[a]	LCL(30)	MCL(31)	LCW(32)	MCW(33)	PEW(34)	PED(35)
P. cookei	UM 87990	86.1	9.66	8.45	6	5.67	14.2	10.7
P. cookei	UM 87990 (L)	--	--	--	--	--	--	--
P. tricuspidens	MNHN BR 218	--	6.82	7.64	4.95	5.06	11.92	8.78
N .gidleyi	AMNH 17379	--	4.99	4.89	3.83	~2.7	~8.3	6.52
N. intermedius	USNM 442229	44.8	--	4.87	--	3.47	--	6.88
N. intermedius	USNM 309900	--	4.6	4.96	3.16	3.64	7.9	6.88

a – numbers in parentheses correspond to measurement numbers in Sargis (2002b)

Table 4.18B. Measurements of the distal ends of plesiadapid tibiae.

Taxon	Specimen	DEW(36)[a]	MML(37)	MMW(38)	TAW(39)	TAD(40)	TbCL(41)	MSW	MSD
P. cookei	UM 87990	8.56	2.04	3.33	4.76	7.36	~17	4.64	5.71
P. cookei	UM 87990 (L)	--	--	--	--	--	--	4.9	5.7
P. tricuspidens	MNHN BR 218	--	--	--	--	--	--	--	--
N .gidleyi	AMNH 17379	4.6	1.7	1.84	2.46	3.6	~11	2.39	3.36
N. intermedius	USNM 442229	4.3	--	--	2.25	--	--	2.46	2.88

a – numbers in parentheses correspond to measurement numbers in Sargis (2002b)

Table 4.19. Measurements of the fibulae of *Plesiadapis cookei*.

Taxon	Specimen	Le(42)[a]	DAL(43)	PED(44)	DED(45)	MSW	MSD
P. cookei	UM 87990 (L)	--	--	--	5.9	3	3.6
P. cookei	UM 87990 (R)	75.9*	--	7.55		2.9	3.5

a – measurement numbers correspond to those of Sargis (2002b)
* measurement does not include epiphyses

Table 4.20A. Measurements 1-10 and neck length variable of the astragali of select mammals (see Fig. 4.31). Ast-**01** – maximum proximodistal length, **02** – body proximodistal length, **03** – head and neck proximodistal length, **04** – fibular facet maximum dorsoplantar height, **05** – fibular facet proximodistal length, **06** – lateral tibial facet maximum proximodistal length, **07** – lateral tibial facet maximum mediolateral width, **08** – medial tibial facet maximum dorsoplantar height, **09** – medial tibial facet maximum proximodistal length, **10** – ectal (posterior calcaneoastragalar) facet proximodistal length, **NV** – neck length variable = Ast-03/Ast-01.

Taxon	**Specimen**	**Ast-01**	**Ast-02**	**Ast-03**	**Ast-04**	**Ast-05**	**Ast-06**	**Ast-07**	**Ast-08**	**Ast-09**	**Ast-10**	**NV**
P. cookei	UM 87990	13.02	8.14	4.64	4.90	6.80	7.25	5.62	3.40	8.40	5.47	0.36
P. tricuspidens	MNHN R 610	10.96	7.80	3.22	4.69	6.61	8.01	5.65	4.00	9.33	5.44	0.29
P. tricuspidens	MNHN R 5347	10.88	7.58	3.45	5.22	6.54	7.07	5.56	3.80	8.68	5.22	0.32
P. tricuspidens	MNHN BR 14537	11.05	7.24	4.16	4.54	6.52	7.35	5.51	3.17	8.42	5.48	0.38
P. tricuspidens	MNHN BR-59-L	--	7.83	--	4.93	6.68	7.88	4.97	3.90	6.96	4.92	--
P. tricuspidens	MNHN nn	9.97	7.47	3.00	4.07	5.82	6.75	4.89	4.24	7.75	4.95	0.30
P. n. sp.	L.Q. 1	11.05	8.10	3.60	4.30	6.39	7.28	5.38	3.71	7.66	5.34	0.33
P. n. sp.	L.Q. 2	10.18	7.68	3.30	4.21	6.21	7.13	4.90	3.37	7.87	5.25	0.32
P. rex	UM 94816	7.94	5.51	2.46	3.39	4.10	5.43	3.86	3.01	6.32	3.49	0.31
N. gidleyi	AMNH 17379	6.84	5.02	2.37	2.43	3.33	3.66	2.92	1.99	4.63	3.25	0.35
Pr. gaoi	UALVP 49120	7.90	5.24	2.68	3.02	4.01	4.76	3.22	2.67	5.83	3.73	0.34
G. moholi	HTB 747	7.50	4.45	2.97	1.94	3.64	6.52	3.01	2.63	5.45	2.69	0.40
L. tardigradus	HTB 750	6.59	4.69	1.91	2.34	2.79	4.55	2.98	1.53	4.63	2.25	0.29
Adapiform	Nn	14.40	9.80	4.30	5.00	6.50	6.9	7.90	4.70	9.60	6.00	0.30
C. volans	YPM 963	8.49	5.92	2.49	3.03	4.72	5.79	4.06	2.90	6.95	2.91	8.49
T. glis	SBU coll.	6.06	3.69	2.20	1.67	2.59	4.02	3.09	1.70	3.59	2.47	0.36
Deccanolestes	VPL/JU/NKIM/79	1.73	1.04	0.67	0.83	0.80	1.07	0.74	0.61	1.31	0.66	0.39

Table 4.20B. Measurements 11-18 of the astragali of select mammals (see Fig. 4.31). Ast-**11** – ectal (posterior calcaneoastragalar) facet mediolateral width, **12** – flexor fibularis groove mediolateral width, **13** – flexor fibularis groove proximodistal length, **14** – sustentacular (anterior calcaneoastragalar) facet proximodistal length, **15** - sustentacular (anterior calcaneoastragalar) facet mediolateral width, **16** - sustentacular (anterior calcaneoastragalar) facet width of contact with navicular facet, **17** – maximum mediolateral diameter of astragalar head, **18** – maximum dorsoplantar height of astragalar head.

Taxon	Specimen	Ast-11	Ast-12	Ast-13	Ast-14	Ast-15	Ast-16	Ast-17	Ast-18
P. cookei	UM 87990	2.92	4.96	4.47	5.72	2.90	3.50	6.94	3.68
P. tricuspidens	MNHN R 610	3.23	3.86	3.32	3.87	3.45	4.47	6.34	3.50
P. tricuspidens	MNHN R 5347	3.42	4.01	3.97	4.55	3.23	3.72	6.25	3.45
P. tricuspidens	MNHN BR 14537	3.08	3.48	3.08	4.21	2.78	2.91	6.45	3.54
P. tricuspidens	MNHN BR-59-L	3.00	nm	nm	nm	nm	--	--	3.18
P. tricuspidens	MNHN nn	2.92	3.20	3.06	3.91	2.81	2.46	5.35	3.58
P. n. sp.	L.Q. 1	2.97	3.97	3.79	4.61	2.97	2.79	6.03	3.41
P. n. sp.	L.Q. 2	2.74	3.85	3.38	4.39	2.80	3.16	5.75	3.30
P. rex	UM 94816	2.71	2.97	2.44	2.98	2.39	2.99	4.79	2.27
N. gidleyi	AMNH 17379	1.57	2.11	1.53	2.43	1.95	2.46	3.86	2.03
Pr. gaoi	UALVP 49120	2.38	3.41	2.36	3.60	2.05	2.58	4.48	2.20
G. moholi	HTB 747	1.79	1.60	1.32	4.06	1.91	2.59	2.88	2.19
L. tardigradus	HTB 750	1.31	1.74	1.54	2.32	1.62	2.23	3.53	1.80
Adapiform	nn	3.11	3.60	3.40	5.30	3.00	3.50	7.00	3.80
C. volans	YPM 963	1.69	2.06	2.24	3.47	1.95	1.97	3.83	2.63
T. glis	SBU coll.	1.67	0.99	1.48	2.47	1.02	1.69	2.79	1.69
Deccanolestes	VPL/JU/NKIM/79	0.45	0.77	0.61	0.73	0.41	0.50	0.80	0.41

Table 4.20C. Measurements 19-24 of the astragali of select mammals (see Fig. 4.31). Ast-**19** – angle between fibular facet and lateral tibial facet, **20** – angle between fibular facet and medial tibial facet, **21** – angle between medial and lateral tibial facets, **22** – angle between ectal (posterior calcaneoastragalar) facet and fibular facet, **23** – angle between ectal (posterior calcaneoastragalar) facet axis and lateral tibial facet axis, **24** – angle between major axis of head and plane of lateral tibial facet.

Taxon	**Specimen**	**Ast-19**	**Ast-20**	**Ast-21**	**Ast-22**	**Ast-23**	**Ast-24**
P. cookei	UM 87990	84	22	115	93	21	14
P. tricuspidens	MNHN R 610	77	37	131	92	23	20
P. tricuspidens	MNHN R 5347	87	53	132	93	21	11
P. tricuspidens	MNHN BR 14537	81	40	119	87	17	16
P. tricuspidens	MNHN BR-59-L	80	40	130	90	23	--
P. tricuspidens	MNHN nn	89	35	116	91	22	21
P. n. sp.	L.Q. 1	81	39	121	92	27	13
P. n. sp.	L.Q. 2	84	47	125	89	36	11
P. rex	UM 94816	92	43	116	93	22	18
N. gidleyi	AMNH 17379	78	27	112	93	26	17
Pr. gaoi	UALVP 49120	91	43	137	97	25	15
G. moholi	HTB 747	86	14	78	112	24	-14
L. tardigradus	HTB 750	84	14	79	100	41	9
Adapiform	Nn	97	31	79	96	22	14
C. volans	YPM 963	110	25	95	94	32	19
T. glis	SBU coll.	72	6	87	105	18	-9
Deccanolestes	VPL/JU/NKIM/79	97	45	97	91	63	5

Table 4.21A. Measurements 1-10 and distal end length variable of the calcanea of select memmals (see Fig. 4.34). Cc-**01** – maximum proximodistal length, **02** – tuber proximodistal length, **03** – distal calcaneum length, **04** – tuber maximum dorsoplantar depth, **05** – tuber proximal end dorsoplantar height, **06** – tuber proximal end mediolateral width, **07** – ectal facet proximodistal length, **08** – maximum length of arc of ectal facet, **09** – ectal facet mediolateral width, **10** – medial projection of sustentaculum from ectal facet lateral margin, **DV** – distal end length variable = Cc-03/Cc-01.

Taxon	Specimen	Cc-01	Cc-02	Cc-03	Cc-04	Cc-05	Cc-06	Cc-07	Cc-08	Cc-09	Cc-10	DV
P. cookei	UM 87990	18.80	11.80	6.50	7.50	6.70	5.50	6.80	7.90	3.31	7.90	0.35
P. tricuspidens	MNHN R 611	16.99	10.88	5.68	6.41	5.46	4.55	5.66	7.05	2.91	7.45	0.33
P. tricuspidens	MNHN R 414	18.39	12.22	6.10	7.40	6.57	5.20	6.43	7.78	3.25	7.53	0.33
P. churchilli	UM nn	12.30	7.94	4.09	4.67	4.39	2.96	4.00	4.93	2.14	5.10	0.33
N. gidleyi	AMNH 17379	10.43	6.48	3.49	4.10	3.84	2.84	3.20	4.60	1.85	4.53	0.33
L. tardigradus	HTB 750	8.62	4.82	3.63	3.64	2.57	1.60	3.57	5.17	1.70	3.54	0.42
C. volans	YPM 963	10.37	5.02	5.36	3.71	3.68	2.13	4.37	4.68	2.13	4.53	0.51
T. glis	SBU coll.	9.02	5.21	3.67	3.27	2.79	2.14	2.46	3.87	1.57	4.03	0.41
Deccanolestes	VPL/JU/IM/38	1.93	1.34	0.70	1.00	0.74	0.55	0.72	1.07	0.62	1.05	0.36

Table 4.21B. Measurements 11-19 of the calcanei of select mammals (see Fig. 4.34). Cc-**11** – proximodistal length from sustentaculum medial apex to distal end, **12** – sustentacular facet proximodistal length, **13** – sustentacular facet mediolateral width, **14** – lateral projection of peroneal tubercle from ectal facet lateral margin, **15** – proximodistal length from peroneal tubercle lateral apex to distal end, **16** – dorsoplantar depth of peroneal tubercle, **17** – diameter of calcaneocuboid facet perpendicular to sustentacular facet, **18** – diameter of calcaneocuboid facet parallel to sustentacular facet, **19** – distance from proximal margin of peroneal tubercle to distal end.

Taxon	Specimen	Cc-11	Cc-12	Cc-13	Cc-14	Cc-15	Cc-16	Cc-17	Cc-18	Cc-19
P. cookei	UM 87990	8.75	7.00	3.65	3.34	4.67	2.19	5.14	5.19	7.63
P. tricuspidens	MNHN R 611	5.52	5.43	3.11	3.00	4.70	2.11	4.23	4.33	6.36
P. tricuspidens	MNHN R 414	6.81	6.43	3.90	3.11	4.20	2.34	4.67	5.26	6.35
P. churchilli	UM nn	4.61	4.29	2.67	2.18	3.01	1.79	2.52	3.30	4.25
N. gidleyi	AMNH 17379	3.60	3.54	2.07	1.37	3.26	1.13	2.03	2.45	3.92
L. tardigradus	HTB 750	3.44	3.41	1.66	0.63	4.49	0.67	2.87	2.35	5.87
C. volans	YPM 963	3.92	4.22	1.84	1.40	2.28	1.46	2.77	3.25	5.49
T. glis	SBU coll.	2.81	2.98	1.36	0.74	3.90	0.53	1.59	1.99	4.88
Deccanolestes	VPL/JU/IM/38	0.78	0.45	0.94	0.49	0.36	0.32	0.66	0.63	0.65

Table 4.21C. Measurements 20-25 of the calcanei of select mammals (see Fig. 4.34). Cc-**20** – angle between ectal facet surface (parallel to its axis) and proximal part of sustentacular facet surface (parallel to its axis), **21** – angle between ectal facet axis and tuber, **22** – angle between peroneal tubercle and sustentaculum, **23** – mediolateral angle between calcaneocuboid facet and tuber axis, **24** – dorsoplantar angle between calcaneocuboid facet and tuber axis, **25** – angle between surface of proximal part of sustentacular facet (parallel to its axis) and distal part of sustentacular facet (parallel to its axis).

Taxon	Specimen	Cc-20	Cc-21	Cc-22	Cc-23	Cc-24	Cc-25
P. cookei	UM 87990	148	73	162	75	103	32
P. tricuspidens	MNHN R 611	150	73	166	73	100	21
P. tricuspidens	MNHN R 414	146	68	172	73	94	21
N. gidleyi	AMNH 17379	145	69	175	81	105	20
P. churchilli	UM nn	152	75	173	75	104	25
L. tardigradus	HTB 750	160	90	180	93	114	9
C. volans	YPM 963	150	69	180	78	101	29
Tupaia	SBU coll.	141	61	158	83	89	9
Deccanolestes	VPL/JU/IM/38	151	43	151	79	108	8

Table 4.22. Measurements and shape variables of plesiadapid cuboids.

Taxon	Specimen	Le	PEW	PED	PtgW	DEW	DED	CfA	GM[a]	PgV
P. cookei	UM 87990	8.22	6.22	4.98	2.04	5.01	5.16	58	4.88	0.42
P. tricuspidens	MNHN R 415	7.95	5.83	5.48	1.90	4.74	4.74	59	4.71	0.40
P. tricuspidens	Pell. Coll.	8.24	6.16	5.11	1.83	4.60	4.60	41	4.65	0.39
N. intermedius	USNM 442229	4.64	3.17	2.76	0.96	2.36	2.54	51	2.48	0.39

a-geometric mean of Le, PEW, PED, PtgW, DEW, and DED.

Table 4.23. Measurements and shape variables of plesiadapid metatarsals.

Taxon	Specimen	Bone	Length	PEW	PED	MSW	MSD	DEW	DED	HSV	SSV
P. n. sp.	MNHN nn	R MT I	16.60	6.00	3.90	2.90	2.60	4.30	Nm	nm	1.80
P. cookei	UM 87990 set 1	R MT I	17.80	5.80	4.20	2.70	2.50	4.40	4.10	0.071	1.92
cf. *P. churchilli*	UM nn	L MT I	12.88	4.15	3.20	2.11	1.81	3.05	2.60	0.160	1.89
N. intermedius	USNM 442229	L MT I	11.38	3.12	2.70	1.66	1.64	2.29	2.03	0.121	1.93
P. n. sp.	MNHN nn	L MT II	24.10	nm	nm	2.70	2.20	Nm	nm	nm	2.29
P. cookei	UM 87990 set 1	R MT II	--	--	--	2.80	2.70	5.10	4.30	0.171	--
P. cookei	UM 87990 set 1	L MT II	--	3.30	4.80	--	--	--	--	--	--
N. intermedius	USNM 442229	L MT II	--	1.71	2.78	1.61	1.21	--	--	--	--
N. intermedius	USNM 442229	?L MT II	--	--	--	--	--	2.67	1.98	0.299	--
P. n. sp.	MNHN nn	R MT III	24.70	3.30	nm	2.70	2.30	3.90	nm	nm	2.29
cf. *P. churchilli*	SMM P77.33.517	L MT III	--	2.08	3.40	1.85	1.68	--	--	--	--
P. cookei	UM 87990 set 1	R MT III	29.10	3.50	5.10	2.40	2.50	4.30	4.00	0.072	2.47
P. cookei	UM 87990 set 1	L MT III	--	3.20	5.10	2.80	2.40	--	--	--	--
N. intermedius	USNM 442229	L MT III	--	1.72	3.00	--	--	--	--	--	--
N. intermedius	USNM 442229	?L MT III	--	--	--	1.73	1.41	2.40	2.01	0.177	--
P. n. sp.	MNHN nn	R MT IV	25.70	4.00	nm	2.70	2.30	3.90	nm	nm	2.33
cf. *P. churchilli*	SMM P77.33.517	R MT IV	x	2.24	3.26	1.65	1.54	--	--	--	--
P. cookei	UM 87990 set 1	R MT IV	31.50	3.30	--	2.50	2.30	4.60	--	--	2.58
P. cookei	UM 87990 set 2	L MT IV	32.30	3.30	--	2.50	2.40	4.80	--	--	2.58
N. intermedius	USNM 442229	L MT IV	--	--	2.61	1.38	1.20	--	--	--	--
N. intermedius	USNM 442229	?L MT IV	--	--	--	1.65	1.38	2.34	1.98	0.167	--
P. n. sp.	MNHN nn	R MT V	19.00	5.20	nm	1.90	nm	3.70	nm	nm	Nm
cf. *P. churchilli*	SMM P77.33.517	L MT V	17.54	--	2.84	1.65	1.40	2.93	2.58	0.127	2.45
P. cookei	UM 87990	R MT V	--	6.40	3.60	3.30	2.40	--	--	--	--
N. intermedius	USNM 442229	L MT V	--	2.80	2.30	--	--	--	--	--	--
N. intermedius	USNM 442229	L MT V	--	--	--	1.30	1.27	2.47	1.98	0.221	--

Table 4.24. Features and measurements of the vertebral column of select mammals.

Taxon	Specimen	DpV	AcV	T#	L#	S#	Ca#	C l	Th l	L-l	S-l	Ca-l	C%l	T%l	L%l	S%l	Ca%l
Plesiadapis cookei	UM 87990	11?	12?	13?	7?	3	>20	43.7	113.9	92.525	31.60	154.72	21	55	45	15	75
Ignacius clarksforkensis	UM 82616	?	11?	12?	7?	3	>20	23.3	58.6	51.3	18.3	92.6	21	53	47	17	84
Tupaia glis	UMMZ 118389	10	9	13	6	3	24	15.4	43.9	41.5	13.1	56.7	18	51	49	15	66
Cynocephalus volans	USNM 56530	9	22	14	8	3-4	18	73.0	118.1	92.4	32.8	158.7	35	56	44	16	75
Cebuella pygmaea	UMMZ 160146	10	10	12	7	3	21	13.8	28.3	32.9	8.9	65.3	23	46	54	15	107
Saguinus mystax	UMMZ 160148	10	10	12	7	3	28	31.7	62.4	68.1	17.3	112.9	24	48	52	13	87
Saguinus oedipus	UMMZ 156437	10	10	12	7	3	32	23.9	62.6	67.5	16.9	117.1	18	48	52	13	90
Callimico goeldii	UMMZ 160149	?	10	12	8	3	29	28.6	59.9	79.2	16.9	106.1	21	43	57	12	76
Saimiri sciureus	UMMZ 122657	11	11	12	7	3	34	29.0	71.8	96.9	25.3	125.7	17	43	57	15	74
Eulemur fulvus	UMMZ 160910	10	11	12	7	3	19	46.5	102.5	104.7	31.8	198.1	22	49	51	15	96
Galago senegalensis	UMMZ 113351	11	11	12	6	3	26	23.1	45.5	40.0	14.9	100.5	27	53	47	17	118
Tarsius philipensis	UMMZ 95741	10	11	12	7	3	26	17.2	22.8	23.6	9.6	69.1	37	49	51	21	149
Sciurus niger	UMMZ TC 269	9	9	12	7	3	26	30.3	75.7	73.8	23.8	66.3	20	51	49	16	44
Spermophilus mexicanus	UMR 1716	9	9	11	7	3	22	15.0	37.6	35.7	11.7	35.4	20	51	49	16	48
Bison bison	UMMZ 114227	?	19	14	5	6	13	453.6	828.2	305	260	313.9	40	73	27	23	28
Hippopotamus amphibius	UMMZ 84041	?	18	14	4	5	9	631	1056	350.6	235.0	216.2	45	75	25	17	15
Petaurus brviceps	UMMZ 160143	10	11	12	7	2	23	15.0	39.1	45.3	9.1	77.9	18	46	54	11	92
Trichosurus vulpecula	UMMZ 157192	10	11	13	6	2	27	52.0	140.9	109.2	26.2	134.7	21	56	44	10	54

Table 4.25. Measurements of plesiadapid atlantes.

Taxon	Specimen	MW[a]	MH	CH	vCW	dCW	crIW	caIW	DL	VL	TPL
P. cookei	UM 87990 (Fig. 4.41A)	24.5	12.6	7.8	6.03	8.44	17.2	12.38	4.7	4.4	5.4
N. intermedius	USNM 442229 (138)*	13.12	6.99	5.65	3.36	5.21	10.22	6.37	2.21	1.38	2.66
N. gidleyi	AMNH 17388	--	--	--	--	--	10.65	7.15	--	1.83	--
N. gidleyi	AMNH 17379	16.4	8.52	6.13	4.39	6.36	11.55	7.67	2.76	2.08	3.75

a - If one half was broken, the mediolateral width of the intact half was measured and doubled to generate MW

*numbers in parentheses following USNM 442229 correspond to unique identifiers of the particular element (i.e., unofficial “sub-specimen” numbers) assigned by P. Houde during preparation of the specimen

Table 4.26. Measurements of plesiadapid cervical vertebrae.

Taxon	Specimen	Pos	Le	PEW[a]	PED	DEW	DED	CH	CW	LML	SPL	TPL
P. cookei	UM 87990 (Fig. 4.41B)	C2	11.9 (9.45)	11.16	4.20	7.12	3.62	5.56	5.40	--	4.92	--
P. cookei	UM 87990 (Fig. 4.41C)	C3?	6.33	6.74	3.11	7.92	3.75	4.27	5.27	5.05	1.05	5.78
P. cookei	UM 87990 (Fig. 4.41D)	C4?	5.92	7.43	2.57	7.99	3.13	--	--	--	--	--
P. cookei	UM 87990 (Fig. 4.41E)	C6	5.66	7.59	2.91	7.57	3.67	4.4	6.54	--	--	--
N. intermedius	USNM 442229 (134)*	C2	6.7 (5.04)	6.49	2.05	4.66	2.25	3.62	4.32	--	--	3.29
N. intermedius	USNM 442229 (144)*	C3?	3.27	3.72	1.7	3.88	1.92	2.85	4.5	--	0.7	--
N. intermedius	USNM 442229 (135)*	C6	3.6	3.65	1.69	3.54	1.63	3.06	4.63	1.92	0.8	--
N. gidleyi	AMNH 17388	C2	? (5.39)	--	--	4.30	--	--	--	--	--	--
N. gidleyi	AMNH 17388	C3	3.86	--	--	4.50	--	--	--	--	--	--
N. gidleyi	AMNH 17388	C4	3.73	--	--	--	--	--	--	--	--	--
N. gidleyi	AMNH 17379	7?	5.01	4.19	1.95	4.97	2.58	--	--	--	--	--

a – for vertebrae, “P” of PEW and PED refers to the cranial end of the element, while “D” of DEW and DED refers to the caudal end

*numbers in parentheses following USNM 442229 correspond to unique identifiers of the particular element (i.e., unofficial “sub-specimen” numbers) assigned by P. Houde during preparation of the specimen

Table 4.27. Measurements of plesiadapid thoracic and lumbar vertebrae.

Taxon	Specimen	Pos	Le	PEW[a]	PED	DEW	DED	CH	CW	LML	SPL	SPW	TPL	APL
P. cookei	UM 87990 (Fig. 4.42A)	T1?	6.59	7.45	3.07	9.24	3.46	--	--	--	--	--	--	na
P. cookei	UM 87990 (Fig. 4.42B)	T2?	--	6.14	2.8	--	--	3.9	4.3	5.93	--	--	--	na
P. cookei	UM 87990 (Fig. 4.42C)	T3?	8.45	6.11	3.25	8.00	3.32	--	4.65	7.44	--	--	--	na
P. cookei	UM 87990 (Fig. 4.42D)	T4?	9.01	--	--	7.34	4.57	--	--	--	--	--	--	na
P. cookei	UM 87990 (Fig. 4.42E)	T5?	8.8	6.8	5.2	7.90	5.24	--	--	--	--	--	5.5	na
P. cookei	UM 87990 (Fig. 4.42E)	T6?	8.55	6.4	4.7	7.71	5.35	--	--	--	--	--	5.3	na
P. cookei	UM 87990 (Fig. 4.42F)	T7?	8	5.67	4.69	--	5.25	--	4.77	--	--	--	--	na
P. cookei	UM 87990 (Fig. 4.42G)	T8?	8.94	5.86	4.8	--	4.78	--	6	--	--	--	5	na
P. cookei	UM 87990 (Fig. 4.42H)	T9?	8.86	5.88	4.94	7.24	4.54	--	5.39	6.62	--	3.62	5.1	na
P. cookei	UM 87990 (Fig. 4.42I)	T10?	9.13	6.3	4.34	8.53	4.19	4	4.04	7.6	4.9	4.14	3.51	na
P. cookei	UM 87990 (Fig. 4.42J)	T12?	10.13	--	--	8.34	5.79	--	4.6	8.45	--	--	na	--
P. cookei	UM 87990 (Fig. 4.42K)	T13?	10.29	7.57	4.62	8.29	--	3.78	--	7.86	4.8	6.46	na	--
N. intermedius	USNM 442229 (146)*	T1?	--	--	--	3.62	1.95	2.6	--	2.45	--	1.62	--	na
N. intermedius	USNM 442229 (145)*	T7?	4.2	3.15	1.93	3.63	1.93	2.73	3.43	3.16	>2.4	1.28	2.71	na
N. intermedius	USNM 442229 (136)*	T12?	5.24	3.46	2.21	4.13	2.23	2.42	3.03	3.8	--	2.94	na	1.3
N. intermedius	USNM 442229 (148)*	T13?	5.68	3.6	2.46	4.48	2.8	2.32	3.11	3.95	2.37	2.3	na	2.78
N. gidleyi	AMNH 17379	T1?	5.35	4.04	2.63	5.1	2.8	2.98	2.92	4.53	2.49	1.2	1.43	na
N. gidleyi	AMNH 17379	T2?	4.9	3.64	2.52	4.32	2.6	2.9	2.95	--	--	1.12	2.36	na
N. gidleyi	AMNH 17379	T12?	6.49	3.87	2.5	5	2.88	2.8	--	5.12	--	--	na	--
N. gidleyi	AMNH 17379	T13?	6.57	4.2	2.5	--	2.8	2.8	3.3	5.49	--	3.64	na	3.61
P. cookei	UM 87990 (Fig. 4.43A)	L1?	11.6	7.4	4.97	8.1	5.16	--	--	8.7	5.42	7.8	--	5.2
P. cookei	UM 87990 (Fig. 4.43B)	L3?	13.06	7.57	5.23	8.46	5.3	4.16	3.8	10.6	5.5	7.4	--	4.41
P. cookei	UM 87990 (Fig. 4.43C)	L4?	13.26	7.5	5.6	8.1	--	--	--	10.8	--	--	--	--
P. cookei	UM 87990 (Fig. 4.43D)	L5?	--	7.74	6.30	--	--	4.12	3.5	9.1	6.98	6.2	--	--
P. cookei	UM 87990 (Fig. 4.43E)	L6?	14.03	8.12	6.05	9.98	6.24	--	--	11.6	--	--	--	--
P. cookei	UM 87990 (Fig. 4.43F)	L7?	14.6	10.7	6.3	11.55	7	--	--	10.10	--	--	--	--
N. intermedius	USNM 442229 (137)*	L1?	5.93	4.1	2.46	4.71	2.78	2.5	3.31	4.97	2.9	2.27	--	2.12
N. intermedius	USNM 442229 (107)*	L7?	7.28	4.76	3.12	5.28	3.42	2.3	3.3	4.46	4.7	2.48	4.8	--
N. gidleyi	AMNH 17379	L1?	7.24	4.74	3	5.12	3.4	2.7	3.4	6.13	--	--	na	4.1
N. gidleyi	AMNH 17379	L2?	7.76	5.42	3.62	5.1	3.42	--	3.6	6.9	--	--	--	>2.7
N. gidleyi	AMNH 17379	L3?	8.3	5.2	3.13	5.46	3.26	2.53	3.75	7.35	3.1	~4.3	--	>2.5
N. gidleyi	AMNH 17379	L6?	9.3	5.63	3.93	5.42	3.75	2.94	3.9	7.56	--		--	--

a – for vertebrae, “P” of PEW and PED refers to the cranial end of the element, while “D” of DEW and DED refers to the caudal end

*numbers in parentheses following USNM 442229 correspond to unique identifiers of the particular element (i.e., unofficial “sub-specimen” numbers) assigned by P. Houde during preparation of the specimen.

Table 4.28. Measurements of plesiadapid sacral vertebrae.

Taxon	Specimen	Pos	Le	PEW[a]	PED	DEW	DED	CH	CW	LML	SPL	TPL
P. cookei	UM 87990	S1	11.8	10.7	4.12	7.9	--	--	--	8.2	>4.25	6
P. cookei	UM 87990	S2	9.6	8.3	--	7.6	--	--	--	9.5	--	5.6
P. cookei	UM 87990	S3	10.2	7.6	--	7.8	4.02	--	--	9.9	>4.5	4.6
N. intermedius	USNM 399898 (72)*	S1	6.1	4.55	2.98	3.74	--	2	3.1	4.8	>2.65	3.6
N. intermedius	USNM 399898 (72)*	S2	6.5	3.82	--	3.71	2.4	--	--	5.03	--	3
N. intermedius	USNM 399898 (72)*	S3	6.1	3.71	2.6	3.9	2.74		1.3	--	--	1.9
N. gidleyi	AMNH 17379	S1	6.92	6.82	3.3	4.78	--	--	3.35	4.45	--	5.67
N. gidleyi	AMNH 17379	S2	7.17	4.84	--	4.64	--	--	--	6.98	--	4.69
N. gidleyi	AMNH 17379	S3	6.55	4.88	--	5.06	2.8	1.75	2.7	--	--	2.22

a – for vertebrae, “P” of PEW and PED refers to the cranial end of the element, while “D” of DEW and DED refers to the caudal end

*numbers in parentheses following USNM 442229 correspond to unique identifiers of the particular element (i.e., unofficial “sub-specimen” numbers) assigned by P. Houde during preparation of the specimen

Table 4.29. Plesiadapid sacrum measurements.

Taxon	Specimen	Le	PEW[a]	DEW	LML	AFL	AFW
P. cookei	UM 87990	32.96	21.7	--	30.5	21.48	6.5
N. intermedius	USNM 399898 (72)*	19.25	11.73	--	--	9.73	4.04
N. gidleyi	AMNH 17379	21.87	17.97	--	--	11.86	4.61

a – for vertebrae, “P” of PEW and PED refers to the superior end of the element, while “D” of DEW and DED refers to the inferior end

*numbers in parentheses following USNM 442229 correspond to unique identifiers of the particular element (i.e., unofficial “sub-specimen” numbers) assigned by P. Houde during preparation of the specimen

Table 4.30. Plesiadapid caudal vertebrae measurements.

Taxon	Specimen	Pos	Le	PEW[a]	PED	DEW	DED	CH	CW	LML	TPL
P. cookei	UM 87990 (Fig. 4.45A)	Ca1	9.7	--	--	--	--	1.4	2.7	7.57	6.9
P. cookei	UM 87990 (Fig. 4.45B)	Ca4?	13.8	5.6	5.6	5.26	5.55	--	2.02	--	--
P. cookei	UM 87990 (Fig. 4.45C)	Ca6	21.3	6.8	5.7	7.9	5.8	--	--	--	--
P. cookei	UM 87990 (Fig. 4.45D)	Ca7	24.72	7.3	5.96	7.98	5.7	na	na	na	2.18
P. cookei	UM 87990 (Fig. 4.45E)	Ca8?	>22.79	7.06	5.14	--	--	na	na	na	--
P. cookei	UM 87990 (Fig. 4.45F)	Ca9?	25.46	6.3	5.6	--	--	na	na	na	--
P. cookei	UM 87990 (Fig. 4.45G)	Ca10?	>25.41	--	--	--	--	na	na	na	--
P. cookei	UM 87990 (Fig. 4.45H)	Ca11?	26.7	5.3	4.6	--	--	na	na	na	1.38
P. cookei	UM 87990 (Fig. 4.45I)	Ca12?	27.8	5.89	4.95	5.27	4.9	na	na	na	0.83
P. cookei	UM 87990 (Fig. 4.45J)	Ca13?	26	--	--	4.93	4.14	na	na	na	--
P. cookei	UM 87990 (Fig. 4.45K)	Ca14?	>21.4	--	--	4.5	4.1	na	na	na	--
P. cookei	UM 87990 (Fig. 4.45L)	Ca15?	21.9	3.57	3.45	3.8	3.34	na	na	na	--
P. cookei	UM 87990 (Fig. 4.45M)	Ca16?	20.88	3.09	3.13	3.43	3.09	na	na	na	na
P. cookei	UM 87990 (Fig. 4.45N)	Ca17?	19.85	3	2.96	3.05	2.9	na	na	na	na
P. cookei	UM 87990 (Fig. 4.45O)	Ca18?	17.84	2.81	2.73	2.7	2.53	na	na	na	na
P. cookei	UM 87990 (Fig. 4.45P)	Ca19?	13.48	2.36	2.32	2.05	2.15	na	na	na	na
P. cookei	UM 87990 (Fig. 4.45Q)	Ca20?	11.48	2.12	1.97	1.84	1.63	na	na	na	na
N. intermedius	USNM 442229 (149)*	Ca6	12.34	3.8	3.34	4.03	3.48	na	na	na	1.43
N. intermedius	USNM 442229 (138)*	Ca7	12.84	3.8	3.67	3.53	3.97	na	na	na	1.17
N. intermedius	USNM 442229 (149)*	Ca>7	12.6	--	--	--	--	na	na	na	--
N. intermedius	USNM 442229 (149)*	Ca>7	8.12	1.7	1.7	--	--	na	na	na	na
N. intermedius	USNM 442229 (149)*	Ca>7	12.4	--	--	--	--	na	na	na	--
N. intermedius	USNM 442229 (149)*	Ca>7	--	--	--	2.3	2.7	na	na	na	na
N. intermedius	USNM 442229 (149)*	Ca>7	--	2.12	2.5	--	--	na	na	na	na
N. gidleyi	AMNH 17379	Ca?1	6.32	3.99	2.98	4.37	3.35	1.48	2.08	4.5	--
N. gidleyi	AMNH 17379	Ca?2	6.35	4.2	2.9	4.8	2.67	1.43	1.99	5.83	--

a – for vertebrae, “P” of PEW and PED refers to the cranial end of the element, while “D” of DEW and DED refers to caudal end

*numbers in parentheses following USNM 442229 correspond to unique identifiers of the particular element (i.e., unofficial “sub-specimen” numbers) assigned by P. Houde during preparation of the specimen

Table 4.31. Measurements of *Plesiadapis cookei* sternebrae.

Taxon	Specimen	Pos	Le	PEW	PED	DEW	DED
P. cookei	UM 87990 (Fig. 4.48A)	Manubrium	17.27	18.6*	--	5.76	4.96
P. cookei	UM 87990 (Fig. 4.48B)	1?	12.5	4.4	5.15	6.02	4.1
P. cookei	UM 87990 (Fig. 4.48C)	2?	11.8	5.98	3.56	5.14	--
P. cookei	UM 87990 (Fig. 4.48D)	3?	--	5.86	3.35	--	--
P. cookei	UM 87990 (Fig. 4.48E)	4?	11.1	4.78	3.9	5.26	3.76

Table 4.32. Measurements of plesiadapid ribs.

Taxon	Specimen	number	side	Le[a]	PEW[b]	PED	NkL	MSW[c]	MSD	DEW	DED
P. cookei	UM 87990 (Fig. 4.49B)	a (2-9)	L	28.50	3.03	2.70	4.70	3.93	2.37	3.25	2.40
P. cookei	UM 87990	b (3-9)	L	>43.7	3.75	2.55	4.61	3.88	2.78	--	--
P. cookei	UM 87990	c (3-9)	L	--	3.67	3.60	3.83	>3.4	2.77	--	--
P. cookei	UM 87990	d (5-10)	L	--	3.38	2.63	3.10	--	--	--	--
P. cookei	UM 87990 (Fig. 4.49C)	e (6-10)	L	59.20	--	--	--	3.56	2.38	3.72	1.71
P. cookei	UM 87990	f (7-12)	L	>50.4	--	--	--	3.71	1.55	3.30	1.05
P. cookei	UM 87990 (Fig. 4.49A)	a (2-9)	R	--	3.23	2.80	4.85	3.86	2.44	--	--
P. cookei	UM 87990	g(?)	R	--	--	--	--	3.50	2.29	--	--
P. cookei	UM 87990	b (3-9)	R	--	3.50	2.27	4.40	--	--	--	--
P. cookei	UM 87990	c (3-9)	R	--	3.20	3.08	3.23	3.50	2.47	--	--
P. cookei	UM 87990	e (6-10)	R	--	3.09	1.80	2.87	--	--	--	--
P. cookei	UM 87990	h(11-13)	R	--	2.26	1.54	na	3.60	1.13	--	--
N. gidleyi	AMNH 17379	?	L	--	1.74	1.40	2.30	--	--	--	--
N. gidleyi	AMNH 17379	?	L	--	1.30	1.90	2.10	1.77	1.43	--	--
N. gidleyi	AMNH 17379	?	L	--	--	--	--	1.95	1.15	--	--
N. gidleyi	AMNH 17379	?	L	--	--	--	--	1.79	1.47	--	--
N. gidleyi	AMNH 17379	?	R	--	1.48	1.84	2.52	--	--	--	--

a – measured between rib tubercle and distal end of rib
b – refers to craniocaudal dimension of rib head
c – refers to maximum diameter of rib shaft in vicinity of angle

Table 4.33. Measurements of plesiadapiform body segments. Abbreviations: **Trk** – trunk (thorax +lumbus), **H** – humerus, **U** – ulna, **R** – radius, **MC III** – metacarpal 3, **F** – femur, **T** – tibia, **MT III** – metatarsal 3

Taxon	Specimen	Trk-L[a]	H-L	U-L	R-L	MC III-L	F-L	T-L	MT III-L
P. cookei	UM 87990	206.00	75.24	88.30	76.30	20.00	86.60	86.10	29.10
P. tricuspidens	Various	--	70.50	85.08	70.10	21.10	76.60	--	--
P. n. sp.	Various	--	--	--	--	19.70	77.80	--	24.70
P. insignis	Gingerich 1976	140.00	36.73	36.00	31.00	11.7	49.00	46.00	--
N. intermedius	USNM 442229	--	--	41.20	32.84	11.51	--	44.80	--
N. gidleyi	Various	--	--	--	--	12.02	--	--	--
C. simpsoni	UM 101963	57.92	21.60	28.12	~24.1	7.18	29.12	30(est)	7.40
I. clarkforkensis	Various	109.00	44.70	44.00	41.82	10.32	53.00	55.00	15.30
Micromomyidae	Various	--	14.58	--	17.13	3.72	15.02	19.03	5.09

Table 4.34. Plesiadapiform limb indices. Abbreviations: **Ltr-I** – limb-trunk index, **Br-I** – brachial index, **Cr-I** – crural index, **Int-I** – intermembral index, **Hf-I** – humerofemoral index, **Rt-I** – radiotibial index. See "other abbreviations" section of Introduction for explanations of indices.

Taxon	Specimen	Ltr-I	Br-I	Cr-I	Int-I	Hf-I	Rt-I
P. cookei	UM 87990	79	101	99	88	87	89
P. tricuspidens	various	--	99	--	--	92	--
P. insignis	Gingerich 1976	58	84	94	71	75	67
N. intermedius	USNM 442229	--	--	--	73	--	73
C. simpsoni	UM 101963	--	112	--	--	74	--
I. clarkforkensis	UM 82616	89	94	104	80	84	76
Micromomyidae	various	--	117	127	93	97	90

Table 4.35. Body segment lengths (mm) for comparison to plesiadapids. Abbreviations: **Trk** – trunk (thorax +lumbus), **H** – humerus, **U** – ulna, **R** – radius, **MC III** – metacarpal 3, **F** – femur, **T** – tibia, **MtIII** – metatarsal 3.

Taxon	Specimen	Trk-L	H-L	R-L	MC III-L	F-L	T-L	MT III-L
Tarsius philipensis	UMMZ 95741	46.39	27.60	35.10	10.49	55.46	53.36	11.63
Glaucomys volans	UMMZ 168356	56.70	26.41	30.34	5.21	31.20	35.34	12.08
Cebuella pygmaea	UMMZ 160146	61.21	30.12	28.40	8.18	34.58	36.70	14.08
Citellus mexicanus	UMR 1716	73.33	24.30	21.43	8.06	31.46	33.70	13.46
Petaurus breviceps	UMMZ 160143	84.40	33.54	41.06	7.34	41.04	44.90	7.14
Tupaia glis	UMMZ 118389	85.38	28.98	27.20	9.60	37.00	37.00	15.90
Galago senegalensis	UMMZ 113351	85.54	35.50	35.70	8.82	70.10	62.50	11.02
Callimico geoldic	UMMZ 160149	139.95	56.70	53.50	16.00	77.50	77.50	29.00
Saguinus mystax	UMMZ 160148	147.70	54.14	50.78	15.02	70.28	71.94	26.26
Sciurus niger	UMMZ TC 29	149.45	48.00	46.20	13.90	62.40	67.90	24.90
Nycticebus coucang	UMMZ 113355	166.68	69.70	67.80	12.00	81.70	76.90	14.30
Ateles geoffroyi	UMMZ 63171	202.50	194.00	207.00	47.30	200.00	187.00	54.60
Eulemur fulvus	UMMZ 160910	207.23	86.19	102.78	22.15	135.53	128.73	31.24
Cynocephalus volans	USNM 56530	210.49	105.40	121.90	28.39	122.96	120.17	24.58
Bradypodus tridactylus	UMMZ 64943	236.00	170.00	152.00	19.05	97.42	90.25	19.76
Trichosurus vulpecula	UMMZ 157192	250.08	80.20	92.90	18.53	104.06	102.02	22.50
Choloepus hoffmani	UMMZ 64940	308.50	125.40	140.00	29.00	126.50	117.54	29.00
Otolemur crassicandatus	UMMZ mean of 2	nm	55.66	68.44	13.21	92.03	85.22	16.15
Nycticebus coucang	UMMZ mean of 3	nm	69.84	76.52	13.66	81.52	79.22	15.90
Alouatta p. mexicana	UMMZ mean of 2	nm	149.79	157.65	31.00	148.61	136.54	38.32
Alouatta p. aequatorialis	UMMZ mean of 2	nm	148.77	160.53	34.20	154.70	136.15	40.46
Ateles geoffroyi	UMMZ mean of 2	nm	194.71	223.43	50.10	195.89	187.73	54.60
Galago senegalensis	UMMZ mean of 2	nm	35.50	35.70	8.82	70.10	62.50	11.02
Ptilocercus lowii	Le Gros Clark 1926	nm	21.53	22.93	6.12	27.16	28.73	8.90
Sciurus carolinensis	SBU MRd-10	nm	42.03	40.16	12.59	54.69	61.06	23.00
Cebuella pygmaea	SBU NC-01	nm	34.70	32.01	9.34	38.68	38.97	15.28
Saguinus oedipus	SBU NSg-06	nm	51.46	45.83	14.22	65.28	65.18	24.63
Tupaia glis	sbu specimen	nm	29.85	26.62	9.33	37.72	38.69	16.14
Saimiri sciureus	UMMZ 122657	nm	74.44	79.97	8.22	92.27	92.46	30.53
Alouatta caraya	UMMZ 124690	nm	136.01	144.30	30.34	145.60	126.30	37.70
Callicebus m. pallesceus	UMMZ 125576	nm	67.60	64.80	9.13	79.65	83.09	24.95
Saguinus oedipus	UMMZ 157195	nm	52.18	52.85	14.81	63.56	64.27	25.18
Petaurus breviceps	UMMZ 160143	nm	33.54	41.06	7.34	41.04	44.90	7.14
Cebuella pygmaea	UMMZ 160146	nm	30.12	28.40	8.18	34.58	36.70	14.08
Saguinus goeffroyi	UMMZ 160147	nm	52.94	55.52	15.27	66.56	69.40	25.58
Hylobates hoolock	UMMZ 160908	nm	220.80	255.10	61.44	203.60	182.00	46.64
Macaca f. mindanensis	UMMZ 161308	nm	119.50	137.20	31.54	141.98	131.85	43.14
Pan troglodytes	UMMZ 167199	nm	285.60	286.68	87.01	281.30	252.10	74.70
Varecia variegata	UMMZ 172669	nm	105.74	122.01	29.57	157.79	140.22	36.65
Cercopihecus cephus	UMMZ 39508	nm	111.32	123.85	28.64	140.88	137.78	42.20
Saimiri s. sciureus	UMMZ 46414	nm	67.68	66.06	15.66	80.91	82.13	27.18
Pan troglodytes	UMMZ 76276	nm	247.00	238.40	75.00	226.40	200.70	65.24
Cebus capucinus	UMMZ 77296	nm	100.91	104.99	22.53	123.72	118.02	37.50
Macaca mulatta	UMMZ 98651	nm	125.84	139.40	30.65	145.40	137.15	37.27

Table 4.36. Measurements for body mass estimation. Abbreviations: **Trk** – trunk (thorax +lumbus), **H** – humerus, **U** – ulna, **R** – radius, **MC III** – metacarpal 3, **F** – femur, **T** – tibia, **MT III** – metatarsal 3. **L** – length, **D** – parasagittal (anterposterior) diameter.

	P. cookei	***tricuspidens***	**n. sp.**	***rex***	***churchilli***	***insignis***	***N. intermedius***	***gidleyi***	***Pr. gaoi***	***Ignacius***	**Micromomyidae**
H-L	75.60	70.50	--	--	--	36.73	--	--	--	44.70	14.58
U-L	88.30	85.08	--	--	--	36.00	41.20	--	--	44.00	--
Mc-L	20.00	21.10	19.70	--	--	11.70	11.51	12.02	15.61	10.32	3.72
F-L	86.60	76.60	77.80	--	--	49.00	--	--	--	53.00	15.02
T-L	86.10	--	--	--	--	46.00	44.80	--	--	55.00	19.03
Mt-L	29.10	--	24.70	--	--	--	--			15.30	5.09
H-D	6.86	7.65	--	3.75	--	6.00	3.28	--	4.89	3.46	1.41
U-D	5.85	5.56	--	3.35	--	4.00	2.94	3.16	--	2.57	--
Mc-D	2.20	2.30	2.07	--	--	--	1.05	1.02	1.51	1.10	--
F-D	6.53	6.21	5.66	--	4.94	6.00	3.69	4.22	--	3.60	--
T-D	5.71	--	--	--	--	5.00	2.88	3.36	--	3.60	--
Mt-D	2.50	--	2.31	--	1.68	--	1.41	--	2.00	1.46	--

Table 4.37A. Parameters for Gingerich (1990) body mass prediction regressions (for use with $\log_{10}$ data). Abbreviations: **Trk** – trunk (thorax +lumbus), **H** – humerus, **U** – ulna, **R** – radius, **MC III** – metacarpal 3, **F** – femur, **T** – tibia, **MT III** – metatarsal 3. **L** – length, **D** – parasagittal (anterposterior) diameter.

Measurement	Slope	Y-intercept	r-square
H-L	2.6752	-1.5579	0.96850
U-L	2.7162	-1.8459	0.97185
Mc-L	2.4746	-0.0636	0.91817
F-L	2.654	-1.7511	0.96504
T-L	3.0581	-2.6904	0.96384
Mt-L	3.0604	-1.3562	0.92179
H-D	2.5984	1.2061	0.99246
U-D	--	--	--
Mc-D	2.7377	2.1836	0.98534
F-D	2.7418	1.0632	0.99138
T-D	2.6828	1.1929	0.98138
Mt-D	2.9932	1.7879	0.9661

Table 4.37B. Parameters for unpublished body mass prediction regressions (for use with $\log_e$ data). Abbreviations: **Trk** – trunk (thorax +lumbus), **H** – humerus, **U** – ulna, **R** – radius, **MC III** – metacarpal 3, **F** – femur, **T** – tibia, **MT III** – metatarsal 3. **L** – length, **D** – parasagittal (anterposterior) diameter.

Measurement	Slope	Y-intercept	r-square
H-L	2.3405	-2.9741	0.9104
U-L	2.3643	-3.2743	0.9008
Mc-L	2.0101	1.3759	0.8585
F-L	2.9254	-6.2301	0.8902
T-L	3.1823	-7.2873	0.8889
Mt-L	2.6293	-1.4216	0.7348
H-D	2.4992	2.8475	0.9451
U-D	2.3251	3.8611	0.901
Mc-D	2.421	5.5167	0.8919
F-D	2.6143	2.4022	0.9028
T-D	2.3251	3.8611	0.901
Mt-D	2.7378	5.0395	0.8938

Table 4.38A. Plesiadapid body mass estimates (gm) based on Gingerich (1990). Abbreviations: **Trk** – trunk (thorax +lumbus), **H** – humerus, **U** – ulna, **R** – radius, **MC III** – metacarpal 3, **F** – femur, **T** – tibia, **MT III** – metatarsal 3. **L** – length, **D** – parasagittal (anterposterior) diameter.

	P. cookei	*P. tricuspidens*	*P.* n. sp.	*P. rex*	*P. churchilli*	*P. insignis*	*N. intermedius*	*N. gidleyi*	*Pr. gaoi*
H-L	2934	2434	--	--	--	425	--	--	--
U-L	2752	2488	--	--	--	241	347	--	--
Mc-L	1432	1635	1379	--	--	372	365	406	776
F-L	2461	1777	1852	--	--	543	--	--	--
T-L	1687	--	--	--	--	248	229	--	--
Mt-L	1330	--	805	--	--	--	--	--	--
H-D	2394	3178	--	498	--	1691	352	--	994
U-D	--	--	--	--	--	--	--	--	--
Mc-D	1321	1492	1118	--	--	--	174	161	472
F-D	1984	1729	1341	--	923	1573	415	599	--
T-D	1670	--	--	--	--	1170	266	403	--
Mt-D	953	--	752	--	290	--	172	--	489

Table 4.38B. Plesiadapid body mass estimates (gm) based on unpublished primate sample. Abbreviations: **Trk** – trunk (thorax +lumbus), **H** – humerus, **U** – ulna, **R** – radius, **MC III** – metacarpal 3, **F** – femur, **T** – tibia, **MT III** – metatarsal 3. **L** – length, **D** – parasagittal (anterposterior) diameter.

	P. cookei	*P. tricuspidens*	*P.* n. sp.	*P. rex*	*P. churchilli*	*P. insignis*	*N. intermedius*	*N. gidleyi*	*Pr. gaoi*
H-L	1274	1082	--	--	--	235	--	--	--
U-L	1509	1383	--	--	--	181	249	--	--
Mc-L	1632	1818	1583	--	--	546	538	586	992
F-L	917	640	670	--	--	173	--	--	--
T-L	984	--	--	--	--	134	123	--	--
Mt-L	1705	--	1108	--	--	--	--	--	--
H-D	2122	2787	--	469	--	1518	336	--	911
U-D	2888	2566	--	790	--	1193	583	690	--
Mc-D	1678	1869	1448	--	--	--	280	261	675
F-D	1492	1308	1026	--	719	1196	335	476	--
T-D	2730	--	--	--	--	2005	556	796	--
Mt-D	1897	--	1528	--	639	--	396	--	1030

Table 4.38C. Summary of plesiadapid body mass estimates (in grams). Abbreviations: **L** – length, **D** – parasagittal (anteroposterior) diameter, **CV** – coefficient of variation.

	P. cookei	*P. tricuspidens*	*P.* n. sp.	*P. rex*	*P. churchilli*	*P. insignis*	*N. intermedius*	*N. gidleyi*	*Pr. gaoi*
Gingerich 1990									
L mean[a]	2099	2084	1345	--	--	366	314	406	776
L CV	33	21	32	--	--	35	24	--	--
D mean	1665	2133	1070	498	607	1478	276	388	651
Diameter CV	34	43	28	--	74	18	39	57	46
Total mean	1898	2105	1208	498	607	783	290	392	682
Total CV	34	29	34	--	74	77	32	46	37
% *P. cookei* (L)	100	99	64	--	--	17	15	19	37
% *P. cookei* (D)	100	128	64	30	36	89*	17	23	39
Primate sample									
L mean	1334	1231	1120	--	--	254	303	586	992
L CV	25	40	33	--	--	66	70	--	--
D mean	2134	2132	1334	630	679	1478	414	556	872
D CV	26	32	20	--	8	26	30	43	21
Total mean	1734	1681	1227	630	679	798	377	562	902
Total CV	35	43	29	--	8	87	41	37	18
% *P. cookei* (L) [a]	100	92	84	--	--	19	23	44	74
% *P. cookei* (D)	100	100	63	29	32	69*	19	26	41
% *P. cookei* (skull)[b]	100	102	--	--	--	11	11	21	19
% *P. cookei* (skull)[b]	100	102	--	--	--	6	6	13	13

a – mass prediction given as a percentage of *P. cookei's* estimated mass

b – percentage body mass of *P. cookei* assuming skull length and body mass scale isometrically

c – percentage body mass of *P. cookei* assuming $\log_{10}$ skull length relates to $\log_{10}$ body mass (in kg) by $y = 3.81x - 7.01$. This regression is based on the "horizontal primate" sample of Silcox et al. (in press)

***** Long bone diameters of *P. insignis* seem exceptionally large for its other dimensions and are likely to have been distorted by being crushed flat during preservation

APPENDIX TABLES

Appendix Table 4.1A. *Plesiadapis cookei* UM 87990 HRxCT scanned elements

Specimen	Type	Taxon	Bone	x-y res	z res	Scan #
UM 87990	fossil	*Plesiadapis cookei*	R scaphoid	18	18	12520
UM 87990	fossil	*Plesiadapis cookei*	R lunate	18	18	12520
UM 87990	fossil	*Plesiadapis cookei*	R astragalus	18	18	12544
UM 87990	cast	*Plesiadapis cookei*	L MC I	18	18	13553
UM 87990	cast	*Plesiadapis cookei*	set 2 L MC II	18	18	13553
UM 87990	cast	*Plesiadapis cookei*	set 2 R MC III	18	18	13553
UM 87990	cast	*Plesiadapis cookei*	set 2 R MC IV	18	18	13553
UM 87990	cast	*Plesiadapis cookei*	set 2 R MC V	18	18	13553
UM 87990	cast	*Plesiadapis cookei*	R pisiform	18	18	13553
UM 87990	cast	*Plesiadapis cookei*	R triquetrum	18	18	13553
UM 87990	cast	*Plesiadapis cookei*	L triquetrum	18	18	13553
UM 87990	cast	*Plesiadapis cookei*	R trapezoid	18	18	13553
UM 87990	cast	*Plesiadapis cookei*	L trapezoid	18	18	13553
UM 87990	cast	*Plesiadapis cookei*	L trapezium	18	18	13553
UM 87990	cast	*Plesiadapis cookei*	L hamate	18	18	13553
UM 87990	cast	*Plesiadapis cookei*	R MT I	18	18	13565
UM 87990	cast	*Plesiadapis cookei*	R distal MT II	18	18	13565
UM 87990	cast	*Plesiadapis cookei*	R MT III	18	18	13565
UM 87990	cast	*Plesiadapis cookei*	R MT IV	18	18	13565
UM 87990	cast	*Plesiadapis cookei*	R proximal mt5	18	18	13565
UM 87990	cast	*Plesiadapis cookei*	R cuboid	18	18	13565
UM 87990	cast	*Plesiadapis cookei*	L ectocuneiform	18	18	13565
UM 87990	cast	*Plesiadapis cookei*	R mesocuneiform	18	18	13565
UM 87990	cast	*Plesiadapis cookei*	R calcaneum	18	18	13565
UM 87990	cast	*Plesiadapis cookei*	L proximal mt2	18	18	13577
UM 87990	cast	*Plesiadapis cookei*	int. phalanx-b	18	18	13577
UM 87990	cast	*Plesiadapis cookei*	int. phalanx-e	18	18	13577
UM 87990	cast	*Plesiadapis cookei*	prox. phalanx-a	18	18	13577
UM 87990	cast	*Plesiadapis cookei*	prox.phalanx-d	18	18	13577
UM 87990	cast	*Plesiadapis cookei*	set 1 L MC II	18	18	13577
UM 87990	cast	*Plesiadapis cookei*	set 1 R MC II	18	18	13577
UM 87990	cast	*Plesiadapis cookei*	set 1 R MC III	18	18	13577
UM 87990	cast	*Plesiadapis cookei*	set 1 L MC III	18	18	13577
UM 87990	cast	*Plesiadapis cookei*	set 1 R MC IV	18	18	13577
UM 87990	cast	*Plesiadapis cookei*	set 1 R MC V	18	18	13577
UM 87990	cast	*Plesiadapis cookei*	dist. phalanx-c	18	18	test scan

Appendix Table 4.1B. *Plesiadapis cookei* UM 87990 medical CT scans

Specimen	Type	Taxon	Bone	x-y res	z res	Scan #
UM 87990	cast	*Plesiadapis cookei*	L femur	187.5	200	med-CT-1
UM 87990	cast	*Plesiadapis cookei*	L radius	187.5	200	med-CT-1
UM 87990	cast	*Plesiadapis cookei*	R fibula	187.5	200	med-CT-1
UM 87990	cast	*Plesiadapis cookei*	R tibia	187.5	200	med-CT-1
UM 87990	cast	*Plesiadapis cookei*	atlas	187.5	200	med-CT-2
UM 87990	cast	*Plesiadapis cookei*	axis	187.5	200	med-CT-2
UM 87990	cast	*Plesiadapis cookei*	lumbar vert 3	187.5	200	med-CT-2
UM 87990	cast	*Plesiadapis cookei*	lumbar vert 6	187.5	200	med-CT-2
UM 87990	cast	*Plesiadapis cookei*	R innominate	187.5	200	med-CT-3
UM 87990	cast	*Plesiadapis cookei*	L humerus	187.5	200	med-CT-3
UM 87990	cast	*Plesiadapis cookei*	L ulna	187.5	200	med-CT-3
UM 87990	cast	*Plesiadapis cookei*	L dent	187.5	200	med-CT-4
UM 87990	cast	*Plesiadapis cookei*	R dent	187.5	200	med-CT-4
UM 87990	cast	*Plesiadapis cookei*	caudal vert g	187.5	200	med-CT-4
UM 87990	cast	*Plesiadapis cookei*	caudal vert h	187.5	200	med-CT-4
UM 87990	cast	*Plesiadapis cookei*	caudal vert I	187.5	200	med-CT-4
UM 87990	cast	*Plesiadapis cookei*	caudal vert j	187.5	200	med-CT-4
UM 87990	cast	*Plesiadapis cookei*	caudal vert k	187.5	200	med-CT-4
UM 87990	cast	*Plesiadapis cookei*	caudal vert l	187.5	200	med-CT-4
UM 87990	cast	*Plesiadapis cookei*	caudal vert m	187.5	200	med-CT-4
UM 87990	cast	*Plesiadapis cookei*	caudal vert n	187.5	200	med-CT-4
UM 87990	cast	*Plesiadapis cookei*	caudal vert o	187.5	200	med-CT-4
UM 87990	cast	*Plesiadapis cookei*	caudal vert p	187.5	200	med-CT-4
UM 87990	cast	*Plesiadapis cookei*	caudal vert q	187.5	200	med-CT-4
UM 87990	cast	*Plesiadapis cookei*	cervical vert 3	187.5	200	med-CT-5
UM 87990	cast	*Plesiadapis cookei*	cervical vert 4	187.5	200	med-CT-5
UM 87990	cast	*Plesiadapis cookei*	cervical vert 6	187.5	200	med-CT-5
UM 87990	cast	*Plesiadapis cookei*	thoracic vert 1	187.5	200	med-CT-5
UM 87990	cast	*Plesiadapis cookei*	thoracic vert 2	187.5	200	med-CT-5
UM 87990	cast	*Plesiadapis cookei*	thoracic vert 3	187.5	200	med-CT-5
UM 87990	cast	*Plesiadapis cookei*	thoracic vert 4	187.5	200	med-CT-5
UM 87990	cast	*Plesiadapis cookei*	thoracic vert 5-6	187.5	200	med-CT-5
UM 87990	cast	*Plesiadapis cookei*	thoracic vert 7	187.5	200	med-CT-5
UM 87990	cast	*Plesiadapis cookei*	thoracic vert 8	187.5	200	med-CT-5
UM 87990	cast	*Plesiadapis cookei*	thoracic vert 9	187.5	200	med-CT-5
UM 87990	cast	*Plesiadapis cookei*	thoracic vert 10	187.5	200	med-CT-5
UM 87990	cast	*Plesiadapis cookei*	thoracic vert 13	187.5	200	med-CT-5
UM 87990	cast	*Plesiadapis cookei*	lumbar vert 1	187.5	200	med-CT-5
UM 87990	cast	*Plesiadapis cookei*	lumbar vert 4	187.5	200	med-CT-5
UM 87990	cast	*Plesiadapis cookei*	lumbar vert 5	187.5	200	med-CT-5
UM 87990	cast	*Plesiadapis cookei*	lumbar vert 7	187.5	200	med-CT-5
UM 87990	cast	*Plesiadapis cookei*	sternebra 5	187.5	200	med-CT-5
UM 87990	cast	*Plesiadapis cookei*	sternebra 6	187.5	200	med-CT-5
UM 87990	cast	*Plesiadapis cookei*	manubrium	187.5	200	med-CT-6
UM 87990	cast	*Plesiadapis cookei*	sternebra 1	187.5	200	med-CT-6
UM 87990	cast	*Plesiadapis cookei*	sternebra 2	187.5	200	med-CT-6
UM 87990	cast	*Plesiadapis cookei*	sternebra 3	187.5	200	med-CT-6
UM 87990	cast	*Plesiadapis cookei*	sternebra 4	187.5	200	med-CT-6
UM 87990	cast	*Plesiadapis cookei*	R clavicle	187.5	200	med-CT-6
UM 87990	cast	*Plesiadapis cookei*	L tibia	187.5	200	med-CT-7
UM 87990	cast	*Plesiadapis cookei*	L innominate	187.5	200	med-CT-7
UM 87990	cast	*Plesiadapis cookei*	R femur	187.5	200	med-CT-7
UM 87990	cast	*Plesiadapis cookei*	L fibula	187.5	200	med-CT-8
UM 87990	cast	*Plesiadapis cookei*	caudal vert a	187.5	200	med-CT-8
UM 87990	cast	*Plesiadapis cookei*	caudal vert c	187.5	200	med-CT-8
UM 87990	cast	*Plesiadapis cookei*	caudal vert d	187.5	200	med-CT-8
UM 87990	cast	*Plesiadapis cookei*	caudal vert e	187.5	200	med-CT-8
UM 87990	cast	*Plesiadapis cookei*	caudal vert f	187.5	200	med-CT-8
UM 87990	cast	*Plesiadapis cookei*	sacrum	187.5	200	med-CT-8
UM 87990	cast	*Plesiadapis cookei*	R humerus	187.5	200	med-CT-8
UM 87990	cast	*Plesiadapis cookei*	R scapula	187.5	200	med-CT-9

Appendix Table 4.2. Other plesiadapid material scanned

Specimen	Sub-spec	Locality	Type	Taxon	Bone	x-y res	z res	Scan #
UM 64588	-	Cedar Point Q, WY	fossil	*Plesiadapis rex*	L humerus	18	18	12544
UM 64588	-	Cedar Point Q, WY	fossil	*Plesiadapis rex*	L ulna	18	18	12544
UM 94816	-	Cedar Point Q, WY	fossil	*Plesiadapis rex*	L astragalus	18	18	12520
UM nn	-	Divide Q, WY	fossil	*Plesiadapis churchilli*	R calcaneum	18	18	12520
UM nn	-	Divide Q, WY	fossil	*Plesiadapis churchilli*	L MT I	18	18	13649
SMM P77.33.517	-	Wannagan Creek, ND	fossil	*Plesiadapis churchilli*	claw	10	10	13064
SMM P77.33.517	-	Wannagan Creek, ND	fossil	*Plesiadapis churchilli*	L MT III	18	18	13649
SMM P77.33.517	-	Wannagan Creek, ND	fossil	*Plesiadapis churchilli*	L MT V	18	18	13649
SMM P77.33.517	-	Wannagan Creek, ND	fossil	*Plesiadapis churchilli*	R MT IV	18	18	13649
AMNH 17379	-	Mason Pocket, CO	fossil	*Nannodectes gidleyi*	radius distal end	10	10	na
USNM 442229	139	Bangtail, MT	fossil	*Nannodectes intermedius*	L hamate	18	18	12520
USNM 442229	139	Bangtail, MT	fossil	*Nannodectes intermedius*	R hamate	18	18	12520
USNM 442229	139	Bangtail, MT	fossil	*Nannodectes intermedius*	R capitate	18	18	12520
USNM 442229	139	Bangtail, MT	fossil	*Nannodectes intermedius*	R scaphoid	18	18	12520
USNM 442229	139	Bangtail, MT	fossil	*Nannodectes intermedius*	R pisiform	18	18	12520
USNM 442229	139	Bangtail, MT	fossil	*Nannodectes intermedius*	L cuboid	18	18	12520
USNM 442229	assoc#2	Bangtail, MT	fossil	*Nannodectes intermedius*	distal phalanx	10	10	13064
USNM 442229	139	Bangtail, MT	fossil	*Nannodectes intermedius*	"lunate"	10	10	13589
USNM 442229	141	Bangtail, MT	fossil	*Nannodectes intermedius*	int. phalanx & sesamoid	10	10	13589
USNM 442229	na	Bangtail, MT	fossil	*Nannodectes intermedius*	R MC I	10	10	13589
USNM 442229	na	Bangtail, MT	fossil	*Nannodectes intermedius*	R MC III	10	10	13589
USNM 442229	na	Bangtail, MT	fossil	*Nannodectes intermedius*	L MC V	10	10	13589
USNM 442229	140	Bangtail, MT	fossil	*Nannodectes intermedius*	L distal MT I	18	18	13649
USNM 442229	140	Bangtail, MT	fossil	*Nannodectes intermedius*	L distal MT II	18	18	13649
USNM 442229	140	Bangtail, MT	fossil	*Nannodectes intermedius*	L distalMT III	18	18	13649
USNM 442229	140	Bangtail, MT	fossil	*Nannodectes intermedius*	L distal MT IV	18	18	13649
USNM 442229	140	Bangtail, MT	fossil	*Nannodectes intermedius*	L distal MT V	18	18	13649
USNM 442229	140	Bangtail, MT	fossil	*Nannodectes intermedius*	L proximal MT I	18	18	13649
USNM 442229	na	Bangtail, MT	fossil	*Nannodectes intermedius*	L proximal MT II	18	18	13649
USNM 442229	na	Bangtail, MT	fossil	*Nannodectes intermedius*	L proximal MT III	18	18	13649
USNM 442229	na	Bangtail, MT	fossil	*Nannodectes intermedius*	L proximal MT IV	18	18	13649
USNM 442229	na	Bangtail, MT	fossil	*Nannodectes intermedius*	L proximal MT V	18	18	13649
USNM 442229	115	Bangtail, MT	fossil	*Nannodectes intermedius*	L radius distal end	10	10	na
UALVP 49114	-	DW1 Alberta	fossil	*Pronothodectes gaoi*	L distal humerus	18	18	12550
UALVP 49120	-	DW2 Alberta	fossil	*Pronothodectes gaoi*	L astragalus	18	18	12520

Appendix Table 4.3. Other plesiadapiform elements scanned

Specimen	Sub-spec	Locality	Type	Taxon	Bone	x-y res	z res	Scan #
UM 101963	-	SC-62, WY	cast	*Carpolestes simpsoni*	L hallucal dist. phalanx	10	10	11370
UM 101963	-	SC-62, WY	cast	*Carpolestes simpsoni*	L hallucal prox phalanx	10	10	11370
UM 101963	-	SC-62, WY	cast	*Carpolestes simpsoni*	L hallucal metatarsal	10	10	11370
UM 101963	-	SC-62, WY	cast	*Carpolestes simpsoni*	L entocuneiform	10	10	11370
UM 101963	179	SC-62, WY	fossil	*Carpolestes simpsoni*	claw	10	10	13064
UM 101963	221	SC-62, WY	fossil	*Carpolestes simpsoni*	claw	10	10	13064
UM 101963	278	SC-62, WY	fossil	*Carpolestes simpsoni*	claw	10	10	13064
UM 101963	309	SC-62, WY	fossil	*Carpolestes simpsoni*	claw	10	10	13064
UM 82616	-	SC-62, WY	fossil	*Ignacius clarkforkensis*	manual claw	10	10	13064

Appendix Table 4.4. Comparative specimens HRxCT scanned

Specimen	Locality	Type	Taxon	Bone	x-y res	z spacing	Scan #
HTB 750	?	extant bone	*Loris tardigradus*	astragalus	18	18	na
HTB 750	?	extant bone	*Loris tardigradus*	calcaneum	18	18	na
SBU coll.	?	extant bone	*Tupaia glis*	astragalus	18	18	10800
SBU coll.	?	extant bone	*Tupaia glis*	calcaneum	18	18	12546
HTB 747	?	extant bone	*Galago moholi*	astragalus	18	18	na
YPM 963	?	extant bone	*Cynocephalus volans*	astragalus	18	18	13903
YPM 963	?	extant bone	*Cynocephalus volans*	calcaneum	18	18	13903
YPM 963	?	extant bone	*Cynocephalus volans*	pedal claw 1	18	18	13903
YPM 963	?	extant bone	*Cynocephalus volans*	pedal claw 2	18	18	13903
VPL/JU/NKIM/52	Naskal intertrappean, India	fossil	*Deccanolestes hislopi*	L astragalus	10	10	12195
VPL/JU/NKIM/38	Naskal intertrappean, India	fossil	*Deccanolestes hislopi*	R calcaneum	10	10	12195
VPL/JU/NKIM/79	Naskal intertrappean, India	fossil	*Deccanolestes hislopi*	L distal humerus	10	10	12195
unpublished	Fayum, Egypt	fossil	adapiform	Astragalus	18	18	12546
SBU MRd-10	?	extant bone	*Sciurus carolinensis*	M & Lt ped. sesamoids	10	10	13589

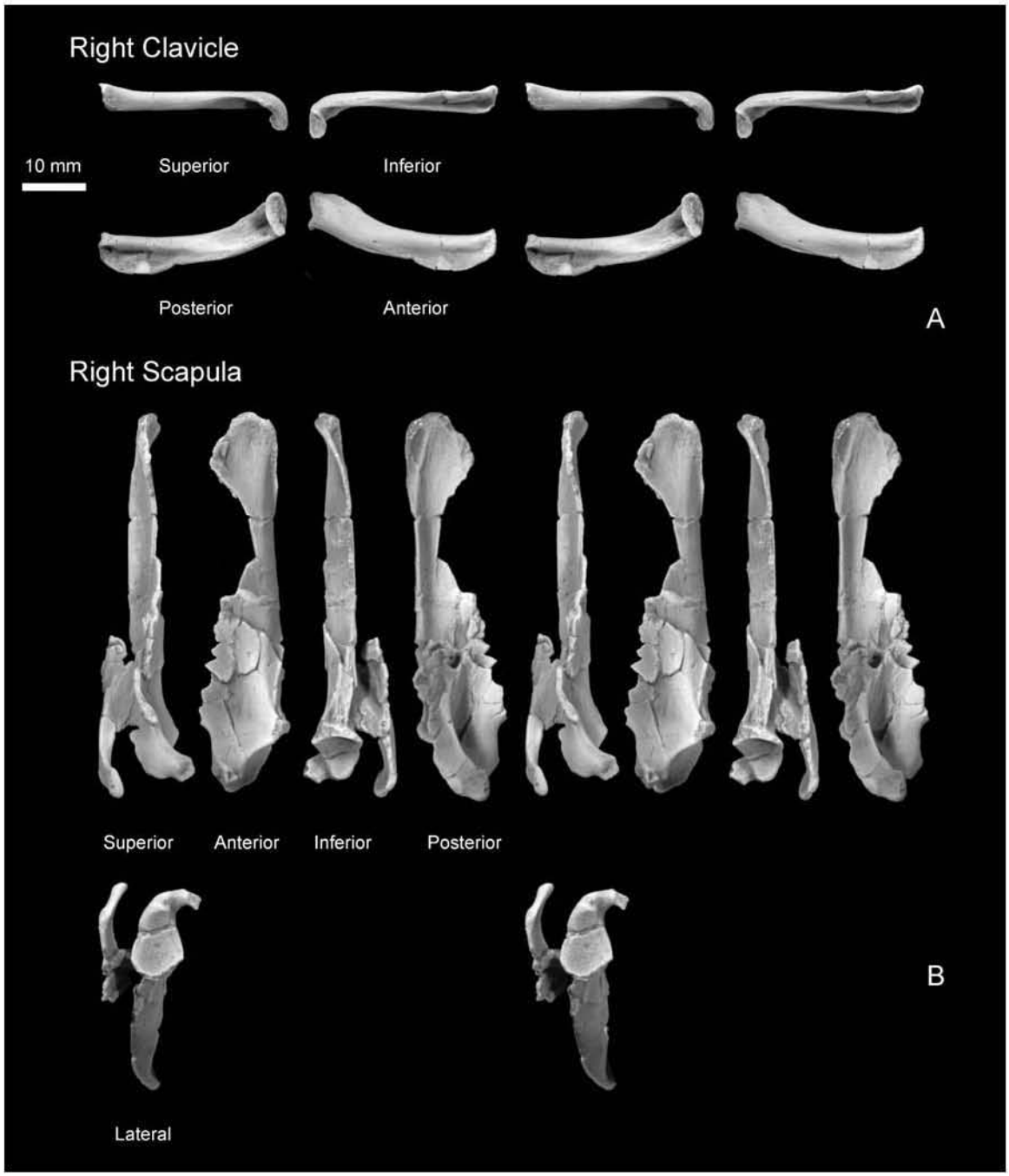

Figure 4.1. *Plesiadapis cookei* (UM 87990). Stereophotographic views of A, right clavicle; and B, right scapula. The left clavicle is represented by the middle third of its shaft, but is not illustrated.

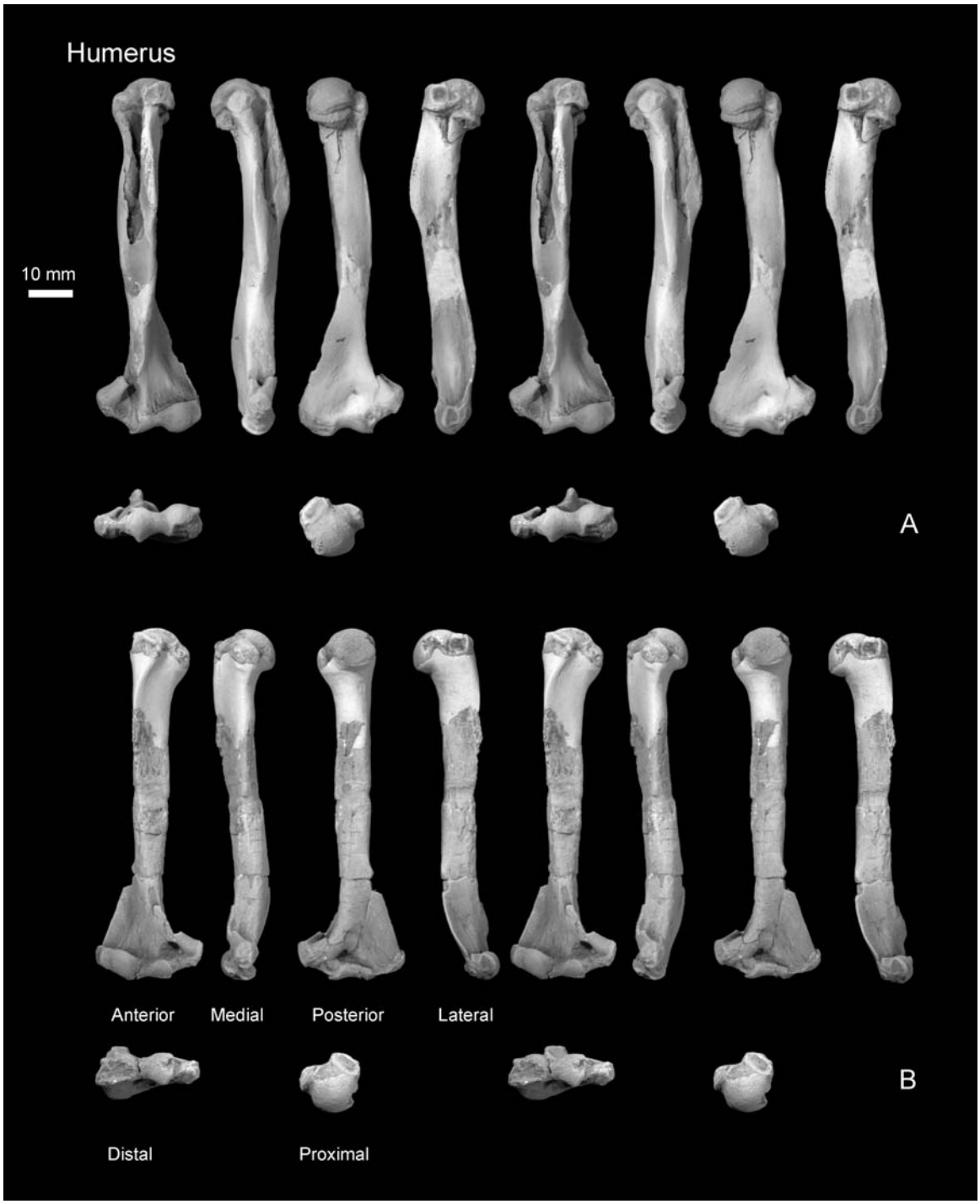

Figure 4.2. *Plesiadapis cookei* (UM 87990). Stereophotographic views of A, left humerus; and B, right humerus. Note that a segment of the left shaft is reconstructed just proximal to the supinator crest. Enough of the shaft remains to be certain that the original length has not been changed and that the proximal segment is correctly oriented with respect to the anteroposterior anatomical plane of the distal segment. The proximal quarter of the right humerus shaft is missing. It is not clear how much evidence supports the details of its reconstruction.

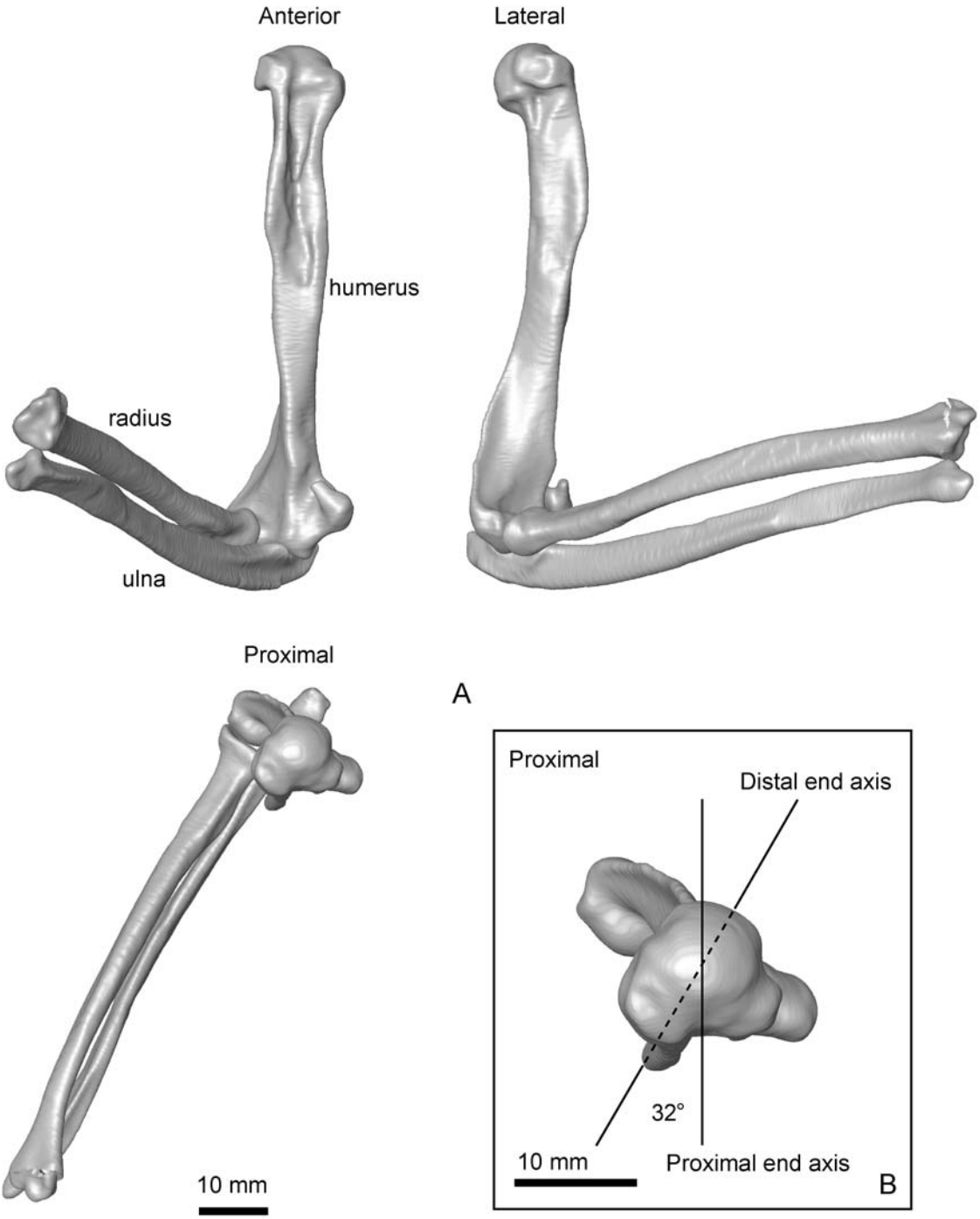

Figure 4.3. Surface reconstructions of the humerus, radius, and ulna of *Plesiadapis cookei* (UM 87990) using CT data (CT image resolution = 0.18(x) x 0.18(y) x 0.20(z) mm). A, the three bones are shown in anterior, lateral, and proximal views, and articulated so that respective joint surfaces are maximally overlapping. Note that the forearm is flexed and projects laterally relative to the proximodistal and anteroposterior axes of the proximal end of the humerus, respectively. B, proximal view of humerus. Note that the axis of the distal end is rotated 32° lateral to the axis of the proximal end, explaining the lateral projection of the radius and ulna.

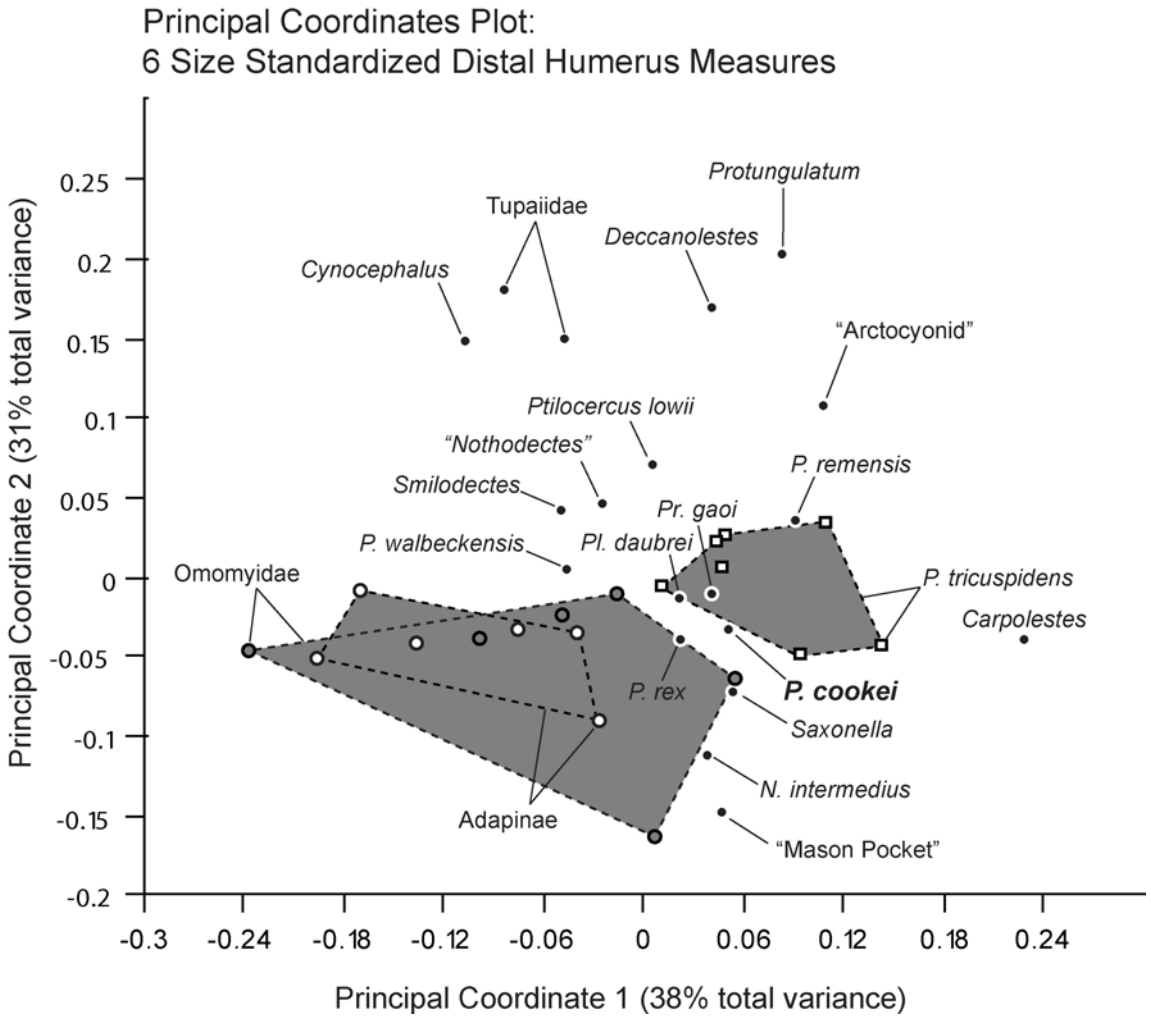

Figure 4.4. Plot of principal coordinates based on an analysis using a Euclidean distance matrix calculated from distal humerus shape variables of Table 5.3C. See Szalay and Dagosto (1980) for some of the raw data. As discussed in methods, shape variables are log ratios of each of six raw measurements (TW, TH, CaW, TL, CaL, and EEC) to the geometric mean of all six measurements for a given specimen. Overlapping gray polygons encompass all omomyoid, adapoid and plesiadapid points. Note that fossil euprimates and plesiadapids overlap with each other. Non-plesiadapid and non-euprimate euarchontans have lower PC II scores, along with primitive eutherians and "*Nothodectes.*" The position of the last noted specimen may indicate that it does not belong to *Nannodectes gidleyi* (AMNH 17379). Another humerus not plotted here (because it is incomplete) is also associated with *N. gidleyi*. It is nearly identical to that of *N. intermedius* and seems more likely to have been a component of the skeleton of *N. gidleyi* than to have been associated with the humerus of "*Nothodectes.*" Non-plesiadapid plesiadapoid plesiadapiforms *Saxonella* and *Carpolestes* plot with higher PC1 and PC2 values than other taxa.

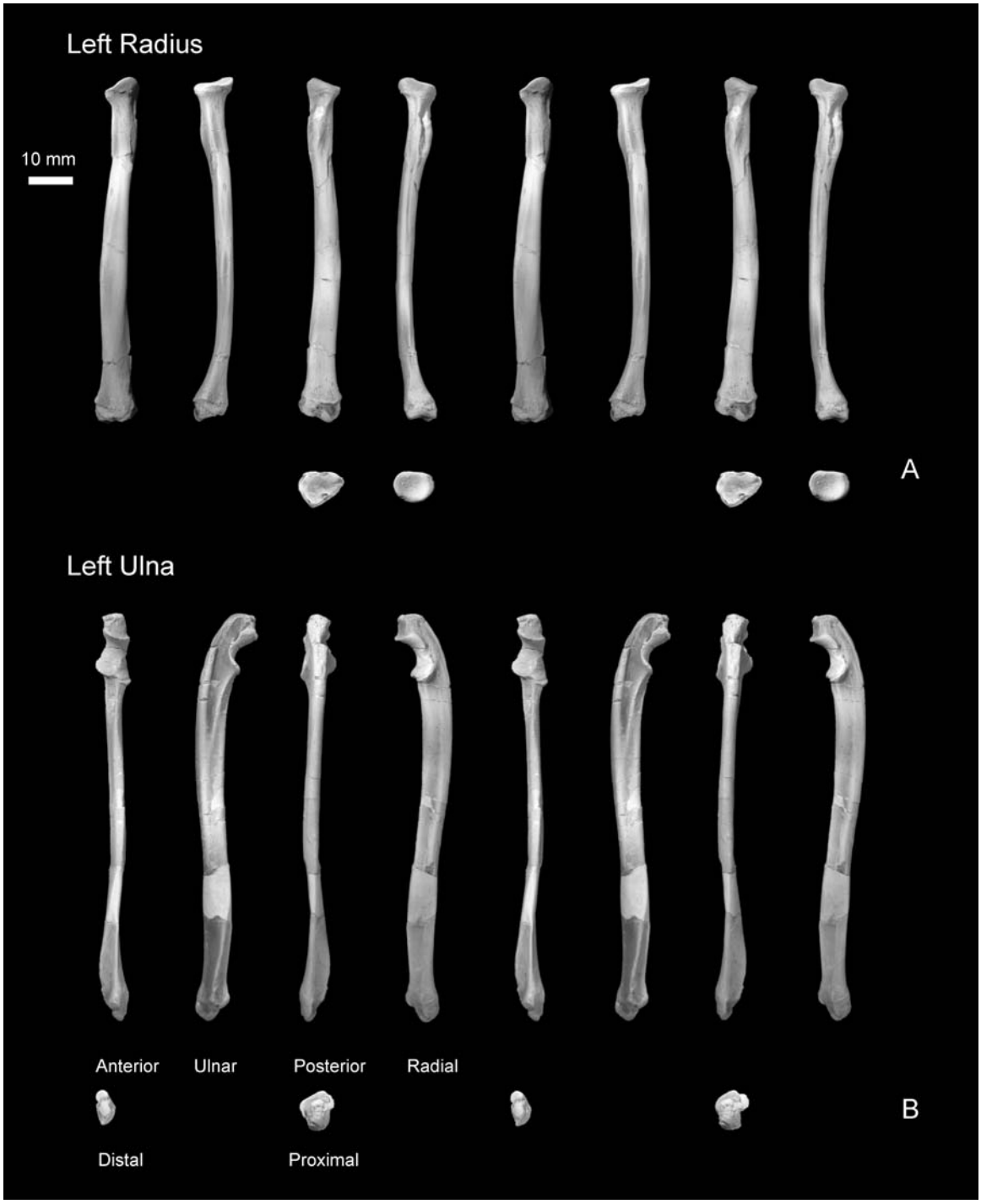

Figure 4.5. *Plesiadapis cookei* (UM 87990). Stereophotographic views of A, left radius; and B, left ulna. Note that the distal epiphysis of the right radius has been attached to the left radius diaphysis. Thus this element does not correctly represent the true morphology of the radius of *P. cookei* (see Fig. 4.6). A distal segment of the ulnar shaft is missing and reconstructed. It is not clear how much evidence supports the details of its reconstruction.

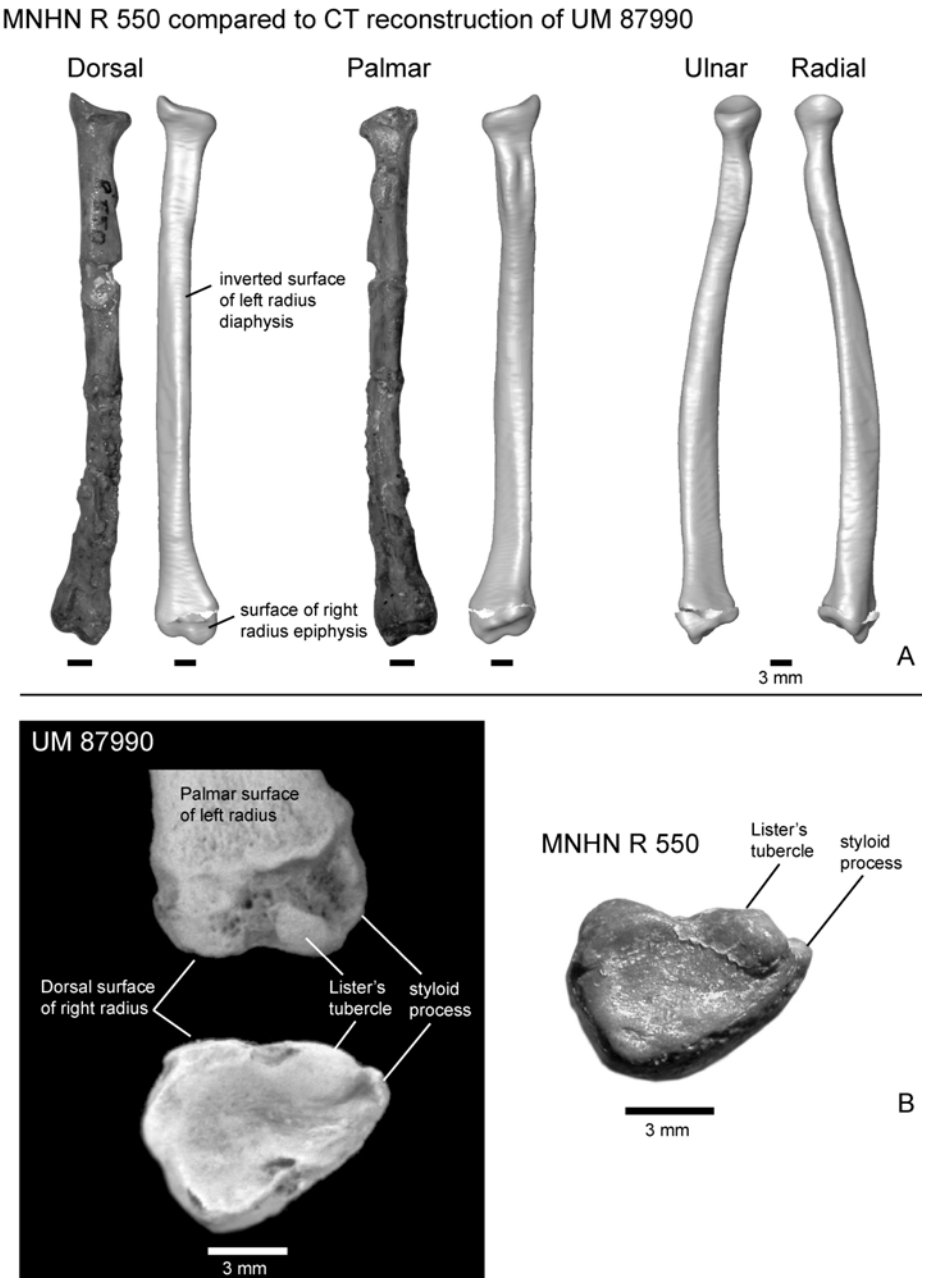

Figure 4.6. Surface reconstructions of the radius of *Plesiadapis cookei* (UM 87990) using CT data [CT image resolution = 0.18(x) x 0.18(y) x 0.20(z) mm] compared to the radius of *P. tricuspidens* (MNHN R 550). A, the diaphysis of the CT reconstruction of the left radius of UM 87990 was separated from the right distal epiphysis and inverted to represent the right diaphysis. These two segments were then repositioned as they are thought to have been in life. Note the similarity between the distal ends of the photograph of *P. tricuspidens* and the reconstructed radius of *P. cookei*. The distal articular surfaces face ulnarly and palmarly to a similar degree. B, detailed comparisons of the distal epiphyses of the radii of *P. cookei* and *P. tricuspidens*. The styloid process, Lister's tubercle and a more ulnarly positioned tubercle allow confident identification of the *P. cookei* element as belonging to the right side.

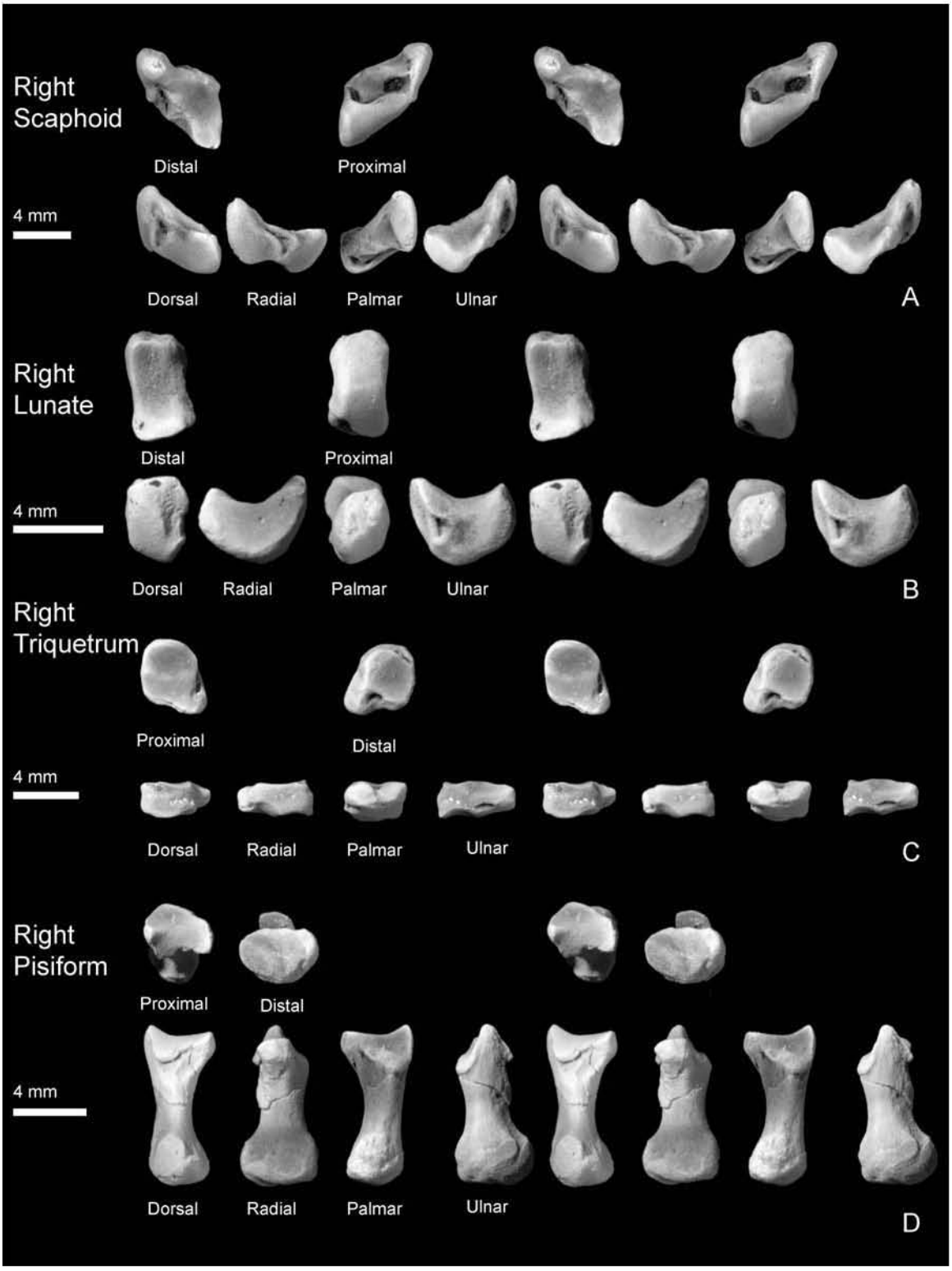

Figure 4.7. *Plesiadapis cookei* (UM 87990). Stereophotographic views of the proximal row of carpal bones. A, right scaphoid; B, right lunate; C, right triquetrum; and D, right pisiform.

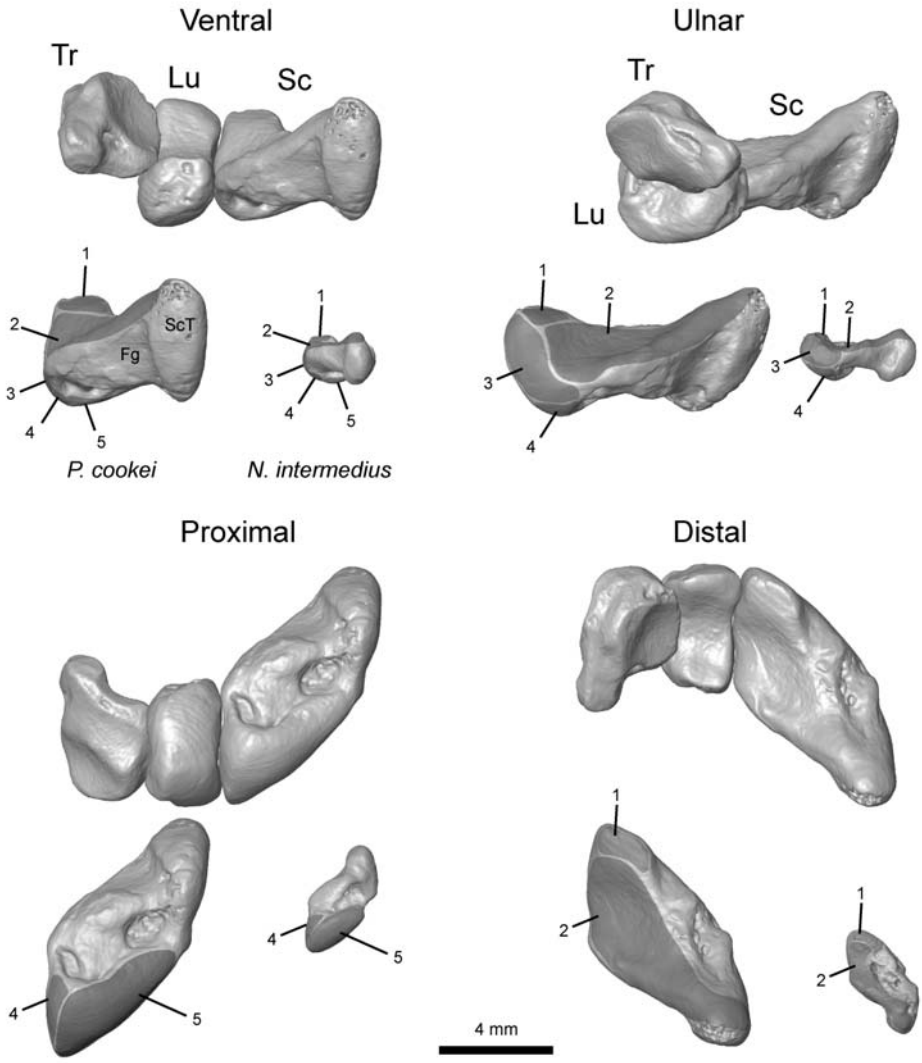

Figure 4.8. Surface reconstructions of the proximal row of carpal bones of *Plesiadapis cookei* (UM 87990), with comparison to the scaphoid of *Nannodectes intermedius* (USNM 442229), based on HRxCT reconstructions [HRxCT resolution = 0.018 mm (cubic voxels)]. Articular surfaces and other regions are identified with gray shading and labeled with numbers on the scaphoids: 1 – shelf-like facet that may contact distal carpal row during dorsiflexed postures of the midcarpal joint, 2 – articular surface for distal carpal bones including hamate, capitate, centrale, trapezoid and trapezium, 3 – lunate facet, 4 – possibly a non-articular area or extension of lunate facet (this appears to be the area Beard (1989) interpreted as the triquetrum facet of the *N. intermedius*, but this interpretation is almost certainly incorrect), and 5 – radius articular facet. Abbreviations: Fg – flexor tendon groove, Lu – lunate, Sc – scaphoid, ScT – scaphoid tubercle, and Tr – triquetrum.

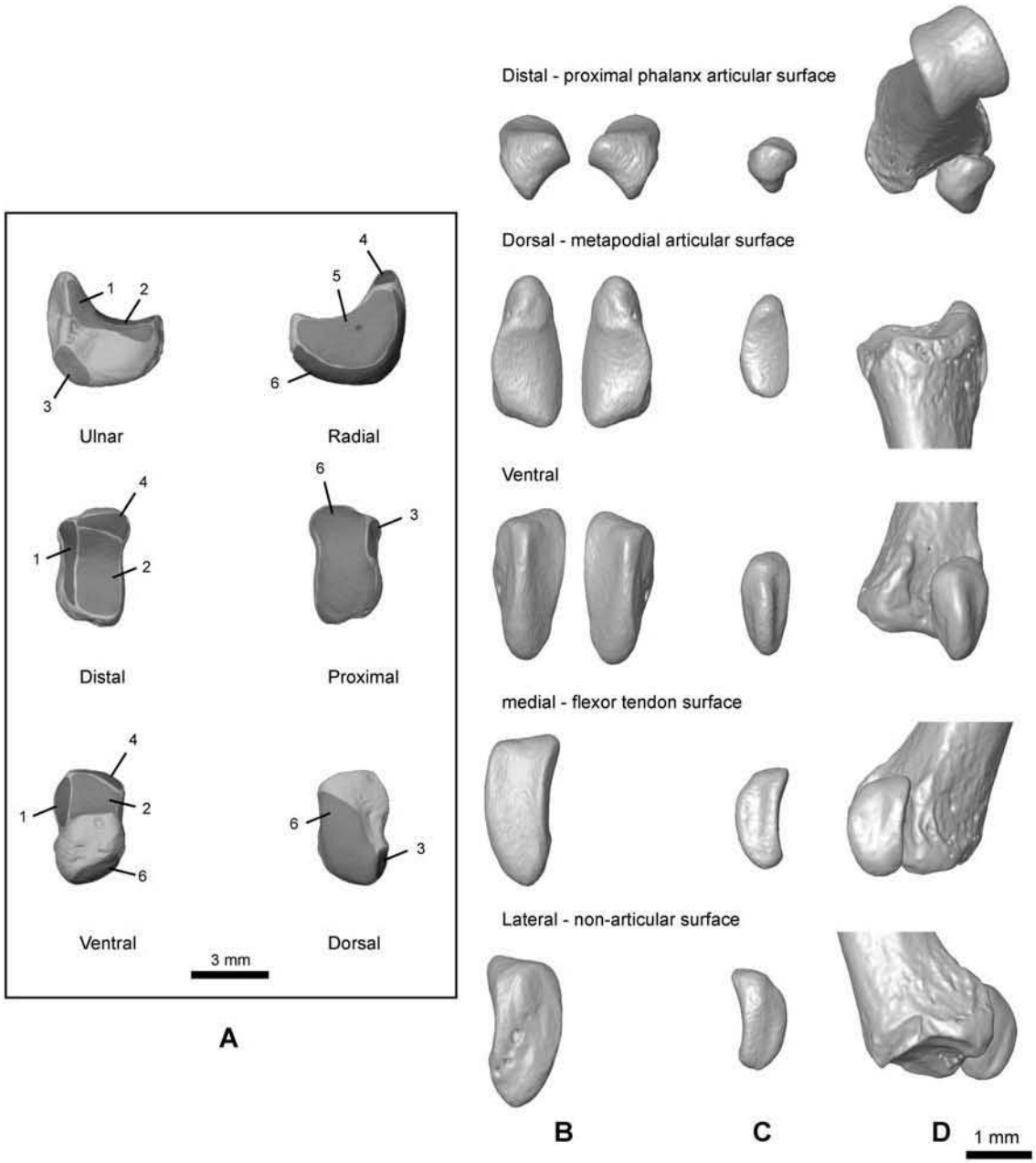
Ulnar
Radial
Distal
Proximal
Ventral
Dorsal
3 mm
A
Distal - proximal phalanx articular surface
Dorsal - metapodial articular surface
Ventral
medial - flexor tendon surface
Lateral - non-articular surface
B
C
D
1 mm

Figure 4.9

Figure 4.9. Surface reconstructions of lunates and sesamoids based on HRxCT data. A, right lunate of *Plesiadapis cookei* (UM 87990). Articular surfaces and other regions are identified with gray shading and labeled with numbers: 1 – triquetrum facet, 2 – hamate facet, 3 – ulna facet, 4 – shelf-like facet that may contact distal carpal row during dorsiflexed postures of the midcarpal joint, 5 – scaphoid facet, and 6 – radius facet. B, medial and lateral pedal sesamoids of *Sciurus carolinensis* SBU MRd-10. C, "lunate" of *Nannodectes intermedius* (USNM 442229) (Beard, 1989). Note the similarity of this bone to the leftmost pedal sesamoid of *Sciurus*. D, a second "lunate" adherent to an intermediate phalanx of USNM 442229, not mentioned in Beard (1989). While slightly different, the bones in C and D appear to represent the same element from the same side. HRxCT resolution for A = 0.018 mm (cubic voxels), and for B-D = 0.010 mm (cubic voxels).

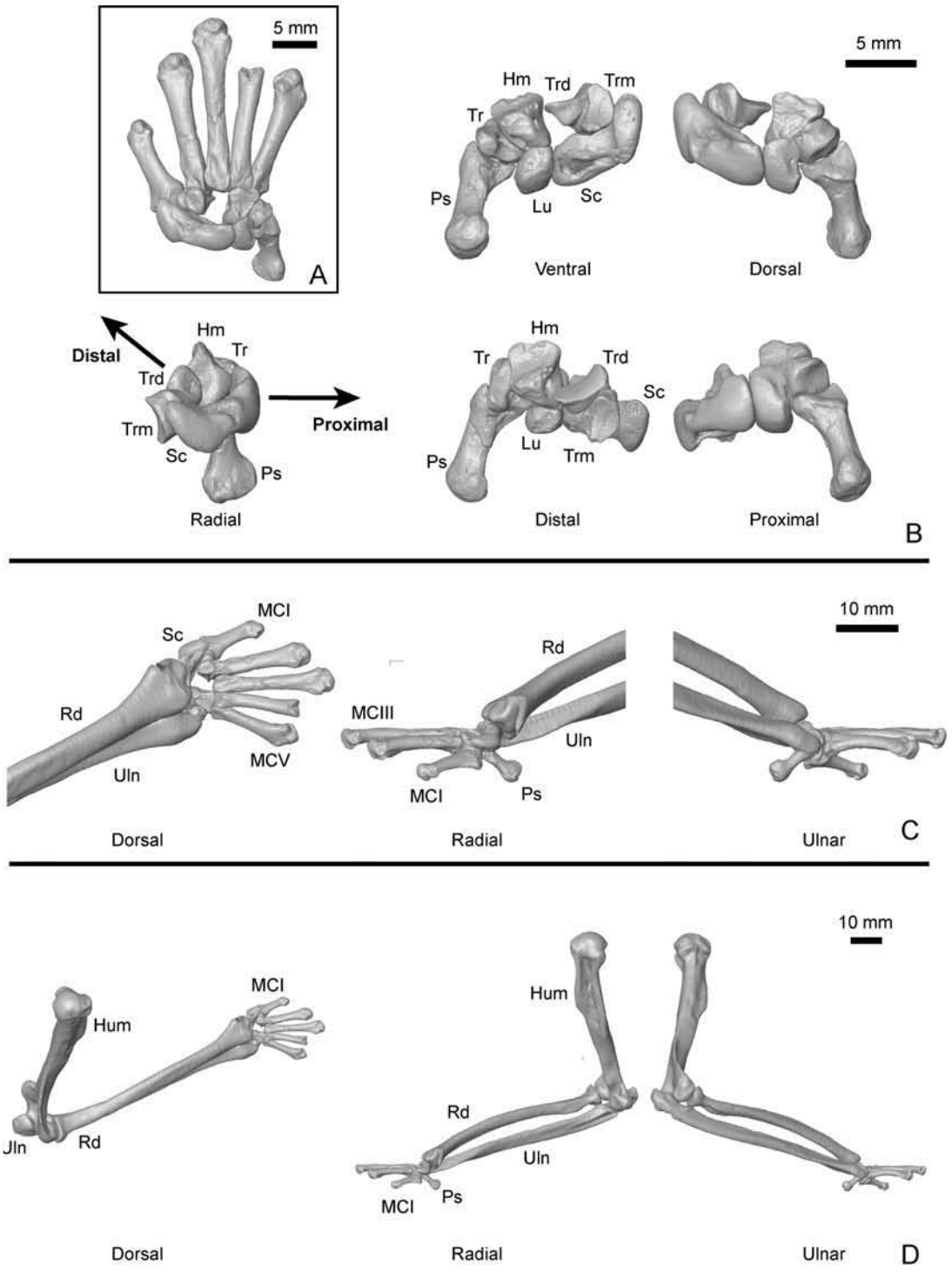
5 mm
A
5 mm
Hm
Trd
Trm
Tr
Ps
Lu
Sc
Ventral
Dorsal
Distal
Hm
Tr
Trd
Proximal
Trm
Sc
Ps
Radial
Hm
Tr
Trd
Sc
Lu
Trm
Ps
Distal
Proximal
B
MCI
Sc
Rd
MCV
Uln
10 mm
Rd
MCIII
Uln
MCI
Ps
Dorsal
Radial
Ulnar
C
10 mm
MCI
Hum
Jln
Rd
Hum
Rd
Uln
MCI
Ps
Dorsal
Radial
Ulnar
D

Figure 4.10

Figure 4.10. Surface reconstructions of forelimb bones from HRxCT data of *Plesiadapis cookei* (UM 87990). A, right carpus and metacarpus [HRxCT resolution = 0.018 mm (cubic voxels)]. The capitate and centrale are not preserved for UM 87990 (this view therefore illustrates how preserved bones of the carpus and metacarpus can be fit together, despite missing elements). B, various views of carpus. Note in radial view that the proximodistal axis of the articular surfaces for the metacarpals face dorsally relative to the articular surface of the radius. This suggests the hand was habitually dorsiflexed. C, reconstructed right forearm with metacarpals (based on 0.018 mm resolution scans with cubic voxels) and forearm bones (based on a 0.18(x) x 0.18(y) x 0.20(z) mm scan). Joint surfaces are positioned so that they are maximally overlapping. Note that because of the palmar orientation of the distal articular surface of the radius, the degree of natural dorsiflexion is muted from what is indicated by analysis of the carpal bones alone. D, views from "C" with right humerus included. Note that the palmar surface of the hand is somewhat supinated relative to the humerus, thus reflecting torsion between the proximal and distal ends of the radius. Abbreviations: Cp – capitate, Hm – hamate, Hum – humerus, Lu – lunate, MC I – pollical metacarpal, MC III – third metacarpal, MC V – fifth metacarpal, Ps – pisiform, Rd – radius, Sc – scaphoid, Tr – triquetrum, Trd – trapezoid, Trm – trapezium, and Uln – ulna.

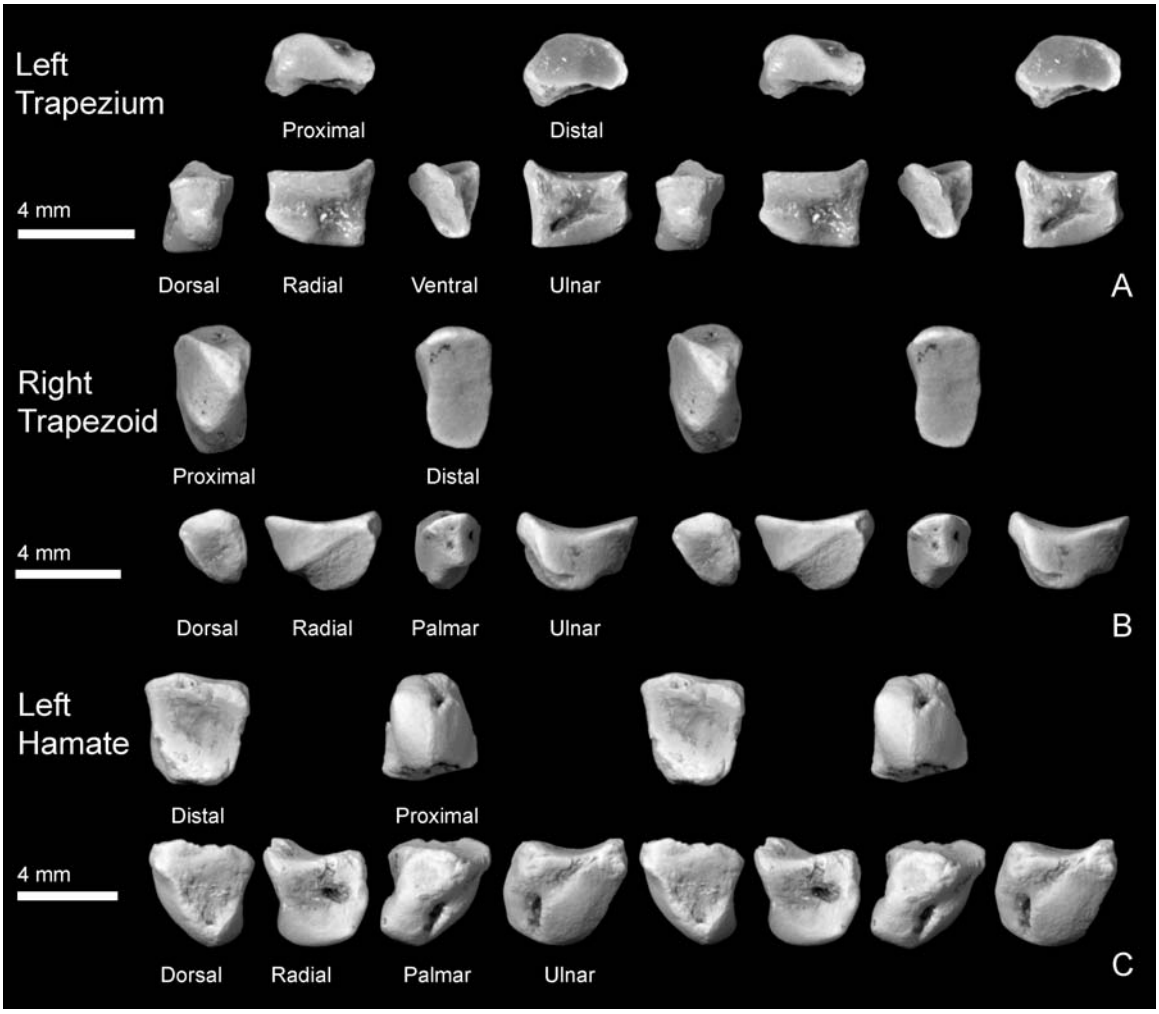

Figure 4.11. *Plesiadapis cookei* (UM 87990). Stereophotographic views of the distal row of carpal bones. A, left trapezium; B, right trapezoid; and C, left hamate.

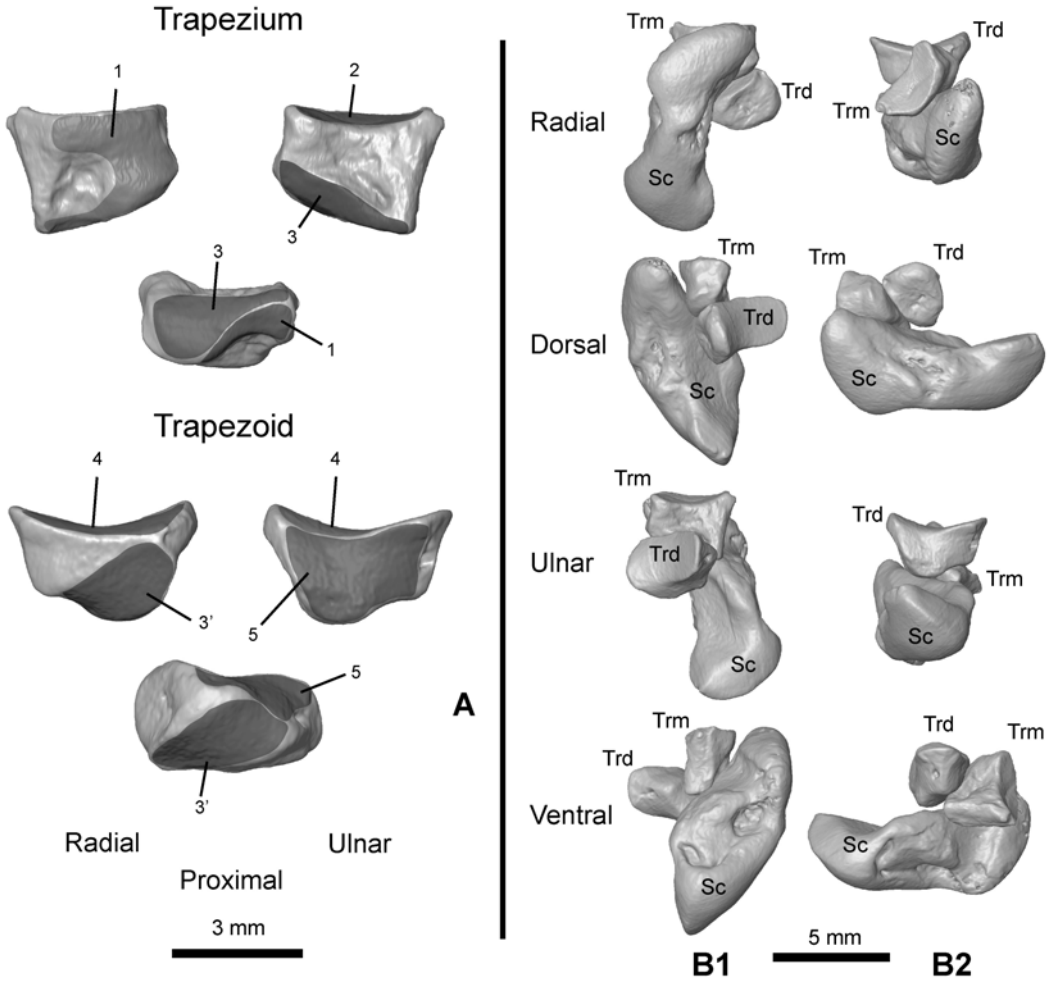

Figure 4.12. Surface reconstructions of the distal row of carpal bones of *Plesiadapis cookei* (UM 87990) based on HRxCT data [HRxCT resolution = 0.018 mm (cubic voxels)]. A, right trapezium and trapezoid. Articular surfaces are illustrated with gray shading and labeled with numbers: 1 – scaphoid facet, 2 – MC I facet, 3-3' – corresponding facets of trapezoid and trapezium, 4 – MC II facet, and 5 – capitate and/or centrale facet. B1, scaphoid (Sc), trapezium (Trm), and trapezoid (Trd) articulated and oriented in several views with respect to idealized anatomical planes of the trapezium (i.e., as used in Fig. 4.11). B2, same bones as in "B1" articulated and oriented in several views with respect to idealized anatomical planes of the trapezoid (i.e., as used in Fig. 4.11). Note the wide separation between the facets for MC I and MC II. MC I and MC II did not contact one another in the articulated hand.

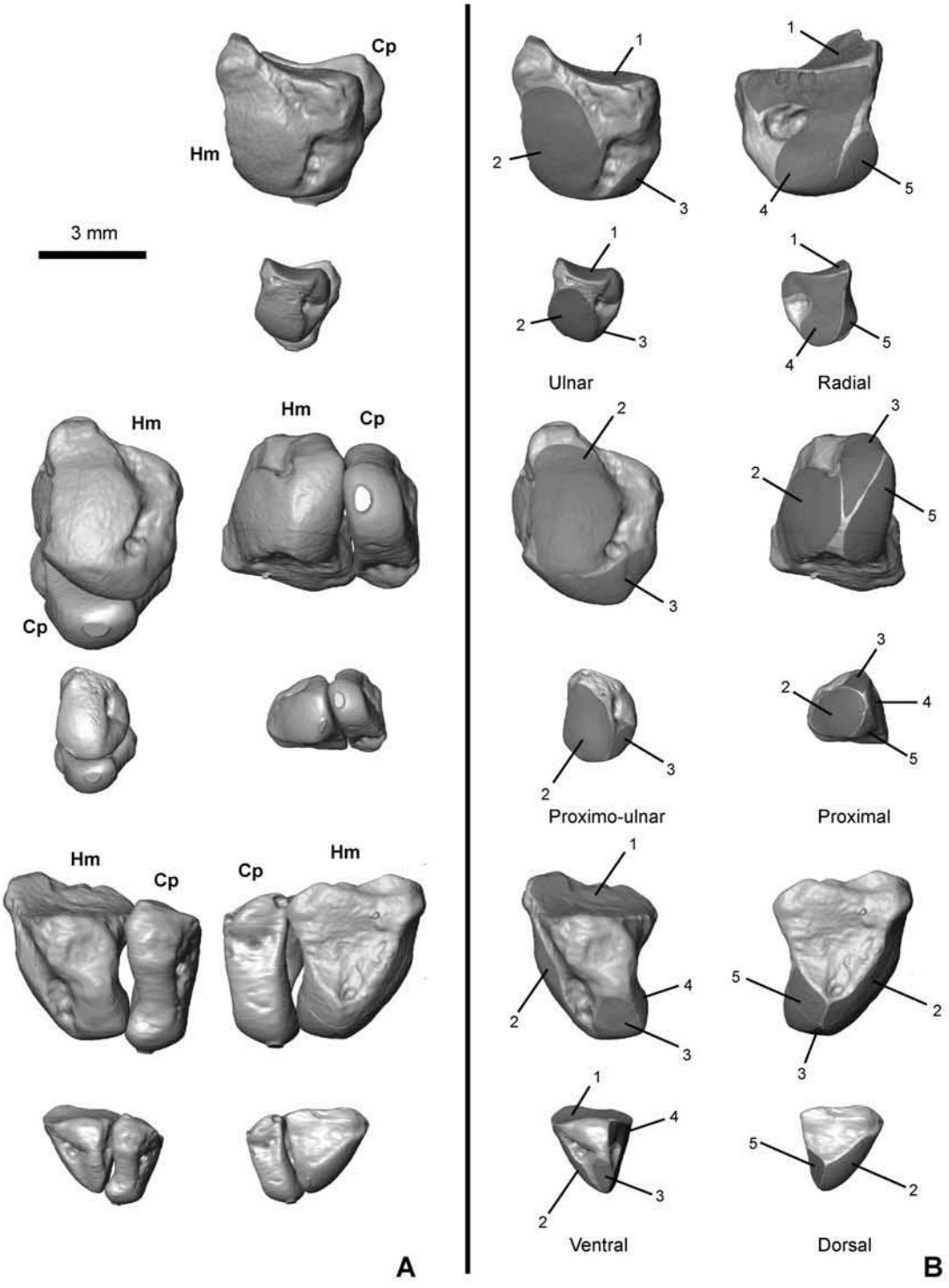
Cp
Hm
3 mm
Hm
Cp
Hm
Cp
Hm
Cp
Cp
Hm
A
1
2
3
1
2
3
4
5
Ulnar
Radial
2
3
2
5
3
2
3
4
5
Proximo-ulnar
Proximal
1
2
3
4
5
2
3
1
2
3
4
5
2
Ventral
Dorsal
B

Figure 4.13

Figure 4.13. Surface reconstructions of hamates (Hm) and capitates (Cp) of *Plesiadapis cookei* (UM 87990) and *Nannodectes intermedius* (USNM 442229) based on HRxCT data [HRxCT resolution = 0.018 mm (cubic voxels)]. Six sets of views are provided of the two taxa with *P. cookei* elements positioned above the same view of those of *N. intermedius*. A, view of the two specimens showing the capitate and hamate articulated. Note that the capitate is not known for *P. cookei*. The surface reconstruction of the hamate of *P. cookei* is articulated with a surface reconstruction of that belonging to *N. intermedius*, but scaled by 1.74 times. B, hamates in six views. Articular surfaces are illustrated with gray shading and labeled with numbers: 1 – MC IV and V facet, 2 – triquetrum facet, 3 – possible ventral accessory facet for scaphoid and/or lunate, 4 – capitate facets, and 5 – possible dorsal accessory facet for scaphoid and/or lunate.

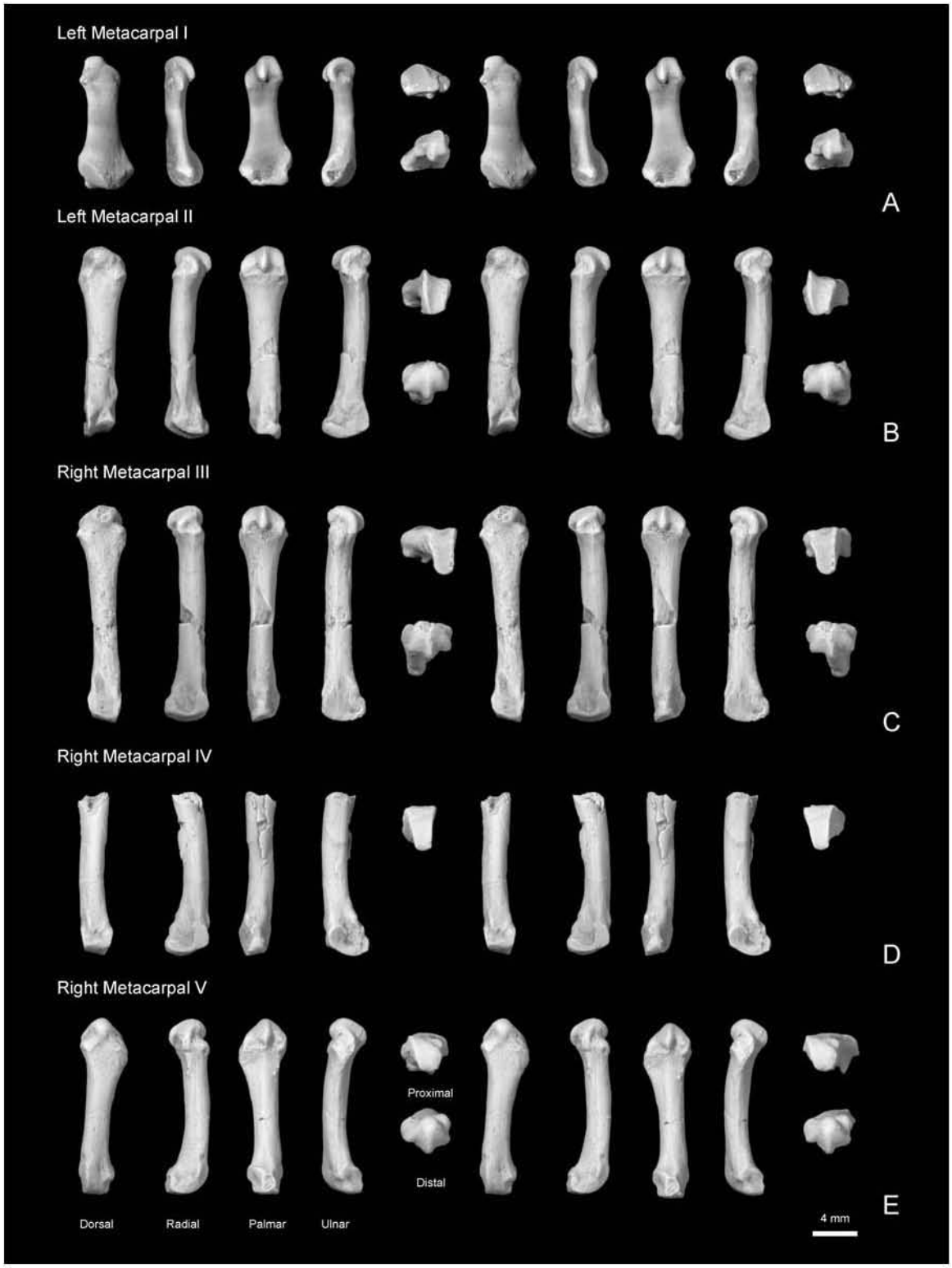
Left Metacarpal I
A
Left Metacarpal II
B
Right Metacarpal III
C
Right Metacarpal IV
D
Right Metacarpal V
Proximal
Distal
E
Dorsal
Radial
Palmar
Ulnar
4 mm
Figure 4.14

Figure 4.14. *Plesiadapis cookei* or *Uintacyon* sp. (UM 87990). Stereophotographic views of “set 1” metacarpals. A, left MC I (pollical metacarpal); B, left MC II; C, right MC III; D, right MC IV; and E, right MC V. Also preserved are proximal fragments of a right MC II and a left MC III.

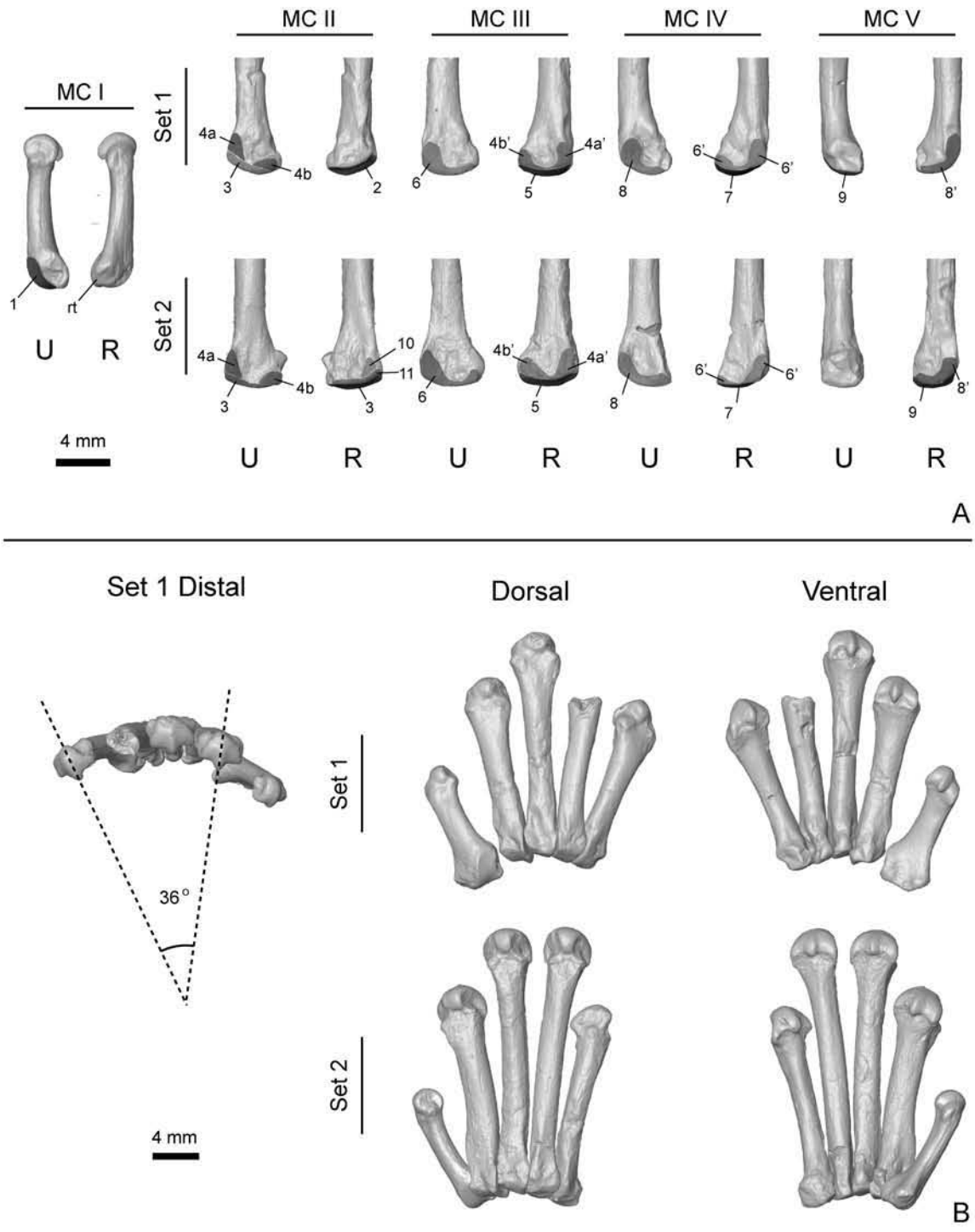
MC I
MC II
MC III
MC IV
MC V
Set 1
Set 2
4a
4b
3
2
4b'
4a'
6
5
6'
8
7
9
8'
10
11
1
rt
U
R
4 mm
A
Set 1 Distal
Dorsal
Ventral
36°
B

Figure 4.15

Figure 4.15. Surface reconstructions of metacarpals of *Plesiadapis cookei* or *Uintacyon* sp. (UM 87990), based on HRxCT data, showing interpretation of articular relationships [HRxCT resolution = 0.018 mm (cubic voxels)]. A, "set 1" and "set 2" metacarpals (MC in radial (R) and ulnar (U) views. Articular surfaces are illustrated with gray shading and labeled with numbers: 1 – trapezium facet, 2 – trapezoid facet, 3 – capitate facet of MC II, 4a-4a' dorsal MC II-III facet, 4b-4b' – ventral MC II-III facet, 5 – capitate facet of MC III, 6-6' – MC III-IV facets, 7 – hamate facet of MC IV, 8-8' – MC IV-V facets, 9 – hamate facet of MC V, 10 – ?MC I-II facet of "set" MC II, and 11 – ?trapezium facet of "set 2" MC II. Abbreviation: rt – radial tubercle for abductor pollicis muscle tendon. B, two alternative reconstructions of the metacarpus of *P. cookei*. One uses the "set 1" elements, the other uses "set 2" elements, and both incorporate the only preserved, undoubted pollical metacarpal of UM 87990. The "set 1" recontruction is also shown in distal view at left. The angle between the axis of flexion at the distal facet of MC II and MC V is shown, illustrating that the metacarpus supported a convergent hand.

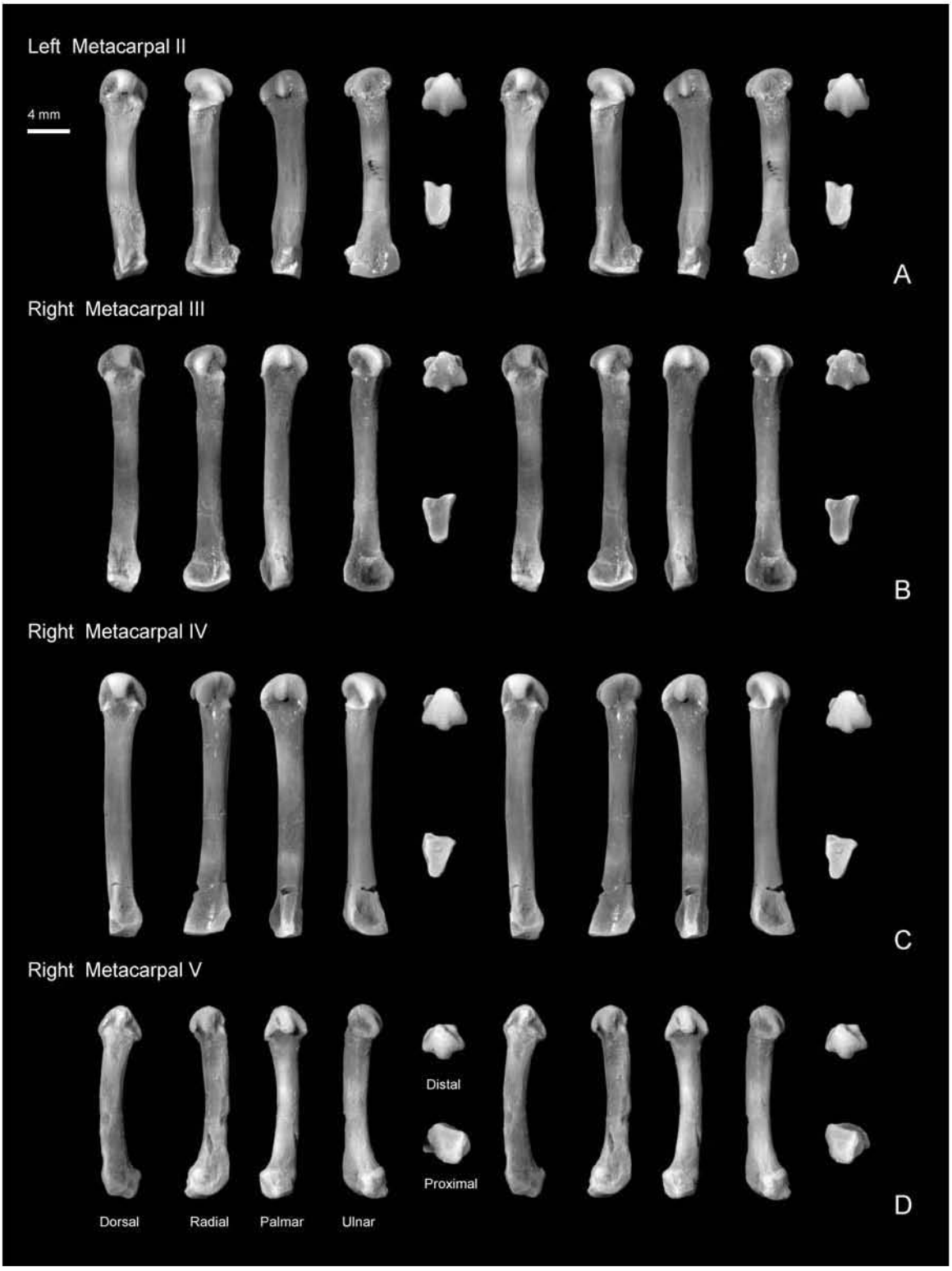

Figure 4.16. *Plesiadapis cookei* or *Uintacyon* sp. (UM 87990). Stereophotographic views of "set 2" metacarpals. A, left MC II; B, right MC III; C, right MC IV; and D, right MC V.

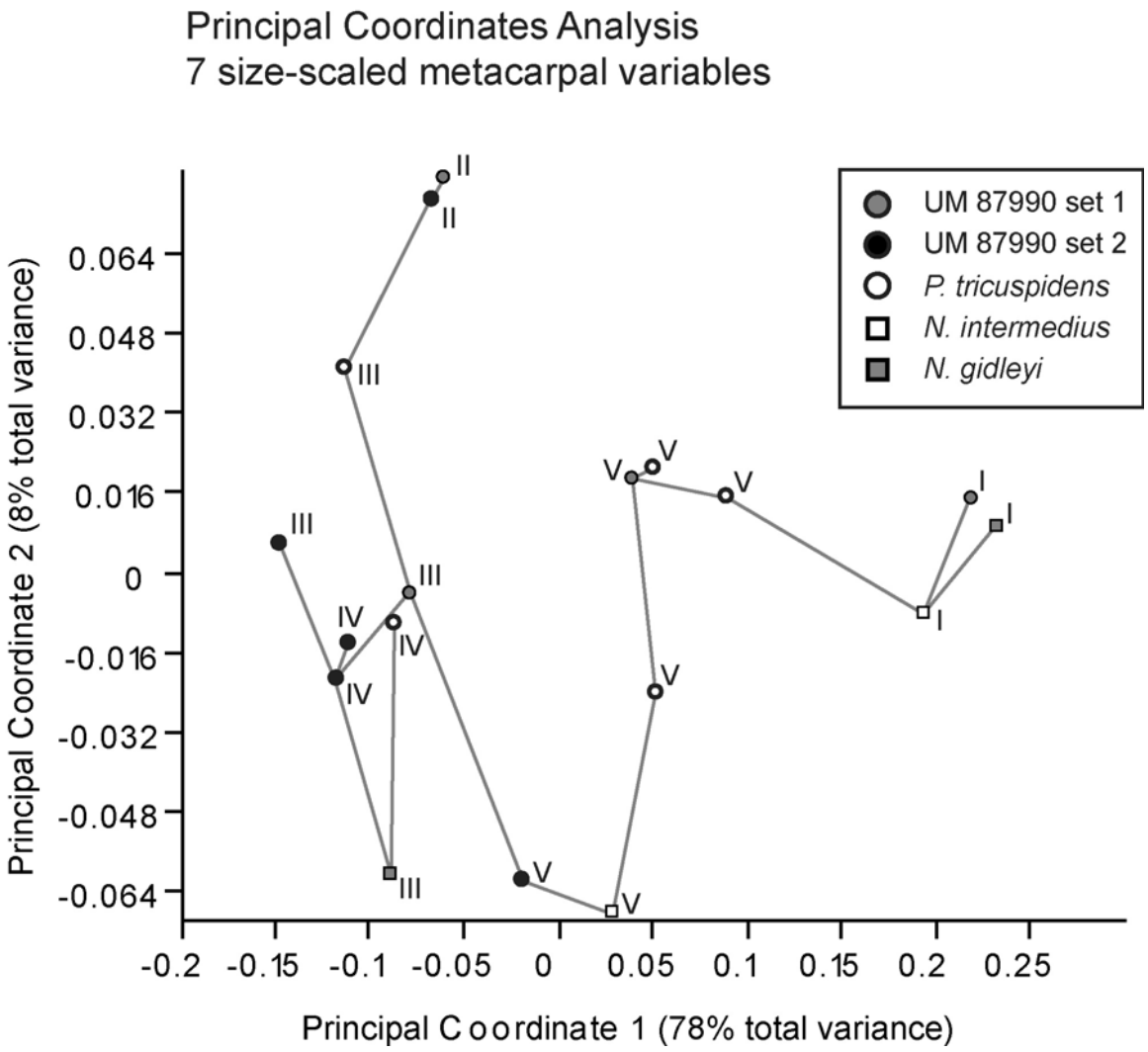

Figure 4.17. Plot of principal coordinates based on an analysis using a Euclidean distance matrix calculated from seven metacarpal shape variables of Table 5.11. As discussed in the methods section these variables were calculated as natural log ratios of each of seven raw measurements from Table 5.10 (Le, PEW, PED, MSW, MSD, DEW, and DED) to the geometric mean of all measurements for a given specimen. Gray line represents a minimum spanning tree between cases. Note that the "set 1" MC V of UM 87990 is closest to the three *P. tricuspidens* MC V's, while the "set 2" MC V is separated from this group by the MC V of *N. intermedius*.

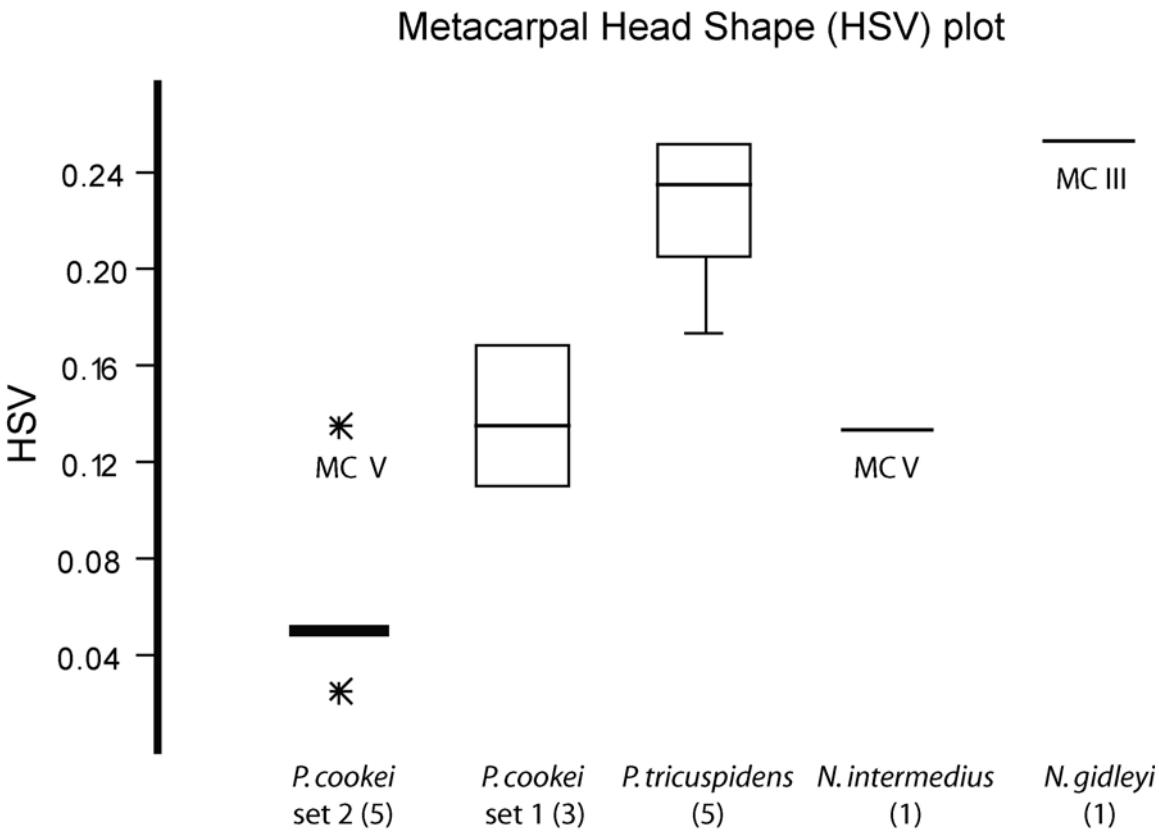

Figure 4.18. Box plot of metacarpal head shapes [HSV = ln(DEW/DED)] of plesiadapids. Note that the metacarpal heads undoubtably attributed to plesiadapids are relatively mediolaterally wide compared to the "set 2" MC II-IV. However, the "set 1" MC II-III and MC V are closer to or in the range of those of certain plesiadapids. Even though the "set 2" MC V head is in the range of known plesiadapids, cluster and principal component analyses effectively rule it out as belonging to *P. cookei*.

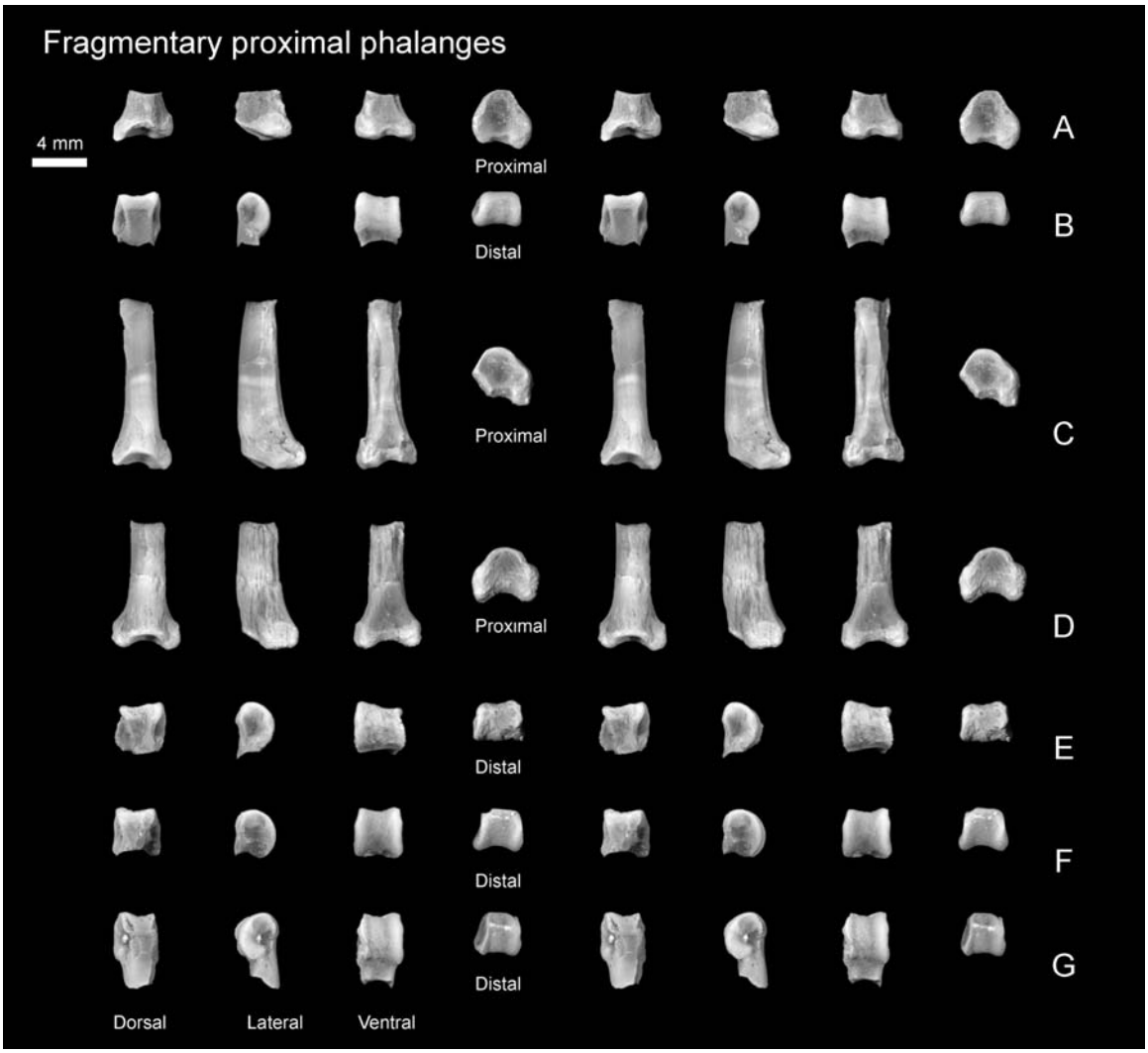

Figure 4.19. *Plesiadapis cookei* (UM 87990). Stereophotographic views of incomplete proximal phalanges. A, proximal end of left hallucal proximal phalanx; B, distal end of a proximal phalanx; C-D, proximal ends of proximal phalanges; and E-G, distal ends of proximal phalanges. Also preserved are a proximal fragment of the right hallucal proximal phalanx and a badly eroded shaft of what may be a pollical proximal phalanx.

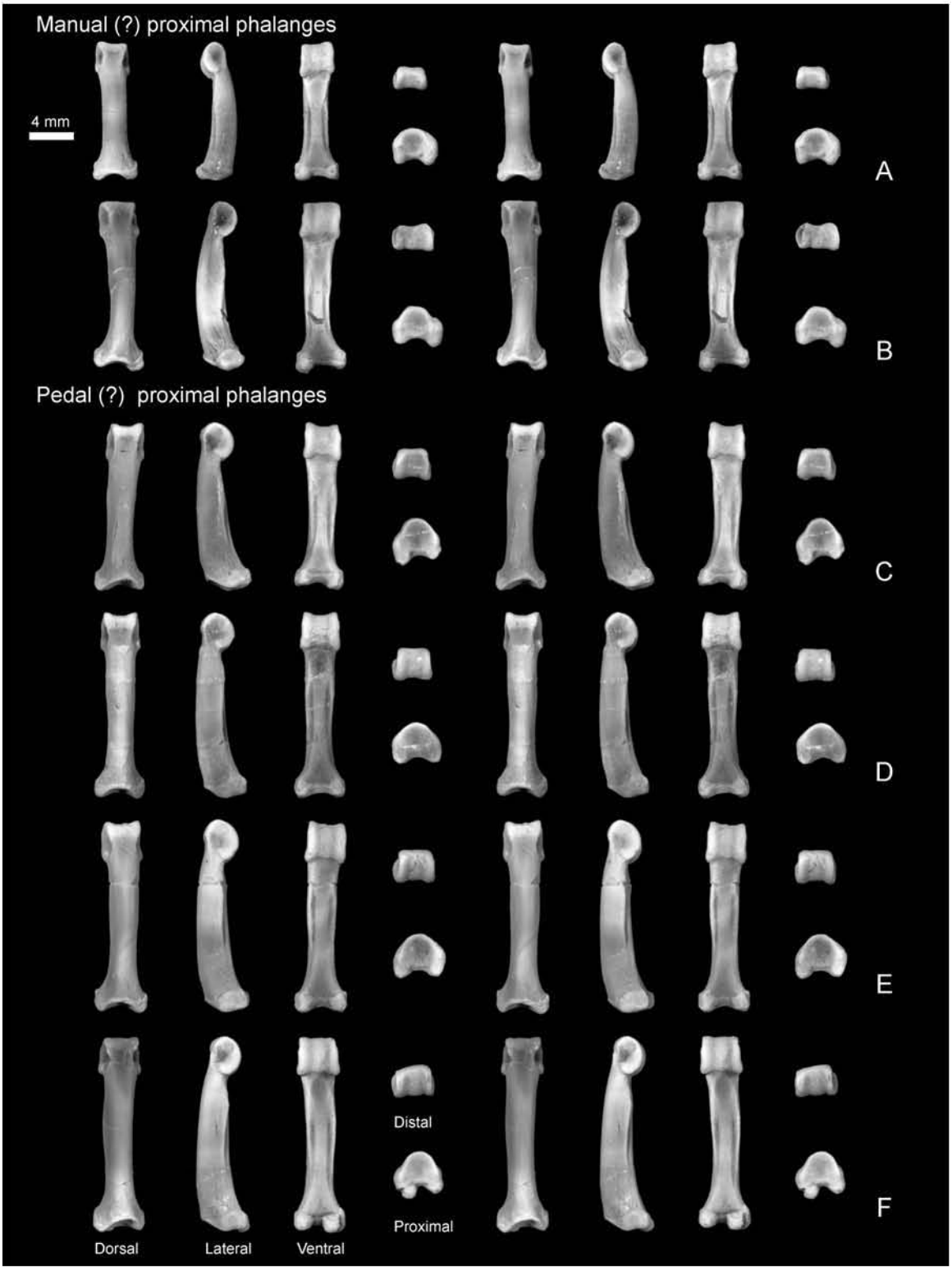

Figure 4.20. *Plesiadapis cookei* (UM 87990). Stereophotographic views of complete proximal phalanges. A-B, possible manual proximal phalanges; and C-F, possible pedal proximal phalanges.

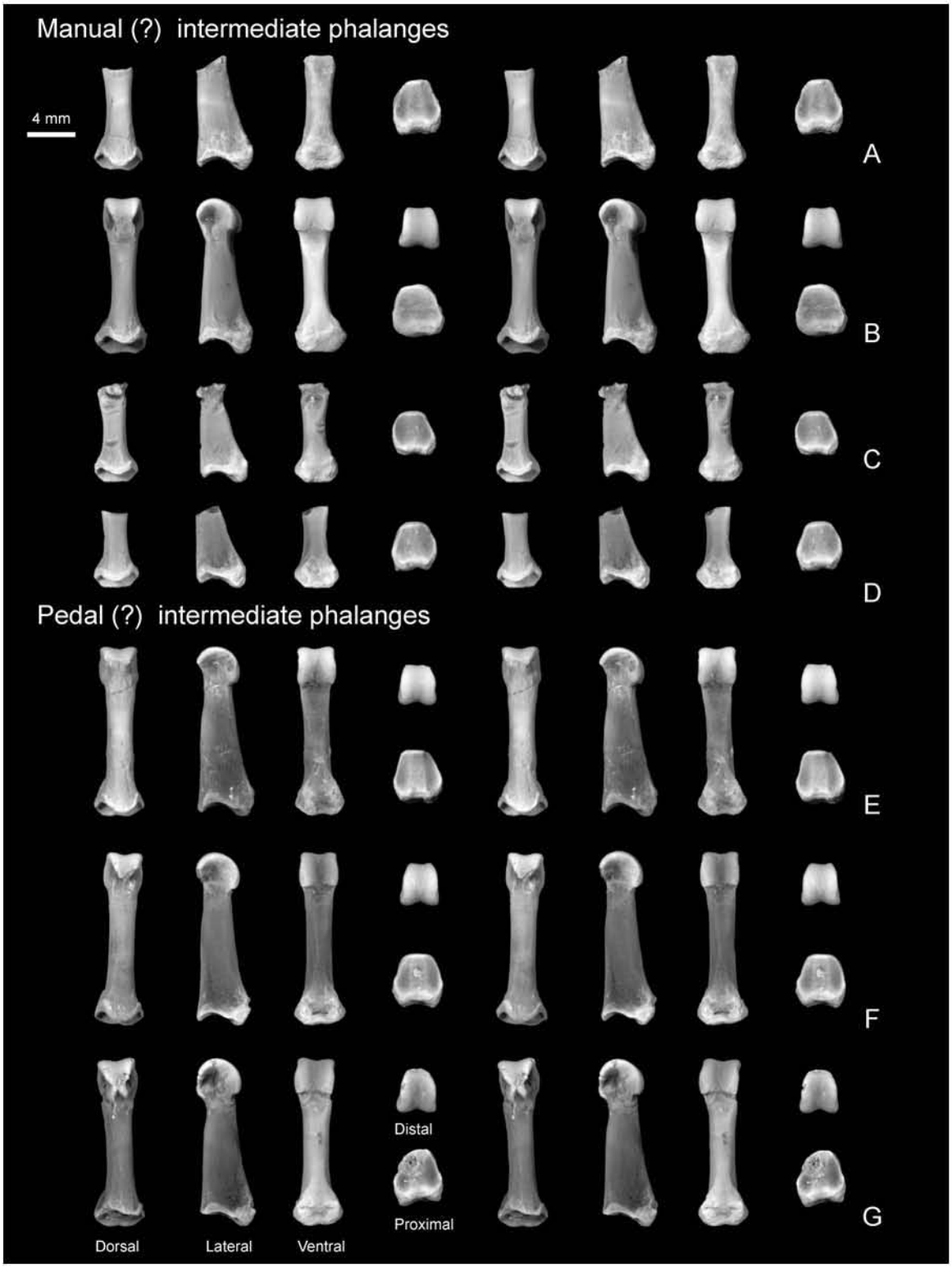

Figure 4.21. *Plesiadapis cookei* (UM 87990). Stereophotographic views of A-D, possible manual intermediate phalanges; and E-G, possible pedal intermediate phalanges.

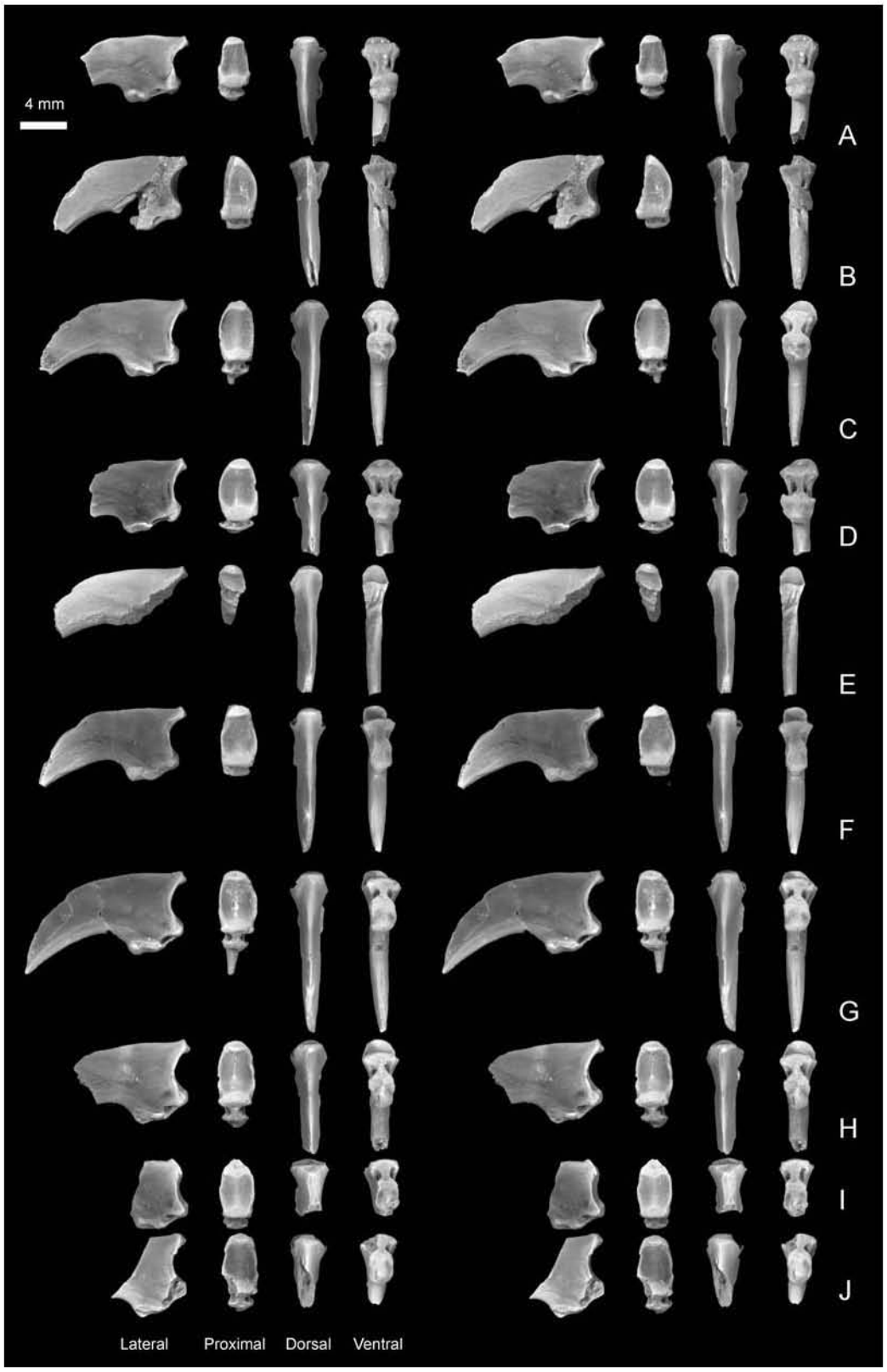

Figure 4.22. *Plesiadapis cookei* (UM 87990). Stereophotographic views of distal phalanges.

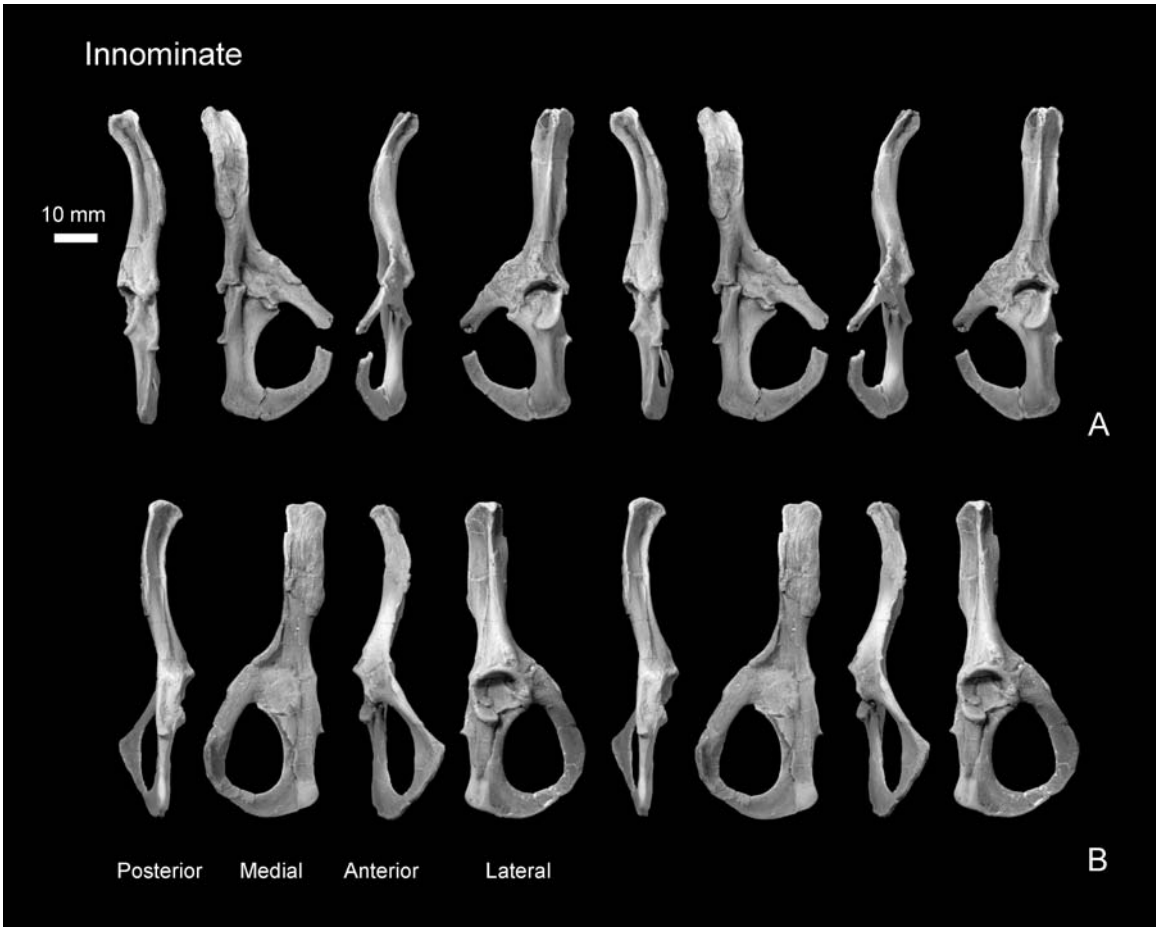

Figure 4.23. *Plesiadapis cookei* (UM 87990). Stereophotographic views of A, left innominate; and B, right innominate. Note that the tip of the right ischial tuberosity is reconstructed.

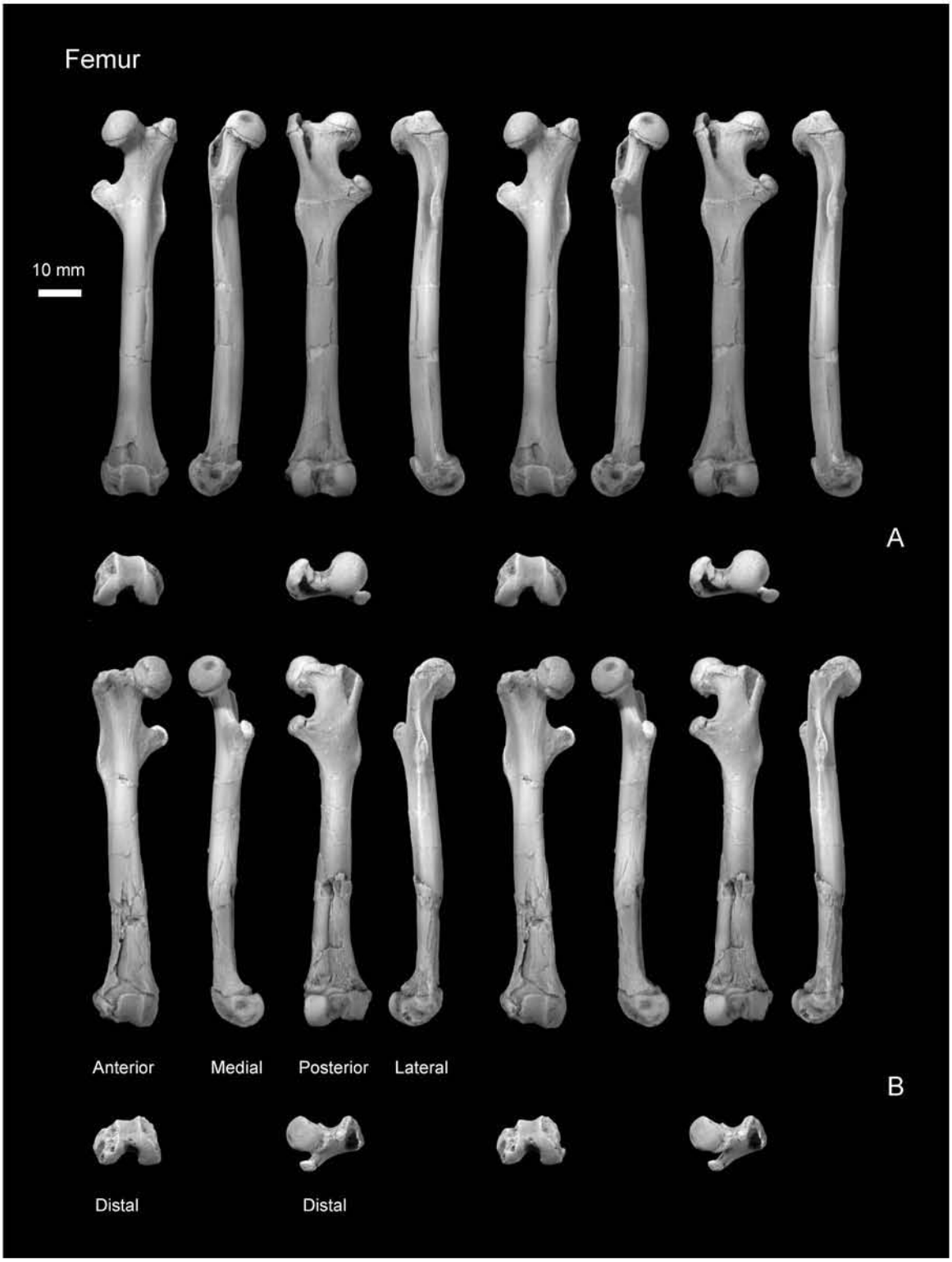
Femur
10 mm
A
Anterior
Medial
Posterior
Lateral
B
Distal
Distal
Figure 4.24

Figure 4.24. *Plesiadapis cookei* (UM 87990). Stereophotographic views of A, left femur; and B, right femur.

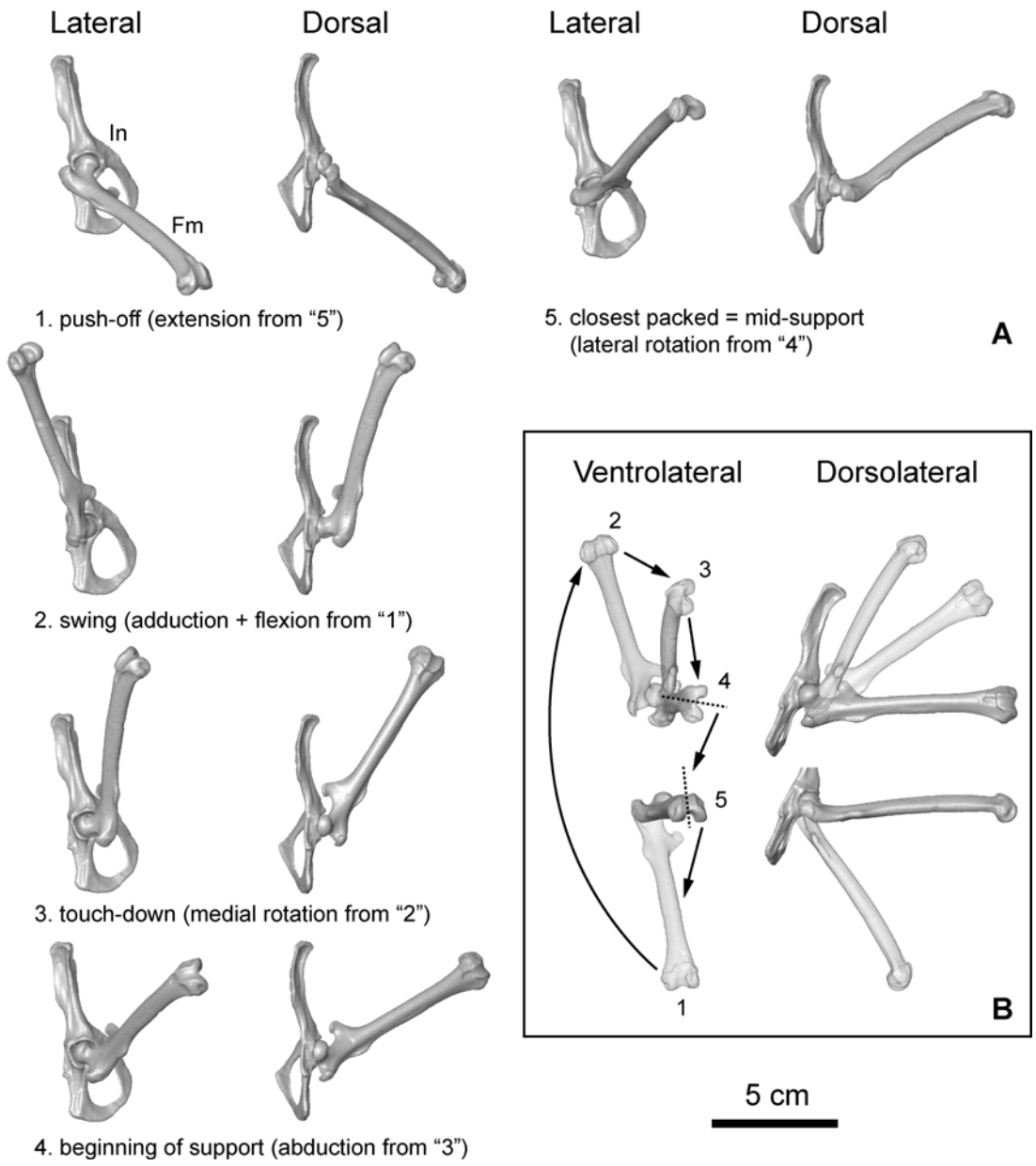
Lateral
Dorsal
In
Fm
1. push-off (extension from “5”)
2. swing (adduction + flexion from “1”)
3. touch-down (medial rotation from “2”)
4. beginning of support (abduction from “3”)
Lateral
Dorsal
5. closest packed = mid-support
(lateral rotation from “4”)
A
Ventrolateral
Dorsolateral
2
3
4
5
1
B
5 cm

Figure 4.25

Figure 4.25. Surface reconstruction of innominate (In) and femur (Fm) of *Plesiadapis cookei* (UM 87990) based on CT data [CT image resolution = 0.18(x) x 0.18(y) x 0.20(z) mm]. A, shows major increments of change in femoral orientation and articulation with innominate during gait cycle. 5 – closest packed posture suggesting that the usual or average posture of the femur is one in which it is flexed, abducted and slightly laterally rotated. Steps 1-5 show how abduction-adduction, mediolateral rotation, and flexion-extension movements combined during the gait cycle to bring the thigh through a large positional and angular excursion, while keeping the joint surfaces of the acetabulum and femur in maximal overlap. Going from the closest-packed position of the hip to pushing off the substrate (5 → 1) would have simply entailed extension the abducted femur. During the swing phase (1 → 2) the thigh was adducted and flexed without any axial rotation. At touch down (2 → 3) the femur was probably medially rotated, especially if the tibia and foot were incorporated into increasing the length of the stride (see below). The beginning of the propulsive phase (3 → 4) likely entailed abduction until the posterolateral extension of the femoral head articular surface abutted the acetabulum. From here, lateral rotation would have brought the femur back to its closest packed position while also causing the body to swing forward (anteriorly) and ventrally on the tibae (4 → 5). From the closest packed position the femur could have extended, thus pushing the body further anteriorly. B, summary of movements in different planes through the gait cycle.

Figure 4.26. *Plesiadapis cookei* (UM 87990). Stereophotographic views of A, left tibia; and B, right tibia. The left tibia is missing its epiphyses. A segment of the proximal part of the shaft has been reconstructed on the left side (evidence for this reconstruction is unknown).

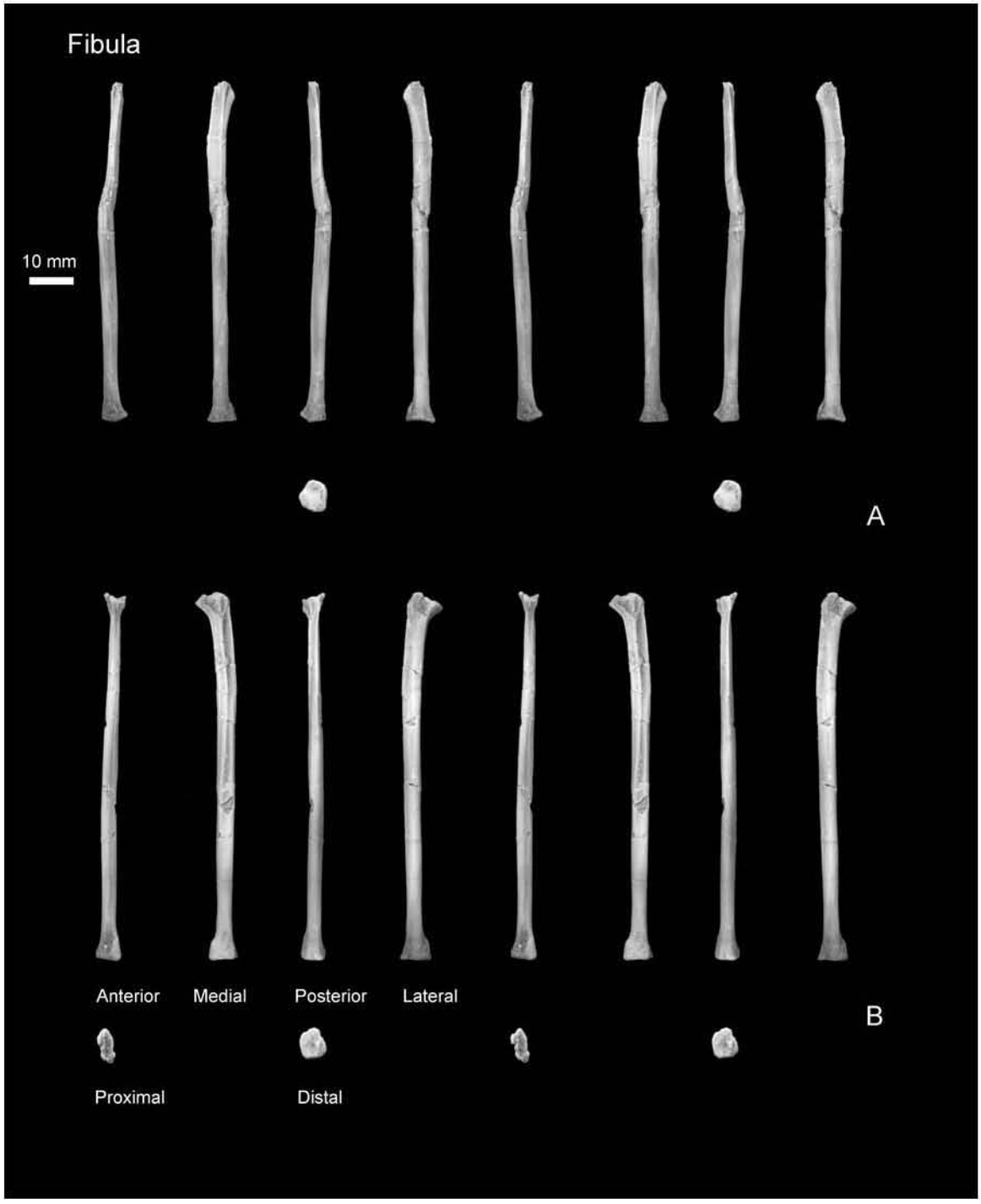

Figure 4.27. *Plesiadapis cookei* (UM 87990). Stereophotographic views of A, left fibula; and B, right fibula. Both fibulae are missing their epiphyses.

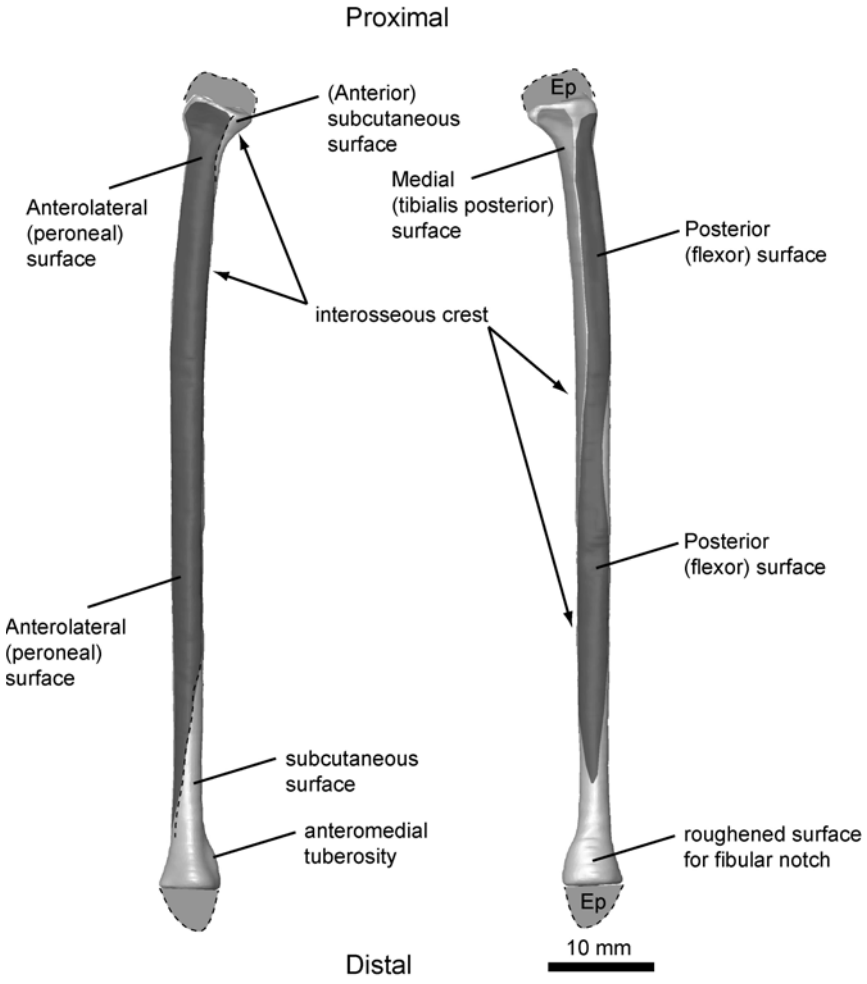

Figure 4.28. Surface reconstruction of right fibula of *Plesiadapis cookei* (UM 87990) based on CT data [CT image resolution = 0.18(x) x 0.18(y) x 0.20(z) mm]. The image is shaded and labeled to aid in understanding statements made in the descriptions. Abbreviation: Ep – epiphysis (reconstructed).

Figure 4.29. *Plesiadapis cookei* (UM 87990). Stereophotographic views of A, right astragalus; and B, right calcaneum.

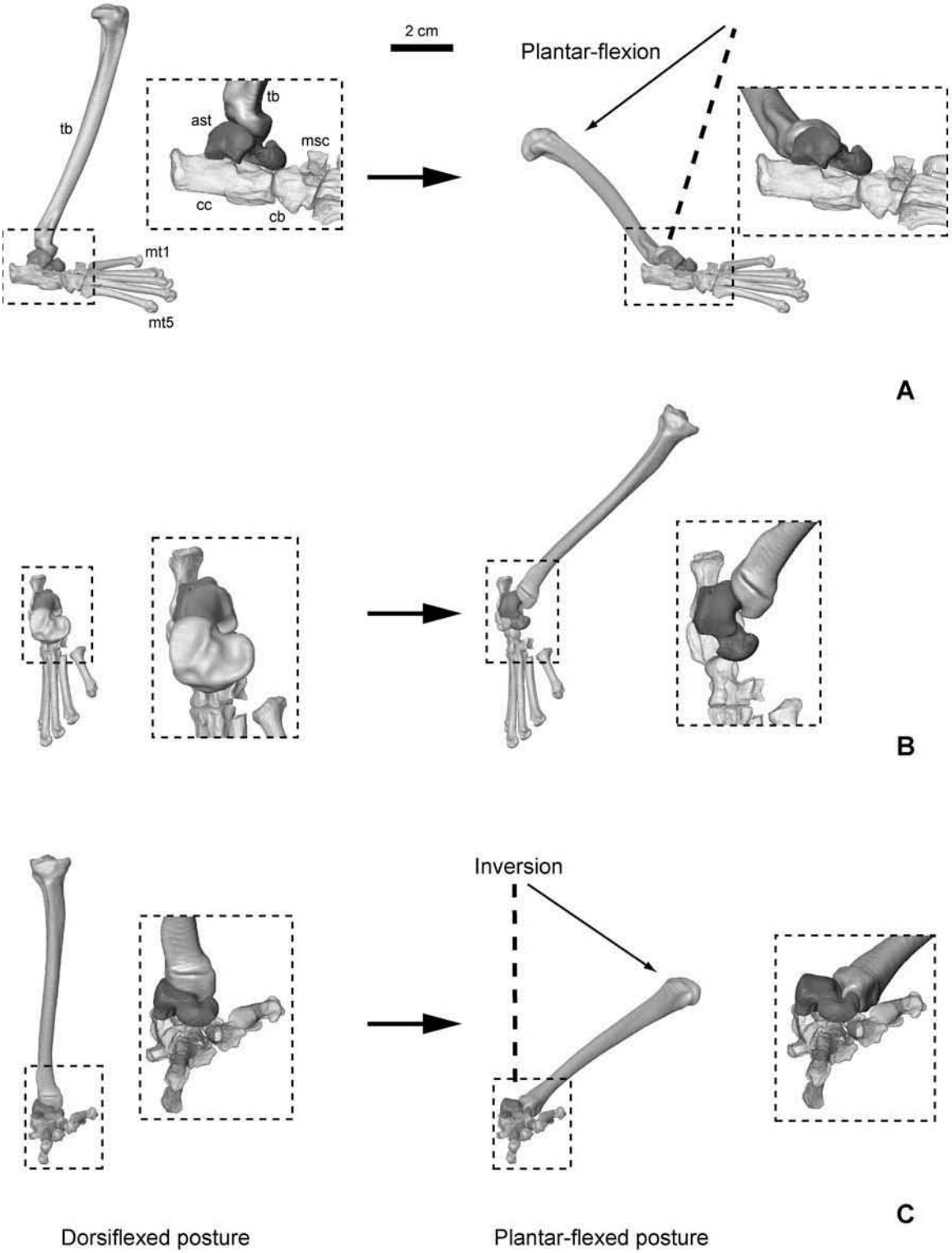
2 cm
Plantar-flexion
tb
ast
msc
cc
cb
mt1
mt5
A
B
Inversion
C
Dorsiflexed posture
Plantar-flexed posture

Figure 4.30

Figure 4.30. Surface reconstruction of tibia (tb) and foot of *Plesiadapis cookei* (UM 87990) based on HRxCT and medical CT data [tibia CT image resolution = 0.18(x) x 0.18(y) x 0.20(z) mm: foot bone HRxCT resolution = 0.018 mm (cubic voxels)]. Three views (A-C) of the foot showing change of orientation and articular relationships of the tibia as the foot is plantar-flexed (left to right). A, lateral view of partly inverted foot. Note that metatarsals and tibia form a slightly acute angle in the image showing dorsiflexion on the left. On the right, the tibia and metatarsals form an obtuse angle, increased by ~60º from the dorsiflexed posture. B, dorsal view of partly inverted foot. Note that anteroposterior axis of the tibial plateau is parallel to the proximodistal axis of the metatarsals in the dorsiflexed image. In the plantar-flexed image the anteroposterior axis of the tibia points out of the plane of the page. Thus the proximodistal axis of the foot now points mediodistal relative to the tibia anatomical orientations. C, anterior view of partly inverted foot. In the dorsiflexed view the proximodistal axis of the tibia is offset from the mediolateral plane of the foot by 60-70º (close to neutral). In the plantar-flexed view the mediolateral plane of foot is aligned with the proximodistal axis of the foot. The complex motion that occurs at the tibioastragalar joint is a consequence of the complexities of the joint surface. Specifically, the medially concave medial tibial facet and the obliquely oriented lateral tibial facet lead to these conjunct motions. Abbreviations: ast – astragalus, cb – cuboid, cc – calcaneum, msc – mesocuneiform, mt1 – first metatarsal, and mt5 – fifth metatarsal.

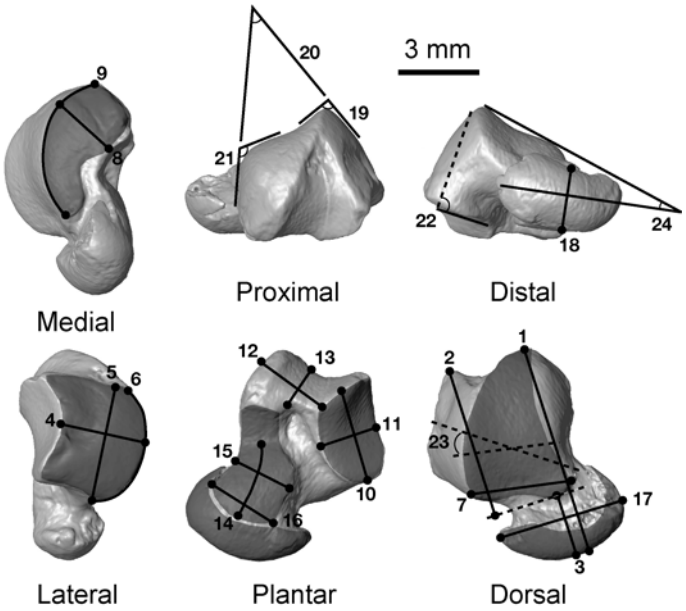

Figure 4.31. Measurements of astragalus. See Table 5.20A-C for measurement descriptions.

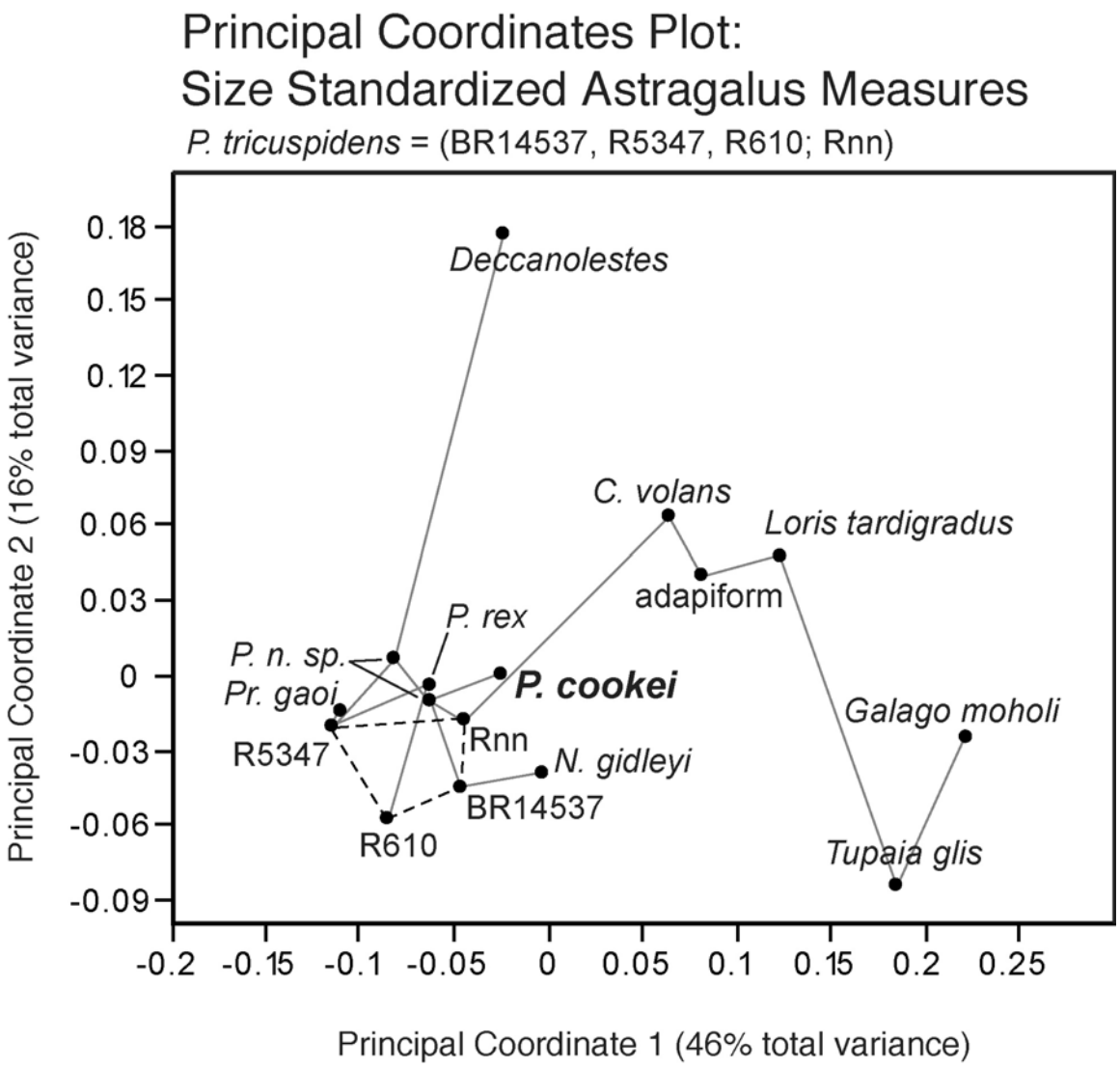

Figure 4.32. Plot of principal coordinates based on an analysis of a Euclidean distance matrix calculated from 24 astragalar shape variables (calculated from raw measurements of Table 5.20A-C). Variables 1-18 are natural log ratios of raw measurements Ast-1 to Ast-18 from Table 5.20A-B to the geometric mean of measurements 1-18. Variables 19-24 are angles in radians (Table 5.20C). All plesiadapids are very similar to each other, while other euarchontans have higher PC 1 scores. *Cynocephalus* is most closely linked with plesiadapids, among euarchontans of the sample; however, the astragalus of *Cynocephalus* is more similar to that of a fossil adapiform and *Loris*, than it is to the plesiadapids. A primitive eutherian, *Deccanolestes hislopi*, is differentiated by higher PC 2 scores, but is most closely linked with plesiadapids among taxa in the sample. It seems likely that other plesiadapiforms would plot in the vicinity of plesiadapids (see Szalay and Decker, 1974). Dashed line encompasses *P. tricuspidens.*

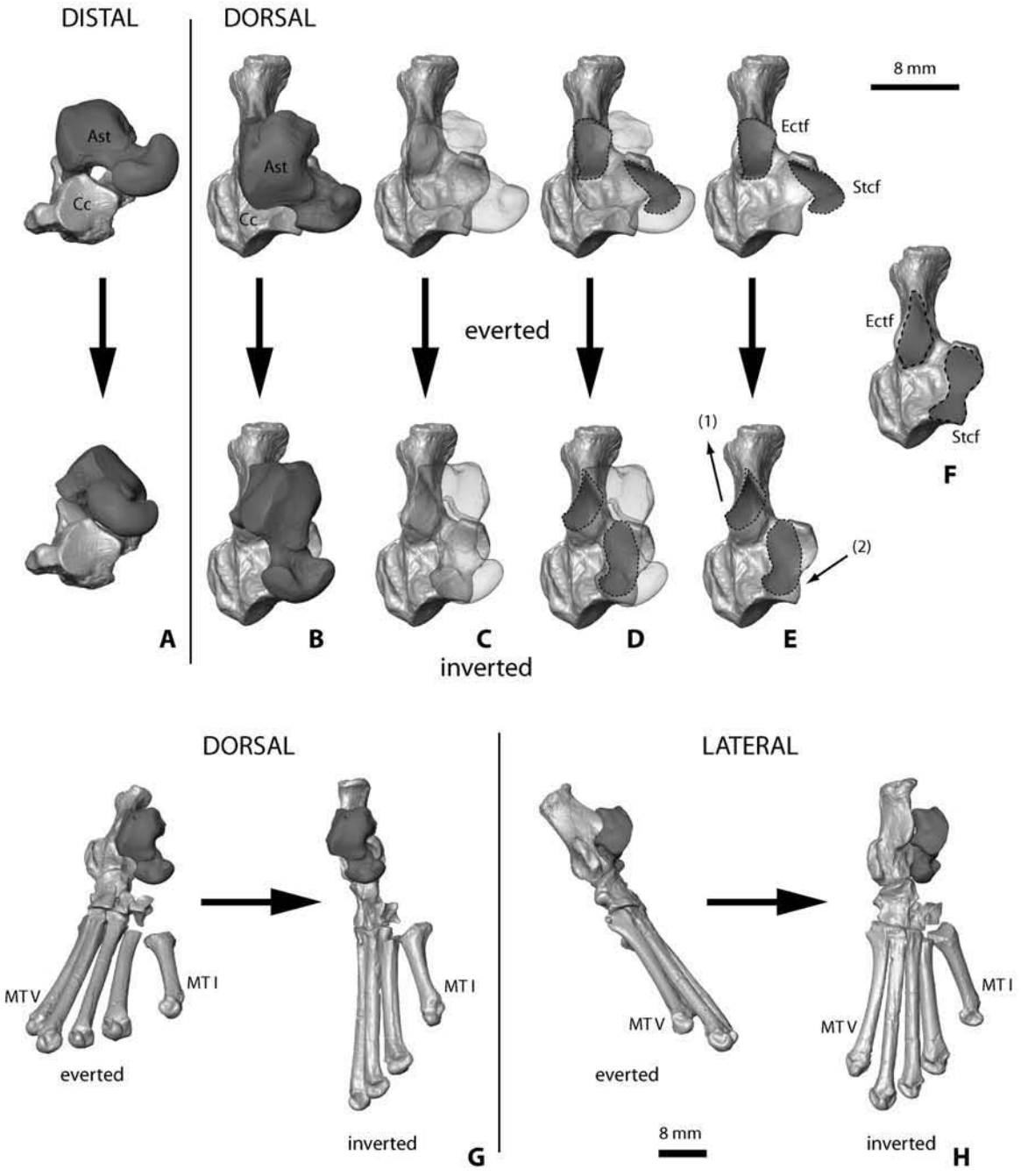
DISTAL
DORSAL
8 mm
Ast
Cc
Ast
Cc
Ectf
Stcf
everted
Ectf
Stcf
F
(1)
(2)
A
B
C
D
E
inverted
DORSAL
LATERAL
MTV
MTI
everted
MTI
inverted
G
MTV
everted
8 mm
MTV
MTI
inverted
H

Figure 4.33

Figure 4.33. Surface reconstruction of astragalus (Ast), calcaneum (Cc) and foot of *Plesiadapis cookei* (UM 87990) based on HRxCT data showing the detailed movements and degree of inversion accomplished at the astragalocalcaneal joint [HRxCT resolution = 0.018 mm (cubic voxels)]. See Szalay and Decker (1974) for detailed discussions of comparisons of mobility among various primitive eutherians. A, distal view of everted (top) and inverted (bottom) astragalocalcaneal joint. Calcaneum orientation held constant. B, dorsal view of everted (top) and inverted (bottom) astragalocalcaneal joint. C, same dorsal views as in "B" with astragalus shown transparent to allow visualization of astragalocalcaneal articular surface. D, same dorsal views as in "C" with astragalus calcaneal facets highlighted. E, same dorsal views as in "D" with astragalus calcaneal facets shown in relation to astragalus facets of calcaneum. Inversion is accomplished by (1) plantar-flexion and medial translation of the calcaneum at the posterior astragalocalcaneal joint (comprised of ectal facets) and (2) medial translation and lateral rotation of the calcaneum at the anterior astragalocalcaneal joint (comprised of sustentacular facets). F, dorsal view of calcaneum with astragalus removed and astragalar facets highlighted. G, dorsal view of astragalus showing change in foot position with inversion (left to right) at astragalocalcaneal joints. H, lateral view of astragalus showing same change in articulation at astragalocalcaneal facet. Note that inversion also leads to substantial conjunct plantar-flexion of the foot.

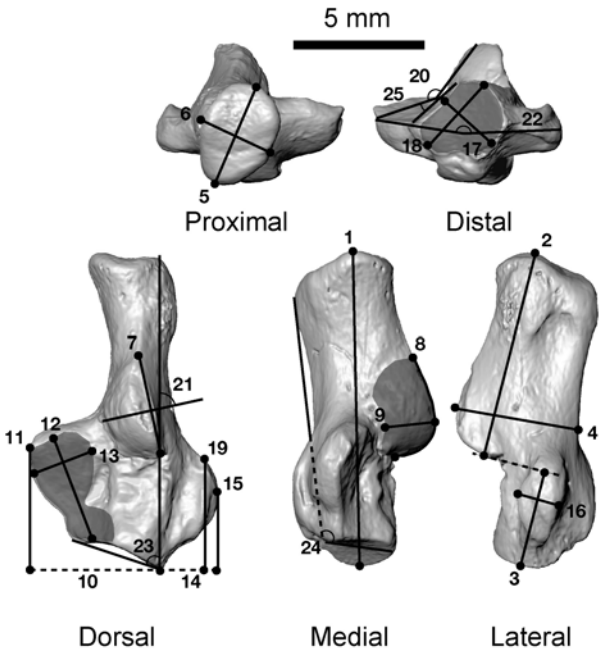

Figure 4.34. Measurements of calcaneum. See Table 5.21A-C for measurement descriptions.

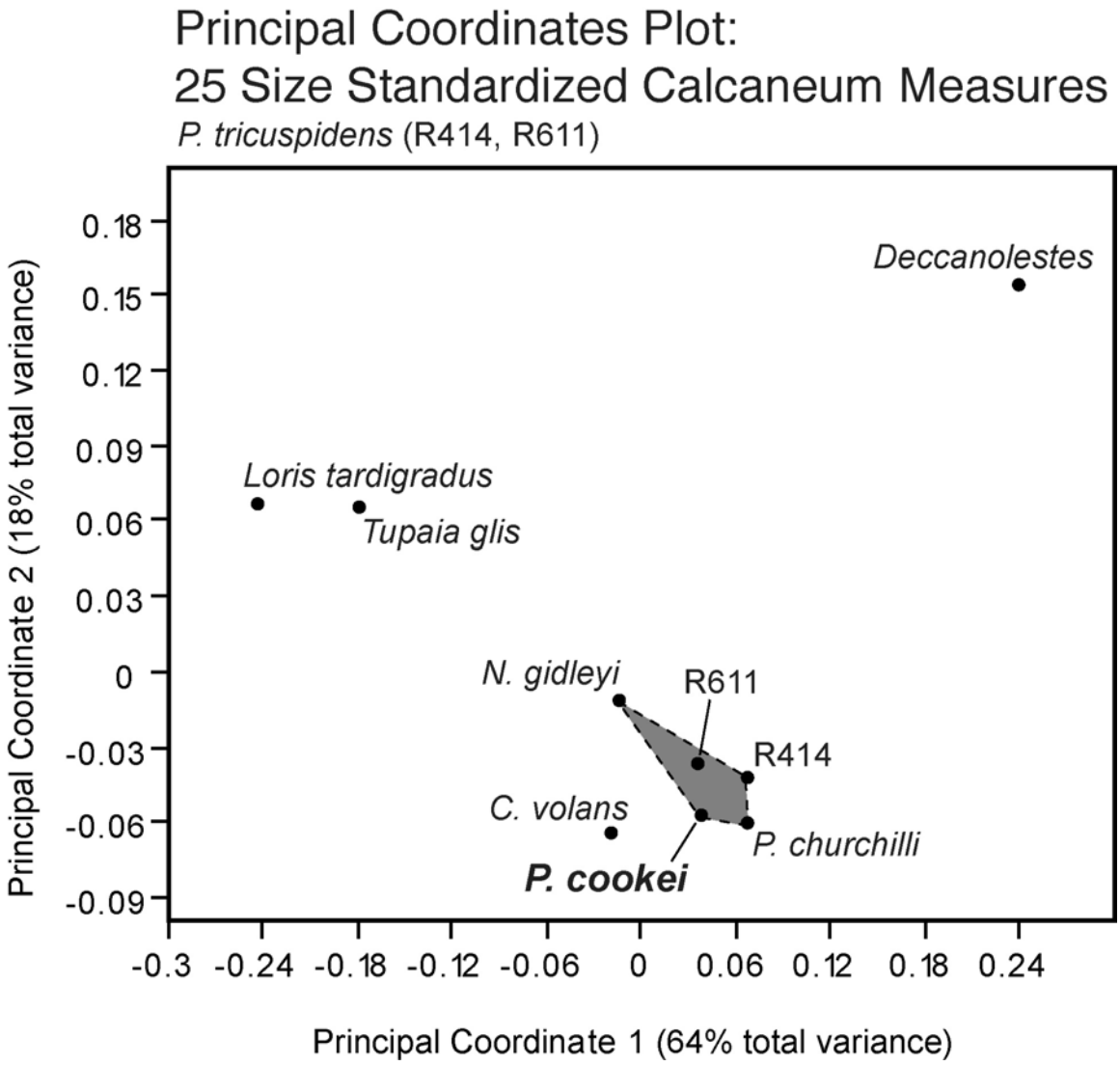

Figure 4.35. Plot of principal coordinate scores based on an analysis of a Euclidean distance matrix calculated from 25 calcaneum shape variables (calculated from raw measurements of Table 5.21A-C). Variables 1-19 are natural log ratios of raw measurements Cc-1 to Cc-19 from Table 5.21A-B to the geometric mean of measurements 1-19. Variables 20-25 are angles in radians (Table 5.21C). All sampled plesiadapids are fairly similar to each other. Other sampled euarchontans and *Deccanolestes* have principal coordinate scores separating them from plesiadapids. *Cynocephalus volans*, on the other hand, plots close to plesiadapids.

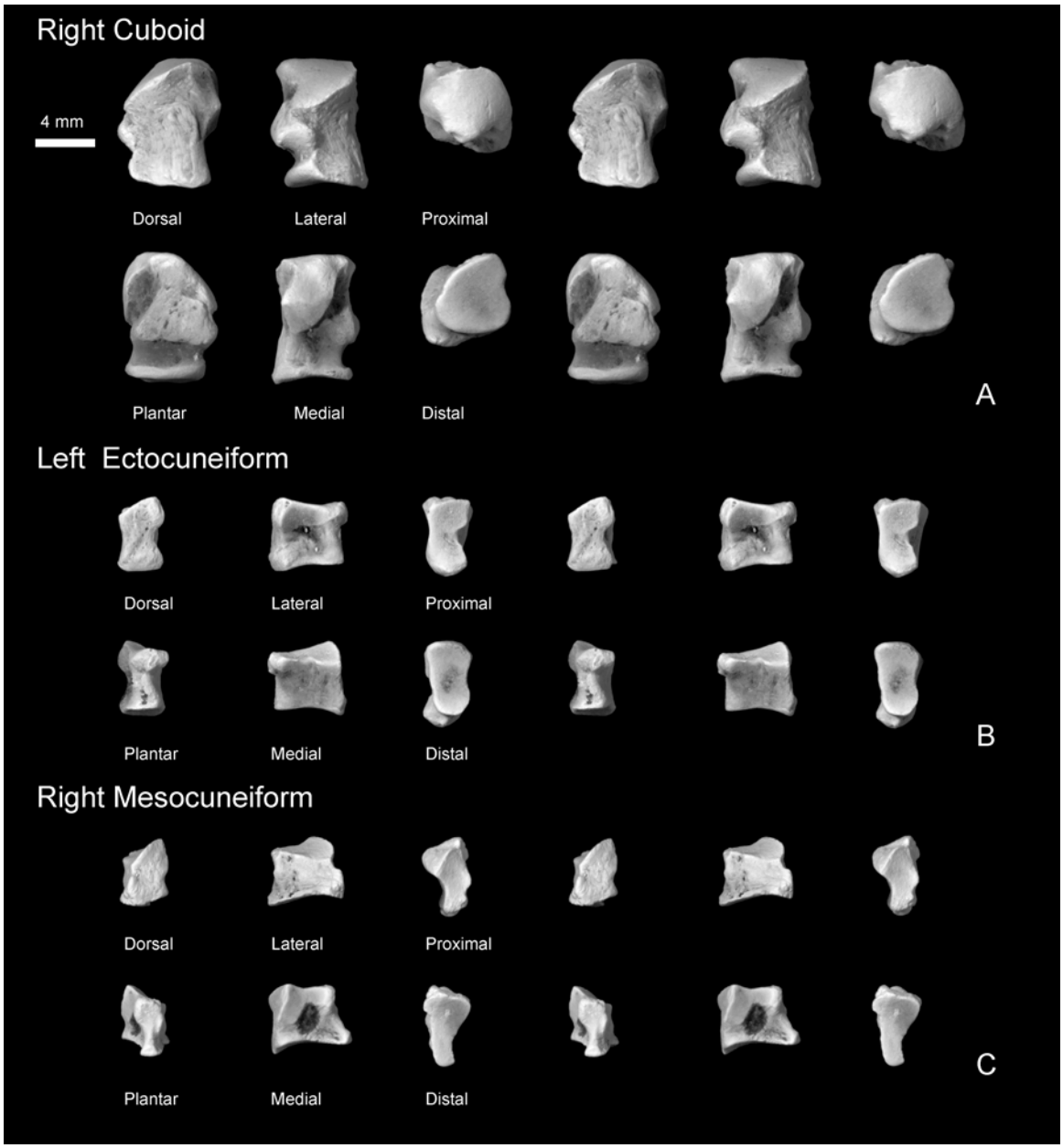

Figure 4.36. *Plesiadapis cookei* (UM 87990). Stereophotographic views of distal tarsal bones. A, right cuboid; B, left ectocuneiform; and C, right mesocuneiform.

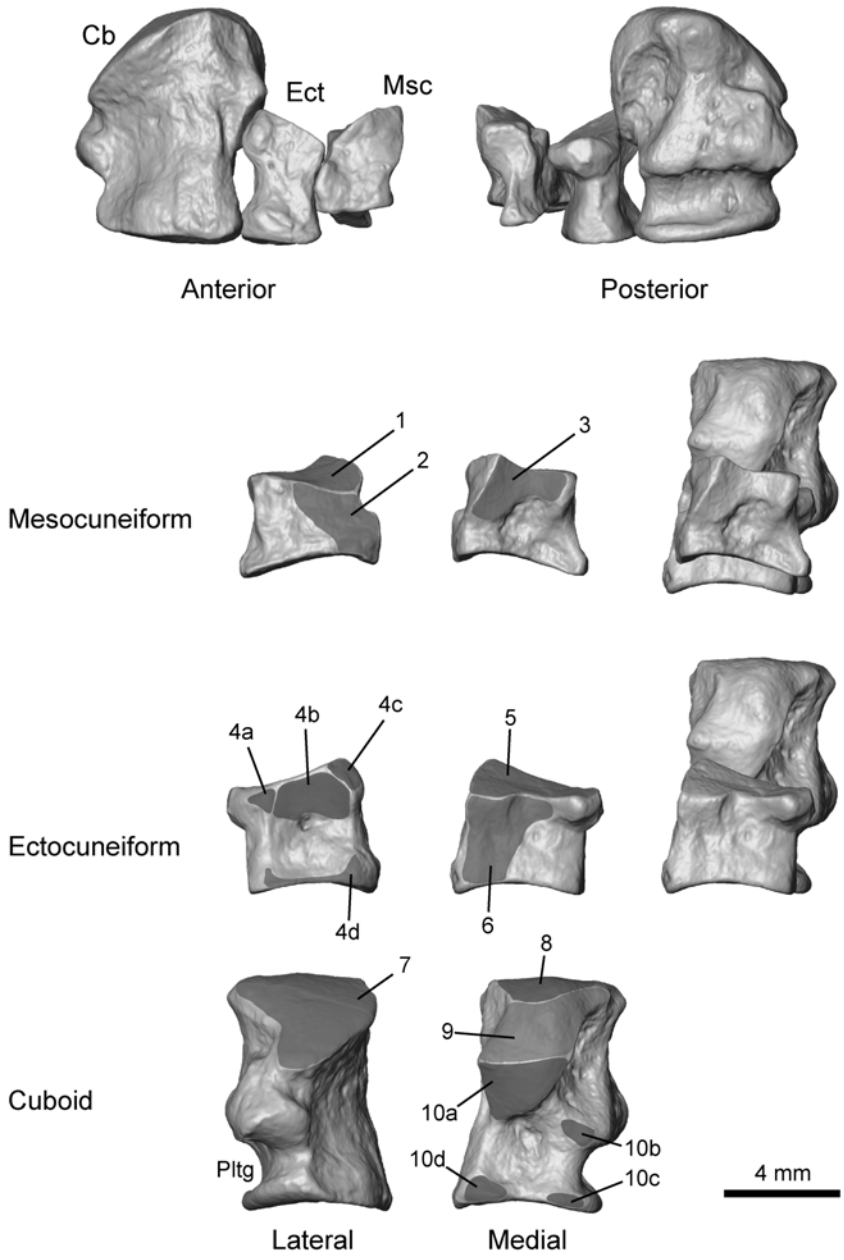

Figure 4.37. Surface reconstruction of distal tarsals of *Plesiadapis cookei* (UM 87990) based on HRxCT data [HRxCT resolution = 0.018 mm (cubic voxels)]. Articular areas shown in gray and labeled with numbers: 1 – navicular articular facet of mesocuneiform (Msc), 2 – ectocuneiform (Ect) facet, 3 – entocuneiform facet, 4a-d – cuboid (Cb), 5 – navicular facet of ectocuneiform, 6 – mesocuneiform facet, 7 – calcaneum facet, 8 – astragalus facet, 9 – navicular facet, and 10a-d – ectocuneiform facets of cuboid. Abbreviation: Pltg – peroneus longus tendon groove. Facet 4a typically contacts 10b. 4b seems to only engage 10a when the ectocuneiform is shifted proximally or dorsally relative to the cuboid. 4c contacts 10a when the bones are positioned as shown in the figure. 4d contacts 10c-d.

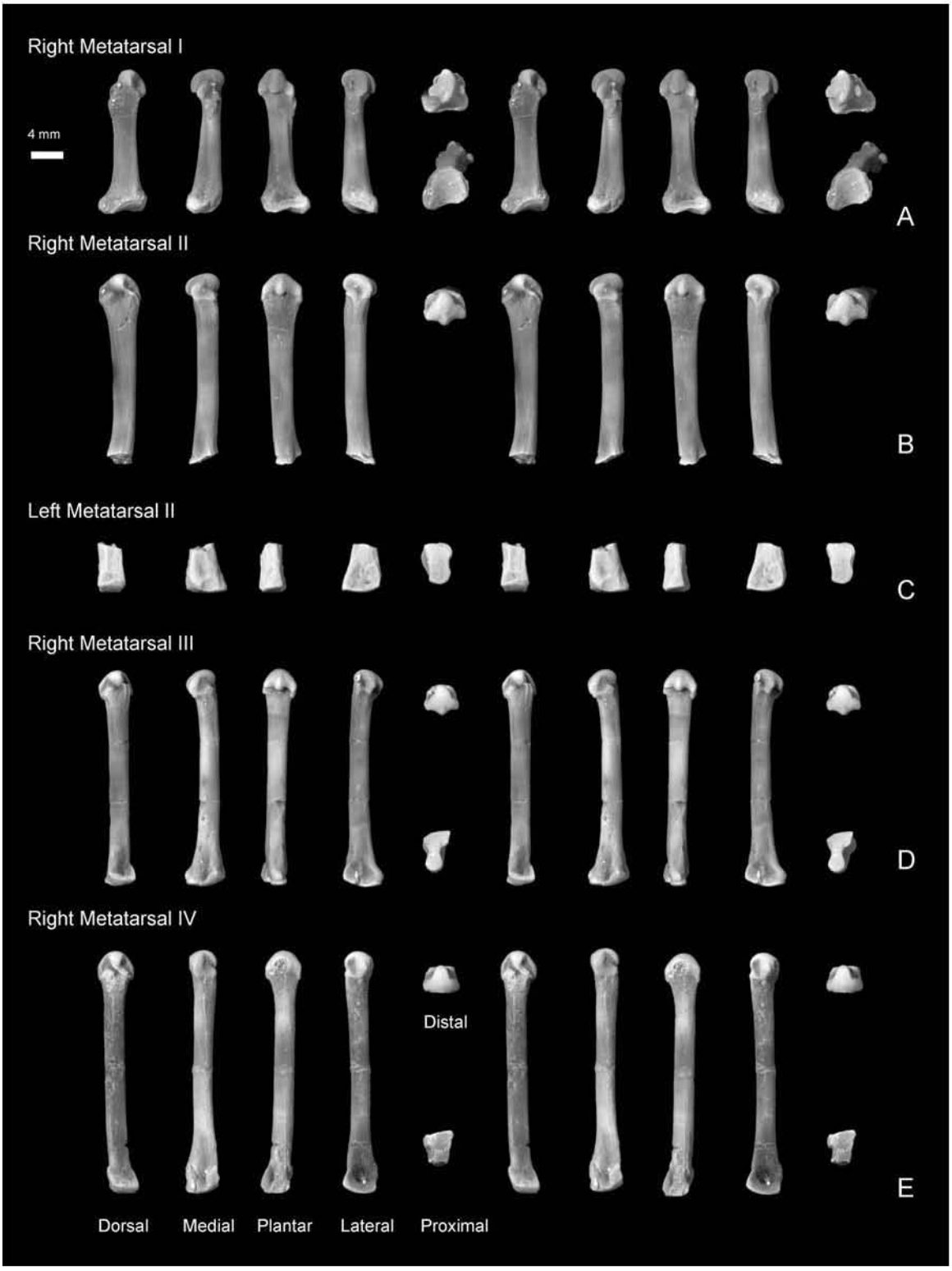

Figure 4.38. *Plesiadapis cookei* (UM 87990). Stereophotographic views of metatarsals. A, right MT I (hallucal metatarsal); B, right MT II; C, left proximal fragment of MT II; D, right MT III; and E, right MT IV.

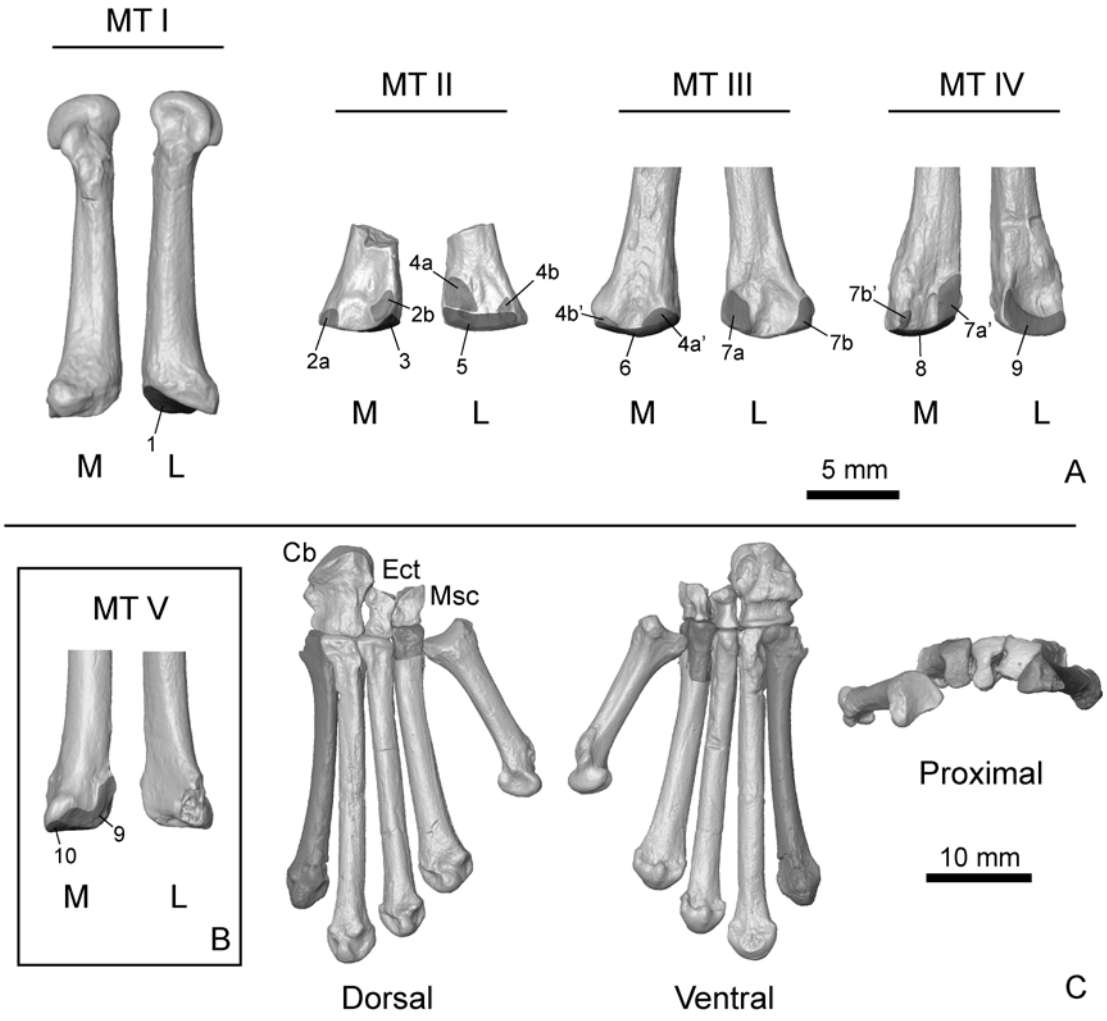

Figure 4.39. Surface reconstructions of metatarsals of *Plesiadapis cookei* (UM 87990) based on HRxCT data showing interpretation of articular relationships [HRxCT resolution = 0.018 mm (cubic voxels)]. A, metatarsals (MT) in medial (M) and lateral (L) views. Articular surfaces are illustrated with gray shading and labeled with numbers: 1 – entocuneiform facet, 2a-b – entoceuniform facets of MT II, 3 – mesocuneiform (Msc) facet, 4a-4a' – dorsal MT II-III facet, 4b-4b' – dorsal MT II-III facet, 5 – ectocuneiform (Ect) facet of MT II, 6 – ectocuneiform facet of MT III, 7a-7a' – dorsal MT III-IV facet, 7b-7b' – ventral MT III-IV facet, 8 – cuboid (Cb) facet of Mt IV, 9 – MT IV-V facet, and 10 – cuboid facet of MT V. B, views of HRxCT reconstruction of MT V belonging to cf. *P. churchilli* (P77.33.517). Lateral view shows this bone to be missing its peroneal tubercle. Otherwise the bone is well enough preserved to reveal that the proximal MT V fragment included in UM 87990 does not belong to *P. cookei* (Fig. 4.40). MT IV is also preserved in P77.33.517. Thus scans of the bones of cf. *P. churchilli* could be magnified together until the size of its MT IV equaled that of UM 87990. cf. *P. churchilli's* magnified MT V was then used in the reconstruction of *P. cookei's* foot. C, composite reconstruction of the metatarsus of *P. cookei*.

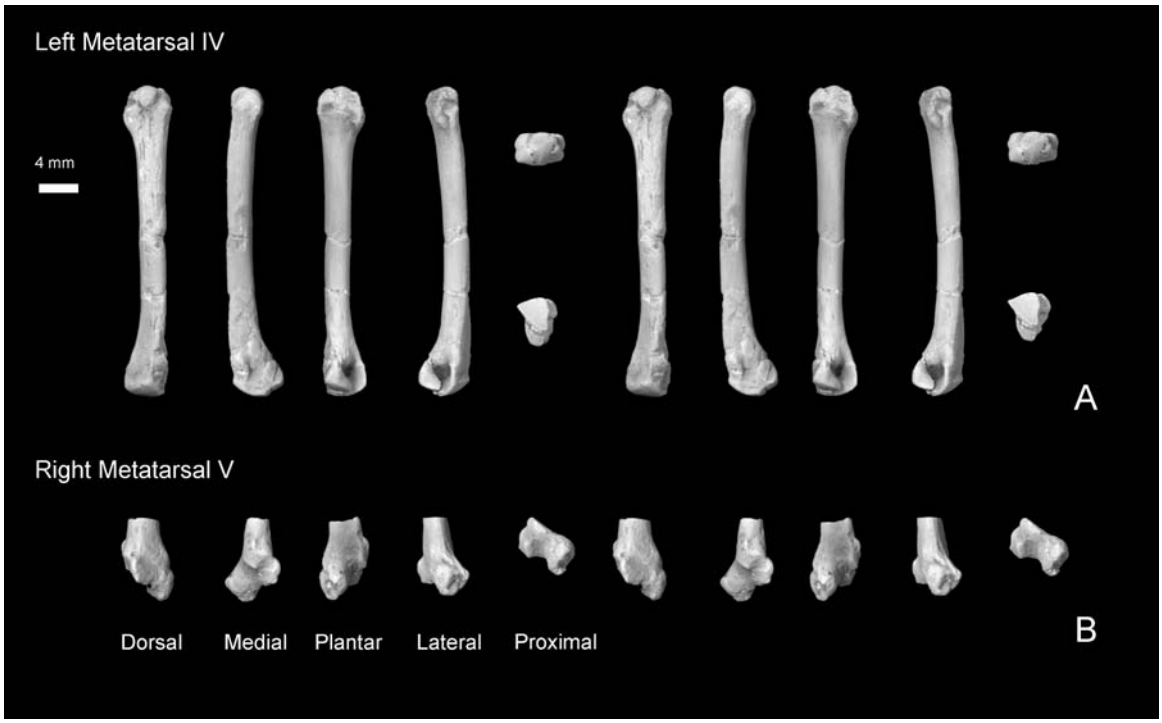

Figure 4.40. Stereophotographic views of metatarsals catalogued as UM 87990 that do not appear to belong to *Plesiadapis cookei*. A, left MT IV; and B, right proximal fragment of MT V.

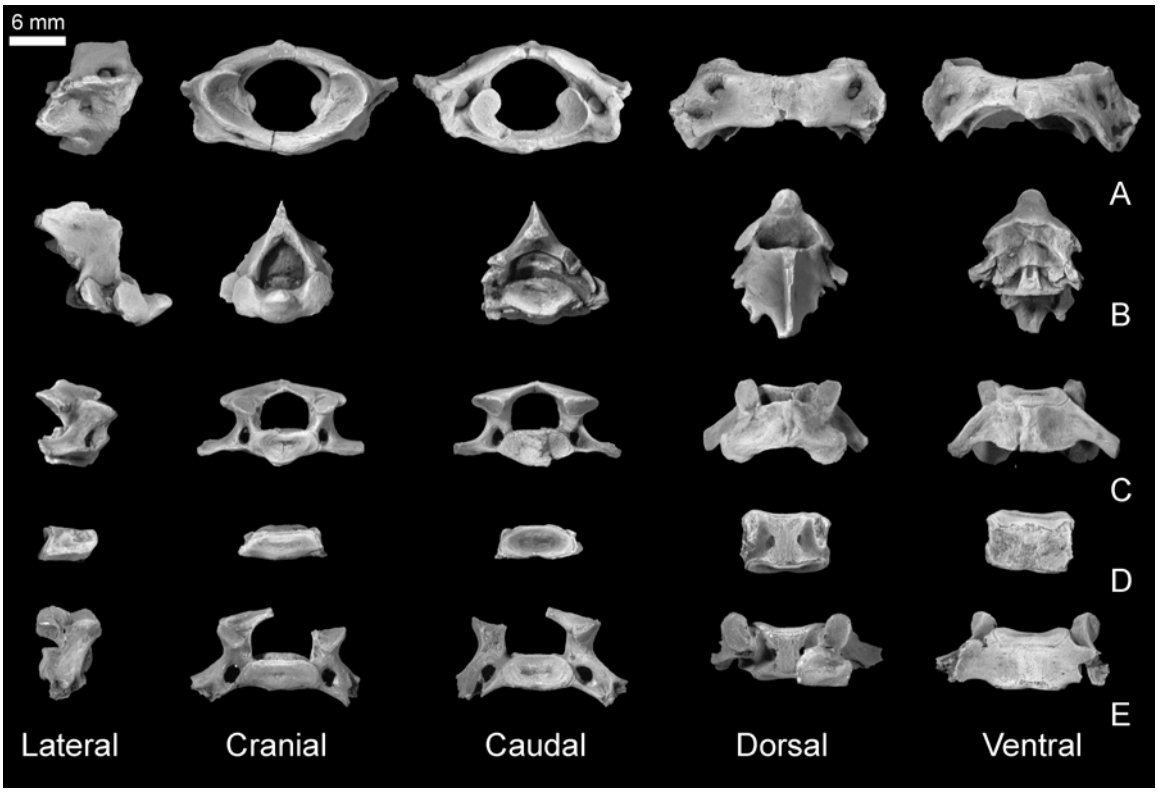

Figure 4.41. *Plesiadapis cookei* (UM 87990). Views of cervical (C) vertebrae. A, atlas; B, axis; C, ?C3; D, ?C4; and E, ?C6.

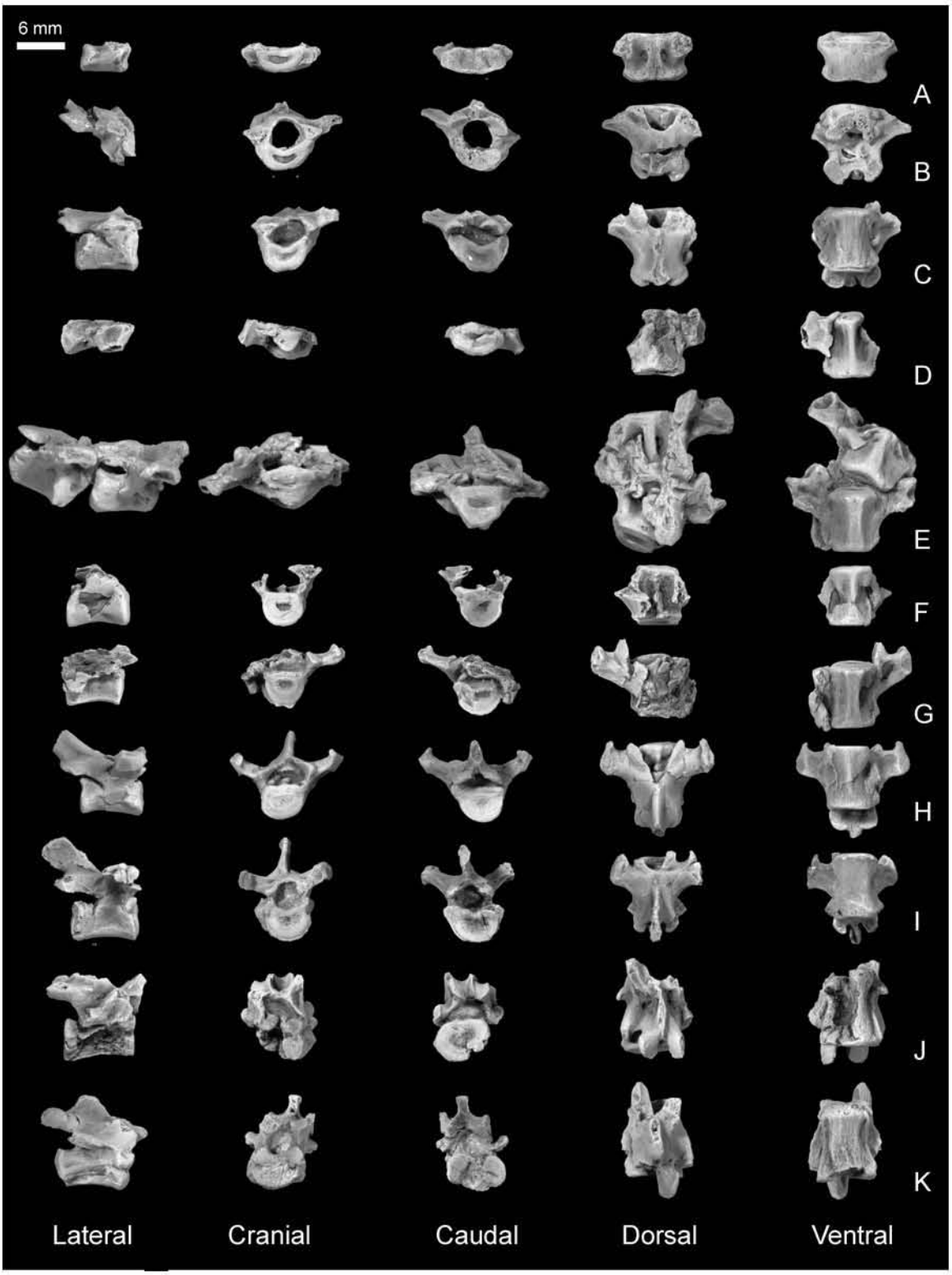

Figure 4.42. *Plesiadapis cookei* (UM 87990). Views of thoracic (T) vertebrae. A, ?T1; B, ?T2; C, ?T3; D, ?T4; E, ?T5-6; F, ?T7; G, ?T8; H. ?T9; I, ?T10; J, ?T12; and K, ?T13. A-I represent pre-diaphragmatic positions, J appears to be postdiaphragmatic and anticlinal, and K is postdiaphragmatic.

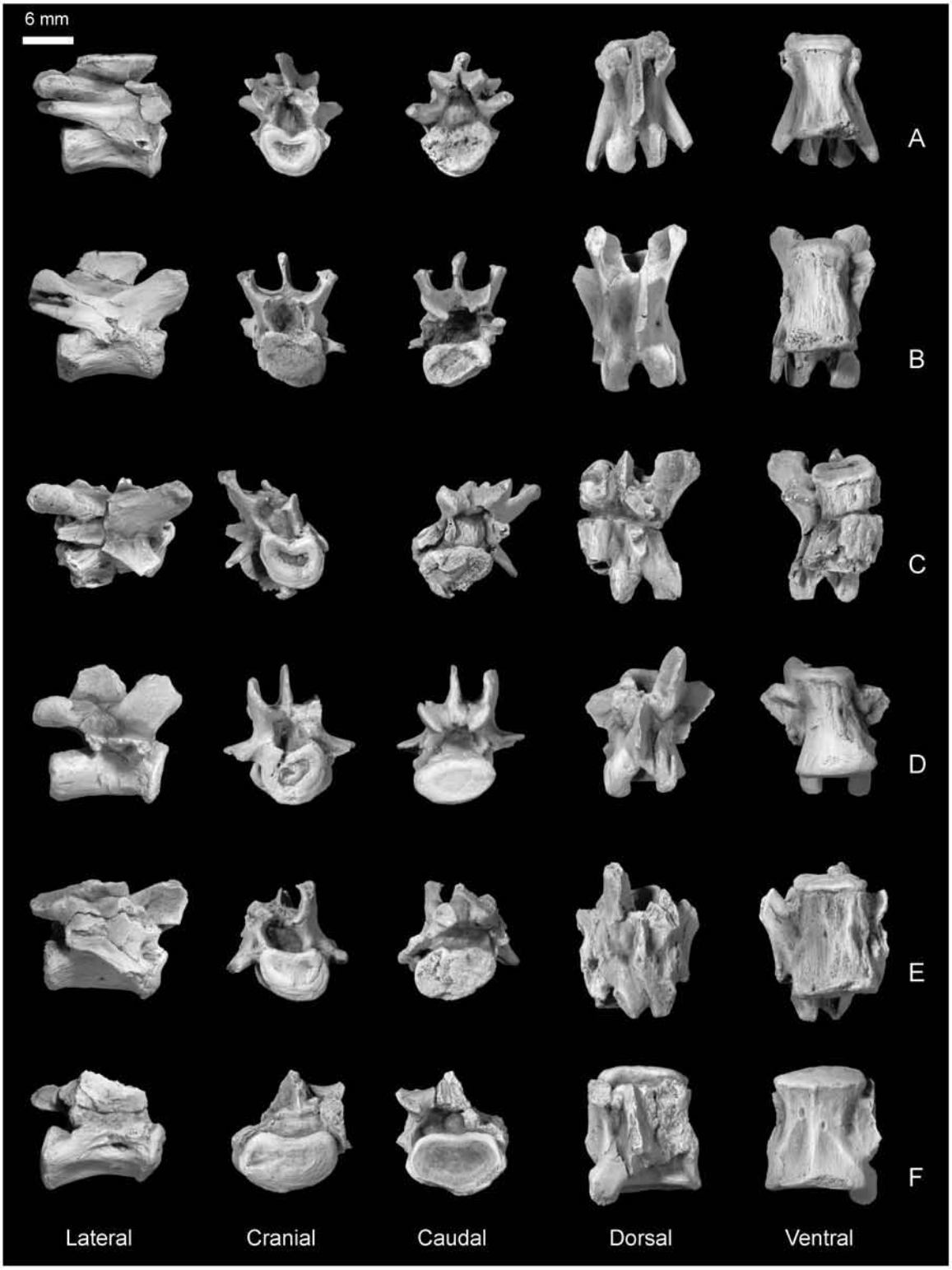

Figure 4.43. *Plesiadapis cookei* (UM 87990). Views of lumbar (L) vertebrae. A, ?L1; B, ?L3; C, ?L4; D, ?L5; E, ?L6; and F, ?L7.

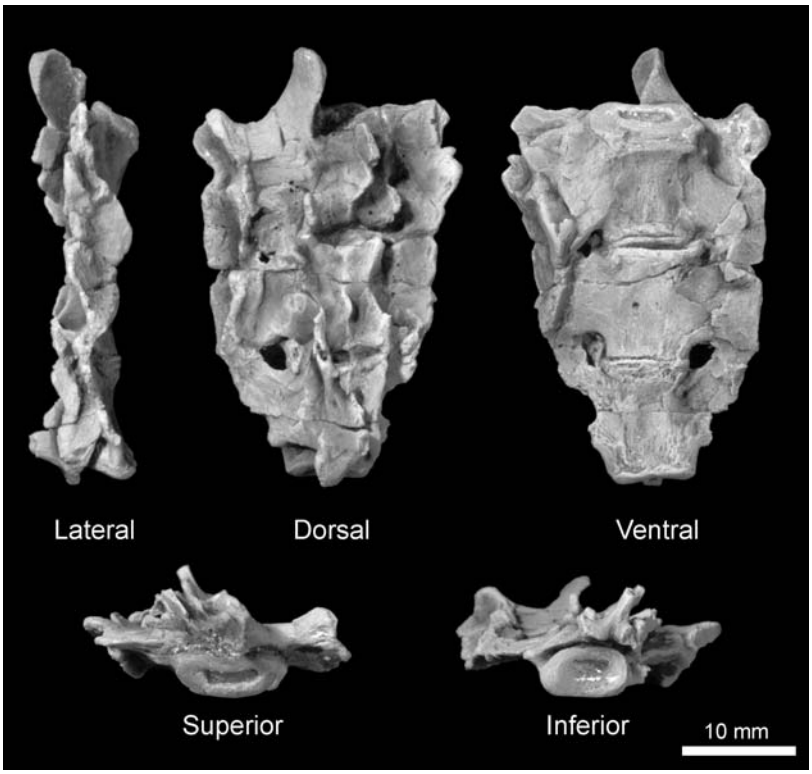

Figure 4.44. *Plesiadapis cookei* (UM 87990). Views of sacrum.

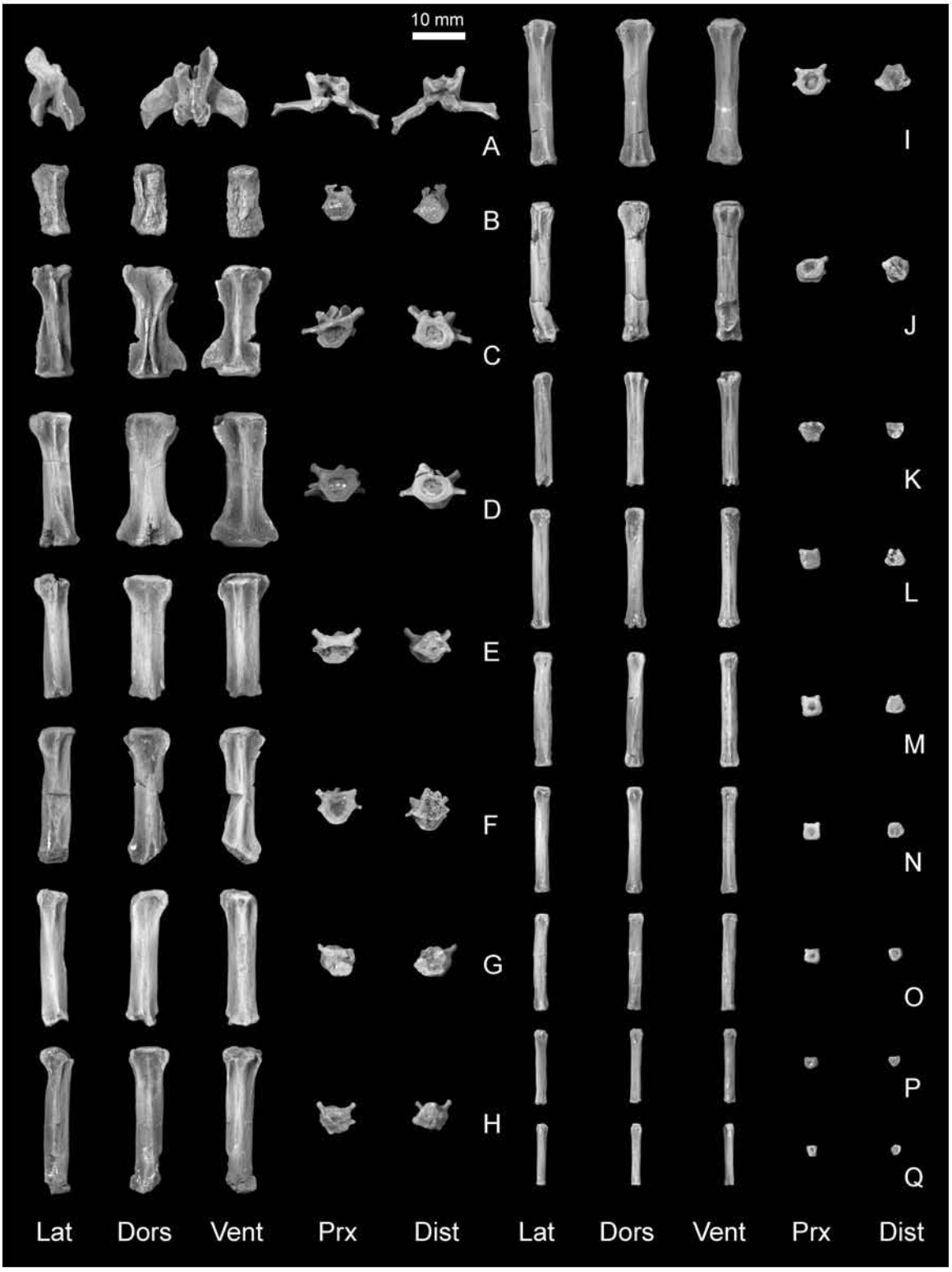

Figure 4.45. *Plesiadapis cookei* (UM 87990). Views of caudal (Ca) vertebrae. A, Ca1, 2 or 3; B, ?Ca4; C, ?Ca6; D, ?Ca7; E, ?Ca8; F, ?Ca9; G, ?Ca10; H, ?Ca11; I, ?Ca12; J, ?Ca13; K, ?Ca14; L, ?Ca15; M, ?Ca16; N, ?Ca17; O, ?Ca18; P, ?Ca19; and Q, ?Ca20.

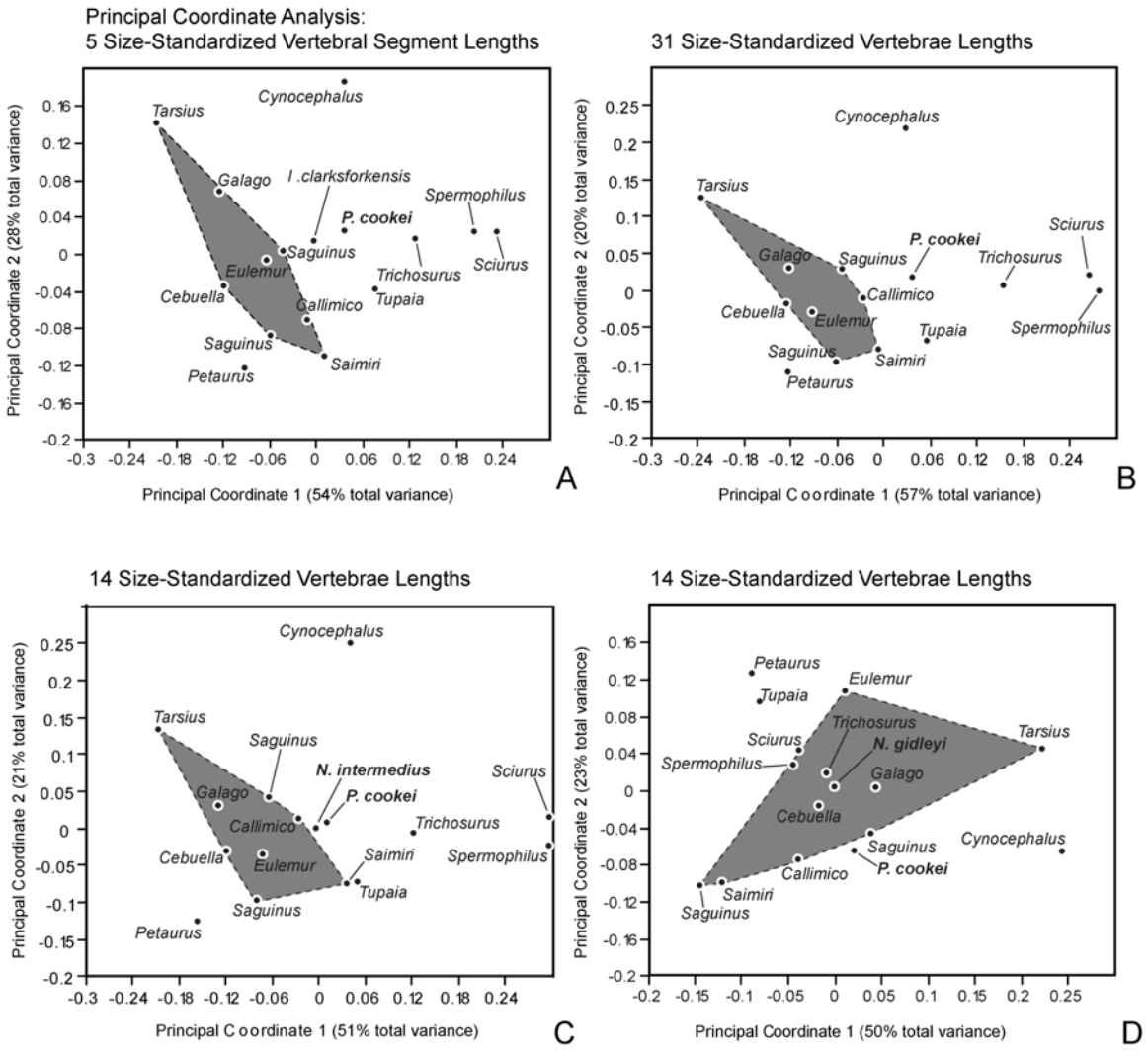
Principal Coordinate Analysis:
5 Size-Standardized Vertebral Segment Lengths
Principal Coordinate 2 (28% total variance)
Principal Coordinate 1 (54% total variance)
Cynocephalus
Tarsius
Galago
I .clarksforkensis
Spermophilus
P. cookei
Saguinus
Sciurus
Eulemur
Trichosurus
Cebuella
Callimico
Tupaia
Saguinus
Saimiri
Petaurus
A
31 Size-Standardized Vertebrae Lengths
Principal Coordinate 2 (20% total variance)
Principal C oordinate 1 (57% total variance)
Cynocephalus
Tarsius
Sciurus
P. cookei
Galago
Saguinus
Trichosurus
Callimico
Cebuella
Eulemur
Tupaia
Spermophilus
Saguinus
Saimiri
Petaurus
B
14 Size-Standardized Vertebrae Lengths
Principal Coordinate 2 (21% total variance)
Principal C oordinate 1 (51% total variance)
Cynocephalus
Tarsius
Saguinus
N. intermedius
Sciurus
Galago
P. cookei
Callimico
Trichosurus
Cebuella
Eulemur
Saimiri
Spermophilus
Tupaia
Saguinus
Petaurus
C
14 Size-Standardized Vertebrae Lengths
Principal Coordinate 2 (23% total variance)
Principal Coordinate 1 (50% total variance)
Petaurus
Eulemur
Tupaia
Trichosurus
Tarsius
Sciurus
N. gidleyi
Spermophilus
Galago
Cebuella
Saguinus
Cynocephalus
P. cookei
Callimico
Saimiri
Saguinus
D

Figure 4.46.

Figure 4.46. Plots of principal coordinate scores based on an analysis of Euclidean distance matrices calculated from vertebrae and vertebral column length shape variables (calculated from raw measurements of Tables 5.24-30). A, plot based on shape variables calculated from measurements of Table 5.24: Cl, Tl, Ll, Sl, and Cal (see introduction for explanation of measurements). B, plot of coordinate scores calculated from 31 vertebral measurements from Tables 5.24-30 including the following craniocaudal lengths: Sl, C1-4, C6, T1, T3-10, T12, L1, L3-5, L7, S1-3, Ca1, Ca4, and Ca6-10. C, plot of coordinate scores calculated from 14 vertebral measurements from Tables 5.24-30 including the following craniocaudal lengths: Sl, C1-3, C-6, T7, L1, L7, S1-3, and Ca6-7. This subset was chosen to allow inclusion of *Nannodectes intermedius* (USNM 442229) vertebrae. D, plot of coordinate scores calculated from 14 vertebral measurements from Tables 5.24-30 including the following craniocaudal lengths: Sl, C1-4, T1, T12, L1, L3-4, S1-3, and Ca1. This subset was chosen to allow inclusion of *N. gidleyi* (AMNH 17379) vertebrae. Comparative sample data are not included here. As discussed in the methods section the variables for each analysis are natural log ratios of each raw measurement to the geometric mean of all measurements of a given specimen included in each analysis. The gray polygons encompass euprimates of the sample.

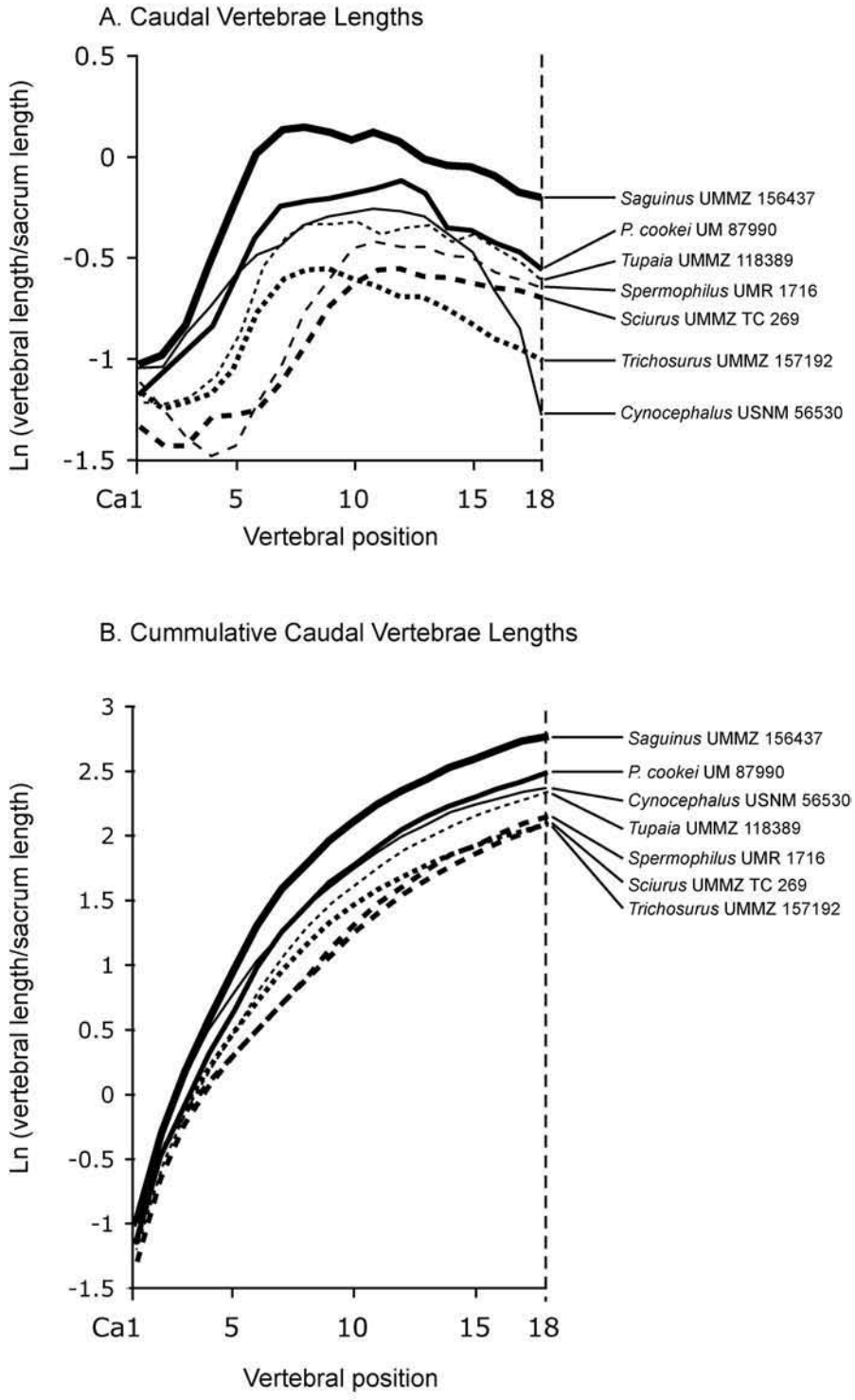
A. Caudal Vertebrae Lengths
Ln (vertebral length/sacrum length)
0.5
0
-0.5
-1
-1.5
Ca1
5
10
15
18
Vertebral position
Saguinus UMMZ 156437
P. cookei UM 87990
Tupaia UMMZ 118389
Spermophilus UMR 1716
Sciurus UMMZ TC 269
Trichosurus UMMZ 157192
Cynocephalus USNM 56530
B. Cummulative Caudal Vertebrae Lengths
Ln (vertebral length/sacrum length)
3
2.5
2
1.5
1
0.5
0
-0.5
-1
-1.5
Ca1
5
10
15
18
Vertebral position
Saguinus UMMZ 156437
P. cookei UM 87990
Cynocephalus USNM 56530
Tupaia UMMZ 118389
Spermophilus UMR 1716
Sciurus UMMZ TC 269
Trichosurus UMMZ 157192

Figure 4.47

Figure 4.47. Caudal vertebrae comparisons. A, proportional length of the first 18 caudal vertebrae of *Plesiadapis cookei, Cynocephalus,* and a subset of the comparative sample (standardized to sacrum length of each specimen by taking the natural log ratio of each vertebral length to the sacrum length). Note that the last several vertebrae of the tail of *Cynocephalus* decrease in proportional length more drastically than in the other taxa. Also note that, after the euprimate *Saguinus, P. cookei* has the proportionally longest inferior caudal vertebrae starting at Ca6. B, cumulative proportional length shows that by the 18th caudal vertebra, *P. cookei* has the second longest tail relative to its sacrum (for the calculation of *P. cookei's* tail length, missing vertebrae Ca2-3 were assumed to each be the same length as Ca1, and missing Ca5 was represented by the average between Ca4 and Ca6). Although *Cynocephalus* has the third longest tail at Ca18, this represents the tip of its tail, while all other taxa in this sample have additional vertebrae, including *P. cookei*.

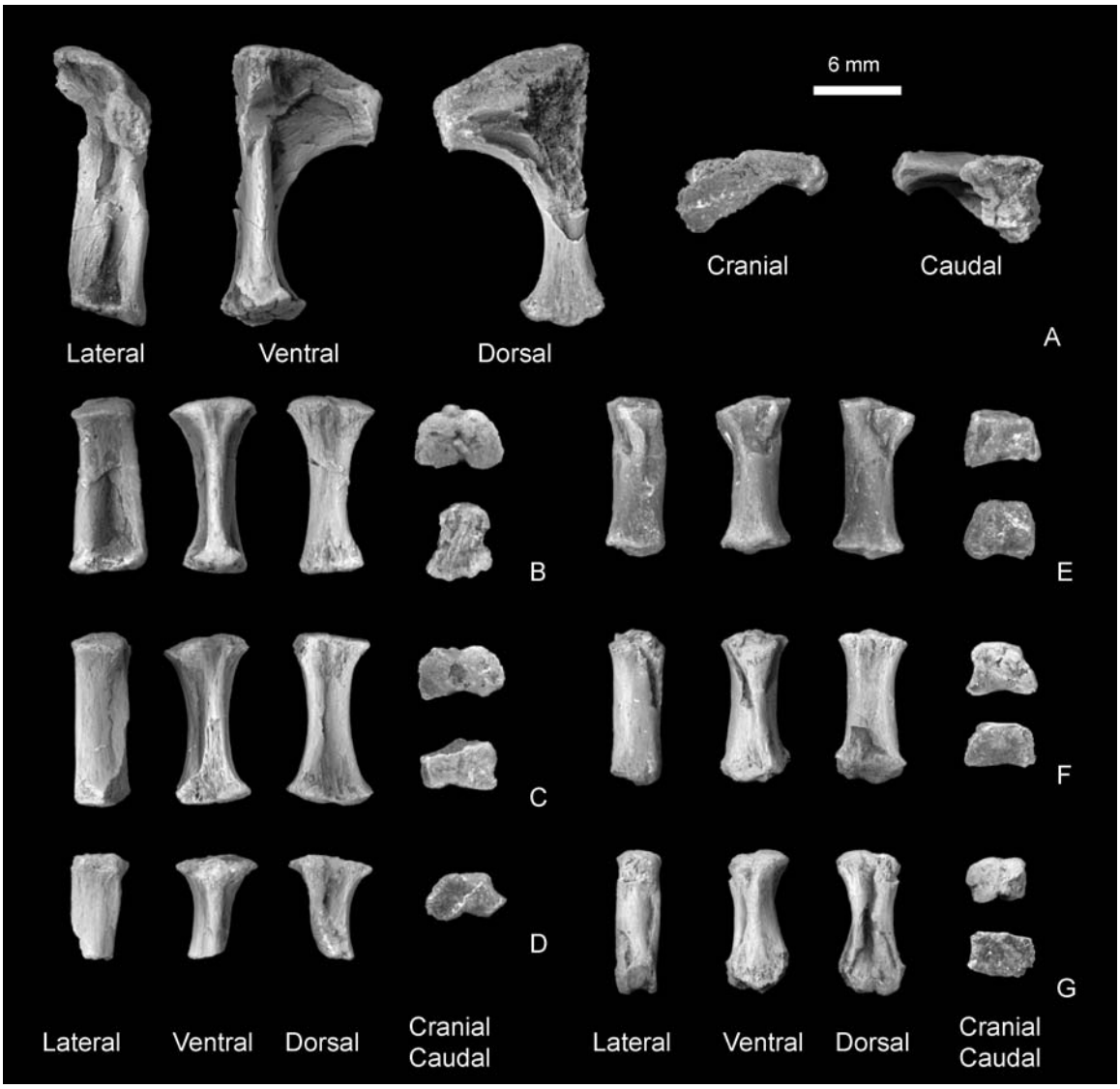

Figure 4.48. *Plesiadapis cookei* (UM 87990). Views of sternebrae (st). A, Manubrium; B, ?St1; C, ?St2; D, ?St3; E, ?St4; F, ?St5; and G, ?St6. ?St6 appears to be the ultimate sternebra because its inferior end does not look like the superior or inferior surfaces on the other sternebrae. It compares well to the ultimate sternebra of articulated museum specimens of primates, treeshrews and squirrels.

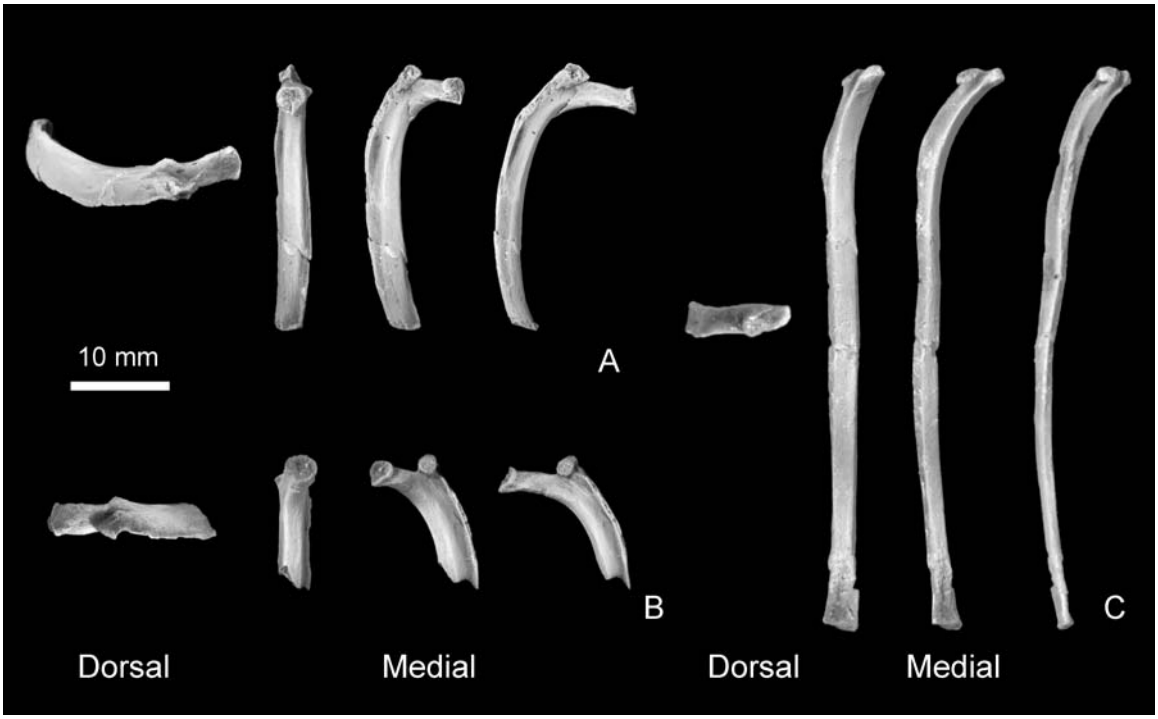

Figure 4.49. *Plesiadapis cookei* (UM 87990). Views of ribs. A, most superior rib preserved from the left side; B, most superior rib preserved from the right side; and C, one of the most inferior rib positions of the left side.

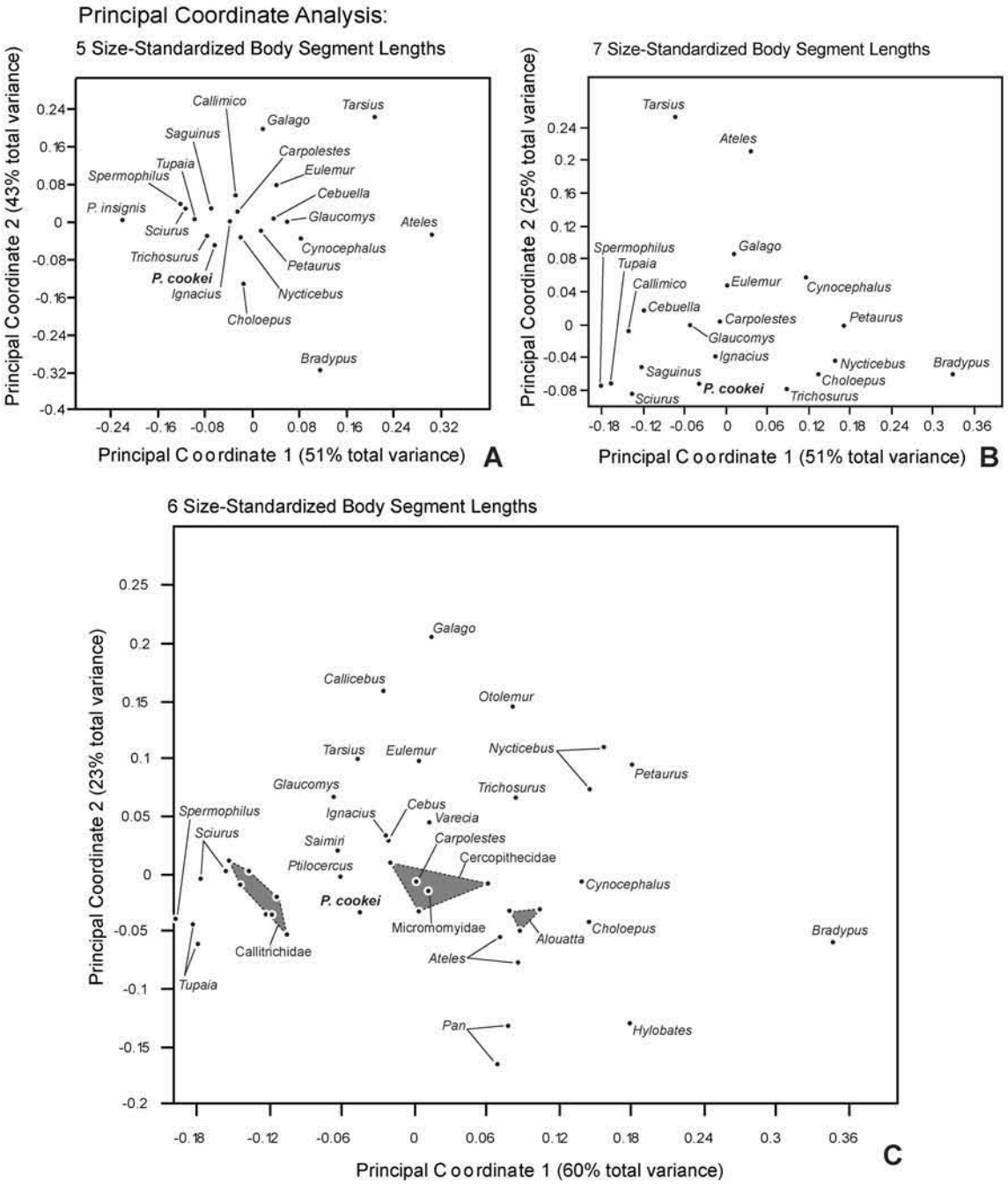
Principal Coordinate Analysis:
5 Size-Standardized Body Segment Lengths
Principal Coordinate 2 (43% total variance)
Principal C oordinate 1 (51% total variance)
A
Callimico
Tarsius
Galago
Saguinus
Carpolestes
Tupaia
Eulemur
Spermophilus
Cebuella
P. insignis
Glaucomys
Ateles
Sciurus
Cynocephalus
Trichosurus
Petaurus
P. cookei
Ignacius
Nycticebus
Choloepus
Bradypus
7 Size-Standardized Body Segment Lengths
Principal Coordinate 2 (25% total variance)
Principal C oordinate 1 (51% total variance)
B
Tarsius
Ateles
Spermophilus
Galago
Tupaia
Callimico
Eulemur
Cynocephalus
Cebuella
Carpolestes
Petaurus
Glaucomys
Ignacius
Nycticebus
Bradypus
Saguinus
Choloepus
P. cookei
Sciurus
Trichosurus
6 Size-Standardized Body Segment Lengths
Principal Coordinate 2 (23% total variance)
Principal C oordinate 1 (60% total variance)
C
Galago
Callicebus
Otolemur
Tarsius
Eulemur
Nycticebus
Petaurus
Glaucomys
Trichosurus
Spermophilus
Ignacius
Cebus
Varecia
Sciurus
Saimiri
Carpolestes
Cercopithecidae
Ptilocercus
Cynocephalus
P. cookei
Micromomyidae
Alouatta
Choloepus
Bradypus
Callitrichidae
Ateles
Tupaia
Pan
Hylobates

Figure 4.50.

Figure 4.50. Plots of principal coordinate scores based on analyses of Euclidean distance matrices calculated from body segment length shape variables (calculated from raw measurements of Tables 5.33, 35). A, plot of coordinate scores calculated from Trk-L, H-L, R-L, F-L, and T-L. B, plot of coordinate scores calculated from Trk-L, H-L, R-L, MC III-L, F-L, T-L, and MT III-L. C, plot of coordinate scores calculated from H-L, R-L, MC III-L, F-L, T-L, and MT III-L. As discussed in the methods section the variables for each analysis are natural log ratios of each raw measurement to the geometric mean of all measurements of a given specimen included in each analysis. Gray areas represent distributions of taxa indicated by labels.

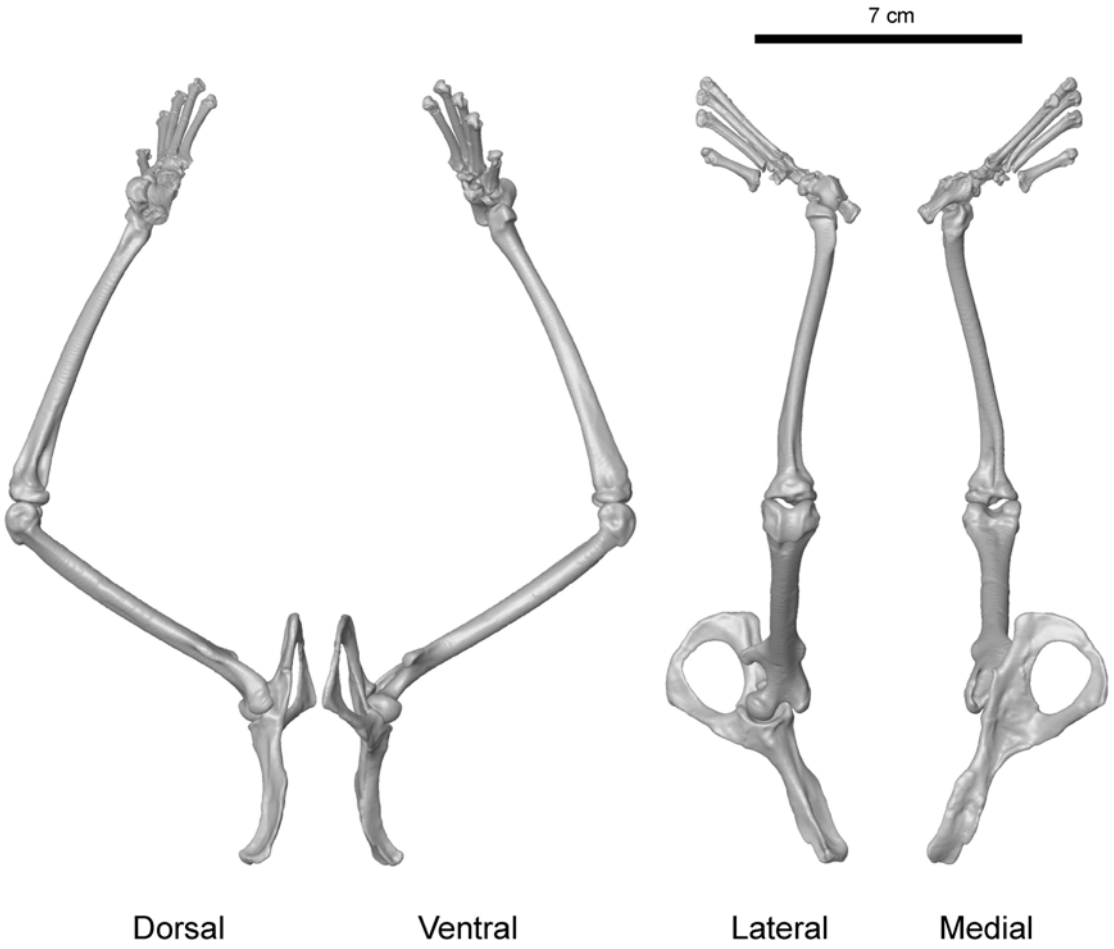

Figure 4.51. Surface reconstruction of hind limb based on HRxCT and medical CT data [innominate, femur, and tibia CT image resolution = 0.18(x) x 0.18(y) x 0.20(z) mm: foot bone HRxCT resolution = 0.018 mm (cubic voxels)]. Reconstruction illustrates a posture possibly utilized in vertical descent of large diameter tree trunks. Note that further inversion of the foot could likely have been accomplished by rotations at the transverse tarsal joint and between the metatarsals and distal tarsals.

CHAPTER 5:
CHARACTER STATE RECONSTRUCTIONS FOR THE ANCESTRAL PLESIADAPID AND EVALUATION OF THEIR PHYLOGENETIC IMPLICATIONS

ABSTRACT

New information on plesiadapid crania and postcrania allows for better-supported interpretations of the morphological characteristics of the common ancestor of the family Plesiadapidae, as well as better-supported inferences regarding soft anatomical structures. The implications of this new information for testing hypotheses of euarchontan (plesiadapiforms, euprimates, scandentians, and dermopterans) phylogenetic relationships are evaluated cladistically in this chapter in the context of previously published matrices. Specifically, a new species-level cladistic analysis based on a matrix of 32 dental characters and 30 taxa was used to reconstruct relationships among plesiadapids. Next, new information on non-dental osteological characters and soft anatomy was optimized onto this cladogram, thus providing an hypothesis for character states in the most basal plesiadapid skull and postcranial skeleton. Finally, the ancestral reconstruction for Plesiadapidae was used to reassess the phylogenetic position of the group with cladistic analysis of a published matrix of 20 taxa and 173 characters that samples the cranium, dentition, and postcranium.

The cranium of the ancestral plesiadapid is reconstructed as having enlarged premaxillae that broadly contact the frontals; a laterally-positioned, intratympanic, transpromontorial route for the internal carotid plexus; a non-functional internal carotid artery; a non-tubular external auditory meatus; and a petrosal bulla. *Plesiadapis cookei* and *P. tricuspidens* appear derived in their tubular external auditory meati and maxillae lacking extensive dorsal exposure of molar tooth roots. *P. tricuspidens* is apparently autapomorphic among plesiadapids in having an increased relative size and posterior projection of the premaxilla, correlated narrowing of the frontal contact of the nasal, an increased relative size of the glenoid fossa and decreased prominence and posterior projection of the nuchal crests. *Nannodectes gidleyi* is autapomorphic in the increased relative size of its glenoid fossa, and the apparent lack of an intratympanic route for the internal carotid plexus. Postcranially, the ancestor of the Plesiadapidae can now be recognized to have had a humerus with a laterally facing deltopectoral crest, and a lateral ridge on the ulnar trochlea; an entocuneiform with a large plantodistal process; claws on all digits; an innominate with a short pubic symphysis; and an axis with a cranially projecting spinous process.

Analyses of a partition of the revised higher level matrix reveals that new information on the cranium alone does not support previous hypotheses for the phylogenetic relationships of some euarchontans. However, analysis of the entire matrix failed to overturn the previously recovered topology for euarchontan relationships.

INTRODUCTION

Bloch et al. (2007) analyzed the relationships among plesiadapiforms using a mixture of species, genus, and family level taxa. They used a family level operational taxonomic unit (O.T.U.) to represent plesiadapids and based their coding primarily on the literature available for the skull and skeleton of *Plesiadapis tricuspidens* (e.g., Russell, 1964; Szalay et al., 1975; Gingerich, 1976), a humerus of *Plesiadapis walbeckensis* (Szalay and Dagosto, 1980), and the postcranium of *Nannodectes* (Simpson, 1935; Beard, 1989), as well as on direct observations of the skeleton of *Plesiadapis cookei* (UM 87990). When different reference species showed variance in character states, Bloch et al. (2007) represented the Plesiadapidae as polymorphic. New information on plesiadapid skeletons presented in chapters 2-4 allows a more accurate coding of the "Plesiadapidae" in the Bloch et al. (2007) matrix. In this study, the use of polymorphic codings for the "Plesiadapidae" is avoided as much as possible: a "composite" Plesiadapidae O.T.U. is generated by optimizing states of characters onto the ancestral node of a newly generated species level tree.

The over arching hypotheses to be tested with the new skeletal material are that (1) plesiadapids are close relatives of carpolestids and (2) these taxa plus saxonellids and *Chronolestes simul* are the sister taxon to Euprimates. The former hypothesis is an apparently fragile aspect of recent phylogenetic analyses (Bloch et al., 2007). While a carpolestid-plesiadapid clade has been favored by specialists familiar with dental morphology (Simpson, 1937; Szalay, 1968; Gingerich, 1976; Fox, 1993; Van Valen,

1994), only one (Bloch et al., 2007) of several (i.e., also Bloch and Boyer, 2002; Bloch and Silcox, 2006) recently published cladistic analyses has recovered unambiguous support for such a grouping.

Bloch and Silcox (2006) described known crania of *Carpolestes simpsoni*. They showed the nasals to have a narrow caudal extent, the frontal and maxilla to have a sutural contact in the orbit, and described the presence of a foramen rotundum. Additionally, they documented the carpolestid basicranium to have the following features: a posteromedially positioned posterior carotid foramen; a large internal carotid canal (proportionally and absolutely larger than that of even the largest plesiadapids: see tables 3.3; 5.7); well developed stapedial and promontorial grooves on the promontorium; a promontorial groove that does not clearly lead to any septa; and a bone that may be either a dividing wall within a two-chambered auditory bulla or an inconspicuously preserved ectotympanic. The cochlea of *Carpolestes* has since been measured and shown to be unusually short (Table 2.3) (Coleman and Boyer, 2008).

In contrast, as demonstrated in chapters 2 and 3, most plesadapids have nasals that are mediolaterally broad at their caudal extent, the nature of suturing in the orbital mosaic is ambiguous, and there is no foramen rotundum. Furthermore, virtually all known plesiadapids have a laterally positioned posterior carotid foramen, an internal carotid plexus foramen of small diameter, no expression of a stapedial system, a narrow promontory groove that leads to an anterior septum (*s1*), no evidence of multi-chambered bullae, no solid evidence of an ectotympanic bone that is distinct from the bullar wall, and a relatively long cochlea (Table 2.3). However, in Chapter 2, two plesiadapids were argued to have a non-tubular ectotympanic, and *Plesiadapis tricuspidens* was shown to

have a lacrimal bone that retains its tubercle. These last two character states are also seen in carpolestids and other plesiadapiforms.

Bloch and Boyer (2002, 2007), Sargis et al. (2007), and Kirk et al. (2008) demonstrated that carpolestids have a number of postcranial specializations for pedal and manual grasping. Bloch and Boyer (2003, 2007), Bloch et al. (2007), and Sargis et al. (2007) acknowledged that if character states considered to be carpolestid and euprimate grasping specializations are homologous, and plesiadapids are the sister taxon of carpolestids, then plesiadapids must have evolved a number of similarities (such as a divergent, but unopposable hallux, and an entocuneiform with a large plantodistal process) to non-carpolestid plesiadapiforms (e.g., paromomyids) convergently or in parallel. This hypothesis predicts that the common ancestor of Plesadapidae and Carpolestidae, and possibly early plesiadapids, should look more like *Carpolestes*. Boyer et al. (2004) claimed that several features of *Nannodectes intermedius* support this hypothesis, but the differences cited to separate larger plesiadapids from *Nannodectes* are either subtle and not statistically significant, or are not clearly directly related to differences in character states reflecting grasping specializations that make *Carpolestes* specifically "euprimate-like." Furthermore, new information from the postcranium of *Plesiadapis cookei* does not add support to the hypothesis that plesiadapids and carpolestids have a common ancestor that is carpolestid-like (Chapter 4).

In all of the ways that plesiadapids differ cranially and postcranially from *Carpolestes*, they are similar to known paromomyids (Kay et al., 1992; Wible, 1993; Bloch and Silcox, 2001; Silcox, 2003). Furthermore, although most plesiadapids have a promontorium that is dorsoventrally deep compared to its mediolateral breadth, the

petrosal of *Nannodectes intermedius* has a configuration more similar to that of a paromomyid (compare "pd" and "pw" in Table 2.3). Finally, many of the features characterizing the carpolestid ear are typically thought to be primitive eutherian features (Novacek, 1986; Bloch and Silcox, 2006), while those characterizing plesiadapids and paromomyids generally appear to be more derived (Kay et al., 1992; Wible, 1993; Bloch and Silcox, 2001; Silcox, 2003). Therefore, because many features reflecting characters coded in the Bloch et al. (2007) matrix now appear to differentiate, rather than unite, Plesiadapidae and Carpolestidae, I predict that a revised characterization of plesiadapid morphology will refute the hypothesis that plesiadapids and carpolestids are sister taxa.

With regard to soft anatomical inference, plesiadapid crania were previously interpreted to differ from those of their proposed sister taxon, the Carpolestidae (Bloch and Silcox, 2006; Bloch et al., 2007), in lacking a functional internal carotid artery (MacPhee et al., 1983; Bloch and Silcox, 2006). As demonstrated in the previous chapters, the posterior carotid foramen and canal exist and the internal carotid plexus has an intratympanic route in virtually all known plesiadapid specimens that are sufficiently well preserved. Even so, the diameter of the posterior carotid foramen has never been used to quantitatively assess the functionality of the artery, though this has been done for other plesiadapiforms (Kay et al., 1992; Bloch and Silcox, 2006). Therefore, this work also evaluates the hypothesis that plesiadapids lack a functional internal carotid artery in a quantitative fashion for the first time using data on posterior carotid foramen diameter and skull size.

Institutional abbreviations

AMNH, American Museum of Natural History, New York; CM, Carnegie Museum of Natural History, Pittsburgh; MNHN, Muséum Nationale d'Histoire Naturelle, Paris; UALVP, University of Alberta Laboratory for Vertebrate Paleontology, Edmonton; UM, University of Michigan, Ann Arbor; USNM, United States National Museum of Natural History, Smithsonian Institution, Washington; YM, Yorkshire Museum, York; YPM-PU, Yale Peabody Museum-Princeton University collection, New Haven.

Generic abbreviations

Ch.- Chiromyoides

E. - Elphidotarsius

I. - Ignacius

P. – Plesiadapis

Pl. - Platychoerops

Pr. – Pronothodectes

N. – Nannodectes

METHODS

Phylogenetic reconstructions

Species level cladistic analysis – A species level tree was generated using parsimony analyses of a matrix consisting of 32 dental characters (Table 5.1) and 30 taxa (Table 5.2), including two outgroups (*Purgatorius janisae*, and *Elphidotarsius*).

Outgroup taxa were scored from the literature including Bloch et al. (2001), Clemens (2004), and Silcox and Gunnell (2008) for *P. janisae*, and Bloch et al. (2001) and Silcox et al. (2001) for *Elphidotarsius*. *Elphidotarsius* is a composite of *E. florencae* and *E. wightoni*, the two most basal species of the Carpolestidae (Bloch et al., 2001; Silcox et al., 2001), because individual species are fragmentarily known. The 28 plesiadapid species included were scored based on Gingerich (1976), Fox (1990), newly available data from the upper dentition of *Pr. gaoi* (Chapter 2), an undescribed upper dentition of *Ch. caesor* (CM 72770), undescribed lower incisors of *Ch. caesor*, and undescribed central incisors of *Nannodectes gazini* (CM 76922, CM 76938).

Gingerich (1976) inferred dental formulae for several poorly preserved plesiadapid species. I follow these inferences in my character coding, unless evidence documented by Gingerich (1976) or elsewhere (i.e., in newly available specimens) contradicts his reconstructions. For instance, Gingerich (1976) inferred that *P. cookei*, *Pl. russelli* and other *Platychoerops* species lacked upper canines, but retained upper second premolars, based on the well-known morphology of *P. tricuspidens*. However, as documented and discussed in Chapter 3, *P. cookei* UM 87990 actually lacks C^1 *and* P^2. Furthermore, it appears to me that the type of *Pl. richardsoni* (YM 550) also lacks these teeth. Therefore, it cannot be assumed that *Pl. russelli* and *Pl. daubrei* retained P^2.

The character matrix was analyzed with the program Nona (Nixon, 1999-2002) in WinClada (Goloboff, 1999) using a heuristic search of ~5,000 replicates.

Character optimization - Cranial and postcranial characters discussed in the preceding three chapters (2-4), as well as characters from Bloch et al. (2007), are optimized onto the ancestral node for Plesiadapidae using the newly generated species

level cladogram. A total of 33 cranial characters and 65 postcranial characters are optimized (Tables 5.3, 5.4A-C). The optimization represents only a "downpass" step of the total optimization exercise (e.g., Wiley et al., 1991) because the ancestral state cannot be assumed as required for the "uppass" step. Furthermore, inclusion of the sister taxon to the Plesiadapidae cannot be used to help reconstruct the ancestral condition of the family because this would allow results of the Bloch et al. (2007) cladistic analysis to influence the reconstruction. Instead, the ancestral node for the Plesiadapidae is left polymorphic for characters that cannot be reconstructed as monomorphic through a "majority rules" criterion on the "downpass" step of the optimization.

Cladistic analysis of matrices using higher level taxa - The character matrix of Bloch et al. (2007) was downloaded from Morphobank.geongrid.org. The character matrix of Bloch and Silcox (2006) was obtained from M. Silcox. The Bloch and Silcox (2006) matrix simply represents the cranial partition of the Bloch et al. (2007) matrix. I re-analyze it here to assess the affect of new cranial material alone on existing phylogenetic hypotheses.

I examined and edited the matrices using the software Mesquite. The matrices were subjected to parsimony analysis using the software Nona (Nixon, 1999-2002) in WinClada (Goloboff, 1999). Parsimony analyses were heuristic searches of 20,000 iterations.

More specifically, I first reanalyzed the matrices of Bloch and Silcox (2006) and Bloch et al. (2007) without revising any character codings. I did this to confirm that I could reproduce the results of the original authors. I was successful at recovering the exact same topologies. Next, I changed codings for the Plesiadapidae O.T.U. in both

matrices based on the results of the optimization described above. I also changed codings for Paromomyidae and Carpolestidae where I disagreed with those of the Bloch and Silcox (2006) and Bloch et al. (2007) based on a re-assessment of the fossil evidence.

In the matrix of Bloch and Silcox (2006), 10 character codings were changed, representing changes in nine characters for two taxa (Tables 5.3, 5.4A, 5.5). One character coding was additionally changed in *Carpolestes simpsoni* based on discussions with J. Bloch that lead me to believe the change represents the morphology more accurately.

In the matrix of Bloch et al. (2007), 17 character codings were changed, representing 16 characters and two taxa (Tables 5.3, 5.4A-C, 5.5). Seven of these characters encode postcranial morphology. The remaining nine characters encode cranial morphology. These nine characters are the same as those changed in the Bloch and Silcox (2006) matrix (Table 5.3).

Reconstruction of internal carotid artery functionality and skull length

Whether the internal carotid plexus canal held a functional internal carotid artery that was responsible for bringing a critical amount of blood to the forebrain has been addressed by measuring the diameter of the posterior carotid foramen (Kay et al., 1992), the internal carotid plexus canal, or groove for the internal carotid plexus on the promontorium (Bloch and Silcox, 2006). Kay et al. (1992) revealed that extant primates without a functional artery have a proportionally and, in most cases, absolutely smaller posterior carotid foramen than those with a functional one. This analysis was designed by Kay et al. (1992) to estimate functionality of the internal carotid artery in the

plesiadapiform *Ignacius graybullianus*. The analysis used information on skull length and posterior carotid foramen diameter. Functionality of the internal carotid artery in the fossil was assessed by comparison to extant taxa with either functional or non-functional internal carotid arteries.

Not all plesiadapids represented by cranial material preserve the posterior carotid foramen. Even so, some of these specimens can be included in the analysis by using the diameter of the groove for the internal carotid artery on the posterior septum where it meets the promontorium, as demonstrated by Bloch and Silcox (2001). This is equivalent to the diameter of the *g1* groove of Chapters 2-3 (Table 2.3). This analysis also requires information on skull length. However, because skull length can be directly measured in only *P. tricuspidens* (MNHN CR 125), where it is 106 mm, skull length must be estimated in other plesiadapid specimens. In Chapter 3, the length of the skull of *P. cookei* (UM 87990) was estimated to be nearly identical to that of MNHN CR 125 using 39 different cranial measurements (Table 3.3). However, the skull of *P. tricuspidens* differs from *P. cookei* and other North American plesiadapids with respect to a number of features discussed in chapters 2 and 3. Therefore, using measurements from MNHN CR 125 to estimate skull length in North American specimens that are more fragmentary than UM 87990 is likely to yield inaccurate results due to differences in shapes of various regions of the skulls (e.g., mediolateral width of the caudal extent of the nasals). Thus, for North American specimens where substantially fewer than 39 points of comparison are available (e.g., there are only 14 measurements available for *Nannodectes intermedius*), skull measurements of *P. cookei* were used to reconstruct cranial length. This was done specifically by calculating the average of logged percentage differences

between each available cranial measurement for a given specimen and that for *P. cookei* (Table 3.3). The anti-logged percentage difference is then multiplied by the length estimate for *P. cookei*'s skull (105.8 mm).

I used logged percentages because I determined that raw (unlogged) percentages yielded inconsistent estimates of size difference and therefore could not be used. I determined this by inter-changing reference specimens. Specifically, when the values of *P. cookei* were calculated as a percentage of those of *P. tricuspidens*, raw percentages estimated *P. cookei* to be, on average, slightly larger than *P. tricuspidens*. However, if *P. tricuspidens* values were calculated as a percentage of those of *P. cookei*, *P. cookei* was estimated to be slightly smaller than *P. tricuspidens*. When logged percentages were used, *P. cookei* was shown to be slightly smaller with either arrangement.

RESULTS

Phylogenetic reconstructions

Species level cladistic analysis – 144 trees resulted from analysis of the dental matrix of 32 characters. The strict consensus of these is shown in Figure 5.1A. Plesiadapidae is monophyletic with *Elphidotarsius* forming the sister taxon of the group. *Pronothodectes* is the most basal genus of the family. *Nannodectes, Chiromyoides,* and *Platychoerops* are monophyletic, and *P. cookei* is recovered as the sister taxon of *Platychoerops.* The length of each most parsimonious tree is 66. The consistency index is 59. The retention index is 83. In most respects the reconstructed phylogeny is congruent with that of Gingerich (1976) based on stratophenetic methodology, if less resolved in some ways. Addition of stratigraphic data will likely resolve many of these polytomies.

Character optimization - Table 5.3 is a list of characters from Bloch et al. (2007) and seven additional characters. These characters were scored for the crania described in chapters 2 and 3, and postcrania described in Chapter 4. Internal carotid artery functionality was also scored (Table 5.4A-B). These character states were optimized onto the consensus cladogram recovered through the species level analysis. The optimized state for the ancestral node is given in the last row of Table 5.4A-C.

A drawing of a cranium based on the ancestral node and *P. tricuspidens* illustrates the differences that appear to distinguish basal, *Pr. gaoi*-like taxa, and more derived, later-occurring *P. tricuspidens*-like taxa (Fig. 5.2).

Various plesiadapid taxa differ from the reconstruction representing the ancestral node for Plesiadapidae. For instance, *N. gidleyi* differs in having an apparently relatively larger glenoid fossa (Table 5.4B: 30) and an internal carotid plexus route that probably did not have an intratympanic route. However, if the posterior carotid foramen is correctly identified in *N. gidleyi* (Chapter 2), the route for the internal carotid plexus was similar to that of other plesiadapids in being relatively laterally positioned on the basicranium. *P. tricuspidens* differs in a number of respects illustrated in Figure 5.2: it exhibits a tubular external auditory meatus (Table 5.4A: 3), a narrow nasal bone (Table 5.4A: 16), a broad premaxilla/frontal contact (Table 5.4B: 27), and an annular component to its ectotympanic that flares substantially beyond the bony struts connecting it to the bullar wall (Table 5.4B: 28). Additionally, *P. tricuspidens* lacks exposure of molar tooth roots other than the distobuccal root of M^3 (Table 5.4B: 29), has a proportionally larger glenoid fossa (Table 5.4B: 30), and appears to have a less posteriorly projecting nuchal crest (Table 5.4B: 31). *P. cookei* is similar to *P. tricuspidens* in the tubular form of its external auditory meatus and in the lack of dorsal exposure of most tooth roots on its maxilla in the orbit.

Major features shared by basal and most derived plesiadapids include a premaxilla that contacts the frontal bone, an apparently petrosal bulla, and an internal carotid artery that has a posterolateral entrance, is non-functional, and crosses the lateral aspect of the promontorium (see chapters 2-3). Plesiadapids have previously been considered to lack a lacrimal tubercle. However, as discussed in Chapter 2, the best preserved lacrimal specimen of *P. tricuspidens* (MNHN CR 126) has a blunt lacrimal tubercle.

Optimization of postcranial traits from Bloch et al. (2007) reveals a few substantial differences in the coding of basal plesiadapids compared to more derived forms. These are discussed in the next section.

Cladistic analysis of character matrices using higher level taxa – As mentioned in the Methods section, the coding of "Plesiadapidae" in Bloch and Silcox (2006) and Bloch et al. (2007) was changed as a result of the character optimization exercise discussed above. Specifically, Bloch and Silcox (2006) and Bloch et al. (2007) coded Plesiadapidae with a "question mark" for cranial character 2 "Relations of entotympanic bone." Given that plesiadapids probably lack an entotympanic bone based on evidence presented in Chapter 2, and that they are extraordinarily similar to Euprimates in this regard, I changed this coding from a "question mark" to a "1" (no entotympanic bone present).

For cranial character 3, "Form of external auditory meatus," Bloch and Silcox (2006) and Bloch et al. (2007) coded Plesiadapidae with a "1" indicating that the external auditory meatus is "expanded into a tube." However, the character optimization shows that the tube form is derived, because basal species like *Pr. gaoi* (UALVP 46685) and *N. intermedius* (USNM 309902) exhibit the unexpanded, "0" state.

For cranial character 5, "Presence of branches of internal carotid artery," Bloch and Silcox (2006) and Bloch et al. (2007) coded Plesiadapidae with a "2" indicating that "evidence for the internal carotid system is absent." Specimens of *Pr. gaoi* (UALVP 46687, 49105), *N. intermedius* (USNM 309902), *P. tricuspidens* (e.g., MNHN CR 125, Pellouin skull, various MNHN isolated petrosals) and *P. cookei* (UM 87990) all show evidence that the internal carotid plexus entered the middle ear cavity. In many of these

specimens the internal carotid plexus left a groove on the lateral aspect of the promontorium (see chapters 2 and 3). These taxa are thus considered to exhibit the "0" state, "groove for at least promontorial branch present." Only *N. gidleyi* (AMNH 17388) appears to lack evidence of the internal carotid plexus. Optimization of this character reveals that Plesiadapidae should be coded with the "0" state.

For cranial character 6, "Position of posterior carotid foramen," Bloch and Silcox (2006) and Bloch et al. (2007) coded Plesiadapidae with a "0" indicating that the foramen had a "posteromedial position." The same set of specimens mentioned for character 5 reveal that the posterior carotid foramen is directly adjacent to the stylomastoid foramen when preserved, which is a criterion for considering the foramen to have a "posterolateral" position. Furthermore, in other taxa with the posteromedial state, the posterior carotid foramen is often medial to the medial edge of the promontorium. In the plesiadapids studied in Chapter 2, the foramen is lateral to the medial edge of the promontorium. In fact it is lateral to the entire promontorium. Therefore, this character is re-coded as "1," "posterolateral" for the Plesiadapidae.

For cranial character 16, "Flaring of nasals," Bloch and Silcox (2006) and Bloch et al. (2007) coded Plesiadapidae with a "1" indicating that the nasals "do not flare at caudal extent and have a narrow contact with frontal." *Pr. gaoi* (UALVP 46685), *N. intermedius* (USNM 309902), *P. anceps* (YPM-PU 19642), and *P. cookei* (UM 87990), however, have nasals that are proportionally much wider mediolaterally than those of *P. tricuspidens* (MNHN CR 125) at their caudal end and even appear to flare slightly compared to the mediolateral width of these bones at their rostrocaudal midpoint.

Therefore, character optimization reveals Plesiadapidae to primitively have exhibited the "0" state, "flaring nasals."

For cranial character 18, "Contact between lacrimal and palatine in the orbit," Bloch and Silcox (2006) and Bloch et al. (2007) coded Plesiadapidae with a "1" indicating that the contact is "obscured by maxillofrontal contact." However, as discussed in Chapter 2, the only plesiadapid specimens (*P. tricuspidens*: MNHN CR 126 and the Pellouin skull, *P. anceps*: YPM-PU 19642) that preserve this region relatively well are still too ambiguous to code the morphology with confidence. Therefore, I changed this character state to a "question mark" for all plesiadapids.

For cranial character 19, "Lacrimal tubercle," Bloch and Silcox (2006) and Bloch et al. (2007) coded Plesiadapidae as "absent." However, as discussed in Chapter 2, my own examination of the only plesiadapid specimen with a well-preserved lacrimal (*P. tricuspidens*: MNHN CR 126) reveals the presence of a poorly defined, blunt tubercle, similar in morphology to that described and illustrated for carpolestids by Bloch and Silcox (2006). Therefore, I changed the character state to "present" for *P. tricuspidens*, which allows the Plesiadapidae to be represented by the "present" state as well.

For cranial character 21, "Foramen rotundum," Bloch and Silcox (2006) and Bloch et al. (2007) coded Plesiadapidae with a "1" indicating that the foramen is "present." As discussed in Chapter 2, my own inspection of specimens of *P. tricuspidens* (MNHN CR 125, MNHN CR 965) leads me to the alternate interpretation. The foramen previously identified as the superior orbital fissure appears to be a suboptic foramen because it does not communicate with the endocranium, is variably present, and is located within the orbitosphenoid. The foramen previously identified as foramen

rotundum appears to be formed between the alisphenoid and orbitosphenoid. These facts suggest the previously identified foramen rotundum is actually a sphenorbital fissure. Therefore, I changed the coding for *P. tricuspidens* to the "0" state (absent). This allows Plesiadapidae to also be represented by a "0."

For, cranial character 23, "Shielding of cochlear fenestra," Bloch and Silcox (2006) and Bloch et al. (2007) coded Plesiadapidae and Paromomyidae as "2," indicating that the fenestra is "shielded by a bony septum." Adapid euprimates, on the other hand were coded by them with a "1," indicating that the fenestra is "shielded by an arterial tube." The bony shield referred to in cranial character 23 is the "posterior septum" of MacPhee (1981). As discussed for plesiadapids and and paromomyids in Chapter 2, a bony tube for the internal carotid plexus runs through the base of the posterior septum. This can be observed directly in *P. tricuspidens* (MNHN CR 125 and the Pellouin skull), *Pr. gaoi* (UALVP 46685, UALVP 46687, UALVP 49105) and *I. graybullianus* (e.g., USNM 482353, USNM 421608). I cannot see how this differs from the state assigned to Adapidae, for instance. Therefore I changed the coding from "2" to "1" for both plesiadapids and paromomyids.

For cranial character 24, "Auditory tube that runs through lateral wall of anterior chamber," Bloch and Silcox (2006) coded carpolestids as having the "present" state. Study of the original specimen of *Carpolestes simpsoni* UM 101963 and discussion with J. Bloch lead me to conclude that the bone separating the carpolestid bulla into an anterior and posterior chamber (the "platform bone" of Bloch and Silcox 2006), is in fact a piece of the ectotympanic bone that has been pushed out of place. Therefore, the

carpolestid bulla is not split into chambers, and carpolestids must be considered as exhibiting the "absent" state for cranial character 24 of Bloch and Silcox (2006).

For postcranial character 4, "Position of deltopectoral crest on humerus," Bloch et al. (2007) coded plesiadapids as polymorphic (0, 1) with some having a laterally positioned crest and others having an anteriorly positioned crest. They based this polymorphic coding on *P. cookei* (UM 87990) exhibiting an anteriorly positioned crest, as contrasted with *P. tricuspidens, P. walbeckensis* and *N. intermedius* (USNM 442229) which exhibit a laterally positioned crest. Additional specimens including those of cf. *Pr. gaoi* (UALVP 49114) and *P. rex* (UM 64588) are observed to also have a laterally positioned crest. This allows the ancestral node for Plesiadapidae to be optimized as having the lateral position state.

For postcranial character 10, "Morphology of the ulnar trochlea on humerus," Bloch et al. (2007) coded Plesiadapidae with the "0" state, indicating "only a medial ridge present." However, *Pr. gaoi* (UALVP 49114), *P. rex* (UM 64588) and many *P. tricuspidens* specimens exhibit a lateral ridge as well. Optimization reconstructs the ancestral node of Plesiadapidae as having a medial and lateral ridge (state "1").

For postcranial character 21, Bloch et al. (2007) coded plesiadapids with a "question mark," indicating that it was not known whether any plesiadapid had a nail on any of its digits. However, the skeleton of *Plesiadapis insignis* in Gingerich (1976) illustrates the presence of claws on all pedal digits, and all manual digits except for the pollex, which is obscured. Furthermore, the form of the hallucal and pollical proximal phalanges of *P. tricuspidens* and *Nannodectes* (see Chapter 4) suggest the presence of claws, rather than nails.

For postcranial character 30, “Plantodistal process of entocuneiform,” Bloch et al. (2007) coded the Plesiadapidae as polymorphic (0, 1) indicating that some taxa have a “strong” process, while others have one that is “reduced or absent.” This was based on the observation that the entocuneiform attributed to the skeleton of *P. cookei* (UM 87990) lacks a strong plantodistal process. However, my reassessment of this bone is that it is so different from the entocuneiform of other plesiadapids (*P. tricuspidens*: MNHN R 416, MNHN R 5359, MNHN R 5331; cf. *P. anceps* AMNH 92011 – see Szalay and Dagosto, 1988) and plesiadapiforms (Sargis et al. 2007), that it must be tentatively considered as incorrectly attributed to UM 87990. Whether or not this is correct, the presence of a strong plantodistal process in *P. tricuspidens* and cf. *P. anceps* allows me to re-code plesiadapids as having the “0” state only.

For postcranial character 32, Bloch et al. (2007) coded Plesiadapidae as polymorphic (0, 1) for the presence of “cranial buttressing” on the acetabulum. However, all plesiadapids known for this morphology (*N. gidleyi* AMNH 17409, AMNH 17379; *P. tricuspidens* MNHN R 448; *P. cookei* UM 87990) exhibit the “1” state as compared to tupaiid treeshrews, for instance. I therefore re-coded the group in this way.

For postcranial character 54, “Length of pubic symphysis,” Bloch et al. (2007) coded plesiadapids with the “0” state, indicating a “long” pubic symphysis. However, the only plesiadapid with a complete symphyseal region on the innominate is *P. cookei* (UM 87990). In Chapter 4, I discuss its morphology, which is revealed to be more like that of *Cynocephalus volans*. *C. volans* has a “short” pubic symphysis compared to those of paromomyid plesiadapiforms, which have a “long” pubic symphysis (Boyer and Bloch

2008). I therefore changed the coding of postcranial character 54 to "1" (short) for *P. cookei*, which allows the Plesiadapidae to also be represented by a "1."

For postcranial character 58, "Orientation of spinous process on axis," Bloch et al. (2007) coded Plesiadapidae with the "0" state, indicating a "caudal" orientation. This coding was based on the axis of *P. cookei* (UM 87990). My study of this specimen suggests to me that it is broken cranially (see Chapter 4), such that whether or not there was a cranial orientation to the process is unknown. However, a specimen of *N. intermedius* (USNM 442229) retains a prominent, cranially-oriented spine. Thus, I re-coded this character for Plesiadapidae with the "1" state, indicating a "cranial" orientation.

A heuristic search of the edited Bloch and Silcox (2006) matrix resulted in only two trees, instead of three (Fig. 5.3). One of these trees (Fig. 5.3A) matched one of the MP trees of Bloch and Silcox (2006: p.26, fig. 23C), with Carpolestidae, Plesiadapidae and Paromomyidae forming successive outgroups to Euprimates. However, the other MP tree has the inverse order for these three groups (Fig. 5.3B). That is, paromomyids form the sister of Euprimates. This means that the consensus tree (Fig. 5.3C) has less resolution than that of Bloch and Silcox (2006). The tree length (TL) decreased from the original results and the consistency index (CI) and the retention index (RI) increased (Table 5.6).

Analysis of the modified Bloch et al. (2007) matrix yielded the same results as the analysis of the original matrix (Fig. 5.3D). TL decreased and CI increased (Table 5.6).

Reconstruction of internal carotid functionality and skull length

Plotting foramen, canal or groove diameters of plesiadapids with those of an extant primate sample from Kay et al. (1992) makes it clear that the artery cannot be inferred to be functional in any plesiadapid (Table 5.7; Fig. 5.4). It should, however, be noted that the widest posterior carotid foramen (belonging to *P. cookei*) is only 1.3-1.43 times the width of that in the rest of the sample (Table 5.7), meaning that there is a lot of *proportional* variation in the diameter of this canal, with the proportionally largest internal carotid plexus groove being found in the smallest individual, *N. intermedius.*

DISCUSSION AND CONCLUSIONS

The species level cladistic analysis of plesiadapids yielded a tree largely consistent with previously constructed phylogenetic hypotheses for the group (Gingerich, 1976), even though these previous hypotheses were not based on cladistic methodology. One interesting result is the recovery of a sister taxon relationship for *P. cookei* and the *Platycheorops* clade. As discussed in Chapter 3, *P. cookei* has been recognized as uniquely similar to *Pl. russelli* and *Pl. daubrei* in a number of features of the dentition. This analysis provides the first cladistic support for such an hypothesis, and suggests that features of the teeth reflecting a folivorous diet were inherited from a common ancestor in *P. cookei* and *Platychoerops*. Features supporting this relationship and distinguishing *P. cookei* and *Pl. daubrei* from *P. tricuspidens* include, on the I^1, reduced-to-absent laterocones, posterocones, mediocones and centroconules; the absence of a P^2; P_4 with a trigonid, and P^{3-4} lacking “premolar type” paraconules.

Re-coding and optimization of cranial and postcranial characters from Bloch and Silcox (2006) and Bloch et al. (2007) for the Plesiadapidae, based on new information and observations, reveals that previous codings for the "Plesiadapidae" by Bloch and Silcox (2006) and Bloch et al. (2007) are inaccurate in many cases. Furthermore, the plesiadapid species that differs most from all of the others and the ancestral node reconstruction is *P. tricuspidens*. This may or may not be a "surprising" result but it is important because previous cladistic analyses have primarily used morphological features of *P. tricuspidens* to characterize the family (Kay et al., 1992; Wible, 1993; Silcox, 2001; Bloch and Silcox, 2006; Bloch et al., 2007). The conclusions that *P. tricuspidens* is cranially derived and that some basic aspects of plesiadapid cranial anatomy differ from previous perceptions, make it necessary to reevaluate the cladistic support for plesiadapid relationships to other plesiadapiforms and euarchontans.

Modification and reanalysis of the Bloch et al. (2007) matrix to reflect this revised characterization of the Plesiadapidae yields no change to the topology recovered. Even so, this investigation reveals that carpolestids and plesiadapids are not as similar as previously believed. Scrutiny of the codings of various taxa is illuminating. In the matrix of characters developed by Bloch et al. (2007), plesiadapids and carpolestids were originally coded alike, to the exclusion of paromomyids, for five of 26 cranial characters (about 19%). These include (in plesiadapids and carpolestids) the following: the presence of a posterior carotid foramen with a posteromedial position (c6), the presence of a foramen rotundum (c21), an orbital contact between the frontal and maxilla (c18), nasals that narrow mediolaterally from anterior to posterior (c16), and a petrosal bulla (c1). Evidence marshaled in chapters 2-4, and in this chapter suggests that Plesiadapidae

is actually distinct from Carpolestidae in lacking the first two features, that plesiadapids might not exhibit the third feature (based on MNHN CR 126 and the Pellouin skull of *Plesiadapis tricuspidens*), and that only *P. tricuspidens* exhibits the fourth character state. A petrosal bulla, the fifth feature, does seem to characterize plesiadapids, but I would consider this interpretation for carpolestids as tentative (better fossil material is needed). Thus, none of the cranial features thought to characterize both plesiadapids and carpolestids in Bloch et al. (2007) can be demonstrated as definite points of similarity after careful scrutiny and reanalysis of the relevant specimens. In light of this conclusion, it is therefore surprising that the modified version of the Bloch et al. (2007) matrix produced results identical to the original.

Further consideration of the Bloch et al. (2007) matrix reveals the likely reason why revisions to the cranial and postcranial codings had no effect on the topologies that resulted: many of the features that phylogenetically link plesiadapids with carpolestids are dental features. In the Bloch et al. (2007) character matrix, there are at least 21 out of 80 (~26%) dental characters in which plesiadapids and carpolestids are similar to one another and different from paromomyid plesiadapiforms. It seems unlikely that most or even many of these could be easily demonstrated as convergences. Another possibility is that many of these dental features are actually primitive retentions — as would be the case in a tree with completely inverted polarity for these characters. Such a phylogenetic hypothesis would be quite radical, however, because the "plesiadapoid + euprimate" node is similar to the paromomyid node in the reconstructed states for most of these characters, meaning that a tree with such an inverted polarity would likely result in plesiadapids and carpolestids being outside of a clade comprised of some other plesiadapoids, euprimates

and paromomyids. This, however, is actually what is suggested by one of the MP trees resulting from revision and reanalysis of the Bloch and Silcox (2006) matrix (Fig. 5.3B), even though it contains no dental characters.

Results of the analysis of modified character matrices notwithstanding, the phylogenetic significance of the foregoing facts regarding morphology of paromomyids, plesiadapids, and carpolestids is unclear. Cranial and postcranial similarities uniting paromomyids and plesiadapids, and postcranial similarities uniting carpolestids and euprimates, may mean that carpolestids along with some other "plesiadapoids" (of Bloch et al., 2007) are closer to Euprimates within a "plesiadapoid + euprimate" clade than to plesiadapids. In other words, Plesiadapoidea may be paraphyletic with respect to Euprimates. In this case a topology similar to that depicted in Figure 5.3A, or that recovered by the cladistic analysis of postcranial characters by Bloch and Boyer (2002) may be closer to the truth.

It is important to note that the decrease in tree length and the increase in consistency index that resulted from analysis of the modified matrices suggest that the recovered topologies are more parsimonious than those of the original matrices. This means that the newly encoded morphology of plesiadapids can be considered as actually strengthening the phylogenetic hypothesis of Bloch et al. (2007), although this may not be intuitive, as revealed by the above discussion.

Clearly, there is much still to be learned regarding the phylogenetic relationships among various plesiadapiforms and extant euarchontan mammals including dermopterans, treeshrews and euprimates. New matrices that more intensively sample

the anatomy of a broader array of relevant taxa, and the discovery of more plesiadapiform fossils are necessary to increase knowledge on this subject

ACKNOWLEDGMENTS

I thank K. C. Beard for access to undescribed material of *Ch. caesor* and *N. gazini* from the Carnegie Museum of Natural History. I thank M. O'Leary for encouraging me to assess features characterizing basal plesiadapids in a more organized, better documented, and more methodologically rigorous fashion than I had done previously. I thank M. Silcox for forwarding me the data from Kay et al. (1992) presented in Table 5.7. D. Krause, M. O'Leary, J. Fleagle, W. Jungers, and P .Gingerich read and enhanced previous versions of this manuscript.

REFERENCES

Beard, K.C., 1989. Postcranial anatomy, locomotor adaptations, and palaeoecology of Early Cenozoic Plesiadapidae, Paromomyidae, and Micromomyidae (Eutheria, Dermoptera). Ph.D. Dissertation, Johns Hopkins University.

Beard, K.C., MacPhee, R.D.E., 1994. Cranial anatomy of *Shoshonius* and the antiquity of Anthropoidea. In: Fleagle, J.G., Kay, R.F. (eds) Anthropoid Origins. Plenum Press, New York, pp. 55-97.

Bloch, J.I., Fisher, D.C., Rose, K.D., Gingerich, P.D., 2001. Stratocladistic analysis of Paleocene Carpolestidae (Mammalia, Plesiadapiformes) with description of a new late Tiffanian genus. Journal of Vertebrate Paleontology 21, 119-131.

Bloch, J.I., Silcox, M.T., 2001. New basicrania of Paleocene-Eocene *Ignacius*: re-evaluation of the plesiadapiform-dermopteran link. American Journal of Physical Anthropology 116, 184-198.

Bloch, J.I., Boyer, D.M., 2002. Grasping primate origins. Science 298, 1606-1610.

Bloch, J.I., Boyer, D.M., 2003. Response to comment on "Grasping Primate Origins." Science 300, 741c.

Bloch, J.I., Silcox, M.T., 2006. Cranial anatomy of the Paleocene plesiadapiform *Carpolestes simpsoni* (Mammalia, Primates) using ultra high-resolution X-ray computed tomography, and the relationships of plesiadapiforms to Euprimates. Journal of Human Evolution 50, 1-35.

Bloch, J.I., Boyer, D.M., 2007. New skeletons of Paleocene-Eocene Plesiadapiformes: a diversity of arboreal positional behaviors in early primates. In: Dagosto, M., Ravosa, M.J. (eds) Primate Origins: Adaptations and Evolution. Plenum Press, New York, pp. 535-582.

Bloch, J.I., Silcox, M.T., Boyer, D.M., Sargis, E.J., 2007. New Paleocene skeletons and the relationship of plesiadapiforms to crown-clade primates. Proceedings of the National Academy of Sciences 104, 1159-1164.

Boyer, D.M., Bloch, J.I., Silcox, M.T., Gingerich, P.D., 2004. New observations on anatomy of *Nannodectes* (Mammalia, Primates) from the Paleocene of Montana and Colorado. Journal of Vertebrate Paleontology 24, 40A.

Boyer, D.M., Bloch, J.I., 2008. Evaluating the mitten-gliding hypothesis for Paromomyidae and Micromomyidae (Mammalia, "Plesiadapiformes") using comparative functional morphology of new Paleogene skeletons. In: Sargis, E.J., Dagosto, M. (eds) Mammalian Evolutionary Morphology: A Tribute to Frederick S. Szalay. Kluwer, New York, pp. 233-284.

Clemens, W.A., 2004. *Purgatorius* (Plesiadapiformes, Primates?, Mammalia), a Paleocene immigrant into northeastern Montana: Stratigraphic occurrences and incisor proportions. Bulletin of Carnegie Museum of Natural History 3, 3-13.

Coleman, M.C., Boyer, D.M., 2008. Evolution of low frequency hearing in primates: evidence from fossils. American Journal of Physical Anthropology Meeting abstracts, 80.

Fox, R.C., 1990. *Pronothodectes gaoi* n. sp. from the late Paleocene of Alberta, Canada, and the early evolution of the Plesiadapidae (Mammalia, Primates). Journal of Paleontology 64, 637-647.

Fox, R.C., 1993. The primitive dental formula of the Carpolestidae (Plesiadapiformes, Mammalia) and its phylogenetic implications. Journal of Vertebrate Paleontology 13, 516-524.

Gingerich, P.D., 1976. Cranial anatomy and evolution of Early Tertiary Plesiadapidae (Mammalia, Primates). University of Michigan Papers on Paleontology 15, 1-141.

Goloboff, P., 1999. NONA (No NAME) ver. 2 Published by the author, Tucumàn, Argentina.

Kay, R.F., Thewissen, J.G.M., Yoder, A.D., 1992. Cranial anatomy of *Ignacius graybullianus* and the affinities of the Plesiadapiformes. American Journal of Physical Anthropology 89, 477-498.

Kirk, E.C., Lemelin, P., Hamrick, M.W., Boyer, D.M., Bloch, J.I., 2008. Intrinsic hand proportions of euarchontans and other mammals: implications for the locomotor behavior of plesiadapiforms. Journal of Human Evolution 55, 278-299.

MacPhee, R.D.E., 1981. Auditory regions of primates and eutherian insectivores, morphology, ontogeny, and character analysis. Contributions to Primatology 18, 1-282.

MacPhee, R.D.E., Cartmill, M., Gingerich, P.D., 1983. New Paleogene primate basicrania and the definition of the order Primates. Nature 301, 509-511.

MacPhee, R.D.E., Cartmill, M., 1986. Basicranial structures and primate systematics. Comparative Primate Biology, Volume 1: Systematics, Evolution, and Anatomy. Alan R. Liss, Inc., pp. 219-275.

Nixon, K. C. 1999-2002. WinClada ver. 1.0000 Published by the author, Ithaca, NY, USA

Novacek, M.J., 1986. The skull of leptictid insectivorans and higher classification of eutherian mammals. Bulletin of the American Museum of Natural History 183, 1-111.

Novacek, M.J., Wyss, A.R., 1986. Higher-level relationships of the recent eutherian orders: morphological evidence. Cladistics 2, 257-287.

Russell, D.E., 1964. Les Mammiferes Paléocènes D'Europe. Mémoires du Muséum National D'Histoire Naturelle, Série C 13, 1-324.

Sargis, E.J., Boyer, D.M., Bloch, J.I., Silcox, M.T., 2007. Evolution of pedal grasping in Primates. Journal of Human Evolution 53, 103-107.

Silcox, M.T., 2001. A phylogenetic analysis of Plesiadapiformes and their relationship to euprimates and other archontans. Ph.D. dissertation, Johns Hopkins University.

Silcox, M.T., 2003. New discoveries on the middle ear anatomy of *Ignacius graybullianus* (Paromomyidae, Primates) from ultra high resolution X-ray computed tomography. Journal of Human Evolution 44, 73-86.

Silcox, M.T., Gunnell, G.F., 2008. "Plesiadapiformes." In: Janis, C.M., Gunnell, G.F., Uhen, M.D. (eds) Evolution of Tertiary Mammals of North America, Volume 2: Small mammals, xenarthrans, and marine mammals. Cambridge University Press, Cambridge, pp. 207-238.

Silcox, M.T., Krause, D.W., Maas, M.C., Fox, R.C., 2001. New specimens of *Elphidotarsius russelli* (Mammalia, ?Primates, Carpolestidae) and a revision of plesiadapoid relationships. Journal of Vertebrate Paleontology 21, 132-152.

Simpson, G.G., 1935. The Tiffany fauna, Upper Paleocene. II.-Structure and relationships of *Plesiadapis*. American Museum Novitates 816, 1-30.

Simpson, G.G., 1937. The Fort Union of the Crazy Mountain Field, Montana, and its mammalian faunas. United States National Museum Bulletin 169, 1-287.

Szalay, F.S., 1968. The beginnings of primates. Evolution 22, 19-36.

Szalay, F.S., 1975. Where to draw the nonprimate-primate taxonomic boundary. Folia Primatologica 23, 158-163.

Szalay, F.S., Tattersall, I., Decker, R.L., 1975. Phylogenetic relationships of *Plesiadapis* - postcranial evidence. Contributions to Primatology 5, 136-166.

Szalay, F.S., Dagosto, M., 1980. Locomotor adaptations as reflected on the humerus of Paleogene primates. Folia Primatologica 34, 1-45.

Szalay, F.S., Dagosto, M., 1988. Evolution of hallucial grasping in the Primates. Journal of Human Evolution 17, 1-33.

Van Valen, L.M., 1994. The origin of the plesiadapid primates and the nature of *Purgatorius*. University of Chicago Evolutionary Monographs 15, 1-79.

Wible, J.R., Covert, H.H., 1987. Primates: cladistic diagnosis and relationships. Journal of Human Evolution 16, 1-22.

Wible, J.R., Novacek, M.J., 1988. Cranial evidence for the monophyletic origin of bats. American Museum Novitates 2911, 1-19.

Wible, J.R., 1993. Cranial circulation and relationships of the colugo *Cynocephalus* (Dermoptera, Mammalia). American Museum Novitates 3072, 1-27.

Wiley, E.O., Siegel-Causey, D., Brooks, D.R., Funk, V.A., 1991. The Compleat Cladist: A Primer of Phylogenetic Procedures. University of Kansas Museum of Natural History, Lawrence, Kansas.

TABLES

Table 5.1. Dental characters for species level analysis of Plesiadapidae.

Incisors

Lower

1. (= character 4 of Bloch et al. 2001) Basal cusp on lingual cingulum of I_1: (0) absent, (1) present.
2. I_1: with squared tip: (0) absent, (1) present
3. I_2: (0) present, (1) absent.
4. (= character 6 of Bloch et al. 2001) I_3: (0) present, (1) absent.

Upper

5. I^1 laterocone: (0) present, (1) reduced, (2) absent. Ordered.
6. I^1 posterocone: (0) present, (1) reduced, (2) absent. Ordered.
7. I^1 mediocone: (0) present, (1) reduced or absent.
8. I^1 centroconule: (0) present, (1) reduced or absent.

Canines

9. C^1: (0) present, (1) absent.
10. C_1: (0) present, (1) absent.

Premolars

11. diastemata between premolars and more anterior teeth: (0) absent, (1) present.
12. P^1 or P_1: (0) present, (1) absent.

Lower

13. Form of P_2: (0) premolariform and procumbent, (1) button shaped, (2) absent. Ordered.
14. (modified from character 14 of Bloch et al. 2001) Metaconid on P_4: (0) absent, (1) present.
15. (d25 of Silcox, 2001) Paraconid on P_4: (0) present, (1) absent.
16. Entoconid on P_4: (0) present, (1) absent.
17. Trigonid of P_4: (0) present, (1) absent.
18. Proportions of P_4: (0) buccolingually broad relative to mesiodistal length, (1) narrow

Upper

19. P^2: (0) present, (1) absent.
20. P^3 paraconule: (0) present, (1) reduced, (2) absent. ordered
21. P^4 paraconule: (0) present, (1) reduced, (2) absent. ordered
22. P^4 molar-type paraconule: (0) absent, (1) present

Molars

Lower

23. Proportions of M_{1-3}: (0) buccolingually broad relative to mediolateral breadth. (1) narrow.
24. Entoconid of M_{1-2}: (0) squared and lacking crest (1) curved with crest
25. Length of M_1: (0) species sample mean less than 3.5 mm, (1) greater than or equal to 3.5 mm.

26. (= d80 of Silcox, 2001) Postvallid of M_1: (0) flush, (1) stepped
27. (modified from d75 of Silcox, 2001) Size of M_3 hypoconulid: (0) small relative to talonid, (1) large
28. Shape of M_3 hypoconulid: (0) rounded and unfissured, (1) squared and fissured

Upper

29. M^{1-2} mesostyles: (0) absent, (1) weakly present, (2) strong. ordered
30. Incisor size relative to molars: (0) slightly larger, (1) greatly enlarged.
31. Upper molars: (0) rectangular, (1) squared, relatively narrow buccolingually compared to mesiodistal length.
32. Premolar and/or molar form: (0) cuspidate, (1) blunt, (2) crestiform. unordered.

Table 5.2. Dental character matrix. See Table 5.1 for character descriptions.

Taxon	1	2	3	4	5	6	7	8	9	10	11	12	13	14	15	16	17	18	19	20	21	22	23	24	25	26	27	28	29	30	31	32
Purgatorius	0	0	0	0	0	0	0	1	?	0	0	0	0	0	0	0	1	0	0	1	1	0	0	0	0	0	0	0	0	0	0	0
Elphidotarsius	0	0	0	1	0	0	0	1	1	0	0	0	1	1	0	1	1	0	0	0	0	0	0	0	0	1	0	0	0	0	0	0
Pr. matthewi	1	0	0	1	0	0	0	1	0	0	0	1	0	0	1	1	1	0	0	0	0	0	0	0	0	1	1	0	0	0	0	0
Pr. jepi	1	0	0	1	0	0	0	1	0	0	0	1	0	0	1	1	1	0	0	0	0	0	0	0	0	1	1	0	0	0	0	0
Pr. gaoi	1	0	0	1	0	0	0	1	0	0	0	1	0	0	1	1	1	0	0	0	0	0	0	0	0	1	1	1	0	0	0	0
N. intermedius	1	0	1	1	0	0	0	1	0	0	0	1	1	0	1	1	1	1	0	0	0	0	1	0	0	1	1	0	0	0	1	0
N. gazini	1	0	1	1	0	0	0	1	0	0	0	1	1	0	1	1	1	1	0	1	0	0	1	0	0	1	1	0	0	0	1	0
N. simpsoni	1	0	1	1	?	?	?	?	0	0	1	1	1	0	1	1	1	1	0	2	0	0	1	0	0	1	1	0	1	0	1	0
N. gidleyi	1	0	1	1	0	0	?	1	0	1	1	1	1	0	1	1	1	1	0	0	0	0	1	0	0	1	1	0	0	0	1	0
P. insignis	1	0	1	1	0	0	0	1	0	1	1	1	1	?	1	1	1	0	0	?	?	0	0	0	0	1	1	0	0	0	0	0
P. praecursor	1	0	1	1	0	0	0	1	0	0	1	1	1	0	1	1	1	0	0	0	0	0	0	0	0	1	1	0	0	0	0	0
P. anceps	1	0	1	1	0	0	0	0	0	1	1	1	1	0	1	1	1	0	0	0	0	0	0	0	0	1	1	0	0	0	0	0
P. walbeckensis	1	0	1	1	0	0	0	1	0	1	1	1	1	0	1	1	1	0	0	0	0	0	0	0	0	1	1	0	0	0	0	0
P. rex	1	0	1	1	0	0	0	0	0	1	1	1	1	0	1	1	1	0	0	0	0	0	0	0	0	1	1	1	1	0	0	0
P. churchilli	1	0	1	1	0	0	0	0	0	1	1	1	2	0	1	0	1	0	0	0	0	0	0	0	0	1	1	1	2	0	0	0
P. fodinatus	1	0	1	1	0	0	0	0	0	1	1	1	2	1	0	0	1	0	0	1	1	0	0	1	0	1	1	1	2	0	0	2
P. dubius	1	0	1	1	0	0	0	1	0	1	1	1	2	?	0	0	1	0	0	1	1	0	0	1	0	1	1	1	2	0	0	2
P. simonsi	?	?	?	?	?	?	?	?	?	?	?	?	?	?	?	?	?	?	?	?	?	0	0	1	1	1	1	1	2	?	0	0
P. gingerichi	?	?	?	?	0	0	0	1	?	1	1	1	2	0	1	0	1	0	?	?	?	0	0	1	1	1	1	1	2	?	0	0
P. remensis	1	0	1	1	0	0	0	0	?	1	1	1	2	0	1	1	1	0	0	0	0	0	0	1	1	1	1	1	2	0	0	0
P. tricuspidens	0	0	1	1	0	0	0	0	1	1	1	1	2	1	1	1	1	0	0	0	0	0	0	1	1	1	1	1	2	0	0	0
P. cookei	0	0	1	1	1	1	1	1	1	1	1	1	2	0	0	0	0	0	1	2	2	0	0	1	1	1	1	1	2	0	0	2
Ch. minor	1	0	1	1	0	0	0	1	?	1	0	?	2	?	?	?	?	?	?	?	?	?	0	?	0	?	?	?	?	1	?	1
Ch. potior	1	1	1	1	0	0	0	1	?	1	1	?	2	?	?	?	?	?	?	?	0	0	0	0	0	?	?	?	?	1	?	1
Ch. caesor	1	1	?	?	0	0	0	1	?	?	?	?	?	?	?	?	?	?	?	0	0	0	0	0	0	0	?	?	1	1	0	1
Ch. major	1	1	1	1	0	0	0	1	?	1	1	?	2	?	?	?	?	?	?	?	?	?	?	?	?	?	?	?	?	1	?	1
Ch. campanicus	1	0	1	1	0	0	0	1	?	1	0	1	2	0	1	1	1	0	0	?	0	0	0	0	0	1	1	0	1	1	0	1
Pl. russelli	?	?	1	1	1	1	1	1	1	1	?	1	2	?	?	?	?	?	?	2	2	1	0	?	1	?	1	1	2	0	0	2
Pl. daubrei	0	0	1	1	2	2	1	1	1	1	1	1	2	1	0	0	0	0	?	2	2	1	0	1	1	1	1	1	2	0	0	2
Pl. richardsoni	?	?	?	?	?	?	?	?	1	1	1	1	?	?	?	?	?	?	1	?	2	1	0	1	1	1	1	1	2	0	0	2

Table 5.3. Cranial and postcranial characters for optimization. All characters unordered.

Cranial characters used by Bloch et al. (2007) - Note that more extensive discussions of most of these characters (83-108; renumbered here to c1 through c26)) are available in Bloch et al. (2007) and Silcox (2001). Sources for the characters in this dataset include Szalay (1975), Wible and Covert (1987), Kay et al. (1992), Wible (1993), Beard and MacPhee (1994) and Silcox (2001).

83 (c1). Structure of auditory bulla: membranous, or bony but non-petrosal in origin (0), or no suture separating bulla from petrosal and/or no developmental evidence for additional elements (1). This character is modified from Beard and MacPhee (1994) and is designed to best employ the data that is available from fossils (i.e., under this definition microsyopids can be coded in spite of the uncertainty about the composition of their bullae).

84 (c2). Relations of entotympanic: no entotympanic present (0), entotympanic contacts petrosal medially (1), entotympanic contacts basioccipital medially (2), or no medial contact (3). This character is modified from Kay et al. (1992), and was scored only in taxa for which an entotympanic could be positively identified.

85 (c3). Form of external auditory meatus: not expanded into bony tube (0), or expanded into bony tube (1). As defined here, this character does not differentiate between tubular external auditory meati that are formed from different bones. This reflects the difficulty of accurately reconstructing the contribution of all of the bones making up the auditory bulla in fossils.

86 (c4). Presence of subtympanic recess (between tympanic ring and bulla): subtympanic recess absent and ectotympanic does not include distinct ring-like element (0), or subtympanic recess present and ectotympanic includes ring-like element separated by annular bridge, membrane or gap between it and bulla (1). This character is modified from a character relating to the annular bridge employed by Beard and MacPhee (1994). See discussion in Silcox (2001). As configured here, this character allows the recognition of the basic similarity of a ring-like ectotympanic even if this is all that is preserved (i.e., as is the case for *Ignacius*; Bloch and Silcox, 2001).

87 (c5). Presence of branches of internal carotid artery: grooves for at least promontorial branch, no tubes (0), tubes present for one or both arteries (1), or internal carotid artery absent (2).

88 (c6). Posterior carotid foramen position (or position of entry of internal carotid artery and/or nerves into middle ear): posteromedial (0), or posterolateral (1).

89 (c7). Subsquamosal foramen: present and large (0), or very small or absent (1). Note that this feature refers to a foramen located at the distal end of the zygomatic arch, making it equivalent to the opening called a suprameatal foramen by Kay et al. (1992; see discussion in Beard and MacPhee, 1994).

90 (c8). Width of central stem and relative size of hypotympanic sinus: broad with hypotympanic sinus restricted (0), or narrow with hypotympanic sinus expansive (1). Beard and MacPhee (1994: p. 79) define the central stem as "the midline keel of the posterior basicranium normally composed of the

basisphenoid and basioccipital bones." Taxa with highly inflated bullae (i.e., an expansive hypotympanic sinus) also by necessity have a central stem, so the expanse of the hypotympanic sinus was not included as a separate character here (by contrast, it was employed as a character by MacPhee and Cartmill, 1986).

91 (c9). Snout: relatively long (0), or short (1). To code this character, the length of the snout was measured from the ventral base of the anterior extent of the zygomatic arch to the front of the premaxilla. This was then compared to total skull length, measured from the caudal-most point on the occiput to the front of the premaxilla. A least-squares regression was performed of snout length on cranial length using SPSS 10.05, with the constraint that it pass through the origin (Silcox, 2001). The resulting line had this equation: snout length=0.039(cranial length). This line was a good fit to the data (r^2=0.971). Character state 1 was assigned to any taxon with a residual more negative than –5.0. This indicates that the snout is at least 5 mm shorter than would be predicted by the equation.

92 (c10). Presence of postorbital bar: absent (0), postorbital process of frontal present but does not meet zygomatic (1), or complete postorbital bar present (2). Although it can be difficult to rule out absolutely the presence of a postorbital bar in damaged specimens, the absence of a process on either the zygomatic or the frontal can demonstrate that there was no complete bar.

93 (c11). Presence of mastoid process: no strong tubercle or inflation in mastoid region (0), or strong tubercle or inflation in mastoid region (1). This character was scored somewhat differently than in Kay et al. (1992) in that it was considered likely that an inflated mastoid region was on the same morphocline as a strong tubercle, rather than being most similar to the complete absence of any expansion of the mastoid.

94 (c12). Number of jugular (=posterior lacerate) foramina: single (0), or dual (1).

95 (c13). Position of caudal midsagittal margin of palate: near M^3 (0), well rostral to M^3 (1), or well caudal to M^3 (2). The states for this character differ somewhat from those used by Kay et al. (1992), who based the character on small variations in the position of the midsagittal margin of the palate.

96 (c14). Number of pterygoid plates: two (0), or one (1).

97 (c15). Supraorbital foramen: absent (0), or present (1).

98 (c16). Nasals: flare laterally at caudal extent with wide contact with frontal (0), or nasals do not flare laterally at caudal extent with narrow contact with frontal (1).

99 (c17). Diameter of infraorbital foramen: large (0), or small (1). For this analysis two measurements were taken from the infraorbital foramen, following Kay et al. (1992): the greatest diameter, and the maximum length perpendicular to the first measurement. These two measurements were then multiplied together to give an approximation of the area of the foramen. A least squares regression analysis was performed of the infraorbital foramen area vs. the logarithm of M^1 (calculated as buccal length * width). Taxa that fell outside the 99% confidence limit for this analysis were grouped together in the "small" category (Silcox, 2001).

100 (c18). Contact between lacrimal and palatine in orbit: present (0), obscured by maxillofrontal contact (1).
101 (c19). Lacrimal tubercle: absent (0), or present (1).
102 (c20). Size of optic foramen: small (0), moderate (1), or large (2). Coding for this character followed the ranges employed by Kay et al. (1992).
103 (c21). Foramen rotundum: absent (0), or present (1).
104 (c22). Position of lacrimal foramen: on orbital rim (0), on face (1), or in orbit (2).
105 (c23). Cochlear window: not shielded (0), shielded by arterial tube (1), or shielded by bony septum (2).
106 (c24). Orientation of fenestra rotunda (=cochlear window): directed posterolaterally (0), or directed posteriorly (1). Although there is some slight variation in the orientation of the fenestra rotunda, the situation in dermopterans and chiropterans, where this opening points directly posteriorly, is particularly distinctive. The derived state of this character has been cited frequently as a volitantian synapomorphy (Novacek, 1986; Novacek and Wyss, 1986; Wible and Novacek, 1988).
107 (c25). Septae in middle ear cavity formed by entotympanic: absent (0), or present (1). The "present" state was only recognized in scandentians, in which the entotympanic forms a dorsal cover to petrosal structures on the roof of the middle ear cavity (MacPhee, 1981).
108 (c26). "Fattened" area on medial promontorium: absent (0), or present (1). This character was suggested by Szalay (1975). The "1" state represents a rounded, bulging promontorium, contrasting with the "deflated" appearance of taxa that exhibit the "0" state.

Additional cranial characters for plesiadapid crania

27. Expansiveness of premaxillary contact with frontal: absent (0), narrow (1), or broad (2).
28. Relative size of annular component of ectoympanic: small, not flaring greatly beyond bony struts by which it is connected to bullar part of ectotympanic (0), or large, flaring well beyond bony struts by which it is connected to bullar part of ectotympanic (1).
29. Exposure of maxillary tooth roots in orbit: present (0), reduced to only distobuccal root of M^3 or absent (1).
30. Glenoid fossa relative size: small (0), or large (1).
31. Nuchal crest length: projects posteriorly (0), or restricted (1).
32. Internal carotid artery functionality: functional (0), or non-functional (1).
33. Presence of *s3* septum on promontorium: present (0), absent (1).

Postcranial characters used by Bloch et al. (2007)

109 (p1). Greater tuberosity on humerus small (0), or prominent (1).
110 (p2). Lesser tuberosity on humerus gracile (0), or protrudes medially away from humeral shaft (1).

111 (p3). Deltopectoral crest of humerus more than 33% total length of the bone (0), or less than 33% total length of bone (1).
112 (p4). Deltopectoral crest of humerus positioned anteriorly (0), or laterally (1).
113 (p5). Radial and/or olecranon fossa of humerus distinct (0), or indistinct to absent (1).
114 (p6). Breadth of medial epicondyle (=entepicondyle) of humerus 30% or more of total distal breadth (0), or less than 30% of total distal breadth (1).
115 (p7). Supinator crest of humerus broad and well developed (0), or reduced to absent (1).
116 (p8). Capitulum of humerus spindle-shaped (0), or ball-like (1).
117 (p9). Attachment for m. teres major on humerus not distinct (0), or present as distinct protrusion on crest leading down from lesser tuberosity (1).
118 (p10). Trochlea of humerus only medial edge present (0), or both medial and lateral edges present and trochlea and capitulum well separated by distinct gap (1).
119 (p11). Bicipital tuberosity on radius clearly distinct from rest of shaft (0), or absent (1).
120 (p12). Radial head ovoid with ratio of mediolateral breadth/anteroposterior breadth greater than 1.26 (0), or round with ratio of mediolateral breadth/anteroposterior breadth less than 1.26 (1).
121 (p13). Radial head with central fossa flat (0), or deeply excavated (1).
122 (p14). Lateral lip on radial head broad but limited to lateral side (0), or narrow and more extensive (1).
123 (p15). Ridge on distal end of anterior radius absent (0), or present, raised and canted (1).
124 (p16). Ulnocarpal articulation mediolaterally and dorsopalmarly extensive, occurring in transverse plane (0), or limited to radial and palmar aspects of distal ulna, lying in proximodistal plane (1).
125 (p17). Olecranon process of ulna similar in length to height of semilunar notch, with ratio of olecranon process length/semilunar notch height greater than 0.8 (0), or very reduced with ratio of olecranon process length/semilunar notch height less than 0.75 (1).
126 (p18). Distal radioulnar articulation unfused (0), or fused (1).
127 (p19). Scaphoid and lunate unfused (0), or fused (1).
128 (p20). Relative length of intermediate phalanges short (0), or long (1).
129 (p21). Nails absent (0), or present on at least one digit (1).
130 (p22). Flexor sheath ridges on manual proximal phalanges absent (0), present but poorly demarcated (1), or present and very well demarcated (2).
131 (p23). Groove for tendon of the flexor fibularis muscle on the astragalus on the midline (0), shifted laterally (1), or absent (2).
132 (p24). Astragalar body shallowly grooved (0), narrow and more deeply grooved (1), not grooved at all, medial and lateral guiding ridges absent (2).
133 (p25). Height of borders of astragalar trochlea subequal (0), or lateral border much higher than medial (1).
134 (p26). Length of astragalar neck less than 30% of total length of bone (0), or more than 30% of total length of bone (1).

135 (p27). Secondary articulation between posterior side of sustentaculum tali and astragalus absent (0), present (1), similar facet on sustentaculum contacts medial malleolus rather than astragalus (2), or sustentaculum reduced or absent (3).
136 (p28). Calcaneocuboid articulation with distal calcaneus flat (0), or with concave pit (1).
137 (p29). Distal end of calcaneus not elongate (0), or elongate (1).
138 (p30). Plantodistal process on entocuneiform strong (0), or reduced to absent (1).
139(p31). Acetabular shape circular with ratio of craniocaudal length/dorsoventral breadth less than 1.1 (0), or with ratio of craniocaudal length/dorsoventral breadth more than 1.1 (1).
140 (p32). Pattern of acetabular bony buttressing even around the entire rim (0), or markedly more emphasized cranially (1).
141 (p33). Greater trochanter on femur taller than femoral head (0), comparable in proximal extent to femoral head (1), or markedly shorter than femoral head (2).
142 (p34). Lesser trochanter on femur not enlarged and not extensive medially (0), or enlarged and extended medially beyond level of head (1).
143 (p35). Third trochanter on femur distal to lesser trochanter (0), or on same level as lesser trochanter (1).
144 (p36). Patellar groove on femur triangular and narrow mediolaterally relative to its distal extent (0), or rectangular and wide mediolaterally relative to its distal extent (1).
145 (p37). Distal femur deep with no anterior extension of patellar ridges (0), very deep with anterior extension of patellar ridges (1), or shallow (2).
146 (p38). Trochanteric fossa on femur deep (0), or shallow to absent (1).
147 (p39). Tibial tuberosity robust (0) or small to absent (1).
148 (p40). Medial malleolus on tibia long (0), or short (1).
149 (p41). Tibial plateau with lateral condyle projecting further proximally than medial condyle (0), or medial and lateral condyles projecting to similar extent proximally (1).
150 (p42). Humerofemoral index [=(humerus length/femoral length)*100)] between 70 and 150 (0), greater than 150 (1), or less than 70 (2).
151 (p43). Brachial index [=(radius length/humerus length)*100] less than 120 (0), or greater than 120 (1).
152 (p44). Centrale unfused (0), or postnatal ossification between scaphoid or lunate and centrale in adults (1).
153 (p45). Capitular tail on humerus present (0), or very reduced to absent (1).
154 (p46). Cross-sectional shape of radial shaft rounded (0), or flattened (1).
155 (p47). Manual intermediate phalanges short and broad (0), or tall and narrow (1).
156 (p48). Non-hallucial terminal phalanges shallow proximally and distally (0), deep proximally and shallow distally (1), deep proximally and distally (2), or mediolaterally wide and dorsoventrally flattened (3).
157 (p49). Manual proximal phalanges longer than intermediate phalanges (0), or shorter than intermediate phalanges (1).

158 (p50). Metatarsal I facet on entocuneiform mediolaterally narrow (0), mediolaterally broad (1), or saddle-shaped (2).
159 (p51). Peroneal process on metatarsal I small (0) or extensive (1).
160 (p52). Medial process of metatarsal I small, medially rather than proximally extended (0), or large, mediolaterally restricted and proximally extended (1).
161 (p53). Ilium blade-like (0), or rod-like (1).
162 (p54). Pubic symphysis long (0), or short (1).
163 (p55). Anterior inferior iliac spine large (0), or very small to absent (1).
164 (p56). Ribs craniocaudally narrow (0), or wide (1).
165 (p57). Atlas craniocaudally narrow (0), or wide (1).
166 (p58). Axis spinous process oriented caudally (0), or cranially (1).
167 (p59). Thoracic spinous processes long and narrow (0), or short and wide (1).
168 (p60). Lumbar transverse processes long and projecting ventrally beyond centrum (0), or short and lateral to centrum, not projecting ventrally beyond centrum (1).
169 (p61). Third trochanter on femur large (0), small (1), or very small to absent (2).
170 (p62). Proximal end of fibula large (0), or reduced (1).
171 (p63). Height of ridges on patellar groove on femur subequal (0), medial higher than lateral ridge (1), or lateral higher than medial ridge (2).
172 (p64). Prehensile hand proportions absent, with proximal phalanx short relative to metacarpal (0), or present, with proximal phalanx long relative to metacarpal (1).
173 (p65). Metatarsal I torsion absent, with distal condyle anteroposterior direction equal to proximal anteroposterior direction (0), or present, with distal condyle anteroposterior direction rotated 90 degrees laterally relative to that of proximal end (1).

Table 5.4A. Cranial characters for Plesiadapidae adopted from Bloch et al. (2007). 1-26 correspond to c1-c26 in Table 5.3.Characters 1-23 are the same in Bloch and Silcox (2006) and Bloch et al. (2007). Character 24 of Bloch and Silcox (2006) is not represented here. Bold cells in the "ancestor" row represent codings that differ from the coding of "Plesiadapidae" in Bloch and Silcox (2006) and Bloch et al. (2007).

Taxon	**1**	**2**	**3**	**4**	**5**	**6**	**7**	**8**	**9**	**10**	**11**	**12**	**13**	**14**	**15**	**16**	**17**	**18**	**19**	**20**	**21**	**22**	**23**	**24**	**25**	**26**
P. tricuspidens	1	0	1	1	0	1	1	1	0	0	1	0	0	1	0	1	0	?	1	0	0	1	1	0	0	1
P. cookei	1	0	1	1	0	1	?	1	0	0	1	0	0	?	?	0	0	?	?	?	?	?	?	0	0	1
*P. rex**	?	?	?	?	?	?	?	?	?	?	?	?	0	?	?	?	0	?	?	?	?	?	?	?	?	?
P. anceps	?	?	?	?	?	?	?	?	0	?	?	?	?	?	?	0	?	?	?	?	?	?	?	?	?	?
N. intermedius	1	0	0	1	0	1	?	1	0	0	1	?	0	?	?	0	0	?	?	?	?	?	?	0	0	1
N. gidleyi	1	0	?	?	?	?	?	1	0	?	1	?	0	1	?	?	0	?	?	?	?	?	?	0	0	1
Pr. gaoi	1	0	0	1	0	1	?	1	0	0	1	0	?	?	0	0	0	?	?	?	?	1	1	0	0	1
Ancestor	1	**0**	**0**	1	**0**	**1**	1	1	0	0	1	0	0	1	0	**0**	0	**?**	**1**	0	**0**	1	**1**	0	0	1

Table 5.4B. New cranial characters for Plesiadapidae – see Table 5.3 for descriptions.

Taxon	**27**	**28**	**29**	**30**	**31**	**32**	**33**
P. tricuspidens	2	1	1	1	1	0	0 1
P. cookei	1	0	1	0	0	0	1
*P. rex**	?	?	0 1	?	?	?	?
P. anceps	1	?	?	?	?	?	?
N. intermedius	1	0	0	0	0	0	1
N. gidleyi	?	?	?	1	?	0	1
Pr. gaoi	1	0	0	0	0	0	0
Ancestor	1	0	0	0	0	0	0 1

**P. rex* codings are based on two maxillary specimens (YPM-PU 21448, YPM-PU 21347) from Cedar Point Quarry

Table 5.4C. Postcranial characters for Plesiadapidae adopted from Bloch et al. (2007). 1-65 correspond to p1-p65 in Table 5.3. Bold cells indicate revisions to coding of Bloch et al. (2007).

Taxon	**1**	**2**	**3**	**4**	**5**	**6**	**7**	**8**	**9**	**10**	**11**	**12**	**13**	**14**	**15**	**16**	**17**	**18**	**19**	**20**	**21**	**22**	**23**	**24**	**25**	**26**	**27**	**28**	**29**	**30**
Pr. gaoi	?	?	?	1	0	0	0	1	?	1	0	1	1	1	?	?	?	?	?	?	?	1	0	1	0	1	?	?	?
N. intermedius	?	?	?	1	0	0	0	1	1	0	0	1	1	1	0	0	0	0	0	0	?	1	?	?	?	?	?	?	?	?
N. gidleyi	?	?	?	1	0	0	0	1	?	?	0	1	1	1	0	0	0	0	?	0	?	1	1	0	1	0	1	1	0	?
P. insignis	?	?	?	?	?	?	?	?	?	?	?	?	?	?	?	?	?	0	?	0	0	?	?	?	?	?	?	?	?	?
P. churchilli	?	?	?	?	?	?	?	?	?	?	?	?	?	?	?	?	?	?	?	?	?	?	?	?	?	?	1	1	0	?
P. rex	?	?	?	1	0	0	0	1	1	1	?	?	?	?	?	?	0	?	?	?	?	?	1	0	1	0	1	?	?	?
*P. anceps**	?	?	?	?	?	?	?	?	?	?	?	?	?	?	?	?	?	?	?	?	?	?	?	?	?	?	?	?	?	0
P. walbeckensis	?	?	?	1	0	0	0	1	1	1	?	?	?	?	?	?	?	?	?	?	?	?	?	?	?	?	?	?	?	?
Pl. daubrei	?	?	?	?	0	0	0	1	?	1	?	?	?	?	?	?	?	?	?	?	?	?	?	?	?	?	?	?	?	?
P. tricuspidens	1	1	0	1	0	0	0	1	1	1	0	1	1	1	0	0	0	0	?	0	?	1	1	0	1	0	1	1	0	0
P. cookei	1	1	0	0	0	0	0	1	1	0	0	1	1	1	0	0	?	0	0	0	?	1	1	0	1	0	1	1	0	?
P. remensis	?	?	?	?	0	0	0	1	?	1	?	?	?	?	?	?	?	?	?	?	?	?	?	?	?	?	?	?	?	?
Ancestor	1	1	0	**1**	0	0	0	1	1	**1**	0	1	1	1	0	0	0	0	0	0	**0**	1	1	0	1	0	1	1	0	**0**

**P. anceps* codings are based on AMNH 92011, which is an entocuneiform from the Bison Bason saddle locality described by Szalay and Dagosto (1988).

Table 5.4C. continued.

Taxon	**31**	**32**	**33**	**34**	**35**	**36**	**37**	**38**	**39**	**40**	**41**	**42**	**43**	**44**	**45**	**46**	**47**	**48**	**49**	**50**	**51**	**52**	**53**	**54**	**55**	**56**	**57**	**58**	**59**	**60**	**61**	**62**	**63**	**64**	**65**
Pr. gaoi	?	?	?	?	?	?	?	?	?	?	?	?	?	?	0	1	1	1	?	?	?	?	?	?	?	?	?	?	?	?	?	?	?	?	?
N. intermedius	?	?	?	?	?	1	2	?	0	1	0	?	?	0	0	1	1	1	0	?	0	0	?	?	?	?	0	1	0	?	?	1	0	0
N. gidleyi	1	1	1	1	0	1	2	0	0	1	0	?	?	?	0	1	1	?	0	?	?	?	?	?	?	1	0	0	?	0	?	1	1	0	?
P. insignis	?	?	?	?	?	?	?	?	?	?	?	0	0	?	?	?	1	1	0	?	?	?	?	?	?	?	?	?	?	?	?	?	?	0	?
P. churchilli	?	?	1	1	0	?	?	0	?	?	?	?	?	?	?	?	?	1	?	?	0	0	?	?	?	?	?	?	?	?	1	?	?	0
P. rex	?	?	?	?	?	?	?	?	?	1	?	?	?	?	0	?	?	?	?	?	?	?	?	?	?	?	?	?	?	?	?	?	?	?
*P. anceps**	?	?	?	?	?	?	?	?	?	?	?	?	?	?	?	?	?	?	1	?	?	?	?	?	?	?	?	?	?	?	?	?	?	?
P. walbeckensis	?	?	?	?	?	?	?	?	?	?	?	?	?	?	0	?	?	?	?	?	?	?	?	?	?	?	?	?	?	?	?	?	?	?
Pl. daubrei	?	?	?	?	?	?	?	?	?	?	?	?	?	?	0	?	?	?	?	?	?	?	?	?	?	?	?	?	?	?	?	?	?	?
P. tricuspidens	0	1	1	1	0	1	2	0	0	1	0	0	0	?	0	1	1	1	0	1	?	?	?	?	0	?	?	?	?	?	1	1	0	?
P. cookei	0	1	1	1	0	1	2	0	0	1	0	0	0	0	0	1	1	1	0	?	0	0	0	1	0	0	0	?	0	?	1	1	0	0
P. remensis	?	?	?	?	?	?	?	?	?	?	?	?	?	?	0	?	?	?	?	?	?	?	?	?	?	?	?	?	?	?	?	?	?	?
Ancestor	0 1	**1**	1	1	0	1	2	0	0	1	0	0	0	0	0	1	1	1	0	1	0	0	0	**1**	0 1	0	0	**1**	0	?	1	1	0	0

**P. anceps* codings are based on AMNH 92011, which is an entocuneiform from the Bison Bason saddle locality described by Szalay and Dagosto (1988).

Table 5.5. Coding changes for plesiadapiform characters.

Matrix	Taxon (OTU)	Character	Original	Final
Bloch and Silcox (2006)	Plesiadapidae	2	?	1
Bloch and Silcox (2006)	Plesiadapidae	3	1	0
Bloch and Silcox (2006)	Plesiadapidae	5	2	0
Bloch and Silcox (2006)	Plesiadapidae	6	0	1
Bloch and Silcox (2006)	Plesiadapidae	16	0	1
Bloch and Silcox (2006)	Plesiadapidae	18	1	?
Bloch and Silcox (2006)	Plesiadapidae	19	1	0
Bloch and Silcox (2006)	Plesiadapidae	21	1	0
Bloch and Silcox (2006)	Plesiadapidae	23	2	1
Bloch and Silcox (2006)	Paromomyidae	23	1,2	1
Bloch and Silcox (2006)	Carpolestidae	24	1	0
Bloch et al. (2007)	Plesiadapidae	c2	?	0
Bloch et al. (2007)	Plesiadapidae	c3	1	0
Bloch et al. (2007)	Plesiadapidae	c5	2	0
Bloch et al. (2007)	Plesiadapidae	c6	0	1
Bloch et al. (2007)	Plesiadapidae	c16	1	0
Bloch et al. (2007)	Plesiadapidae	c18	1	?
Bloch et al. (2007)	Plesiadapidae	c19	0	1
Bloch et al. (2007)	Plesiadapidae	c21	1	0
Bloch et al. (2007)	Plesiadapidae	c23	2	1
Bloch et al. (2007)	Paromomyidae	c23	2	1
Bloch et al. (2007)	Plesiadapidae	p4	0,1	1
Bloch et al. (2007)	Plesiadapidae	p10	0	1
Bloch et al. (2007)	Plesiadapidae	p21	?	0
Bloch et al. (2007)	Plesiadapidae	p30	0,1	0
Bloch et al. (2007)	Plesiadapidae	p32	0,1	1
Bloch et al. (2007)	Plesiadapidae	p54	0	1
Bloch et al. (2007)	Plesiadapidae	p58	0	1

Table 5.6. Most parsimonious tree parameters.

Variable	Matrix	Original	Final
Tree length	Bloch and Silcox (2006)	55	52
Consistency Index	Bloch and Silcox (2006)	60	63
Retention Index	Bloch and Silcox (2006)	60	62
Tree length	Bloch et al. (2007)	502	500
Consistency Index	Bloch et al. (2007)	44	45
Retention Index	Bloch et al. (2007)	54	54

Table 5.7. Posterior carotid foramen (PCF) and groove diameters and skull lengths (mm) of selected Mammalia. Abbreviations: Func. – functionality of internal carotid artery. 1 – supplies forebrain with blood, 2 – does not contribute to brain's blood supply. Le – prosthion-inion length of skull.

Taxon	Func	Specimen/reference	PCF	Skull Le
Erinaceus sp.	1	Kay et al. 1992	0.43	45.00
Tupaia glis	1	Kay et al. 1992	0.62	49.10
Tupaia tana	1	Kay et al. 1992	0.81	59.40
Nycticebus coucang	2	Kay et al. 1992	0.45	59.20
Perodicticus potto	2	Kay et al. 1992	0.18	61.90
Galago senegalensis	2	Kay et al. 1992	0.16	40.66
Galago senegalensis	2	Kay et al. 1992	0.20	46.80
Galago demidovii	2	Kay et al. 1992	0.14	37.30
Eulemur fulvus	1	Kay et al. 1992	0.68	87.30
Lemur sp.	1	Kay et al. 1992	0.75	83.70
Tarsius sp.	1	Kay et al. 1992	0.56	39.30
Callithrix argentata	1	Kay et al. 1992	0.74	45.70
Callicebus sp. (Bolivia)	1	Kay et al. 1992	1.05	59.00
Saguinus mystax	1	Kay et al. 1992	0.99	50.70
Saimiri sciureus	1	Kay et al. 1992	1.24	59.70
Aotus trivirgatus	1	Kay et al. 1992	1.30	62.70
Cebus paella	1	Kay et al. 1992	2.00	95.50
Pithecia pithecia	1	Kay et al. 1992	1.37	82.60
Ateles geoffroyi	1	Kay et al. 1992	2.42	102.90
Alouatta pigra	1	Kay et al. 1992	2.50	104.40
Plesiadapis tricuspidens	?	MNHN CR 125	0.34	106.36
Plesiadapis tricuspidens	?	Pellouin skull	0.30	106.50[B]
Plesiadapis cookei	?	UM 87990	0.40[A]	105.80 [B]
Nannodectes intermedius	?	USNM 309902	0.29[A]	50.40 [B]
Pronothodectes gaoi	?	UALVP 49105	0.28	61.20 [B]
Carpolestes simpsoni	?	Bloch & Silcox 2006	0.53	39.56
Ignacius graybullianus	?	Kay et al. 1992	0.17	48.20

A – measurement represents g1 groove of these specimens
B – estimate from Table 3.3

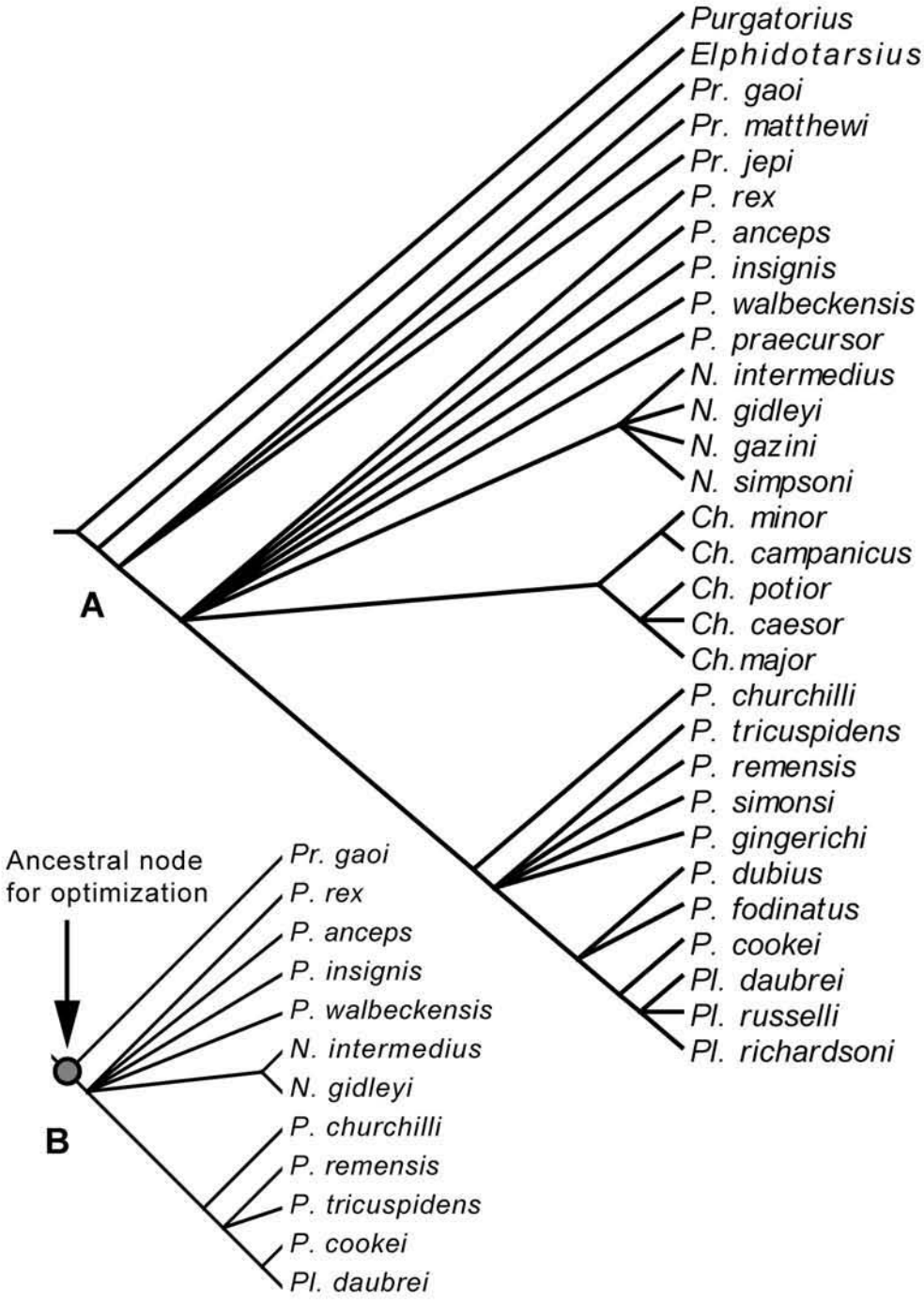

Figure 5.1. A. Consensus cladogram of all well-known plesiadapid species. The topology is the result of a dental analysis consisting of 32 characters listed in Tables 5.1 and 5.2. See introduction for genus abbreviations. B. Cladogram culled to taxa for which cranial data and/or postcranial data are available and which were used to reconstruct the ancestral node as indicated.

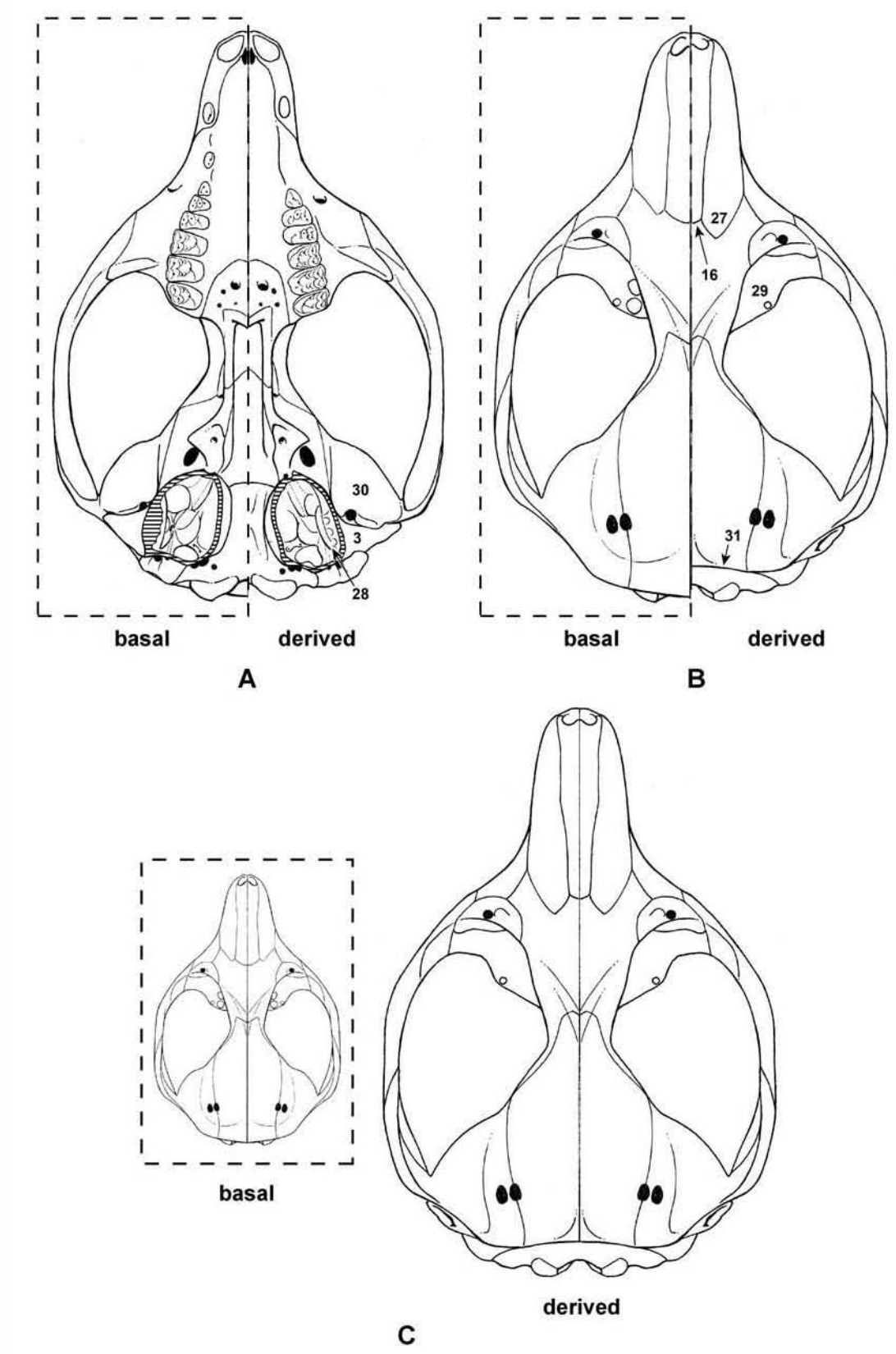
30
3
28
basal
derived
A
27
16
29
31
basal
derived
B
basal
derived
C

Figure 5.2.

Figure 5.2. Illustration of plesiadapid skulls based on character state reconstructions. Comparison of the reconstructed skulls of basal (based on ancestral node reconstruction) and derived (based on *Plesiadapis tricuspidens*) Plesiadapidae in A, ventral, and B, dorsal views. Numbers correspond to characters listed in Table 5.3. The derived form was reconstructed using measurements from skulls of *P. tricuspidens*, which are complete enough to reveal overall cranial proportions. This reconstruction was then modified by using all available measurements and morphology from *Pronothodectes gaoi* (Table 2.5), which matches the ancestral node reconstruction in most respects (Table 5.4A-B). In order to transform the skull of *P. tricuspidens* into that of *Pronothodectes*, all bones were re-scaled according to nasal length, but this re-scaling could have been done using a single dimension on any other bone that was preserved without distortion in both taxa. Wherever there was no morphological information on basal plesiadapids, the reconstruction was left similar to the image of the derived form. Thus, these comparisons probably under-represent the full morphological disparity separating basal, *Pr. gaoi*-like and derived, *P. tricuspidens*-like plesiadapids. Numbers correspond to features in which derived *P. tricuspidens* (and in some cases *P. cookei*) differ from primitive ones (Table 5.3). C, Size comparison of reconstructed skulls of basal and derived Plesiadapidae in dorsal view. The more derived skull is shown at 210% the size of the basal one, which approximates the difference in size between early, *Nannodectes intermedius*-sized taxa and late-occurring *P. tricuspidens*. The only plesiadapid that has been estimated to be substantially larger is *P. cookei* (but see Table 3.3, 5.7 and Chapter 4). The only smaller plesiadapids are *Pr. matthewi* and *N. gazini* (Gingerich, 1976). Still, most of the size range for the family Plesiadapidae is illustrated by the two reconstructed skulls in this figure.

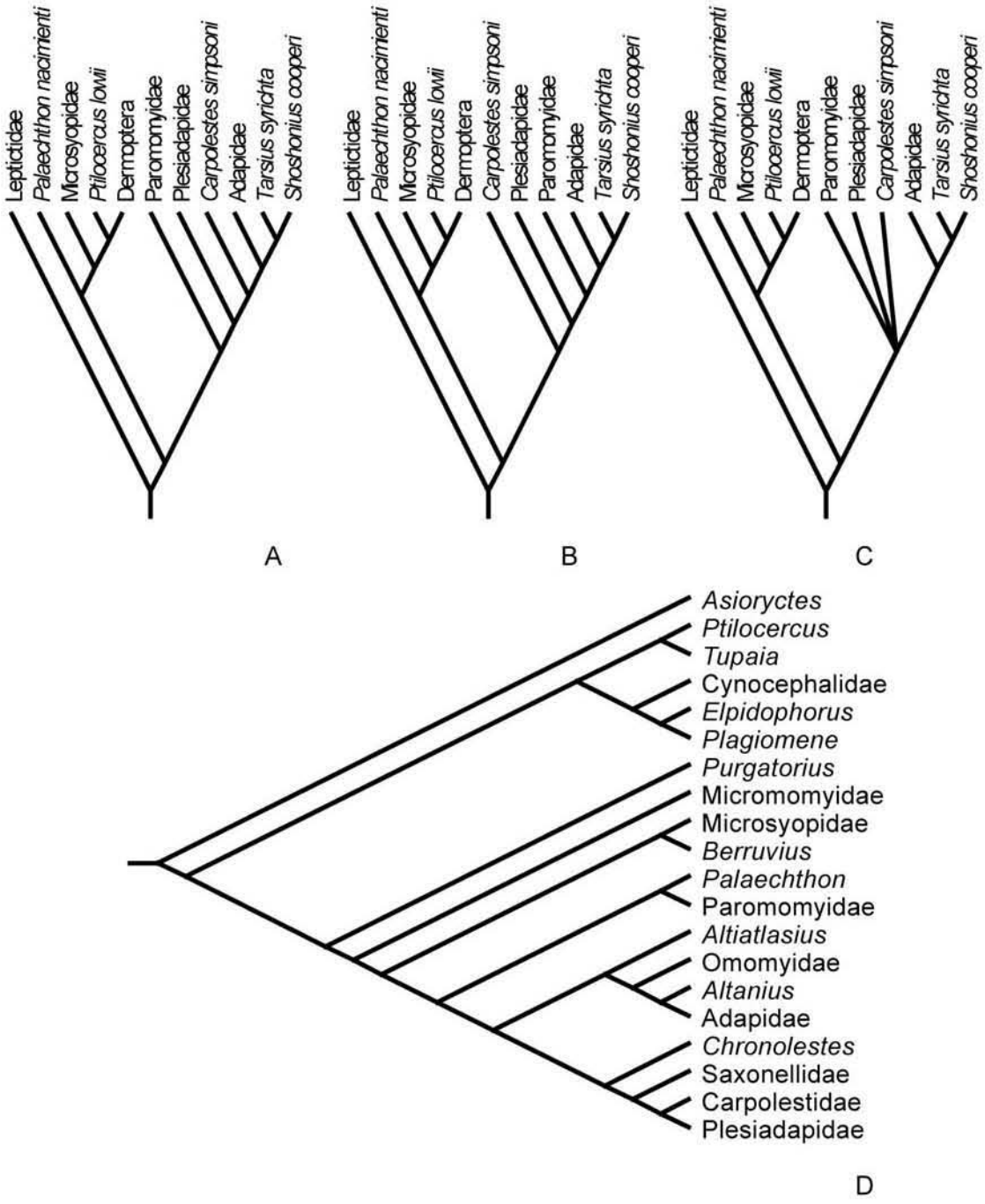
Lepticidae
Palaechthon nacimienti
Microsyopidae
Ptilocercus lowii
Dermoptera
Paromomyidae
Plesiadapidae
Carpolestes simpsoni
Adapidae
Tarsius syrichta
Shoshonius cooperi
A
B
C
Asioryctes
Ptilocercus
Tupaia
Cynocephalidae
Elpidophorus
Plagiomene
Purgatorius
Micromomyidae
Microsyopidae
Berruvius
Palaechthon
Paromomyidae
Altiatlasius
Omomyidae
Altanius
Adapidae
Chronolestes
Saxonellidae
Carpolestidae
Plesiadapidae
D

Figure 5.3

Figure 5.3. Most parsimonious (MP) trees resulting from modified character matrices. A, MP tree 1 from analysis of modified matrix of Bloch and Silcox (2006), with topology matching one of the MP trees of the original matrix. B, MP tree 2 from analysis of modified matrix of Bloch and Silcox (2006), with a novel topology that was not supported by the original matrix. C, strict concensus of A and B. D, MP tree from analysis of modified matrix of Bloch et al. (2007).

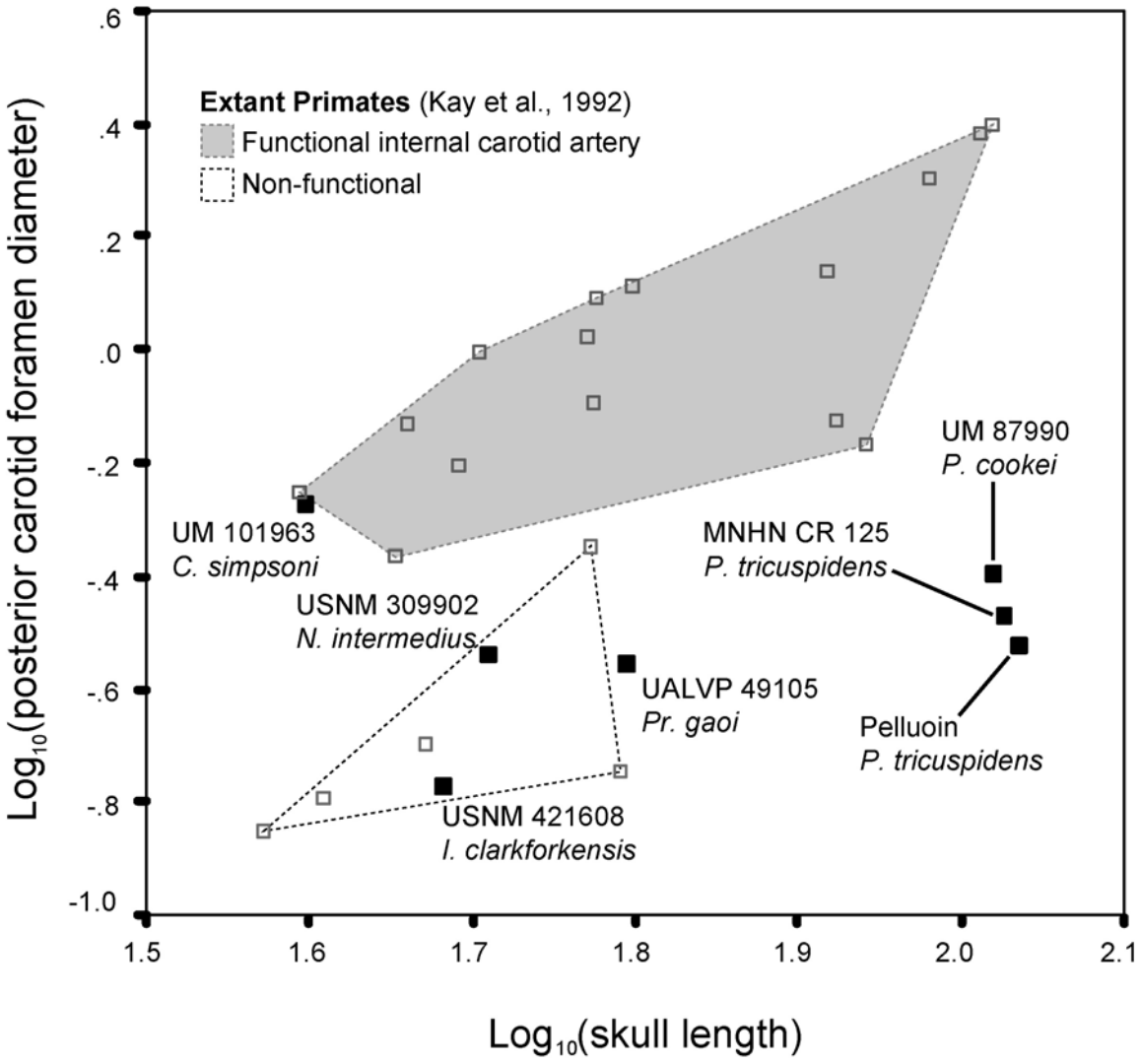

Figure 5.4. Plot of posterior carotid foramen sizes of selected plesiadapiforms (solid squares) relative to those of extant primates (open squares) measured by Kay et al. (1992). The posterior carotid foramen or *g1* groove for internal carotid plexus (y axis represents one or other of these measurements, which are equivalent – Bloch and Silcox, 2001, 2006) in all plesiadapids is smaller than that of extant primates with a functional internal carotid artery and *Carpolestes simpsoni* (Bloch and Silcox, 2006), but larger than in *Ignacius* (Kay et al., 1992). Skull length estimates for fragmentary specimens were based on *Plesiadapis tricuspidens* and *P. cookei* (see Chapter 3) and were generated as described in text. See Table 5.7 data. Though the method of generating skull length estimates is crude, it is clear that skull length is not critical for interpretation of functionality reflected by the foramen in this sample. Regardless of skull length, foramina of taxa with functional arteries are generally larger than those of taxa with non-functional arteries.

CHAPTER 6:
SUMMARY AND CONCLUSIONS

This section serves to summarize and emphasize major contributions and conclusions of the foregoing chapters.

New crania of plesiadapids and reassessment of cranial stucture

Chapter 2 provides the first description of crania referred to a member of the genus *Pronothodectes* (Fox, 1990). Furthermore, it provides the most extensive and detailed documentation and description of plesiadapid cranial morphology heretofore available. Finally, it examines a larger sample of better preserved cranial material, with more advanced visualization techniques than any other study on plesiadapid crania. The fossil and analytical resources of this work allowed me to describe distinctive features of taxa traditionally thought to represent basal plesiadapids (such as *Pronothodectes* and *Nannodectes*) and more derived plesiadapids (such as *Plesiadapis tricuspidens*), as well as similarities shared by them. These new observations revealed the morphology of basal plesiadapids to be different from previous perceptions in some ways (e.g., Russell, 1964; Bloch et al., 2007). Major findings include the following: (1) the bony composition of the plesiadapid tympanic bulla is uncertain, but best interpreted as petrosal in origin given available evidence (including that presented here); (2) all known plesiadapids other than *P. tricuspidens* appear to have nasals that exhibit a slight lateral flaring at their caudal extent (as compared to the mediolateral width of either the rostrocaudal midpoint or the

rostral end of the nasals) and premaxillae with a relatively mediolaterally narrow caudal extent; (3) small plesiadapids have an unexpanded external auditory meatus, unlike large plesiadapids in which the external auditory meatus is expanded, or tube-like; (4) *P. tricuspidens* appears to have a more caudally restricted nuchal crest than other known plesiadapids; (5) there is no separate foramen rotundum for cranial nerve V2 in specimens of *P. tricuspidens* (the foramen previously interpreted as the superior orbital fissure appears to be a suboptic foramen, meaning that the foramen previously considered the foramen rotundum [Russell, 1964; Bloch and Silcox, 2006] is actually the sphenorbital fissure [Kay et al., 1992]); (6) the internal carotid neurovascular plexus entered the skull from a posterolateral (not posteromedial) position and traveled to the promontorium through a bony tube supported by the posterior septum [of MacPhee (1981)] in most plesiadapid taxa; (7) the internal carotid plexus is identifiable on the promontorium as a laterally positioned groove, or pair of grooves, that leads from the anterior end point of bony tube mentioned above to the anterior septum [of MacPhee (1981)]; (8) the tube for the internal carotid plexus is narrow (0.28-0.40 mm) in all plesiadapids, indicating that it did not contain a functional artery; (9) *Pronothodectes gaoi* and some specimens of *P. tricuspidens* have one more tympanic cavity septum (*s3*) than other plesiadapids; and (10) the annular component of the ectotympanic bone of *P. tricuspidens* is more expanded than that of the smaller *N. intermedius*.

Craniodental material of *Plesiadapis cookei* and its implications for paleobiological distinction from *P. tricuspidens*

Chapter 3 provides the first extensive descriptions and comparisons of a skull of *Plesiadapis cookei*, the largest, and one of the latest occurring North American plesiadapid taxa (Gingerich, 1976). It is compared extensively to the similarly well preserved skulls of *P. tricuspidens* from France. Previously known similarities betwee*n* *P. cookei* and *P. tricuspidens* include features such as large size, a penecontemporaneous existence and dental features such as lack of a margoconid on the lower central incisor (Jepsen, 1930; Gingerich, 1976). The skull of *P. cookei* possesses a unique mixture of features, some representing similarities to other North American plesiadapids, as described in Chapter 2, and others representing similarities to *P. tricuspidens*. *P. cookei* is similar to *P. tricuspidens* in having a tube-like external auditory meatus and limited exposure of molar tooth roots on the dorsum of its maxilla in its orbit, but otherwise it looks more like other North American plesiadapids in features 2, 4 and 10 from above, and in having proportionally smaller glenoid fossae than *P. tricuspidens*.

Quantitative comparison of 39 skull measurements confirms that *P. cookei* and *P. tricuspidens* had skulls of virtually identical size. This constitutes strong evidence that they had similar body sizes in life. This conclusion appears to be at odds with evidence from molar teeth, which suggest that *P. cookei* was much larger than *P. tricuspidens*. An investigation of the dentition was therefore undertaken. Metrics reflecting molar tooth function, including orientation patch count and relief index, solidly support the hypothesis that *P. cookei* was more specialized for eating leafy, fibrous foods than was *P. tricuspidens*. If *P. cookei* was more specialized to folivory, then having larger teeth for

its body size would fit predictions based on the observation that euprimate folivores have larger teeth than more dietarily-generalized relatives of the same body size (Kay, 1975).

The postcranial skeleton of *Plesiadapis cookei* and evidence for a suspensory, arboreal locomotor repertoire

Chapter 4 represents the most comprehensive description and documentation of plesiadapid postcranial morphology yet. Beard's (1989) work is more thorough in that it has a larger and (in some ways) better distributed extant comparative sample. However, more fossil material is considered in this chapter than in Beard's study and raw measurements comprehensively representing the postcranium are presented for virtually all available plesiadapid specimens known. Furthermore, HRxCT imagery allows a more complete view of carpal, metacarpal, tarsal, and metatarsal complexes because it provides the capacity to invert left side bones into right side bones, and to scale elements from any given species for articulation with bones of *P. cookei*. Medical and HRxCT scan images are also used to thoroughly illustrate complex morphology and articulations of the elbow, wrist, hip, knee, and ankle joints, as well as the carpus, metacarpus, tarsus and metatarsus. Finally, quantitative comparisons among bones attributed to different plesiadapid species allow some of the first concrete statements regarding interspecific differences in the morphology of the plesiadapid postcranium.

Major points demonstrated in this chapter include the following: (1) the plesiadapid clavicle is distinctively superoinferiorly expanded; (2) most plesiadapid humeri have a lateral keel on the ulnar trochlea; (3) humeri of large-bodied plesiadapids exhibit lateral torsion of the distal end; (4) the humerus of *Plesiadapis cookei* is

absolutely longer and absolutely smaller in cross-sectional dimensions, and thus more slender than that of *P. tricuspidens*; (5) the wrist of *P. cookei* exhibits a relatively large lunate that intervenes between the triquetrum and scaphoid, and contacts the radius and ulna; (6) the bone previously identified as a lunate in *Nannodectes intermedius* is actually a sesamoid of the metacarpophalangeal joint; (7) the pollical metacarpal did not contact the second metacarpal at its proximal end and was mobile with respect to it; (8) the metacarpus is shorter than previously thought, meaning the fingers were proportionally longer than previously determined; (9) the intermediate phalanges of large-bodied plesiadapids are more robust than those of smaller plesiadapids; (10) the intermediate phalanges of *P. cookei* and *P.* n. sp. are proportionally mediolaterally narrower than those of other plesiadapids; (11) the innominate of *P. cookei* has a caudally positioned, craniocaudally narrow pubic symphysis; (12) the femur of *P. cookei* has a shaft distal to the lesser trochanter that is absolutely longer than that of *P. tricuspidens*, but which is otherwise metrically identical; (13) the astragalotibial joint had a limited capacity for plantarflexion but enhanced capacities for conjunct medial rotation and inversion; (14) the calcaneocuboid joint has its greatest mobility in abduction and adduction, not rotation; (15) the axis of the vertebral column of all known plesiadapids probably had a cranially projecting spinous process; (16) the neck of plesiadapids appears to have been relatively short compared to the trunk; (17) there appear to have been at least 13 thoracic, 7 lumbar, 3 sacral, and 20 caudal vertebrae in *P. cookei*; (18) the anticlinal spinous process appears to have been situated on T12 while the diaphragmatic vertebra appears to have been T11 in *P. cookei*; (19) the sacrum of plesiadapids has a large, cranially-projecting first spinous process, a rudimentary second spinous process, and a large,

vertically-to-caudally projecting third spinous process; and (20) the tail of *P. cookei* was relatively long with the longest vertebrae of the tail occurring at the 11^{th} or 12^{th} position.

Estimation of body mass based on the postcranium and using different sets of regressions reveals plesiadapids to have ranged from between around 300 g (*Nannodectes intermedius*) to 2000-3000 g (both *P. cookei* and *P. tricuspidens*) in mass. This is basically consistent with, although slightly lower than, estimates of mass range derived from cranial material.

Consideration of morphology, joint mobility and likely habitual postures strongly supports previous contentions that *P. cookei* was committed to an arboreal lifestyle (Gunnell and Gingerich, 1987; Bloch et al., 2007), although they do not necessarily add strong support to the idea that it had "suspensory tendencies" (Bloch and Boyer, 2007; Boyer and Bloch, 2008).

Phylogenetic implications of new observations

Chapter 5 provides the first species level cladistic analysis focused on members of the Plesiadapidae. The analysis of 30 species generates a cladogram that is consistent with phylogenetic hypotheses of Gingerich (1976) in most respects. Some polytomies in this cladogram may only be resolvable by incorporation of stratigraphic evidence. States for cranial and postcranial morphological characters are optimized onto the ancestral node of this species level cladogram. The optimized codings for the ancestral node are then used to revise the codings for a higher level "Plesiadapidae" taxon in recently published matrices (Bloch and Boyer, 2002, 2007; Bloch and Silcox, 2006). Revision of these codings for Plesiadapidae reveals that the previous phylogenetic signal in these

matrices is (for the most part) supported by the findings of this dissertation. This means that the traditional view of plesiadapids and carpolestids as sister taxa (e.g., Fox, 1993) is upheld, as well as the more recent hypothesis that a clade consisting of plesiadapids, carpolestids, saxonellids, and *Chronolestes simul* is the sister taxon to anatomically modern primates (Bloch et al., 2007). This was somewhat surprising, however, because many of the new observations relating to the crania of plesiadapids refute previous perceptions of similarity to carpolestid plesiadapiforms. Furthermore, no evidence from the postcranium was found to support the prediction that the common ancestor of plesiadapids and carpolestids, as well as possibly the earliest plesiadapids, should be similar to *Carpolestes simpsoni* in features suggesting specialized grasping capacity (Bloch and Boyer, 2002). It therefore appears that the majority of the evidence for a carpolestid-plesiadapid sister taxon relationship does indeed come from the dentition, as previously noted (e.g., Fox, 1993).

Overall conclusion

With regard to the overarching hypothesis presented in the introductory chapter of this dissertation, new plesiadapid fossil material does not explicitly refute the idea that euprimate pedal grasping features were inherited from a "plesiadapiform" lacking euprimate visual system features. This is because previous phylogenetic hypotheses including plesiadapids, carpolestids, and euprimates were not altered as a result of any analyses performed here. Therefore, the "angiosperm exploitation hypothesis" (e.g., Sussman, 1991) for primate-euprimate origins remains the best supported explanation for the evolution of features that characterized the ancestral member of Euprimates.

More generally speaking, this dissertation finds the Plesiadapidae to represent a group of mammals that are unusually similar to euprimates in many aspects of their detailed morphology and inferred arboreal lifestyle (Fig. 6.1). Thus, consideration of their fossil record is integral to further studies that aim to address questions regarding the phylogenetic and ecological origins of extant primates.

REFERENCES

Beard, K.C., 1989. Postcranial anatomy, locomotor adaptations, and palaeoecology of early Cenozoic Plesiadapidae, Paromomyidae, and Micromomyidae (Eutheria, Dermoptera). Ph.D. Dissertation, Johns Hopkins University.

Bloch, J.I., Boyer, D.M., 2002. Grasping primate origins. Science 298, 1606-1610.

Bloch, J.I., Silcox, M.T., 2006. Cranial anatomy of the Paleocene plesiadapiform *Carpolestes simpsoni* (Mammalia, Primates) using ultra high-resolution X-ray computed tomography, and the relationships of plesiadapiforms to Euprimates. Journal of Human Evolution 50, 1-35.

Bloch, J.I., Boyer, D.M., 2007. New skeletons of Paleocene-Eocene Plesiadapiformes: a diversity of arboreal positional behaviors in early primates. In: Dagosto, M., Ravosa, M.J. (eds) Primate Origins: Adaptations and Evolution. Plenum Press, New York, pp. 535-582.

Bloch, J.I., Silcox, M.T., Boyer, D.M., Sargis, E.J., 2007. New Paleocene skeletons and the relationship of plesiadapiforms to crown-clade primates. Proceedings of the National Academy of Sciences 104, 1159-1164.

Boyer, D.M., Bloch, J.I., 2008. Evaluating the mitten-gliding hypothesis for Paromomyidae and Micromomyidae (Mammalia, "Plesiadapiformes") using comparative functional morphology of new Paleogene skeletons. In: Sargis, E.J., Dagosto, M. (eds) Mammalian Evolutionary Morphology: A Tribute to Frederick S. Szalay. Kluwer, New York, pp. 233-284.

Fox, R.C., 1990. *Pronothodectes gaoi* n. sp. from the late Paleocene of Alberta, Canada, and the early evolution of the Plesiadapidae (Mammalia, Primates). Journal of Paleontology 64, 637-647.

Fox, R.C., 1993. The primitive dental formula of the Carpolestidae (Plesiadapiformes, Mammalia) and its phylogenetic implications. Journal of Vertebrate Paleontology 13, 516-524.

Gingerich, P.D., 1976. Cranial anatomy and evolution of Early Tertiary Plesiadapidae (Mammalia, Primates). University of Michigan Papers on Paleontology 15, 1-141.

Gunnell, G.F., Gingerich, P.D., 1987. Skull and partial skeleton of *Plesiadapis cookei* from the Clark Fork Basin, Wyoming. American Journal of Physical Anthropology 72, 206a.

Jepsen, G.L., 1930. Stratigraphy and paleontology of the Paleocene of northeastern Park County, Wyoming. Proceedings of the American Philosophical Society 69, 463-528.

Kay, R.F., 1975. The functional adaptations of primate molar teeth. American Journal of Physical Anthropology 43, 195-216.

Kay, R.F., Thewissen, J.G.M., Yoder, A.D., 1992. Cranial anatomy of *Ignacius graybullianus* and the affinities of the Plesiadapiformes. American Journal of Physical Anthropology 89, 477-498.

MacPhee, R.D.E., 1981. Auditory regions of primates and eutherian insectivores, morphology, ontogeny, and character analysis. Contributions to Primatology 18, 1-282.

Russell, D.E., 1964. Les Mammifères Paléocènes d'Europe. Mémoires du Muséum National d'Histoire Naturelle, Série C 13, 1-324.

Sussman, R.W., 1991. Primate origins and the evolution of angiosperms. American Journal of Primatology 23, 209-223.

Figure 6.1. CT reconstruction of *Plesiadapis cookei's* skeleton (UM 87990) in antipronograde posture with life reconstruction superimposed below it. The purpose of placing the skeleton in this posture on a branch of such girth and orientation is to provide a summary of results of analyses and comparisons: *P. cookei* and other plesiadapids were better suited to cling and climb on large diameter supports than small ones, given the configuration of their limb joints. All known plesiadapids probably used pronograde, orthograde, and antipronograde postures on large trees trunks and branches. However, aspects of *P. cookei's* skeleton suggest that it may have used antipronograde postures more frequently than others. Perhaps it even used suspensory postures sometimes. Study of the dentition reconstructs *P. cookei* as folivorous, but leaves do not typically grow directly from tree trunks, like that in the figure. *P.cookei* probably used pronograde and orthograde postures when resting or traveling on large tree trunks or branches. When foraging, it must have ventured out into the terminalia of branches where leaves grow. As it progressed to narrower and narrower branches it probably assumed antipronograde, and then suspensory postures. I thank P. Gingerich who gave me this synthetic perspective at my dissertation defense. In the picture, one may imagine that *P. cookei* is returning from, or venturing to engage in a bout of foraging and feeding. The life reconstruction is a photoshop generated image. I sampled photographs of pelage of lemurs, and rodents to create that of *P. cookei*. The bushy tail is based on that preserved for *P. insignis*.

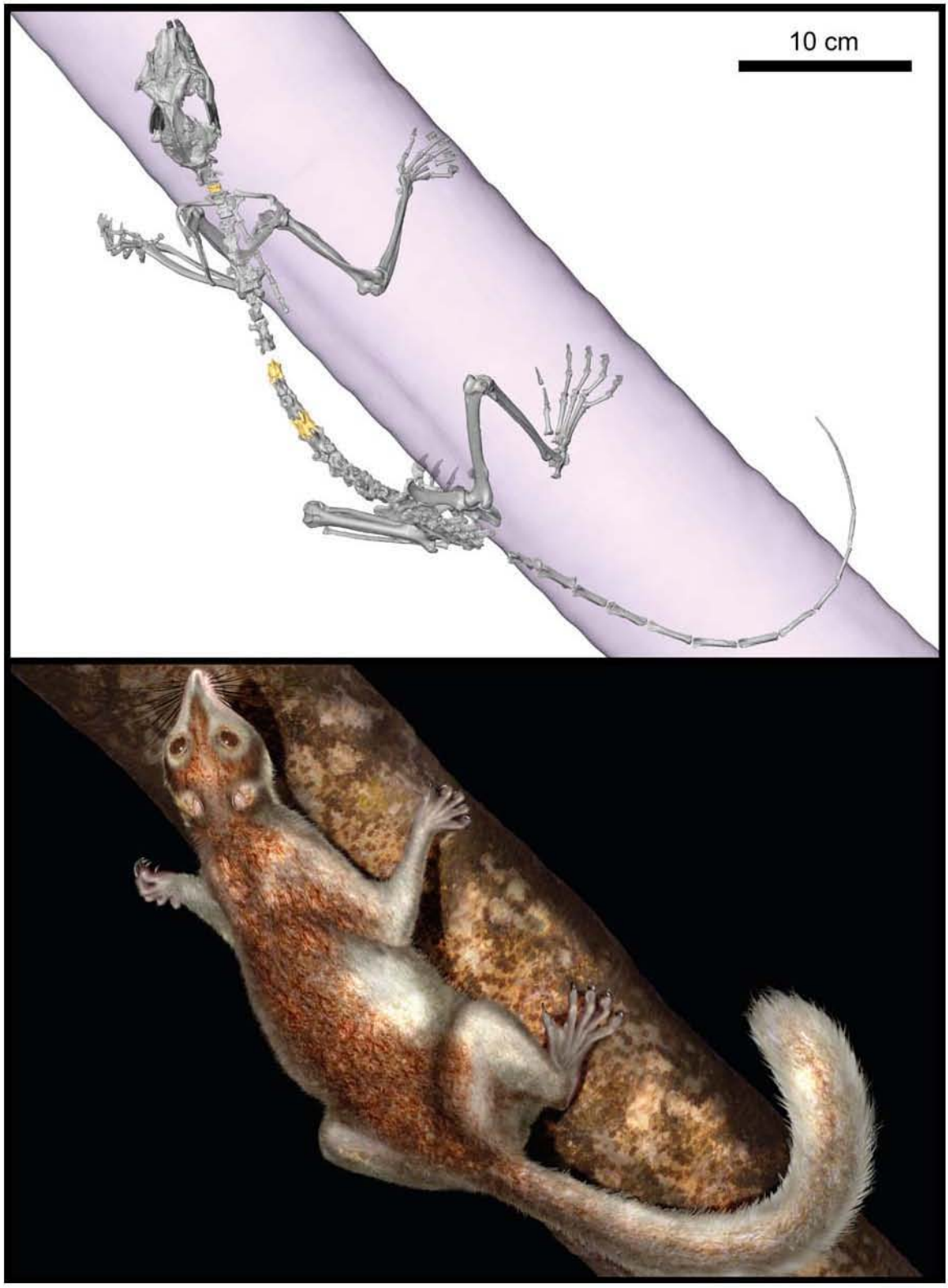
10 cm

BIBLIOGRAPHY

Alexander, R.M., Jayes, A.S., Maloiy, G.M.O., Wathuta, E.M., 1979. Allometry of limb bones of mammals from shrews (*Sorex*) to elephant (*Loxodonta*). Journal of Zoology, London 189, 305-314.

Argot, C., 2002. Functional-adaptive analysis of the hindlimb anatomy of extant marsupials and the paleobiology of the Paleocene marsupials *Mayulestes ferox* and *Pucadelphys andinus*. Journal of Morphology 253, 76-108.

Beard, K.C., 1989. Postcranial anatomy, locomotor adaptations, and palaeoecology of Early Cenozoic Plesiadapidae, Paromomyidae, and Micromomyidae (Eutheria, Dermoptera). Ph.D. Dissertation, Johns Hopkins University.

Beard, K.C., 1990. Gliding behavior and paleoecology of the alleged primate family Paromomyidae (Mammalia, Dermoptera). Nature 345, 340-341.

Beard, K.C., 1993a. Phylogenetic systematics of the Primatomorpha, with special reference to Dermoptera. In: Szalay, F.S., McKenna, M.C., Novacek, M.J. (eds) Mammal Phylogeny: Placentals. Springer-Verlag, New York, pp. 129-150.

Beard, K.C., 1993b. Origin and evolution of gliding in Early Cenozoic Dermoptera (Mammalia, Primatopmorpha). In: MacPhee, R.D.E. (ed) Primates and Their Relatives in Phylogenetic Perspective. Plenum Press, New York, pp. 63-90.

Beard, K.C., MacPhee, R.D.E., 1994. Cranial anatomy of *Shoshonius* and the antiquity of Anthropoidea. In: Fleagle, J.G., Kay, R.F. (eds) Anthropoid Origins. Plenum Press, New York, pp. 55-97.

Bloch, J.I., Boyer, D.M., 2001. Taphonomy of small mammals in freshwater limestones from the Paleocene of the Clarks Fork Basin. In: Gingerich, P.D. (ed) Paleocene-Eocene stratigraphy and biotic change in the Bighorn and Clarks Fork basins, Wyoming. University of Michigan Papers on Paleontology 33, 185-198.

Bloch, J.I., Boyer, D.M., 2002. Grasping primate origins. Science 298, 1606-1610.

Bloch, J.I., Boyer, D.M., 2003. Response to comment on "Grasping Primate Origins". Science 300, 741c.

Bloch, J.I., Boyer, D.M., 2007. New skeletons of Paleocene-Eocene Plesiadapiformes: a diversity of arboreal positional behaviors in early primates. In: Dagosto, M., Ravosa, M.J. (eds) Primate Origins: Adaptations and Evolution. Plenum Press, New York, pp. 535-582.

Bloch, J.I., Silcox, M.T., 2001. New basicrania of Paleocene-Eocene *Ignacius*: re-evaluation of the plesiadapiform-dermopteran link. American Journal of Physical Anthropology 116, 184-198.

Bloch, J.I., Silcox, M.T., 2006. Cranial anatomy of the Paleocene plesiadapiform *Carpolestes simpsoni* (Mammalia, Primates) using ultra high-resolution X-ray computed tomography, and the relationships of plesiadapiforms to Euprimates. Journal of Human Evolution 50, 1-35.

Bloch, J.I., Fisher, D.C., Rose, K.D., Gingerich, P.D., 2001. Stratocladistic analysis of Paleocene Carpolestidae (Mammalia, Plesiadapiformes) with description of a new late Tiffanian genus. Journal of Vertebrate Paleontology 21, 119-131.

Bloch, J.I., Silcox, M.T., Boyer, D.M., Sargis, E.J., 2007. New Paleocene skeletons and the relationship of plesiadapiforms to crown-clade primates. Proceedings of the National Academy of Sciences 104, 1159-1164.

Boyer, D.M., 2008. Relief index of second mandibular molars is a correlate of diet in Primates and other euarchontan mammals. Journal of Human Evolution 55, 1118-1137.

Boyer, D.M., Bloch, J.I., 2008. Evaluating the mitten-gliding hypothesis for Paromomyidae and Micromomyidae (Mammalia, "Plesiadapiformes") using comparative functional morphology of new Paleogene skeletons. In: Sargis, E.J., Dagosto, M. (eds) Mammalian Evolutionary Morphology: A Tribute to Frederick S. Szalay. Kluwer, New York, pp. 233-284.

Boyer, D.M., Bloch, J.I., Silcox, M.T., Gingerich, P.D., 2004. New observations on anatomy of *Nannodectes* (Mammalia, Primates) from the Paleocene of Montana and Colorado. Journal of Vertebrate Paleontology 24, 40A.

Boyer, D.M., Patel, B.A., Larson, S.G., Stern, J.T.J., 2007. Telemetered electromyography of peroneus longus in *Varecia variegata* and *Eulemur rubriventer*: implications for the functional significance of a large peroneal process. Journal of Human Evolution 53, 119-134.

Cartmill, M., 1972. Arboreal adaptations and the origin of the order Primates. In: Tuttle, R. (ed) The Functional and Evolutionary Biology of Primates. Aldine, Chicago, pp. 97-122.

Cartmill, M., 1992. New views on primate origins. Evolutionary Anthropology 1, 105-111.

Clemens, W.A., 2004. *Purgatorius* (Plesiadapiformes, Primates?, Mammalia), a Paleocene immigrant into northeastern Montana: Stratigraphic occurrences and incisor proportions. Bulletin of Carnegie Museum of Natural History 3, 3-13.

Coleman, M. N. and Boyer, D.M. 2008. A new line of evidence for investigating cerebral circulation patterns in fossils. Journal of Vertebrate Paleontology 28, 66A.

Conroy, G.C., Wible, J.R., 1978. Middle ear morphology of *Lemur variegatus*: Some implications for primate paleontology. Folia Primatologica 29, 81-85.

Evans, A.R., Wilson, G.P., Fortelius, M., Jernvall, J., 2007. High-level similarity of dentitions in carnivorans and rodents. Nature 445, 78-81.

Evans, H.E., 1993. Miller's Anatomy of the Dog. W. B. Saunders, Philidelphia.

Fleagle, J.G., 1999. Primate Adaptation and Evolution. Academic Press, New York.

Fleagle, J.G., Anapol, F.C., 1992. The indriid ischium and the hominid hip. Journal of Human Evolution 22, 285-305.

Fox, R.C., 1990a. *Pronothodectes gaoi* n. sp. from the late Paleocene of Alberta, Canada, and the early evolution of the Plesiadapidae (Mammalia, Primates). Journal of Paleontology 64, 637-647.

Fox, R.C., 1990b. The succession of Paleocene mammals in western Canada. Geological Society of America Special Paper 243, 51-70.

Fox, R.C., 1991. Systematic position of *Pronothodectes gaoi* Fox from the Paleocene of Alberta: reply. Journal of Paleontology 65, 700-701.

Fox, R.C., 1993. The primitive dental formula of the Carpolestidae (Plesiadapiformes, Mammalia) and its phylogenetic implications. Journal of Vertebrate Paleontology 13, 516-524.

Fu, J.-F., Wang, J.-W., Tong, Y.-S., 2002. The new discovery of the Plesiadapiformes from the early Eocene of Wutu Basin, Shandong Province. Vertebrata PalAsiatica 40, 219-227.

Gambaryan, P.P., 1974. How Mammals Run. Wiley, New York.

Gaudin, T.J., Wible, J.R., 1999. The entotympanic of pangolins and the phylogeny of Pholidota (Mammalia). Journal of Mammalian Evolution 6, 39-65.

George, R.M., 1977. The limb musculature of the Tupaiidae. Primates 18, 1-34.

Gervais, M.P., 1877. Enumération de quelques ossements d'animaux vertébrés, recueillis aux environs de Reims par M. Lemoine. Journal de Zoologie 6, 74-79.

Gidley, J.W., 1923. Paleocene primates of the Fort Union, with discussion of relationships of Eocene primates. Proceedings of the U S National Museum 63, 1-38.

Gingerich, P.D., 1971. Cranium of *Plesiadapis*. Nature 232, 566-&.

Gingerich, P.D., 1973. First record of the Paleocene primate *Chiromyoides* from North America. Nature 244, 517-518.

Gingerich, P.D., 1975a. Systematic position of *Plesiadapis*. Nature 253, 111-113.

Gingerich, P.D., 1975b. New North American Plesiadapidae (Mammalia, Primates) and a biostratigraphic zonation of the middle and upper Paleocene. University of Michigan Papers on Paleontology 24, 135-148.

Gingerich, P.D., 1976. Cranial anatomy and evolution of Early Tertiary Plesiadapidae (Mammalia, Primates). University of Michigan Papers on Paleontology 15, 1-141.

Gingerich, P.D., 1990. Prediction of body mass in mammalian species from long bone lengths and diameters. Contributions from the Museum of Paleontology 28, 79-92.

Gingerich, P.D., 1991. Systematic position of *Pronothodectes gaoi* Fox from the Paleocene of Alberta. Journal of Paleontology 65, 699.

Gingerich, P.D., 2000. Arithmetic or geometric normality of biological variation: an empirical test of theory. Journal of Theoretical Biology 204, 201-221.

Gingerich, P.D., Gunnell, G.F., 1992. A new skeleton of *Plesiadapis cookei*. The Display Case University of Michigan 6, 1, 3.

Gingerich, P.D., Gunnell, G.F., 2005. Brain of *Plesiadapis cookei* (Mammalia, Proprimates): surface morphology and encephalization compared to those of Primates and Dermoptera. University of Michigan Museum of Paleontology Contributions 31, 185-195.

Gingerich, P.D., Krause, D.W., Houde, P., 1983. A new earliest Tiffanian (Late Paleocene) mammalian fauna from Bangtail Plateau, western Crazy Mountain Basin, Montana. Journal of Paleontology 57, 957-970.

Gingerich, P.D., Smith, B.H., Rosenberg, K., 1982. Allometric scaling in the dentition of primates and prediction of body weight from tooth size in fossils. American Journal of Physical Anthropology 58, 81-100.

Goloboff, P., 1999. NONA (No NAME) ver. 2 Published by the author, Tucumàn, Argentina.

Godinot, M., Beard, K.C., 1991. Fossil primate hands: a review and an evolutionary inquiry emphasizing early forms. Human Evolution 6, 307-354.

Gradstein, F.M., Ogg, J.G., Smith, A.G., 2004. A Geologic Time Scale 2004. Cambridge University Press, Cambridge.

Gregory, W.K., 1920. On the structure and relations of *Notharctus*, an American Eocene primate. Memoires of the American Museum of Natural History 3, 45-243.

Gunnell, G.F., 1989. Evolutionary history of Microsyopoidea (Mammalia, ?Primates) and the relationship between Plesiadapiformes and Primates. University of Michigan, Papers on Paleontology 27, 1-157.

Gunnell, G.F., Gingerich, P.D., 1987. Skull and partial skeleton of *Plesiadapis cookei* from the Clarks Fork Basin, Wyoming. American Journal of Physical Anthropology 72, 206a.

Haines, R.W., 1955. The anatomy of the hand of certain insectivores. Proceedings of the Zoological Society of London 125, 761-776.

Hamrick, M.W., Rosenman, B.A., Brush, J.A., 1999. Phalangeal morphology of the Paromomyidae (?Primates, Plesiadapiformes): The evidence for gliding behavior reconsidered. American Journal of Physical Anthropology 109, 397-413.

Hamrick, M.W., 2001. Primate origins: evolutionary change in digit ray patterning and segmentation. Journal of Human Evolution 40, 339-351.

Hoffstetter, R., 1977. Phylogénie des primates. Confrontation des resultats obtenus par les diverses voies d'approche du probleme. Bulletins and Mémoires Société d'Anthropologie de Paris t.4, série XIII, 327-346.

Hooker, J.J., 1994. A new species of *Platychoerops* (Plesiadapiformes, Mammalia) from the latest Palaeocene of the Paris, London and Belgian basins. Geobios 27, 343-352.

Hooker, J.J., Millbank, C., 2001. A Cernaysian mammal from the Upnor Formation (Late Palaeocene, Herne Bay, UK) and its implications for correlation. Proceedings of the Geologists' Association 112, 331-338.

Jenkins, F.A., 1974. Tree shrew locomotion and the origins of primate arborealism. In: Jenkins, F.A. (ed) Primate Locomotion. Academic Press, New York, pp. 85-115.

Jepsen, G.L., 1930. Stratigraphy and paleontology of the Paleocene of northeastern Park County, Wyoming. Proceedings of the American Philosophical Society 69, 463-528.

Jernvall, J., Gilbert, C.C., Wright, P.C., 2008. Peculiar tooth homologies of the greater bamboo lemur (*Prolemur = Hapalemur simus*): When is a paracone not a paracone? In: Fleagle, J.G., Gilbert, C.C. (eds) Elwyn Simons: A Search for Origins. Springer, New York, pp. 335–342.

Jungers, W.L., 1985. Body size and scaling of limb proportions in primates. In: Jungers, W.L. (ed) Size and Scaling in Primate Biology. Plenum Publishing Corporation, New York, pp. 345-381.

Jungers, W.L., Falsetti, A.B., Wall, C.E., 1995. Shape, relative size, and size-adjustments in morphometrics. Yearbook of Physical Anthropology 38, 137-161.

Kay, R.F., 1975. The functional adaptations of primate molar teeth. American Journal of Physical Anthropology 43, 195-216.

Kay, R.F., Thewissen, J.G.M., Yoder, A.D., 1992. Cranial anatomy of *Ignacius graybullianus* and the affinities of the Plesiadapiformes. American Journal of Physical Anthropology 89, 477-498.

Kirk, E.C., Cartmill, M., Kay, R.F., Lemelin, P., 2003. Comment on "Grasping primate origins". Science 300, 741.

Kirk, E.C., Lemelin, P., Hamrick, M.W., Boyer, D.M., Bloch, J.I., 2008. Intrinsic hand proportions of euarchontans and other mammals: implications for the locomotor behavior of plesiadapiforms. Journal of Human Evolution 55, 278-299.

Le Gros Clark, W.E., 1926. On the anatomy of the pen-tailed tree-shrew. Proceedings of the Zoological Society of London 1926, 1179-1309.

Lemoine, V., 1893. Etude sur les os du pied des mammifères de la faume cernaysienne et sur quelques pieces osseuses nouvelles de cet horizon paléontologique. Bulletin de la Societe Géologique de France (3eme ser) 21, 353-368.

Linnaeus, C., 1758. Systema naturae per regna tria natureae secundum classes, ordines genera, species cum characteribus, differentris, synonymis, locis, Editis decima, reformata edn. Laurentii Salvii, Stockholm.

Lofgren, D.L., Lillegraven, J.A., Clemens, W.A., Gingerich, P.D., Williamson, T.E., 2004. Paleocene biochronology: the Puercan through Clarkforkian land mammal ages. In: Woodburne, M.O. (ed) Cenozoic Mammals of North America: Geochronology and Biostratigraphy, 2nd edn. University of California Press, Berkeley, pp. 43-105

MacPhee, R.D.E., 1981. Auditory Regions of Primates and Eutherian Insectivores: Morphology, Ontogeny, and Character Analysis. Contributions to Primatology 18, 1-282.

MacPhee, R.D.E., Cartmill, M., Gingerich, P.D., 1983. New Paleogene primate basicrania and the definition of the order Primates. Nature 301, 509-511.

MacPhee, R.D.E., Cartmill, M., 1986. Basicranial structures and primate systematics. Comparative Primate Biology, Volume 1: Systematics, Evolution, and Anatomy. Alan R. Liss, Inc., pp. 219-275.

Maiolino, S.A., Boyer, D.M., 2007. Evidence from claw morphology for a diversity of positional behaviors in plesiadapid "plesiadapiforms." Journal of Vertebrate Paleontology 27, 111A.

Mosimann, J.E., Malley, J.D., 1979. Size and shape variables. In: Orloci, L., Rao, C.R., Stiteler, W.M. (eds) Multivariate Methods in Ecological Work. International Cooperative, Fairland, pp. 175-189.

Napier, J.R., 1961. Prehensility and opposability in the hands of primates. Symposia of the Zoological Society of London 5, 115-132.

Napier, J.R., Walker, A.C., 1967. Vertical clinging and leaping - a newly recognized category of locomotor behavior of primates. Folia Primatologica 6, 204-219.

Nixon, K. C. 1999-2002. WinClada ver. 1.0000 Published by the author, Ithaca, NY, USA

Nomina Anatomica, 5th edition.1983. Williams & Wilkins, Baltimore.

Nomina Anatomica Veterinaria, 4th edition.1994. Adolf Holhauzen's Successors, Vienna

Novacek, M.J., 1977. Aspects of the problem of variation, origin and evolution of the eutherian auditory bulla. Mammal Review 7, 131-149.

Novacek, M.J., 1986. The skull of leptictid insectivorans and higher classification of eutherian mammals. Bulletin of the American Museum of Natural History 183, 1-111.

Novacek, M.J., Wyss, A.R., 1986. Higher-level relationships of the recent eutherian orders: morphological evidence. Cladistics 2, 257-287.

Piton, L.-E., 1940. Paléontologie du gisement éocène de Menat (Puy-de-Dôme) (Flore et Faune). Vallier, Clermont-Ferrand, 301p.

Rose, K.D., 1981. The Clarkforkian land-mammal age and mammalian faunal composition across the Paleocene-Eocene boundary. University of Michigan Papers on Paleontology No 26, 197 pp.

Rose, K.D., Bown, T.M., 1982. New plesiadapiform primates from the Eocene of Wyoming and Montana. Journal of Vertebrate Paleontology 2, 63-69.

Roach, H.I., Mehta, G., Oreffo, R.O.C., Clarke, M.P., Cooper, C., 2003. Temporal analysis of rat growth plates: cessation of growth with age despite presence of a physis. Journal of Histochemistry and Cytochemistry 51, 373-383.

Runestad, J.A., Ruff, C.B., 1995. Structural adaptations for gliding in mammals with implications for locomotor behavior in paromomyids. American Journal of Physical Anthropology 98, 101-119.

Russell, D.E., 1959. Le crâne de *Plesiadapis.* Bulletin de la Société Géologique de France, pp. 312-314

Russell, D.E., 1962. Essai de reconstitution de la vie Paléocène au Mont de Berru. Bulletin du Muséum National d'Histoire Naturelle 34, 101-106.

Russell, D.E., 1964. Les Mammifères Paléocènes d'Europe. Mémoires du Muséum National d'Histoire Naturelle, Série C 13, 1-324.

Russell, D.E., 1967. Sur *Menatotherium* et l'age Paléocène du gisement de Menat (Puy-de-Dôme). Problèms Actuels de Paléontologie, College International de Centre National de Recherche Scientifique, Paris 163, 483-490.

Sargis, E.J., 2001. A preliminary qualitative analysis of the axial skeleton of tupaiids (Mammalia, Scandentia): functional morphology and phylogenetic implications. Journal of Zoology 253, 473-483.

Sargis, E.J., 2002a. Functional morphology of the forelimb of tupaiids (Mammalia, Scandentia) and its phylogenetic implications. Journal of Morphology 253, 10-42.

Sargis, E.J., 2002b. Functional morphology of the hindlimb of tupaiids (Mammalia, Scandentia) and its phylogenetic implications. Journal of Morphology 254, 149-185.

Sargis, E.J., 2004. The postcranial morphology of *Ptilocercus lowii* (Scandentia, Tupaiidae): An analysis of primatomorphan and volitantian characters. Journal of Mammalian Evolution 9, 137-160.

Sargis, E.J., Boyer, D.M., Bloch, J.I., Silcox, M.T., 2007. Evolution of pedal grasping in Primates. Journal of Human Evolution 53, 103-107.

Savage, D.E., Russell, D.E., 1983. Mammalian Paleofaunas of the World. Addison-Wesley Publishing Company, Reading, Massachusetts.

Shapiro, L.J., Simons, C.V.M., 2002. Functional aspects of strepsirrhine lumbar vertebral bodies and spinous processes. Journal of Human Evolution 42, 753-783.

Silcox, M.T., 2001. A phylogenetic analysis of Plesiadapiformes and their relationship to Euprimates and other archontans. Ph.D., Johns Hopkins.

Silcox, M.T., 2003. New discoveries on the middle ear anatomy of *Ignacius graybullianus* (Paromomyidae, Primates) from ultra high resolution X-ray computed tomography. Journal of Human Evolution 44, 73-86.

Silcox, M.T., Gunnell, G.F., 2008. "Plesiadapiformes." In: Janis, C.M., Gunnell, G.F., Uhen, M.D. (eds) Evolution of Tertiary Mammals of North America, Volume 2: Small mammals, xenarthrans, and marine mammals. Cambridge University Press, Cambridge, pp. 207-238.

Silcox, M.T., Bloch, J.I., Boyer, D.M., Godinot, M., Ryan, T.M., Spoor, F., Walker, A. in press. The semicircular canal system in early primates, Journal of Human Evolution.

Silcox, M.T., Krause, D.W., Maas, M.C., Fox, R.C., 2001. New specimens of *Elphidotarsius russelli* (Mammalia, ?Primates, Carpolestidae) and a revision of plesiadapoid relationships. Journal of Vertebrate Paleontology 21, 132-152.

Simons, E.L., 1960. New fossil primates: a review of the past decade. American Scientist 48, 179-192.

Simons, E.L., 1964. The early relatives of man. Scientific American 211, 51-62.

Simons, E.L., 1967. Fossil primates and the evolution of some primate locomotor systems. American Journal of Physical Anthropology 26, 241-254.

Simons, E.L., 1972. Primate Evolution, An Introduction to Man's Place in Nature. Macmillan, New York.

Simpson, G.G., 1935. The Tiffany fauna, upper Paleocene. II.-Structure and relationships of *Plesiadapis*. American Museum Novitates, 1-30.

Simpson, G.G., 1937. The Fort Union of the Crazy Mountain Field, Montana, and its mammalian faunas. United States National Museum Bulletin 169, 1-287.

Sokal, R.R., Rohlf, J.F., 1997. Biometry, The Principles and Practice of Statistics in Biological Research. W. H. Freeman and Company, New York.

Stafford, B.J., Thorington, R.W.J., 1998. Carpal development and morphology in archontan mammals. Journal of Morphology 235, 135-155.

Stafford, B.J., 1999. Taxonomy and Ecological Morphology of the Flying Lemurs (Dermoptera, Cynocephalidae). Doctor of Philosophy, City University of New York.

Stern, J.T.,Jr., 1988. Essentials of Gross Anatomy. F. A. Davis, Philadelphia.

Straus, W.L., Jr., 1930. The foot musculature of the highland gorilla (*Gorilla beringei*). Quarterly Review of Biology 5, 261-317.

Sussman, R.W., Raven, P.H., 1978. Pollination by lemurs and marsupials: an archaic coevolutionary system. Science 200, 731-736.

Sussman, R.W., 1991. Primate origins and the evolution of angiosperms. American Journal of Primatology 23, 209-223.

Szalay, F.S., 1968. The beginnings of primates. Evolution 22, 19-36.

Szalay, F.S., 1971. Cranium of the Late Palaeocene primate *Plesiadapis tricuspidens*. Nature 230, 324-325.

Szalay, F.S., 1972. Cranial morphology of the Early Tertiary *Phenacolemur* and its bearing on primate phylogeny. American Journal of Physical Anthropology 36, 59-76.

Szalay, F.S., 1972. Paleobiology of the earliest primates. In: Tuttle, R.H. (ed) Functional and Evolutionary Biology of Primates. Aldine, Chicago, pp. 3-35.

Szalay, F.S., 1975. Where to draw the nonprimate-primate taxonomic boundary. Folia Primatologica 23, 158-163.

Szalay, F.S., 1984. Arboreality: is it homologous in metatherian and eutherian mammals? In: Hecht, M.K., Wallace, B., Prance, G.T. (eds) Evolutionary Biology, Vol 18. Plenum, New York, pp. 215-258.

Szalay, F.S., Dagosto, M., 1980. Locomotor adaptations as reflected on the humerus of Paleogene primates. Folia Primatologica 34, 1-45.

Szalay, F.S., Dagosto, M., 1988. Evolution of hallucial grasping in the Primates. Journal of Human Evolution 17, 1-33.

Szalay, F.S., Decker, R.L., 1974. Origins, evolution and functon of the tarsus in Late Cretaceous Eutheria and Paleocene primates. In: Jenkins, F.A. (ed) Primate Locomotion. Academic Press, New York, pp. 223-259.

Szalay, F.S., Drawhorn, G., 1980. Evolution and diversification of the Archonta in an arboreal milieu. In: Luckett, W.P. (ed) Comparative Biology and Evolutionary Relationships of Tree Shrews. Plenum Press, New York, pp. 133-169.

Szalay, F.S., Rosenberger, A.L., Dagosto, M., 1987. Diagnosis and differentiation of the order Primates. Yearbook of Physical Anthropology 30, 75-105.

Szalay, F.S., Tattersall, I., Decker, R.L., 1975. Phylogenetic relationships of *Plesiadapis* - postcranial evidence. Contributions to Primatology 5, 136-166.

Tambareau, Y., Russell, D.E., Sigogneau-Russell, D., Villatte, J., 1992. Decouverte de vertébrés dans le Paléocène de Campo (Pryenees aragonaises). Bulletin de la Societe d'Histoire Naturelle de Toulouse 128, 73-76.

Teilhard de Chardin, P., 1922. Les mammifères de l'éocène inférieur francais et leurs gisements. Annales de Paléontologie 11, 9-116.

Thewissen, J.G.M., Williams, E.M., Hussain, S.T., 2001. Eocene mammal faunas from northern Indo-Pakistan. Journal of Vertebrate Paleontology 21, 347-366.

Trouessart, E.L., 1897. Catalogues des Mammalium tam Viventium quam Fossilium. R. Friedlander und Sohn, Berlin.

Van der Klaauw, C.J., 1931. The auditory bulla in some fossil mammals with a general introduction to this region of the skull. Bulletin of the American Museum of Natural History 62, 1-352.

Van Valen, L., 1971. Adaptive zones and the orders of mammals. Evolution 25, 420-428.

Van Valen, L.M., 1982. Homology and causes. Journal of Morphology 173, 305-312.

Van Valen, L.M., 1994. The origin of the plesiadapid primates and the nature of *Purgatorius*. University of Chicago Evolutionary Monographs 15, 1-79.

Wible, J.R., 1993. Cranial circulation and relationships of the colugo *Cynocephalus* (Dermoptera, Mammalia). American Museum Novitates 3072, 1-27.

Wible, J.R., Covert, H.H., 1987. Primates: cladistic diagnosis and relationships. Journal of Human Evolution 16, 1-22.

Wible, J.R., Gaudin, T.J., 2004. On the cranial anatomy of the yellow armadillo *Euphractus sexintus* (Dasypodidae, Xenarthra, Placentalia). Annals of the Carnegie Museum 73, 117-196.

Wible, J.R., Novacek, M.J., 1988. Cranial evidence for the monophyletic origin of bats. American Museum Novitates 2911, 1-19.

Wible, J.R., 2008. On the cranial osteology of the hispaniolan solenodon *Solenodon paradoxurus* Brandt, 1833 (Mammalia, Lipotyphla, Solenodontidae). Annals of the Carnegie Museum 77, 321-402.

Wiley, E.O., Siegel-Causey, D., Brooks, D.R., Funk, V.A., 1991. The Compleat Cladist: A Primer of Phylogenetic Procedures. University of Kansas Museum of Natural History, Lawrence, Kansas.

Witmer, L.M., 1995. The extant phylogenetic bracket and the importance of reconstructing soft tissues in fossils. In: Thomason, J.J. (ed) Functional Morphology in Vertebrate Paleontology. Cambridge University Press, Cambridge, pp. 19-33.

Youlatos, D., Godinot, M., 2004. Locomotor adaptations of *Plesiadapis tricuspidens* and *Plesiadapis* n. sp. (Mammalia, Plesiadapiformes) as reflected in selected parts of the postcranium. Journal of Anthropological Sciences 82, 103-118

Zachos, J., Pagani, M., Sloan, L., Thomas, E., Billups, K., 2001. Trends, rhythms, and aberrations in global climate 65 Ma to present. Science 292, 686-693.